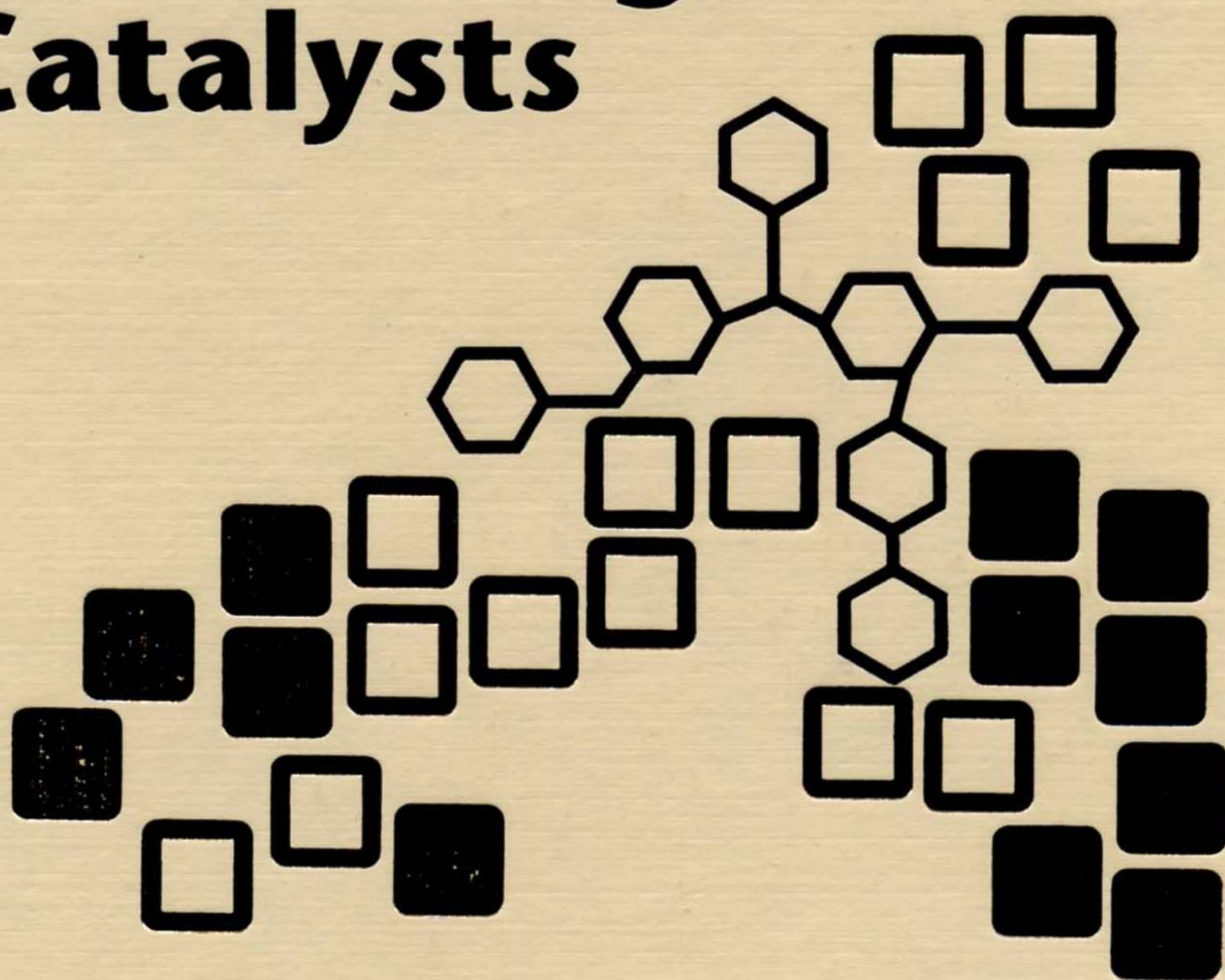


Deactivation and Testing of Hydrocarbon-Processing Catalysts



EDITED BY

**Paul O'Connor, Toru Takatsuka,
and Geoffrey L. Woolery**

ACS Symposium Series 634

Deactivation and Testing of Hydrocarbon-Processing Catalysts

Paul O'Connor, EDITOR
Akzo Nobel Catalysts

Toru Takatsuka, EDITOR
Chiyoda Corporation

Geoffrey L. Woolery, EDITOR
Mobil Technology Company

Developed from a symposium sponsored
by the Division of Petroleum Chemistry, Inc.
at the 210th National Meeting
of the American Chemical Society,
Chicago, Illinois,
August 20–25, 1995





Library of Congress Cataloging-in-Publication Data

Deactivation and testing of hydrocarbon-processing catalysts / Paul O'Connor, editor, Toru Takatsuka, editor, Geoffrey L. Woolery, editor.

p. cm.—(ACS symposium series, ISSN 0097-6156; 634)

“Developed from a symposium sponsored by the Division of Petroleum Chemistry, Inc., at the 210th National Meeting of the American Chemical Society, Chicago, Illinois, August 20–25, 1995.”

Includes bibliographical references and indexes.

ISBN 0-8412-3411-6

1. Petroleum—Refining—Congresses.
2. Catalysts—Congresses.
3. Catalyst poisoning—Congresses.

I. O'Connor, Paul. II. Takatsuka, Toru, 1948— . III. Woolery, Geoffrey Logan. IV. American Chemical Society. Division of Petroleum Chemistry. V. American Chemical Society. Meeting (210th: 1995: Chicago, Ill.) VI. Series.

TP690.A1D43 1996
665.5'33—dc20

96-17665
CIP

This book is printed on acid-free, recycled paper.



Copyright © 1996

American Chemical Society

All Rights Reserved. The appearance of the code at the bottom of the first page of each chapter in this volume indicates the copyright owner's consent that reprographic copies of the chapter may be made for personal or internal use or for the personal or internal use of specific clients. This consent is given on the condition, however, that the copier pay the stated per-copy fee through the Copyright Clearance Center, Inc., 222 Rosewood Drive, Danvers, MA 01923, for copying beyond that permitted by Sections 107 or 108 of the U.S. Copyright Law. This consent does not extend to copying or transmission by any means—graphic or electronic—for any other purpose, such as for general distribution, for advertising or promotional purposes, for creating a new collective work, for resale, or for information storage and retrieval systems. The copying fee for each chapter is indicated in the code at the bottom of the first page of the chapter.

The citation of trade names and/or names of manufacturers in this publication is not to be construed as an endorsement or as approval by ACS of the commercial products or services referenced herein; nor should the mere reference herein to any drawing, specification, chemical process, or other data be regarded as a license or as a conveyance of any right or permission to the holder, reader, or any other person or corporation, to manufacture, reproduce, use, or sell any patented invention or copyrighted work that may in any way be related thereto. Registered names, trademarks, etc., used in this publication, even without specific indication thereof, are not to be considered unprotected by law.

PRINTED IN THE UNITED STATES OF AMERICA

Advisory Board

ACS Symposium Series

Robert J. Alaimo
Procter & Gamble Pharmaceuticals

Mark Arnold
University of Iowa

David Baker
University of Tennessee

Arindam Bose
Pfizer Central Research

Robert F. Brady, Jr.
Naval Research Laboratory

Mary E. Castellion
ChemEdit Company

Margaret A. Cavanaugh
National Science Foundation

Arthur B. Ellis
University of Wisconsin at Madison

Gunda I. Georg
University of Kansas

Madeleine M. Joullie
University of Pennsylvania

Lawrence P. Klemann
Nabisco Foods Group

Douglas R. Lloyd
The University of Texas at Austin

Cynthia A. Maryanoff
R. W. Johnson Pharmaceutical
Research Institute

Roger A. Minear
University of Illinois
at Urbana–Champaign

Omkaram Nalamasu
AT&T Bell Laboratories

Vincent Pecoraro
University of Michigan

George W. Roberts
North Carolina State University

John R. Shapley
University of Illinois
at Urbana–Champaign

Douglas A. Smith
Concurrent Technologies Corporation

L. Somasundaram
DuPont

Michael D. Taylor
Parke-Davis Pharmaceutical Research

William C. Walker
DuPont

Peter Willett
University of Sheffield (England)

Foreword

THE ACS SYMPOSIUM SERIES was first published in 1974 to provide a mechanism for publishing symposia quickly in book form. The purpose of this series is to publish comprehensive books developed from symposia, which are usually "snapshots in time" of the current research being done on a topic, plus some review material on the topic. For this reason, it is necessary that the papers be published as quickly as possible.

Before a symposium-based book is put under contract, the proposed table of contents is reviewed for appropriateness to the topic and for comprehensiveness of the collection. Some papers are excluded at this point, and others are added to round out the scope of the volume. In addition, a draft of each paper is peer-reviewed prior to final acceptance or rejection. This anonymous review process is supervised by the organizer(s) of the symposium, who become the editor(s) of the book. The authors then revise their papers according to the recommendations of both the reviewers and the editors, prepare camera-ready copy, and submit the final papers to the editors, who check that all necessary revisions have been made.

As a rule, only original research papers and original review papers are included in the volumes. Verbatim reproductions of previously published papers are not accepted.

ACS BOOKS DEPARTMENT

Contents

Preface	ix
----------------------	-----------

OVERVIEW

1. Philosophical Overview of Testing	2
Paul O'Connor, Geoffrey L. Woolery, and Toru Takatsuka	
2. Advantages, Possibilities, and Limitations of Small-Scale Testing of Catalysts for Fixed-Bed Processes	6
S. T. Sie	
3. Evaluating Pore Structure and Morphology of Hydrocarbon-Conversion Catalysts	42
R. Mann, K. Khalaf, and A. Al-Lamy	

CATALYST DEACTIVATION BY COKE

4. Deactivation of Zeolite Catalysts by Coke	62
T. Masuda and K. Hashimoto	
5. Modes of Coking and Deactivation of Acid Zeolite Catalysts	77
M. Guisnet, P. Magnoux, and K. Moljord	
6. Catalyst Coking, Activation, and Deactivation	91
P. A. Sermon, M. S. W. Vong, and M. Matheson	
7. NMR Techniques for Studying the Coking of Zeolite-Based Catalysts	99
J. L. Bonardet, M. C. Barrage, and J. Fraissard	
8. Characterization of Fluid Catalytic Cracking Catalyst Coke by ¹³C NMR and Mass Spectrometry	117
B. J. McGhee, J. M. Andresen, C. E. Snape, R. Hughes, C. L. Koon, and G. Hutchings	

DEACTIVATION OF FLUID CATALYTIC CRACKING
CATALYSTS

9. **Catalyst Decay as a Side Reaction of the Chain Processes of Catalytic Cracking**..... 134
B. W. Wojciechowski and N. M. Rice
10. **Catalyst Deactivation in Fluid Catalytic Cracking: A Review of Mechanisms and Testing Methods** 147
Paul O'Connor, E. Brevoord, A. C. Pouwels, and
H. N. J. Wijngaards
11. **Sodium Deactivation of Fluid Catalytic Cracking Catalyst** 159
Xinjin Zhao and Wu-Cheng Cheng
12. **Contaminant-Metal Deactivation and Metal-Dehydrogenation Effects During Cyclic Propylene Steaming of Fluid Catalytic Cracking Catalysts**..... 171
Lori T. Boock, Thomas F. Petti, and John A. Rudesill

DEACTIVATION OF REFORMING CATALYSTS

13. **Catalyst Deactivation in Adiabatic Prereforming: Experimental Methods and Models for Prediction of Performance** 186
Thomas S. Christensen and Jens Rostrup-Nielsen
14. **Mechanism of Deactivation in Reforming Catalysts at Start of Run** 201
Yaofang Liu, Guoqing Pan, and Jiujin Yang

DEACTIVATION OF HYDROPROCESSING CATALYSTS

15. **Catalyst Deactivation in Commercial Residue Hydrodesulfurization** 208
Hiroki Koyama, Eiichi Nagai, and Hideaki Kumagai
16. **Deactivation of Light Naphtha Aromatization Catalyst** 219
S. Fukase, N. Igarashi, K. Aimoto, and K. Kato
17. **Effect of Process Conditions and Catalyst Properties on Catalyst Deactivation in Residue Hydroprocessing**..... 229
M. Absi-Halabi and A. Stanislaus

- 18. Catalyst Deactivation in Hydrodemetallization..... 238**
 J. P. Janssens, A. D. van Langeveld, S. T. Sie,
 and J. A. Moulijn

TESTING OF CATALYST PERFORMANCE

- 19. Activity and Coking Rate of Catalysts Deactivated
 by Fast-Coking Species Added to the Feed 254**
 Dady B. Dadyburjor, Zhenyu Liu, Shigeki Matoba,
 Shinichi Osanai, and Tetsuya Shirooka
- 20. Pilot Reactor Testing of the Effect of Naphtha Boiling
 Point in Catalytic Reforming..... 268**
 K. Moljord, K. Grande, I. Tanem, and A. Holmen
- 21. Vanadium Mobility in Fluid Catalytic Cracking..... 283**
 Richard F. Wormsbecher, Wu-Cheng Cheng, Gwan Kim,
 and Robert H. Harding
- 22. Improved Methods for Testing and Assessing Deactivation
 from Vanadium Interaction with Fluid Catalytic Cracking
 Catalyst 296**
 Bruce Lerner and Michel Deeba
- 23. Riser Simulator: Testing of Adsorption Effects..... 312**
 Jacek Pruski, Ahmet Pekediz, and Hugo de Lasa
- 24. Development of a Bench-Scale Fluid Catalytic Cracking
 Microriser..... 322**
 M. P. Helmsing, M. Makkee, and J. A. Moulijn
- 25. Evaluation of Coke Selectivity of Fluid Catalytic Cracking
 Catalysts 340**
 E. Brevoord, A. C. Pouwels, F. P. P. Olthof,
 H. N. J. Wijngaards, and Paul O'Connor
- 26. Correlation of Catalyst Performance Between Laboratory
 Tests and Commercial Units for Hydrotreating Residual Oil 354**
 Yoshimitsu Miyauchi, Takeshi Hashiguchi, Naoto Kimbara,
 and Katsuhisa Fujita
- 27. Life Testing of Light Hydrocarbon Aromatization Catalysts 367**
 K. Hirabayashi, F. Igarashi, and T. Kondou

28. Performance Testing of Hydroconversion Catalysts.....	379
W. H. J. Stork	
29. Development of a Test Procedure To Evaluate Fluid Catalytic Cracking Catalyst Regenerability	401
V. L. N. Murthy, S. Debnath, M. Rama Rao, S. K. Ray, A. K. Das, and S. Ghosh	

MODELING OF CATALYST PERFORMANCE

30. A Catalyst Deactivation Model for Residual Oil Hydrodesulfurization and Application to Deep Hydrodesulfurization of Diesel Fuel	414
Toru Takatsuka, Yukitaka Wada, and Shin-ichi Inoue	
31. Modeling Catalytic Deactivation of Benzene Hydrogenation	428
Paul F. Meier and Marvin M. Johnson	

INDEXES

Author Index	439
Affiliation Index	440
Subject Index.....	440

Preface

CRUDE PETROLEUM CONSISTING OF HEAVY HYDROCARBONS is converted into many products in large refineries, usually in processes that make use of specific heterogeneous catalysts. Selecting the correct catalyst for a specific application is a complex and difficult task, and accurate and reliable laboratory tests need to be developed for this purpose. As time passes the catalysts used in the various processes lose their activity, and selectivity also declines. Therefore, evaluating hydrocarbon conversion catalysts requires a good simulation of the catalyst deactivation behavior. This is a field of great interest to the scientists and engineers who are trying to test catalysts in a proper way in order to improve key hydrocarbon-conversion processes such as catalytic cracking and hydroconversion.

The field of testing is one in which most companies are willing to share their knowledge and procedures and one in which the need for education, exchange, and standardization is clearly present. Also the large growth of hydrocarbon-conversion processes in the Asia Pacific region implies that many new scientists and engineers are becoming involved in this field. At the moment there are no clear reference works other than occasional symposium proceedings, which are often too broad or too theoretical or cover only part of the topic and mainly report on recent developments.

The objective of this book is to serve as a practical reference work on testing for the main hydrocarbon-conversion processes applied in oil refineries: catalytic cracking, hydroprocessing, and reforming. These fields were combined because of the clear analogies and congruence between the areas, such as deactivation of active sites by coke, mass-transfer phenomena of hydrocarbons into solid catalysts, hydrocarbon chemistry and reaction kinetics, and downscaling of commercial conditions to realistic small-scale tests.

As the title reveals, this volume focuses on deactivation and testing; however, analytical methods and characterization techniques and process modeling are also discussed, as these vital disciplines deserve attention in order to design a proper evaluation protocol.

This book will be warmly welcomed not only by the people directly working in this dynamic field, but it will also be of significant interest to scientists and engineers involved in the general areas of heterogeneous catalysis, catalyst characterization and preparation, chemical reaction engineering, and hydrocarbon processing.

Acknowledgments

We thank the authors for the effort they made both in presenting their work at the symposium upon which this book is based and in preparing the camera-ready manuscripts used in this volume. The views and conclusions expressed in this book are those of the authors. We express our gratitude to all our colleagues who acted as technical referees and to W. A. Wachter in particular, who took on the gigantic task of editing all the manuscripts.

We thank the ACS Division of Petroleum Chemistry, Inc., for sponsoring the symposium and in particular John Reynolds and Herman Lovink for their continuous personal support of this project. We also thank Anne Wilson of ACS Books, whose friendly coaching helped us meet our deadlines.

We are indebted to Chiyoda Corporation, Mobil Technology Company, and Akzo Nobel Catalysts for allowing us to participate in this project. And last but not least, we are grateful to Karin Haitzma-Atema from Akzo Nobel Catalysts who enthusiastically organized and directed the enormous flow of paper that started as a call for papers in 1993 and continued until the final manuscripts were ready early in 1996.

PAUL O'CONNOR
Akzo Nobel Catalysts
P.O. Box 37650
1030 BE Amsterdam
Netherlands

TORU TAKATSUKA
Chiyoda Corporation
3-13 Moriya-cho
Kanagawa-Ku
Yokohama 221
Japan

GEOFFREY L. WOOLERY
Mobil Technology Company
P.O. Box 480
Paulsboro, NJ 08066-0480

January 23, 1996

OVERVIEW

Chapter 1

Philosophical Overview of Testing

Paul O'Connor¹, Geoffrey L. Woolery², and Toru Takatsuka³

¹Akzo Nobel Catalysts, Nieuwendammerkade 1–3, P.O. Box 37650,
1030 BE Amsterdam, Netherlands

²Mobil Technology Company, P.O. Box 480, Paulsboro, NJ 08066–0480

³Chiyoda Corporation, 3–13 Moriya-cho, Kanagawa-Ku,
Yokohama 221, Japan

The proper testing of hydrocarbon conversion catalysts is of interest for the catalyst producers as well as the catalyst users. The decision on whether or not to continue the development of a new catalyst technology, or to use a new catalyst in a commercial situation will often depend on the results we see in a laboratory test.

It is in the interest of both the catalyst producer and the catalyst user, that the proper tests are used, and we feel that this is an area in which an open communication will definitely benefit both, yielding a Win-Win situation.

A philosophical introduction to testing.

The need for having good and realistic catalyst performance testing capabilities is obvious (1): For the catalyst producer, effective catalyst innovation is only possible if the many possible ideas and developments can be effectively checked. The costs of catalyst development are. Therefore a critical screening of the many leads generated is required.

For the catalyst user, it is crucial that on one hand no catalysts are used which endanger the continuity of operations, while on the other hand the best catalyst available to suit the unit should be selected at the earliest stage as possible, in order to maximize the benefits that the catalyst brings.

Having established the need for testing, it may be interesting to consider and reflect on some philosophical issues on the topic of testing.

In the Myth of Inductive Hypothesis Generation Karl Popper (2) states that the belief that we can start with pure observations alone without anything in the nature of a theory is absurd. As he illustrated by the story of the man who dedicated his life to natural science, wrote down everything he could observe and gave his

priceless collection of observations to the Royal Society to be used as inductive evidence. Popper himself started a lecture to physics students with the following instructions:

Take pencil and paper; carefully observe, and write down what you have observed!

They asked of course what he wanted them to observe. Clearly the instruction "Observe!" is absurd. Observation is always selective ! It needs a chosen object, a definite task, an interest, a point of view, a problem.

As remarked by Albert Einstein (3) Theory cannot be fabricated out of the results of observation, but it can only be invented; Observation as such cannot be prior to theory as such, since some theory is presupposed by any observation.

In Science, Pseudo-Science and Falsifiability Popper tackles the problem of the strength of a theory. He remarked that the apparent strength of theories which can explain everything was in fact their weakness. The impressive thing about strong theories is the risk involved in their predictions ! The criterion of the scientific status of a theory is its falsifiability, or refutability, or testability !

This places Testing in the middle of this discussion:

Also the instruction Test ! is absurd. A test implies a theory which needs to be proven or disapproved. A test should be a procedure of submitting a theory to such conditions as an attempt to falsify it or to refute it;

Testability is Falsifiability. Some theories are more testable, more exposed to refutation than others, they take greater risks !

The hypothesis, the testing protocol, collecting meaningful data and extracting conclusions.

A few years ago, at a previous ACS Symposium Dr.Flank (4) stated the following:

In testing a minimal degree of structuring is commonly employed, and there are numerous pitfalls that must be avoided if the conclusions drawn are to be worth very much. Is there a better way?

Ofcourse there is; Much of what should be done takes place before going into the lab ; each step along the way should be planned in advance and should be part of a coherent overall strategy. The process comprises a hypothesis, a testing protocol that has been constructed to meet perceived needs, collecting of meaningful responses, analysis of those responses in a number of ways, and extracting significant conclusions.

Flank remarks that the criteria for proving or disproving the hypothesis are often changed after the fact to accomodate poor data or a pre-conceived conclusion. This should be avoided by setting specific criteria in advance.

How to generate meaningful data in a laboratory?

The ultimate objective of a catalyst testing program is to evaluate the catalyst for performance in a commercial process (5). The challenge then becomes to generate

data in the laboratory which will be relevant for the large scale commercial operation.

Dautzenberg (6) and many others (1,5) propose guidelines to ensure effective catalyst testing on a laboratory and/or pilot plant scale; and ofcourse this area is also the main focus of this symposium. The choice of the proper catalyst pretreatment and/or deactivation conditions obviously also is a key issue to be addressed.

The trend towards testing on a smaller scale (miniaturization).

As stated by Sie (6), testing on a smaller scale can give significant benefits in terms of cost reduction (less investment, maintenance and labour costs) as well as safety; while the number of catalysts tested can be dramatically increased. Ofcourse testing on a smaller scale can only be feasible if the results remain relevant and meaningful for the assessment of the commercial performance of catalysts. The following table gives an example of this trend at the R&D centre of a large oil company (6):

Table 1. Units used for Hydrocarbon Process R&D at the Royal Dutch Shell Laboratories in Amsterdam

<i>Plant</i>	<i>Scale</i>	<i>Plants in 1970</i>	<i>Plants in 1987</i>
Pilot Plant	> 1 l	~30	~10
Bench Scale	30-100ml	~10	~35
Microflow	5-10ml	~ 5	~45

A combination of certain well chosen small scale tests with a good process model can also be effective as a replacement of large pilot plant testing. A point can also be made that a proper small scale test can sometimes give more insight into the process involved than certain large scale units; "Big is not always better".

The evolution of testing in hydrocarbon conversion processes.

It may be interesting to end this introduction with some thoughts about the way testing has evolved over the years in the hydrocarbon conversion field.

Starting in the first half of this century, catalyst testing was very empirical, mainly aimed at generating some basic data in the laboratory, often trials in commercial plants were needed to really prove or disprove the benefits of a new catalyst development.

With time the interest for a better simulation of the commercial situation started to dominate the development of new more realistic test and deactivation methods. Realistic information on what to expect of the catalyst tested became the real target.

With the advent of more sophisticated testing methods and a better understanding of testing phenomena, we can expect to see more interest for the basic understanding of the underlying processes involved, such as: Hydrocarbon Conversion Kinetics, Catalyst Deactivation Mechanisms, Multiphase Mass Transfer and Diffusion, etc.

More and more the test will become an integral part of the catalyst or process hypothesis which we wish to test.

Literature cited.

1. O'Connor, P. and Pouwels, A.C.
Realistic FCC Commercial Catalyst Testing in the Laboratory
Proc of 8th Int Symp on Large Chemical Plants, October 1992
2. Popper, K.
from *Conjectures and Refutations* (1962), Routledge & Kegan Paul (1978)
3. Einstein, A.
from *Logik der Forschung*
4. Flank, W.H.
A Philosophy for Testing
ACS Symposium Series 411, Washington 1988, edited by S.A. Bradley, M.J. Gathuso and R.J. Bertolacini
5. Heinemann, H.
Catalysis Today, 22 (1994) p281
6. Dautzenberg, F.M.
Ten Guidelines for Catalyst Testing
ACS Symposium Series 411, Washington 1988, edited by S.A. Bradley et al.
7. Sie, S.T.
Procestechologie, 3 (1991) p11 (in Dutch).

Chapter 2

Advantages, Possibilities, and Limitations of Small-Scale Testing of Catalysts for Fixed-Bed Processes

S. T. Sie

Faculty of Chemical Technology and Materials Science, Delft University
of Technology, Julianalaan 136, 2628 BL, Delft, Netherlands

An analysis is made of the factors which pose a limit to representative downscaling of catalyst testing in continuous fixed-bed reactors operated with either gas or gas-liquid flow. Main limiting factors are the axial dispersion and, in the case of gas-liquid operation, also the contacting of the catalyst. The effects of catalyst and reactor geometries are quantified, and boundaries for safe operation are indicated.

By taking advantage of radial diffusion to wipe out the effect of uneven velocity distributions and by resorting to catalyst bed dilution with fine inert particles, representative experiments are possible on a very small scale, with amounts of catalyst down to a few grams or even less. Results obtained on such a small scale are shown to be in good agreement with those obtained in industrial reactors under comparable conditions.

Fixed-bed reactors are among the most widely used reactors in the hydrocarbon processing and petrochemical industry. These reactors are mostly operated as continuous reactors with a stream of gas or cocurrent streams of gas and liquid in the trickle-flow regime. The large total capacity of industrial plants using fixed-bed processes implies that even relatively modest performance differences are of great economic importance. Laboratory tests, e.g., to evaluate new or regenerated catalysts, to monitor the commercial production of catalysts or to assess the effect of changes of feedstock or operating variables on process performance must therefore give accurate results which can discriminate between catalysts with relatively small, yet commercially significant performance differences and which results are meaningful for industrial practice.

In fundamental catalysis studies catalysts are quite often tested under conditions which differ widely from the industrial practice of a continuous process, e.g., tests are carried out in batch using model feedstocks, in stirred reactors, with powdered catalyst or single pellets at conversions that are quite different from those in practice (e.g., differential conversions). While such tests can yield valuable

mechanistic and kinetic information, it is seldom possible to use the test results to accurately and reliably predict the catalytic performance in terms of conversion rates, selectivities and deactivation behaviour under industrial conditions. Therefore, a need remains for laboratory catalytic tests which simulate the commercial operations close enough to give results on catalytic process performance that are directly meaningful for industrial practice, preferably without requiring translations of which the validity is uncertain.

The present paper discusses laboratory catalytic tests in the latter context, dealing mostly with fixed-bed processes that are applied in the hydrocarbon processing industry. More specifically, the consequences and limitations of scale reduction of laboratory tests will be examined.

Incentives for Scale Reduction in Catalyst Testing

Reducing the scale of experiments in the laboratory has a number of important advantages, such as

- lower cost of construction and installation of equipment
- less consumption of materials and less waste products to be disposed off
- reduced demands on laboratory infrastructure because of lower space requirement, lower utility requirements, less facilities for storage and transport of feeds and products
- increased intrinsic safety: reduced hazards of fire, explosions and emission of toxic materials
- generally reduced manpower needs.

Table I lists the categories of laboratory reactors used for catalyst testing and catalytic process studies, viz., in the order of decreasing size: pilot-plant, bench-scale and microflow reactors. Table II compares the feed requirements of some representative examples of these three classes for a typical case of oil hydroprocessing. The large effect of scale is evident: whereas the pilot plant consumes monthly amounts of liquid and gas that require supply on a periodic basis by tank car and tube trailers, the microflow needs can be covered by a small drum or can and a few gas bottles. The size of the test reactor does not only have consequences for the logistics of supply, storage and disposal of feeds and products, but can also dictate the scale of preparation of special feedstocks and catalysts.

The enhanced intrinsic safety as a benefit of scale reduction may be illustrated by the maximum hazards associated with the operation of a sub-micro reactor containing a few tenths of a gram of catalyst: when working with flammable gases or liquids, the low flow rates would only sustain a flame of the size of a small candle. In the case of a toxic gas such as carbon monoxide, the emission associated with a typical flow rate would be less than the amount of CO given off by a burning cigarette.

In the event of a mechanical failure when operating under high pressure, the gas inventory released would be less than that from a punctured bicycle tire, and in the case of explosion of this amount of gas its detonating power would be comparable with that of a small firecracker.

Against the above background, it seems a logic policy to carry out catalyst testing on the smallest possible scale whilst ensuring the meaningfulness of results for commercial practice. In the following parts the limits to such a downscaling will be examined.

Table I. Categories of Laboratory Test Reactors

	Pilot Plant (PP)	Bench-Scale (BS)	Microflow (MF)
Total bed length, cm	400 - 800	20 - 100	5-20
Bed diameter, cm	4 - 8	2 - 3	0.8 - 1.5
Bed volume, mL	5,000 - 40,000	60 - 700	2.5 - 25

Table II. Effect of Reactor Scale on Liquid Velocities and on Feed Requirements in Oil Hydroprocessing

	Pilot Plant	Bench-Scale	Microflow
Total bed length, cm	800	50	10
Bed diameter, cm	4	2	1
Catalyst volume, L	10	0.15	0.008
u_L , cm/s	0.44	0.028	0.0056
Re_L	22	1.4	0.3
Liquid feed required per month, L	15,000	220	12
Hydrogen required per month, Nm ³ (no recycle)	15,000	220	12

LHSV = 2, Hydrogen/oil = 1000 NL/L, $d_p = 1.5$ mm, $v_L = 3 \cdot 10^{-7}$ m²/s.

Simulation of an Industrial Reactor on Laboratory Scale

In principle, the safest way to represent an industrial reactor on a laboratory scale is to reduce the diameter while keeping the bed length the same. In a well-designed industrial fixed-bed reactor where proper care is taken to ensure uniform distribution of feed over the cross section of the bed, there are theoretically no cross sectional differences. Hence, a more slender but equally tall test reactor would be a good representation of the commercial reactor, provided that the diameter of the test reactor is not so small that wall effects become appreciable (to be discussed later).

Reducing the bed length while keeping the space velocity the same will reduce the fluid velocity proportionally. This will affect the fluid dynamics and its related aspects such as pressure drop, hold-ups in case of multiphase flow, interphase mass and heat transfer and dispersion. Table II shows the large variation in fluid velocity and Reynolds number in reactors of different size. The dimensionless Reynolds number ($Re = u * d_p * \rho / \eta$, where u is the superficial fluid velocity, d_p the particle diameter, ρ the fluid density and η the dynamic viscosity) generally characterizes the hydrodynamic situation.

Even when the laboratory test reactor is intended to be representative in a reaction kinetic sense only (thus waiving the demand for correspondence in terms of pressure drop and hold-ups), the process performance data can be affected by differences in mass transfer and dispersion caused by scale reduction. When interphase mass transfer and chemical kinetics are both important for the overall conversions, the above test reactor, which is a relatively large pilot plant reactor, cannot be further reduced in size unless one accepts deviations in test results.

Fortunately, in most catalytic conversions of interest to the hydrocarbon processing industry the interphase mass transfer plays a rather insignificant role in comparison with chemical reaction rates and intraparticle diffusion. For practical reasons, transformation rates in industrial catalytic processes are confined to a range of space-time-yields which has been called the Weisz window on reality (*1*). The useful space-time-yield is rarely much below 10^{-6} or much above 10^{-5} mol/(mL.s). Fixed-bed reactors are generally chosen for processes with relatively low intrinsic reaction rates since for very fast reactions other reactor technologies such as riser reactors become preferable. Therefore, most fixed bed processes operate under conditions where within the above window the catalyst effectiveness is 1 or not very much below 1, implying that the diffusion paths of reactant molecules inside the catalyst particles are not much shorter than the particle dimensions. Since in general the effective film thicknesses for interphase mass transfer in fluid flow through a bed of particles will be much smaller than the particle dimensions, it follows that the transformations in most practical fixed-bed processes are mainly governed by chemical reaction rates and intraparticle diffusion.

The above practical restriction provides considerable freedom for downscaling of test reactors. As a starting point, the assumption can be made that a well-designed industrial fixed-bed reactor is a close approximation of an ideal integral reactor which fulfills the following criteria

- (1) All volume elements of the feed contribute equally to the overall conversion, which implies that they have to spend the same time in the reactor. This

criterion applies to conversions with a reaction order greater than zero, i.e. conversions for which the fixed-bed reactor is an appropriate choice. (For reactions of a negative order a stirred tank would be the preferred reactor).

(2) All parts of the catalyst bed must contribute maximally to the overall conversion, which means that all catalyst particles must be adequately contacted by the reactant.

To be representative of such an industrial reactor, the test reactor has to fulfill the same requirements, i.e., it has to be a close approximation of such an ideal integral reactor as well. Even though commercial reactors may occasionally perform more poorly as a result of improper design, it does not make much sense to try and mimic a malfunctioning commercial reactor on a laboratory scale.

In the following parts the effect of scale parameters on compliance with the above requirements will be examined in more detail.

Allowable Spread in Residence Time and Effect of Reactor Variables on Residence Time Distribution

Allowable Spread in Residence Time. Other ways of stating the requirement of equal residence time of all parts of the reactant is that the flow through the reactor should approach plug flow or that the residence time distribution (RTD) should be equivalent to that in a large number of mixers in series. An often used rule of thumb is that this requirement is met when the equivalent number of mixers (N_c) exceeds a certain value, say 5. However, this criterion is at best a semi-quantitative one, since the minimum value of N_c is dependent upon the accepted deviation from the ideal reactor, and on the degree of conversion and the reaction order.

A more quantitative criterion for the allowed spread in residence time is given by the following equation

$$Pé = L * u / D_{ax} > 8 * n * \ln \{ 1/(1-X) \} \quad (1)$$

in which $Pé$ is a dimensionless number which is a measure for the spread in residence time in the reactor and which is approximately twice the equivalent number of mixers in series (for $Pé \gg 1$), L the reactor length, u the superficial fluid velocity, D_{ax} the (apparent) axial diffusivity, n the (positive) reaction order and X the fraction converted.

The above criterion, which has been proposed by Gierman (2) is based on the argument that the temperature required for a given conversion in the test reactor should not exceed the theoretical one by more than 1 °C, which can be considered to be within the accuracy of temperature definition in practice. A similar, but more conservative criterion has been proposed earlier by Mears (3) based on a maximum increase of 5% in bed length or catalyst volume to effect the same conversion as in an ideal reactor. In the criterion of Mears, the coefficient 8 in Equation 1 should be replaced by 20.

Figure 1 shows the minimum $Pé$ number and equivalent number of mixers for a first and second order reaction as a function of conversion depth according to Equation 1. It clearly follows that a fixed number of mixers (e.g. 5 or 10) as a criterion for an acceptable deviation from an ideal plug flow reactor is a gross oversimplification which can be misleading.

Axial Molecular Diffusion. Molecular diffusion can be an important cause of a spread in residence time, particularly at low velocities (low space velocities and short bed lengths) and with fluids of high diffusivity. Therefore, it is important in microreactors with gas flow.

Figure 2 shows the Péclet numbers measured for a microreactor of about 10 cm length and 0.8 cm diameter with nitrogen gas as flowing medium. It can be seen that Pé increases about proportionally with the gas velocity and that the particle size of the packing (varied by a factor of 8) hardly has an influence. Thus, for the case investigated, D_{ax} as defined in Equation 1 is apparently no function of particle size or velocity, which is in line with the idea that it is mainly based on molecular diffusion.

Table III shows some data on dispersion of nitrogen flowing through a similar microreactor filled with particles of typical fixed-bed catalysts, at a gas hourly space velocity (GHSV) of 450 NL/(L.h). The measured axial diffusivity proved to be in good agreement with the molecular diffusivity of the binary mixture of nitrogen and helium tracer gas (corrected for porosity and tortuosity), which supports the above idea. It can also be seen that the reactor is not very far from a plug-flow reactor (Pé about 100) notwithstanding the rather low space velocity, the short bed, and the fact that the catalyst of practical size had not been diluted. Hence, it can be concluded that with gaseous reactants a microflow reactor of the present dimensions can be considered to be a sufficiently close approximation of an ideal plug flow reactor for most practical cases of catalyst testing.

Figure 3 shows the minimum bed lengths calculated for some cases of fixed-bed processes with flowing gas as a function of conversion for reactions obeying first and second-order kinetics. It can be concluded that for such gas phase processes microflow reactors with dimensions indicated in Table I are generally suitable.

Axial Convective Diffusion. The variation in width, length and direction of individual channels formed by the interstices of the packing give rise to a dispersion which can be characterized by the dimensionless Bodenstein number, Bo, which is a similar number as the Péclet number but with the particle diameter as characteristic dimension

$$Bo = d_p * u / D_{ax} \quad (2)$$

Combining Equations 1 and 2 gives as condition for a good test reactor

$$Bo * L / d_p > 8 * n * \ln \{1/(1-X)\} \quad (3)$$

For single phase and two-phase flow through randomly packed beds the Bodenstein number is a function of the Reynolds number. A global correlation between Bo and Re, established by Gierman (2) on the basis of published data, is shown in Figure 4.

According to this correlation, Bo decreases as Re decreases until it attains a more or less constant value in the range of interest for small laboratory reactors, viz., about 0.4 for single phase flow and 0.04 for the liquid in trickle flow. Substituting these values in Equation 3 yields

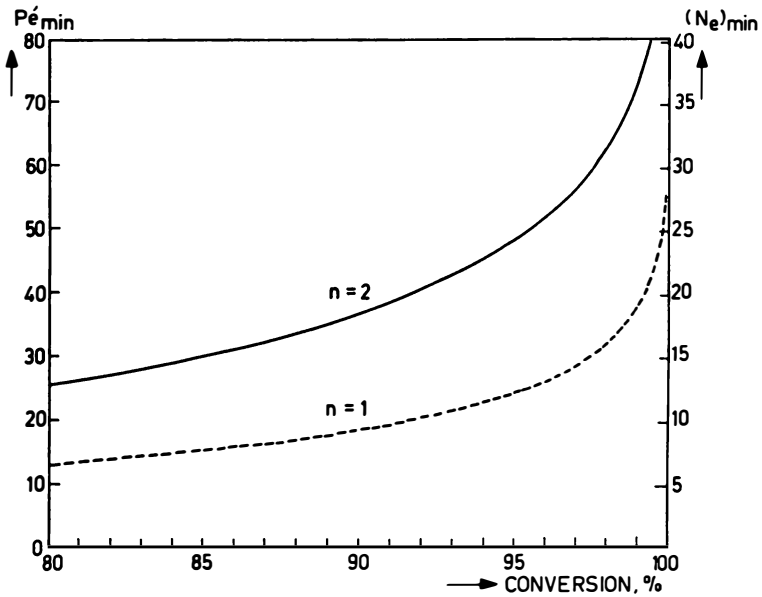


Fig. 1. Minimum required Péclet number and equivalent number of mixing stages as a function of conversion, for reactions following first and second order kinetics.

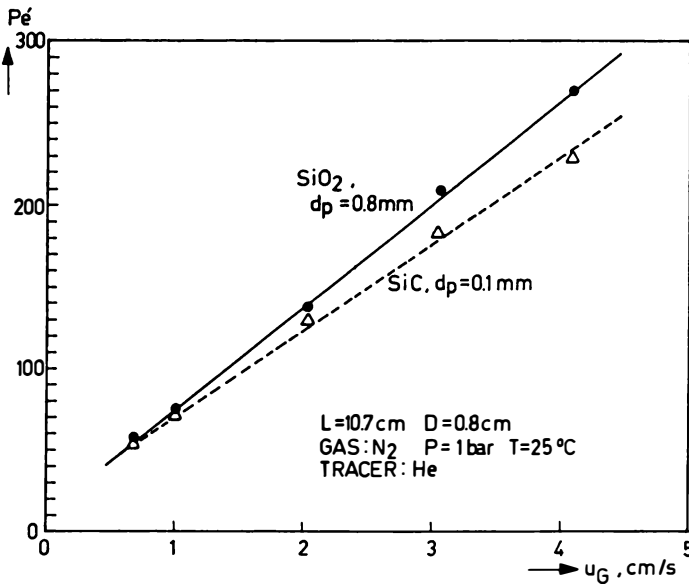


Fig. 2. Measured axial dispersion in a microflow reactor with flowing gas as a function of superficial velocity.

Table III. Measured Axial Dispersion in a Microflow Reactor with Gas Flow through an Undiluted Bed

Packing	$P\epsilon$	N_e	D_{ax} , cm^2/s	$\epsilon D_m / \tau$, cm^2/s
Spheres, $d = 1.5 \text{ mm}$ $\epsilon = 0.40$	105	53	0.132	0.137 *)
Cylinders, $d = 1.5 \text{ mm}$, $L = 3 \text{ mm}$ $\epsilon = 0.44$	97	49	0.143	0.15 *)

*) Based on a binary diffusion coefficient for N_2/He of $0.687 \text{ cm}^2/\text{s}$ and an assumed tortuosity factor τ of 2.

$L=10.2 \text{ cm}$, $D = 0.8 \text{ cm}$, $V(\text{bed}) = 5 \text{ mL}$. Gas: Nitrogen. $P = 1 \text{ bar}$, $T = 25 \text{ }^\circ\text{C}$,
 $\text{GHSV} = 450 \text{ NL}/(\text{L.h})$, $u_G = 1.36 \text{ cm/s}$. Tracer: He

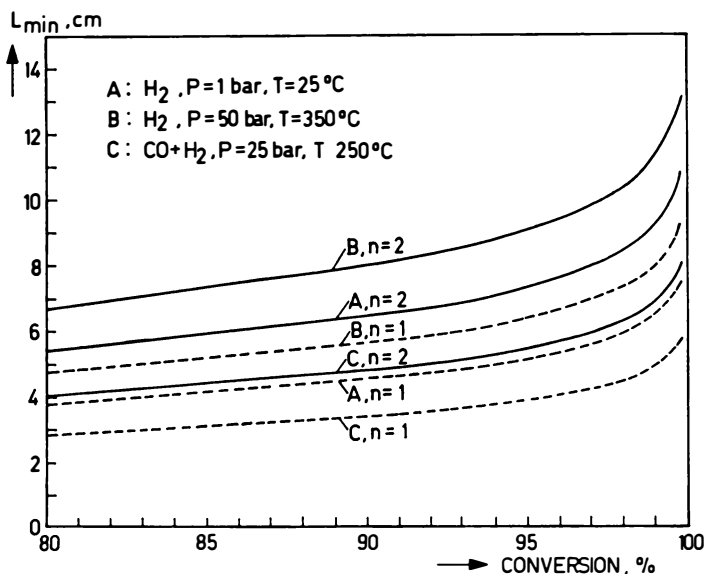


Fig. 3. Minimum bed length as a function of conversion as determined by axial molecular diffusion in flowing gas.

($\text{GHSV} = 1000 \text{ NL}/(\text{L.h})$, $\epsilon = 0.4$, $\tau = 2$).

$$L/d_p > 20 * n * \ln \{1/(1-X)\} \quad (4A)$$

for single phase flow, and

$$L/d_p > 200 * n * \ln \{1/(1-X)\} \quad (4B)$$

for the liquid in trickle flow.

It is of interest to note that the ratio L/d_p is the important quantity that has to exceed a certain minimum value. An established rule-of-thumb states that this ratio should be above 50. However, this rule-of-thumb is an oversimplification as it does not discriminate between single and two-phase flow and does not take into account the reaction order and conversion depth.

Figure 5 shows the calculated required bed lengths as a function of conversion for single-phase and trickle flow, with reaction order and particle size as parameters. It can be seen that in the case of a process with gaseous reactant (single-phase flow) short reactor beds are suitable, i.e., testing of catalysts with particle sizes as large as 3 mm in bench-scale reactors is generally possible, and neither should there be a problem with testing of catalyst particles of about 1 mm diameter in microreactors.

In two-phase, trickle flow the minimum bed lengths for an acceptably low axial dispersion of the liquid are an order of magnitude greater. (In most oil conversion processes axial dispersion in the gas is generally relatively unimportant since hydrogen gas is used in large excess and recycled, with consequently low conversion per pass). As can be seen from Figure 5, testing of catalysts with particle diameters above 1 mm generally should be done in reactors with beds of the order of metres. Hence, for testing of such catalysts of practical size a pilot plant reactor seems indicated. Microflow reactors are clearly unsuitable, whereas bench-scale reactors are marginally applicable only in rather undemanding cases (relatively low conversions and not too large particles). However, as Figure 5 also shows, the two latter categories of reactors should be quite acceptable for particles of very small size, e.g., of 0.1 mm diameter. This forms the basis of the catalyst dilution technique to be discussed in a later part of this paper.

Transverse Macroscopic Velocity Profiles: The Wall Effect. The axial dispersion discussed above is caused by the more or less random variations of fluid velocity at the scale of the particle diameter and is an intrinsic property of a random packing of particles. Aside from these microscopic fluctuations of velocity, there can be more systematic differences of fluid velocities in the bed. A transverse velocity profile extending from wall to wall may be present as a consequence of uneven packing, e.g., unequal compaction of the packing in different parts of the bed or, in the case of a catalyst having a size distribution, unequal average particle size caused by segregation during filling of the reactor.

Whereas such non-uniformity in the packing need not exist if the reactor is filled with sufficient care, the perturbation of the random packing by the reactor wall is a cause of velocity differences which cannot be avoided.

Figure 6 shows a computed radial voidage profile in a packing of spheres. It can be seen that in the region close to the wall, i.e. 0-2 particle diameters away from the wall, there is a much greater voidage than in the interior. As a result of the greater permeability in this wall zone and the flow-retarding effect of the reactor wall, a

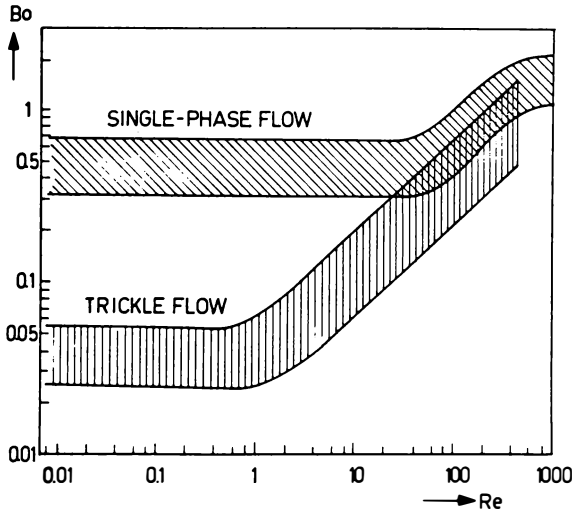


Fig. 4. Correlation of Bodenstein and particle Reynolds number for single-phase flow and for the liquid in trickle flow. After Gierman (2).

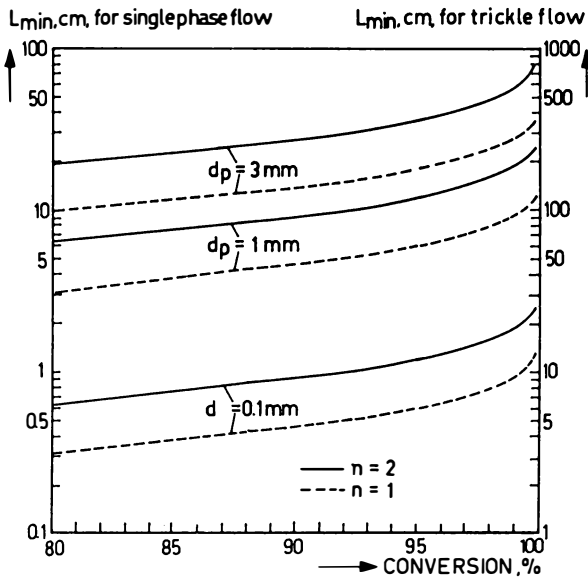


Fig. 5. Role of axial dispersion in the bed for single-phase and trickle flow. Minimum bed length as a function of conversion for first and second order reactions and for different catalyst sizes.

transversal velocity profile will be present with velocity zero at the wall and a higher than average velocity some distance away from it. Figure 7 shows experimentally measured radial velocity profiles for different ratios of tube over particle diameter. It can be inferred that there is a maximum velocity at a distance from the wall of approximately twice the particle diameter. At a diameter ratio of 5, the velocity profile is quite pronounced and even at a ratio of 10 flow is far from even. Only at a diameter ratio of 25 there is a flat velocity profile in the greater central part of the bed.

The wall effect will result in an appreciable spread in residence time of the reactant, unless its contribution is relatively unimportant at a sufficiently large ratio between bed and particle diameter (say, greater than 20) or unless there is a sufficiently strong effect of radial diffusion, as will be discussed below.

Interaction of Radial Diffusion and Trans-bed Velocity Differences.

Radial diffusion can be effective in reducing the effect of a transverse velocity profile by mass exchange between regions of fast and slow forward velocities. If this mass exchange is sufficiently effective, the overall result is a dispersion which can be described as an axial diffusivity (Taylor diffusivity).

Erasure of a trans-bed velocity profile by molecular diffusion in radial direction requires that the available time, i.e., the average residence time in the bed, is sufficiently long in comparison with the time needed for diffusion in radial direction. Figure 8 shows the ratio of the average residence time over the time needed for diffusion over a distance equal to the bed radius for a few typical cases of gas and liquid flow. It can be seen that this ratio is above 1 for gas flow through fixed beds with diameters below 2 cm, i.e., the diameters of bench-scale and microflow reactors. Hence, for these reactors, radial diffusion in the gas can reduce the effect of macroscopic velocity profiles. For a liquid, on the other hand, the diffusivity is so low that notwithstanding the longer residence time in the reactor the ratio between this time and the radial diffusion time is above 1 only for very small bed diameters, viz., in the order of millimetres. Therefore, for processes involving liquid flow the performance of bench-scale and microflow reactors of the usual dimensions are likely to be affected by trans-bed velocity profiles including those resulting from the wall effect.

An often used criterion for an acceptably small effect of macroscopic velocity profiles is

$$L * D_{rad} / (R^2 * u) \gg 1/8 \quad (5)$$

in which D_{rad} is the effective diffusivity in a radial direction and R the bed radius. However, this criterion is only a semi-quantitative one since it does not state how large the deviation from ideal plug flow may be.

A more quantitative expression of the dispersion caused by flow profiles interacting with radial diffusion may be derived from investigations in chromatography (preparative gas chromatography and liquid chromatography). This stands to reason since the requirements for a good chromatographic column are exactly the same as for an ideal fixed-bed reactor as defined earlier, viz., minimum axial dispersion and complete contacting of the solid.

The length equivalent to one mixing stage caused by the interaction of a radial velocity profile and radial diffusion can be written as

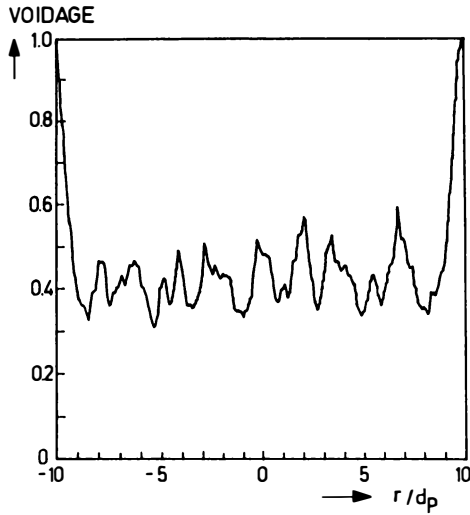


Fig. 6. Computed lateral voidage profile for a three-dimensional column randomly packed with uniform spheres. After Zimmerman and Ng (4).

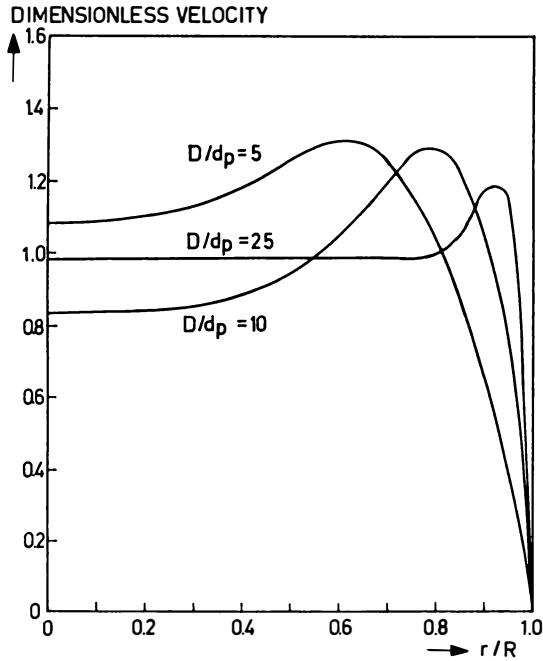


Fig. 7. Radial velocity profiles for flow through packed beds at different ratios of bed diameter to particle diameter. After Fahien and Stankovic (5).

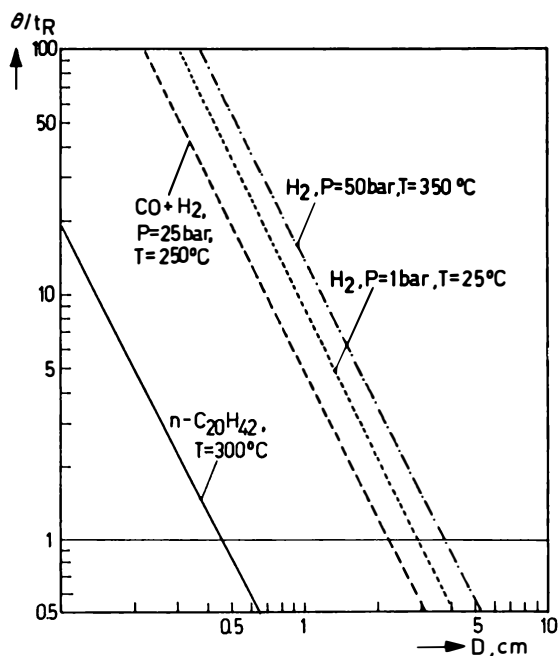


Fig. 8. Ratio between the average residence time and the time required for diffusion over a distance equal to the tube radius, as a function of bed diameter. (Hydrogen or syngas : gas phase, GHSV = 1000 NL/(L.h). n-Dodecane : liquid phase, WHSV = 1 kg/(L.h). $\epsilon = 0.4$, $\tau = 2$).

$$L / N_e = 2 \kappa * R^2 * v / D_{rad} \quad (6)$$

in which v is the average fluid velocity in the bed and κ a dimensionless number which is a characteristic measure for the velocity profile (for the parabolic Poiseuille profile of laminar flow in a tube $\kappa = 1/48$). Combined with Equation 1, this yields

$$L * D_{rad} / (R^2 * u) > 8 (\kappa / \epsilon) * n * \ln \{1/(1-X)\} \quad (7)$$

which is a more precise expression than Equation 5.

Figure 9 shows the value of κ as a function of the ratio of bed diameter over particle diameter, as determined from packed gas chromatographic columns (6). It can be seen that κ tends to decrease as the diameter ratio increases, which implies that flow becomes more uniform. Whereas at low ratios κ is inevitably high (of the same order of magnitude as in laminar flow through empty tubes) due to the wall effect, at higher diameter ratios κ can vary more widely since its value depends upon whether the column is well or badly packed.

To determine the effectiveness of radial diffusion for erasing radial velocity profiles in small columns suffering from the wall effect, calculations have been made assuming $\kappa = 0.04$ for bed to particle diameter ratios below 5 (see Figure 9), and assuming molecular diffusion to be the only mechanism for radial mass exchange (this rather conservative assumption is valid with the relative low velocities in microflow and bench-scale reactors). Figure 10 shows thus calculated maximum diameters for a few typical cases of gas and liquid flow through the packed beds. It can be seen that with gas as the flowing medium microreactors with a maximum diameter of 1.5 cm will in general be applicable even at the low D/d_p ratio of less than 5 assumed. This means that there should be no problem in testing catalyst particles of practical size in such a reactor. The same is true for bench-scale reactors with bed diameters in the 1.5 - 3 cm range, although a diameter ratio below 5 may be problematic in some cases.

For liquid as the flowing medium, the maximum bed diameter allowed is in the millimetre range, and this implies that one cannot rely on liquid diffusion to erase velocity profiles in microflow and bench-scale reactors of the usual size.

From the foregoing it appears that the generally applied rule-of-thumb stating that D/d_p should be larger than 10 to avoid wall effects is questionable. For liquid flow, this rule is too optimistic and a minimum value of 20 seems preferable (c.f. Figure 7). For gas flow, the rule is unduly restrictive and even a diameter ratio of less than 5 is still acceptable. This is, in fact, demonstrated by the earlier discussed data given in Table III. The microflow reactor filled with catalysts of practical size (D/d_p about 5) and operated with gas showed a good approach to plug flow with a dispersion mainly determined by axial molecular diffusion.

Catalyst Contacting

Aside from the requirement of a sharp residence time distribution, the ideal fixed-bed reactor should also allow all parts of the catalyst bed to fully participate in the overall conversion, i.e., all catalyst particles must be contacted by the reactant fluid. With a single fluid phase, this condition is generally met when the plug flow criterion is obeyed since in this case there is a uniform flow through the bed. However, in two

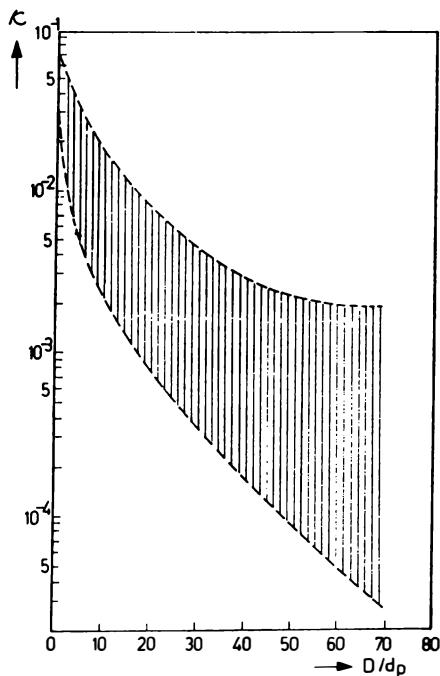


Fig. 9. Effect of the ratio between bed and particle diameter on the irregularity of the packing causing macroscopic velocity profiles. After Sie (6).

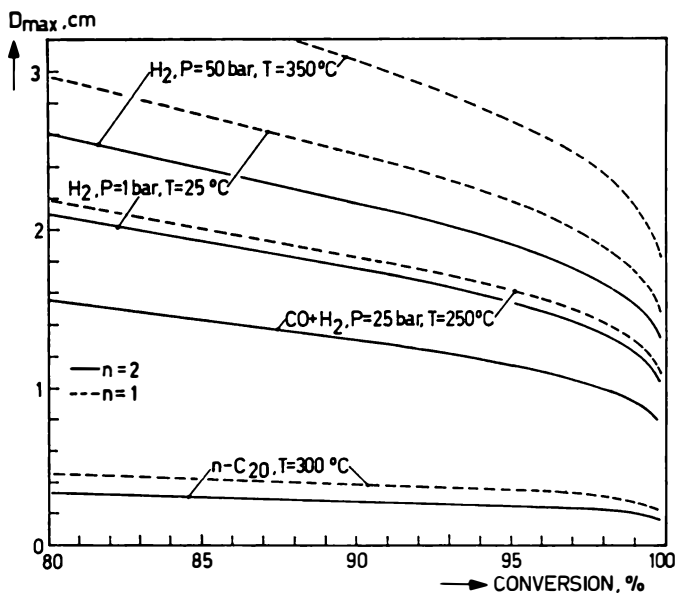


Fig. 10. Maximum allowable bed diameter as a function of conversion and reaction order, for reactors with a significant wall effect. ($D/d_p < 5$; Conditions as stated in Figure 8).

phase flow such as cocurrent trickle flow the ratio of liquid to gas flow may be different in different parts of the bed: a situation may prevail where liquid flows preferentially through a certain part of the bed, while gas flows predominantly through the other parts. This maldistribution is commonly referred to as incomplete wetting of the catalyst, which is an appropriate description of an extreme situation in which certain parts of the catalyst bed see no liquid at all. However, even if all catalyst particles are "wetted" in the sense that they are all covered by a thin film of liquid, the performance of the reactor is still suboptimal if the liquid in this film is not refreshed at a sufficient rate. Therefore, the requirement for an ideal reactor is better stated as "even irrigation" of all parts of the catalyst bed (7).

A criterion for even irrigation is the following one proposed by Gierman and Harmsen (2)

$$W = \eta_L * u_L / (\rho_L * d_p^2 * g) > 5 \cdot 10^{-6} \quad (8)$$

in which η_L and ρ_L are the dynamic viscosity and density of the liquid, and g the gravity constant. W is a dimensionless number which compares the frictional force for flow with the gravity force. When the former force predominates, there will be a tendency to correct any liquid maldistribution since the liquid then seeks to flow through every available channel. The numerical value in Equation 8 has been established by Gierman and Harmsen (2) on the basis of a large amount of experimental data, but can also be made plausible by simple considerations (7).

From Equation 8 it follows that the important variables for even irrigation are the particle diameter, the liquid kinematic viscosity ($\nu_L = \eta_L / \rho_L$), and liquid velocity determined by LHSV and bed length. Figure 11 shows the maximum allowable particle diameter as function of liquid kinematic viscosity for beds of different lengths. From this figure it can be deduced that testing of particles with a diameter of 2 mm will be acceptable in a pilot plant with a 5 m long bed, but will be very problematic in a 10 cm long microflow reactor. E.g., at a LHSV of 1 L/(L.h) and for a liquid kinematic viscosity of $3 \cdot 10^{-7} \text{ m}^2/\text{s}$ (typical value for a heavy gasoil under hydrotreating conditions), the maximum allowable particle diameters are 0.4, 1.3 and 2.9 mm for a 10 cm long microflow reactor, a 1 m bench-scale reactor, and a 5 m long pilot-plant reactor, respectively.

Catalyst Bed Dilution with Fine Inert Particles

From the foregoing discussion it will be clear that except for fixed-bed reactors with gas flow, particle size is the major limiting factor for the applicability of small laboratory reactors for representative catalyst testing. In testing catalysts for trickle flow processes, only relatively small particles can be used in a bench-scale or microflow reactor to comply with the criteria for axial convective dispersion in the packing (see Figure 5), the wall effect, and even irrigation (see Figure 11). Particles of such small size (diameter below 0.5 mm) give rise to unacceptably high pressure drops in industrial fixed-bed reactors and practical catalysts for these reactors generally have particle diameters in the range of 1 to 3 mm.

When the effectiveness factor of such practical catalysts is 1, i.e., there is no intraparticle diffusion limitation at all, crushing or grinding the catalyst to obtain smaller particles can be a way to assess catalyst performance in small-scale laboratory

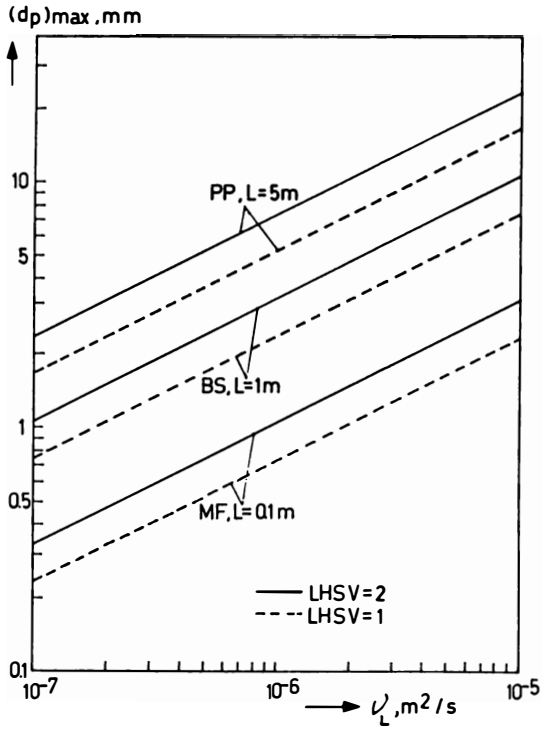


Fig. 11. Condition for uniform irrigation in trickle flow. Maximum particle size as a function of liquid kinematic viscosity for different bed lengths and different space velocities.

reactors. However, even if the main reaction is not limited by diffusion, other reactions (side reactions or consecutive reactions involving larger molecular species) can still be diffusion limited. In this case, testing of catalysts in crushed form may give misleading results on selectivity or stability of the catalyst even when activity data are correct.

In many processes of interest to the hydrocarbon processing industry the size and shape of the catalyst has been chosen as a compromise between catalyst effectiveness and pressure drop. Hence, with effectiveness factors for the main reaction somewhat below 1, intraparticle pore diffusion is generally a factor to be reckoned with. Its effect is not easily quantified since the processing of a practical feedstock involves the conversion of a large variety of molecules with widely different reaction rates and therefore the translation of catalyst performance data obtained with crushed particles to that of the actual catalyst may be difficult and of questionable validity.

A way out of the dilemma to use a bed of small particles in small laboratory reactors and yet determine the performance of a practical catalyst of much larger particle size is to embed the latter particles in much finer inert particles, with diameters in the range 0.05 - 0.2 mm. Thus, by diluting the catalyst bed with 1-3 times its volume of fine inert material, the hydrodynamics will be largely dictated by the packing of the fine inert particles, whereas the performance measured is that of the catalyst in the actual form. A schematic picture illustrating such a diluted catalyst bed is shown in figure 12.

Table IV presents some data on liquid residence time distributions measured under conditions of hydrocracking in trickle flow. It can be seen that bed dilution with fine inert particles results in a considerable improvement in the plug-flow character of the reactor, which supports the idea that the dispersion is largely determined by the packing of fine particles. Since in the range of Re numbers of interest the Bodenstein number is approximately a constant (see Figure 4), the Péclet numbers for beds of equal length should be inversely proportional to the particle diameter. Dilution of the 1.5 mm particles with 0.2 mm particles should raise Pé by a factor of about 7, which is approximately in line with the data in Table IV.

The catalyst bed dilution technique is an effective way for meaningful testing of practical catalysts in their original size in small reactors. This technique has been discussed in a number of papers (7-11). Evidence for the meaningfulness of test data thus obtained will be presented in a later part of this paper.

Accuracy of Temperature Definition

Fixed-bed reactors can in principle be operated in two different ways, viz.,

- isothermally, i.e. the temperature is the same in every part of the bed, or
- adiabatically, i.e., the reaction heat is taken up or supplied by the reactant stream without heat being released or supplied to the environment.

A commercial fixed-bed reactor is generally operated as an adiabatic reactor since at this scale heat losses to the surroundings are generally insignificant and removal or supply of heat in the bed requires special arrangements. In laboratory reactors operated above ambient temperatures natural heat losses are quite appreciable and heaters are required to maintain temperatures at desired levels.

Small laboratory reactors are most easily operated as isothermal reactors. To simulate a commercial adiabatic reactor, the temperature in the isothermal laboratory

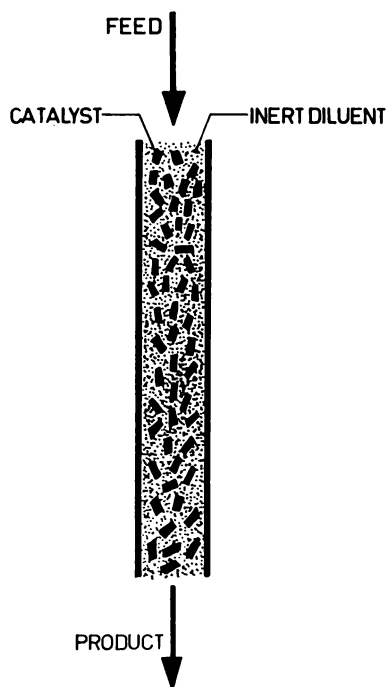


Fig. 12. Schematic representation of a diluted catalyst bed.

Table IV. Effect of Bed Dilution with Fine Particles on Residence Time Distribution of Oil in a Bench-scale Reactor under Conditions of Trickle-flow Hydrocracking

bed	Diluted		Undiluted	
	a	b	a	b
Experiment				
Mean residence time (arbitrary units)	16.8	17.9	9.1	7.9
Axial bed Pé number	80.0	66.9	6.2	10.3

LHSV = 1, P = 125 bar, T = 366 °C, Hydrogen/oil = 1000 NL/kg.

Feed: vacuum gasoil. Radiotracer: ¹⁴C-labelled dotriacontane.

Bed length: 0.9 m, bed diameter: 2 cm.

Reactor filling: glass beads, d = 1.5 mm. Diluent: Silicon carbide, d = 0.2 nm.

reactor is generally chosen to be the same as the weighted average bed temperature (WABT) of the commercial adiabatic reactor.

For large (pilot plant) laboratory reactors, on the other hand, the adiabatic mode of operation is generally preferable since natural heat losses play a lesser role and heat removal or supply through the bed is more difficult. In the following part the accuracy of temperature definition in both modes of operation will be analyzed.

Isothermally Operated Reactors. In an isothermal reactor the temperature of the reactant stream is constant in axial direction. Hence this stream does not take up reaction heat (in the case of an exothermic reaction) and all heat generated within the bed must be transported radially to the reactor wall. If the bed radius is too large and the effective heat conductivity of the bed too low, a radial temperature profile will develop with appreciable differences between the centre of the bed and near the wall. The temperature profile will be more pronounced as the radial distances are longer and as fluid velocities are lower, hence, wide and short reactors are likely to suffer most from radial temperature inhomogeneity.

Figure 13A shows some calculated radial temperatures within catalyst beds for some typical cases of hydroprocessing of oils in either a gas phase or a trickle-flow process. In these calculations, effective radial thermal conductivities were used that have been determined from existing correlations involving both static and convective mechanisms of heat transfer. It can be seen that whereas deviations from true isothermicity are reasonably small for a bed diameter of 1 cm, isothermal operation is hardly possible at the diameters in the range of pilot-plants, especially if the reactor is relatively short and operated with gas only. Under the latter circumstances, the reactor may even be unstable and temperature may run away.

An effective way to improve the isothermicity of reactors is to dilute the catalyst with inert particles, preferably of a material with a high heat conductivity, such as silicon carbide (heat conductivity in the solid state about 40 times that of porous alumina). In the diluted bed, the heat generated per unit volume of bed will be lowered, and together with an increased effective heat conductivity this will result in a more even radial temperature distribution.

Figure 13B shows the calculated temperature differences for the same cases as considered before, but with catalyst beds diluted with silicon carbide to one third of the original catalyst concentration. It can be seen that the temperature differences are appreciably smaller than in the undiluted case (note the differences in temperature scale between Figures 13A and 13B). The dilution with good thermally conducting material is particularly effective at the low velocities in short beds because the convective contribution to the effective heat conductivity is then relatively small. It can be inferred that in microflow reactors ($D = 1$ cm; $L = 10$ cm) and in bench-scale reactors ($D = 2$ cm; $L = 1$ m) with diluted beds radial temperature differences are less than 1-2 °C for the considered cases, which is quite acceptable.

Axial temperature differences in isothermally operated laboratory reactors can be minimized by installing a sufficiently large number of independently controlled heating zones along the reactor, e.g., 3 or more in the case of a microreactor and at least 5 for a bench-scale reactor of 1 metre length, with pre- and post-reactor heating elements. A thick reactor wall will promote temperature equalization in axial direction.

For isothermal reactors, it is advisable to have a central thermowell which

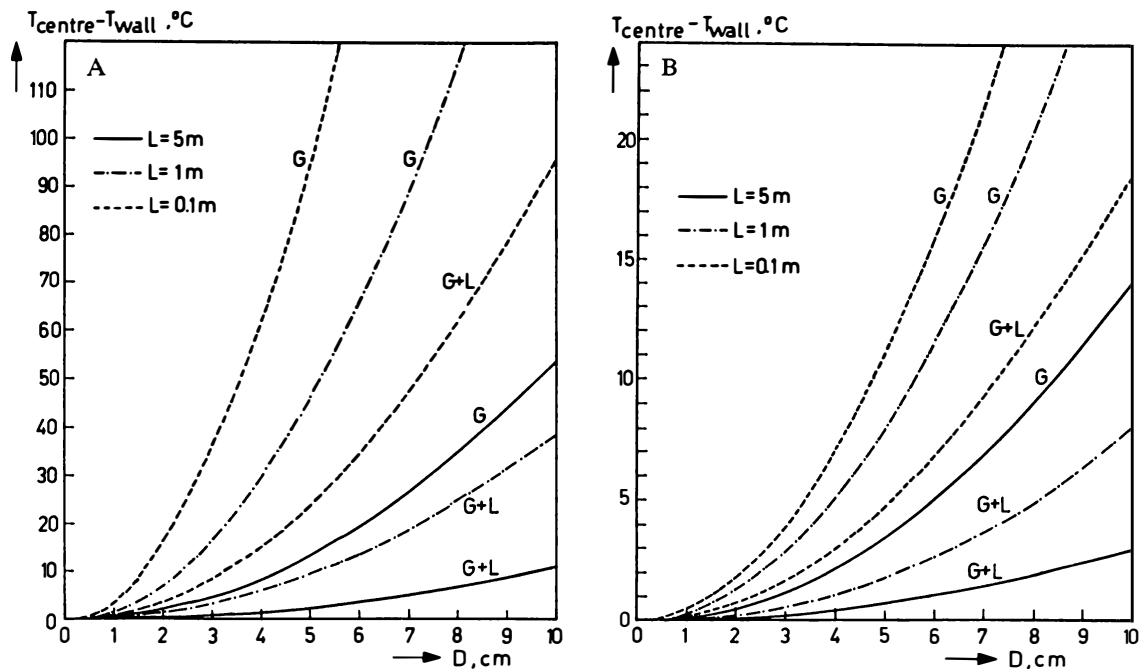


Fig. 13A and B. Effect of bed diameter on temperature differences between centre and wall region of the bed in "isothermally" operated test reactors with undiluted (A) and diluted (B) beds, at an axial position where the heat generated per unit volume of bed is the same as the average for the total bed.

(Vapor-phase hydroprocess: WHSV = 2 kg/(L.h), H_2/oil = 1000 NL/kg, 2 %w H_2 consumption, $\Delta T_{\text{ad}} = 150$ °C. Trickle-flow hydroprocess: WHSV = 1 kg/(L.h), H_2/oil = 500 NL/kg, 1 %w H_2 consumption, $\Delta T_{\text{ad}} = 80$ °C. B : Dilution with 2 volumes of SiC particles).

allows to verify the absence of unacceptably large radial and axial temperature differences. Figures 14 A and B demonstrate the closeness to isothermicity of microflow reactors used in catalyst testing for a gas-phase and a trickle-flow process.

Adiabatically Operated Reactors. In a true adiabatic reactor there is no flow of reaction heat to or from the surroundings, and the reaction heat (in the case of an exothermic reaction) heats up the reactant stream so that the temperature difference between the outlet and inlet stream is equal to the theoretical adiabatic temperature rise ΔT_{ad} . In a laboratory reactor, one attempts to obtain this situation by surrounding the reactor with heating zones to compensate for natural heat losses. However, even when the heating power is adjusted in such a way that the net heat loss from the reactor is zero and consequently the temperature difference between the outgoing and incoming stream equals the theoretical adiabatic temperature rise, the temperature distribution in the bed may still deviate from that in a true adiabatic reactor when the number of heating zones is limited and their temperature setting is nonoptimal.

This is illustrated in Figure 15, which compares calculated temperatures in the fluid and reactor wall with the true adiabatic profile for a specific case. It can be seen that the temperature deviations are quite appreciable, notwithstanding the fact that the reactor system is "adiabatic" in the sense that the temperature difference between the outgoing and incoming stream equals the adiabatic temperature rise and the net overall heat loss is zero. The deviations are caused by a significant axial heat conduction through the metal wall of the reactor which tends to flatten the temperature profile and by radial conduction of heat from the interior of the bed to the wall. Furthermore, end effects play a role as well, and the actual temperature of the fluid when it enters the reaction zone does not necessarily have to be equal to the temperature of the reactor wall or the fluid temperature at the reactor inlet, as can be seen in Figure 15. It will be clear that deviations from true adiabaticity as shown in this figure may seriously affect the results of catalyst testing, particularly as regards selectivity and deactivation behavior.

The effect of geometric parameters on the adiabaticity of a test reactor can be deduced from Table V. It can be seen that for improperly designed laboratory reactors the axial and radial heat flows can be quite appreciable even when the net heat loss is zero. From this table it follows that the radial heat flow is reduced as the bed diameter is increased, whereas the axial heat flow diminishes as the reactor length is increased. Hence, long pilot plant reactors of wide diameter will perform best as adiabatic reactors even with suboptimal design of compensation heaters.

Although construction of a good adiabatic reactor on a small scale is more difficult, it is by no means impossible. Figure 16 shows an adiabatic microreactor with catalyst bed volume of only 10 mL. At some distance from the reactor tube a metal screen is mounted with a large number (10 or more) independently controlled electric heaters. These heaters are controlled by the temperature difference between the reactor tube and the screen at the respective axial positions. By setting the temperature differences equal to zero, the axial temperature profile is duplicated on the metal screen so that radial flow of heat is prevented at any axial position. Axial flow of heat through the tube wall is minimized by opting for a slender reactor, while the still occurring axial flow of heat will affect the power input to the individual heating sections, but not the axial temperature profile. To prevent heat losses at the

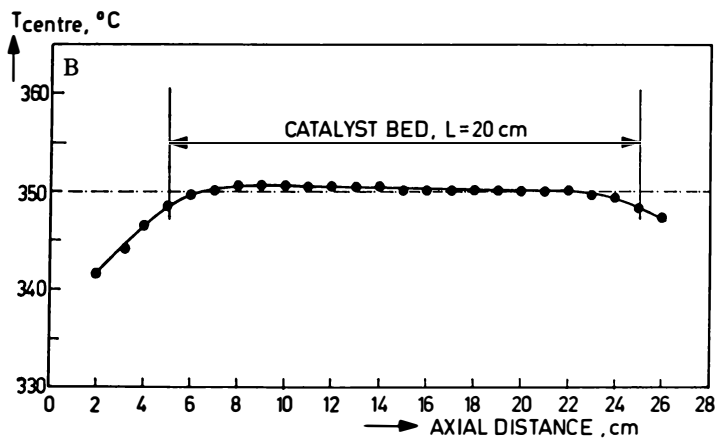
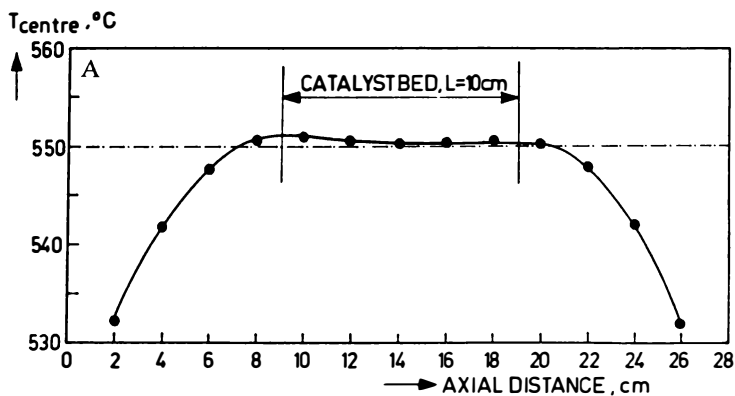


Fig. 14A and B. Examples of measured temperature profiles along the central axis of microflow reactors used in catalyst testing for a vapor phase (A) and a trickle-flow process (B).

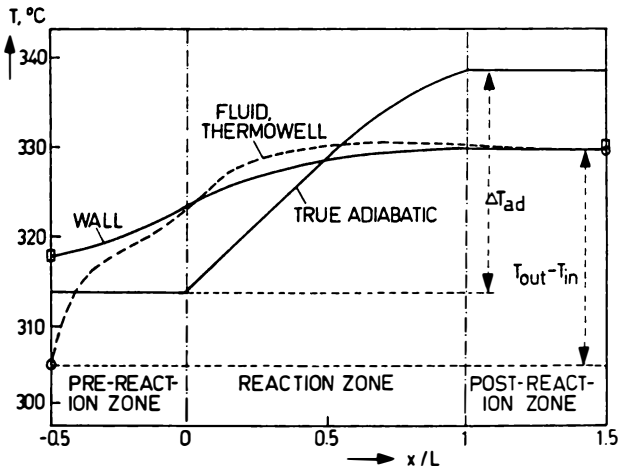


Fig. 15. Temperature profiles in an "adiabatically" operated test reactor, as determined with a computer simulation model by Anderson and Sapre (13). ($L = 0.3$ m, $D = 2.5$ cm, wall thickness 0.65 cm, $WHSV = 2$, $\Delta T_{ad} = 25$ °C).

Table V. Effect of Geometric Parameters on Adiabaticity of Pilot Reactors According to a Computer Simulation Model by Anderson and Sapre (13)
(Parameters varied relative to base case are underlined)

Case	A (base)	B	C	D
Inner diam., m 0.0417		0.0417	0.0417	<u>0.417</u>
Wall thickness, m	0.021	<u>0.004</u>	0.021	0.021
Length, m	0.30	0.30	0.30	<u>7.6</u>
Δ (ad), % *	215	77	8	54
Δ (ad,app), % *)	199	32	16	0.3

*) Δ (ad) = deviation from true adiabaticity, given by the heat transfer rate between bed and metal walls as a percentage of total heat generation rate.

Δ (ad, app) = deviation from true adiabaticity, deduced from axial heat conduction rate through the wall, as a percentage of total heat generation rate.

For a true adiabatic reactor Δ (ad) and Δ (ad, app) are zero.

Reaction: $k_0 = 2 \cdot 10^{16} \text{ h}^{-1}$, $WHSV = 2$, $E/R = 17,500 \text{ K}$, Adiab. temp. rise = 28 K for 100 % conversion. Bed: Effective radial heat conductivity = 0.260 W/(m.K). Reactor: Steel wall, insulation thickness = 0.03 m.

reactor ends, the catalyst containing, adiabatic part of the reactor is preceded and followed by an isothermal part filled with inert material.

Figure 17 compares the actually measured axial temperature profile with the theoretical one in the simulation of the first reactor of a catalytic reformer by such a microreactor. It can be seen that the deviations from the theoretical profile are within a few degrees centigrade, even in this demanding test case where the reaction heat is only of the order of 5 W at a temperature level of about 500 °C.

Although a small adiabatic reactor can be constructed, isothermal reactors are in most cases preferred for small scale catalyst testing because of their greater simplicity. For processes operating in a relatively narrow range of temperatures, catalyst testing in an isothermal reactor at a temperature equal to the average temperature of an adiabatic one will in most cases be acceptable. For highly exo- or endothermic processes the industrial plant will have several adiabatic beds in series so as to limit the temperature rise or drop per bed within the operating range and an adiabatic laboratory test unit should have several reactors as well. This gives rise to a rather complicated test unit with many temperature control loops. An example of such a miniadiabatic unit for catalytic reforming has been described earlier (12).

Accuracy of Catalytic Tests in Laboratory Units and Comparison with Industrial Data

Processes with Reactants in the Gas Phase. As discussed in the preceding parts, for such processes there is hardly a problem in catalyst testing on a scale as small as that of microreactors, even with undiluted beds of catalyst of actual size. Hence, in this case testing on a larger scale than microflow reactors will seldom be necessary.

The latter conclusion is supported by the data of Table VI, which demonstrate that testing in a bench-scale and microflow reactor gives almost identical results for light naphtha isomerization over undiluted catalyst of actual size. The absence of a noticeable effect of bed length and gas velocity is in line with the assumption that in this case extraparticle mass transfer effects are relatively unimportant, as discussed earlier.

With properly designed equipment and careful execution of the tests, the accuracy of small-scale testing can be quite high. Table VII shows some data on the reproducibility of microflow tests on light naphtha isomerization carried out in several reactor units during a period of about half a year. The agreement between results of individual tests is sufficiently good for practical purposes of catalyst evaluation and optimization of process conditions.

Table VIII compares microflow test results on light naphtha isomerization with catalyst performance as found in industrial plants. It can be seen that there is a satisfactory agreement between the activities found in laboratory tests and in commercial operation.

Trickle-flow Processes. Figure 18 shows a comparison of test results obtained in relatively large pilot plant reactors with data of an industrial gasoil hydrodesulfurization unit operating with the same feed and catalyst under the same conditions. These data show that the large pilot plant with a total bed length of 4.8 m and a diameter of 8 cm gives rather similar results as the industrial unit, the difference in reaction rate found being about 6%. This is in line with earlier published data (14) in

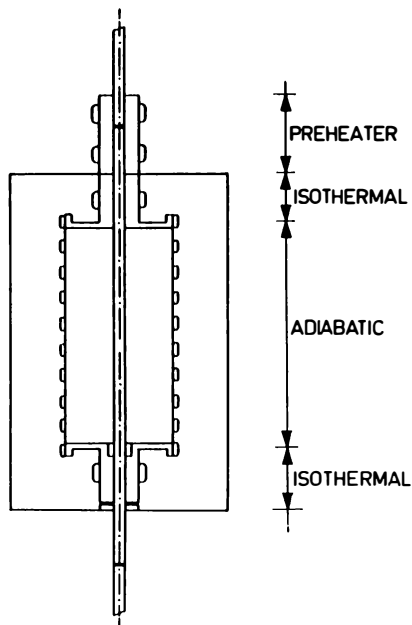


Fig. 16. Schematic drawing of an adiabatic microreactor.

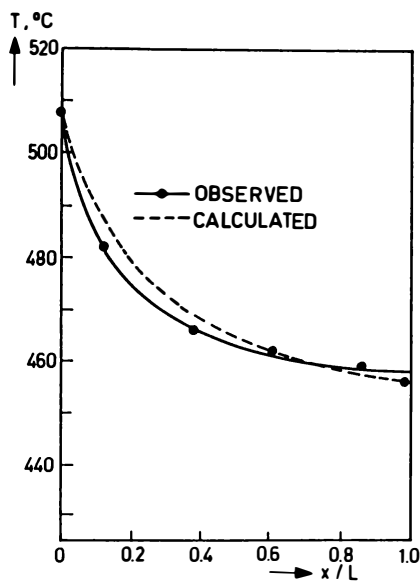


Fig. 17. Axial temperature profile in an adiabatic microreactor operating as the first bed of a catalytic reformer. ($V_r = 10$ mL, Naphtha feed, LHSV = 13.8 L/(L.h), $H_2/\text{feed} = 6.8$ mol/mol, $P = 10.8$ bar).

Table VI. Comparison of Test Results on Light Naphtha Isomerization in Bench-scale and Microflow Reactors

Reactor	Bench-Scale	Microflow
Reactor i.d., mm	20	10
Thermowell o.d., mm	6	5
Bed length, cm	25	7
Catalyst charge, g	37.9	2.1
Yield of C ₅₊ , %w	97.3	97.8
isoC ₅ /tot.C ₅ par., %	64.6	64.2
isoC ₆ /tot.C ₆ par., %	81.8	81.9
RON-0 of C ₅₊ (calcd.)	79.4	79.6

Catalyst: Pt/H-Mordenite, cylindrical extrudates, d = 1.6 mm, L/d = 4.

Feed: Middle East light naphtha, RON-0 = 69.0, isoC₅/tot.C₅par. = 38.5 %, isoC₆/C₆par. = 58.7%. P = 25 bar, T = 250 °C, Hydrogen/feed = 2.5 mol/mol, WHSV = 1.00 kg/(L.h).

Table VII. Reproducibility of Catalyst Testing in Microflow Reactors for Isomerization of Light Naphtha

Experiment	191/A7	192/C5	192/N6	193/A5	194/B4	194/E6
Yield of C ₅₊ , %w	97.5	97.3	97.3	97.6	96.9	97.4
iC ₅ /C ₅ p., %	68.0	67.9	68.0	66.5	68.3	68.5
iC ₆ /C ₆ p., %	72.7	72.6	72.3	72.4	72.5	72.5
RON-0 C ₅₊ , calcd.	80.4	80.2	80.2	80.0	80.3	80.4

Catalyst: Pt/H-Mordenite, cylindrical extrudates, d = 1.5 mm, L/d = 4.5.

Feed: Middle East light naphtha. RON-0 = 67.3, isoC₅/tot.C₅par. = 38.1, isoC₆/tot.C₆par. = 55.4. Other conditions as given in Table VI.

Table VIII. Comparison of Microflow Test Results with Data from Commercial Plants on Light Naphtha Isomerization over Pt/H-Mordenite Catalysts

	Catalyst activity	
	Plant data	Microflow test
Commercial plant Y	73.9	69.4
Commercial plant K	65.2	67.5
Commercial plant O	54.3	54.4

Catalyst activity on a weight basis determined from process data by means of a kinetic process model

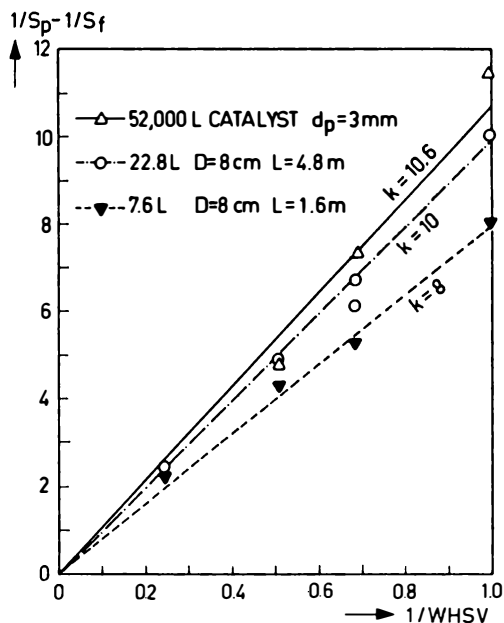


Fig. 18. Comparison of a commercial reactor with pilot reactors of different lengths in gasoil hydrodesulfurization.

(S_f and S_p are the sulfur contents of feed and product, respectively. k is the second-order rate constant).

which a close agreement is demonstrated between results obtained in a pilot plant of similar dimensions, and another industrial plant. From Figure 18 it can also be inferred that results obtained in the shorter pilot plant ($L = 1.6$ m) deviate significantly: the reaction rate is some 20 to 30 % lower than in the two other units, which is an unacceptably large difference.

The unsatisfactory performance of the 1.6 m long pilot plant reactor containing an undiluted bed of particles of 3 mm diameter can be understood: from Figure 5 it can be deduced that for a sufficiently low axial dispersion a minimal reactor length of 2.7 m would be required (90 % conversion, $n = 2$). Also from the point of view of catalyst irrigation the 1.6 m reactor with 3 mm particles is suboptimal: from Figure 10 a maximum particle diameter of 1.6 mm can be inferred ($LHSV = 1, v_L = 3 \cdot 10^{-7} \text{ m}^2/\text{s}$). In contrast with this relatively short reactor, the 4.8 m long pilot plant satisfies the criteria on minimum bed length for acceptable dispersion as well as on the maximum particle diameter for even irrigation. It also has a sufficiently large diameter to meet the criterion for the wall effect ($D/d_p = 26$) and is therefore an acceptable test reactor, as experimentally found.

The above unsuccessful attempt at downscaling of a laboratory trickle-flow reactor which was made some 30 years ago, suggests that representative testing of practical catalysts for trickle-flow processes can only be done in relatively large pilot plant reactors. However, as will be clear from the discussion in earlier parts of this paper, the technique of catalyst bed dilution with fine inert particles has opened the way to small-scale testing of catalysts for these processes as well.

Figure 19 shows some results on gasoil hydrodesulfurization in bench-scale reactors with diluted catalyst beds of different lengths. It can be seen that, in contrast to the above experiments with undiluted beds, the shortening of the diluted bed has no effect within the experimental accuracy. This not only supports the view that both reactors with diluted beds are acceptable as regards axial dispersion and catalyst contacting, but is also in line with the idea that extraparticle mass transfer effects play a minor role only, as discussed before.

Figure 20 presents some results of comparative tests on hydrodesulfurization of a heavy gasoil in a bench-scale and a microflow reactor over two catalysts, both diluted with small particles of silicon carbide. It can be inferred that results are the same irrespective of the reactor scale, the same difference in relative performance of the two catalysts being observed in both reactor types.

Quantitative information on the reproducibility of tests with diluted catalyst beds in microflow reactors was obtained from a series of tests with a standard catalyst and feedstock carried out in the context of monitoring catalyst quality in commercial catalyst production. From the data listed in Table IX it can be inferred that a good reproducibility can be obtained provided due attention is given to experimental details of the testing procedure such as reactor filling, start up and control of reaction conditions.

Data obtained on trickle-flow processes obtained in microflow tests with diluted catalyst beds are not only reproducible, but are also meaningful for industrial practice. This is demonstrated in Table X by the direct comparison of microflow test results with data from an industrial gasoil hydrodesulfurization unit.

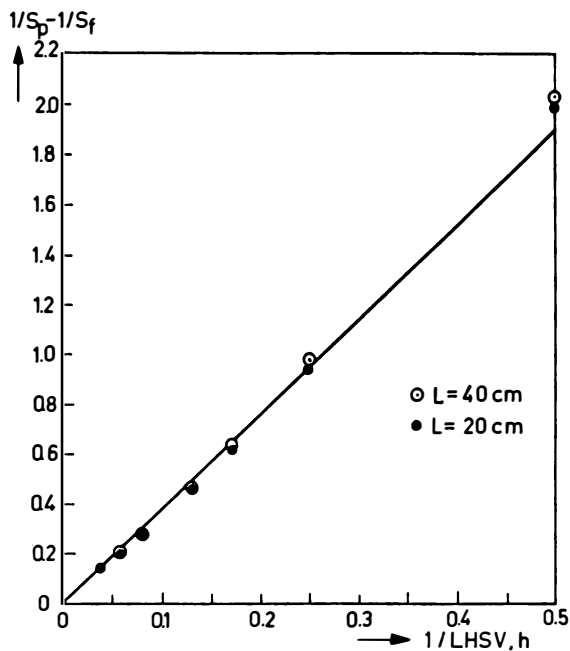


Fig. 19. Hydrodesulfurization of gasoil in a bench-scale reactor with diluted catalyst beds of different lengths.

(Catalyst: Co/Mo/Alumina, 1.5 mm diameter cylindrical extrudates, $L/d_p = 4$. $D = 2$ cm).

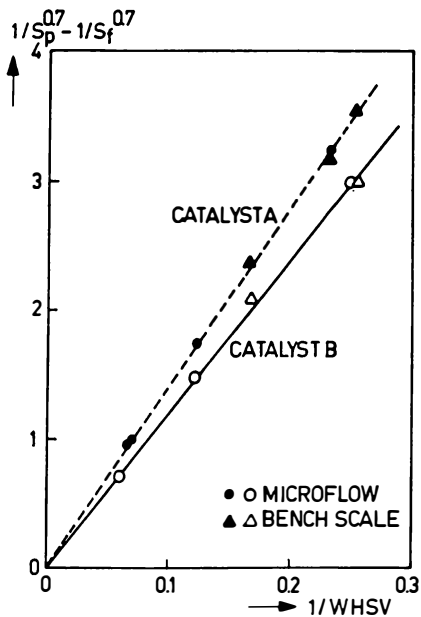


Fig. 20. Comparison of bench-scale and microflow reactors for hydrodesulfurization of a heavy gasoil over diluted catalyst beds. (A and B are Co/Mo/Alumina catalysts shaped as cylindrical extrudates of 1.5 mm diameter).

Table IX. Reproducibility of Catalyst Testing in Microflow Reactors with Diluted Catalyst Beds for Hydrodesulfurization of Gasoil in Trickle Flow

Number of tests	21
Number of reactor units	5
Number of operators	4
Time span	2 years
Average activity	15.4
Maximum activity	16.1
Minimum activity	14.6
Standard deviation	0.54 (=3.5%)

Catalyst: Co/Mo/Alumina, 1.5 mm diam. cylindrical extrudates.

Table X. Comparison of Microflow Test Results with Commercial Plant Data on Hydrodesulfurization of Gasoil in Trickle-flow Operation

	Commercial operation	Microflow test
Catalyst inventory	122 m ³	20 mL (diluted)
S in product, %w	0.082	0.075
% Desulfurization	95.0	95.4
2-nd order HDS rate constant	20.9	23.5

Catalyst: Co/Mo/Alumina, 1.2 mm diam. Trilobe extrudates, L/d = 3.

Diluent in microflow test: Silicon carbide, d = 0.05 mm. Feed: Middle East heavy gasoil, 1.64 %w S. Operating conditions: WHSV, WABT, hydrogen/oil ratio, partial pressures of hydrogen and hydrogen sulfide same in commercial and microflow reactor.

Concluding Remarks

Reducing the scale of experimentation has many advantages in terms of cost and safety and hence there is no merit in catalyst testing on a larger scale than necessary. In the present paper the limiting factors for downscaling of test reactors for fixed-bed processes have been analyzed and quantitative criteria have been given for the parameters of interest to ensure meaningful results.

Due to the beneficial effect of radial diffusion in gas-phase processes in counteracting transverse velocity profiles caused, for instance, by the perturbation of packing homogeneity near the reactor wall, and by taking advantage of the improvements in axial dispersion and catalyst irrigation resulting from dilution of the catalyst bed with fine inert material, it is possible to obtain reproducible and meaningful results from tests in microreactors.

Microflow reactors as shown in Figures 21 and 22 are now capable of generating most of the catalytic performance data for fixed-bed processes applied in the hydrocarbon process industry, a task that some 25 years ago had to be reserved for large pilot plants with catalyst volumes of 10 L or more which required tank farms and gas holders and even on-site production of hydrogen to enable their operation.

From the analysis of limiting factors as discussed in this paper, it follows that even smaller reactors than microreactors may be used, since the bed diameter of the latter can be further reduced without adverse consequences, as long as the reactor tube can still accommodate the catalyst particles. Thus, catalyst testing may be done in reactors having diameters in the millimeter range containing less than one gram of catalyst.

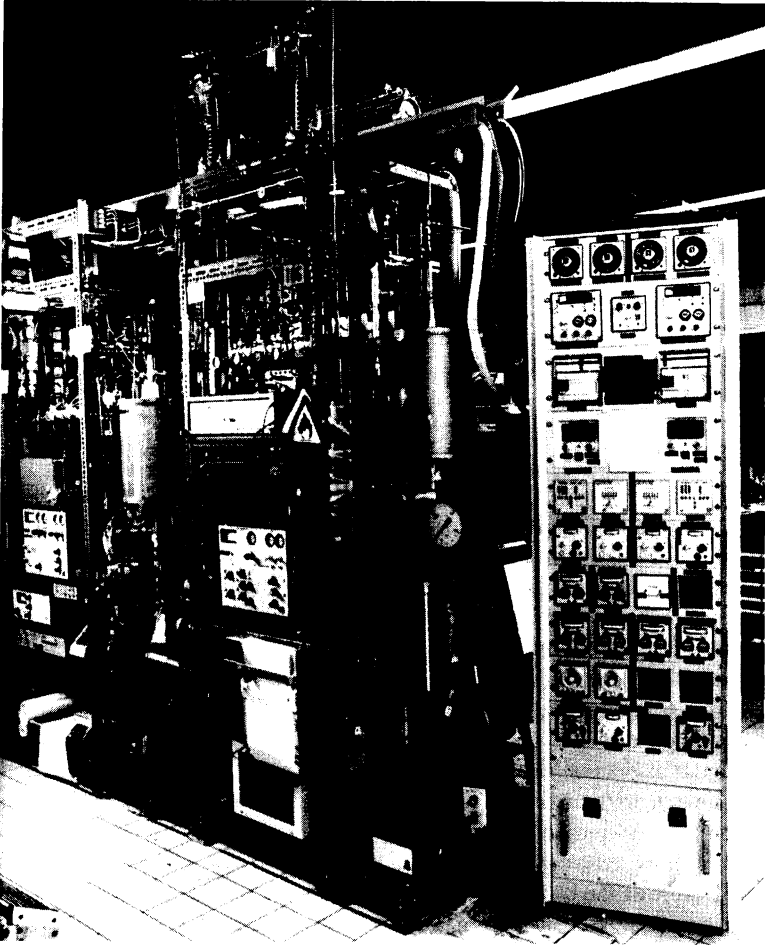


Fig. 21. Picture of microflow reactors for testing catalysts for gas-phase processes, build in the eighties. The reactor units are equipped with on-line GLC analyzers.

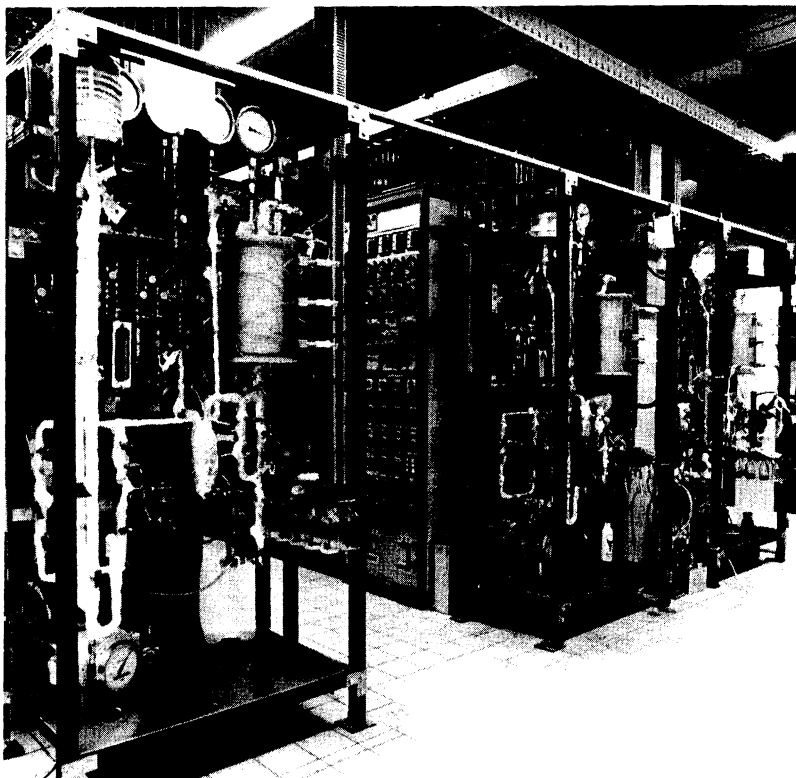


Fig. 22. Picture of microflow reactors for testing catalysts for trickle-flow processes, build in the eighties. The reactor units are equipped with automatic collectors for liquid samples.

Large pilot plants remain indispensable only when in the development of an unconventional process sufficient amounts of novel product have to be made available for application studies, or when complex interactions between elements of the process have to be studied in an integrated way. In the latter case, a pilot plant will be a scaled-down version of an actual complex industrial plant, rather than just a reactor unit as required in catalyst performance testing or kinetic process studies.

Notation

Bo	Bodenstein number
d	diameter of cylindrical particle
d_p	particle diameter (equivalent sphere diameter)
D	bed diameter
D_{ax}	effective diffusivity in axial direction
D_m	molecular diffusivity
D_{rad}	effective diffusivity in radial direction
E	activation energy
g	gravity constant
GHSV	gas hourly space velocity
k	reaction rate constant
L	length of reactor or cylindrical particle
LHSV	liquid hourly space velocity
n	reaction order
N_e	equivalent number of ideal mixers
P	pressure
Pé	Péclet number
r	radial coordinate
R	bed radius or gas constant
Re	Reynolds number
RTD	residence time distribution
S_f	sulfur content in feed
S_p	sulfur content in product
T	temperature
u	superficial fluid velocity
v	average fluid velocity in bed
V	catalyst volume
W	wetting number
WHSV	weight hourly space velocity
WABT	weighted average bed temperature
x	axial coordinate
X	conversion
<u>Greek letters</u>	
ΔT_{ad}	adiabatic temperature rise
Δ (ad)	deviation from true adiabaticity related to radial heat flow
Δ (ad,app)	deviation from true adiabaticity related to axial heat conduction
ϵ	voidage

η	dynamic viscosity
θ	average residence time of fluid in the bed
κ	dimensionless constant describing transverse velocity profile
ν	kinematic viscosity
ρ	density
τ	tortuosity factor

Subscripts

G	gas
L	liquid

Acknowledgments

The author gratefully acknowledges the contributions of his former coworkers at the Koninklijke/Shell Laboratory at Amsterdam where most of this work has been carried out. Thanks are in particular due to Ir M. Sonnemans and Mr J. Glezer for carrying out the dispersion measurements in microreactors with gas flow, to Ir J. van Klinken who was responsible for the liquid dispersion measurements under trickle-flow conditions, to Mr. M. Winter for carrying out the tests on light naphtha isomerization, to Ir. H. Gierman and Ing. D. Pultrum for their work in the development of the adiabatic microreactor, and to Mr. P.A. van Weeren and Mr. A.F. de Vries for the gasoil hydrodesulfurization experiments.

Literature Cited

1. Weisz, P.B. *Chem. Technol.* **1982**, 12 (7), 424.
2. Gierman, H. *Appl. Catal.* **1988**, 43, 277.
3. Mears, D. *Chem. Eng. Sci.* **1971**, 26, 1361.
4. Zimmerman, S.P.; Ng, K.M. *Chem. Eng. Sci.* **1986**, 41, 861.
5. Fahien, R.W.; Stankovic, I.M. *Chem. Eng. Sci.* **1979**, 34, 1350.
6. Sie, S.T. *Anal. Chim. Acta* **1967**, 38, 3.
7. Sie, S.T. *Rev. Inst. Franç. Pétrole* **1991**, 46 (4), 501.
8. De Bruijn, H. *Proc. 6th Int. Symposium on Catalysis* **1976**, 951.
9. Van Klinken, J.; Van Dongen, R.H. *Chem. Eng. Sci.* **1980**, 35, 59.
10. Koros, R.M. *Proc. 4th Symposium Chem. Reaction Eng.* **1976**, 372.
11. Carruthers, J.D.; Dicamillo, D.J. *Appl. Catal.* **1988**, 43, 253.
12. Sie, S.T.; Blauwhoff, P.M.M. *Catal. Today* **1991**, 11, 103.
13. Anderson, D.H.; Sapre, A.V. *Chem. Eng. Progress* **1989**, 85 (7), 54.
14. LeNobel, J.W.; Choufour, J.H.,. *Proc. 5th World Petroleum Congress* **1959**, Sect. III, 233.

Chapter 3

Evaluating Pore Structure and Morphology of Hydrocarbon-Conversion Catalysts

R. Mann, K. Khalaf, and A. Al-Lamy

Department of Chemical Engineering, University of Manchester Institute of Science and Technology, Manchester M60 1QD, United Kingdom

Porosimeter tests on FCC catalyst powder and pellets of different sizes are interpreted using 3-D stochastic pore networks to elucidate an improved measure of the powder's internal pore structure. The elucidated pore structure can be evaluated against image analysis of low melting point alloy penetration sections examined on a scanning electron microscope (SEM), whereby the state of penetration of the internal pores is frozen into a 2-D sectional image. Actual SEM images can be compared directly with 'theoretical' random sections of 3-D stochastic networks. In this way stochastic pore networks form a suitable coherent structural framework for reconciling mercury porosimetry and low melting point alloy penetration. The more realistic description of the pore structure provided by 3-D stochastic networks is directly suited to the analysis of diffusion, reaction and coke laydown processes in cat cracker operation.

Gas adsorption and mercury porosimetry are two principal experimental methods for quantifying the nature of the porosity of a particle. Figure 1 shows an SEM image of a typical particle of fluid cat cracking (FCC) catalyst. Such particles are used in fluid bed processes, for cracking heavier distilled fractions down to lighter liquid fuels in the C₈ carbon number range. The performance of such cat crackers is crucially dependent on the porous properties of these fine powdered 70 μm diameter particles. Three aspects of their pore structure are important; resistance to attrition, high activity for cracking and resistance to deactivation by coke/metals deposition.

The range of pore sizes important to good catalytic function are from around 10 Å in the supported zeolite to perhaps 100,000 Å (10 μm) in the zeolite/silica-alumina composite. The technique of gas adsorption is of little use beyond about 250 Å, so that by far the largest range of important pore sizes (and related interactions between pores which constitute the 'pore structure' of the particle) are assessable only through the mercury porosimetry technique. Many practitioners in catalyst characterisation claim that

pores above 250Å (ie. outside the range of gas adsorption) are irrelevant, but there are strong grounds for believing that pores in the range of 0.1 to 1 µm are important to transport and diffusion processes (1) and moreover, probably control the interaction of permeability and particle mechanical strength. It is therefore important to be able to measure, characterise and describe pores in this size range.

Pore networks in 2-D and 3-D are still being developed as computer-aided representations of real porous materials since the idea was first proposed some 40 years ago (2). Subsequently, 2-D networks were applied to porosimetry (3) and low-temperature gas adsorption (4), and 2-D and 3-D models have been compared (5). More recent work has applied 3-D networks to porosimetry (6), to flow and transport behaviour (7), as well as to diffusion and reaction in catalysis (8). The equivalence of pore networks to a continuum representation for porosity has lately been established (9) and a review of recent developments and applications is available (10).

Mercury Porosimetry Results

Figure 2 shows a set of results for a catalyst powder (Super-D), manufactured by Crosfields Chemicals, Warrington, made from pellets by grinding with a pestle and mortar. Figure 2 portrays the extent of penetration of the pore volume as the pressure of mercury is increased. Also shown in the same figure are the results for pellets fractured into half-size and quarter-size fragments. These results for powder, fractured pellets and whole pellets are to be used as a measurement framework for distinguishing the basic pore structure/pore size distribution of the interior porosity of the micro-porous particles and the intra-pellet pore spaces of the full pellet.

The nature of the problem can be illustrated with respect to the schematic diagrams of Figures 3 and 4. Figure 3 shows schematically that in penetrating a mass of powder of micro-porous particles, mercury invades spaces between the particles (shown white) simultaneously with penetration of the particles themselves. Thus in Figure 2, the powder result indicating a high pore volume at the highest pressures, arises from a potentially large contribution from spaces between the micro-porous particles. By contrast, Figure 4 shows (also schematically) that as mercury penetrates an assembly of pellets it is vital to discriminate the inter-pellet space (white) from the intra-pellet porosity (black) whilst recognising that both inter-pellet and intra-pellet mercury penetration might occur simultaneously with intra-particle penetration of the mercury. The pellet curve in Figure 2 includes these three distinct volume contributions.

In principle it should be possible to discriminate the pore structure of the basic particles from just the powder and whole pellet results, and the results for 0.5 and 0.25 pellet fragments are available to check and substantiate assumptions made. The full treatment of these results has been reported separately (11), but for the purposes of the present treatment, attention will be confined to the powder/whole pellet penetration curves.

The interpretation of these two porosimeter curves relies upon the nature of the pore space structure adopted. Classical treatments have traditionally applied the Washburn equation



Figure 1. SEM view of an FCC catalyst particle (Reproduced with permission. Copyright 1993 Institution of Chemical Engineers.)

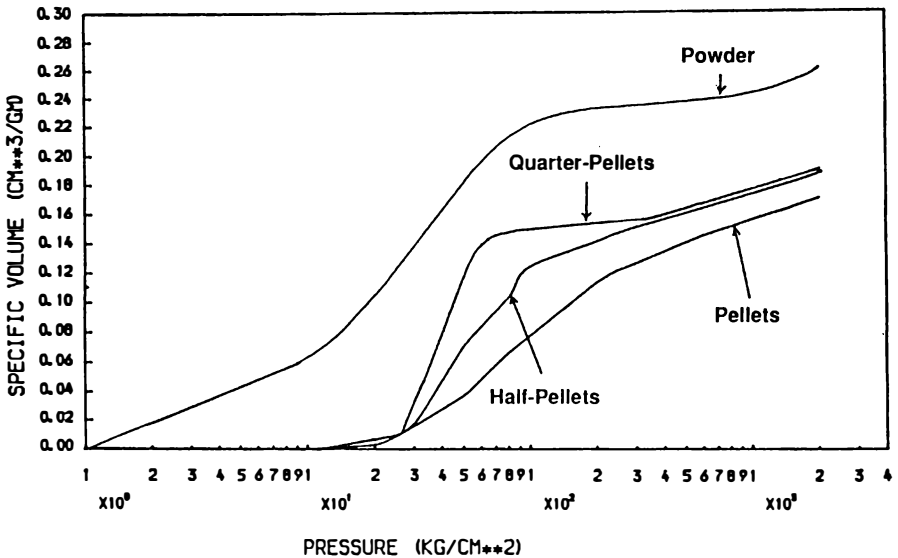


Figure 2. Mercury porosimeter results

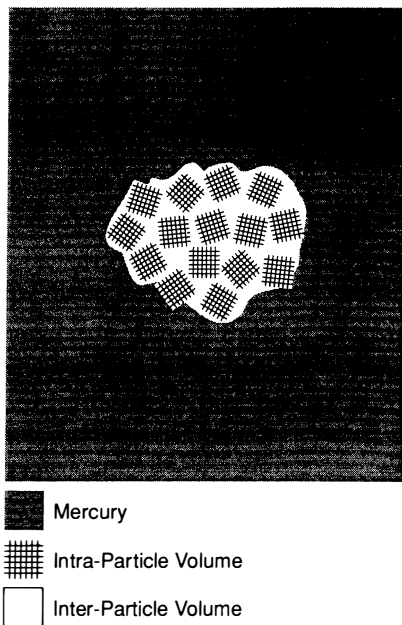


Figure 3. Mercury penetration into micro-porous particles

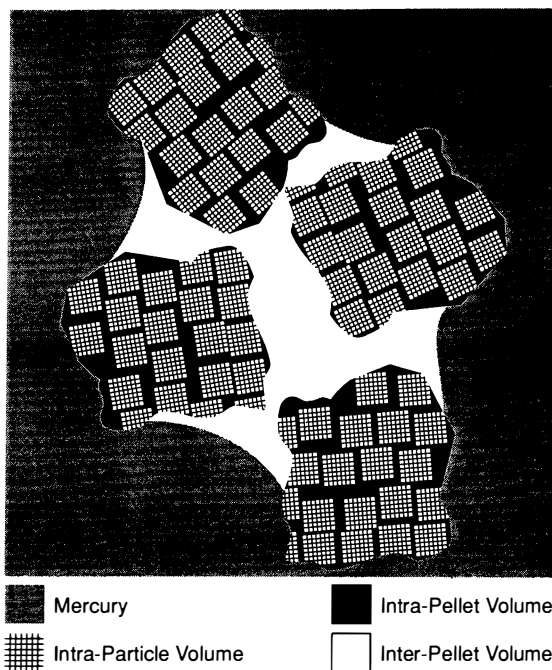


Figure 4. Mercury penetration into an assembly of pellets

$$P = \frac{4\gamma \cos \theta}{D} \quad (1)$$

in conjunction with a parallel bundle structure. Research at UMIST (3,12,13,14) has sought to develop more realistic structure models based upon so-called stochastic networks of pores.

A full analysis of intra-particle and intra-pellet porosity based on stochastic networks remains to be completed (11). For the present, we seek the application of a stochastic network to the intra-particle spaces based upon a discrimination of this porosity via a parallel bundle analysis of the results of Figure 2.

The parallel bundle analysis of Figure 2 furnishes the results presented in Figure 5. The key to this analysis is the recognition that whatever the distribution of pore sizes is for each category of porosity (intra-particle, inter-pellet and intra-pellet) the actual amounts of pore volumes are integrals of those distributions. These take values specified by the density of the solid materials (zeolite, plus silica/alumina support) and the pore volumes per gm indicated by the porosimeter results in Figure 2. Thus the final penetration for the powder is the sum of inter-particle and intra-particle and intra-particle porosity. By the same token, the final penetration for the pellet comprises the sum of the intra-particle volume added to the intra-pellet and inter-pellet volumes.

From Figure 5 it is deduced that these integral pore volume constraints require the intra-particle pore volume to be distributed in an approximately negative exponential distribution with the highest frequencies of pores towards the smallest detectable size (35Å), with the frequency declining towards zero around 1.2 µm. Somewhat similarly, it appears that the inter-pellet volume is greatest towards the smaller size pores and vanishingly small approaching 1 µm. The intra-pellet volume is largest around 0.3 µm, vanishes at the small and large pores, but is skewed towards 1 µm pores.

Hence at around 1 µm the detected pore volume arises almost entirely from spaces within the pellets. In contrast around 0.1 µm, the pore volume due to inter-pellet spaces is dominant. The integral values of pore volume per gm are then 0.140 cm³ for intra-particle porosity, with values of 0.086 cm³ and 0.045 cm³ for intra-pellet and inter-pellet spaces respectively.

Application of Stochastic Pore Networks

Parallel bundles of pores (in which all pores of a given size or radius are bound to be equally accessible) are a highly unrealistic structural configuration. Stochastic networks are arrangements of pores into fully accessible inter-connected frameworks within which pores are assumed to be distributed randomly. In this way, the size of any pore is taken to be independent of its neighbours. A network may then be constructed to obey any stipulated distribution function by assigning pores from the distribution randomly to positions in the network. Stochastic networks are an attempt to incorporate the elements of randomness and chaos which are implicit to many porous media, in such a way as to retain a feasible computability. Modern computers (and now micro-computers) can readily compute mercury porosimetry into networks comprised of up to millions of pores (11,15).

It has also long been recognised that pore size distributions deduced from a parallel bundle are skewed towards small pores. The physical reason for this is that whenever a large pore is penetrated by mercury through a small pore, its volume will be erroneously attributed to the small pore size through which access occurred. This distortion can be severe and the overlap (or agreement) between parallel bundles and networks can be as little as 25%. In other words the error introduced or discrepancy can be as high as 75% (13,14).

Figure 6 shows a pictorial representation of a regular cubic 3-D pore network in which all the pores are of the same length (7). The network shown is referred to as a 10x10x10 network and pores of different diameters are evident in Figure 6. Also shown in Figure 7 is the counterpart irregular cubic network, created by allowing random displacement of pore nodes about their positions. Such irregular networks have the important property of allowing pore length to be varied independently of pore diameter. In the event that length and diameter for pores are completely uncorrelated, the regular and irregular networks have been shown to have identical porosimeter curves (11). Such a result has also been demonstrated in 2-D (16).

Low Melting Point Alloy Impregnation

The technique of impregnation with low melting point alloy results in a freezing of the state of penetration in 3-dimensions amongst the pore spaces. An impregnated sample of powder can then be sectioned and polished and, if viewed on an SEM, affords a view of a 2-D random plane through the 3-D pore spaces. The alloy used melts at 47°C. Impregnation has been performed at around 60°C (in a hot water bath) so that samples are 'solid' at room temperature.

Figure 8 shows a part of a section of an impregnated powder sample with a field size of approximately 500 μm x 500 μm . This field contains sections through about 250 powder particles, and it is clear that the extent of penetration amongst individual particles shows a very great variance. Indeed, about 50 particles (around 1/5th of the total) show negligible penetration of low melting point alloy. For the purposes of the present analysis, attention will be focused on the typical particle shown in Figure 9. This particle is the one located just lower than, and left of the centre of Figure 8. It has a typical penetrated porosity of 0.33 and an apparent diameter of about 60 μm . The section in Figure 9 probably passes close to the particle centre, since particles are of this order of diameter.

The results of an image analysis of this particle on a Joyce-Loebl analyser are presented in Figure 10 in number distribution terms over the size range zero to 9.6 μm . The total number of detected features is 84, although 51 of them are detected to be less than 1.2 μm . These small (more or less sub-micron) pores are relatively very numerous and form some 65% by number of the total. Their numerical proportion is beyond the so-called percolation threshold (17) so that they can be expected to control the penetration processes for both mercury porosimetry and low melting point alloy impregnation. Thus for a parallel bundle interpretation (pores of all sizes equally accessible), all the large pores bigger than 1.2 μm would inevitably be interpreted as belonging to pores in the size range zero to 1.2 μm . Hence in Figure 5, observations of the mercury penetrated, results in the conclusion that the largest pores could not be bigger than 1.2 μm . It is also deduced from Figure 5 that pores within the micro-porous particles could not exceed this size.

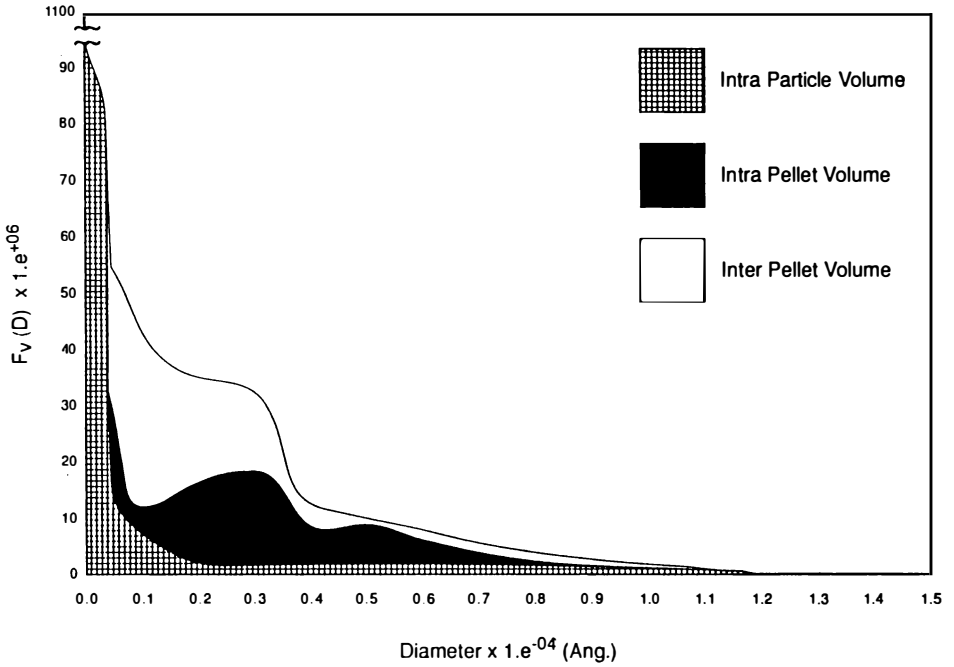


Figure 5. Probable distribution of intra-particle pore volume

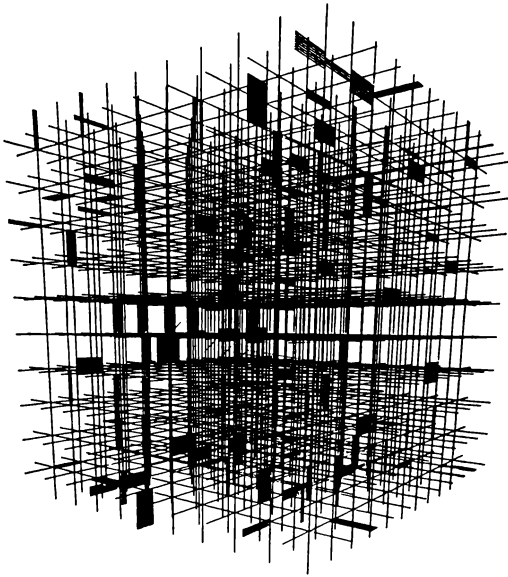


Figure 6. Regular cubic 3-D stochastic pore network (10x10x10) (Reproduced with permission. Copyright 1993 Institution of Chemical Engineers.)

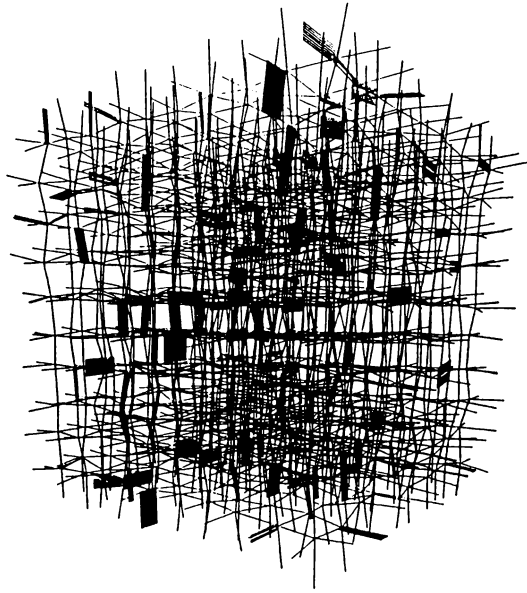


Figure 7. Irregular cubic 3-D stochastic pore network (10x10x10)
(Reproduced with permission. Copyright 1993 Institution of Chemical Engineers.)

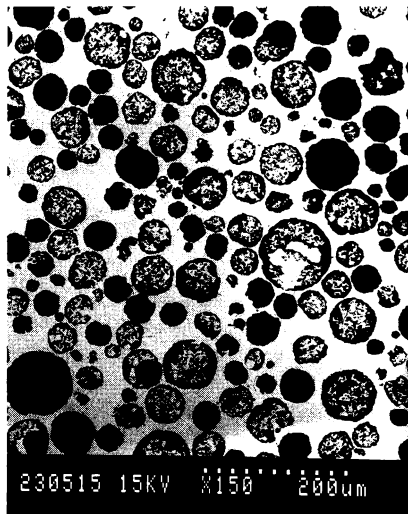


Figure 8. Low melting point alloy (LMPA) impregnation at 50 atmos
(Reproduced with permission. Copyright 1993 Institution of Chemical Engineers.)

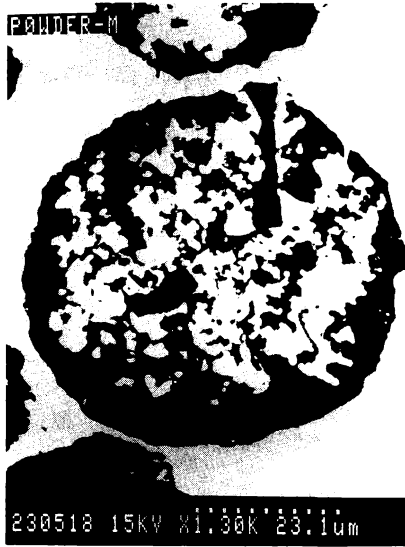


Figure 9. Alloy impregnation for a typical particle

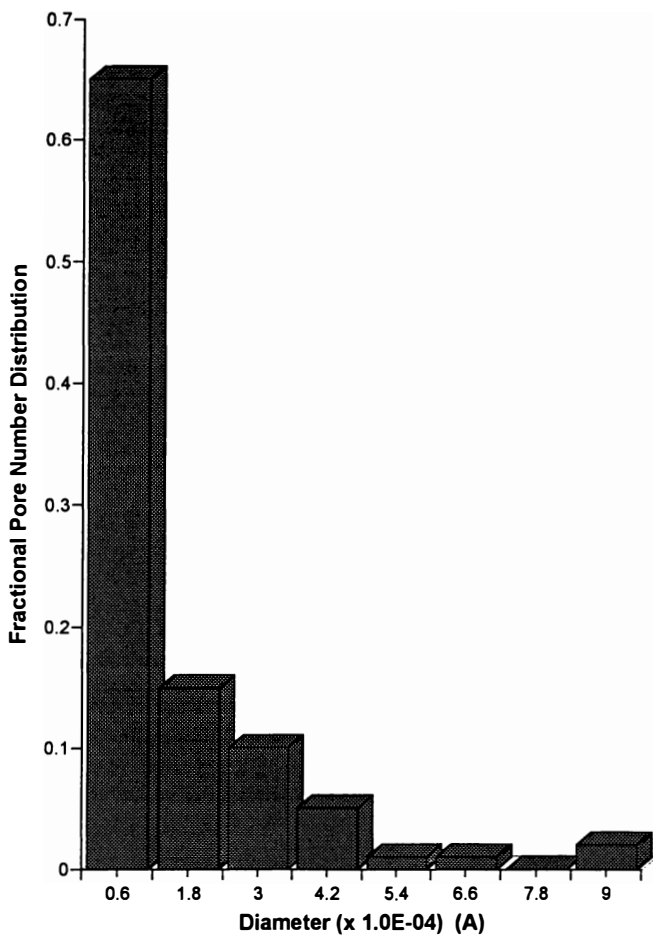


Figure 10. Image analysis of impregnated pore spaces in Figure 9

Such a conclusion is apparently refuted by the visualisation of the penetration of the interior of a typical particle in Figure 9 where pores clearly larger than $1.2\ \mu\text{m}$ can be seen. The quantification of the number size distribution of detected features (pore penetrated by alloy) in Figure 10 shows a very low number count of the largest features with one in the range 6-7.2, none in the range 7.2-8.4, and 2 in the range 8.4-9.6. Although low in number, these largest features dominate the visual appearance of the section.

Pore Size Distribution for a 3-D Stochastic Network

The powder mercury penetration curve in Figure 2 has been corrected for inter-particle pore spaces (via Figure 5) so that the penetration of mercury into the FCC powder particles is known. It corresponds to the hatched area in Figure 5. However, the pore volume distribution in Figure 5 (approximately negative exponential decay in shape) refers to a parallel bundle interpretation. It is necessary to deduce the network pore size distribution that gives rise to the same mercury penetration curve. The deduced distribution of pore volume according to a $23 \times 23 \times 23$ network (containing 38,000 pores) is presented in Figure 11. Also shown in Figure 11 is the parallel bundle result. The shielding of large pores behind small one gives rise to a significant distortion in the parallel bundle result. The 3-D network analysis indicates that the pore volume is to be attributed largely to the largest pores. Thus for a network analysis, almost 50% of the pore volume is contained in pores between 1 and $1.2\ \mu\text{m}$.

In contrast, a parallel bundle interpretation would allocate only 10% of pore volume to the range 0.8 to $1.2\ \mu\text{m}$. Figure 11, displaying the two distributions side-by-side, shows the small overlap of the two approaches. This overlap amounts to about 10%, so that there is a 90% disparity between the parallel bundle and the network analysis. In short, the network predicts that there should be many larger pores.

Computer Images of a Sectioned 3-D Stochastic Network

Now that a 3-D network has been deduced to represent the pore spaces within the FCC particle of Figure 9, it is possible to execute a random slice through the network to examine the pores so sectioned that are calculated to have been penetrated by low melting point alloy. Figure 12 presents a sectional image of a $15 \times 15 \times 15$ window (the maximum achievable with UMRCC computer graphics) of the $23 \times 23 \times 23$ network used to simulate a typical FCC power particle. One immediately significant feature of Figure 12 is that, although the network sectioned contains only cylindrical pores up to $1.2\ \mu\text{m}$ in diameter, Figure 12 contains features significantly larger than $1\ \mu\text{m}$ because pore sections appear aggregated together close to junctions of pores. In fact the largest feature in Figure 12 is $4.2\ \mu\text{m}$ (equivalent circular) diameter. It is clear that this coalescence of intersecting pores adjacent to the junctions causes the feature size distribution in a section to be larger than the basic pore space sizes that form the network. Stochastic pore networks enable us to begin to decompose feature sizes and shapes into the basic pore 3-D space geometrics that give rise to them in a 2-D section.

However, from Figure 12 it is evident that even though an interpretation of the porosimeter curve via a 3-D stochastic pore network gives rise to much larger estimates

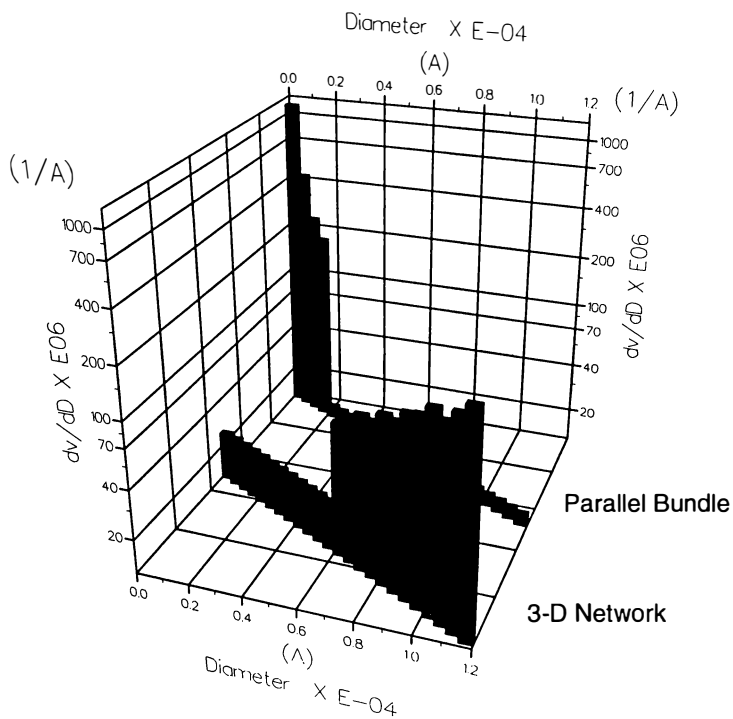


Figure 11. Intra-particle pore volume from a pore network

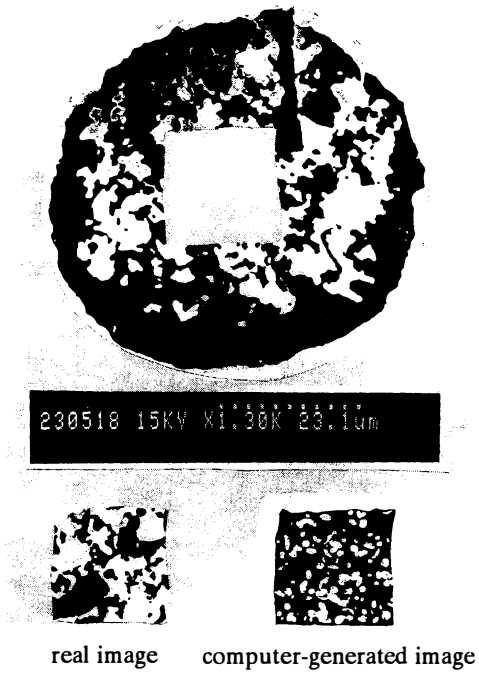


Figure 12. Comparison of real and "virtual" section images

for pore sizes than the parallel bundle (by almost a factor of 10 according to Figure 11), the pore features presented on sectioning a 3-D network are still very much smaller than those seen in a real typical particle image.

The features in the computer generated section in Figure 12 have been subjected to image analysis and the result is shown in Figure 13 for comparison with the result for the real SEM section. From the comparison in Figure 13, the actual features on the real microscope section are mainly larger and smaller. The real image has features up to 9.6 μm in size as well as greater number of small features below 0.5 μm . In contrast, the computer synthesised section has a greater proportion of pores in the range 0.5 to 1.5 μm with a maximum feature size just over 4 μm .

A much better reconciliation between the real image and 3-D stochastic network sections is achieved by a simple extension of the basic pore size distribution of the pore segments forming a 3-D network. Figure 14 shows a pore volume distribution for network segments extended from a maximum of 1.2 μm to 3.0 μm . If a 3-D aggregation of these pores is performed, the resulting computer section image of size 15 x 15 x 15 is presented in Figure 15, alongside a corresponding section from the real particle. In this case, the maximum feature in the computer generated section has now increased to a size of 9 μm , which is close to the largest feature seen in the real image.

Image analysis of the real and computer images of Figure 15 is presented in Figure 16. There is now a much improved correspondence between the number distribution of feature sizes in each case, although as with Figure 13, there is still an excess of features in the computer image in the intermediate range of sizes from 1 to 5 μm . By contrast, the real image has an excess of features below 0.5 μm , which was also the case in Figure 13. Furthermore, this imaging approach has clearly indicated that mercury porosimetry is somewhat insensitive in identifying and quantifying larger pores. The extension of the largest pore sizes to 3 μm from 1.2 μm obviously has a pronounced effect on the pore volume distribution which can be clearly seen from Figure 14. However, the penetration of mercury into the network with the larger pores is extremely close to that observed with the smaller (1.2 μm) pores, small only differences arising at initial penetration. This is because although small pores only contribute marginally to the overall pore volume, they provide a dominating proportion of the pore number distribution. Correspondingly, these small pores control the penetration process into the network. The sizes of the large pores hidden behind and amongst the small pores cannot be sensitively deduced from a porosimeter curve. It seems therefore essential to consolidate inferences from porosimetry by actual visual observation. The low melting point alloy technique appears admirably suitable to do this. It should be noted that the use of images and porosimetry gives most pores between 2 and 3 μm , whereas a parallel bundle analysis (as in Figures 11 and 14) would give pores mostly below 0.1 μm . This inherent error in porosimetry can therefore be seen in this case to amount to a factor of between 20 and 30.

In addition, it is clear that the computer synthesised features appear quite realistic in several respects. The sectional appearance uses a roughness generator (which is a tuneable parameter) as well as a tortuosity parameter (also tuneable) applied to individual sections of pores. Using random node displacements then leads to quite contorted sectional features where pores interact randomly at or close to junctions. Individual features, especially the larger ones, thereby have a reassuringly realistic appearance which is nevertheless perfectly quantitative. The incorporation of roughness and tortuosity

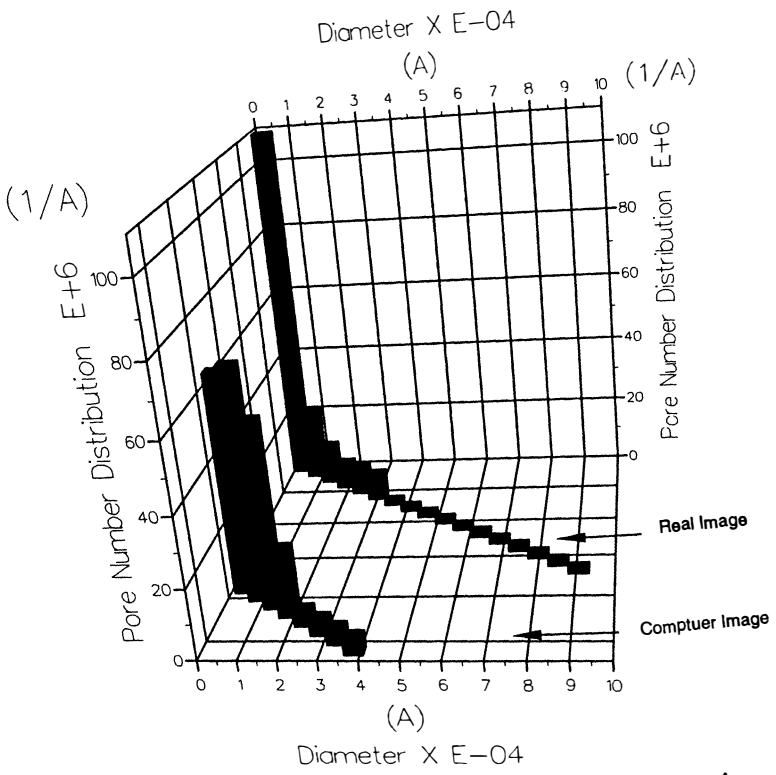


Figure 13. Image analysis of "virtual" computer section

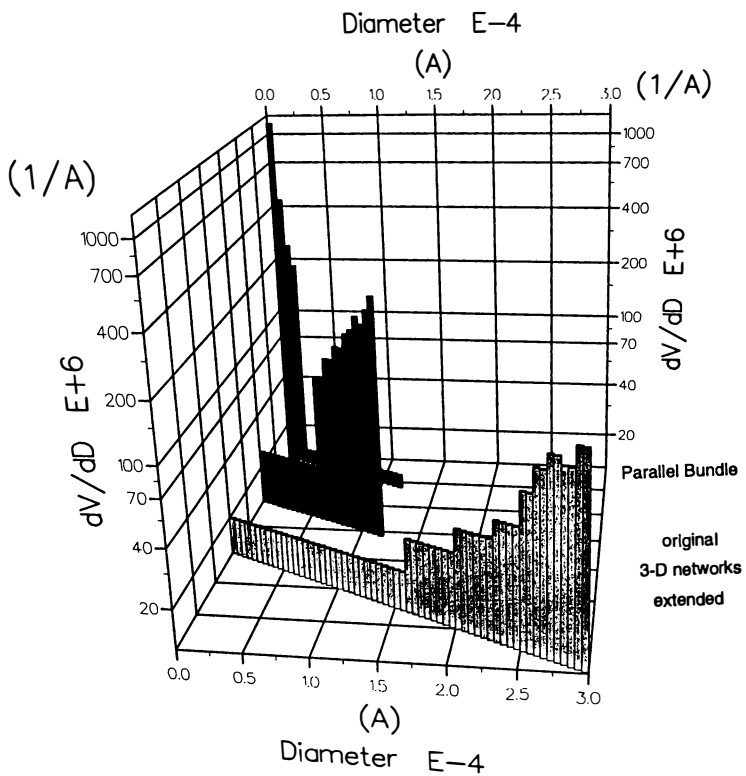


Figure 14. Intra-particle pore volume for a network extended to 3 μ m

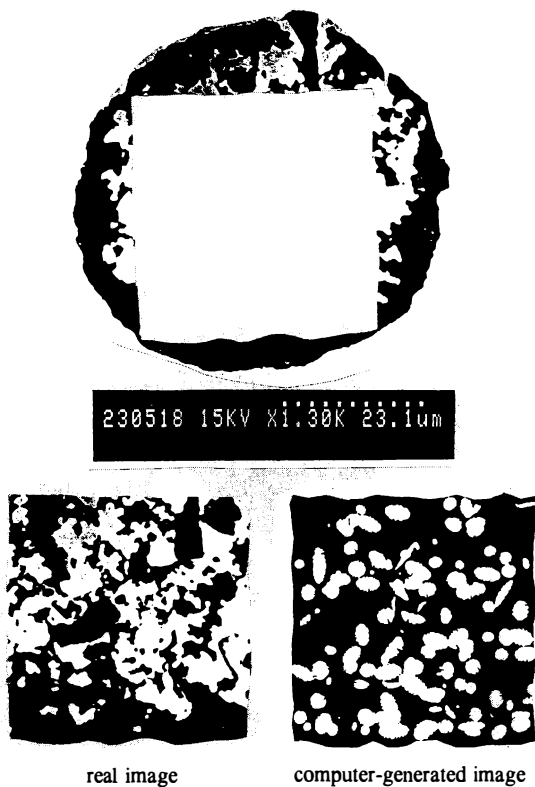


Figure 15. Real and "virtual" sections with pore sizes extended to $3\mu\text{m}$

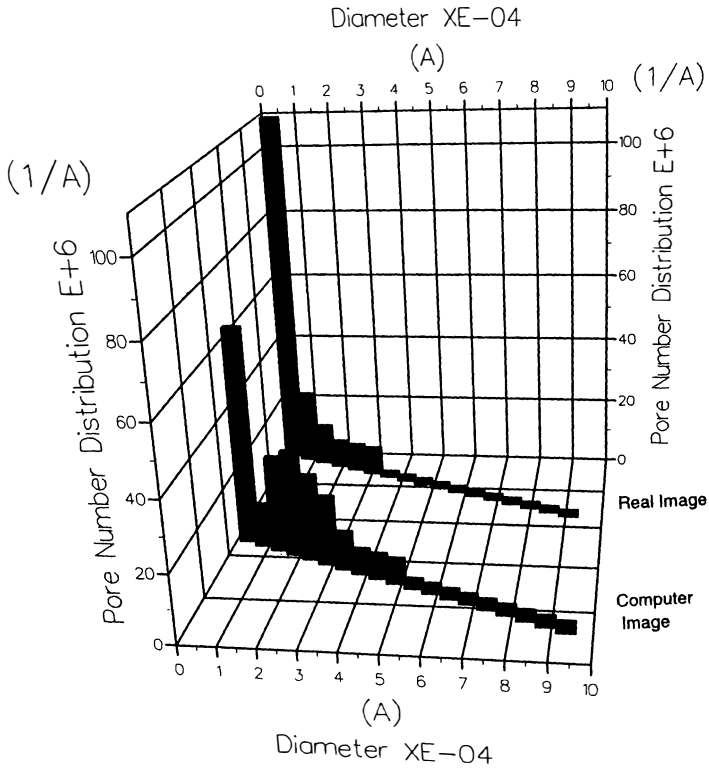


Figure 16. Image analysis of "virtual" section (pores up to $3\mu\text{m}$)

distortion is assumed not to affect the basic mercury penetration and low melting point alloy impregnation processes. More complete details have recently been published (18).

Therefore, the section shown in Figure 15, and the pore network in 3-D from which it arises, are both absolutely defined in a quantitative way. Inasmuch as the 3-D networks are felt to be a realistic representation of random pore spaces, it is feasible to compute directly several important macroscopic properties for the FCC powder particles. Amongst these properties are permeability and effective diffusivity, so that diffusion and reaction calculations relevant to gas-oil cracking in the FCC particles can be directly undertaken. Also important in this respect are calculations of deactivation due to coke laydown within the particles. It is also possible that the pore networks could be used to deduce strength and abrasion resistance of the particles.

In conclusion it would appear that the combination of 3-D stochastic pore networks with mercury porosimetry and low melting point alloy impregnation offers a new framework for the description and calculation of the role of pore spaces in typical porous catalyst particles.

Literature Cited

- [1] Yanik, S.J.; O'Conner, P.; Bradt, M.F.; Abner, D.K.; Friedrich, M.C.; 1992, *AIChE Symp. Series No. 291*, 88, 9-20
- [2] Fatt, I., 1956, *Petr. Trans. AIME*, 207, 164
- [3] Androustopoulos G.P.; Mann, R., 1979, *Chem Eng Sci*, 34: 1203-1212
- [4] Mann, R.; Thomson, G., 1989, *Science & Technology* (Eds A.E. Rodrigues et al), Kluwer Academic Publishers, 63-77.
- [5] Chatzis, I.; Dullien, F., 1985, *Int. Chem. Eng.* 25, 47
- [6] Day, M.; Parker, I.B.; Bell, J.; Fletcher, R.; Duffie, J.; Sing, K.S.W.; Nicholson, D.; 1994, *Studies in Surface Science and Catalysis* 87, 225-234
- [7] Sahimi, M.; and Stauffer, D.; 1991, *Chem Eng Sci*, 46, 2225
- [8] Hollewand, M.; Gladden, L.F.; 1992, *Chem Eng Sci*, 47, 1761
- [9] Zhang, L.; Seaton, N.A.; 1994, *Chem Eng Sci*, 49, 41
- [10] Mann, R., 1993, *Trans. I. Chem.E.*, 71(A), 551-562
- [11] Khalaf, K., 1988, "Application of 3-D stochastic pore networks to FCC particles", Ph.D. Thesis, UMIST
- [12] Mann, R.; Androustopoulos, G.P.; Golshan, H., 1981, *Chem Eng Sci*, 36, 337-346
- [13] Mann, R.; Golshan, H.; 1981, *Chem Eng Commun*, 12: 377-391
- [14] Mann, R.; Sharratt, P.N.; Thomson, G., 1986, 41, 711-718
- [15] Sbaiti, B., 1985, "Modelling of porous media using 3-D stochastic pore networks", Ph.D. Thesis, UMIST
- [16] Mann, R.; Almeida, J.; Mugerwa, M., 1986, *Chem Eng Sci*, 41: 2663-2671
- [17] Broadbent, S.R.; Hammersley, J.M., 1957, *Proc. Camb. Philos. Soc.*, 53, 629-641
- [18] Mann, R.; Al-Lamy, A.; Holt, A., 1995, *Trans. I.Chem.E.*, 73 (A), 147-153

CATALYST DEACTIVATION BY COKE

Chapter 4

Deactivation of Zeolite Catalysts by Coke

T. Masuda and K. Hashimoto

Department of Chemical Engineering, Faculty of Engineering,
Kyoto University, Kyoto 606, Japan

Zeolite catalysts are widely used in conversion processes of hydrocarbons, because of their high activity and shape selectivity. The conversion rate and the shape selectivity are closely related to intracrystalline diffusion rate and acidic properties of the zeolite catalyst. Carbonaceous materials called coke deposit on the catalyst during reactions, leading to changes in catalytic properties (diffusivity and acidic properties) as well as the reaction performance. This presentation reviews the mechanisms of the deactivation of zeolite catalysts caused by coke deposition from the following points of view. (1) Characterization of coke. Examination of the location of coke formation. (2) Relationship between the changes in acidic properties, and the acid strength and the acid amount. Prediction of the reduction of diffusion rate taking account of pore structure and molecular size. (3) Development of models for predicting the change in the activity and the shape selectivity.

Zeolites are solid acid catalysts which are widely used in hydrocarbon processing, such as naphtha cracking, isomerization, disproportionation and alkylation. During reactions carbonaceous materials called coke deposit on the zeolite and reduces its activity and selectivity. Coke deposited not only covers the acid sites of the catalyst, but also blocks the pores, and restrain reactants from reaching the acid sites, leading to the decrease in the apparent reaction rate (1, 2). Here, we will mainly deal with the intracrystalline diffusivity of zeolites, and will discuss the relationship between it and the change in catalyst selectivity.

THE PORE STRUCTURES OF ZEOLITES AND THE MODES OF COKE DEPOSITION

Zeolites are composed of crystals of alumino silicate with the size of 0.1-5 micron. The pores of HY type zeolites consist of super cages and windows (0.74 nm). ZSM-

5 (MFI type) zeolites have straight channels and zigzag channels which connect them. The cross sections of these pores have the sizes of 0.51×0.55 nm and 0.54×0.56 nm, respectively (3). The intersections of these channels have space which just two butene molecules can occupy (4). Mordenite has a porous structure, in which the supercages and their windows are connected in a straight line. The pore sizes of zeolites are close to the minimum molecular sizes of light hydrocarbons. Hence, zeolites have the ability to sieve molecules (shape selectivity).

The mode of coke deposition is closely related to the pore structure of the zeolite (5-8). Figure 1 shows how coke deposits on typical zeolites. In the case of ZSM-5, coke deposits at intersections of the straight and zigzag channels, and also on the outer surface of the crystal. Whereas, Y type zeolites and mordenites have supercages whose sizes are almost equal to the molecular sizes of aromatic compounds composed of a few benzene rings, and coke is easily formed in the supercages. These differences in the manner of the coke formation reflect on mode of the deactivation.

Figure 2 shows the relationship between the amount of coke deposition (D_C) and relative activity (A_R) for several zeolites for the reaction of *n*-hexane (5). Mordenite has straight pore structures. When once coke is formed at a position in a pore, the reactants cannot make contact with the active sites in the deeper region of the pore. Therefore the active sites in the pore is completely deactivated, even though the amount of coke deposition is relatively small. Since Y type zeolites have a three-dimensional pore structure and the size of the pores is relatively large, the decrease in activity proceeds quickly, but the time required for complete deactivation is long. Coke is formed through cyclization and dehydrogenation (9), such as the sequence of paraffins \rightarrow olefins \rightarrow naphthene \rightarrow aromatics \rightarrow poly-aromatics (10). The pore size of ZSM-5 (MFI type) is almost equal to the minimum size of a benzene molecule, and hence there is no space available within the pores for aromatics. Therefore there is not enough space for cyclization reactions to proceed. Thus, a large amount of coke is probably formed on the outer surface of the crystal. Hence, the activity of ZSM-5 zeolite is fairly stable in comparison with other zeolites.

Coke is composed of carbon and hydrogen, and is expressed as the formula, CH_n . Figure 3 shows the change in *n* value of coke with coke loading for several reactions; reaction of methanol to gasoline and the methylation of toluene with methanol using ZSM-5 (MFI type) zeolite, and the cracking of cumene using silica-alumina catalyst (11, 12). The *n* values can be well correlated by a single curve, as shown in Fig. 3.

From electron microscope observations, it was found that whisker-like material comes out of coked ZSM-5, indicating that polymers formed within the pores diffuse to the outer surface of the zeolite crystals. Even though the coke formed inside the zeolite crystal are mobile polymers, their diffusion rates are extremely slow in comparison with the reactant molecules and they can be regarded as immobile species. On the other hand, the coke formed on the outer surface of the crystal was reported to be carbonaceous materials from the observation of TEM spectroscopy (13).

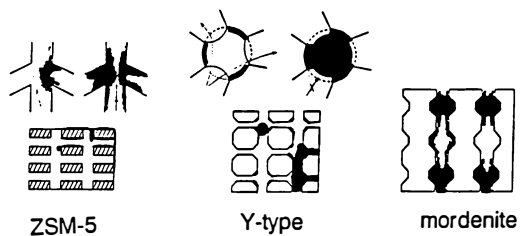


Figure 1. Modes of coke deposition.

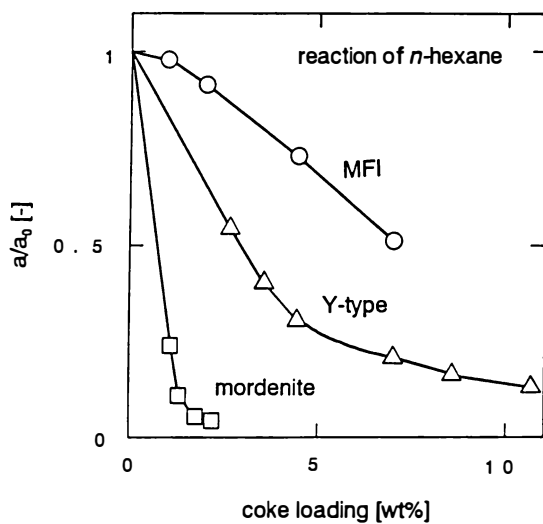


Figure 2. Reduction of activity with coke deposition. (reaction of *n*-hexane) (Reproduced with permission from reference 5. Copyright 1989 Elsevier.)

THE CHANGE OF CATALYTIC PROPERTIES DUE TO COKE DEPOSITION

The activity and shape selectivity of zeolites are closely related to their acidic properties and diffusivities, which change with coke deposition (14-17). Here, we will briefly explain how the shape selectivity is related to the above properties and will discuss about the change of it due to coke deposition.

The Dependency of Shape Selectivity on Diffusivity. The methylation of toluene to produce xylene isomers using ZSM-5 (MFI type) zeolite catalyst is a typical reaction, in which the shape selectivity is observed. In this reaction, xylene isomers once produced inside the zeolite crystal diffuse to the outer surface of the crystal, and the shape selectivity is ascribed to the difference of the diffusivity among the isomers.

Figure 4 shows typically the effect of the half of crystal size (L) on the relationship between methanol conversion and the selectivity toward *para*-xylene (17). The κ value represents the ratio of the acid amount outside crystal to that inside crystal. The decrease in the crystal size leads to the reduction in the selectivity, because the reaction conditions shift from diffusion control to reaction control.

The above results shows that the diffusivity of zeolites has a strong influence on the shape selectivity, as well as the acidic properties. During the coke deposition, the magnitude of the diffusivity is changed, leading to the change in the shape selectivity. In the next section, we discuss about how the diffusivity of zeolites is measured and how that changes due to coke deposition.

Diffusivity of Zeolite.

Fresh Zeolite. The diffusivities within usual porous catalyst (pore radius; a few nm) can be estimated by the parallel pore model (18) or the random pore model (19). However, configurational diffusion occurs within the pores of zeolites (pore diameter < 1 nm) and there are only a few reports on the measurement or estimation methods of the diffusivities of zeolites, especially at higher temperature range (20,21). Here we will review the results of ZSM-5, which first explains the diffusivity of fresh ZSM-5, then the results of coke loaded ZSM-5.

Figure 5 shows the Arrhenius plot of the diffusivities of aromatics. The diffusivities of benzene, toluene and *para*-xylene, minimum molecule sizes of which are the same and are close to that of the pore diameter. Whereas, those of *meta*-, *ortho*-xylene, which minimum molecule sizes are larger than the size of the pores, are almost 1/10 of the former group. This difference among the diffusivities is the reason why ZSM-5 shows shape selectivity.

The mechanism of the diffusion within ZSM-5 zeolite crystal is thought to be analogous to that of impurities in the lattice of metals. This analogy gives the relation of the intracrystalline diffusivity, D , to the molecular size and the pore size, as follows:

$$D = D_0 \cdot \exp[-E/(RT)] \quad (1)$$

$$E = K_E(L_m/d_m)[(f-x)d_z]^2 \quad (2-a), \quad D_0 = K_D(L_m/d_m)^{1/2}[(f-x)d_z] \quad (2-b)$$

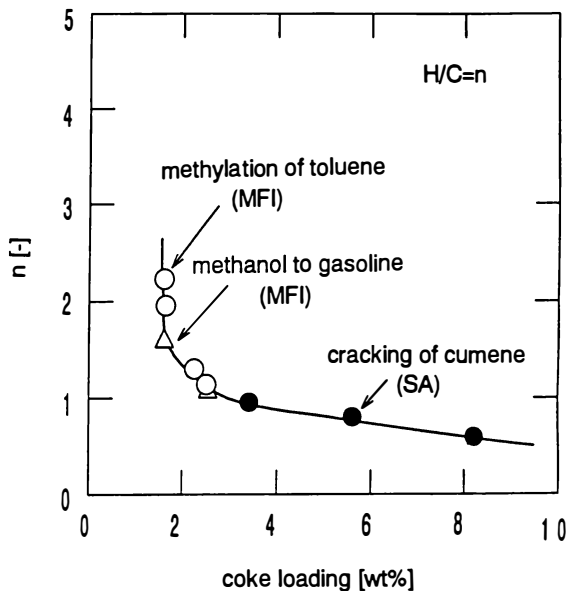


Figure 3. Change in H/C value with coke deposition.

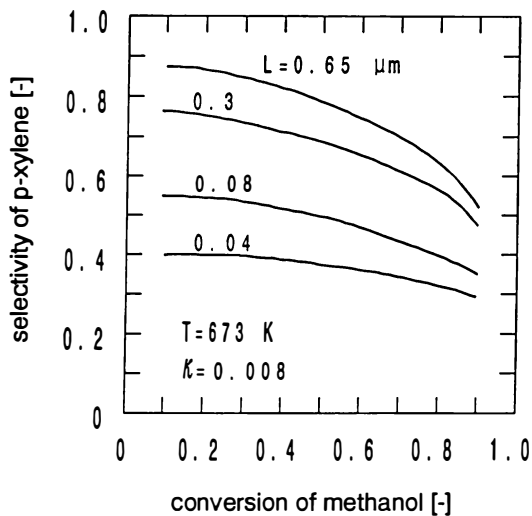


Figure 4. Effect of zeolite crystal size on relationship between methanol conversion and selectivity toward *para*-xylene.

where E is the activation energy, D_0 is the frequency factor, d_m is minimum molecular diameter, L_m is molecular length, f and x are functions of d_m and d_z (pore diameter). The calculated results (D_c) using Eqs. (1) and (2) and the experimental results (D_e) of five aromatics, three *n*-paraffins and one *i*-paraffin well agree in the temperature range of 373-773 K (Fig. 6).

Coked Zeolite. The change in the diffusivities due to coke deposition could be reviewed using the above results. Figure 7 shows the Arrhenius plot of the intracrystalline diffusivity of *para*-xylene in coked ZSM-5 zeolite. The diffusivity decreases with the amount of coke deposition, but the change in activation energy is small. This fact can be explained as follows: when coke deposits at a position in the pore, the effective pore opening becomes smaller than the size of the diffusing molecule. The molecule simply cannot pass through that position in the pore, and must diffuse through other positions. Hence, the energy needed for the molecule diffusion does not increase.

Figure 8 shows the transient changes in the intracrystalline diffusivities of *n*-heptane and *n*-octane inside crystals of coked Y type zeolite with the coke deposition. Figure 9 also shows those of benzene and *para*-xylene. There are small differences among diffusivities in different temperatures, indicating that only a small energy is needed for molecules to diffuse through windows in the pore structure. The reduction of the diffusivity is ascribed to the decrease in the effective pore openings of the windows. From Figs. 7-9, the manner of the change in the diffusivity is dependent on the pore structure of the zeolite.

There are a few reports on models for predicting the change in diffusivity with the coke deposition (14, 15, 22). Figure 10 shows the lattice model for representing the pore structure of ZSM-5 (22). The solid lines represent pores, and their intersections represent the intersections of the pores. The symbols ● and ○ represent coke and diffusing molecules, respectively. Their distribution at intersections corresponds to the amount of coke deposition, and the number of adsorbed molecules in the zeolite. All of the diffusing molecules walk randomly, and when a molecule reaches the border of the lattice, it is regarded as desorbed.

Figure 11 shows the simulation of this random movement as a plot of the change in the amount desorbed against the number of iterations. The results of theoretical equations (23) are also shown as broken curves. The comparison of the ratio of the diffusivity of fresh catalysts (D_0) to coked catalysts (D_c) between the calculated and the experimental data are shown in Fig. 12, where suffixes "*cal*" and "*exp*" denote "*calculated*" and "*experimental*", respectively. The calculated values well agree with the experimental data. On the basis of this lattice model, the change of diffusivity due to coke deposition was found to be expressed by

$$(D_c/D_0) = 1/(1+0.23C_c) \quad (3)$$

Here C_c means the coke amount. The intracrystalline diffusivity of a fresh catalyst (D_0) can be estimated by Eqs. (1) and (2). Hence, the intracrystalline diffusivity (D_c) of coked catalyst can be calculated by employing Eq. (3), as shown in Fig. 13 (22).

During a reaction, many types of components diffuse within the zeolite crystal. In this case, the diffusion rate of fast molecules is hindered by slow molecules. The

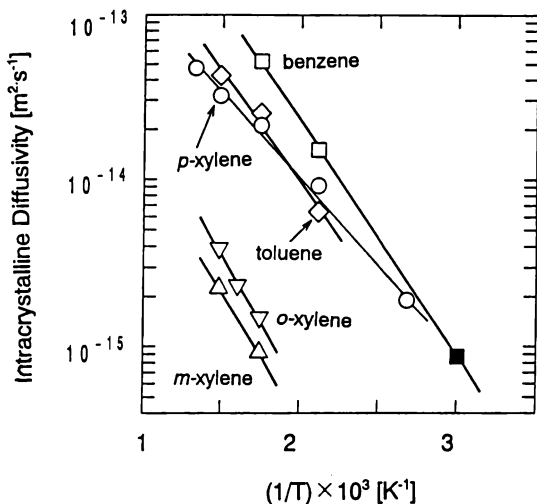


Figure 5. Arrhenius plots of diffusivities of aromatics in MFI type zeolite crystal. (Reproduced with permission from reference 20. Copyright 1991 Elsevier.)

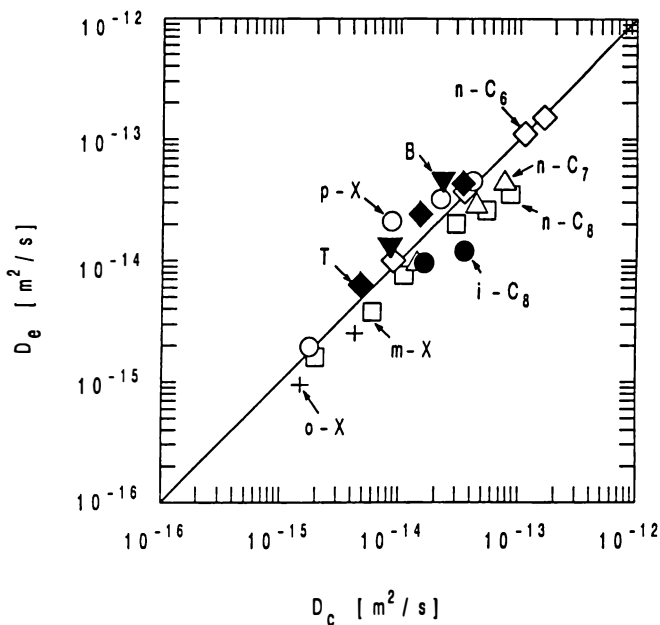


Figure 6. Comparison of diffusivities of MFI type between calculated by lattice model and the experimental data. B: benzene, T: toluene, p-X: *para*-xylene, m-x: *meta*-xylene, o-x: *ortho*-xylene, n-C_i (i=6-8): *n*-paraffin of carbon number i, i-C₈: *iso*-octane. (Reproduced with permission from reference 20. Copyright 1991 Elsevier.)

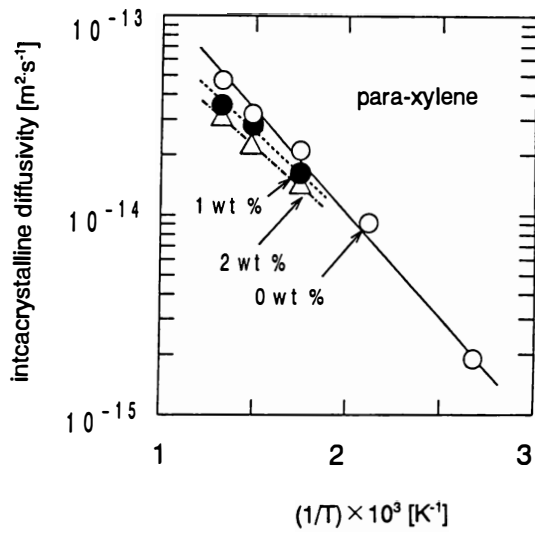


Figure 7. Arrhenius plots of diffusivity of *para*-xylene in coked MFI type zeolite.

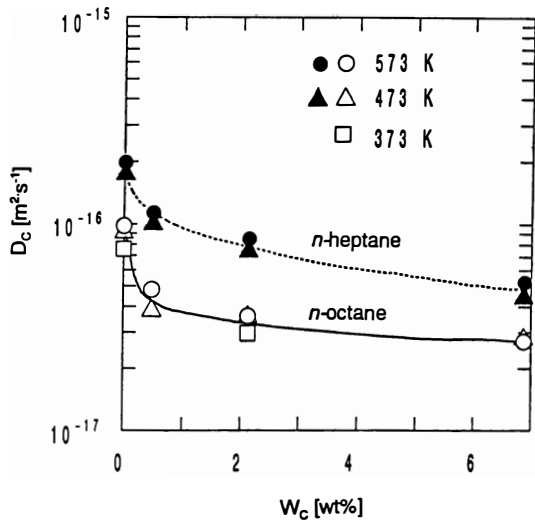


Figure 8. Changes in diffusivities of paraffins inside Y type zeolite with coke deposition.

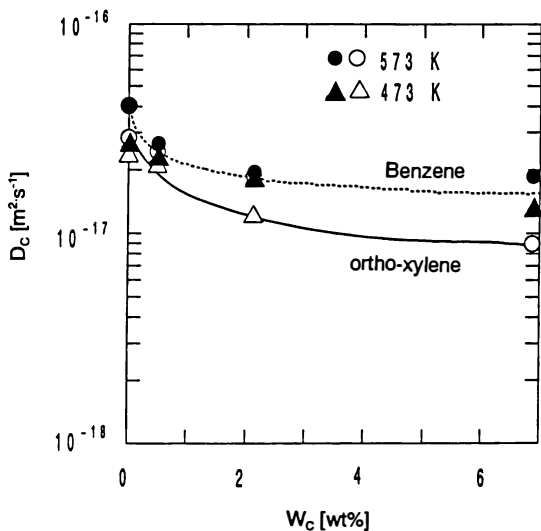


Figure 9. Changes in diffusivities of aromatics inside Y type zeolite with coke deposition.

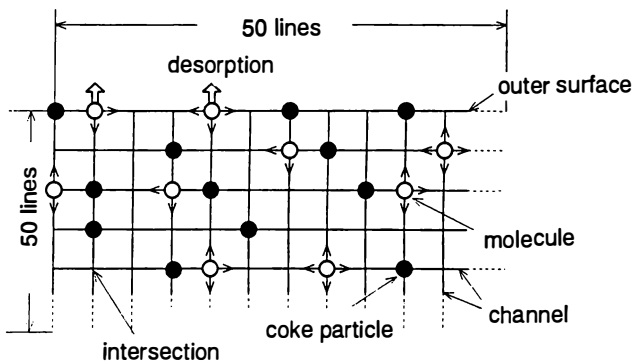


Figure 10. Lattice model for MFI type zeolite pore structure.
(Reproduced with permission from reference 22. Copyright 1992 Elsevier.)

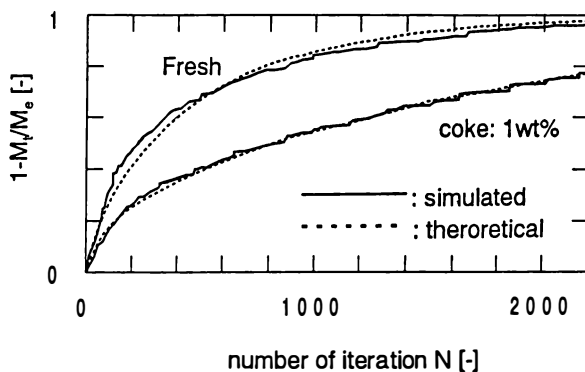


Figure 11. Transient change of amount desorbed calculated by lattice model. (Reproduced with permission from reference 22. Copyright 1992 Elsevier.)

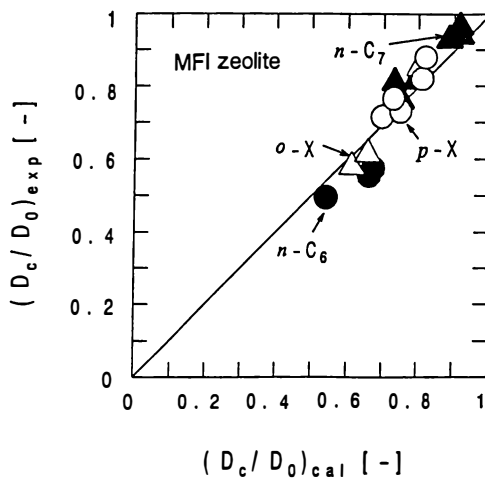


Figure 12. Comparison of diffusivity of coked MFI type zeolite between calculated and the experimental data. (Reproduced with permission from reference 22. Copyright 1992 Elsevier.)

lattice model (Fig. 10) can be expanded to simulate this process. Figure 14 shows the change of the diffusivities of *para*-xylene (fast molecule) D_p and *meta*-xylene (slow molecule) D_m due to coke deposition simulated by the lattice model. When the D_p and the D_m values are measured separately in a fresh ZSM-5 catalyst, the D_p/D_m value was about 10. However, in a bi-component system, this ratio drops to about 5, because of *meta*-xylene hinders the diffusion of *para*-xylene. Furthermore, this ratio decreases with the amount of coke deposition. This change well represents the selectivity toward *para*-xylene in the methylation of toluene, as shown in Fig. 15.

Figure 16 shows the changes in the product yields of the catalytic cracking of the oil obtained by the pyrolysis of the waste polyethylene using the rare earth-exchanged Y type zeolite (REY) at 673 K (24, 25). Oil is cracked to produce gasoline, gas and coke, and gasoline is converted to gas and coke. Thus, the gasoline is an intermediate product. During the reaction, the diffusivity of oil and the acidic properties are rapidly changed by the coke deposition, leading to the increase in the oil yield. Figure 17 shows the change in the temperature-programmed desorption spectra of ammonia (TPD) with the amount of coke. Acid sites corresponding to a peak above 573 K are strong acid sites. The acid sites, especially strong acid sites which act as active sites for the reaction, are decreased. This reduction would affect the deactivation (25). Figure 18 shows the changes in the amount of the strong acid sites, G_m , and the overall reaction rate, k , with coke loading. In the region of small coke amount, the change in the reaction rate is similar to that in the acid amount. Above 2 wt% of coke amount, the reaction rate rapidly decreases. These results suggest that the decrease in the effective pore opening is the dominant factor in deactivation in the region of high coke loading, because of the large molecular weight of the reacting oil. Unfortunately, there are no reports on the estimation of the change in the diffusivity of coked Y type zeolite. However, the changes in the product yield may be caused by changes in the diffusivity, as described above.

We have shown that the changes in the shape selectivity can be explained by changes in diffusivity by using ZSM-5 (MFI type) and Y type zeolites as model zeolites. However, it is very difficult to derive the model equations for representing the deactivation mechanisms for every types of zeolites, since each type of zeolite has different pore structure. Hence, the mechanism of deactivation should be clarified for each type of zeolites. Reports on the activity of zeolites which were determined experimentally are omitted here. However, it is still impossible to evaluate physico-chemical properties of a catalyst from the spectrum of ammonia TPD, which is usually employed to evaluate the acidic properties of a catalyst, since the spectrum is affected by various factors. Therefore, it is difficult to obtain the exact relationship between acidic properties and the change in activity due to deactivation. However, if an accurate method to evaluate the acidic properties is developed, it is expected that we can clarify whether the coverage of acid sites or pore blockage is the dominant factor of decrease in the activity due to coke deposition.

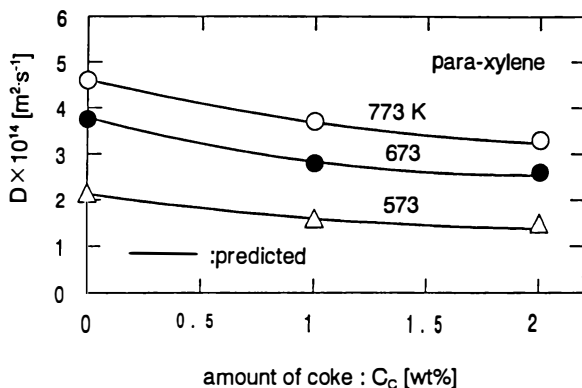


Figure 13. Transient change in intracrystalline diffusivity of *para*-xylene inside MFI type zeolite crystal.
(Reproduced with permission from reference 22. Copyright 1992 Elsevier.)

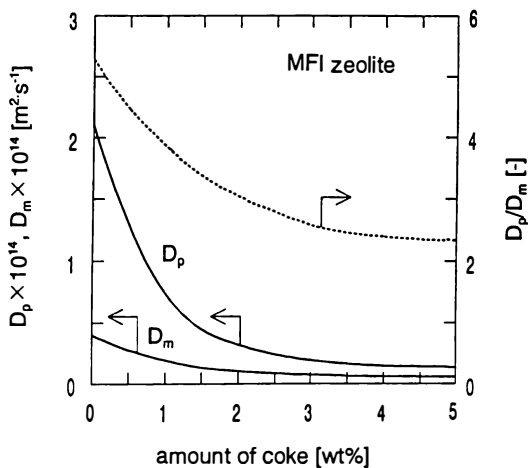


Figure 14. Change in diffusivities in MFI type zeolite with coke deposition,
 —: *para*-xylene (D_p) and *meta*-xylene (D_m)
: ratio of D_p to D_m

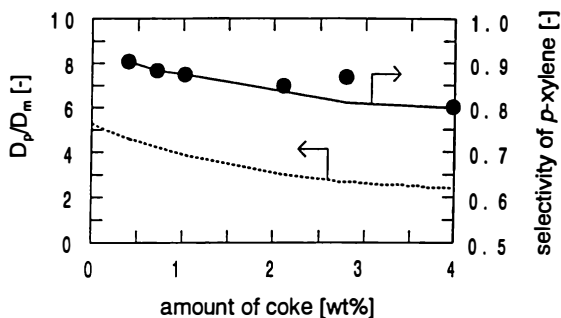


Figure 15. Transient changes of diffusivities and selectivity toward *para*-xylene of MFI type zeolite with coke loading,
 —: selectivity toward *para*-xylene
 - - - - -: ratio of diffusivity of *para*-xylene (D_p) to that of *meta*-xylene (D_m)

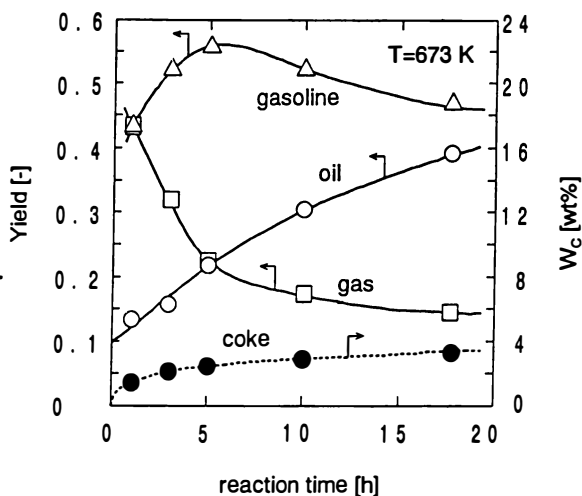


Figure 16. Changes in product yields of catalytic cracking of heavy oil obtained by the pyrolysis of poly-ethylene using REY zeolite.

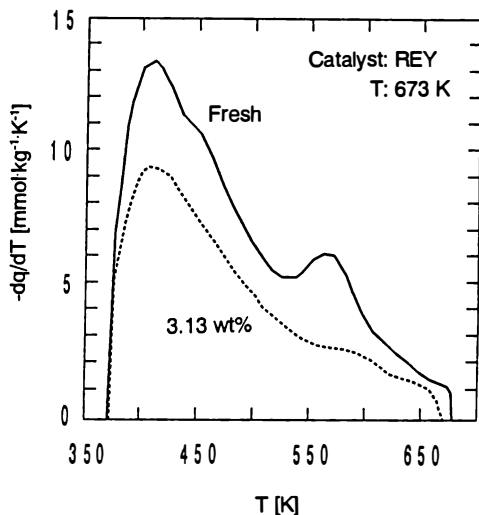


Figure 17. Comparison of ammonia TPD spectra of fresh REY zeolite with that of coked zeolite. reaction: catalytic cracking of oil obtained by the pyrolysis of polyethylene.

—: fresh REY zeolite
 - - - - -: REY zeolite with 3.13 wt% coke loading

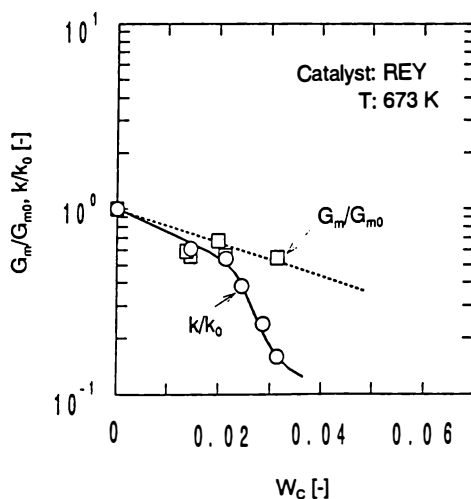


Figure 18. Transient changes in amount of strong acid sites and catalytic activity with coke deposition. reaction: catalytic cracking of oil obtained by pyrolysis of polyethylene.

—: overall reaction rate constant (k) normalized by that of fresh catalyst (k_0)
 - - - - -: amount of strong acid sites (G_m) normalized by that of fresh catalyst (G_{m0})

REFERENCES

1. Hughes R., **Deactivation of Catalysts**, Academic Press, 1984.
2. Bibby, D.M., Howe, R.F. and McLellan, G.D., **Appl.Catal.**, **A93**, 1, 1992.
3. Meier, W.M. and Olson, D.H., **Atlas of Zeolite Structure Typs**, 2nd, Butterworths, London, 1987.
4. Haag, E.O., Lago, R.M. and Weisz, P.B., **Farad.Dis.Chem. Soc.**, **72**, 317, 1981.
5. Guisnet, M. and Magnoux, P., **Appl. Catal.**, **54**, 1, 1989.
6. Magnoux, P., Canaff, C., Machado, F. and Guisnet, M., **J.Catal.**, **134**, 286, 1992.
7. Hammon, U., Kototailo, G.T., Riekert, L. and Zhon, J.Q., **Zeolites**, **8**, 338, 1988.
8. Mantha, R., Bhatia, S. and Rao, M., **Ind.Eng.Chem.Res.**, **30**, 281, 1991.
9. Groten, W.A., Wojciechowski, B.W. and Hunter, B.K., **J.Catal.**, **138**, 343, 1992.
10. Liu, Z. and Dadyburjor, D.B., **J.Catal.**, **134**, 583, 1992.
11. Hashimoto, K., Takatani, K., Iwasa, H. and Masuda, T., **Chem.Eng.Sci.**, **27**, 177, 1983.
12. Hashimoto, K., Masuda, T., and Mori, T., **Chem.Eng.Sci.**, **43**, 2275, 1988.
13. Behrsing, T., Jaeger, H. and Sanders, J.V., **Appl.Catal.**, **54**, 289, 1989.
14. Wei, J., **J.Catal.**, **76**, 433, 1982.
15. Mo, W.T. and Wei, J., **Chem.Eng.Sci.**, **41**, 703, 1986.
16. Hashimoto, K., Masuda, T. and Hariguchi, Y. **Bull.Chem.Soc. Jpn.**, 575, 1989
17. Masuda, T., Mizota, H. and Hashimoto, K., **Kagaku kougaku Ronbunshu**, **20**, 170, 1994.
18. Scott, D.S. and Dullien, F.A., **AIChE J.**, **8**, 113, 1962.
19. Wakao, N. and Smith, J.M., **Ind.Eng.Chem., Fundam.**, **3**, 123, 1964.
20. Hashimoto, K., Masuda, T. and Murakami, N., **Stud.Surf.Sci.Catal.**, **69**, 477, 1991.
21. Masuda, T. and Hashimoto, K., **Stud.Surf.Sci.Catal.**, **83**, 225, 1994.
22. Masuda, T., Murakami, N. and Hashimoto, K., **Chem.Eng. Sci.**, **47**, 2775, 1992.
23. Ruthven, D.M., **Principle of Adsorption & Adsorption processes**, John Wiley & Sons, Tronto, 1984.
24. Songip, A.R., Masuda, T., Kuwahara, H. and Hashimoto, K., **Energy & Fuels**, **8**, 131, 1994.
25. Masuda, T., Mukai, R.S., Akiyama, T., Fujikata, Y. and Hashimoto, K., **Kagaku kougaku Ronbunshu**, **21**, 1133, 1995.

Chapter 5

Modes of Coking and Deactivation of Acid Zeolite Catalysts

M. Guisnet¹, P. Magnoux¹, and K. Moljord²

¹Laboratoire de Catalyse en Chimie Organique, Unité de Recherche Associé au Centre National de la Recherche Scientifique 350, Université de Poitiers, 40 avenue du Recteur Pineau, 86022 Poitiers Cedex, France

²SINTEF Applied Chemistry, N-7034 Trondheim, Norway

The formation of coke during hydrocarbon conversion on zeolite catalysts can be considered as a nucleation-growth process. Nucleation is due to the retention in the zeolite micropores of coke precursors (heavy secondary reaction products). At high temperature the retention is due to trapping in the cavities or at channel intersections ; condensation and hydrogen transfer reactions are involved both in the formation of coke precursors and in their growth. As with other catalysts, deactivation of zeolite catalysts occurs either through site coverage or through pore blockage. Pore blockage is the only mode of deactivation of monodimensional zeolites and of zeolites with trap cavities (large cavities with small apertures), both types deactivating very rapidly. With the other types of zeolites at low coke contents deactivation is due to site coverage, while at high coke contents it is due to a blockage of the pores by coke deposits on the outer surface of the crystallites.

Owing to their strong acidity and/or to their shape selective properties, zeolites are the most employed catalysts in refining (cracking, hydrocracking, hydroisomerization etc) and petrochemical processes (alkylation, isomerization, disproportionation of aromatics etc) (1,2). The deactivation of zeolite catalysts can be extremely rapid : e.g. 5-10 seconds in catalytic cracking (FCC) or very slow : e. g. 3-5 years in hydroisomerization of C₅-C₆ alkanes. The rate of deactivation depends on the feed composition, on the operating conditions and on the zeolite characteristics such as acidity and presence of redox sites. However, coking is generally the main cause of deactivation of zeolite catalysts (3,4). First of all, coke can poison the active sites or block their access. Secondly, the removal of coke during the catalyst regeneration, which is carried out through oxidative treatment at high temperatures (e.g. up to 800°C in FCC), has detrimental effects such as dealumination of the zeolite, structure alteration, sintering of supported metals .

The aim of this paper is to describe coking and deactivation of acid zeolite catalysts during hydrocarbon transformations at high temperatures ($\geq 450^\circ\text{C}$). It is our objective that this description will serve for a true modeling of the deactivation of zeolite catalysts and even of all the porous catalysts. Indeed zeolites constitute excellent models of porous catalysts, i.e. catalysts in which the reactions (hence coking) occur almost exclusively in the pores, whose surface is much greater than the outer surface of the particles or pellets. The characteristics of the pores - size, shape, apertures - are perfectly defined as are those of the acid sites - location and strength. The characteristics of both can be adjusted by various methods, e.g. ion exchange and dealumination. Lastly, coke molecules formed inside the zeolite pores are relatively simple and the composition of coke (not only the chemical identity of the components, but also their distribution as a function of their nature and their size) can be obtained (4). To call "coke" "simple" molecules (not even necessarily polyaromatic) as is done here may appear surprising. However, as these simple molecules contribute with the polyaromatic molecules to deactivation, we prefer to use "coke" for all the secondary products responsible for zeolite catalyst deactivation.

Methods for Determining Coke Composition

The major difficulty in the determination of the modes of coke formation and deactivation is to establish the composition of coke. Until recently the characterization of zeolite coke was limited most often to the measurement of its hydrogen to carbon ratio (H/C). Information on the change in coke composition with operating conditions (e.g. temperature, time-on-stream) can be obtained from H/C values. Various spectroscopic techniques, such as IR, UV-VIS, ^{13}C NMR, EPR have been used for an "in situ" characterization of coke. These techniques, which have the great advantage of being non-destructive, give important information on the chemical nature of coke (3,5). Some of these techniques and in particular FTIR spectroscopy have been successfully employed for investigating simultaneously the deactivation of the catalyst (the IR cell being used as a flow reactor), the amount of coke and its effect on the acidic OH groups (3). Unfortunately, the information on the nature of coke and in particular at high reaction temperatures remains very limited (4).

The only way to obtain the coke composition consists in recovering all the coke from the coked zeolites and analyzing it through adequate techniques. A simple method has been developed in our laboratory (6). It consists of treating the coked zeolites with a solution of hydrofluoric acid in order to dissolve the zeolite and to liberate the coke trapped in the pores. Part of the coke is soluble in organic solvents (generally methylene chloride) and can be characterized by standard techniques, such as NMR, IR, GC, and MS. Of these, GC/MS coupling provides the composition of this soluble coke, i. e. not only the chemical identities of the components, but also their distribution as a function of their nature and of their size. Unfortunately, this is not the case with the insoluble part of coke for which only the elemental composition and some elements of information about the chemical nature, the size and the shape of the component molecules can be obtained. However, it will be shown later that because insoluble coke molecules result generally from the transformation of soluble coke molecules this limitation in the characterization of insoluble coke does not constitute a major obstacle in the determination of the modes of coking and deactivation. The dissolution of zeolites in the hydrofluoric acid

solution does not modify coke composition : i) there is a good agreement between the H/C values measured by coke combustion and those estimated from coke composition ii) samples of an inert solid (SiO₂) impregnated with very reactive organic molecules : 1-tetradecene, 9-methylphenanthrene, etc, were submitted to this treatment. The GC of the compounds recovered in CH₂Cl₂ was identical to the GC of the starting materials (5).

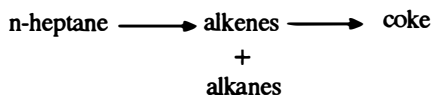
As an example the degree of information obtained by the above methods on the coke formed from propene at 400-450°C on a HZSM-5 zeolite is presented. For a coke content of 3.5 wt% the atomic H/C ratio of coke is close to 1, i. e. comparable to that of benzene. IR spectroscopy shows the presence of aromatics (7). All the coke components are soluble in methylene chloride after dissolution of the zeolite in a hydrofluoric acid solution. Two families of compounds are found : naphthalenes with 2 to 4 methyl groups (about 60 wt%) and fluorenes with 1 to 3 methyl groups (40 wt%) (8).

Modes of Coke Formation

General. Coking can be considered as a transformation of the reactant(s) and/or of the reaction products. However, the coking reaction is very complex, involving many successive and in general bimolecular reactions (condensation and hydrogen transfer). Moreover coke not being a desorbed product its formation needs in addition to reaction steps that the coke precursors are retained in or on the zeolite. Hence the diffusion steps of intermediates will often determine the rate of coking.

Therefore, the formation of coke requires the reactant(s) to undergo bimolecular reactions and the carbonaceous products to be retained in or on the zeolite. This retention occurs either because the products are not volatile enough to be eliminated from the zeolite under the operating conditions or because their size is greater than the pore aperture (hence a steric blockage in the cavities or at channel intersections). Obviously, the first mode of retention concerns not only the coke molecules deposited within the micropores, but also those deposited on the outer surface of the crystallites.

Mode of Coke Formation During n-Heptane Cracking at 450°C on Protonic Zeolites. The formation of coke was investigated during n-heptane cracking at 450°C on four protonic zeolites : two large pore-size zeolites HUSY and HMOR, the third with an intermediate-pore size, HZSM-5 and the fourth one with small pores, HERI (8). The percentages of protonic exchange were chosen so as to have similar initial cracking activities ($55-65 \times 10^{-3} \text{ mol. h}^{-1} \cdot \text{g}^{-1}$). While C₃ and C₄ were the major products (70-90%) with all the zeolites, the i-C₄/n-C₄ and olefins/alkanes (o/s) ratios were quite different. However, whatever the zeolite, o/s was smaller than 1, indicating secondary transformations of olefinic cracking products. Coking, which is one of these transformations, is therefore consecutive to n-heptane cracking :

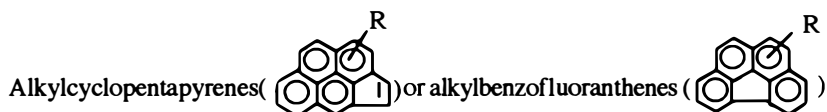


The initial rate of coking, very high with HUSY, HMOR and HERI, was much lower with HZSM-5. This lower coking rate is mainly due to the lower

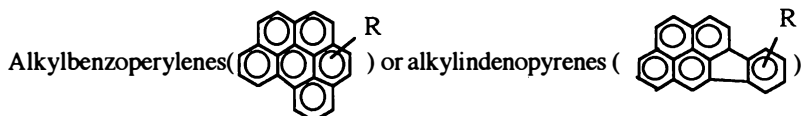
density of the acid sites of HZSM-5, the rate of coking being practically the same for a dealuminated HY zeolite with an acid site density similar to that of HZSM-5 (9).

The composition of coke was determined for various coke contents. With all zeolites the H/C ratio and R, the yield of solubilization of the coke components in methylene chloride (after dissolution of the zeolite in a hydrofluoric acid solution), decreased when the coke content increased. For low coke contents H/C was greater than 1 and R equal to 100%, for high contents H/C was smaller than 1 and R below 100% (e. g. HUSY, Figure 1).

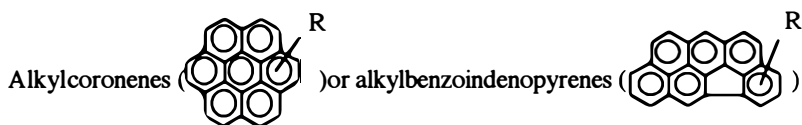
The analysis of the soluble part of coke by GC/MS showed that the size and the degree of aromaticity of the coke components increased with time on stream (hence with the coke content). This is shown in figure 2 for HUSY. With this zeolite, the components of the soluble coke can be classified into three main families :



with a C_nH_{2n-26} general formula.



with a C_nH_{2n-32} general formula.



with a C_nH_{2n-36} general formula.

The C_nH_{2n-26} family appears to be a primary coke product while the C_nH_{2n-32} , the C_nH_{2n-36} families and the insoluble coke (which are more polyaromatic) are secondary coke products (Figure 2).

For similar coke contents the composition of coke depended very much on the zeolite, which confirmed that coking is a shape-selective process (9-10). At low coke contents, the major components were alkylbenzenes in the case of HZSM-5 and HERI, while they were polyaromatic compounds with HUSY and HMOR. At high coke contents the coke components were polyaromatic with all zeolites. However, the size and the shape of coke molecules were different :

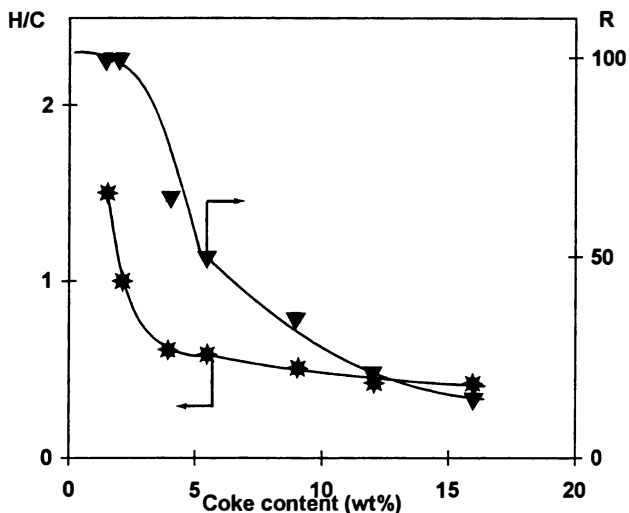


Figure 1 . Formation of coke during n-heptane cracking at 450°C over a HUSY zeolite. Atomic hydrogen to carbon ratio (H/C ★) and yield of coke recovered in methylene chloride (R (%) ▼) as functions of the coke content.

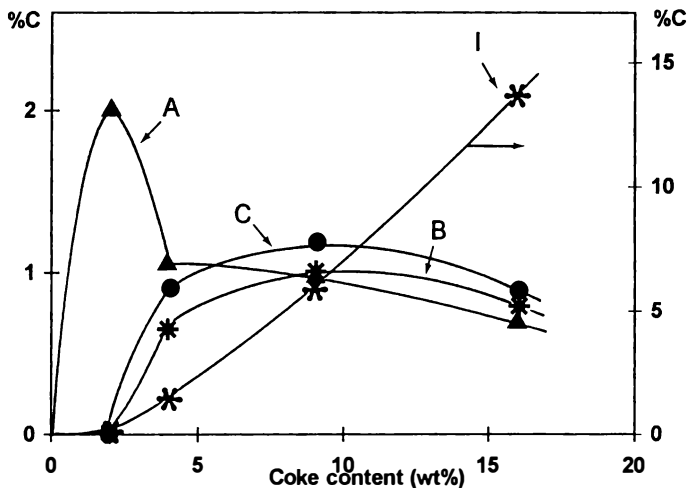
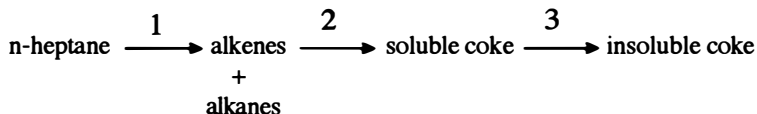


Figure 2 . Formation of coke during n-heptane cracking at 450°C over a HUSY zeolite. Amounts of soluble coke families with formulae C_nH_{2n-26} (A), C_nH_{2n-32} (B), C_nH_{2n-36} (C) and of insoluble coke (I) as functions of total coke content.

alkylpyrenes with HZSM-5, "linear" polyaromatics such as chrysene and benzo-chrysene with HERI and condensed polyaromatics with HUSY.

Whatever the zeolite and the coke content, most of the soluble coke molecules were too volatile and too weakly basic to be retained on the outer surface of the crystallites. This is confirmed by the very low yield of solubilization of coke by direct soxhlet treatment (without dissolution of the zeolite in hydrofluoric acid solution) of the coked zeolite samples. The size of the soluble coke molecules was between the size of the pore apertures and that of the cavities (or of the channel intersections). Moreover, these coke molecules took the shape of the cavities. It can therefore be concluded that the soluble coke molecules were trapped in the cavities.

With all the zeolites insoluble coke results from the secondary transformation of soluble coke (see figure 2 for HUSY). Moreover, it has been shown in the case of HUSY with a high coke content, that coke is present in the form of filaments of about 1 nm wide, protruding from the zeolite micropores (11). Coke formation occurs therefore according to the following scheme :

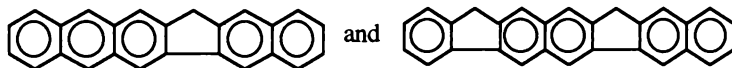


Olefins resulting from n-heptane cracking (step 1) are transformed into soluble coke molecules, which are sterically trapped in the cavities or at channel intersections (step 2). The soluble coke molecules are transformed into insoluble molecules (step 3), that overflow onto the outer surface of the zeolite crystallites. Whatever the zeolite, coke formation occurs probably through the same reactions, involving carbenium ions as intermediates : oligomerization of the olefinic cracking products, cyclization of oligomers (after hydrogen transfer), transformation through hydrogen transfer of the naphthenes into monoaromatics, alkylation of these monoaromatics, then cyclization and hydrogen transfer giving biaromatics, triaromatics and so on (5). Bimolecular reactions of naphthenes could also occur. However their concentration in the reaction products is low.

Besides the simple growth of coke molecules according to the alkylation-cyclization-hydrogen transfer process, another mode of formation of insoluble coke molecules, the dehydrogenative coupling of polyaromatic species located in adjacent supercages, was recently proposed to explain the behaviour of a highly dealuminated HY zeolite (framework Si/Al ratio estimated equal to 100) during coking with propene at 450°C (12). As was expected, considering the low density of the acid sites, the coking activity of this sample was very low, but surprisingly the selectivity to insoluble coke was very high (Figure 3). It was therefore suggested, that the formation of insoluble coke molecules could be governed by the residence time of the coke molecules in the supercages. This was demonstrated by treating a sample of a HY zeolite (framework Si/Al ratio of 30) which was coked for a short time (20 minutes), with a nitrogen flow at the coking temperature (450°C) for about 6 hours. While there was practically no change in the coke content (3.3 wt%) the percentage of insoluble coke rose from 10% on the non-treated sample to 60% on the treated sample and the H/C ratio of coke decreased from 0.63 to 0.46 (12). The same

phenomenon occurred during the stripping of FCC catalysts (Forissier, M. U.M. CNRS. Elf Solaize unpublished data).

The two modes of growth of the coke molecules were found to coexist during the aromatization of propene at 450°C on HZSM-5 catalysts (13). Indeed the soluble coke components could be classified into four families : alkylfluorenes (C_nH_{2n-16}) and alkylpyrenes (C_nH_{2n-22}), which appear as primary products and more highly unsaturated compounds : C_nH_{2n-34} and C_nH_{2n-38} which appear only at high coke contents. These latter compounds which have most likely the following linear structures,



can only result from dehydrogenative coupling of alkylfluorenes and of coke precursors (alkylnaphthalenes, anthracenes or phenanthrenes which were found in the coke retained in the HZSM-5 pores at lower temperatures (250-350°C)). On the other hand fluorenic and pyrenic compounds result most likely from the classical mode of growth of coke precursors, which involves a succession of alkylation, cyclization and hydrogen transfer steps.

The relative significance of the two modes of growth of coke molecules depends probably on the coking activity, hence on the number and strength of acid sites (12). Indeed the lower the coking activity and the longer the residence time of coke molecules in the zeolite pores, the greater is the probability of coupling between the molecules of coke or coke precursors. This could explain why insoluble coke molecules are already formed at lower coke contents on the least active zeolite for coke formation (Figure 3).

Conclusion. The mode of coke formation during hydrocarbon conversion at high temperatures can be deduced from the change in the coke composition with time-on-stream (or with coke content). During n-heptane cracking at 450°C on protonic zeolites, coke results from secondary rapid transformation of olefinic cracking products (oligomerization, alkylation, cyclization, hydrogen transfer) into aromatics and polyaromatics. Dehydrogenative coupling of aromatics trapped in the zeolite pores participates also to the growth of coke molecules.

Coking of zeolites can be considered as a nucleation-growth process. The key step is the retention of secondary reaction products in the micropores (nucleation). At high reaction temperatures this retention is generally due to a steric blockage (trapping), while at low temperatures it is mainly due to the low volatility of the secondary products (5).

Modes of Deactivation

General. It is generally accepted that coke affects the activity of porous catalysts in two different ways (13) : site coverage (active sites poisoned by coke adsorption) and pore blockage (active sites rendered inaccessible to reactants by coke deposits). In the case of site coverage, one coke molecule poisons one active site. However, one can associate to this mode of deactivation the inhibition of activity due to a competition for adsorption on the acid sites between reactant and coke molecules. The activity decrease is less in this case than in the case of site coverage. Pore blockage has generally a more pronounced deactivating effect than site coverage. Indeed one coke molecule can block the access to more than one active site. To this mode of

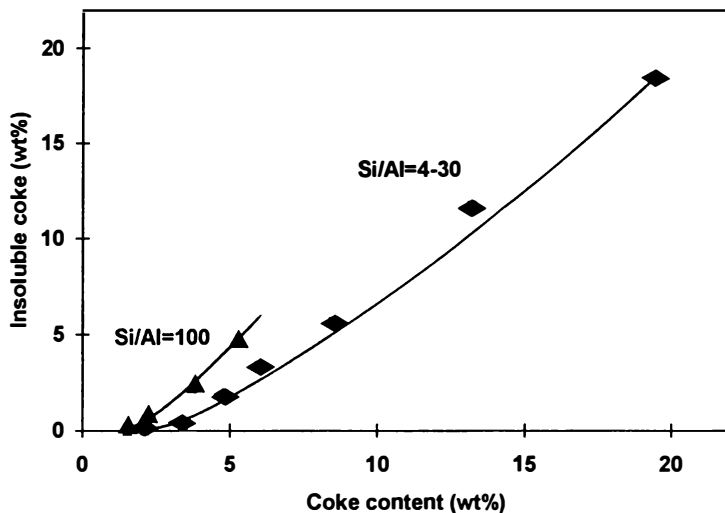


Figure 3 . Formation of coke from propene at 450°C over zeolites with various Si/Al ratios. Amount of insoluble coke as function of total amount of coke. Reproduced with permission from ref 12.

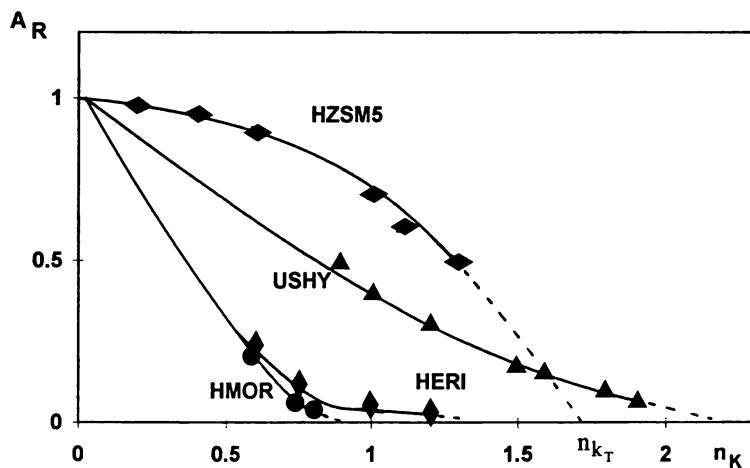


Figure 4 . n-Heptane cracking at 450°C over various protonic zeolites. Deactivating effect of coke molecules. Residual activity A_R versus the number of coke molecules n_K (10^{20} molecules g^{-1}). Reproduced with permission from ref 9.

deactivation one can associate limitation of the access of the reactants to the pores by coke molecules. In this case the deactivating effect of coke molecules is less pronounced than with total pore blockage.

As the composition of zeolite coke can be defined, the number of coke molecules can be estimated and their physical properties (size, volatility, solubility) specified. This makes it easier to determine the modes of deactivation. Indeed the number of coke molecules can be compared to the number of cavities (or of channel intersections) and to the number of acid sites of the zeolite (9). Moreover the deactivating effect of coke molecules (not just the deactivating effect per gram of coke as is the case with the other catalysts) can be determined. The location and the cause of retention of coke molecules can be obtained from their physical properties. Thus, as already mentioned, the coke molecules which are formed during n-heptane cracking at 450°C on protonic zeolites and which are soluble in methylene chloride can only be located in the cavities or at the channel intersections, because of their properties. With zeolites, such as offretite, which present different types of pores, it is even possible to determine from the coke composition in what kind of pore the formation of coke molecules begins. Thus during n-heptane cracking at 450°C on an H offretite, due to their physical properties, the first coke molecules are trapped in the cages with small apertures (gmelinite cages). This is confirmed by adsorption experiments with adsorbates of different molecular sizes (14,15).

The effect of the coke content on the adsorption capacity of zeolite catalysts gives more essential information for determining the mode of deactivation (9). Indeed when V_A , the volume apparently occupied by coke (estimated from adsorption experiments with adsorbates having size similar to that of the reactant) is close to V_R , the volume really occupied by coke molecules (estimated from the amount of coke and its composition) it can be concluded that deactivation does not result from pore blockage. Two adsorbates were used for characterizing the samples of protonic zeolites coked during n-heptane cracking at 450°C : n-hexane which has the same kinetic diameter as the reactant and nitrogen, which is a less bulky molecule. Indeed at the high reaction temperature (450°C) the effect of coke is probably less pronounced than at the temperature chosen for n-hexane adsorption (0°C).

Modes of Deactivation. During n-heptane cracking at 450°C HZSM-5 deactivates very slowly. On the contrary, HMOR and above all HERI rapidly lose nearly all their activity. HUSY has an intermediate behaviour. The deactivating effect of the coke molecules depends on the zeolite and on the coke content (Figure 4). Initially this effect is limited on HZSM-5 (limited decrease of the residual activity A_R with n_K the number of coke molecules), average on HUSY and very pronounced on HMOR and HERI. At high coke contents it is smaller than at low coke contents for HUSY, HMOR and HERI, but more pronounced for HZSM-5. From the extrapolation of the curves of figure 4 to zero activity, the number n_{K_T} of coke molecules which cause the complete deactivation of the zeolites can be estimated. n_{K_T} is close to the number of strong acid sites n_{A_2} (responsible for n-heptane cracking) in the case of HUSY and HZSM-5, while on HMOR and HERI it is about 7 times smaller, which is characteristic of pore blockage.

This blockage is confirmed in figure 5 where the decrease in activity is plotted vs n_K/n_{A_2} . At low coke content, one coke molecule deactivates over 20 strong acid sites of HERI or of HMOR (provided all of these acid sites have

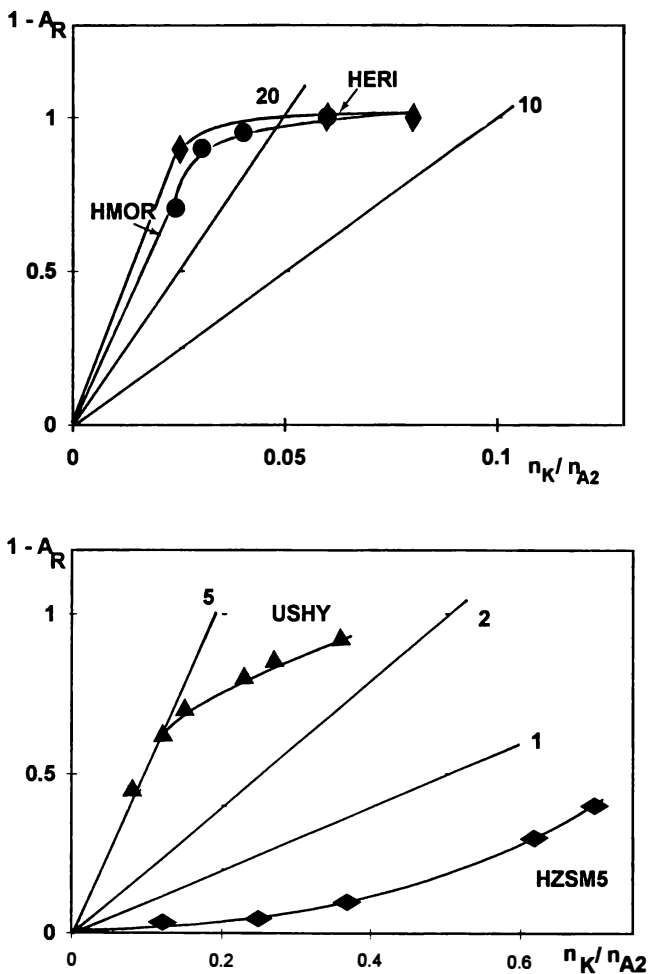


Figure 5 . n-Heptane cracking at 450°C over various protonic zeolites. Relative decrease in activity ($1 - A_R$) as a function of the ratio of the number of coke molecules to the number of strong acid sites (n_K/n_{A2}). Experimental values : USHY (\blacktriangle) HZSM-5 (\blacklozenge) Straight lines with slope = 1, 2, 3 ; HMOR (\bullet) HERI (\blacklozenge) slope = 10,20. Reproduced with permission from ref.9.

the same activity). Adsorption experiments also confirm this pore blockage. With HMOR for n-hexane adsorbate and with HERR for nitrogen and n-hexane adsorbates $V_R/V_A = 0.1$. However with HMOR, V_R/V_A nitrogen = 1 for low coke contents (Figure 6). This is due to the fact that nitrogen can diffuse through the narrow channels of HMOR, therefore reaching the free volume of the large channels. However, V_R/V_A decreases rapidly and at 4.5 wt% coke is equal to the value found with n-hexane. Coke molecules covering the outer surface of the crystallites thus block the access of nitrogen to the pore volume.

With HZSM-5, at low coke contents, 4 coke molecules are apparently needed to deactivate one strong acid site (Figure 5). This can be explained if we consider the composition of coke. Coke is constituted by alkyl mono and biaromatics (8) i.e. by molecules which are neither very basic (hence not strongly adsorbed on the acid sites) nor very bulky (hence do not block the access of the reactant to the channel intersections). This low deactivating effect of coke is characteristic of a competition between the reactant and the coke molecules for adsorption on the acid sites or of a limitation of the access of the reactant to these sites. Whatever the adsorbate, V_R/V_A is close to 1 at low coke contents (Figure 6), which confirms that no pore blockage occurs. However, V_R/V_A decreases when the coke content increases. Thus for 7 wt% coke, $V_R/V_A = 0.3$, which means that coke blocks the access of the adsorbates and probably of the reactants to a volume much greater than the volume which is occupied by coke itself. It must be noted that a significant decrease of V_R/V_A is observed as soon as bulky insoluble coke compounds appear. Deactivation results probably from pore blockage due to these insoluble coke molecules, which surround the zeolite crystallites. This is confirmed by an increase in the deactivating effect of coke molecules (Figure 4).

With HUSY the situation is more complex. Indeed at low coke contents, one coke molecule neutralizes apparently the activity of 5 strong acid sites. Yet nitrogen can fill all the pore volume not occupied by coke (illustrated by V_R/V_A being about 1). This excludes the possibility of pore blockage. The large deactivating effect of coke molecules is most likely due to the heterogeneity in strength of the HUSY acid sites (16). As coke molecules are preferentially formed on the strongest (hence the more active) acid sites the significant decrease in activity observed could correspond to the deactivation of only one strong acid site. At high coke contents the deactivating effect of coke molecules decreases (Figure 4) probably because then deactivation affects acid sites with an average strength. However V_R/V_A nitrogen becomes lower than 1 showing a pore blockage most likely created by the insoluble coke molecules.

Conclusion. As with the other catalysts deactivation of zeolites by coking can occur in two main ways. The first mode of deactivation, generally called site coverage, corresponds to the situation in which coke molecules are adsorbed on the active sites of the cavities (or of the channel intersections) and limit or block the access of the reactants to these acid sites. The degree of deactivation depends on the strength of adsorption of the coke molecules (hence on their basicity) compared to that of the reactant molecules, or on the size of coke molecules compared to those of the reactant molecules and of the cavities. It depends also on the distribution in strength of the acid sites, the strongest, hence the more active, being generally the first deactivated. The second mode of deactivation corresponds to the limitation or the blockage of the access of the reactants to cavities (hence to the acid sites which are located there) in

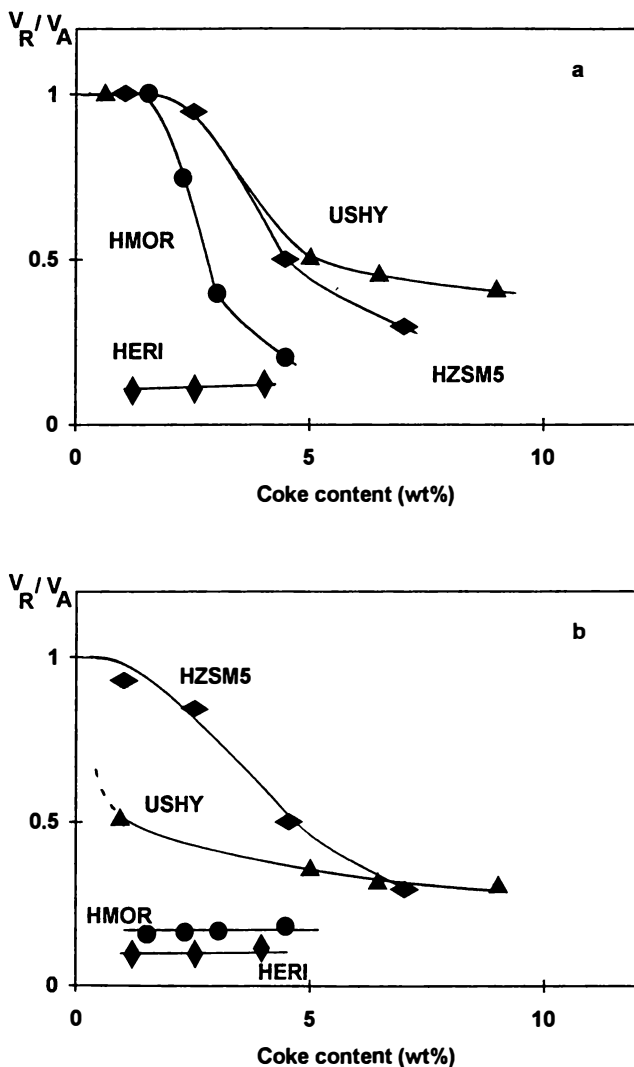


Figure 6 . n-Heptane cracking at 450°C over various protonic zeolites. Ratio (V_R/V_A) of the pore volume really occupied by coke to the volume made inaccessible to nitrogen (a) and to n-hexane (b) as a function of the coke content (wt%). Reproduced with permission from ref.9.

which no coke molecules are present. This mode of deactivation is superimposed on the site coverage. The deactivating effect of the coke molecules is very pronounced.

Deactivation occurs mainly by pore blockage in the case of monodimensional zeolites, such as mordenite and with zeolites presenting trap cavities (i. e. large cavities with small apertures), such as erionite. Because of the large deactivating effect of coke molecules in the case of pore blockage, these zeolites can only be used as catalysts for reactions which are accompanied by a slow formation of coke (e. g. reactions of bifunctional catalysis, such as alkane hydroisomerization). In case of the other zeolites, at low coke contents, deactivation occurs through site coverage, since coke molecules are deposited in the pores of the zeolite and homogeneously in the crystallites. At high coke content pore blockage occurs because of the formation of coke on the outer surface of the zeolite crystallites.

Literature cited

- (1) Rabo, J.A. ; *Zeolite Chemistry and Catalysis* ; ACS Monograph 171 ; American Chemical Society : Washington, 1976.
- (2) Maxwell, I.E ; Stork, W.H.J. In *Introduction to Zeolite Science and Practice* ; Van Bekkum, H. et al. Eds. ; Studies in Surface Science and Catalysis ; Elsevier : Amsterdam, 1991, vol.58, pp 571-630.
- (3) Karge, H.G. In *Introduction to Zeolite Science and Practice* ; Van Bekkum, H., et al. Eds. ; Studies in Surface Science and Catalysis ; Elsevier : Amsterdam, 1991, vol.58, pp.531-570.
- (4) Guisnet, M. ; Magnoux, P. In *Catalyst Deactivation* , Delmon, B. and Froment, G.F. Eds.; Studies in Surface Science and Catalysis ; Elsevier Amsterdam, 1994, vol.88, pp 53-68.
- (5) Guisnet, M. ; Magnoux, P. In *Zeolite Microporous Solids : Synthesis, Structure and reactivity* ; Derouane, E.G. et al. Eds; NATO ASI Series C ; Kluwer Academic Publishers : Dordrecht, Boston, London, 1992, pp 437-456.
- (6) Magnoux, P. ; Roger, P. ; Canaff, C. ; Fouché, V. ; Gnep, N.S. ; Guisnet, M. In *Catalyst Deactivation* ; Delmon, B. and Froment, G.F. Eds ; Studies in Surface Science and Catalysis ; Elsevier : Amsterdam, 1987, vol.34, pp 317-330.
- (7) Ghosh, A.K ; Kydd, R.A. *J. Catal.* 1986, 100, pp. 185.
- (8) Guisnet, M. ; Magnoux, P. ; Canaff, C. ; In *New Developments in Zeolite Science Technology* ; Murakami, Y. et al. Eds ; Proceeding of the 7 th International Zeolite Conference ; Elsevier : Amsterdam, 1987, pp. 701-707.
- (9) Guisnet, M. ; Magnoux, P. *Appl. Catal.*. 1989, 54, pp.1.
- (10) Rollmann, L.D ; Walsh, J. *J. Catal.*. 1987, 56, pp.139.

- (11) Gallezot, P. ; Leclerc, C. ; Guisnet, M. ; Magnoux, P. *J. Catal.* 1989, *117*, pp.100.
- (12) Moljord, K. ; Magnoux, P. ; Guisnet, M. *Appl. Catal* , 1995, *122*, pp.21.
- (13) Beeckman, J.W ; Froment, G.F. *Ind. Eng. Chem. Fundam.* , 1979, *18*, pp.245.
- (14) Magnoux, P. ; Guisnet, M. ; Mignard, S. ; Cartraud, P. *J. Catal.* 1989, *117*, pp.495.
- (15) Mignard, S. ; Cartraud, P. ; Magnoux, P. ; Guisnet, M. *J. Catal.* 1989, *117*, pp.503.
- (16) Magnoux, P. ; Cartraud, P. ; Mignard, S. ; Guisnet, M. *J. Catal.* 1987, *106*, pp.235.

Chapter 6

Catalyst Coking, Activation, and Deactivation

P. A. Sermon, M. S. W. Vong, and M. Matheson

Fractal Solids and Surfaces Research Group, Department of Chemistry,
Brunel University, Uxbridge, Middlesex UB8 3PH, United Kingdom

Alumina-supported Pt, initially able to chemisorb hydrogen, no longer does so once it commences catalysis of hexane conversion to benzene, when the surface metal sites *which remain active* have been blocked to molecular hydrogen by carbonaceous deposits (while the acidic support surface sites remain available to ammonia adsorption). Silica-supported Pt *lost* activity in cyclohexene hydrogenation as a result of the build-up of such deposits, but activity of polymeric (m/e 238) carbonaceous residues on silica-alumina (whose formation was facilitated by spilt-over hydrogen) was *stable* and was related to paramagnetic species therein. It is concluded that the hydrocarbon reactions occurred, wholly or at least partly on the carbonaceous over-layer on the surface; this coking must now be turned to advantage.

Coking, widely experienced in the catalysis of hydrocarbon conversion (1), can deactivate both metallic and acid catalytic sites for hydrocarbon reactions (2). Accumulation of such carbonaceous deposits affects selectivity in hydrocarbon conversion (3). Adsorbed ethene even inhibits facile o-p-H₂ conversion over Ni or Pt (4,5), the surface of which it appears is very nearly covered at lower temperatures in such deposits. H spillover may enhance hydrocarbonaceous residue formation (6). Accumulated carbonaceous residues can be removed by temperature programmed oxidation, reduction and hydrogenation TPO, TPR, TPH, etc (7) as part of catalyst regeneration.

Results and Discussion on Development and Properties of Carbonaceous Deposits

Pt/Alumina. A sample (0.5g) of 0.3% Pt/alumina EUROPT-3 was used to promote hexane to benzene conversion in a Micromeritics 2900 flow reactor system which permitted *in-situ* TPR, TPD, TPO and pulse hydrogen chemisorption etc. The exit stream from the reactor was analysed via a residual gas analyser and an FID gas

chromatograph. Figure 1 illustrates the results that were obtained in sequence. Following calcination and TPR-TPD, 6l mm³ STP of hydrogen were chemisorbed on the sample, suggesting 70% dispersion of the Pt. In addition NH₃ adsorption-TPD showed 5.1cm³ STP NH₃ to be adsorbed on acid sites and then thermally desorbed. Immediately afterwards the Pt/alumina exhibited increasing isothermal activity in hexane conversion to benzene (but decreasing hydrogenolysis activity) at 773K in 1.7 kPa n-C₆H₁₄ and 99.6 kPa H₂ flowing at 40 cm³/min. However, afterwards the *active* catalyst had substantially lost its ability to chemisorb hydrogen. Although (i) an NH₃-TPD experiment showed that the lay-down of carbonaceous deposits had little effect on the number or nature of the surface acid sites, and (ii) TPO-TPR-N₂ flushing removal of reaction-generated carbonaceous deposits restored the hydrogen chemisorption capacity. Apparently the coked (and yet active) Pt surface could not chemisorb molecular hydrogen directly under these conditions, although the acid sites were unaffected, and even the free Pt sites were easily regenerated by coke removal. This required further study using the intermediate cyclohexene as described below. Interestingly (7) surface allylic species may be attacked by H from the metal side or H₂ from the gas phase side, but whether the latter was responsible for the sustained activity seen here remains to be ascertained, as does the precise structure or H/C ratio in the surface residues.

Pt/silica. Pt/silica (D; 5.3 nm \bar{d}_p) showed declining activity in cyclohexene hydrogenation (see Figure 2a) when tested isothermally in a micro-reactor (shown in Figure 2b) where H₂ and cyclohexene entered at the base and products were analysed at the exit as a function of time by gas chromatography under conditions (i.e. 101 kPa total pressure; C₆H₁₀:N₂:H₂ = 1.7:89.5:10.1; 200 cm³/min) similar to those (8) thought to result in structure insensitivity (i.e. when the surface is covered by more than a hydrocarbon overlayer). Therefore it is not surprising that at 295K the order of reaction with respect to cyclohexene was zero. Grinding increased the specific rate which might therefore have been diffusion-controlled, and at higher reaction temperature activity decreased more rapidly as carbonaceous material accumulated on metal surface sites (see Figure 2a).

Silica-alumina. Fluidised beds (9) were used to study the properties of carbonaceous deposits accumulating on oxide surfaces, taking silica-alumina (75%/25%) (BDH) fluidised upon 1.7% Pt/alumina pellets in the reactor shown in Figure 2c (10) as a specific example. In this pre-purified hydrogen entered at relatively high flow rate at 1 past the pre-reduced pellets (0.4g) fluidising the silica-alumina (3g) above, which was then in contact with cyclohexene in nitrogen entering at 2 at relatively low volume flow rate (to meet with any spillover H and gaseous hydrogen). The alkene concentration around the Pt pellets at the base of the reactor at various flow-rates was low and contributed less than 0.7% of the observed hydrogenation. The possibility of migration of Pt from the pellets to the oxide powders was disregarded since atomic absorption of the oxide showed no trace of Pt after (or before) reaction.

Continuous hydrogenation of cyclohexene using spilt-over hydrogen from Pt/Al₂O₃ pellets was performed on SiO₂-Al₂O₃ at 323K (see Figure 2d). Fluidised silica-alumina darkened with the deposition of carbonaceous material and showed significant and stable hydrogenation activity (i.e. 162.33 x 10¹⁵ molecules/ g/min) for as long as 10h, but after the removal of the platinum pellets (see Figure 2d) activity was reduced to a low but significant level when spilt-over hydrogen was no longer available.

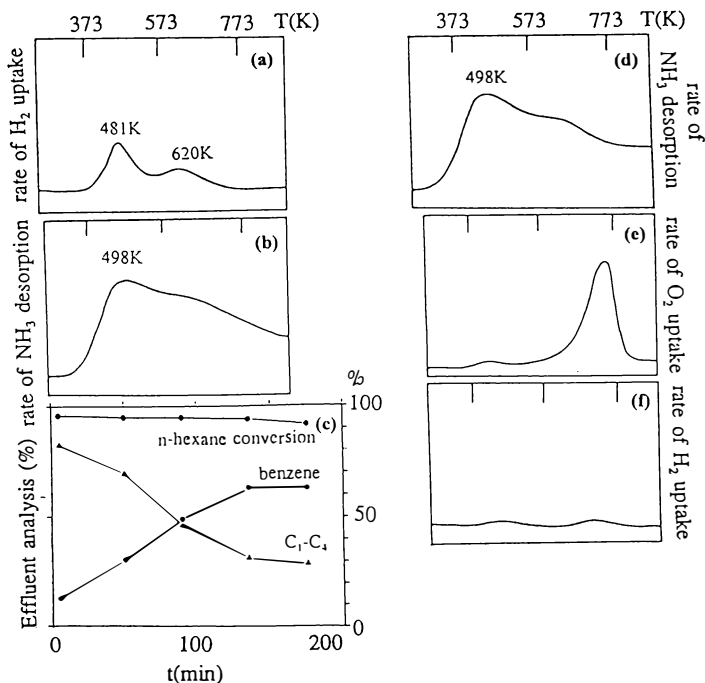


Figure 1. Results a-f were obtained in sequence for a sample (0.5g) of 0.3%Pt/alumina in a flow microreactor system allowing in-situ TPO-TPD-TPR and pulse chemisorption at intervals into its catalysis of hexane (m/e 86) conversion to benzene (m/e 78). The sample was calcined (773K; 4h; air flowing at 30cm³/min) and (a) subjected to TPR in 6%H₂/N₂ where reduction was at a maximum rate at 481K and 620K and involved consumption of 0.52cm³ STP H₂. It was then N₂ flushed (60cm³/min; 873K; 1h) and subjected to pulse chemisorption of hydrogen at 273K in which 61mm³ STP was adsorbed, suggesting a 70%Pt dispersion. Then after N₂ flushing it was subjected to (b) TPD of 5.1cm³ STP NH₃ preadsorbed at 398K into He (15cm³/min) which occurred at a maximum rate at 493K. Then after N₂ flushing its isothermal activity at 773K was measured (c) in conversion of n-hexane (1.7kPa) in H₂ (99.6kPa) flowing at a total rate of 40cm³/min. Then after N₂ flushing it was subjected to pulse chemisorption of H₂, which was limited to 9mm³ STP H₂ at 273K, but (despite suppression of H₂ adsorption) after N₂ flushing TPD of 5.0cm³ STP NH₃ (which had been preadsorbed at 398K) took place into He (d) (i.e. NH₃ adsorption showed no suppression). Subsequently, (e) it was subjected to TPO in 2%O₂/He which occurred at a maximum rate of 716K. Then after N₂ flushing it was again subject to TPR, that involved only a hydrogen consumption of 0.10m³ STP. Finally after N₂ flushing it was subject to pulse H₂ chemisorption and now took up 57mm³ STP H₂ at 273K.

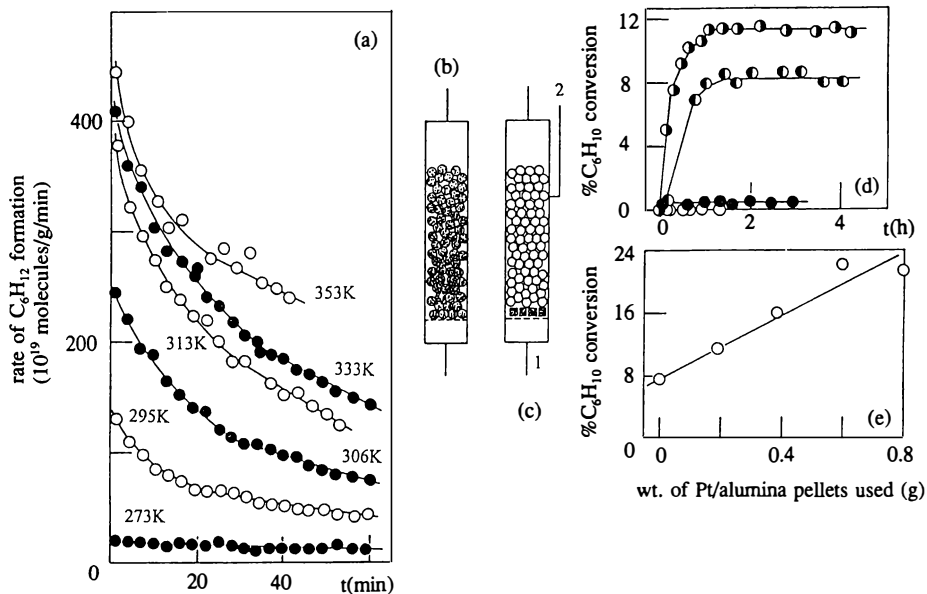


Figure 2 (a) Deactivation of Pt/silica (D) in isothermal cyclohexene hydrogenation under conditions mentioned in the text in the reactor shown in (b). (c) Fluidised bed reactor in which H_2 entered at 1 and passed by 1.7%Pt/alumina pellets and fluidised 3g silica-alumina powder thereon (which also received C_6H_{10}/N_2 entering at a low rate at 2) in which the activity of the silica-alumina shown in (d) was recorded at 323K. These data were measured in the absence (○) and the presence (● first run; ◐ second run) of the Pt/alumina pellets, and after the removal of these pellets (●). The dependence of the activity (d) of this silica-alumina on the weight of pellets used in re-testing is shown in (e)

The rate of cyclohexene hydrogenation increased linearly with the number (or weight) of Pt/Al₂O₃ pellets used (see Figure 2e), suggesting that the rate of hydrogen spillover depends on the amount of contact between the Pt pellets and the oxide.

TPO profiles typical of those obtained from the above SiO₂/25%Al₂O₃ used in cyclohexene hydrogenation (in Figure 2d) with spillover hydrogen are shown in Figure 3a; a maximum was observed at 713-773K. Integration of such profiles gave the amount of carbon held in carbonaceous deposits on the silica-alumina. These were found to increase with the number of reaction cycles in cyclohexene hydrogenation (see Figure 2d) and reached 10¹⁹⁻²⁰ C atoms/g oxide; a figure which may correlate with the number of OH groups (~10²⁰ per g) on the oxide surface.

The SiO₂-25% Al₂O₃ sample so catalytically-used (see Figure 3b) also gave an EPR signal, while none was detected on the unused oxide, and the signal may therefore be associated with the surface carbonaceous deposits. Table I shows that there was good correlation between the intensities of the EPR signals and the surface carbon density on the SiO₂-Al₂O₃ built up with the help of spillover hydrogen as determined by TPO.

Table I. Analysis of Carbonaceous Deposits on SiO₂-Al₂O₃ (25%) used in Cyclohexene Hydrogenation at 343K in the presence of Spillover Hydrogen and Activity Estimated by the Turnover Numbers for each Unpaired Electron Site seen by EPR (N_{EPR})

<i>No. of C atoms revealed by TPO (10¹⁸ C atoms/g)</i>	<i>No. of EPR Spins (10¹⁴ spins/g)</i>	<i>N_{EPR} (molecules/site/sec)</i>
113.20	12.70	11.20
52.51	8.25	13.60
61.43	7.12	10.53
32.90	5.28	13.30
20.70	0	0

Hence the catalytic activity of the fluidised SiO₂/Al₂O₃ (75/25%) in cyclohexene hydrogenation was found to increase with the concentration of EPR spins/g oxide associated with carbonaceous deposits. Moreover, the turnover number for cyclohexene hydrogenation at 343K on SiO₂/25% Al₂O₃ fluidised upon 1.7% Pt/Al₂O₃ (N_{EPR}; 11-14s⁻¹; Table I) was similar to the value for Pt/SiO₂ catalysts at the same reactant partial pressures (11) and the value for Pt(223) crystal surfaces measured at lower hydrogen pressure (12). That carbonaceous deposits built up on the oxide by spillover hydrogen are active in their own right is remarkable.

Mass spectrometry of exhaust gases emerging from the SiO₂-25% Al₂O₃ used in cyclohexene hydrogenation during heating in vacuo (see Figure 3c) revealed species corresponding to m/e=238 (possibly associated with hydrocarbonaceous polymers) which is consistent with carbonaceous deposits seen on Ni/Al₂O₃ (13). Anthracene, pyrene and naphthalene have been identified previously in the CCl₄-extracts of catalysts for n-butane steam-reforming (12). Such polymers would have a greater ease of

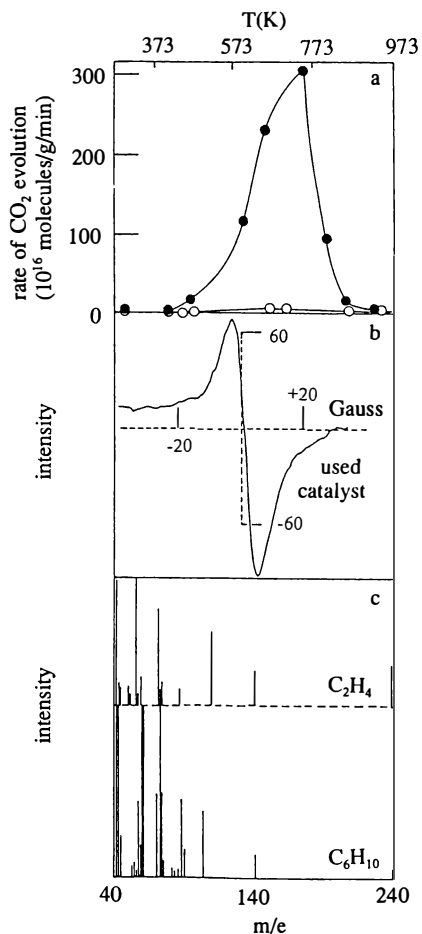


Figure 3 (a,b) TPO and EPR (air, 298K) profiles for a silica-alumina sample unused (O) and used (●) as in Figure 2 (d-e) in cyclohexene hydrogenation when fluidised upon 1.7%Pt/alumina pellets. **(c)** Mass spectrometric evidence for the nature of carbonaceous species built up on this silica-alumina sample during ethene hydrogenation at 483K or cyclohexene hydrogenation at 296-393K when fluidised upon 1.7%Pt/alumina pellets as the sample is now heated in vacuo to 523K.

forming electron donor acceptor complexes which could catalyse hydrocarbon hydrogenation reactions (14).

Discussions and Conclusion

Here hydrocarbon conversion reactions occur wholly or at least partly on the carbonaceous overlayer on the metal and oxide surfaces, as reported by others (13,15-20). Poly-condensed EDA complexes may behave as 'giant alkenes' in which by reversible catalytic hydrogenation/dehydrogenation occurs. This mechanism is similar to the intermolecular hydrogen transfer mechanism proposed (13) for hydrogenation of unsaturated hydrocarbons.

In alkene hydrogenation the formation of different types of surface carbonaceous species can 'poison' the surface metal sites, but on the other hand can create new catalytically active sites on the oxide support while possibly leaving access to its acidic sites. The latter mode of operation of carbonaceous deposits may allow a wide range of hydrocarbon reactants which normally *poison* supported metals to be transformed in the presence or absence of metals (which might only be required to initiate the formation of the carbonaceous over-layer, which having matured, then takes over responsibility for shepherding the reaction along itself, the metal no longer being accessible to all reactants). It is interesting that ethene and cyclohexene produce similar types of carbonaceous deposits (see Figure 3(c)) and this hints at a common intermediate.

Acknowledgements

The authors gratefully acknowledge the support of MSWV by SRC and of MM by EPSRC and BP.

Literature Cited

- 1 Houk, B.G., Coker, R.L., Larson, D.E., Graham, A.H. and Williams, S. *Chem. Tech. Europe*, Jan/Feb 1995, 20.
- 2 Sermon, P.A., Vong, M.S.W. and Luengo, M.A.M. in *Catalyst Deactivation 1994*, Delmon, B. and Froment, G.F., Eds. Stud. Surf. Sci. Catal., 1994, Vol. 88, 319.
- 3 Webb, G., Matheson, I.M., Jackson, S.D. and Grenfell, J. in *Catalyst Deactivation 1994*, Delmon, B. and Froment, G.F., Eds. Stud. Surf. Sci. Catal., 1994, Vol. 88, 297
- 4 Farkas, A., Farkas, L. and Rideal, E.K. *Proc. Roy. Soc.*, 1934, CXLVIA, 297.
- 5 Farkas, A. and Farkas, L. *J. Amer. Chem. Soc.* 1938, 60, 22.
- 6 Vong, M.S.W. and Sermon, P.A. in *New Aspects of Spillover Effect in Catalysis*. Inui, T., Fujimoto, K., Uchijima, T. and Masai, M. Ed., 1993, 385; Vong, M.S.W. and Sermon, P.A. in *Catalyst Deactivation 1991*, Bartholomew, C.H. and Butt, J.B., Eds.; Stud. Surf. Sci. Catal.; Elsevier, 1991, Vol. 68, 235.
- 7 Rooney, J.J., Gault, F.G. and Kembal, C. *Proc. Chem. Soc.* 1960, 407; Rooney J.J., *J. Catal.* 1963, 2, 53.
- 8 Schlatter, J.C. and Boudart, M. *J. Catal.* 1972, 24, 482.
- 9 Teichner, S.J., Mazabrard, A.R., Pajonk, G., Gardes, G.E.E. and Hoang-Van, C. *J. Coll. Interf. Sci.* 1977, 58, 88.

- 10 Lau, M.S.W. and Sermon, P.A. *J. Chem. Soc. Chem. Commun.* **1978**, 891.
- 11 Segal, E., Madron, R.J. and Boudart, M. *J. Catal.* **1978**, *52*, 45.
- 12 Bhatta, K.S.M. and Dixon, G.M. *Trans. Far. Soc.* **1967**, *63*, 2217; Akers, W.W. and Camp, D.P. *J. Am. Inst. Chem. Eng.* **1955**, *1*, 4, 471.
- 13 Webb, G., Thomson, S.J. and Jackson, S.D. *J. Catal.* **1981**, *70*, 249.
- 14 Tamaru, K. and Ichikawa, M. in *Catalysis by Electron Donor-Acceptor Complexes*; Halstead Press: 1975.
- 15 Gardner, N.C. and Hansen, R.S. *J. Phys. Chem.* **1970**, *74*, 3298.
- 16 Somorjai, G.A. and Nieuwenhuys, B.E. *J. Catal.* **1977**, *46*, 2517.
- 17 Blakely, D.W. and Somorjai, G.A. *J. Catal.* **1976**, *42*, 181.
- 18 Somorjai, G.A. *Catal. Rev. Sci. Eng.* **1978**, *18*, 173.
- 19 Bonzel, H.P. and Krebs, H.J. *Surf. Sci.* **1980**, *91*, 499.
- 20 Thomson, S.J. and Webb, G. *J. Chem. Soc. Chem. Comm.* **1976**, 526

NMR Techniques for Studying the Coking of Zeolite-Based Catalysts

J. L. Bonardet, M. C. Barrage, and J. Fraissard

Laboratoire de Chimie des Surfaces, Unité de Recherche Associé
au Centre National de la Recherche Scientifique 1428, Université Pierre
et Marie Curie, Tour 55, 4 place Jussieu, Paris 75252, Cedex 05, France

This article is a brief review of the state of the art in the use of Nuclear Magnetic Resonance for studying deactivation of zeolite based catalysts which occurs during cracking, hydrocracking, reforming and isomerization reactions. ^{13}C , ^{29}Si , ^{27}Al , ^1H and ^{129}Xe are the nuclei studied to obtain information about the nature of the coke, pore blocking, location of the coke, diffusion of reactants, loss of crystallinity, or appearance of defects after coking. Sophisticated techniques such as CP/MAS, DOR (double rotation) or NMR imaging can enhance resonance lines or directly visualize the coke profile in a deactivated coked sample.

One of the major technological and economic problems of the petroleum industry is the deactivation of FCC catalysts during oil transformation. Among the numerous techniques used for studying coking phenomena, (IR, UV-Visible absorption, XRD, XPS, chemical analysis...) NMR occupies a particularly important position because of the diversity of the nuclei which can be studied (^{13}C , ^{27}Al , ^{29}Si , ^1H , ^{129}Xe , etc.) and the development of sophisticated techniques (Magic Angle Spinning, CRAMPS, Cross-Polarization, DOR, NMR imaging, etc.) allowing high resolution NMR in solids.

Of the results in the literature, we report here some examples considered as typical for each nucleus.

Results and discussion.

^{13}C NMR. The first nucleus used to characterize the coke in zeolite based catalysts was of course ^{13}C . Despite low detection sensitivity ($10^{-2}/^1\text{H}$)

the large chemical shifts observed (0-300 ppm) and the use of strong magnetic fields make it easy to distinguish the different types of carbonaceous residues formed during the deactivation of zeolites. Most ^{13}C NMR studies on coking concern Y, ZSM-5 and H-mordenite which are the principal catalysts used in the petroleum industry. The pioneers of the ^{13}C NMR studies were Derouane et al. (1) at the beginning of the 80's. They studied methanol and ethylene conversion on HZSM-5 and H-mordenite zeolites. As shown in Figure 1-A, the conversion of methanol on HZSM-5 leads to a wide distribution of aliphatic compounds ($10 < \delta < 40$ ppm), to some aromatics ($125 < \delta < 145$ ppm) and to straight-chain and branched olefins ($\delta = 150$ ppm). The weak resonance line at 59.9 ppm is characteristic of CH_3O - groups attached to the surface produced by alkylation of the acidic sites with methanol. The narrow signal at 50.2 ppm is due to unreacted methanol. On H-mordenite, (Figure 1-B) the distribution of aliphatics is more limited ($13 < \delta < 25$ ppm) but that of aromatics is broader. As previously, the intense signal at 60.7 ppm is attributed to superficial methoxy groups. The entities observed are trapped in the zeolite intracrystalline volume because of pore blockage. The difference observed in the distribution of aliphatic and aromatic compounds between the two catalysts results from the difference in the internal pore size : the absence of isoparaffins and C_5 aliphatics for H mordenite is due to larger pore size of the latter which make the conversion of C_4 - C_6 olefins into aromatics easier ; the broad aromatic line can be explained by the formation of fused-ring aromatics. In the case of ethylene reacting on HZSM-5, straight-chain polymers are formed rapidly at ambient temperature. These first results show that it is easy to identify the nature of the coke, which depends on the zeolite structure, the type of reactant and the operating conditions. Nevertheless, it is not possible to distinguish between internal and external coke; moreover in-situ study does not allow a distinction between the products of the reaction and the carbonaceous residues.

A few years later, Lange et al. (2) performed in-situ experiments in which the reaction products and the coke were distinguished. Studying ethylene conversion on H-mordenite, they showed that there are two types of coke : the first is low temperature coke formed after adsorption of ethylene and heating to $T < 500$ K ; it consists of small paraffinic molecules ($9 < \delta < 25$ ppm). Above 500K, the coke consists of alkylbenzenes and small polynuclear aromatics ($\delta = 185$ and 130 ppm) The lines observed at 310 and 245 ppm were attributed by the authors to alkyl $((\text{CH}_3)_3\text{C}^+$ or $(\text{CH}_3)_2\text{C}^+(\text{C}_2\text{H}_5)$) and allyl carbocations (Figure 2). Similar results were obtained by White et al.(3) for propene 1- ^{13}C and propene 2- ^{13}C cracking on HY zeolites.

In the same way, Maixner et al. (4) claimed that the most important parameters for the formation of coke are the reaction temperature and the nature of reactants. They studied the conversion of

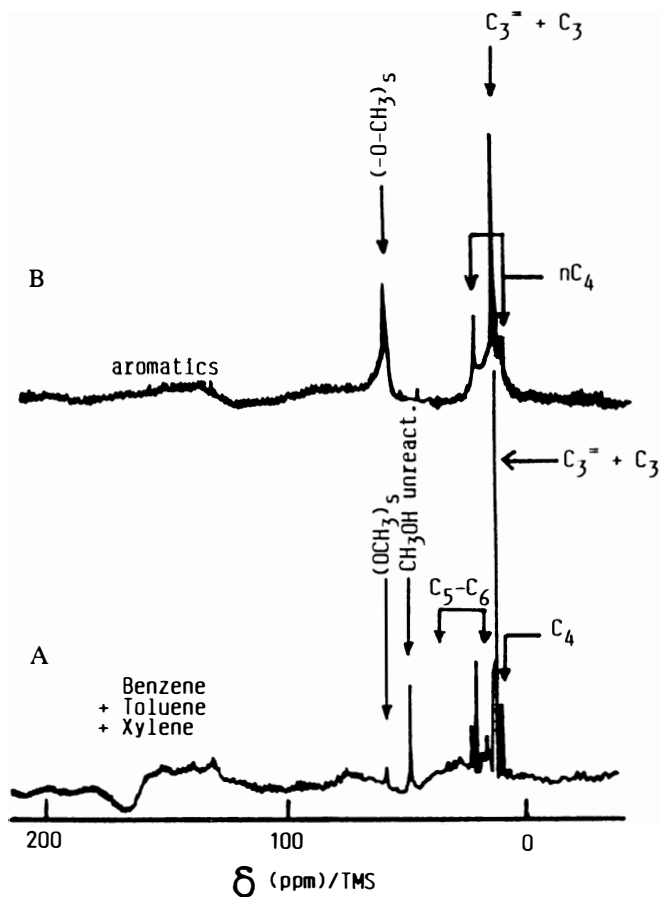


Figure 1) - ^{13}C -MAS-NMR spectra of carbonaceous deposits formed by reaction of methanol over ZSM-5 (A) and H-Mordenite. (B) (adapted from reference 1)

three types of reactants (toluene, hex-1-ene and 2,2,4-trimethylpentane) over LaNa Y zeolite, under the same reaction conditions. As shown by Table I, the amount of coke in the conversion of hex-1-ene is always high, whatever the temperature. At low temperature (373K) the CP/MAS ^{13}C NMR spectrum does not present any line in the 100-200 ppm region characteristic of olefinic and aromatic residues, carbonaceous deposits are only isoparaffins. At higher temperatures, the H/C ratio of coke, decreases and the spectra feature a broad line between 110 and 150 ppm due to the formation of aromatics. In the cracking of 2,2,4-trimethylpentane the same changes are observed in the ^{13}C NMR spectra; the only difference is in the amount of coke formed, which is lower at low temperature (373 and 473K). In the case of toluene cracking, the coke loading is weaker and passes through a minimum for $T = 473\text{K}$. At 373K the H/C ratio is close to that of pure toluene, showing that this latter is only adsorbed in the zeolite with a relatively large mobility in the internal microporous volume (as shown by the absence of rotational side-bands in the CP/MAS NMR spectrum.) At this temperature, the catalyst is inactive in the cracking reaction. At higher reaction temperatures ^{13}C CP/MAS NMR spectrum exhibit a strong resonance line in the 110-140 ppm range with the appearance of side-bands. In agreement with the low H/C ratio, the authors estimated that aromatic coke occluded in the framework consists of dealkylated polynuclear aromatics whose the size severely limits the mobility within the internal micropores.

Richardson et al. (5), studying the conversion of butadiene on HY zeolites, confirm that coke aromaticity increases with the temperature. For $T > 773\text{K}$ the coke is totally aromatic or graphitic. Moreover, using the spin counting technique proposed by Hagaman (6) and ^{13}C -CP/MAS they showed that the spectra could be analysed quantitatively when the reaction temperature is low. As the temperature increases, the fraction of aromatic carbon atoms is underestimated: at 423K less than 80% of the C atoms are detected by NMR. This is due to the presence of organic free radicals (leading to a broadening of the resonance lines by decreasing the relaxation time) and/or of proton-deficient regions (CP is inefficient in the graphitic region).

In the same way, Meinhold and Bibby (7) studying coke formation on HZSM-5 zeolites during the conversion of methanol to gasoline showed that the amount of "NMR-visible carbon" depends on the coke level (Figure 3). If the coke loading is lower than 1% w/w all the coke carbons are visible. From 1 to 5% of coke only half the additional coke is detected and from 5 to 23% of coke only 1 in 5 additional carbons is "NMR visible". Possible explanations are the same as Richardson's: rapid relaxation and broadening by paramagnetic species; regions of the sample with no protons (no possibility of cross-polarization); probe detuning by conducting samples (graphitic coke).

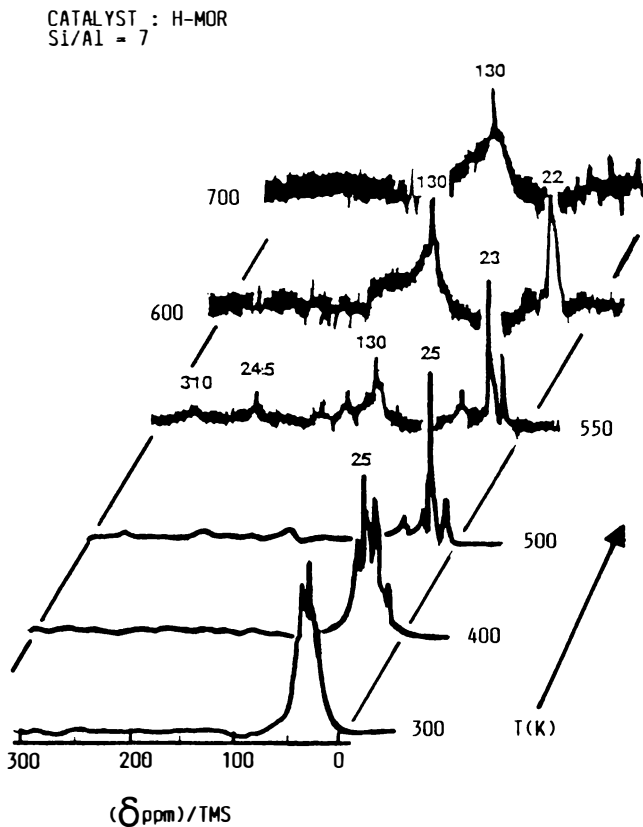


Figure 2) - ^{13}C -MAS-NMR spectra of carbonaceous deposits formed by reaction of ethene over H-Mordenite (reproduced with the permission from reference 2)

Table I Coke loadings of deactivated LaY and H/C atomic ratios in the carbonaceous deposits. (from reference 4)

Feed	T = 373 K		T = 473 K		T = 623 K	
	w-%	H/C	w-%	H/C	w-%	H/C
2,2,4-trimethylpentane	12.1	1.93	14.8	1.17	18.4	0.73
Hex-1-ene	20.4	1.93	19.8	1.29	20.1	0.77
Toluene	9.3	1.18	2.9	1.17	5.1	0.55

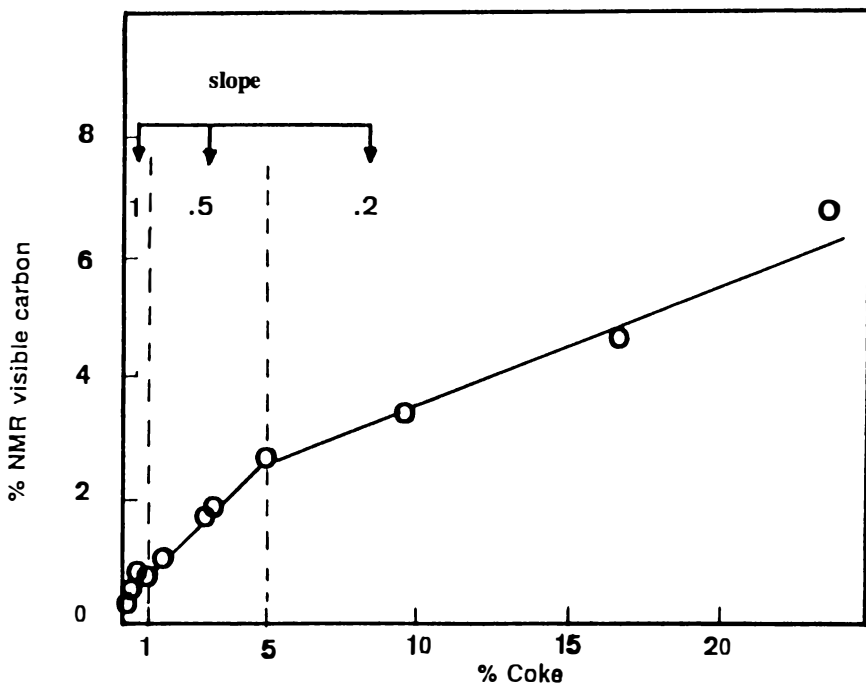


Figure 3) -Percentage of carbon detected by NMR versus coke content (reproduced with the permission from reference 7)

These examples show that ^{13}C NMR spectroscopy makes it easy to identify the nature of the coke but it is sometimes difficult to distinguish the reaction products from the carbonaceous residues. Moreover, if sophisticated methods such as CP or MAS lead to better sensitivity and resolution of the spectra, quantitative analysis can only be performed under restrictive conditions.

^{29}Si and ^{27}Al NMR. Though less used than ^{13}C -CP/MAS NMR, ^{29}Si and ^{27}Al nuclei have a certain interest for determining the effect of coking on the zeolitic framework. Meinhold and Bibby (8) used the NMR of these two nuclei to estimate the volume occupied by the coke formed in HZSM-5 during the conversion of the methanol. They showed that there is a linear relationship between the position and the width of the ^{27}Al signal. By comparing the position, the width and the intensity of a HZSM-5 sample with various levels of hydration they estimated the amount of water remaining in the channels after coking. Combining this with ^{29}Si NMR, they measured the H/C ratio to obtain an average size for the "coke molecules". For example, a sample with a 9.6% coke loading contains about 44 carbon atoms/u.c., the Si-CP.MAS NMR signal implies 22 protons/u.c. leading to a H/C ratio equal to 0.5; this value is close to that previously obtained by chemical analysis (0.7). In the case of a sample with a high coke level (23%) the total number of cross-polarizing protons is considerably reduced, and the H/C ratio is 0.1 if all the coke is internal and cross-polarized. It is evident that this low value totally disagrees with chemical analysis; consequently, this result proves that a large part of the coke is located on the external surface and has a graphitic structure. Echevskii et al. (9) only used ^{27}Al NMR to examine the role of extra-framework Al species (Al_{NF}) in the formation of coke on dealuminated pentasil zeolites. They found no direct relationship between the $\text{Al}_{\text{NF}}/\text{Al}_{\text{F}}$ ratio and the deactivation rate, indicating that most of the Al_{NF} species are not involved in coke formation. These results disagree with ours (10). Indeed, we found that an increase in the coke level in partially dealuminated HZSM-5 coked during acetone conversion leads to a decrease in the $^{27}\text{Al}_{\text{NF}}$ signal. Moreover, studying coking of dealuminated HY zeolites by cracking n-hexane or ortho-xylene, we observed the appearance of an intermediate signal at 30 ppm (between those of Al_{F} (60 ppm) and Al_{NF} (0 ppm)) whose intensity increases with the amount of carbonaceous residue. This signal has been already observed by several authors. By example, Gilson (11) or Nagy (12) attributed this signal to pentacoordinated Al atoms. In our case we think that this additional line corresponds rather to tetrahedral aluminum of the framework highly distorted and destabilized by the coke (13). This interpretation is confirmed by the additional dealumination of the HY lattice occurring after total elimination of coke by oxidation (14).

¹H-NMR Despite the low range of usual chemical shifts ($0 < \delta < 10\text{ppm}$) MAS makes it possible to distinguish between acidic and non-acidic protons. It is possible then to obtain interesting information about the number of Bronsted acid sites still active after coking as, for example, in the work of Ernst et al. (15) on dealuminated HZSM-5 zeolites deactivated during n-hexane cracking. Figure 4 shows the spectra of non-coked (A) and coked samples (B). Considerable changes in the ¹H NMR spectra can be seen. Firstly, the relative intensity of peak "b" at 4.2 ppm (corresponding to the protons of Brønsted acid OH groups, relatively to peak "a", which corresponds to non-acidic silanol groups), is markedly affected by coking. The fall in the relative intensity of this peak can be used to calculate the number of acidic groups still free after coking and proves that carbonaceous residues poison Bronsted sites. Secondly, a very broad line appears after coking. This signal, not affected by magic angle spinning, is characteristic of a strong homonuclear dipolar proton-proton interaction due to the weak mobility of "coke molecules" blocked in the channel of the zeolite.

On the other hand, Lechert et al. (16), by proton relaxation time measurements, showed that coke formed by butadiene conversion at 530K on dealuminated HY zeolites consists of molecules with about 20 C atoms on average. Pulse field gradient measurements of self-diffusion performed by Karger (17) and Volter (18) give information about the location of the coke. These authors used methane or propane as probes to determine the self-diffusion coefficient of these molecules in HZSM-5 zeolites coked by n-hexane cracking. For example, Figure 5 presents the variations of the intracrystalline self-diffusion coefficient D_i of methane versus the time of stream (i.e. coke loading). At the beginning of the cracking reaction, D_i decreases sharply, but after approximately 2 h, and despite continuous coke formation, it remains constant, showing that the intracrystalline mobility of the guest molecule is no longer affected. In contrast, the desorption rate D_d continues to decrease slightly, indicating an increasing transport resistance near or on the external surface. These results show that after blockage of the internal channels, further coke is preferentially formed on the outside surface of the crystallite blocking the external pore openings. It is, therefore, possible to distinguish internal and external coke by this technique, and to demonstrate the effect of second order pores in polycrystalline samples.

In 1994 Cheah et al. (19) studied the formation of coke deposits during the dehydration of ethanol over alumina pellets at 873K, using an NMR imaging technique applied to the ¹H nucleus (20). They demonstrated that NMR imaging offers a unique way by visualizing coke deposition within catalyst pellets. Samples with different coke loading were prepared by impregnating pellets with deionised water for 3h at ambient temperature; excess water is then removed. Figure 6 shows the variations of image intensity from the centre to the edge of more or less deactivated alumina pellets. The curve relative to aluminum 98 (98%

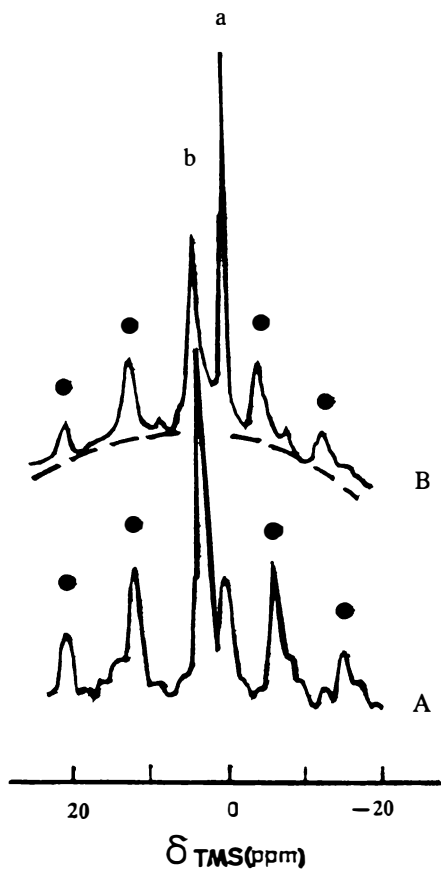


Figure 4) - 1-H-MAS NMR spectra of a non steamed H-ZSM5 zeolite. A) before coking; B) after coking. a) non-acidic OH groups; b) Bronsted acid OH groups. ● spinning sidebands (reproduced with the permission from reference 15).

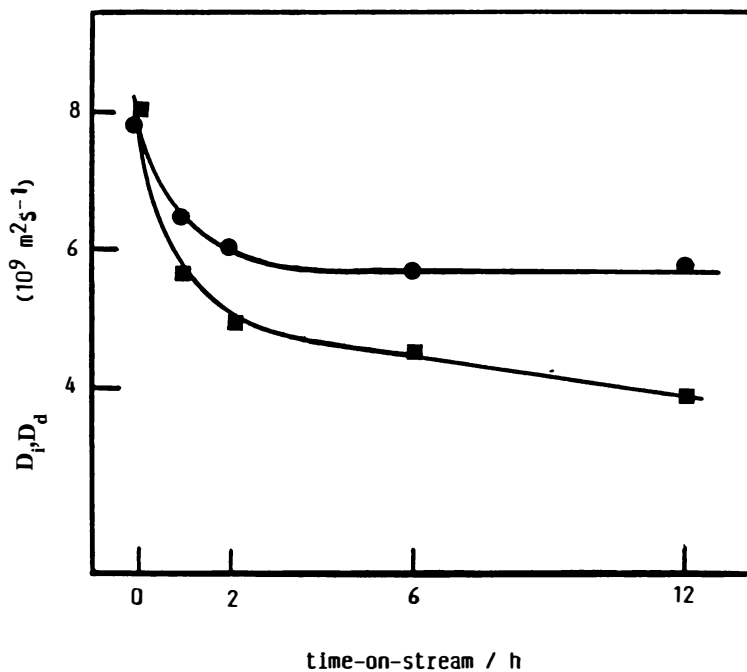


Figure 5) - NMR intracrystalline self-diffusion coefficient D_i (●) and NMR desorption diffusivity D_d (■) of methane sorbed in ZSM5 with increasing coking time. (reproduced with the permission from reference 18)

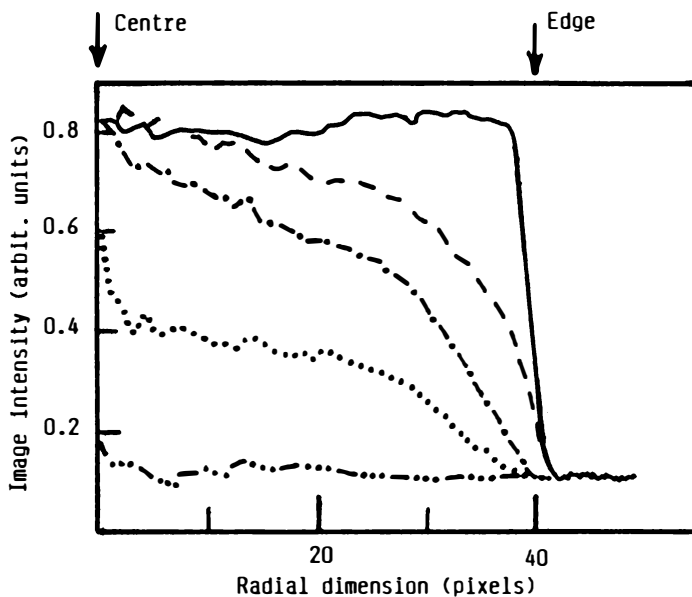


Figure 6) -Radial intensity profile of fresh (----), and coked pellets: Alumina 98 (- - -), Alumina 85 (- · - ·), Alumina 70 (·····) and Alumina 50 (- ····) (reproduced with the permission from reference 19)

ethanol conversion) shows low intensity pixel at the outer edge of the pellet indicating that coke begins to form in the external region of the pellet; it is possible, by NMR imaging to study catalysts at various levels of deactivation up to an ethanol conversion of 50%. For this sample, the image intensity is reduced to near-zero; the attenuation of the NMR signal intensity and the contrast within the image are due to a combination of pore blockage (impregnated water cannot penetrate the pores) and enhanced proton relaxation properties resulting from coke deposition in the pore of the catalyst. The conclusions of this study can be summarized as follows :

- The deposition of coke within alumina pellet is not uniform and depends markedly on the heterogeneities in the porosity of the catalyst.
- The distribution of coke is strongly affected by the position of a given pellet in the reactor.

^{129}Xe NMR. The most interesting nucleus for following pore blocking and the location of coke in FCC catalysts seems to be ^{129}Xe . ^{129}Xe NMR of adsorbed xenon, a technique developed by Fraissard et al. (21) at the beginning of the 80s, has proved to be particularly fruitful for the study of certain zeolite properties such as short-range crystallinity, structure defects, etc. (22) In the 90s we have successfully extended this technique to the study of coking phenomena.

The information provided by the xenon probe is obtained by inspection of the $\delta = f(n_{\text{Xe}})$ curve where δ is the ^{129}Xe chemical shift of adsorbed xenon and n_{Xe} the number of xenon atoms adsorbed per gram of anhydrous solid. The most general form of the Fraissard's equation can be written : $\delta = \delta_0 + \delta_s + \delta_{\text{SAS}} + \delta_{\text{Xe-Xe}}$

- δ_0 is the chemical shift of gaseous xenon extrapolated at zero pressure, taken as reference; therefore $\delta_0 = 0$.

- δ_s expresses the xenon-lattice interaction. In the absence of strong adsorption sites (SAS) it can be obtained by extrapolation of the δ -curve to zero concentration. As shown by Fraissard et al. (23), this term depends on the dimensions of the internal micropores of the zeolites and on the ability for xenon atoms to diffuse from one cavity to another.

- δ_{SAS} expresses the contribution of strong adsorption sites in the pores including the eventual contribution of the electric or (and) magnetic field created by the compensating cations.

- $\delta_{\text{Xe-Xe}}$ corresponds to the chemical shift due to Xe-Xe collisions. This term predominates at high pressure.

- In the case of an isotropic Xe distribution (large cavities), the slope $d\delta/dn$ of the straight section of the d-curve is inversely proportional to the free volume of the cavities accessible to the xenon atoms.

It is possible then to gain information about the internal free volume, the presence of strong adsorption sites in the micropores, the ability for xenon to diffuse from one cavity to another, etc.

We performed a complete study for HY zeolite coked by n-heptane

cracking (24). Figure 7 represents the $\delta = f(n_{Xe})$ variations for samples not coked, 3%, 10% and 15% coked. The more or less pronounced minimum observed at low xenon concentration is characteristic of strong adsorption sites attributed, in agreement with ^{27}Al NMR spectra, to extra-framework aluminum species. Even at low coke level (3%) this curvature disappears, showing that the coke is deposited first of all on or near the Al_{NF} species, masking the interactions between them and the xenon atoms. As HY zeolites lose, at the same time, more than half their activity in heptane cracking we deduced that Al_{NF} species may have a role in the cracking activity, perhaps in relation with the acidity of the catalysts. Comparison of 3% and 10% coked samples shows that the slope of the δ -curve increases markedly and that δ_s (the chemical shift at zero xenon concentration) increases somewhat less. From these results, we deduced that once the strong adsorption sites are covered with coke, this latter forms more homogeneously, affecting the windows between supercages and restricting xenon diffusion from one supercage to another ($\delta_s \uparrow$) as well as the free volume of these supercages (slope \uparrow). At very high coke content (15%) δ_s shows a marked increase, indicating very restricted diffusion of xenon atoms between cavities, but the identity of the slopes proves that supplementary coke mainly affects the external surface of the crystallites. This interpretation is confirmed by the ^{129}Xe spectrum of the 15% coked sample (Figure 8) which presents, at high xenon equilibrium pressure, three resonance lines: one broad and very shifted, corresponding to xenon adsorbed in the residual internal volume; a component, whose chemical shift (40 ppm) is independent of the concentration of xenon adsorbed, is due to xenon present in micro or meso-cavities of coke formed on the external surface of the crystallites; a third signal at 0 ppm, due to xenon gas whose relaxation time has been seriously reduced by the presence of paramagnetic centres on the external carbon deposits. The results of a complementary study at variable adsorption temperature are presented in Figure 9. For a low coke level, the parameters of the δ -curves, δ_s (strongly) and the slope (slightly) depend on the adsorption temperature. These results allow to conclude that coke is formed at first heterogeneously and located mainly at the windows between the supercages. At higher coke content (10%) δ_s and the slope become independent of the adsorption temperature; this result is similar to that obtained for zeolites with narrow channels such as ZSM5 (25). This proves that coke lines the micropores of the zeolites uniformly, strongly reducing the microporous volume, as confirmed by xenon adsorption measurements at low temperature (211K) which show that the total amount of xenon adsorbed at saturation is divided by 2.5 compared to the non coked reference sample. The residual internal volume can be considered as more or less interconnected channels whose diameter is close to that of the xenon atom.

^{129}Xe NMR can also be used to follow the regeneration of the

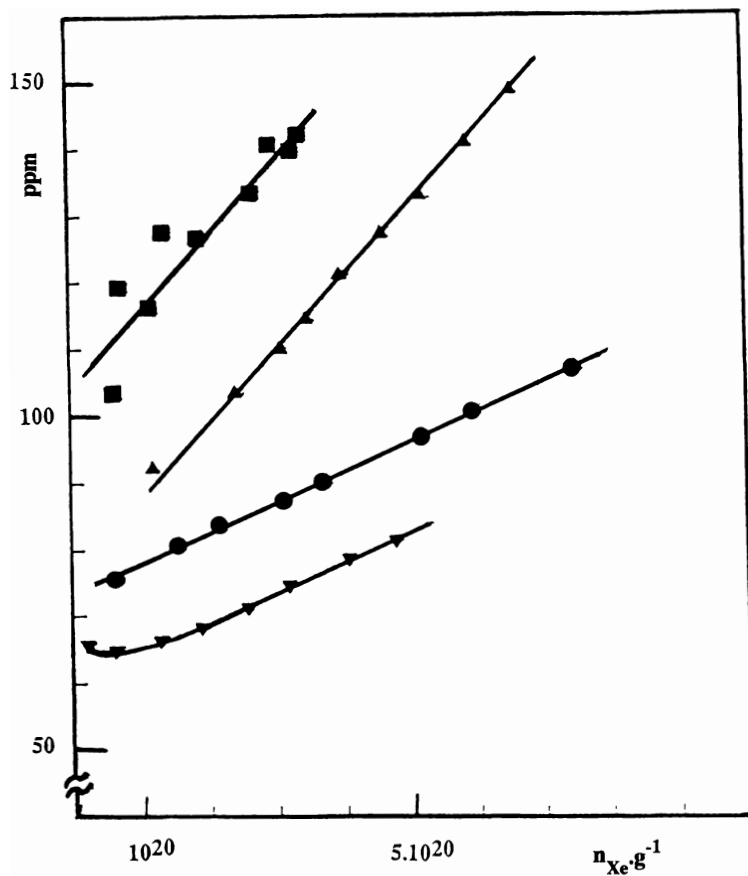


Figure 7) - ^{129}Xe NMR chemical shift as a function of sorbed Xe of dealuminated HY zeolites at 300 K. ∇ fresh sample; \bullet 3% coked sample; \blacktriangle 10.5% coked sample; \blacksquare 15% coked sample. (reproduced with the permission from reference 24)

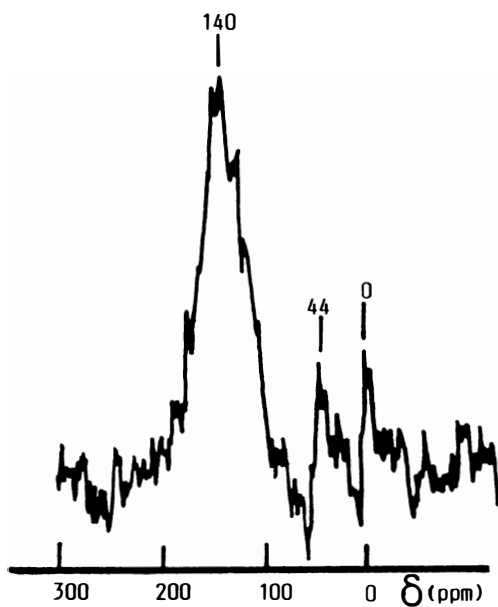


Figure 8) -NMR spectrum of xenon adsorbed ($p = 1000$ torrs) on highly coked HY zeolite (15% coked)

catalyst by partial or total oxidation of the coke (14). We showed that the first step of oxidation eliminates mostly external coke blocking the pore openings (same slope, δ_s decreases). A second oxidation step (>80% of coke eliminated) restores the free internal volume (slope identical to that of the fresh catalyst), remaining coke being located at the windows of

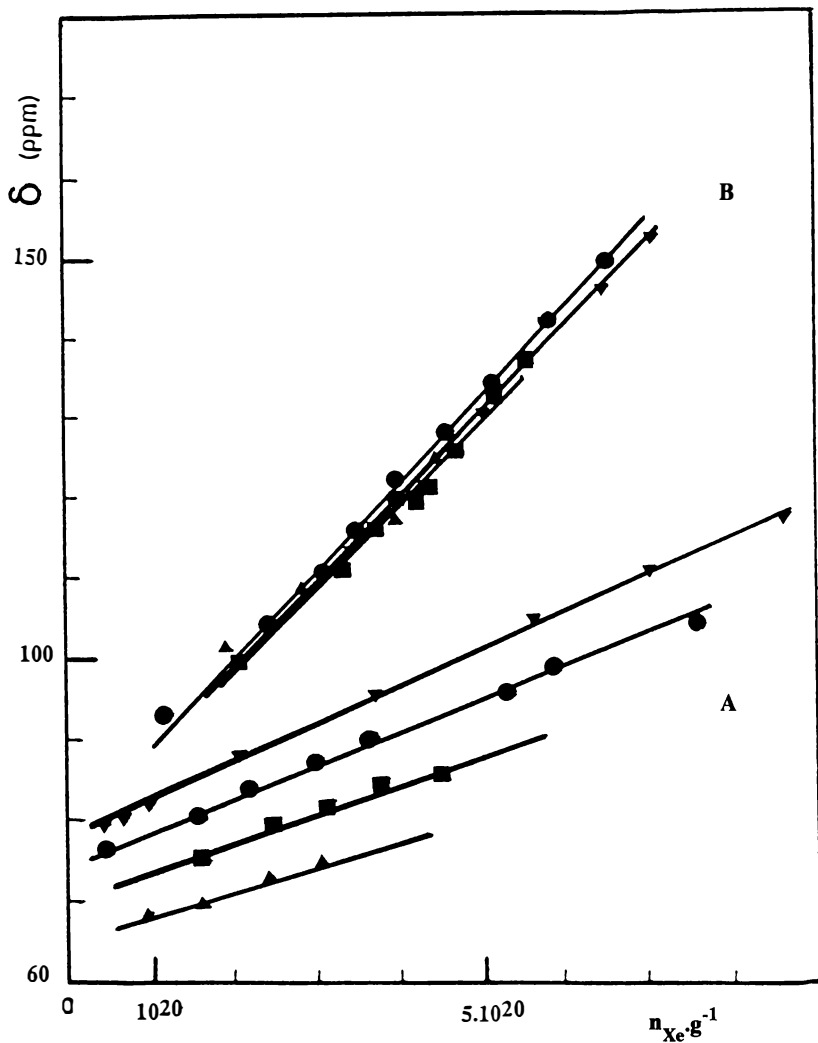


Figure 9) - ^{129}Xe NMR chemical shift as a function of sorbed Xe of dealuminated HY zeolites .A) 3% coked sample; B) 10.5% coked sample. ∇ 273 K; \bullet 300 K; \blacksquare 319 K; \blacktriangle 338 K (adapted from reference 24)

the cages ($\delta_S > \delta_S$ (fresh sample)) on or close to the $AlNF$ species (no curvature). The last oxidation step completely eliminates the residual coke ($\delta_S = \delta_S$ (fresh sample)) but the slope of the linear section is multiplied by 2.3 (Figure 10). At the same time the amount of xenon adsorbed at saturation is divided by 2.4 and the internal microporous volume is therefore divided by the same factor. Moreover, the curvature of the δ -curve at low xenon concentration is accentuated relative to that of the fresh sample: total oxidation cause further dealumination of the lattice, confirming the results obtained by ^{27}Al NMR, and creates defects in the pore structure and/or makes the lattice partially amorphous.

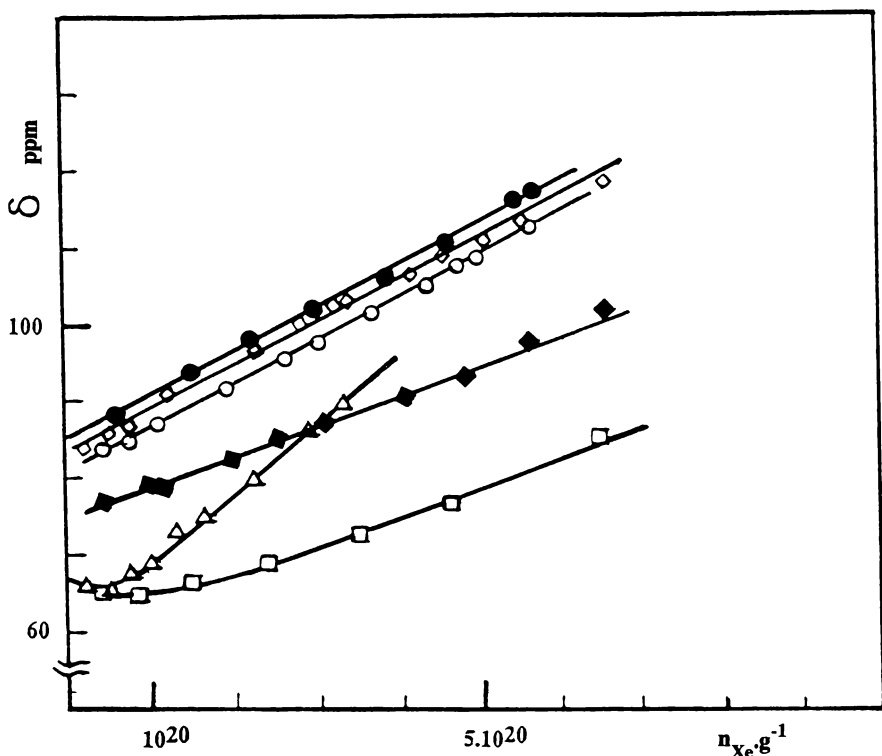


Figure 10) - ^{129}Xe NMR chemical shift as a function of sorbed Xe of dealuminated HY zeolites coked during orthoxylene cracking then partially and totally reoxidized. \square : fresh sample; \bullet : 8.7 % coke; \diamond : pyrolyzed; \circ oxidized, 4.8% coke; \blacklozenge oxidized, 1.6% coke; \triangle oxidized, 0% coke.: (from reference 14).

Literature Cited.

- 1 Derouane, E.G.; Gilson, J.P.; Nagy, J.B. *Zeolites*, **1982**, *2*, 42.
- 2 Lange, J.P.; Gutsze, A.; Allgeier, J.; Karge, H.G. *Appl. Catal.*, **1988**, *45*, 345
- 3 White, J.L.; Lazo, N.D.; Richardson, B.R.; Haw, J.F. *J. Catal.* **1990**, *125*, 260
- 4 Maixner, S.; Chen, C.Y.; Grobet, P.J.; Jacobs, P.A.; Weitkamp, J. in *"New Developments in Zeolite Science and Technology"*. Eds: Y Murakami et al. *Stud. Surf. Sc. Catal.*, Elsevier. Amsterdam, the Netherlands, 1986, Vol. 28, p693
- 5 Richardson, B.R.; Haw, J.F.; *Anal. Chem.*, **1989**, *61*, 1821
- 6 Hagaman, E.W.; Chambers, R.R.; Woody, M.C. *Anal. Chem.* **1986**, *58*, 38
- 7 Meinhold, R.H.; Bibby, D.M.; *Zeolites*, **1990**, *10*, 121
- 8 Meinhold, R.H.; Bibby, D.M. *Zeolites*, **1990**, *10*, 146
- 9 Echevskii, G.V.; Nekipelov, V.M.; Ione, K.I.; Zamaraev K.I. *React. Kinet. Catal. Lett.*, **1987**, *33*, n°1, 233
- 10 Bonardet, J.L.; Barrage, M.C.; Fraissard, J.; Kubelkova, L.; Novakova, J.; Ernst, H.; Freude, D. *Collect. Czech. Chem. Commun.*, **1992**, *57*, 733
- 11 Gilson J.P.; Edwards C.; Peters A.; Koppuswamy R.; Womsbecker R.F., Roberie T.G., and Shatlock M.P. *J. Chem. Soc., Chem.*, **1987**, 91
- 12 Dumont N.; Ito T.; Nagy J.B.; Gabelica Z.; Derouane E.G. in *"catalysis and adsorption in zeolites"* Eds G. Ohlmann et al.; *Stud. Surf. Sc. Catal.*, Elsevier: Amsterdam, Netherlands, 1991, Vol. 65, p591
- 13 Bonardet, J.L.; Barrage, M.C.; Fraissard, J. in *"Proc. 9th Int. Zeolite Conf."* Eds R. von Ballmoss et al, Butterworth-Heinemann: U.S.A., 1993, Vol. II, p475
- 14 Bonardet, J.L.; Barrage, M.C.; Fraissard, J.F. in *"Fluid catalytic cracking III"* Eds M. Ocelli and P O'Connor, ACS Symposium Series, Petroleum Division, U.S.A., 1994, Vol. 571, p230
- 15 Ernst, H., Freude, D., Hunger, M. and Pfeifer, H., in *"catalysis and adsorption in zeolites"* Eds G. Ohlmann et al.; *Stud. Surf. Sc. Catal.*, Elsevier: Amsterdam, Netherlands, 1991, Vol. 65, p397
- 16 Lechert, H.; Basler, W.D.; JIA, M. *Catal. Today*, **1988**, *3*, 23
- 17 Kärger, J.; Hunger, M.; Freude, D.; Pfeifer, H.; Caro J.; Bülow M.; Spindler H.; *Catal. Today*, **1988**, *3*, 493
- 18 Völter, J.; Caro, J.; Bülow, M.; Fahlke, B.; Härger, J.; Hunger, M.; *Appl. Catal.*, **1988**, *42*, 15
- 19 Cheah, K.Y.; Chiaranussati, N.C.; Hollewand, M.P.; Gladden, L.F.; *Appl. Catal.*, **1994**, *115*, 147
- 20 Wolf E.E.; Alfani F. *Cat. Rev. Sc. Eng.*, **1982**, *24*, 329
- 21 Ito, T.; Fraissard, J.; in *"Proc. Vth Int. Conf. Zeolites."* Eds. L.V. Rees; Heyden, London, Great-Britain, *Napoli*, 510 (1980).
- 22 Fraissard, J.; Ito, T. *Zeolites*, **1988**, *8*, 350
- 23 Demarquay J.; Fraissard J. *Chem. Phys. Lett.* **1987**, *136*, 314
- 24 Barrage, M.C.; Bonardet, J.L.; Fraissard, J. *Catal. Lett.*, **1990**, *5*, 143
- 25 Chen, Q.J.; Fraissard, J.; *J. Phys. Chem.*, **1992**, *96*, 1809

Characterization of Fluid Catalytic Cracking Catalyst Coke by ^{13}C NMR and Mass Spectrometry

B. J. McGhee¹, J. M. Andresen¹, C. E. Snape¹, R. Hughes²,
C. L. Koon², and G. Hutchings³

¹Department of Pure and Applied Chemistry, University of Strathclyde,
Glasgow G1 1XL, United Kingdom

²Department of Chemical Engineering, University of Salford,
Salford M5 4WT, United Kingdom

³Department of Chemistry, Leverhulme Centre for Innovative Catalysis,
Liverpool University, Liverpool L69 3BX, United Kingdom

Coke has been concentrated from deactivated FCC catalysts via demineralisation to facilitate characterisation by solid state ^{13}C NMR and mass spectrometry. The catalysts were obtained from refinery operations with a residue feed and a hydrotreated vacuum gas oil and from microreactivity runs with n-hexadecane and various additives. As for solid fuels, the use of a low-field spectrometer in conjunction with the single pulse excitation (or Bloch decay) technique has enabled quantitative carbon skeletal parameters to be obtained from ^{13}C NMR for the cokes. Internal standard measurements demonstrated that most of the carbon is detectable by SPE and, therefore, NMR-invisible graphitic layers are not thought to be major structural features of the cokes. Differences in feedstock composition were reflected in the structure of the cokes with the aromatic nuclei being most highly condensed in the residue-derived coke and corresponding to 15-20 peri-condensed aromatic rings.

In view of the importance of fluid catalytic cracking (FCC) to petroleum refining, the deactivation of cracking catalysts via coke deposition has been the subject of considerable investigation over the past 50 years (1-3). As well as being formed via the actual cracking reactions associated with the strongly acidic catalytic sites, coke can arise in FCC units from (i) normal thermal reactions, (ii) dehydrogenation reactions promoted by metals - Ni and V in heavy feeds and (iii) entrained catalyst products, symptomatic of incomplete stripping in the regenerator. The contributions of these different mechanisms is clearly going to be dependent on the type of feedstock, together with the design and operation of particular FCC units. However, the lack of detailed basic knowledge on the chemical nature of coke is preventing progress towards a proper overall mechanistic understanding and a clear identification of the different coke-forming routes in FCC operations.

Fundamental deactivation studies involving NMR on zeolites thus far have generally involved excessively high concentrations of coke in relation to normal FCC operation where catalysts are regenerated typically after only α 1% w/w of carbon has been deposited. The high concentrations have been necessary to achieve sufficient sensitivity for characterising the coke on the deactivated catalysts by solid state ^{13}C NMR. For example, Groten et al (4) have investigated coke formation on zeolite USHY with 1-hexene as the feed with coke levels of α 5% w/w. Lange and coworkers (5) used ^{13}C -enriched ethene to follow the formation of polyaromatic structures on H-mordenite. Deactivated γ -alumina-supported hydroprocessing catalysts have also been characterised by solid state ^{13}C NMR (6) but, again due to the relatively low sensitivity, the spectra have been obtained by cross polarisation (CP) which fails to observe all the carbon in coals and oil shales and usually discriminates heavily against aromatic carbon (7). Further problems are posed by high magnetic field strengths where, to eliminate spinning sidebands, special pulse sequences or extremely rapid magic-angle spinning (MAS, >10 kHz) are needed.

There is a general consensus that the use of low field strengths with Bloch decay or single pulse excitation (SPE) offers the best compromise for quantitative ^{13}C NMR analysis of coals and solid fuels (7-10), albeit with a considerable sacrifice in sensitivity since long recycle times (with 90° pulses, 5 times the ^{13}C thermal relaxation times $-T_{1s}$) are required to ensure that the ^{13}C magnetisation fully regains equilibrium. In principle, the only carbon not observed is that in the vicinity of paramagnetic centres which obviously includes graphite. The only way this methodology can be applied successfully to deactivated catalysts is by demineralising the aluminosilicate matrices to concentrate the coke. This approach has been used to characterise two coke concentrates isolated from deactivated FCC catalysts containing only α 1% w/w carbon. The samples chosen for investigation were from refinery runs with an atmospheric residue and a hydrogenated vacuum gas oil (HVGO) in order to ascertain whether the use of these two vastly different feedstocks had a significant effect on coke composition. The degree of condensation of the aromatic structure has been assessed from the proportions of non-protonated aromatic carbon derived by the SPE ^{13}C NMR technique. Information on the coke concentrates from the refinery catalysts and the MAT runs with n-hexadecane has also been obtained by mass spectrometry. The latter extends our earlier study on the roles of quinoline and phenanthrene as poisons and coke inducers in n-hexadecane cracking where only the whole catalysts, as opposed to coke concentrates, were characterised by mass spectrometry (11, 12). A laboratory-scale fluidised-bed reactor has been used to enable sufficiently large quantities of deactivated catalyst containing α 1% coke (α 80 g) to be obtained from n-hexadecane for the demineralisation-quantitative ^{13}C NMR methodology.

Experimental

Catalysts and their demineralisation. The FCC catalysts were typical commercial formulations and the deactivated samples were obtained from units processing (i) a heavy feedstock containing α 1.5% sulphur, a Conradson carbon content of 5.0% w/w and Ni and V contents of 5 ppm each and (ii) a HVGO containing only 0.1% sulphur and below 2 ppm of Ni and V. The catalyst samples deactivated in the MAT reactor were from a series runs with n-hexadecane as the base feed with either phenanthrene or quinoline as a co-feed present at concentrations of 1 and 10% v/v (11, 12). The all-silica laboratory-scale fluidised-bed reactor used had a 4 cm diameter bed and, during each run, α 30 g n-hexadecane was fed into the reactor containing 80 g of catalyst.

The catalysts "as received" all had carbon contents close to 1%. They were

first refluxed in chloroform for 3 hours to remove any entrained molecular species and then vacuum-dried prior to demineralisation. This initial treatment reduced the carbon content of the catalyst deactivated with the atmospheric residue from 1.08 to only 1.00% (estimated error of $\pm 0.05\%$), indicating that molecular species only account for an extremely small proportion of the coke. This observation is consistent with the fact that both catalysts were removed from the FCC units after stripping (collected at the base of the stripper). The cokes were concentrated by applying the standard demineralisation procedure for solid fuels (13,14) to the chloroform-extracted catalysts. This involved successive extraction with 2M hydrochloric acid (stirring overnight at 60°C) and 40% hydrofluoric acid (HF), the HCl-extracted sample being stirred at room temperature for 4 hours with 20 cm³ of HF being used per gram of sample. The coke concentrates were finally washed with dilute hydrochloric acid to remove any remaining inorganic paramagnetics prior to collection in plastic filtration equipment. The vacuum-dried coke concentrates recovered from the refinery catalysts deactivated by the residue and HVGO feedstocks had carbon contents of 55 and 39%, respectively. The n-hexadecane-derived coke concentrate had a carbon content of 33%.

¹³C NMR. The CP and SPE ¹³C NMR measurements on the coke concentrates were carried out as previously for coals (8-10) at 25 MHz on a Bruker MSL100 spectrometer with MAS at 4.5-5.0 kHz to give spectra in which the sideband intensities are only ca 3% of the central aromatic bands. Known weights of tetrakis(trimethylsilyl)silane (TKS) were added to the samples as the internal reference and to facilitate estimation of the fraction of the total carbon observed by SPE. Approximately ca 150 mg of sample was packed into the zirconia rotors. The ¹H decoupling and spin-lock field was ca 60 kHz and, for SPE, the 90° ¹³C pulse width was 3.4 ms. A recycle delay of 50 s was employed between successive 90° pulses in SPE since the ¹³C T₁ for the non-protonated aromatic carbons were 10 s as measured by Torchia's CP-based method (15) for both coke concentrates (Table 1). Normal CP spectra of the residue-derived coke were obtained using a range of contact times between 0.05 and 8 ms for the residue-derived coke to facilitate determination of the time constants for CP (T_{CH}) and ¹H rotating-frame relaxation (T_{1r}). The CP spectrum of the HVGO and n-hexadecane-derived cokes were obtained using a contact time of 1 ms.

Dipolar dephasing (DD) was combined with both SPE and CP to estimate the proportions of protonated and non-protonated aromatic carbon, and at least 8 separate dephasing periods in the range 5-500 ms were used (500 scans each). In order to check that the tuning had remained virtually constant throughout the duration of the DD experiments, the delays were arranged in a random order and between 500 and 1000 scans were accumulated for each delay. The spectra were processed using exponential line broadening factors of either 30 or 50 Hz. No background signal was evident in the SPE spectra from the Kel-F rotor caps. The measurement of aromatic and aliphatic peak areas manually was found to be generally more precise than using the integrals generated by the spectrometer software.

Mass Spectrometry. Mass spectrometry was conducted on the coke concentrates using a VG instrument in which the probe was heated from ambient to 500°C at a rate of 20°C min⁻¹ and spectra over the mass range 50-600 were recorded every 5 s. Spectra were recorded in both electron impact (EI) and chemical ionisation (CI, with ammonia) modes. Field ionisation (FI) spectra of some of the deactivated catalysts from the n-hexadecane MAT runs were obtained at the Stanford Research Institute as described elsewhere (16).

^{13}C NMR analysis of the cokes from the refinery feeds

Quantitative aspects. Figures 1 and 2 compare the CP and SPE ^{13}C spectra of the highly aromatic refinery coke concentrates and Figure 3 presents the decays of the aromatic peak intensities in the CP and SPE-DD experiments on the residue-derived coke. The carbon skeletal parameters obtained from the SPE and CP ^{13}C NMR experiments for both samples are summarised in Table 1. The first coke concentrate obtained from the catalyst deactivated with the residue feedstock gave a broad aromatic band, possibly due to the incomplete removal of the rare-earth during the HCl wash. Indeed, it was found that, after the final HCl wash, much narrower spectral bands were obtained and the quality of the spectra shown are comparable to those obtained for low-volatile coals and anthracites (with similar aromaticities as the cokes, see following).

The sensitivity is obviously superior in the CP spectra (7-10,000 scans for CP compared to 1000-2000 for SPE, Figures 1 and 2) but, as found for many coals⁽⁹⁻¹¹⁾, CP significantly underestimates the carbon aromaticity using relatively short contact times (Table 1, CP values for 1 ms contact, estimated error ± 0.01). This arises from the non-protonated aromatic carbons, in particular, cross polarising much more slowly than the aliphatic carbons (both CH_2 and CH_3 in the residue coke have much shorter T_{CH_3} than the aromatic carbon, Table 1). At longer contact times, the discrimination against aromatic carbon is not quite as acute, but the aromaticity values obtained are still lower than that by SPE (Figure 4). This is indicative that some aromatic carbon, presumed to be in the vicinity of free radicals, is polarised at all (^1H $T_{1\rho}$ s are too short - $< \alpha 0.2$ ms, the values in Table 1 are only for hydrogens adjacent to the carbons being polarised). The fact that 70 and 90% of the carbon in the residue and HVGO-derived coke concentrates, respectively, has been observed by SPE demonstrates that the procedure is reasonably quantitative and that graphitic layers are probably not present in significant amounts. If these were major structural features, the resultant paramagnetism would have detuned the probe resulting in little of the carbon being detectable.

Aromatic structure. As for the total aromaticity, CP also grossly underestimates the fraction of non-protonated aromatic carbon determined by dipolar dephasing (Table 1, estimated error ± 0.02). This can be seen in the decay of the aromatic peak intensity (Figure 3); the faster relaxing Gaussian component for the protonated aromatic carbon has virtually decayed completely after $\alpha 60$ ms with the slower relaxing exponential component from the non-protonated carbon having a time constant of over 500 ms. After the initial decay of the protonated aromatic carbon, the intensity of the remaining non-protonated carbon is modulated by the rotation of the rotor at 5 kHz, this effect being particularly evident in Figure 3 for the CP experiment (note that this modulation is not encountered in variable contact time CP measurements due to the much longer timescale). From the fractions of non-protonated aromatic carbon derived by SPE (Table 1), it is estimated that bridgehead aromatic carbons ($C_{\text{BR}}/C_{\text{AR}}$) account for $\alpha 67$ and 56% of the total aromatic carbon in the residue and HVGO-derived cokes, respectively. The only assumptions needed are that (i) each aliphatic carbon is bound to one aromatic carbon, which is not unreasonable in light of the distribution of aliphatic carbon (see following) and (ii) the concentrations of heteroatoms in the cokes are relatively small (total concentration corresponding to less than $\alpha 2$ mole % carbon).

If peri-condensed aromatic structures are drawn to fit the $C_{\text{BR}}/C_{\text{AR}}$ values (Table 1), 15-20 rings are required for the residue feedstock coke compared to only 8-12 rings for the HVGO sample. This represents a significant difference in aromatic structure which is considered to arise primarily from the major differences in feedstock

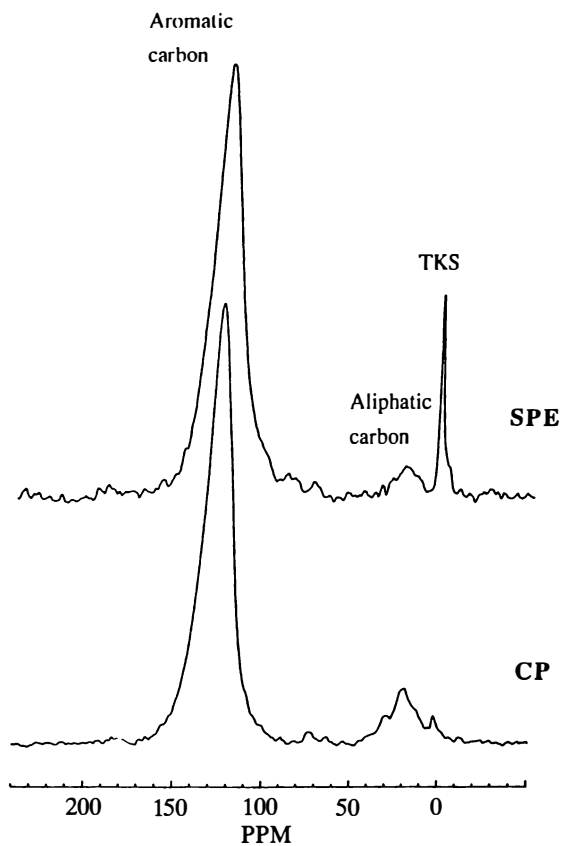


Figure 1 CP (1 ms contact time) and SPE ^{13}C NMR spectra of the coke concentrate from FCC catalyst deactivated using the residue feedstock.

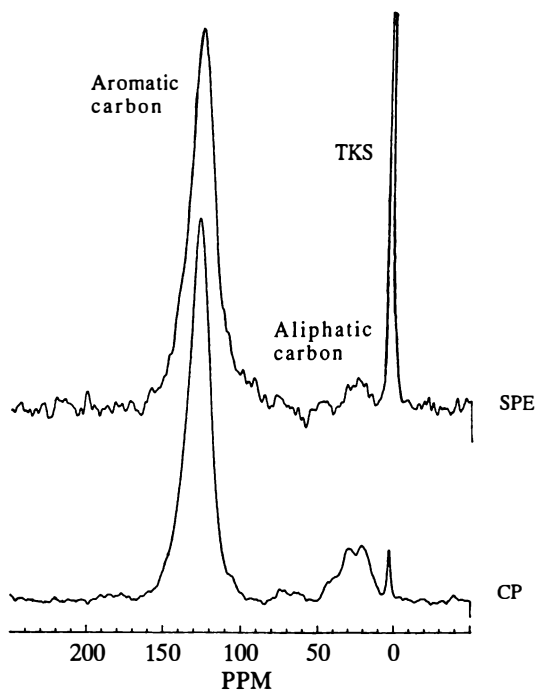


Figure 2 CP (1 ms contact time) and SPE ^{13}C NMR spectra of the coke concentrate from FCC catalyst deactivated using the HVGO feedstock.

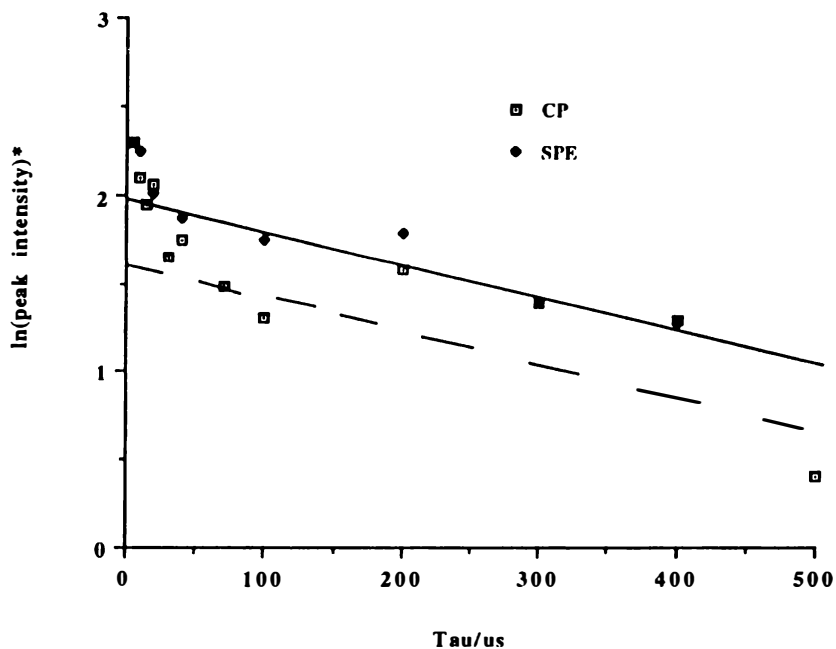


Figure 3 Decay of the natural logarithm of the aromatic peak intensity in the CP and SPE ^{13}C NMR dipolar dephasing experiments on the coke concentrate from FCC catalyst deactivated using the residue feedstock (initial intensity assigned value of 10).

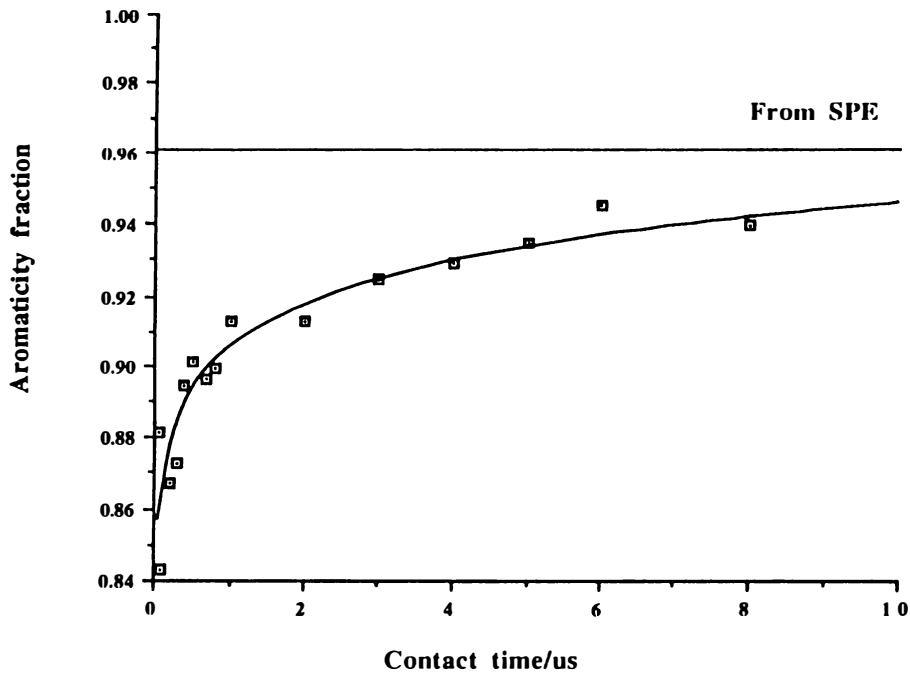


Figure 4 Variation of aromaticity as function of contact time in CP ^{13}C NMR for the coke concentrate from FCC catalyst deactivated using the residue feedstock.

composition and, along with other factors, particularly the Ni and V concentrations, could well affect combustion behaviour in the regenerator.

Table 1. NMR and other structural parameters for the coke concentrates

<i>Parameter</i>	<i>Residue feedstock</i>	<i>HVGO feedstock</i>
¹³ C T ₁ /s for non-protonated aromatic carbon.	10.0	11.5
CP-derived parameters obtained from variable contact time experiment,		
T _{CH} / ms, aromatic C ^b	330	N.D.
CH ₂	40	N.D.
CH ₃	70	N.D.
T _{1r} / ms, aromatic CH	8	N.D.
CH ₂	6	N.D.
CH ₃	5	N.D.
Carbon aromaticity, f _a , (± 0.01) ^a		
CP (1 ms)	0.91	0.85
SPE	0.97	0.96
Fraction of aromatic carbon that is non-protonated from dipolar dephasing experiments (± 0.02) ^a , CP (1 ms)		
SPE	0.55	N.D.
	0.67	0.56
Fraction of aromatic carbon that is bridgehead, C _{BR} /C _{AR} (SPE, ± 0.03) ^a		
	0.63	0.51
Fraction of aliphatic carbon that is CH ₃ (10-24 ppm range, SPE, ± 0.1 ^a)		
	0.75	0.50
% of carbon observed by SPE		
	70	90

N.D. = not determined. SPE = single pulse excitation. CP = cross-polarisation
^a = estimated errors. ^b = average value for protonated and non-protonated carbons.

Aliphatic structure. Although the cokes are clearly highly aromatic in character, some information on the distribution of aliphatic groups can also be obtained from the ¹³C NMR spectra. Intuitively, one would expect virtually all the aliphatic carbon to be adjacent to aromatic rings in either arylmethyl or diarylmethylene groups. The fraction of aliphatic carbon present as methyl has been estimated from the intensity of the 10-24 ppm chemical shift range (Table 1, a fairly clear separation between CH₂ and CH₃ chemical shifts for the aliphatic structures in high-rank coals occurs at 23-24 ppm). Figure 1 indicates that CP overestimates the fraction of CH₃ for the residue-derived coke; CH₃ cross polarises at a slower rate than CH₂ which is reflected in characteristic time constants, T_{CH} (Table 1). The SPE spectrum (Figure 1)

suggests that arylmethyl groups account for α 75% of the aliphatic carbon in the residue-derived coke (Table 1). Although the signal to noise levels of the aliphatic bands are not good, this fraction appears to be much higher than for the HVGO-derived coke where CH_3 accounts for approximately only half of the aliphatic carbon (Figure 2 and Table 1). The larger proportion of CH_2 (and CH if present) in the HVGO-derived coke is again consistent with the differences in composition between the two feedstocks. By definition, the more aliphatic HVGO contains higher concentrations of both long chain alkyl and naphthenic moieties than the atmospheric residue.

Mass Spectrometry

Cokes from the refinery feeds. Figure 5 shows two of the probe EI mass spectra obtained from the refinery coke concentrate prepared from the residue feedstock. Very little material evolved below 100°C which is probably an indication that the chloroform extraction was reasonably successful at removing the entrained products. Those which evolved were characteristic of alkylated species (major peaks at 55 and 57 obtained in spectrum at 55°C) and clearly, in view of the extremely high aromaticity of the coke (Table 1), these represent only a negligible quantity of the total organic matter. Most of the volatiles from the coke evolved above 400°C and gave a series of peaks characteristic of 4-8 ring polynuclear aromatics (Figure 5, bottom spectrum). Again, these volatile species represent only a small fraction of the organic matter and are clearly much less condensed than the bulk of the coke structure (15-20 rings, see earlier).

Cokes from n-hexadecane MAT runs. Mass spectrometry indicates that the coke concentrate from n-hexadecane possesses considerably more aliphatic character than the refinery cokes (Figure 6). Even at high probe temperatures, the EI mass spectra are still dominated by fragments characteristic of alkylated species (m/z 43 and 44) and 1 and 2 ring aromatics (e.g. m/z 77, 91, 105 and 117) with only minor peaks being observed for >3 ring polynuclears. It should be noted that the coke concentrates gave far better sensitivity than previously obtained for the whole coked catalysts (11, 12), allowing the higher molecular mass aromatic fragments to be observed.

FIMS has the advantage of giving parent ions for the volatiles evolved from the coke and the principal classes of species identified are alkanes, mono and di-alkenes and alkylbenzenes up to C_{20} . Two catalyst samples coked using n-hexadecane were analysed, the first sample being cooled immediately after reaction under a nitrogen purge. The second was deactivated with a feed containing 10% w/w phenanthrene in n-hexadecane and was left for 30 minutes at reaction temperature under a nitrogen purge before cooling to simulate the stripping action of an FCC unit. Figure 7 compares the relative ion intensities of dialkene alkyl benzene species from both samples and it can be seen that the stripping action simulated with the phenanthrene-derived coke gives rise to increasing proportions of both the dialkene and alkyl benzene species. Although, just as for EI, FIMS data are clearly not representative of the total coke, these results clearly suggest that there is a considerable increase in aromatic content during the stripping period used here in the MAT.

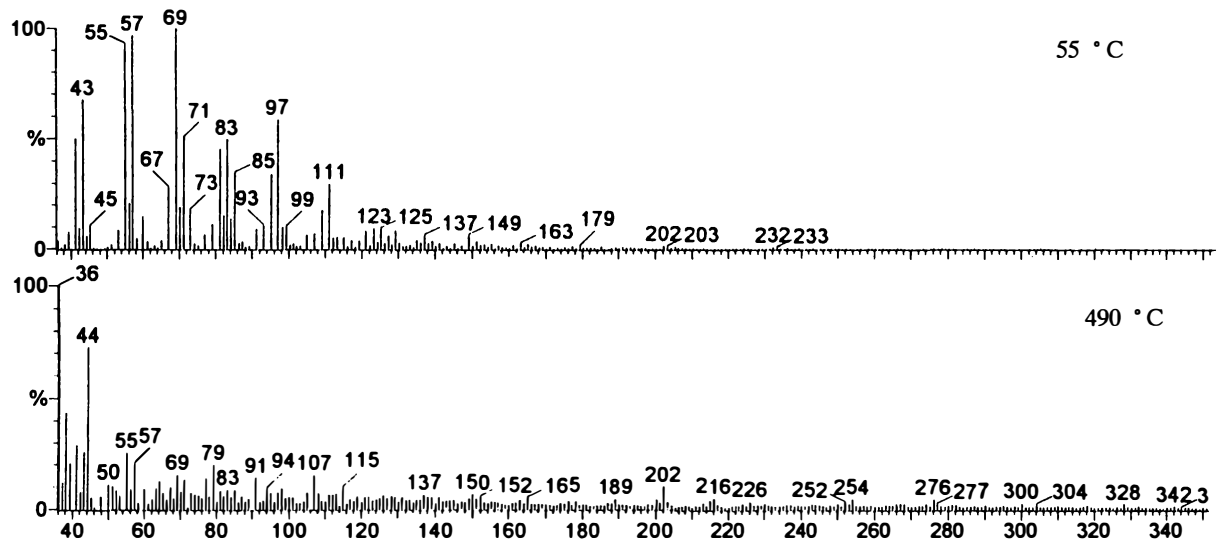


Figure 5 EI mass spectra of coke concentrates obtained from the residue refinery feed, top scan taken at 55°C and the bottom scan at 490°C.

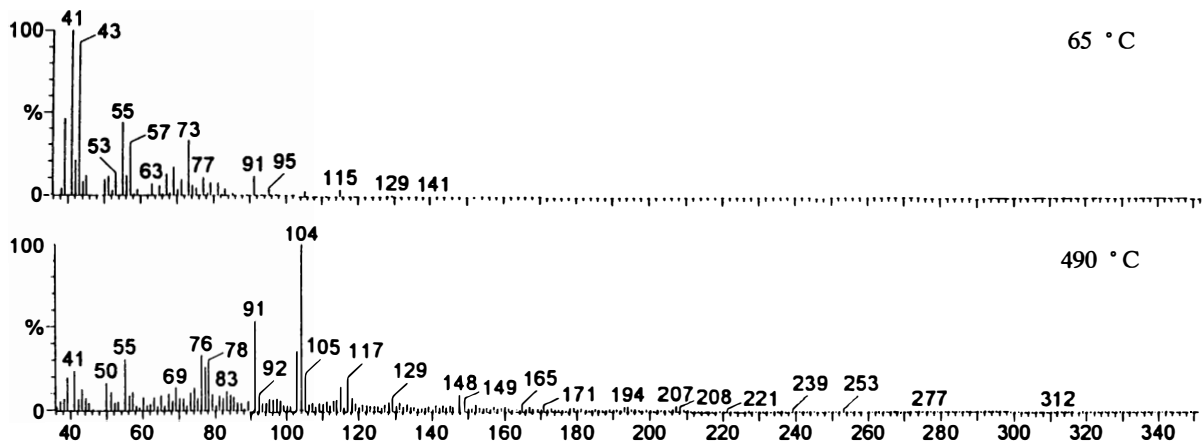


Figure 6

EI mass spectra of coke concentrates obtained from n-hexadecane as the feed in a MAT run, top scan taken at 65°C and the bottom scan at 490°C.

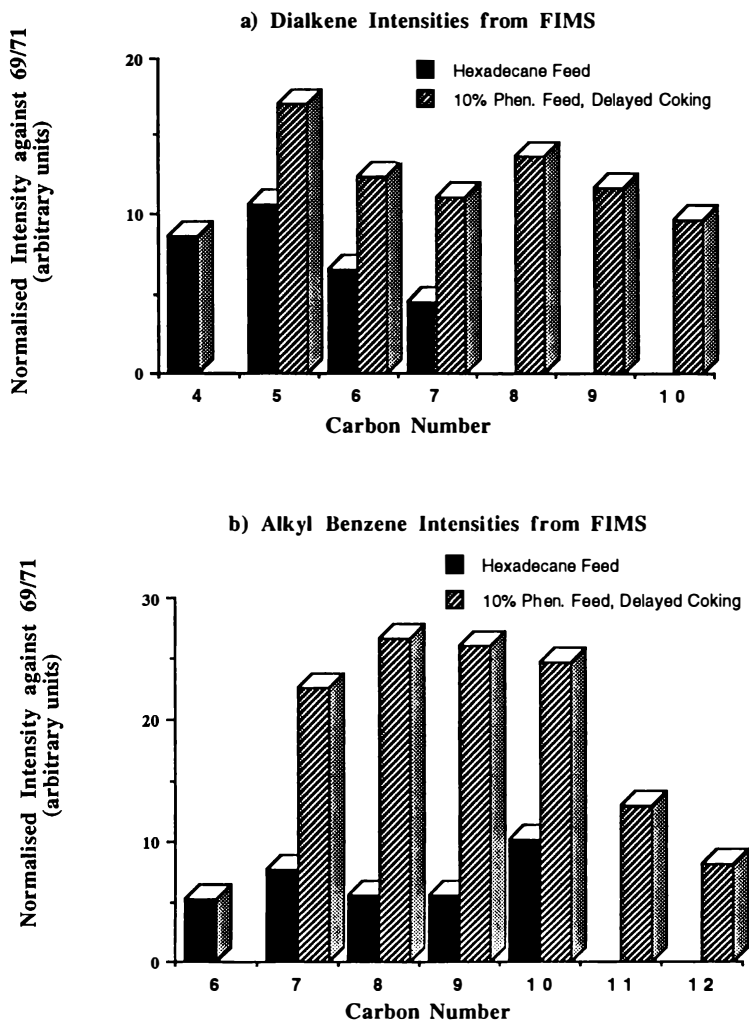


Figure 7

FI mass spectra relative intensities of a) dialkenes and b) alkyl benzenes from coke concentrates obtained from neat n-hexadecane and 10% w/w phenanthrene in n-hexadecane as the feeds in MAT runs.

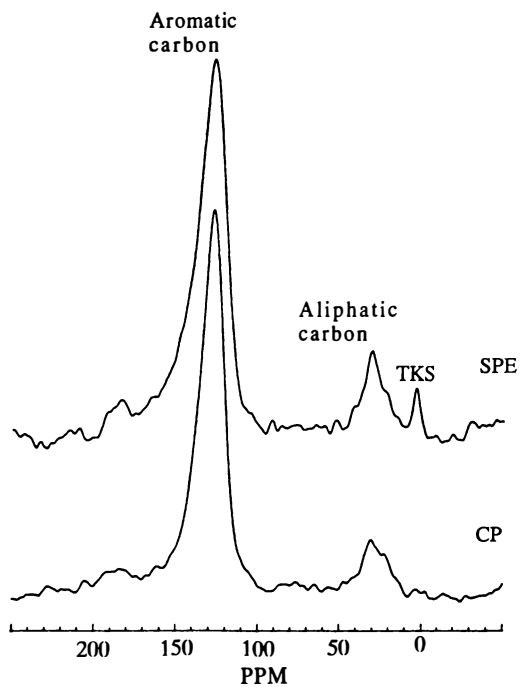


Figure 8

CP (1 ms contact time) and SPE ^{13}C NMR spectra of the coke concentrate from FCC catalyst deactivated using n-hexadecane in the fluidised-bed reactor.

¹³C NMR analysis of coke from n-hexadecane feed

Figure 8 shows the CP and SPE ¹³C NMR spectra of the n-hexadecane-derived coke concentrate obtained from the fluidised-bed reactor. The coke is again largely aromatic but to a much lesser degree than for the refinery cokes with the aromaticity (total sp² carbon) values derived from the CP and SPE spectra both being close to 0.80. The sp² carbon envelope contains a small contribution from carboxyl and carbonyl groups (Figure 8, ~ 5 mole % carbon, 175-205 ppm). These probably arose from accidental exposure of the coked catalyst to hot air during recovery from the fluidised-bed reactor. The presence of a reasonably high proportion of aliphatic carbon is consistent with the EI mass spectrometry results where alkyl fragments were the most intense for the corresponding MAT cokes. The distribution of intensity in the aliphatic envelope which is centred at *ca* 30 ppm indicates that CH₂ dominates over methyl which is again in agreement with the mass spectrometry results where the major alkyl fragments observed arise from chains of at least 4/5 carbons.

Conclusions

The coke formed in FCC refinery operations is highly aromatic in nature and comprises large polynuclear groups. This structure is dependent, however, on the nature of the feedstock. n-Hexadecane in MAT and fluidised-bed tests gives rise to a coke with a considerable greater degree of aliphatic character with only small contributions from polynuclears being observed in probe mass spectrometry. The demineralisation-quantitative ¹³C NMR methodology successively demonstrated here for refinery catalysts is now being extended to other cokes prepared from n-hexadecane in the laboratory-scale fluidised-bed reactor to further elucidate the influence of different compound classes on coke structure.

Acknowledgements

The authors thank the Engineering & Physical Sciences Research Council (EPSRC) for financial support of this work through Grant No. GR/H/24990 (including a studentship for B.J. McGhee) and the Mass Spectrometry Service Centre at the University of Wales. Dr. N.J. Guddle of BP Oil International Ltd. (Oil Technology Centre, Sunbury-on-Thames, Middlesex TW16 7LN, UK) supplied the deactivated refinery catalysts. The authors are indebted to Dr. R. Malhotra of Stanford Research Institute for obtaining the FIMS results.

Literature Cited

1. Butt, J.B., Catalyst Deactivation, *Adv. Chem. Ser.* **1972**, 109, 259.
2. Hughes, R. *Deactivation of Catalysts*, Academic Press, London 1984.
3. Wolf, E.H.; Alfani, A, *Cat. Rev. Sci. Eng.*, **1982**, 24, 329 and references therein.
4. Groten, W.A.; Wojciechowski, B.W.; Hunter, B.K., *J. Catal.* **1990**, 125, 311.
5. Lange, J.P.; Gutsze, A.; Allgeier, J.; Karge H.G., *Appl. Catal.* **1988**, 45, 345.
6. Egiebor, N.O.; Gray, M.R.; Cyr, N. *Appl. Catal.* **1989**, 55, 81.

7. Snape, C.E.; Axelson, D.E.; Botto, R.E.; Delpuech, J.J.; Tekely, P., Gerstein, B.C.; Pruski, M.; Maciel, G.E.; Wilson, M.A., *Fuel*, **1989**, 68 547 and references therein.
8. Franz J.A.; Garcia R.; Linehan J.C.; Love G.D.; Snape C.E. *Energy & Fuels*, **1992**, 6 , 598.
9. Love G.D.; Law R.V.; Snape C.E., *Energy & Fuels*, **1993**, 7 , 639.
10. Maroto-Valer M.M.; Love G.D.; Snape C.E., *Fuel*, **1994**, 73, 1926.
11. Hughes R.; Hutchings G.; Koon C.L.; McGhee B.J.; Snape C.E., *Preprints, Am. Chem. Soc., Div. of Petrol. Chem.*, 39, **1994**(3) , 379.
12. Hughes, R.; Hutchings; G., Koon, C.L.; McGhee, B.; Snape, C.E., in *Catalyst Deactivation*, Elsevier, 1994 , Delmon, B.; Froment, G.F., Eds., *Studies in Surface Science and Catalysis*, 1994, 88, 377.
13. Saxby, J.B *Chem. Geol.*, **1970**, 6 , 173 and in Yen T.F.; Chilingarian G.V. (Eds.), *Oil Shale*, Elsevier, 1976, 103.
14. Durand B.; Nicaise G., *Kerogen-insoluble organic matter from sedimentary rocks*; Durand B. Ed., Editons Technip, Paris, 1980, 35.
15. Torchia D.A., *J. Magn. Reson.*, **1978**, 30 , 613.
16. Malhotra, R., McMillen, D.F. and Huestis, D.L., *Preprints, Am. Chem. Soc. Div. Fuel Chem.*, **1991**, 36(3), 1252.

DEACTIVATION OF FLUID CATALYTIC CRACKING CATALYSTS

Catalyst Decay as a Side Reaction of the Chain Processes of Catalytic Cracking

B. W. Wojciechowski¹ and N. M. Rice²

¹Department of Chemical Engineering and ²Department of Mathematics and Statistics, Queen's University, Kingston, Ontario K7L 3N6, Canada

The rapid loss of catalyst activity in catalytic cracking has had a profound influence on the engineering and commercialization of cat cracking. In this work we propose a plausible chemical mechanism for catalyst decay and derive an expression for the kinetics of the decay process based on this mechanism.

We propose that there are two principal causes of decay in cracking catalysts. One is the *pyrolytic* (thermal) elimination of hydrogen, or of a small paraffin, from a large carbenium ion - an ion which would normally take part in the chain propagating steps of the "fruitful" processes of catalytic cracking. This is strictly an undesirable side-reaction of ions engaged in the mainline process of catalytic cracking.

The other cause is the *catalytic* disproportionation of two normal adjacent carbenium ions to yield a paraffin and a site-spanning di-ion which deactivates two sites. This is a minor catalytic process; it can form coke, but at the same time it yields valuable complex products, notably aromatics. In fact, this process can in principle be engineered not to form coke if an appropriate reaction environment can be arranged.

Both decay processes are due to minor side reactions of some of the same carbenium ions as those propagating the "fruitful" reactions of cracking and isomerization. Their effects combine to yield an equation for the kinetics of catalyst decay which can be anywhere from first to second order in site concentration. In practice, small molecules of the type studied as model compounds generally exhibit almost pure second-order decay in site concentration, while the large molecules found in gas oils tend to show a lower kinetic order, often approaching first-order decay.

The specifics of the chemistry and mathematics which follow from our proposal are presented below in some detail. The consequences of the mechanism we have proposed agree with the observed facts regarding the kinetic behaviour of the feed conversion process in catalytic cracking, with the kinetics of the simultaneous catalyst decay, and with the chemical nature of the major and minor products found in catalytic cracking, including coke.

The loss of catalyst activity in catalytic cracking must be connected in some way with one or both of the following root causes:

1. the complete loss of active sites; and/or;
2. various degrees of reduction in the activity of all or some sites.

We also note that the process of decay in catalytic cracking has been amply demonstrated(1)(2)(3) to be a function of the time of exposure of the catalyst to the reactants: i.e. of the time on stream. Such time-dependent behaviour indicates that the kinetics of the process of catalyst decay are the same as those to be expected in a batch reaction. On reflection, it is obvious that the situation of the catalyst charge in a steady-state reactor is in fact that of a batch of reactant (the catalyst) undergoing a chemical process (catalyst decay) as a function of the time on stream: i.e. the time it spends at reaction conditions - at reaction temperature and in the presence of an atmosphere of feed, products and potential poisons.

From these considerations we can see an outline of the kinetics and mechanism of catalyst decay. While the catalyst remains in the presence of the reactant-product stream, on each active site the processes which dominate are the "fruitful" processes of the attached carbenium ions, involving protolysis, β -cracking, disproportionation, and the reversible adsorption-desorption of product olefins. These events, in combination, constitute the *chain mechanism of cracking*(4) and yield the major products of the "cracking" reaction. None of these processes results in an irreversible reduction of catalyst activity, although the various carbenium ions present will undergo various mainline reactions at different rates.

However, as in most chemical reactions, other less-common "side-reactions" or "minor-but-unavoidable" reactions occur. This is certainly to be expected in the obviously complex process of catalytic cracking. We propose that some of these minor or side reactions lead to a decrease or even a complete loss of activity on the sites where they occur, and are therefore responsible for the observed loss of overall catalyst activity.

Since the sites themselves are not altered in any permanent way, and their original activity can be fully restored by burning off a carbonaceous deposit formed on the catalyst during the cracking reaction, it is reasonable to suppose that it is "coke" that poisons, shields or otherwise deactivates the active sites. However, the total carbonaceous deposit found on the catalyst at the end of a reaction contains "coke" which is formed by a variety of processes, some of which may not lead to a loss of activity. For example, the mass of coke due to products adding on to multilayers or to whiskers of graphitic carbon(5) will contribute to the amount of coke formed, but contributes little or nothing to catalyst deactivation.

The processes which *do* lead to a loss of activity will consist of one or more of the following:

1. the deposition of poison molecules which, once adsorbed on an active site, do not desorb or propagate reaction chains;
2. monomolecular poison-producing thermal decompositions of ions participating in the mainline reactions of catalytic cracking;
3. bimolecular poison-producing catalytic reactions between otherwise normal ions present on the catalyst during reaction.

These processes may vary in importance, depending on reaction conditions, the catalyst, and the feed. However, in the early stages of the cracking of pure

compounds with small molecular weights, chemical reactions of relatively small species are the only ones which can produce the observed coke and deactivate individual catalyst sites; there are no poisonous impurities present. We must therefore accept that some rare undesirable reactions of the small and otherwise ordinary surface-resident carbenium ion species cause the observed loss of activity.

Once we accept this view, we can attempt to envision a chemistry whereby some or all of the participating carbenium ions in the chain mechanism of cracking stray from the path of fruitful reactions, undergo undesirable reactions, cause the buildup of coke, and bring about catalyst decay.

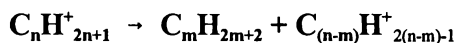
The Mechanism of Coke and Minor Product Formation

There is a broad range of reactions that can occur on each active site in the course of catalytic cracking(6). All these reactions, good and bad, share a common characteristic: all involve an interaction with various *saturated* carbenium ions which are resident on conjugate Brønsted bases. In the case of the pristine Brønsted acid site, the saturated ion is a proton (in a sense, a saturated carbenium ion with carbon number zero) which initiates the cracking reactions of paraffinic and other molecules(7). This species does not contribute to catalyst decay. Subsequently, in the course of reaction, a variety of other *saturated* carbenium ions reside on the conjugate Brønsted base. These react mainly by disproportionating with the feed, or by β -cracking, until such time as a desorption of the resident carbenium ion takes place, reconstituting the pristine Brønsted acid site(8).

Many varieties of *saturated* ions are involved in the fruitful reactions of cracking, all participating in cycles of reactions which preclude deactivation. In order to explain catalyst decay, we must envision the formation of some other type of surface species. This must be a species which occasionally arises from the carbenium ions which normally participate in the mainline reactions. Where else could it come from? Such a species - the species we believe to be responsible for decay - is *unsaturated* carbenium ions. Unsaturated ions may be expected to differ in their desorption and reactivity properties from the more common *saturated* ions; perhaps these differences are sufficient to explain the accumulation of deactivating species.

Unsaturated carbenium ions are not formed by the adsorption of product olefins on pristine acid sites; nor are they formed by the addition of olefins to saturated carbenium ions. Both are minor processes which form saturated carbenium ions and play a part only at higher conversions in the chain mechanism of cracking. Rather, they must be formed by aberrant side-reactions of the main conversion processes, reactions by which normal, *saturated* carbenium ions generate site-poisoning *unsaturated* carbenium ions.

One can postulate two principal routes to the formation of unsaturated carbenium ions from the dominant population of saturated ions. The first is a straightforward four-centre *pyrolytic* (and hence thermal and not catalytic) elimination of a saturated molecule from a saturated carbenium ion:



Such elimination reactions have been reported(9), and there is no reason to think that they are precluded from occurring in the carbenium ions residing on Brønsted bases. The species $C_{n-m}H_{2(n-m)-1}$ is a carbenium ion with a double bond as well as a positive charge and is therefore *unsaturated*. In principle, the process of elimination from a given ion can continue, with the elimination of a succession of paraffins with various values of $m \geq 0$ (hydrogen for this purpose is a paraffin with carbon number $m=0$) until an ion incapable of the desorption necessary to reconstitute the active site, or incapable of disproportionating with a feed molecule to propagate the chain reaction, is formed and the site is completely deactivated. Along the way, at various stages of this process of progressive unsaturation, the resident ions will have successively lower activity levels towards both disproportionation and desorption. In this way they will inhibit the site and contribute to an overall loss of catalyst activity without removing the site from all participation in the conversion process.

We note at this point that it is possible for an olefin-ion to cyclize by reacting with its own double bond to form a *cyclic, saturated* carbenium ion. Such an ion can desorb as a cyclic monoolefin, or, after further H_2 eliminations, as a cyclic diolefin or aromatic. Since few cyclic olefins or linear or cyclic diolefins are observed in the products of cracking (10) it seems that unsaturated carbenium ions either continue to eliminate smaller molecules until they deactivate the site completely, or cyclize and eliminate small molecules until the residual fragment desorbs as a monocyclic aromatic or a more complex minor product. This is probably the process by which all of the small amounts of aromatics, indenenes etc. found in the cracking products of pure paraffins are formed. Notice that the desorption which results in the formation of an aromatic in this way "rejuvenates" a site and returns it to a pristine high activity condition.

Cyclic products, and hence cyclic carbenium ions, seem to form more rapidly at higher conversion. This is probably due to product olefin addition (alkylation) to small surface-resident ions, followed by cyclization and elimination reactions. The process of addition, cyclization and elimination can continue if no desorption takes place, until a large and undesorbable aromatic is formed on the surface, resulting in the complete deactivation of a site by "aromatic coke". Each such addition of an olefin changes the character of the adsorbed species and, in particular, its reactivity. Notice that in the processes proposed so far, only one active site will be deactivated per deactivating event.

A second important process of unsaturated ion formation is that via the *catalytic* interaction of *adjacent saturated* carbenium ions. If such ions are large enough, the end furthest from the centre of charge is scarcely aware that it is part of an ion. Two such ends, colliding in the course of the normal waving about their points of attachment, will simply undergo an elastic collision. However, if a neutral end of one ion comes into collision with the charge centre of the second ion, the consequent configuration should be no different from that encountered in the transition state of a neutral gas-phase saturated molecule undergoing a disproportionation reaction with a carbenium ion. One of the products of this type of reaction is a saturated gas-phase molecule. The other is an ion; in the case of the reaction between two carbenium ions, it is a di-ion spanning the two sites where the two reactant ions used to reside. If the di-ion manages to desorb from one of the two

attachment sites by releasing a proton to it, it will rejuvenate one Brønsted site and form an olefin-ion on the other site.

There will be an equilibrium between olefin-ions on single sites and bridging di-ions tying up two sites, so that the original source of the olefin-ion, whether it is due to catalytic or thermal reactions, becomes moot. It may equally well come from the thermal elimination of a paraffin (or H_2) from a saturated carbenium ion attached on one site, or from a catalytic disproportionation between two adjacent ions. The difference between the two forms is that either two sites are deactivated (by the di-ion), or one site is inhibited by an olefin mono-ion. On all the USHY catalysts studied in our laboratories(11)(12) and elsewhere(13), all the pure feed cracking reactions cause decay which is close to second order in site concentration, implying that di-ions are the principal agents of catalyst decay. Gas oils, on the other hand, cause decay with an order between one and two in site concentration, and often decay by a process which is close to first order(14).

One is led to suspect that the larger and more complex ions which arise in gas oil cracking eliminate paraffins or hydrogen from their singly-attached ions more readily than do the simple ions of the paraffins we have studied as model compounds. In those reactions, the formation of ions which are sufficiently large to poison sites one by one will involve successive additions of product olefins to the small carbenium ions which form from the feed. The reaction mechanism summarizing the processes described above is shown in Figure 1.

Using this picture of the chemical events involved in catalyst decay, we can quantify the consequences of such behaviour *without any prior knowledge* of the activity of each of the many species which may be formed in this way. To do this, we use the concept and the mathematics of Markov chains, a mathematical construct which allows for the wide variety of processes described above to be systematized and considered in quantitative terms.

Formulating the Kinetics of Deactivation

There are three cases of decay kinetics which need to be explained. They differ in their dependence on the concentration of active sites remaining on the surface. They are:

1. first-order decay kinetics;
2. second-order decay;
3. mixed first- and second-order decay.

We will assume that sites on a catalyst can be in different states of activity, corresponding to the nature of the attached species. Some sites will have singly-attached species (mono-ions) and some will have doubly-attached species (di-ions). Singly-attached species may change in length or chemical nature as time passes and the ongoing chain propagating reactions, or occasional thermal eliminations, change the nature of the ion resident on those sites. The activity for chain propagation, desorption and other "mainline" propagation reactions differs from the ion to ion; in particular, we expect that the activity of olefin-ions is very different from that of the saturated carbenium ions. Each such transition from one species to another on a given site has some fixed probability of occurring in any one period of time.

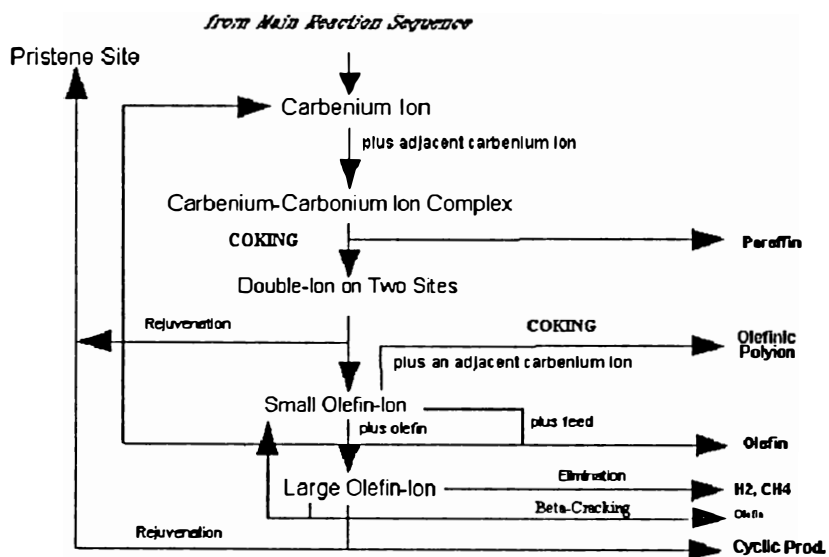


Figure 1. Minor and coke-forming reactions.

Moreover, some of the singly-attached species might become doubly attached. The probability of such a transition depends on the nature (we will call it "state") of the singly-attached species and on the availability of neighbouring sites to which it may attach. It will generally be much smaller than the probability of a transition between single-site states. The di-ions will in general remain on the surface as coke and lead to the complete deactivation of their sites of attachment. Only occasionally (i.e. with a relatively small probability) will such species detach from one of the two sites, producing one pristine site and one site with an olefinic mono-ion attached.

Each type of ion species (state) will have associated with it some level of activity for the mainline reactions, and the overall activity of the catalyst is the average activity of all the sites at that instant. We suspect that mono-ions will generally have much higher activity levels than di-ions, but one can investigate other suppositions by implementing our methods with the appropriate transition probabilities.

The above physical situation may be modelled by a modified Markov process, where the states represent the various ions attached at the catalytic sites, and the transition probabilities are the above-mentioned probabilities of an ion being replaced or modified within a period of time. This will not be an ordinary Markov process, because the transition probabilities are not all constant. In particular, those probabilities corresponding to the transition of single sites to double sites depend not only on the states in question, but also on the availability of other single sites. That probability in turn, changes, as sites are removed by irreversible decay events.

First-Order Decay Kinetics

We first consider the special case where there is no double-site attachment at all. We suppose for this case that there is some small probability b_j of a singly-attached site dropping directly from an active state j to the dead state. These probabilities may vary from state to state, but do not change over time, so in this special case we have a true Markov process. It is natural to classify the states as active or dead (there is one dead state), and to partition the transition probability matrix correspondingly:

$$P = \begin{bmatrix} P_{11} & \mathbf{0} \\ b^t & 1 \end{bmatrix} = \begin{bmatrix} P_{11} & P_{12} & \cdot & \cdot & \cdot & 0 \\ P_{21} & P_{22} & \cdot & \cdot & \cdot & 0 \\ \cdot & \cdot & \cdot & \cdot & \cdot & \cdot \\ \cdot & \cdot & p_{ij} & \cdot & \cdot & 0 \\ \cdot & \cdot & \cdot & \cdot & \cdot & \cdot \\ b_1 & b_2 & \cdot & \cdot & \cdot & 1 \end{bmatrix}$$

where p_{ij} is the probability of transition (per unit time) from an active state j to an active state i , and P_{ii} is the whole submatrix of these probabilities. The 1 in the bottom right corresponds to the assumption that a dead state always remains dead.

Similarly, the vector giving the distribution of sites in the various states at time n can be partitioned as:

$$\begin{bmatrix} s(n) \\ z(n) \end{bmatrix} = \begin{bmatrix} s_1(n) \\ s_2(n) \\ \vdots \\ z(n) \end{bmatrix}$$

where $z(n)$ gives the proportion of sites in the dead state, and $s(n)$ the proportions of active (mono-ion) states. For each time step we have $s(n+1) = P_{11}s(n)$, so in general $s(n) = P_{11}^n s(0)$.

Since dead sites have zero activity, the overall activity of the catalyst is $\bar{a}(n) = a's(n)$, where a is the vector giving the activity levels of the active states. In order to see how overall activity \bar{a} changes over time, first consider what happens if one starts with a "quasi-steady-state" distribution of active states, i.e., let $v(0) = e_1$, the eigenvector of P_{11} corresponding to the dominant eigenvalue λ_1 of P_{11} . In this case $P_{11}e_1 = \lambda_1 e_1$, so $s(n) = P_{11}^n e_1 = \lambda_1^n e_1 = \lambda_1^n s(0)$. Thus the relative proportions of sites in active states remain unchanged over time; there is simply an overall exponential decrease in the total population of active sites. Similarly, in this quasi-steady-state case we have $\bar{a}(n) = a's(n) = \lambda_1^n a'e_1 = \lambda_1^n \bar{a}(0)$: i.e., the overall activity decreases exponentially. The decay constant λ_1 is very close to 1 since the columns of P_{11} all have a sum very close to 1. In fact, if the columns of P_{11} all have identical sums β , then $\lambda_1 = \beta$; this corresponds to the situation where the probability of sudden death is the same from each active state, namely $b = 1 - \beta$.

Next, consider the more general case of an arbitrary initial distribution $s(0)$. Denote by $\{e_1, e_2, \dots\}$ a basis of eigenvectors of P_{11} with corresponding eigenvalues λ_i arranged in decreasing magnitude. Then $s(0)$ can be written as some linear combination $s(0) = \sum \alpha_i e_i$, so $s(n) = P_{11}^n s(0) = \sum \alpha_i P_{11}^n e_i = \sum \alpha_i \lambda_i^n e_i$. Since λ_1 is very close to 1 and the other eigenvalues are much smaller, the first term in the sum soon becomes dominant as n increases. Thus the distribution $s(n)$ is soon essentially proportional to the dominant eigenvector e_1 . The speed of approach to this quasi-steady-state is governed by the rate at which $|\lambda_2/\lambda_1|^n$ tends to 0. After quasi-steady-state is reached, $s(n)$ continues to decrease, but now decreases exponentially at the much slower rate λ_1^n .

Similarly, the overall activity starting from an arbitrary $s(0)$ is given by $\bar{a}(n) = a's(n) = \sum \lambda_i^n \alpha_i a'e_i$. This decreases quickly at first, but soon all the terms in the sum become negligible compared to the first term. After this we have $\bar{a}(n) \approx \lambda_1^n \alpha_1 a'e_1$, a purely exponential decrease.

Second-Order Decay Kinetics

Turning to the more general case, where double-site attachments may occur, we identify three types of sites: types 1, 2, 3 are respectively single-site states, double-site states, and the dead state with zero activity and no escape. Types 1 and 2 each comprise many states; type 3 comprises just one state. For the various transitions we denote by P_{ij} the submatrix of transition probabilities from states of type j to states of type i . That is, we partition the overall probability transition matrix P according to the types of states as:

$$P = \begin{bmatrix} P_{11} & P_{12} & P_{13} \\ P_{21} & P_{22} & P_{23} \\ P_{31} & P_{32} & P_{33} \end{bmatrix} = \begin{bmatrix} P_{11} & P_{12} & 0 \\ P_{21} & P_{22} & 0 \\ 0 & P_{32} & 1 \end{bmatrix}$$

The magnitudes of the individual entries in each P_{ij} reflect the physical assumptions stated above; for example, the whole matrix $P_{31} = 0$, since in this model we are assuming no direct transitions from single-sites to dead sites; also $P_{13} = P_{23} = 0$ since there is no recovery from a dead state; also individual entries in P_{21} are much smaller than those of P_{11} . Because of the gradual disappearance of single-sites it becomes more difficult over time for doubly-attached sites to form. Thus the entries of P_{21} decrease over time, and there is some compensating increase in P_{11} . Now that we see that P changes over time, it will be more proper to denote it as $P(\mathbf{n})$.

As indicated above, the entries of P_{21} vary over time, according to the availability of single sites. Fortunately there is an easy way to get an overall measure of this availability, and hence an easy way to modify P_{21} and P_{11} to take account of it. Because P_{11} is much larger than P_{21} , the model corresponds to a rapid mixing of single-site states, with slow leakage to double-site states. Consequently the system very rapidly approaches a quasi-steady-state with respect to the population of single sites, with a continuing slow drift to double sites. As indicated above, this quasi-steady-state is given by the dominant eigenvector of P_{11} . Strictly speaking, this eigenvector changes over time, but since the change in P_{11} is slow, the corresponding change in the eigenvector is slow.

Once this quasi-steady-state is reached and the corresponding overall average activity level calculated, any subsequent change in average activity is due to the slow drift to doubly-attached sites as described by P_{21} . Their formation is responsible for the observed catalyst decay at times on stream beyond the few seconds or less required to establish the mono-ion quasi-steady-state. Since these double sites have a much lower activity level than single sites, they contribute much less to the overall catalyst activity. Thus once quasi-steady-state has been reached by the mono-ions, the overall average activity level $\bar{a}(\mathbf{n})$ at time \mathbf{n} provides a good measure of the availability of single sites.

As a result of this useful coincidence we may use $\bar{a}(\mathbf{n})$ to modify the \mathbf{P}_{21} transition probability matrix as follows: with $\mathbf{P}(\mathbf{0})$ given, and with $\bar{a}(\mathbf{n})$ normalized so that the overall activity equals 1 for purely single-site quasi-steady-state, it follows from the preceding that:

$$\mathbf{P}_{21}(\mathbf{n}) \approx \bar{a}(\mathbf{n})\mathbf{P}_{21}(\mathbf{0})$$

Since $\mathbf{P}(\mathbf{n})$, the overall probability matrix, must have column sums equal to 1, each column of $\mathbf{P}_{11}(\mathbf{n})$ must be adjusted accordingly as follows:

$$\text{kth column of } \mathbf{P}_{11}(\mathbf{n}) = [(1 - \bar{a}(\mathbf{n})\beta)/(1 - \beta)](\text{kth column of } \mathbf{P}_{11}(\mathbf{0})).$$

where

$$\begin{aligned} \beta &= \text{sum of the kth column of } \mathbf{P}_{21}(\mathbf{0}) \\ &= \text{probability of a single-site in state k transiting to a} \\ &\quad \text{double-site in unit time.} \end{aligned}$$

We believe that each such β is very close to 0 so that $\mathbf{P}_{11}(\mathbf{n})$ changes very slowly over time.

Computer simulations of this discrete mathematical model show that after the initial rapid approach to a quasi-steady-state, the activity level $\bar{a}(\mathbf{n})$ decreases as a second-order process in terms of the remaining activity i.e., for some β ;

$$\Delta\bar{a}(\mathbf{n}) \approx -\beta\bar{a}(\mathbf{n})^2$$

or equivalently, for some constant A ;

$$\bar{a}(\mathbf{n}) \approx (A + \beta\mathbf{n})^{-1}.$$

This may be proven analytically, at least in the special case where each column of $\mathbf{P}_{21}(\mathbf{0})$ has the same sum β . That is to say, when each mono-ion has the same probability β of transiting to a di-ion. In this case all the columns of $\mathbf{P}_{11}(\mathbf{0})$ have the same sum $(1 - \beta)$, and hence $\mathbf{P}_{11}(\mathbf{0})$ has dominant eigenvalue $(1 - \beta)$. Let q be the eigenvector of $\mathbf{P}_{11}(\mathbf{0})$ corresponding to this dominant eigenvalue, so that:

$$\mathbf{P}_{11}(\mathbf{0})q = (1 - \beta)q.$$

From the equation above giving the kth column of $\mathbf{P}_{11}(\mathbf{n})$ it follows that:

$$\mathbf{P}_{11}(\mathbf{n}) = [(1 - \bar{a}(\mathbf{n})\beta)/(1 - \beta)]\mathbf{P}_{11}(\mathbf{0})$$

Hence,

$$\mathbf{P}_{11}(\mathbf{n})q = [(1 - \bar{a}(\mathbf{n})\beta)/(1 - \beta)]\mathbf{P}_{11}(\mathbf{0})q = (1 - \bar{a}(\mathbf{n})\beta)q.$$

Thus q is also an eigenvector of $P_{11}(n)$, with eigenvalue $(1 - \bar{\alpha}(n)\beta)$.

Now suppose at time n we have a population distribution:

$$p(n) = [s(n), d(n), z(n)].$$

From the chemical assumptions, reflected in the relative sizes of the transition probabilities p_{ij} , it follows that $P_{22}(n)$ is much smaller than $P_{11}(n)$ and $d(n)$ is no bigger than $s(n)$. Consequently:

$$s(n+1) = P_{11}(n)s(n) + P_{12}(n)d(n) \approx P_{11}(n)s(n)$$

On the other hand, since the system is in quasi-steady-state we have, for some decay factor λ ,

$$s(n+1) = \lambda s(n).$$

Thus, as expected, $s(n)$ is essentially the dominant eigenvector q , with eigenvalue $\lambda = (1 - \bar{\alpha}(n)\beta)$, i.e.:

$$s(n+1) \approx (1 - \bar{\alpha}(n)\beta)s(n).$$

Denote by:

$$a = [a_1, a_2, \theta]^t,$$

the vector of activity levels corresponding respectively to single-site, double-site, and dead states. Since the model assumes a_2 is much smaller than a_1 , we see that the overall average activity level is:

$$\bar{a}(n) = a_1' s(n) + a_2' d(n) + \theta z(n) \approx a_1' s(n).$$

This simply reiterates the supposition stated above: most of the cracking activity comes from single-sites. But combining it with the expression obtained for $s(n+1)$ we get:

$$\begin{aligned} \bar{a}(n+1) &= a_1' s(n+1) \approx a_1' (1 - \bar{\alpha}(n)\beta) s(n) \\ &= (1 - \bar{\alpha}(n)\beta) \bar{a}(n). \end{aligned}$$

Thus we have the expected second-order decay:

$$\bar{a}(n+1) - \bar{a}(n) \approx -\beta \bar{a}(n)^2.$$

Computer simulations show that second-order decay occurs even when the column sums of P_{21} are not all the same; in fact, they may differ by orders of magnitude, but no analytic proof of this is available yet.

The situation described by the above considerations in all probability corresponds to that responsible for the second-order kinetics of catalyst decay observed in the cracking of small molecules on most catalysts. The ions formed in such reactions are probably too small and too simple to allow a significant rate of monomolecular elimination of saturated fragments to form the unsaturated site poisoning species. Rather, pairs of adjacent small ions seem to disproportionate and produce di-ions which stick to the surface and irreversibly deactivate two sites per event.

Mixed-Order Decay Kinetics

In the first-order case we have supposed that no di-ions exist and that there is some chance of mono-ions undergoing sudden death. In the second-order case we suppose that di-ions do exist, and the dead state is reached only via these states. The most general case is therefore the one where both types of processes take place simultaneously. One can expect such a case to arise if the feed consists of a mixture of widely varying molecular types, as it does for example in gas-oil cracking.

No example of pure first-order kinetics of decay has been confirmed, but gas-oil cracking often shows decay kinetics which approach first-order behaviour(15). In such cases we envision a mixture of first- and second-order decay taking place in proportions which yield an overall order lying between one and two; often close to one. Computer simulations of the behaviour of mixtures of the first- and second-order processes formulated in the manner described above support this view.

The reason that gas-oil cracking has such a large component of first-order decay and the model compounds do not is no doubt connected to the presence of much more complex carbenium ions in gas-oil cracking processes. The ions present in these systems may well be able to form non-desorbable and therefore poisonous species by a series of monomolecular eliminations of various small paraffinic molecules (or hydrogen).

Conclusions

The kinetics of feed conversion, minor product formation, and catalyst decay in catalytic cracking are well-described in a unified hypothesis by quantifying the fates of the carbenium ions which one expects to find in a given catalytic cracking reaction.

Aberrant side reactions of these ordinary ions, such as thermal decomposition and ion-ion disproportionation, can lead to the formation of a great variety of complex, less-active, or even totally inactive, species. With no prior knowledge of the reactivity of these many different types of ions, or of their chances of undergoing any given reaction, merely by assuming that the various possibilities of side reactions *do* exist, we have formulated equations which describe the changes in the overall activity of the catalyst.

Our equations consistently predict that decay can proceed by first-order kinetics, second-order kinetics or, in the case of mixed feeds, with an order between first and second. This behaviour persists under a great variety of assumptions

regarding the transition probabilities between the many states assumed by the surface species. Most importantly, the predictions agree exactly with experimentally-observed non-physical causes of decay and selectivity behaviour of all cases of model compound cracking studied to date.

Literature Cited

1. Pachovsky, R.A. and Wojciechowski, B.W., *Can. J. Chem. Eng.* 49, 365 (1971)
2. Best, D.A. and Wojciechowski, B.W., *J. Catal.*, 47, 343 (1977)
3. Corma, A. and Wojciechowski, B.W., *Cat. Rev., Sc. and Eng.*, 24(1), 1 (1982)
4. Zhao, Y-X., Bamwenda, G.W., Groten, W.A. and Wojciechowski, B.W., *J. Catal.*, 140, 243 (1993)
5. Blackmond, D.G., Goodwin, J.G. Jr. and Lester, J.E., *J. Catal.*, 78, 34 (1982)
6. Cumming, K.A. and Wojciechowski, B.W., to be published
7. Haag, W.O. and Dessau, R.M., *Proceedings of the 8th International Congress on Catalysis, Berlin, 1984, vol 2, p 305, Dacheima, Berlin, 1984*
8. Hall, W.K., Lombardo, E.A. and Engelhardt, J., *J. Catal.*, 115, 611 (1989)
9. Groten, W. and Wojciechowski, B.W., *J. Catal.*, 125, 311 (1990)
10. Groten, W. and Wojciechowski, B.W., *J. Catal.*, 122, 362 (1990)
11. Corma, A. and Wojciechowski, B.W., *J. Catal.*, 60, 77 (1979)
12. Abbot, J. and Wojciechowski, B.W., *J. Catal.*, 115, 1 (1989)
13. Corma, A., Miguel, P.J. and Orchilles, A.V., *J. Catal.*, 145 58 (1994)
14. Viner, M.R. and Wojciechowski, B.W., *Can. J. Chem. Eng.*, 60, 127 (1982)
15. Pachovsky, R.A. and Wojciechowski, B.W., *Can. J. Chem. Eng.*, 53, 308 (1975)

Catalyst Deactivation in Fluid Catalytic Cracking

A Review of Mechanisms and Testing Methods

Paul O'Connor, E. Brevoord, A. C. Pouwels, and H. N. J. Wijngaards

**Akzo Nobel Catalysts, Nieuwendammerkade 1–3, P.O. Box 37650,
1030 BE Amsterdam, Netherlands**

The consequences of deactivation on FCC catalyst activity and selectivity are reviewed and possible relations between the various deactivation phenomena are qualitatively indicated.

A few cases of FCC catalyst deactivation are highlighted, specifically addressing the question how to simulate the deactivation phenomena properly.

Mechanisms of FCC catalyst deactivation.

Deactivation of FCC catalysts does not only yield a drop in activity, but usually also a change in selectivity. Basically, three types of phenomena should be considered when studying the changes in catalyst activity and selectivity:

Catalyst Aging: How does the catalyst change its behaviour in time.

Catalyst Poisoning: How do external poisons affect catalyst behaviour in time.

Catalyst Fouling: How does formation of coke and/or metal deposits affect catalyst behaviour.

One can also distinguish between reversible and irreversible forms of deactivation as illustrated in Table 1.

Hydrothermal Deactivation.

With amorphous silica-alumina catalysts [5, 6], the primary mode of aging involves steam-induced loss of surface area by the growth of the ultimate gel particles, resulting also in loss of porosity.

While amorphous catalysts deactivate thermally as well as hydrothermally, thermal deactivation is a significantly slower process.

The introduction of zeolites in cracking catalysts combined with various non-zeolite matrix types (a.o. higher stability silica-alumina types) certainly complicates the picture of FCC hydrothermal deactivation.

Letzsch et al [7] have shown that like amorphous catalysts the zeolite is more strongly deactivated hydrothermally than purely thermally.

The first 10 to 25% of steam has the greatest influence[4].

The zeolite unit cell size reduction, which should give an indication of the zeolite activity loss by dealumination [8] is not very sensitive to steam partial pressure, with the exception that some steam is necessary for cell size shrinkage.

Chester et al [6] indicate that the relative contributions of zeolite deactivation (e.g. loss of crystallinity) and matrix deactivation (e.g. loss of porosity) in different temperature ranges can be significantly different. They therefore conclude that increasing temperature as a means of increasing catalyst steam deactivation severity can give misleading estimates of overall catalyst stability. This has also been confirmed with "today's" FCC catalysts [10].

As the relative contribution of zeolite and matrix activity will have an impact on catalyst selectivity, we can conclude that the foregoing is also valid for catalyst selectivity.

Deactivation by Poisons and deposits.

Basic and polar molecules e.g. nitrogen compounds which are readily adsorbed on to the catalyst acidic sites, lead to an instantaneous, but temporary deactivation [1, 2].

Also polycyclic aromatics and other organic and non-strippable molecules which lead to coke formation are considered reversible (regenerable) catalyst poisons [11,12].

Irreversible catalyst poisons (or deposits) can even influence the catalyst during the first passage through the reactor, but are not (easily) removed during the stripping and/or regeneration stages. Examples are the heavy metals in feed as vanadium and nickel and other poisons such as alkali components, iron and copper.

If we assume that the poisoning effect will increase with the concentration of poisons on the catalyst [13,14,15], we can model this effect by for instance assuming steady state addition and removal of catalyst, see for example Leuenberger [14].

The catalyst poisoning effect will then be proportional to the ratio between catalyst replacement and feed rate.

Unfortunately, the metal level on FCC catalysts is hardly ever in equilibrium and as catalyst deactivation by vanadium does not take place in isolation, but combined with and influenced by hydrothermal deactivation [14, 15], more sophisticated dynamic equations[4] will be needed to describe this behaviour by including the effects of the catalyst age distribution [15, 16, 17].

In principle the poisoning effect of vanadium on the FCC catalyst can be partially reversed [9], this type of regeneration however does not usually take place in conventional FCC operations.

With the deposits of catalyst poisons as coke and heavy metals, fouling and pore mouth plugging phenomena can be observed [18, 19].

Fouling can result in bigger differences in selectivity of various catalysts, because of changes in pore architecture [2, 10].

The catalysts which are relatively less accessible for large hydrocarbons will be more sensitive to pore mouth blocking and plugging [18].

Khouw et al [20] report that catalysts contaminated to high vanadium levels are still capable of converting light feeds, but not heavier feeds (see Table2)

Apparently catalyst poisons can block access for the larger hydrocarbon molecules to the most accessible sites.

The foregoing can be explained with a simple supply and demand model of cracking [4,10]: if a larger fraction of the sites are more accessible, the detrimental effect of poisons on the resid cracking selectivity will be less as both the poisons and the large molecules compete for the most accessible sites.

How to simulate a low metals catalysts deactivation.

Assuming that the metals and other poisons on catalyst are low, we may expect that traditional catalyst steaming will be sufficient to simulate catalyst deactivation.

Keyworth et al [16] recommend making a composite of several steamings in order to address the age distribution of equilibrium catalyst in a commercial unit.

Beyerlein et al [17, 21] critically question the possibility of improving catalyst aging procedures, which rely only on steam treatment at constant temperature for varying times.

We find [10, 22] that the decay behaviour of zeolite catalysts by steaming differs significantly from the activity and selectivity results after cyclic deactivation without metals.

One of the typical features of the FCC operation is the continuous regeneration of the catalyst which is being circulated. The average catalyst goes undergoes 10.000 to 50.000 regeneration cycles.

As described by Gerritsen et al [23] in a Cyclic Deactivation procedure the catalyst is deactivated by means of several reaction and regeneration (coke burning) cycles. This is essential for the realistic deposition and aging of the metals.

Strangely enough our data consistently shows that even without metals, the catalyst seems to deactivate differently by Cyclic Deactivation compared to steaming.

Table 1. Forms of Deactivation [1, 2, 3, 4]

<i>Deactivation</i>	<i>Reversible</i>	<i>Irreversible</i>
Catalyst Aging		Hydrothermal
Catalyst Poisoning	Coke, N, S, O (Polars)	Na, V, Ni, etc.
Catalyst Fouling	Coke deposits	Metal deposits

Table 2. Vanadium contamination has higher effect on conversion of residue feed

<i>Feedstock</i>	<i>Activity Loss in wt%</i>	<i>Conversion per 1000 ppm V From [20]</i>	<i>Own Data</i>
VGO, CCR << 1 wt%		1	0.7
RESID, CCR = 3-4 wt%		3	1.8

CCR: %wt Conradson Carbon Residue in feed.

An example is given in the next Table:

Table 3. Ranking changes dependent on deactivation conditions

<i>Method</i>	<i>ST</i>	<i>CD-1</i>	<i>CD-2</i>
<u>Catalyst A</u>			
Conversion, %wt	67.7	72.5	68.5
Coke, %wt	2.1	2.5	3.4
C ₄ -olefinicity	0.64	0.60	0.61
<u>Catalyst B</u>			
Conversion, %wt	67.0	72.7	69.2
Coke, %wt	2.2	2.6	3.9
C ₄ -olefinicity	0.69	0.60	0.57

ST Steaming 5 hours at 788°C, 100% steam
 CD-1 Cyclic deactivation, 50 hrs, no metals
 CD-2 Cyclic deactivation, 50 hrs, 1000 ppm Ni, 1000 ppm V
 For CD 1 and 2 regeneration temperature 788 C, 50% Steam

This example shows that a significant change in ranking is obtained with respect to C₄-olefinicity (total C₄ = olefins / total C₄) and hence hydrogen transfer activity of the catalyst.

A possible explanation for this is that while dealumination in a commercial unit is fast, migration of Non-Framework Alumina (NFA) from within the zeolite structure will be a function of temperature and steam partial pressure [24].

In traditional high temperature steaming methods NFA will migrate quickly, while under commercial conditions we do not encounter these conditions. Here the Cyclic Deactivation method approaches the commercial conditions much more closely than traditional steaming methods.

The presence of coke and coke burning in the regenerator stage may also have an effect on the mobility and aging of the non-framework alumina species. This has also been demonstrated to be the case for vanadium [1, 25].

How to simulate a catalyst poisoned by metals.

The literature on FCC catalyst deactivation by vanadium and nickel is extensive [1, 2, 10, 13, 14, 26, 27]. Basically nickel and vanadium influence the catalyst via four main reactions:

<u>Mechanism</u>	<u>Metal Potency</u>
Destruction or neutralization of active catalyst sites	(V > Ni)
Dehydrogenation reactions leading to coke and gas formation	(Ni > V)
Oxidation promotion, a higher CO ₂ /CO ratio in the regenerator [28]	(Ni > V)
Pore mouth blockage	(Ni > V)

The following table gives a rough impression of the relative poisoning power and dehydrogenation activity of some fresh compounds based on several literature sources available [10, 26, 27, 29, 30, 31, 32].

Table 4. Indications for Fresh Poisoning Power and Dehydrogenation Activity

	<i>Relative Activity Loss^{*)} per ppm weight</i>	<i>Relative Activity Loss^{*)} per ppm moles</i>	<i>Relative H₂Production^{**)} per ppm weight</i>
V	1.0	1.0	0.3
Ni	0.1	0.1	1.0
Fe	0.1	0.1	0.3
Cu	0.1	0.1	0.4
Na	0.9	2.0	<0.1
K	0.9	1.2	<0.1
Mg	0.5	1.0	<0.1
Ca	0.5	0.6	<0.1
Ba	0.1	<0.1	<0.1
C (Coke) ^{***)}	0.8	0.2	<0.1
N (Nitrogen) ^{***)}	> 1.2	> 4.0	0.1

*) Defined as 1.0 for Vanadium

**) Defined as 1.0 for Nickel

***) Very rough indications, for comparison only

Unfortunately, this information is not sufficient. The method in which the poisons are deposited [2, 23, 33] and the rate with which the poisons are (de)activated, affect the dehydrogenation activity of Ni and V.

The mobility and acid site poisoning by vanadium also must be taken into account.

Consequently, we fully agree with Tatterson et al [33] who conclude that the ability of the FCC catalyst to rapidly deactivate deposited metals will be an important factor in resid cracking.

Vanadium also interacts with nickel in a manner which inhibits the deactivation behaviour of nickel; therefore, metals resistant cracking catalysts must be evaluated in the presence of both nickel and vanadium.

Considering the importance of these metal-metal and metal-catalyst support interactions, a Cyclic Deactivation procedure will be preferred in order to simulate the actual metal distribution and interactions on the catalyst surface and to mimic the correct metal age distribution [2, 23, 27, 34].

Furthermore, the presence of SO_x during the regeneration stage seems to be a factor [35] as the SO_x in the regenerator flue gas may compete with vanadium oxide in the reaction with certain compounds to non-mobile vanadate species.

We normally apply high sulphur feedstocks (High SO_x generation) in the Cyclic Deactivation procedure to include this effect in our simulation.

Also extra SO_x can be added to the catalyst during the regeneration stage.

There is only a limited amount of information on the deactivation mechanisms and rates of vanadium and nickel. The formation of metal silicates and/or aluminates have been proposed [26, 33, 34, 36], which seem to form more easily by reduction and oxidation cycles [37].

Tatterson et al [33] indicate that the sites in which nickel is easily reduced are the sites in which nickel generates the most coke and find that Ni ions in tetrahedral sites are far less active than in the octahedral sites.

Cheng et al [37] report that also for vanadium the coke selectivity can be correlated with the reducibility of vanadium.

Rajagopalan et al [38] confirm that methods involving cyclic redox aging of metals in the presence of sulphur are needed for screening metals-tolerant catalysts.

A simplified cyclic test (Mitchell method followed by cyclic propylene steaming) has been proposed which addresses the redox aging of the metal, but not the non-uniform laydown and age distribution of metals on the catalyst.

Under actual FCC conditions, the penetration and age profile of the metals will influence the efficiency of the catalyst metal trapping function [23,39,40] and consequently catalyst activity and selectivity.

Therefore, our opinion is that it is essential to simulate and/or consider the metal profile over the catalyst.

How to evaluate the high poisoning power of nitrogen.

From Table 4 we observe that nitrogen in feedstock can have a big impact on the activity of a catalyst [10, 32].

The large effect of nitrogen may be explained by blockage of a number of sites through coke formation, related to the adsorption of the nitrogen containing hydrocarbon molecules.

Ho et al [41] show that the poisoning power of a nitrogen aromatic (polar) compound is primarily determined by a balance between its size (steric hindrance) and basicity.

The former may be measured by molecular weight, the latter by proton affinity.

We have confirmed that [10] at end of run conditions of FCC pretreatment, the nitrogen left in feed can have a much higher poisoning power (smaller molecules containing nitrogen) than in the case of a non-treated nitrogen containing feedstock (nitrogen still in larger, less mobile molecules).

Catalyst testing with the high nitrogen feedstock concerned and at the relevant catalyst-to-oil ratios is essential in order to arrive at a realistic assessment of the effect of nitrogen in a specific situation.

How to evaluate catalyst deactivation by coke.

Coke is a typical example of a reversible catalyst poison.

The deactivation influence of coke depends very much on the nature of the coke, its structure and morphology and the exact location of its deposition on the catalyst surface [42, 43, 44]. Coke formation follows the adsorption of coke precursors on the catalyst surface. The adsorption depends on the strength of the interaction and the volatility of the species.

Polar sulphur, nitrogen and oxygen containing compounds will tend to be adsorbed more strongly than neutral hydrocarbons [3].

Catalyst age distribution is also a factor here as the coke deactivation is more severe for the relatively fresh catalyst, because of a larger surface area available for adsorption.

Various mechanisms of coke poisoning: active site coverage, pore filling as well as pore blockage have been observed in FCC [18, 19, 43] and percolation theory concepts have been proposed for the modelling here of [45, 46, 47, 48]. This approach provides a framework for describing diffusion and accessibility properties of randomly disordered structures.

We can model the FCC catalyst system as a combination of a shrinking core of sites not yet deactivated by coke and a progressing shell of large hydrocarbon molecules and metal contaminants, penetrating into the catalyst particle. The relative velocities of these fronts will be of great importance and will be strongly determined by the accessibility of the various functional sites of the catalyst [40].

A poor coke selectivity resulting in a high delta coke (or low cat-to-oil ratio) will aggravate the poisoning effect of the fraction of the Conradson Carbon Residue, which is converted to coke.

The amount of "soft" coke or hydrocarbons entrained to the regenerator without being stripped [3, 10] will have a significant effect on the overall coke selectivity and will depend on the surface area and pore size architecture of the aged catalyst [10, 49].

It is well known that nickel acts as a dehydrogenation agent and forms a lot of coke and hydrogen in FCC [36, 37]. The case for vanadium however is less clear.

We have confirmed that fully oxidized vanadium can be just as active as nickel for dehydrogenation.

In Table 5 the effect of a mild calcination (1hr 600 C) and more severe calcination (1hr 788 C) on the yields of two high vanadium containing equilibrium catalysts (E-cat's) are given, showing the strong increase in dehydrogenation.

Note that the effect seems more pronounced on the catalyst coming from a unit running on partial CO Combustion.

As the catalysts are not identical in composition and deactivation history we must be careful with this preliminary conclusion.

It does raise the question on what the oxidation state of Vanadium is in a commercial FCC unit, and if or how fast the vanadium is reduced and hence deactivated in the reactor riser.

Table 5. The effect of Vanadium Oxidation State on Dehydrogenation

<i>Method</i>	<i>As such</i>	<i>Calcined 600 C</i>	<i>Oxidized 788 C</i>
<u>E-cat, Partial CO Combustion</u>			
Conversion, %wt	61.1	63.2	59.8
Coke @ 68wt% conv	4.6	4.2	6.4
H ₂ @ 68wt% conv	0.30	0.23	0.53
<u>E-cat Complete CO Combustion</u>			
Conversion, %wt	61.6	58.5	60.3
Coke @ 68wt% conv	4.2	4.4	5.4
H ₂ @ 68wt% conv	0.29	0.28	0.38

References

1. Mauleon, J.L. and Sigaud, J.B.; "Characterization and selection of heavy feeds for upgrading through FCC", 12th WPC, Houston 1987, John Wiley & Sons Ltd.
2. O'Connor, P., Gevers, A.W., Humphries, A.P, Gerritsen, L.A. and Desai, P.H.; "Concepts for Future Residue Catalyst Development", ACS Symposium Series 452, Chapter 20, pg. 318, M.L. Occelli, editor, ACS Washington DC 1991.
3. Furimsky, E.; Erdöl und Kohle, Bd. 32, Heft 8, August 1979, pg. 383.
4. O'Connor, P. and Pouwels, A.C. "FCC Catalyst Deactivation: A Review and Directions for further Research" Studies in Surface Science and Catalysis, vol 88, Catalyst Deactivation 1994 Elsevier, B. Delmon and G.F. Froment (Editors)
5. John, G.S/ and Mikovsky, R.J.; Chem. Eng. Sci (1961) 15, 161, 172.
6. Chester, A.W. and Stover, W.A.; Ind. Eng. Chem., Prod. Des. Dev. (1977) vol 16, no. 4.
7. Letzsch, W.S, Ritter, R.E and Vaughn, E.V; O&GJ, 130, January 1976, pg. 130.
8. Pine, L.A., Maher, P.J. and Wachter, W.A.; J. Catal (1984) 85, pg. 466.
9. Yoo, J.S., Burk, E.H, Karch, J.A. and Voss, A.P.; Ind. Eng. Chem. Res. (1990) 29, pg. 1183.
10. O'Connor, P., Pouwels, A.C. and Wilcox, J.R.; "Evaluation of Resid FCC Catalysts" Symposium on Catalytic Cracking of Heavy Oils, paper 242E, 1992 AIChE, Annual Meeting, Miami Beach, 1-6 November 1992.
11. Voorhies, A.; Ind. Eng. Chem. (1945) 37, pg. 318-322.
12. Fu, C. and Schaffer, A.M.; Ind. Eng. Chem. Prod. Res. Dev. (1985) 24, pg. 68-75.
13. Tolen, D.F.; O&GJ, 30 March 1981, pg. 90.
14. Leuenberger, E.L.; O&GJ, 15 July 1985, pg. 125.
15. Rawlence, D.J. and Gosling, K.; Catalysis Today (1991) 11 pg. 47.
16. Keyworth, D.A., Turner, J and Reid, T.A.; O&GJ, 14 March 1988, pg. 65.
17. Beyerlein, R.A., Tamborski, G.A., Marshall, C.L., Meyers, B.L., Hall, J.B. and Higgins; B.J. "Monitoring FCC Deactivation Profile by Equilibrium Catalyst Separation", ACS Symposium Series 452, Chapter 8, pg. 109, M.L. Occelli, editor, ACS Washington DC 1991.
18. Mann, R., El-Kady, F.Y.A. and Marzin, R.; Chem. Eng. Sci. (1985) 40, no. 2, 249.

19. O'Connor, P. and van Houtert, F.W.; Paper F-8, Akzo Catalyst Symposium 1986,
The Netherlands, H.Th. Rijnten and H.J. Lovink, editors.
20. Khouw, F.H.H, Nieskens, M.J.R.C., Borley, M.J.H. and Roebischlaeger, K.H.W.;
"The Shell Residue FCC Process Commercial Experiences and Future Developments",
1990 NPRA Annual Meeting, 25-27 March '90, paper AM-90-42.
21. Beyerlein, R.A., Feng, C.C, Hall, J.B., Higgings, B.J. and Ray, G.J.;
Evolution of NFA Species during hydrothermal dealumination of USY Catalysts
Symposium Series 571, Chapter 7, pg. 81,
M.L. Occelli and P. O'Connor, editors, ACS Washington DC 1993.
22. O'Connor, P. and Pouwels, A.C.;
"Realistic FCC Commercial Catalyst Testing in the Laboratory", 8th
International Symposium on Large Chemical Plants, page 241, October
1992, Antwerpen, Belgium.
Proceedings by Royal Flemish Society of Engineerings, G. Froment,
editor.
23. Gerritsen, L.A., Wijngaards, H.N.J., Verwoert, J. and O'Connor, P.;
Catalysis Today (1991) 11, pg. 61.
24. Meyers, B.J., Fleisch, T.H. and Marshall, C.L;
Applied Surface Science (1986), 26, pg. 503.
25. Hettinger, W.P., Beck, H.W., Cornelius, E.B., Doolin, P.K., Kmecak, R.A., and Kovack, S.M.;
"Hydrothermal Screening of Reduced Crude Conversion Catalysts",
Symposium on Advances in FCC, ACS Washington, August 1983,
American Chem. Soc. Div. Petr. Chem. 28 (4), 920 (1983).
26. Occelli, M.L; "Metal Resistant FCC: Thirty Years of Research",
ACS Symposium Series 452, Chapter 21, pg. 343,
M.L. Occelli, editor, ACS Washington DC 1991.
27. Chester, A.W.; Ind. Eng. Chem. Res. (1987) 26, pg. 863-869.
28. Doolin, P.K., Hoffman, J.F. and Mitchell Jr, M.; Applied Catalysis
(1991) 71, pg. 223.
29. Pine, L.A.; J. Catal (1990) 125, pg. 514.
30. Nielsen, R.H. and Doolin, P.K.;
"Metals Passivation" in Fluid Catalytic Cracking: Science and Technology
Studies in Surface Science and Catalysis, vol. 76, 1993 Elsevier Science
Publishers B.V.
J.S. Magee and M.M. Mitchell Jr., editors.
31. Letzsch, W.S. and Wallace, D.N.; O&GJ, 29 November 1992, pg. 58.
32. Scherzer, J. and Mac Arthur, D.P.; "Ind. Eng. Chem. Res. (1988) 27, pg. 1571.
33. Tatterson, D.F. and Mievillie, R.L; "Ind. Eng. Chem. Res. (1988) 27, pg. 1595.

34. Roth, S.A., Iton, L.E., Fleisch, T.H., Meyers, B.L., Marshall, C.L. and Delgass, W.N.;
J. Catal (1987) 108, pg. 214.
35. Wormsbecher, R.F., Peters, A.W., and Maselli, J.M.; J. Catal (1986) 100, pg. 130.
36. Lam, C., O'Connor, P. and Smit, C.P.; "The Advance Catalyst Series", Akzo Catalyst Symposium 1988, The Netherlands, H.J. Lovink, editor.
37. Cheng, W.C. Juskelis, M. and Suarez, W.; Applied Catalysis A. General (1993) 103, pg. 87.
38. Rajagopalan, K.R., Cheng, W.C., Suarez, W. and Wear; C.C.; "Resid FCC Catalyst Technology: Today and Future", 1993 NPRA Annual Meeting, March 1993, AM-93-53.
39. Stockwell, D.M., Koermer, G.S. and Jaglowski, W.M.; United States Patent, 5082814, 21st January 1992.
40. O'Connor, P. and Humphries, A.P.; "Accessibility of Functional Sites in FCC", Symposium on Advances in FCC, ACS Chicago, August 1993. American Chem. Soc. Div. Petr. Chem. (1993) 38, no. 3, pg. 598.
41. Ho, T.C., Katritzky A.R. and Cato, S.J.; Ind. Eng. Chem. Res. (1992) 31, pg. 1589.
42. Menon, R.G.; J. of Mol Catalysis (1990) 59, pg. 207.
43. Dean, J.W. and Dadyburjor, D.B.; Ind. Eng. Chem. Res. (1989) 28, pg. 271.
44. Ho, T.C.; Ind. Eng. Chem. Res. (1992) 31, pg. 2281.
45. Uguina, M.A., Serrano, D.P., van Grieken, R. and Venes, S.; Applied Catalysis A: General (1993) 99, pg. 97.
46. Froment, G.F; "A quantitative Approach of Catalyst Deactivation by Coke Formation", Proceedings International Symposium on Catalyst Deactivation, Elsevier, Amsterdam 1980.
47. Sahimi, M.A. and Tsotsis; T.T.; J. Catal (1985) 96, pg. 552.
48. Reyes, S.C. and Scriven, L.E.; Ind. Eng. Chem. Res. (1991) 30, pg. 71.
49. O'Connor, P. and Yanik, S.J.
Resid FCC Operating Regimes and Catalyst Selection
Akzo Nobel Catalyst Symposium, Noordwijk 1991 edited by S. Docter

Sodium Deactivation of Fluid Catalytic Cracking Catalyst

Xinjin Zhao and Wu-Cheng Cheng

Washington Research Center, Grace Davison, W. R. Grace and Company—Conn., 7500 Grace Drive, Columbia, MD 21044

The mechanism of FCC catalyst deactivation by sodium is addressed in this paper. In commercial units, sodium is found to deactivate the matrix surface area significantly but no significant trend was observed for the effect of sodium on the zeolite surface area of equilibrium catalysts. On the other hand, the effect of sodium is more pronounced on zeolite and much less severe on matrix surface area in the typical laboratory deactivation protocol. The differences are explained by the mobility of sodium on catalysts. Significant interparticle migration of sodium is observed both commercially and in laboratory deactivated catalysts. The loading of sodium is associated with the available sites of the particular fraction of that catalyst. In commercial units, sodium preferentially migrates to the freshly added catalyst due to its greater availability of exchange sites. The effect of catalyst sodium and feed sodium are simulated in the laboratory and their effect on catalyst activity and cracking yields are discussed.

Sodium on fluid cracking catalyst, FCC, comes from the raw materials used in the catalyst manufacturing process as well as salt contamination in the feedstock. Sodium can deactivate cracking catalysts by poisoning the acid sites on the matrix and zeolite and by promoting sintering of silica-alumina (1). Sodium can act synergistically with vanadium to accelerate the destruction of zeolite (2).

The relationship between cracking activity and sodium level of zeolites is complicated and seems to depend on the type of feedstock and catalyst

pretreatment conditions. Sodium addition drastically reduces the activity of dealuminated Y-zeolite (USY) for alkane cracking (3-5). This is consistent with the notion that cracking of small alkanes requires strong Brønsted acid sites, and the addition of sodium effectively neutralizes these sites. Several authors have found that sodium addition does not decrease the activity of USY for gas oil cracking, a much more facile reaction. However, sodium addition on USY does influence gasoline composition and product selectivity of gas oil cracking (5-8). Differences in activity and selectivity have been observed for sodium added to zeolite before and after hydrothermal deactivation, implying that sodium on fresh catalyst and sodium from feedstock behave differently (7).

Investigations of sodium poisoning of amorphous silica-alumina catalysts show that activity loss is not a linear function of sodium content, being more rapid at low Na concentration and leveling off at higher Na concentration. This suggests that the strongest and most accessible sites are poisoned by Na first (1,9). Physical blocking of adjacent sites has also been proposed (10).

The present day FCC catalyst consists typically of a USY zeolite in a silica-alumina matrix. The matrix can have a range of surface area and cracking activity (11). At the regenerator temperature, sodium has a solid state diffusion coefficient of 10^{-6} to 10^{-7} cm^2s^{-1} (12) and is expected to move easily within a catalyst particle. The distribution of Na between zeolite and matrix and its effect on the stability of each component under these conditions is of interest. Furthermore, in the presence of steam, interparticle migration of volatile Na species is expected. The mechanism of this process has not been investigated. A greater understanding of these processes will aid catalyst manufacturers in designing a more sodium-tolerant catalyst.

In this paper we have examined commercial equilibrium catalysts (Ecat) to look for correlations between zeolite and matrix area stability of various catalyst families as a function of sodium. We have performed density separation of Ecat samples to measure the sodium distribution as a function of catalyst age. Finally, we have revisited the issue of whether fresh catalyst sodium is equivalent to feedstock sodium in its influence on zeolite stability, catalytic activity and selectivity.

Experimental Methods

Commercially deactivated FCC Ecats of varying matrix types and containing a wide range of sodium were characterized by t-plot surface area (ASTM D4365-85) to determine the effect of Na on zeolite and matrix area stability. The Ecats were also examined by electron microprobe (Cameca SX50) to determine the Na distribution within a catalyst particle. Some of the Ecats were separated into eight age fractions based on a modified sink/float procedure described in the literature (13,14). Each age fraction was analyzed by ICP, t-plot and zeolite unit cell size (ASTM D3942-91).

To determine if we could simulate in the laboratory the effect of sodium on commercially deactivated FCC catalysts, we prepared catalysts containing Na in the range of 0.22 to 0.41 wt% by modifying the catalyst washing procedure and deactivated the samples at 1088 K for 4 hours under 1 atm of steam. This steaming procedure is commonly used to prepare deactivated catalysts with physical properties (zeolite and matrix surface areas and unit cell size) that match commercial Ecats.

The above procedure of incorporating sodium to fresh catalyst has an inherent shortcoming. Sodium from FCC feedstock accumulate on catalysts which have been hydrothermally aged. During hydrothermal aging, the zeolite unit cell size decreases from above 24.50 Å to typically lower than 24.30 Å, the surface area of both zeolite and matrix decreases and transformation of kaolin clay to metakaolin occurs.

To demonstrate this effect we prepared the following two catalysts. Catalyst A was a 50 wt% USY silica sol catalyst, washed and exchanged with ammonium sulfate to 0.49 wt% Na₂O on catalyst. Catalyst B was the same catalyst, washed and exchanged with ammonium sulfate to 0.17 wt% Na₂O on catalyst. Both catalysts were steamed for 4 hours at 1088 K. Subsequently, the steam-deactivated Catalyst B was impregnated with sodium carbonate, to bring its sodium content to the same level as Catalyst A, and calcined in air for 2 hours at 810 K. These samples, which we shall refer to as Catalyst A' and Catalyst B', were evaluated by standard microactivity (ASTM D-3907) on a Sour Imported Heavy Gas Oil (SIHGO). Properties of the feedstock are shown in Table 1. To determine if and how rapid the impregnated sodium would redistribute on the catalyst under FCC regenerator conditions, we further steamed Catalyst A' and Catalyst B' for 4 hours at 1088 K. These samples, which we shall refer to as Catalyst A'' and Catalyst B'' were again evaluated by microactivity.

Results and Discussion

Effect of Sodium on FCC Ecat Matrix and Zeolite Surface Areas As part of our technical service program, Grace Davison analyzes commercially deactivated equilibrium catalysts from FCC units worldwide. Due to differences in feed quality and unit operation, equilibrium catalysts from different FCC units contain varying levels of sodium, even though the sodium on fresh catalyst may be similar.

Figure 1 shows the matrix surface area of commercially aged Ecat for four types of cracking catalyst. Each set of data represents one type of cracking catalyst deactivated in different commercial FCC units. The four types of catalysts were chosen for their wide range of matrix surface areas. Although the fresh catalyst matrix surface area for each catalyst type is similar, the equilibrium matrix surface area decreases by as much as fifty percent with increasing Na. The variation of matrix surface could be attributed to other

Table 1. Properties of Sour Imported Heavy Gas Oil

API Gravity, @ 289 K	22.5	Simulated Distillation, Vol%, K	
Aniline Point, K	346	IBP	490
			20
			616
Sulfur, wt%	2.59	40	655
Total Nitrogen, wt%	0.086	60	696
Basic Nitrogen, wt%	0.034	80	745
		FBP	826
n-d-m Analysis			
Cp	59.5	K Factor	11.52
Cn	18.0		
Ca	22.4	Conradson Carbon, wt%	0.25

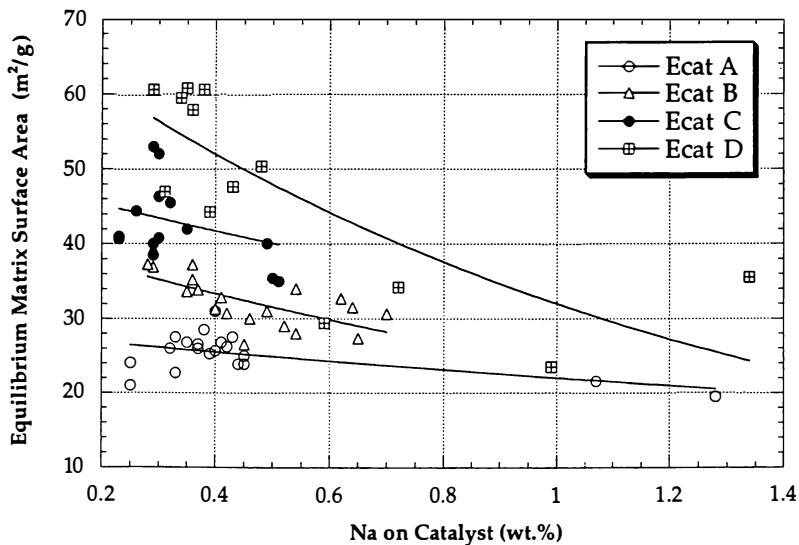


Figure 1. Effect of Sodium on Ecat Matrix Surface Area

causes, but comprehensive analyses of a vast amount of data showed that sodium level on the equilibrium catalysts had the most significant effect on the matrix surface area. Analyses also showed that the effects of nickel or vanadium on matrix surface areas were minimal for this particular catalyst (Figures 2-3). Similar results were observed for all four catalyst families. These results indicate that sodium is very effective in promoting the sintering of FCC matrices.

Figure 4 shows the effect of sodium on Ecat zeolite surface area. It is clear that zeolite surface area does not correlate well with the level of sodium on catalysts. Part of the reason for the poor correlation could be due to the differences in fresh catalyst addition rates for different commercial units. It might also mean that matrix surface area is mostly affected by sodium level, while zeolite surface area is more determined by other factors. Since the equilibrium catalysts were from many different commercial units, the severity in the units can have a strong influence on the zeolite stability. A typical fresh FCC catalyst contains about 0.3 wt.% sodium on catalyst. Most of the sodium in fresh catalysts is ion-exchanged on the acid sites of the zeolite. During use, under commercial conditions, the number of acid sites in the zeolite decreases due to dealumination, and the sodium migrates out of the zeolite. Most of the loss in zeolite surface area occurs early in the life of the catalyst, when the zeolite unit cell is high and the sodium is concentrated on the zeolite. Our results suggest that once the zeolite reaches its equilibrium cell size, it is very stable with respect of gradual sodium build-up.

Matrix and Zeolite Deactivation for Laboratory Deactivated Catalysts

Figure 5 shows the measured zeolite and matrix surface areas of a series of catalysts, with varying exchanged sodium content, after laboratory hydrothermal deactivation for 4 hours at 1088K. Surprisingly, the matrix surface area did not change at all with increasing sodium level. However, the steamed zeolite surface area was significantly reduced with increasing level of sodium. An increase of Na from 0.22 wt.% to 0.41 wt.% reduced the steamed zeolite surface area from 86 m²/g to 62 m²/g.

There are several possible explanations for the difference in commercial and laboratory deactivation by sodium. One possibility is that sodium on commercially aged and laboratory impregnated samples resides on different sites of the catalyst. Impregnated sodium on fresh catalyst tends to be concentrated on the zeolite due to its much greater availability of exchange sites, where upon steam deactivation, it destroys the zeolite but not the matrix. Feed sodium builds up gradually on catalyst, causing sintering of the matrix but not the zeolite. Consequently, the observed deactivation effect would be different. Another reason may be that the activation energy for matrix sintering and zeolite destruction are very different. Therefore, the high temperature laboratory deactivation protocol preferentially deactivates zeolite.

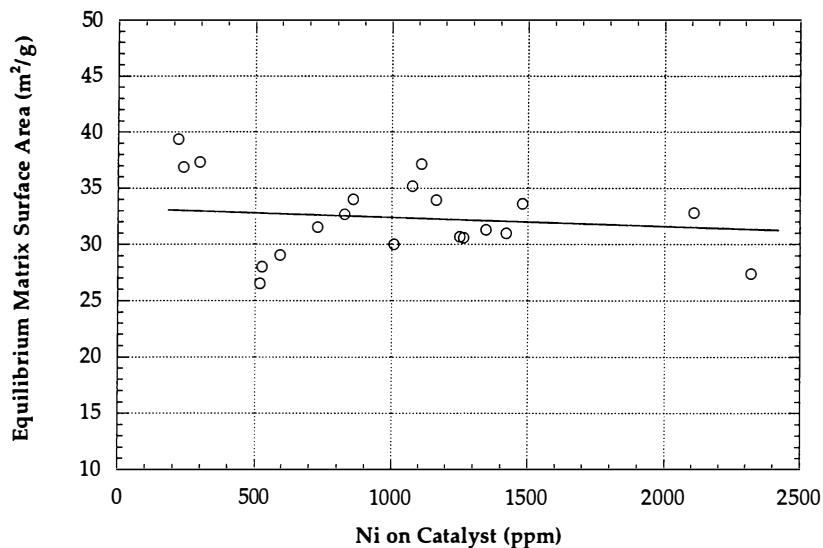


Figure 2. Effect of Nickel on Ecat Matrix Surface Area

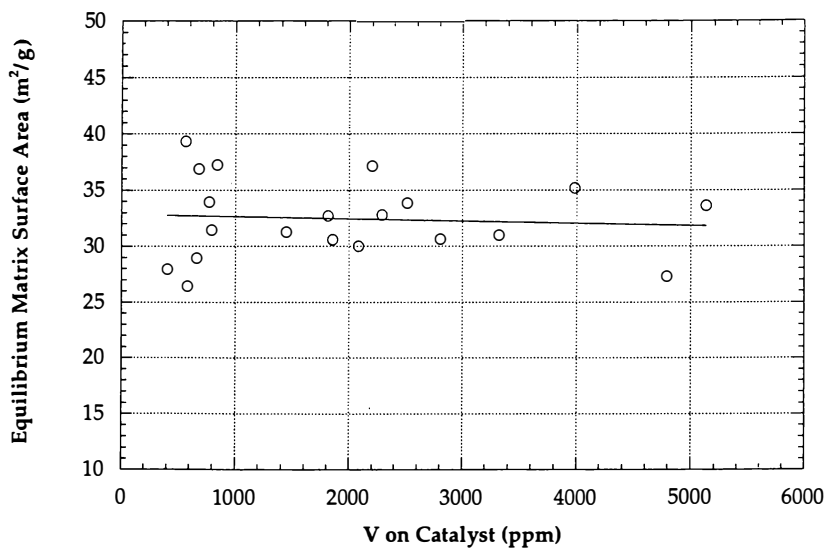


Figure 3. Effect of Vanadium on Ecat Matrix Surface Area

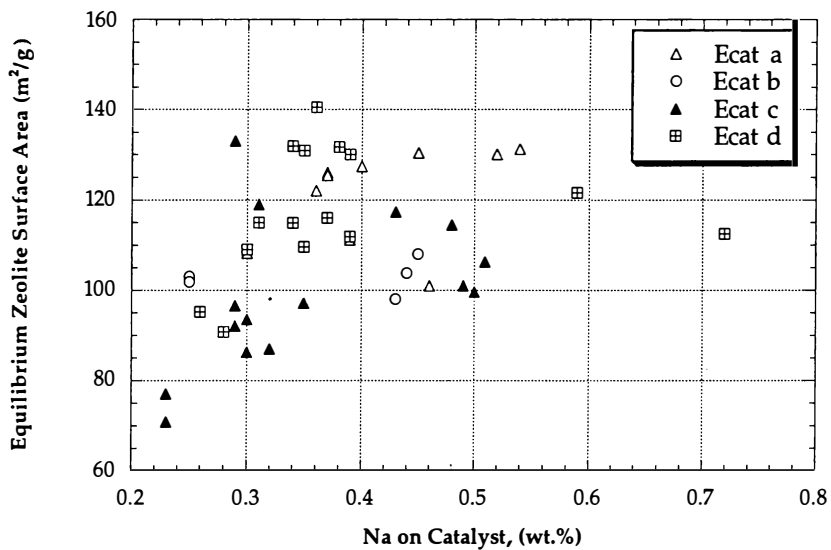


Figure 4. Effect of Sodium on Ecat Zeolite Surface Area

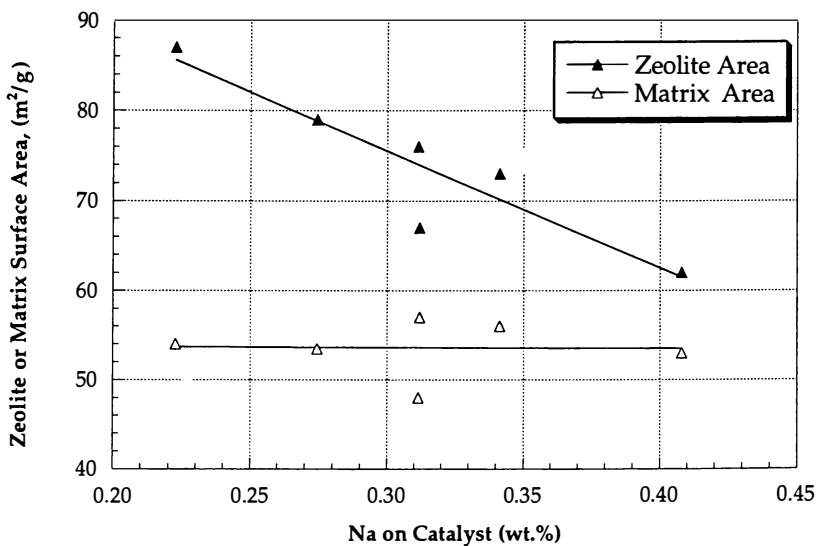


Figure 5. Effect of Sodium on Laboratory Catalyst Deactivation

Interparticle and Intraparticle Mobility of Sodium In order to explore the distribution of sodium on catalysts, we separated an Ecat sample with 0.3 wt% Na into eight age fractions and analyzed each fraction by ICP, t-plot and zeolite unit cell size. We had chosen an FCC unit which had been on the same catalysts for an extended period of time to ensure that the inventory had been completely turned over at the time the sample was withdrawn. Table 2 shows the analysis of all the fractions. Intuitively, one would expect the heavier fraction, or the older fractions, to contain more sodium than the lighter, or the younger fractions. The results indicate the exact opposite. As shown in Table 2, the lightest fraction (fraction A) contains almost 60% more sodium than the heaviest fraction (fraction H). This indicates that the feed added sodium does not accumulate on catalysts. Rather, it is very mobile and only deposits or accumulates on preferred sites. Since the lighter or the younger fractions contain more zeolite and more exchange sites, they have a higher capacity to adsorb sodium. Although fraction A showed over three times more zeolite surface area than fraction H, it did not contain three times as much sodium as fraction H. This suggests that not all sodium species are mobile. Some of the sodium must be trapped in the matrix. We will discuss later that sodium may have reacted with alumina or kaolin to form some stable species in the matrix.

A typical electron microprobe analysis of FCC Ecat is shown in Figure 6. Sodium tends to be uniformly distributed across an FCC particle, even on a sample with as high as 1.4 wt% Na. This suggests that surface or bulk diffusion of Na on FCC catalyst is very rapid.

Effect of Na on Fresh and Steam Deactivated Catalysts Properties of the two USY silica sol catalyst samples, having different method of sodium incorporation, are shown in Table 3. Both samples had similar zeolite and matrix surface areas and zeolite unit cell size after 4 hours at 1088K steaming. However, Catalyst A' had a significantly higher microactivity--about 50% higher on a second order kinetic conversion basis than Catalyst B'. Moreover, upon further steaming of both of these samples for 4 hours at 1088K, Catalyst A'' still maintained 37% higher kinetic conversion than Catalyst B'', although again the two samples had similar zeolite and matrix areas and zeolite unit cell size. The method of sodium addition also has an effect on the product selectivity and gasoline octane (Table 4). By and large however, these results are very similar to that reported by Edwards et. al. (7).

These results, along with the data in Figure 2, strongly suggest that the addition of Na to hydrothermally aged catalysts has minor destabilizing effect on the zeolite structure. Its primary effect is to poison the acid sites, and thus lower the catalytic activity. The results also indicate that sodium on fresh catalyst is less of a poison to catalytic activity than sodium added after hydrothermal aging. The diffusivity of sodium ions in silica aluminas at 1088K is in the order 10^{-6} to 10^{-7} cm^2s^{-1} (12). If all Na species were mobile, we would expect Na to be uniformly distributed throughout all the sites in the order of

Table 2. Density Separation of Equilibrium Catalyst

Fraction	A	B	C	D	E	F	G	H	E-cat
Wt% in Fraction	15.9	9.3	20.0	12.0	13.6	9.7	11.1	7.9	100.0
CHEMICAL ANALYSES:									
Al ₂ O ₃ : Wt%	42.4	42.8	43.3	43.5	43.6	43.5	43.5	44.6	44.1
Na : Wt%	0.37	0.34	0.33	0.31	0.30	0.28	0.26	0.23	0.30
Ni : ppm	368	607	757	1111	1366	1773	2042	2684	1240
V : ppm	1710	2250	2500	2760	2890	3080	3390	4020	3190
PHYSICAL ANALYSES:									
Sa : M2/GM	202	181	169	150	136	113	93	62	143
Zeolite : M2/GM	169	151	142	126	115	96	78	51	121
Matrix : M2/GM	33	30	27	24	21	17	15	11	22
Unit Cell : A	24.29	24.24	24.25	24.23	24.22	24.24	24.20	24.21	24.25

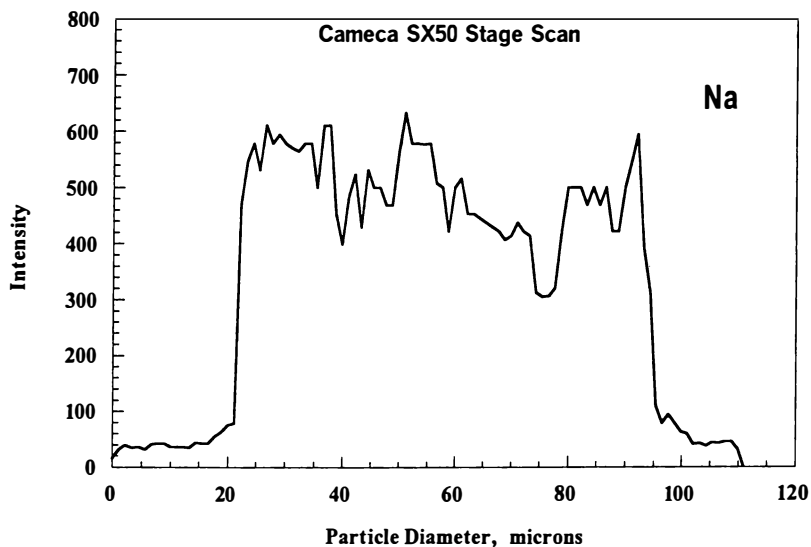


Figure 6. Microprobe Analysis of Sodium Distribution in Ecat

minutes. However, even after 4 hours of steaming at 1088K, the sample which had been post-impregnated with sodium was still less 37% less active than the sample with all of the sodium on the fresh catalyst.

This evidence suggests that not all Na species are mobile. Some Na species must in fact have reacted irreversibly with components on the catalyst, leaving it unavailable to poison the acid sites. It is likely that these reactions occur during the early stages of hydrothermal deactivation. The exact mechanism is unclear, but may involve reactions with extraframework alumina. As the zeolite dealuminates from 24.55 to 24.25Å unit cell size, approximately 65% of the initial framework alumina (about 15 wt% of the zeolite) comes out of the zeolite structure. Sodium, which also must leave the exchange sites as the zeolite dealuminates may react with this very reactive form of alumina. The other possibility is that as kaolin undergoes its transition to metakaolin at 800K

Table 3. Catalyst Properties: Effect of Na on Fresh Catalyst vs. Na Impregnation After Hydrothermal Aging

	Catalyst A	Catalyst B
Analyses		
%Na ₂ O	0.49	0.17
%Al ₂ O ₃	25.50	26.40
%RE ₂ O ₃	0.04	0.02
Zeolite Area (m ² /g)	279	281
Matrix Area (m ² /g)	48	49
Treatment	Catalyst A' 4 Hr at 1088 K Steam of Catalyst A	Catalyst B' 4 Hr at 1088 K Steam of Catalyst B Na ₂ CO ₃ Impreg 2 Hr at 810 K Calcination
Analyses		
%Na ₂ O	0.47	0.47
Zeolite Area (m ² /g)	176	184
Matrix Area (m ² /g)	29	31
Unit Cell Size (Å)	24.23	24.25
MAT Activity (C/O=4)	61	51
Kinetic Conversion	1.56	1.04
Treatment	Catalyst A'' 4 Hr at 1088 K Steam of Catalyst A'	Catalyst B'' 4 Hr at 1088 K Steam of Catalyst B'
Analyses		
Zeolite Area (m ² /g)	158	164
Matrix Area (m ² /g)	24	23
Unit Cell Size (Å)	24.22	24.23
MAT Activity (C/O=4)	52	44
Kinetic Conversion	1.08	0.79

(15) it reacts with sodium to form sodium metakaolin. High temperature stable $\text{Na}_2\text{O}-\text{Al}_2\text{O}_3-\text{SiO}_2$ are known (16). However, once the extraframework alumina and the metakaolin have aged and sintered, they become less reactive to added sodium.

Conclusions

Sodium deactivates FCC catalysts by three separate mechanisms: poisoning of acid sites, enhancing the sintering of matrix, and accelerating the destruction of

Table 4. Microactivity Yield Comparison: Effect of Na on Fresh Catalyst vs. Na Impregnation After Hydrothermal Aging

	Catalyst A'	Catalyst B'
Wt % Conversion	60.0	60.0
Catalyst/Oil Ratio	3.9	5.2
Interpolated Yields		
H2	0.05	0.07
Tot C1+C2	1.7	1.8
C3=	3.8	3.8
Total C3s	4.6	4.4
Isobutylene	1.5	1.8
Total C4=	5.4	5.8
iC4	2.8	2.1
Total C4s	8.7	8.4
C5+Gaso	43.1	43.3
LCO	23.0	24.2
640+Btms	17.0	15.8
Coke W% Feed	1.9	2.1
Gasoline Composition		
n-Paraffins	4.9	4.7
Iso.Paraffins	32.3	29.6
Olefins	22.0	26.3
Naphthenes	8.8	8.8
Aromatics	32.0	30.6
GC RON	90.6	91.0
GC MON	80.3	80.1

zeolite. The predominant mechanism depends on the method of sodium addition. Sodium added to the fresh catalyst (above 1% on zeolite) tends to decrease zeolite but not matrix surface area. Sodium added after hydrothermal dealumination act mainly as an acid site poison for the zeolite. Sodium in commercially aged Ecat decreases the matrix surface area. Interparticle transport of sodium occurs readily in commercial FCC units. Sodium tends to migrate to particles with greatest number of acid sites. One has to be careful in interpreting results on laboratory simulated sodium effects on FCC catalyst deactivation.

Acknowledgments

The authors are grateful to P. M. Erbe for laboratory assistance and Grace Davison for permission to publish this work.

References

1. Letsch, W. S., and Wallace, D. N., *Oil & Gas J.*, 80, 56 (1982).
2. Pine, L. A., *J. Catal.*, 125, 514 (1990).
3. Fritz, P. O., and Lunsford, J. H., *J. of Catal.*, 118, 85, (1989).
4. Shertukde, P. V., Marcelin, G., Sill, G. A., and Hall, W. K., *J. Catal.*, 136, 446 (1992).
5. Kumar, R., Cheng, W.-C., Rajagopalan, K., Peters, A. W., and Basu, P., *J. Catal.*, 143, 594 (1993).
6. Pine, L. A., Maher, P. J., and Wachter, W. A., *J. of Catal.*, 85, 466 (1984).
7. Edwards, G. C., Rajagopalan, K., Peters, A. W., Young, G. W., and Creighton, J. E., *ACS Symposium Series*, 375, 101 (1988).
8. Corma, A., *Catal. Lett.*, 22, 39 (1993).
9. Benesi, H. A., and Winquist, H. C., *Adv. Catal.*, 27, 97 (1978).
10. Fort, T. and Nebesh, E., *J. Catal.*, 11, 91 (1968).
11. Rajagopalan, K., and Habib, E. T. Jr., *Hydrocarbon Processing*, Sept., 43, (1992).
12. Johnson, J. R., Bristow, R. H., and Blau, H. H., *J. Am. Ceram. Soc.*, 34, 165 (1951).
13. Beyerlein, R. A., Tamborski, R. A., Marshall, C. L., Meyers, B. L., Hall, J. B., and Huggins, B. J., *ACS Symposium Series*, 452, 694 (1990).
14. Palmer, J. L., and Cornelius, E. B., *Appl. Catal.* 35, 217 (1987).
15. Brindley, G. W. and Nakahira, M., *J. Am. Ceram. Soc.*, 42, 314 (1959).
16. de Pablo, L., and Foster, W. R., *J. Am. Ceram. Soc.*, 42, 491, (1959)

Contaminant-Metal Deactivation and Metal-Dehydrogenation Effects During Cyclic Propylene Steaming of Fluid Catalytic Cracking Catalysts

Lori T. Boock, Thomas F. Petti, and John A. Rudesill

Washington Research Center, Grace Davison, W. R. Grace and Company—Conn., 7500 Grace Drive, Columbia, MD 21044

Recent work on laboratory catalyst deactivation in the presence of Ni and V by cyclic propylene steaming (CPS) has shown that a number of conditions affect the dehydrogenation activity and zeolite destruction activity of the individual metals. These conditions include final metal oxidation state, overall exposure of the metal to oxidation, the catalyst composition, the total metal concentration and the Ni/V ratio. Microactivity data, which show dramatic changes in coke and hydrogen production, and surface area results, which show changes in zeolite stability, are presented that illustrate the effect each of these conditions has on the laboratory deactivation of metals. The CPS conditions which are adjustable, namely final metal oxidation state and overall exposure of the metal to oxidation are used as “variables” which can control the metal deactivation procedure and improve the simulation of commercial catalyst deactivation. In particular, the CPS procedure can be modified to simulate both full combustion and partial combustion regeneration.

One of the challenges in evaluating new FCC catalyst technologies has been in simulating how the catalyst will perform after being deactivated in a commercial FCC unit. As resid processing becomes more prevalent, the issue of metal contaminants and metal deactivation takes on even more importance. In a commercial FCC unit, metal contaminants, particularly Ni and V are deposited on the catalyst from the feedstock. These metals initially have high dehydrogenation activity. They can also react with and destroy the zeolite in the catalyst (1). As the catalyst ages,

the dehydrogenation activity and the zeolite destruction activity is greatly reduced. However, even the most complex laboratory deactivation procedures take only 2-3 days; thus, these metals are typically much more active than in a commercial unit. Development of a laboratory deactivation procedure that better simulates Ecat (equilibrium catalyst) performance is the objective of this work. Zeolite surface area, microactivity (MA) and MA coke and hydrogen yields are the tools which measure our success.

An early attempt to simulate metals deactivation was the introduction of the Mitchell method steam deactivation procedure (2). This procedure involved impregnation of catalysts with Ni and V naphthenates, followed by steaming in the presence of air. While this method was easy to implement and did allow comparison of catalysts in the presence of metal contaminants, both the destruction of the zeolite and the metal dehydrogenation activity was greatly over-predicted (3, 4) in both MAT and riser testing.

Cyclic methods which mimic commercial fluid, such as cyclic metal impregnation (CMI) have also been introduced (3). These methods improve on the Mitchell method procedure by exposing the catalyst to both oxidation and reduction conditions and imposing an age distribution on the metals. This greatly reduces the destruction of the zeolite (4), but the metal dehydrogenation activity is still higher than on an Ecat, particularly in MA testing. Additionally, methods such as CMI, which use a feedstock to deposit the metals on the catalyst, are time-consuming, difficult to implement and have less than satisfactory reproducibility.

In an earlier work, we introduced cyclic propylene steaming (CPS) as an alternative to CMI (5). This procedure gave large improvements over the Mitchell method deactivation procedure but is just as easy to implement. Catalyst evaluated by the CPS procedure gave similar yields and activities to the CMI procedure, with much better reproducibility. However, when compared to Ecats, particularly high metal Ecats, CPS still over-predicts MA coke and hydrogen yields. Despite this drawback, this tool is the most promising for catalyst evaluations in the presence of metals. Developments which address the shortcomings and improve on the CPS procedure will be described herein.

An additional complication in simulating laboratory deactivated catalysts that match commercial Ecats is the fact that commercial FCC units are operated very differently. One difference which may have dramatic effects on ZSA retention, activity, and coke and hydrogen yields (especially for high metals operations) is full versus partial combustion regeneration. The laboratory deactivation procedures discussed above are all based on mimicking full combustion regeneration and comparisons are to Ecats from full combustion units. However, in developing the CPS deactivation procedure, we are targeting the ability to simulate Ecats from both full and partial combustion FCC units.

CPS Deactivation

Procedure The standard CPS procedure involves impregnating the catalysts with metal naphthenates before steaming, followed by alternate exposure of the catalyst to streams containing oxidizing and reducing gases. The standard redox cycles consist of:

- 10 minutes 50 wt% nitrogen, 50 wt% steam
- 10 minutes 50 wt% 5% propylene in nitrogen, 50 wt% steam
- 10 minutes 50 wt% nitrogen, 50 wt% steam
- 10 minutes 50 wt% 4000 ppm SO₂ in air, 50 wt% steam

These cycles are repeated up to 30 times to give a total run time of 20 hours.

Both CPS deactivated catalysts and Ecats are tested in the microactivity unit (modified ASTM D 3907-87) where activity and yields are measured. Catalyst surface areas (total, zeolite and matrix) are also measured by the t-plot procedure (6)

Comparison of CPS to Ecat Ecats from two different FCC units was compared to the same catalyst that was deactivated by standard CPS at comparable metal levels. Both units were operated in full combustion. The two catalysts were different grades with similar Ni (≈ 700 ppm), but different V (600 vs. 2000 ppm) levels. Figures 1 and 2 display the MA coke and hydrogen yields, at constant conversion versus V levels. At the low V level, the CPS deactivated catalyst produced $\approx 5\%$ more coke and $\approx 45\%$ more hydrogen than the Ecat, whereas at the high V level, the CPS deactivated catalyst produced 40% more coke and 70% more hydrogen than the Ecat. Since the Ni levels were similar, we conclude that this additional coke penalty is due to V dehydrogenation activity.

Thus one weakness of the standard CPS procedure is that it over-emphasizes the V dehydrogenation activity compared to the corresponding Ecat as measured in MA testing. Figure 3 shows a graphical representation of the current CPS status summarizing the data shown in Figures 1 and 2 and Table I. It is clear from this figure that the ability to independently control the position of the CPS envelope on both the activity and the coke/hydrogen axes by varying the laboratory deactivation conditions is a desirable objective.

Factors that Influence Metals Tolerance Differences

Catalysts As any catalyst manufacturer will divulge, there are clear differences in the metals tolerance behavior of different catalyst grades. Catalysts are often designed to be tolerant to a specific metal, such as Davison's Ni tolerant technology. Thus, in addition to the ability to

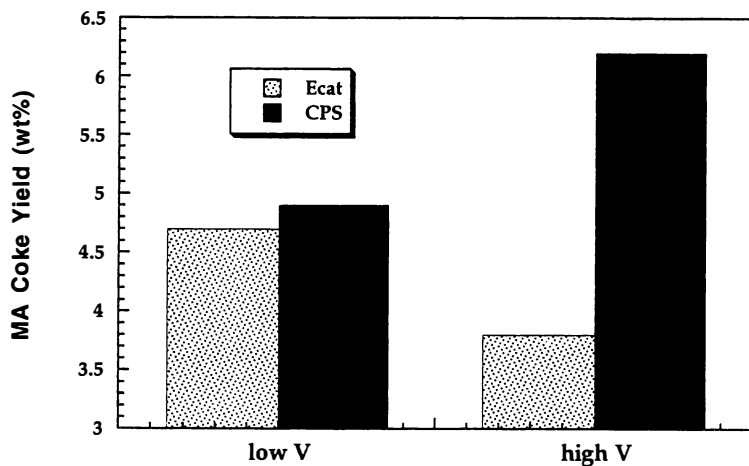


Figure 1. Comparison of Ecat and CPS Deactivated Catalyst MA Coke Yields vs. V Level, illustrating poor match at high V levels

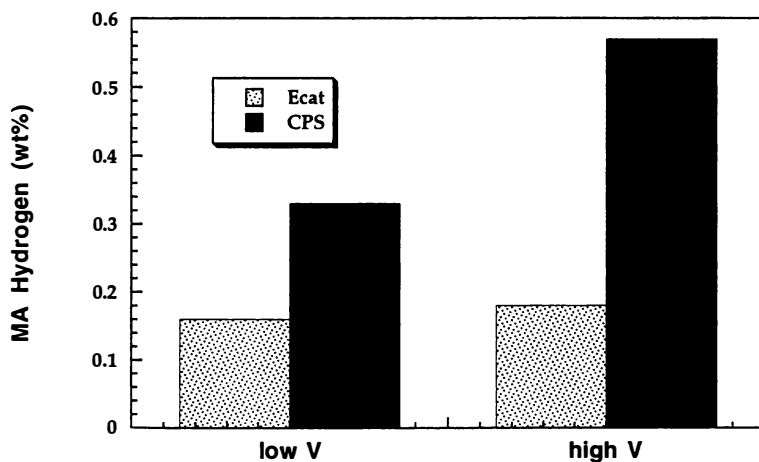


Figure 2. Comparison of Ecat and CPS Deactivated Catalyst MA Hydrogen Yields vs. V Level, illustrating poor match at high V levels

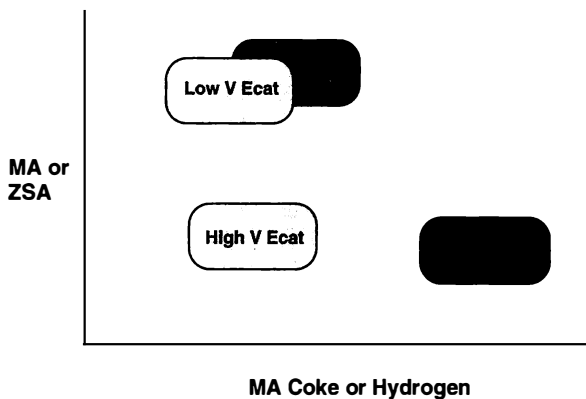


Figure 3. The Current Status of CPS

Table I. Comparison of Ecat and CPS Deactivated Catalyst MA Activity and Catalyst Properties, illustrating poorer match at high V levels

	Low V Ecat	CPS	High V Ecat	CPS
MA	70	70	65	65
C/O	4.5	5.0	3.4	4.9
ZSA	172	163	152	132
MSA	47	43	33	33
unit cell size, μ	24.25	24.23	24.23	24.23

simulate commercial Ecats, a laboratory deactivation procedure must also be able to resolve differences in the metal tolerance of different catalysts. This is necessary if commercial performance of the catalyst is to be predicted.

The standard CPS procedure is able to discern how the different catalysts respond to both Ni and V. A series of experiments were performed comparing a conventional catalyst with a Ni-tolerant catalyst, at varying Ni and V levels. The resulting coke factors (slope of MA coke vs. kinetic activity) were fit to a model and the resulting curves are shown in Figures 4 and 5. The contaminant coke produced by the conventional catalyst from Ni increases rapidly at low Ni levels, only leveling off at very high Ni levels. However, on the Ni-tolerant catalyst, the contaminant coke from Ni is very flat at all Ni concentrations. The V contaminant coke curves are similar for both catalysts, with the conventional catalyst producing more coke from V at high V levels and the Ni tolerant catalyst producing more coke at low V levels.

These differences in the contaminant coke produced by the individual metals on the two catalysts result in very different Ni/V dehydrogenation ratios (DHR), also shown on the plots in Figures 4 and 5. At low metal levels, the DHR is high on the conventional catalyst, but it decreases as the coke produced by Ni levels off and the coke produced by V increases. Here again we see the over-emphasis of V activity at high V levels. However, the DHR is always greater than one at the conditions studied. On the other hand, the DHR for the Ni-tolerant catalyst is relatively constant and always less than one. This is due in part to the high Ni-tolerance of the catalyst and in part to the over-emphasis of V by the CPS procedure. An important consequence of this work is that the industry accepted Ni/V dehydrogenation ratio of "4" may not be applicable for all catalysts, and will vary with metal levels and FCC operating conditions.

Metal Oxidation State In a commercial FCC unit, the catalyst is exposed to oxidizing and reducing conditions numerous times. It is this oxidation/reduction which is believed to have a large impact on the deactivation of the metals (4, 7). This is why both CMI and CPS deactivation give improved metal deactivation over the Mitchell Method. Additionally, early patents (8) have suggested oxidizing or reducing a metal containing catalyst after steaming can also have a large affect on coke and hydrogen selectivities. Thus it seems that the final oxidation state of the metals may be an important factor affecting the metal tolerance of catalysts.

In order to explore this hypothesis, we examined the oxidation state of the metals on the catalyst after CPS as compared to Ecats using temperature programmed reduction (TPR). We found that the metals on the CPS catalysts (both V, and to a lesser extent Ni) were in a higher oxidation state than the metals on Ecat, even for a high excess oxygen FCC regenerator. Based on this result, the standard CPS procedure was

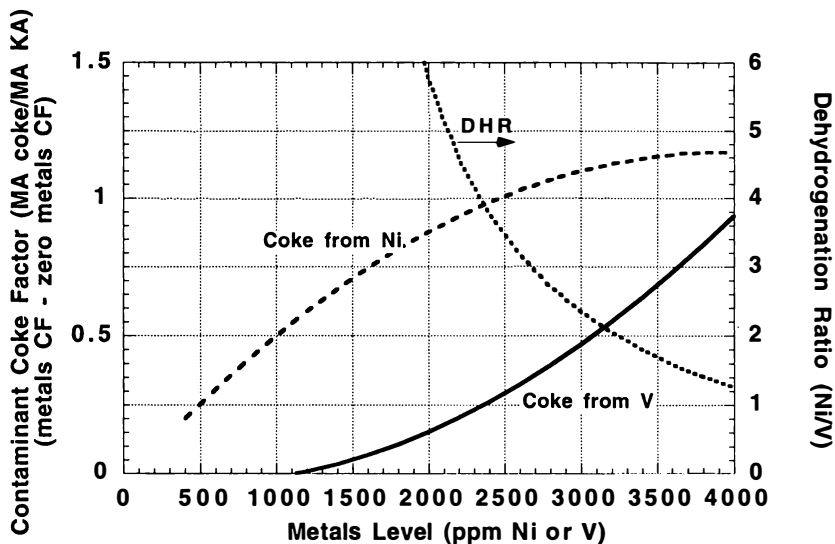


Figure 4, Comparison of Contaminant MA Coke from Ni and V (Conventional Catalyst) - Calculated dehydrogenation ratio (DHR) varies

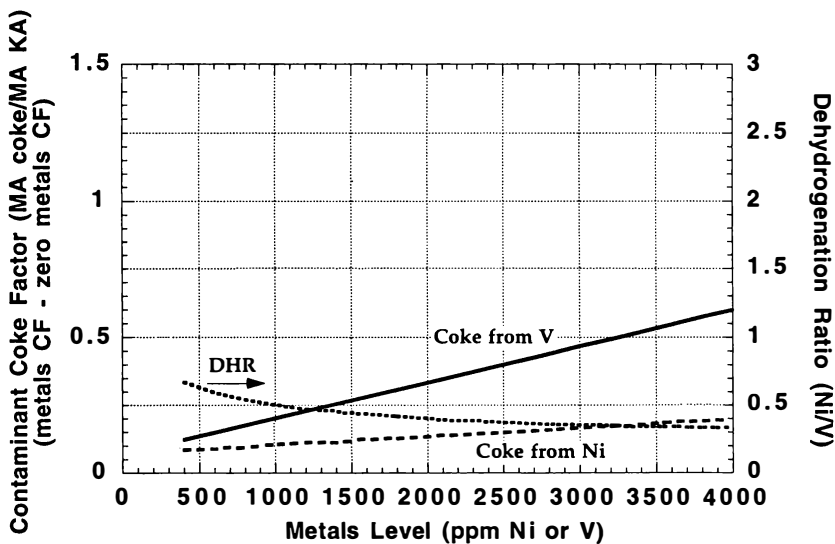


Figure 5. Comparison of Contaminant MA Coke from Ni and V (Ni-Tolerant Catalyst) - Calculated DHR varies (and is <1)

modified to end on a reduction cycle (propylene in nitrogen) rather than an oxidation cycle (air). This procedure should better simulate a commercial FCC unit, since our findings showed that even the best "full burn" FCC regenerator does not fully oxidize all the metals, whereas the CPS regeneration cycle does.

The effect of this change in CPS procedure was explained with a Ni-tolerant catalyst impregnated with either 3000 ppm Ni or 3000 ppm V. The catalyst was steamed by both the standard and modified CPS procedure. Figures 6 and 7 display the resulting MA coke and hydrogen selectivities, respectively. Clearly, on this Ni-tolerant catalyst, changing the final oxidation state of the V from oxidized to reduced has a dramatic effect on MA coke and hydrogen yields. The decrease in both MA coke and hydrogen is in effect de-emphasizing the role of V as a dehydrogenation catalyst, bringing the CPS procedure more in line with commercial Ecats. However, changing the state of the Ni from oxidized to reduced has a much smaller effect (and may even be in the opposite direction). The small effect of Ni may be attributed to the high Ni-tolerance of this catalyst. A conventional catalyst may show a larger coke and hydrogen effect as the oxidation state of the Ni is varied. The overall result is that a modification in only the final cycle of the CPS procedure results in a drastic change in the Ni/V DHR, as measured by the MA test. This gives us an excellent "variable" which can be used to control the DHR during CPS deactivation of catalysts for MA and once-through riser testing. It should be noted, however, that the final oxidation state of the metals after CPS deactivation is unimportant when the catalysts are evaluated in a continuous pilot plant, because the regenerator reactor are constantly varying the metal oxidation state.

Low Oxygen CPS Deactivation As noted earlier, commercial results (7) indicate that there is a large difference in both activity and selectivity of catalysts from full combustion and partial combustion FCC units. The variation in yields is due to the oxidation states of both Ni and V, as described in the previous section; however, the variation in activity is primarily due to the oxidation state of the V, which is very destructive to the zeolite in its oxidized form. Therefore, modifications to laboratory deactivation procedures are required to simulate the deactivation of catalysts from full and partial combustion FCC units. All of the standard deactivation procedures discussed so far have been aimed at simulating full combustion. The modified CPS procedure described in the previous section does change the final metal oxidation state to a reduced state similar to what one would expect from a partial combustion unit; however, throughout most of the deactivation, the metals on the catalyst are exposed to full combustion conditions. As such, the zeolite destruction is higher than that expected from a partial combustion unit.

A low oxygen CPS procedure has been developed where all cycles are run in an oxygen starved state with no added air; only atmospheric oxygen is present. This simulates partial combustion throughout the deactivation process. A standard Si-sol catalyst was

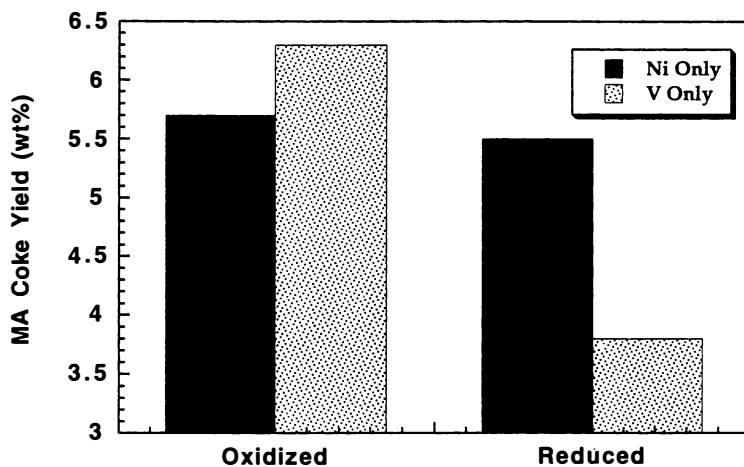


Figure 6. The Effect of the Metal Oxidation State on MA Coke Yields Ni Only vs. V Only

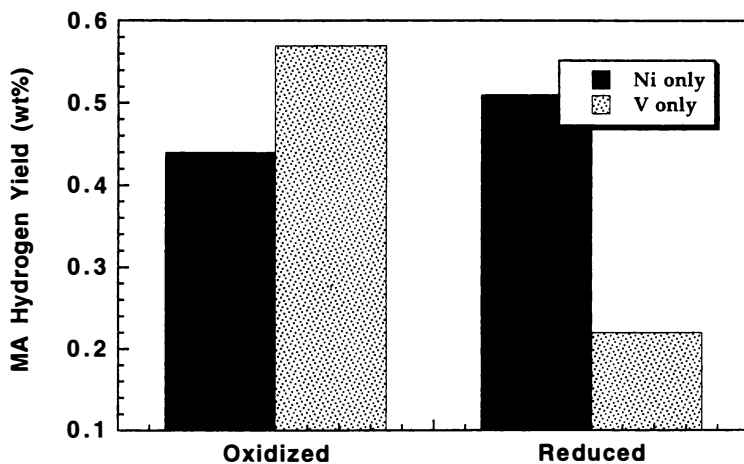


Figure 7. The Effect of the Metal Oxidation State on MA Hydrogen Yields Ni Only vs. V Only

deactivated by both the standard CPS procedure and this low oxygen CPS procedure at varying V levels. Results are shown in Figure 8 as a plot of the natural log of the ratio of V-contaminated kinetic activity to zero-V kinetic activity (9) versus V. This plot shows that the catalyst deactivation is very dependent on the V concentration under standard CPS conditions, but that the effect of V is greatly reduced under low oxygen CPS conditions. This is consistent with commercial observations (7) and gives us yet another “variable” which can be used to modify the laboratory deactivation conditions.

Implications on the Development of the CPS Deactivation Procedure

In the previous sections, two “variables” have been identified which can be used to control the CPS deactivation procedure. The first “variable” is the final oxidation state of the metals. By adjusting the CPS conditions during the last cycle only, we can adjust the oxidation state of the metals. This in turn gives us a method to control the Ni/V DHR, independent of catalyst type or metal level. Figure 9 graphically represents this control with the horizontal line moving along the MA coke or hydrogen axis.

The second “variable” is the oxidation state of the V throughout the CPS deactivation. By reducing the oxygen during all cycles, we can control the V oxidation state throughout the procedure and thus independently control the zeolite destruction by V. This is shown in Figure 9 as the vertical line along the ZSA or MA axis. Together, these two variables give us the ability to control the CPS deactivation to achieve either extreme in activity and coke and hydrogen selectivity, as well as any intermediate condition.

As an example of the use of modified CPS, a catalyst evaluation study was performed comparing a Ni-tolerant catalyst with a conventional catalyst. The two catalysts were impregnated with 1000 ppm Ni and 1700 ppm V and deactivated by standard CPS and the low oxygen last cycle CPS procedure. Figures 10 and 11 display the MA coke and hydrogen yields from the two catalysts under the two CPS conditions.

The effect of changing the metal oxidation state from oxidized to reduced gives a dramatic improvement in the MA coke and hydrogen selectivities for the Ni tolerant catalyst. Since this catalyst is very Ni tolerant, most of the contaminant coke is being produced by the V; reducing the V therefore de-emphasizes this coke and hydrogen. On the contrary, the conventional catalyst produces similar to slightly more coke and hydrogen when the final oxidation state is reduced. Here, the contribution from V is overshadowed by the coke and hydrogen from Ni. In the reduced state, the Ni may actually produce more MA coke and hydrogen, offsetting any benefits from the reduced V. It is our belief that the reduced CPS procedure better simulates most commercial FCC full combustion units, and that the results observed here for the “reduced” CPS are what would be observed in a commercial trial of these two catalysts. Furthermore, these results demonstrate that the ability to

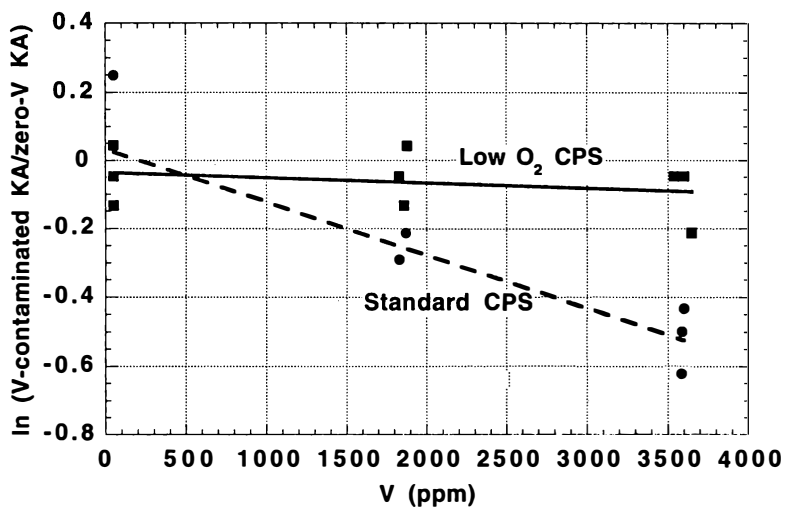


Figure 8. Vanadium Tolerance of FCC Catalyst Standard vs. Low O₂ CPS - MA Retention with V Level

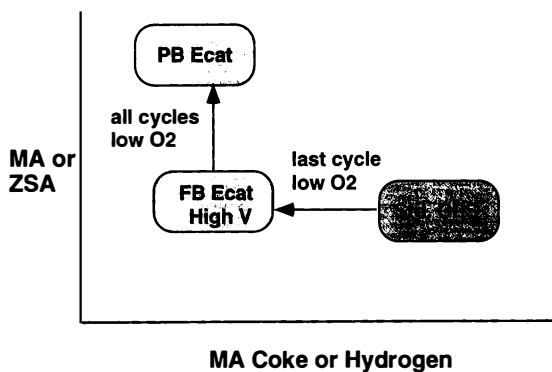


Figure 9. Implications on the Development of CPS Two Variables to Control Activity and Selectivities

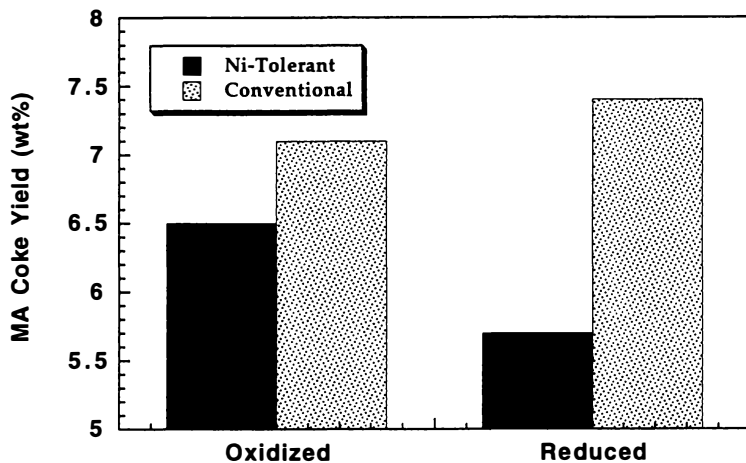


Figure 10. A Typical Catalyst Evaluation
The Effect of CPS Deactivation Conditions on MA Coke Yields

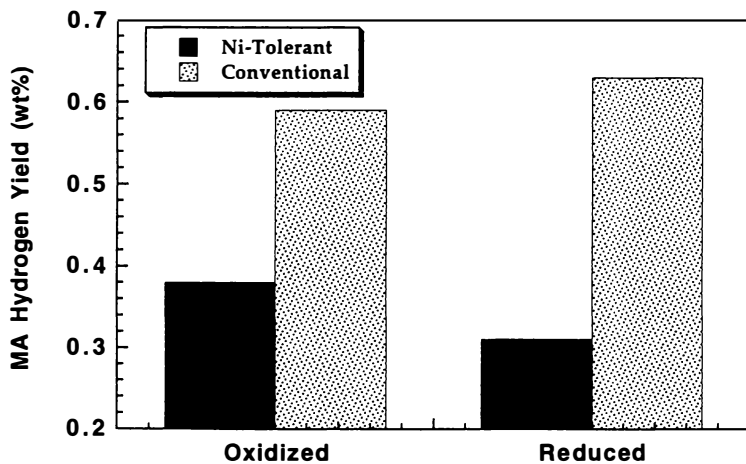


Figure 11. A Typical Catalyst Evaluation
The Effect of CPS Deactivation Conditions on MA Hydrogen Yields

control laboratory deactivation procedures to simulate different commercial FCC conditions is important in evaluating catalysts. Additionally, these results confirm that specific catalysts may be more appropriate for full combustion or partial combustion units depending on the metal levels and the Ni/V ratio. It is fundamental that a laboratory deactivation procedure discern these differences.

Conclusions

The CPS catalyst deactivation procedure is the most promising procedure for simulating commercial FCC equilibrium catalysts due to its ease of implementation, excellent reproducibility and good simulation results. However, the CPS procedure does over-emphasize the importance of V on catalysts in MA testing. Minor modifications to the procedure have been made which de-emphasize the role of V and give a better match to commercial Ecat yields. Additionally, these minor modifications have given us two "variables" which can be used to tailor the CPS procedure to different commercial operations, such as full combustion versus partial combustion regeneration. This enables us to simulate commercial FCC deactivation and better predict catalyst performance in a specific FCC unit.

Literature Cited:

1. Wormsbecher, R.F., Peters, A.W. and Masselli, J.M., *J. Catal.*, 100,130 (1986).
2. Mitchell, B.R., *Ind. Eng. Chem. Prod. Res. Dev.*, 19, 209 (1980).
3. Haas, A.W., Suarez, W. and Young, G.W., *AIChE Symp. Series*, 88, 133, (1992).
4. Rajagopalan, K., Cheng, W.-C., Suarez, W., and Wear, C.C., *NPRA Annual Mtg.*, San Antonio, TX, (1993).
5. Cheng, W.-C., Juskelis, M.V. and Suarez, W., *AIChE Annual Mtg.*, Miami Beach, FL, (1992).
6. Rajagopalan, K., Peters, A.W., and Edwards, G.C., *Appl. Catal.*, 23, 69, (1986).
7. Dougan, T.J., Alkemade, U., Lakhanpal, B. and Boock, L.T., *Oil & Gas J.*, 92, 81, (1994).
8. Bearden, R. and Stunz, G.F., *US Patent* 4 280 896 (1981).
9. Leuenberger, E.L., *Oil & Gas J.* July 15, 125, (1985).

DEACTIVATION OF REFORMING CATALYSTS

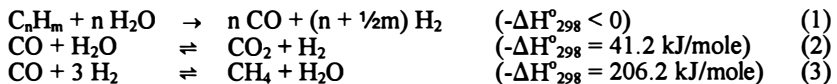
Catalyst Deactivation in Adiabatic Prereforming: Experimental Methods and Models for Prediction of Performance

Thomas S. Christensen and Jens Rostrup-Nielsen

Haldor Topsøe A/S, Nymøllevej 55, DK-2800 Lyngby, Denmark

Adiabatic prereforming has become an established process step in the production of syngas. The main deactivation phenomena for the prereforming catalyst are sulphur poisoning and carbon formation. Carbon formation proceeds either as carbon whiskers at high temperature or as gum at low temperature. Trouble free operation is ensured by selecting operating conditions and catalyst type. Experimental methods are used to characterize the deactivation phenomena. Prereforming catalysts have been investigated by use of Temperature Programmed Reaction (TPR) showing the presence of different carbon morphologies. Application of the pseudo-adiabatic reactor principle has ensured reliable adiabatic bench-scale tests providing data for industrial design. Methods based on intrinsic activity measurement have been developed to reveal the impact of the deactivation phenomena. Sulphur adsorption isotherms and mathematical models describing the complex interaction between pore diffusion, poisoning rate and reaction kinetics have been established and are used for design and performance prediction.

Adiabatic prereforming is a low-temperature steam reforming process (1,2) which is used in modern syngas production to reduce energy consumption and investment (3). The prereforming process was earlier used in the manufacture of methane-rich gases for town gas and SNG (substitute natural gas) (2,4). Today prereforming is an integrated part of the plants producing hydrogen, ammonia, methanol, and CO/H₂ mixtures. In the prereformer, all higher hydrocarbons are converted over a nickel catalyst into methane, carbon oxides and hydrogen. The methane reforming and shift equilibria are established at the reactor exit at the adiabatic equilibrium temperature:



For natural gas, the overall process is endothermic and the actual ΔT depends on the contents of higher hydrocarbons and on the operating conditions, especially the steam-to-carbon ratio. For heavier feedstocks, the overall process is slightly exothermic and typical temperature profiles for operation with naphtha feed are shown in Figure 1.

The prereformer is installed upstream the tubular reformer furnace as shown in Figure 2 (3,5). It is both an economic and operational advantage for the syngas production to include a prereforming step. One advantage is its very flexible use of feedstock, which especially can be utilized in H₂-production at refineries where the same unit can handle feedstocks ranging from refinery off-gas and LPG to naphtha and kerosene (3,6). At the same time, the use of a prereformer makes it possible to increase the preheat temperature of the tubular reformer, without the risk of thermal cracking of higher hydrocarbons in the preheater (3,7) and without the risk of whisker carbon formation from higher hydrocarbons on the tubular reformer catalyst (2). A higher preheat temperature means a lower fired duty in the tubular reformer and hence a smaller furnace and a cheaper process unit.

Deactivation of Prereforming Catalyst

In the design of adiabatic prereforming units it is important to consider catalyst deactivation and the low temperature operation requires a high-activity catalyst with resistance to poisoning. Excessive deactivation can be avoided through a proper selection of operating conditions and catalyst. The installed catalyst volume must be dimensioned so that the required conversion of the higher hydrocarbons can be obtained also when the catalyst is partly deactivated at end-of-life, typically after 2-3 years. Deactivation of the catalyst can be caused by various sources, as listed in Table I. Sulphur poisoning and gum formation are the most common deactivation phenomena. The poisoning of the catalyst results in a continuously progressive movement of the temperature profile in the flow direction, as seen on Figure 1.

Table I. Deactivation Phenomena in Adiabatic Prereforming

Type	Effect and Critical Parameters
<i>Sintering</i>	Loss of surface area $T > T_{\text{Tammann}} = 591^{\circ}\text{C}$ for Ni
<i>Poisoning</i> Sulphur Silica Alkali Metals (K, Na)	Partly coverage of Ni surface. Pore mouth poison Decrease of reaction rate
<i>Carbon Formation</i> Whiskers Gum	Pellet breakage (high temperature) Coverages of active catalyst surface (low temperature)

Sintering. According to the Tammann's rule (2) sintering is expected above a certain temperature equal to 50% of the melting point of the metal (in degree Kelvin); $T_T = \frac{1}{2} T_m$ (K). Sintering of the nickel crystals is not taking place at prereforming conditions because the operating temperature is below the Tammann temperature ($T_{T,\text{Ni}} = 591^{\circ}\text{C}$) (2). Although the metal is not subjected to sintering, a carrier system with high surface area and thermal stability is required as support.

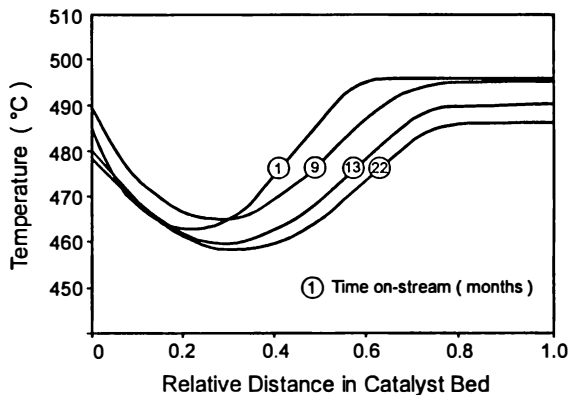


Figure 1. Temperature profiles in an industrial, adiabatic prereformer operating on naphtha feed in a H_2 -plant. $H_2O/C = 3.5$; $P = 26$ bar; Topsøe RKNR Catalyst.

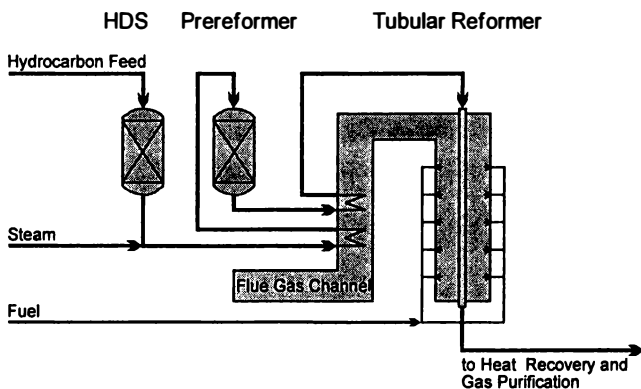


Figure 2. Typical installation of an adiabatic prereformer unit.

Sulphur Poisoning. Sulphur is the most common poison for steam reforming catalysts. Sulphur is a natural component of all hydrocarbon feedstocks, but the sulphur contents of the feed is reduced to a few ppb by hydro-desulphurization followed by absorption over zinc oxide. The remaining sulphur, normally below the analytical detection limit, will slowly poison the catalyst (1). The mechanisms of sulphur poisoning are described in detail in the literature (2,8). The sulphur compounds are chemisorbed dissociatively on the nickel surface; equation 4.



At equilibrium, the sulphur coverage of the nickel surface, θ , can be calculated by a Temkin-like adsorption isotherm dependent on the temperature and the $\text{H}_2\text{S}/\text{H}_2$ -ratio (1,9) with the parameters found by Alstrup *et al.* (9); equation 5.

$$\theta = 1.45 - 9.53 \cdot 10^{-5} \cdot T + 4.17 \cdot 10^{-5} \cdot T \cdot \ln \left[p_{\text{H}_2\text{S}} / p_{\text{H}_2} \right] \quad (5)$$

Rostrup-Nielsen found that the intrinsic reaction rate, r_i , for methane steam reforming is correlated with the sulphur coverage by equation 6 (2). In the adiabatic prereformer, the sulphur acts as a pore mouth poison and as the reactions are restricted by pore diffusion (2,8), the effective activity of the sulphur poisoned catalyst pellet can be described by an empirical relation, equation 7, between the effective pellet reaction rate, r_p , and the average sulphur coverage, θ_{av} (1).

$$r_{i,\text{pois}} = (1-\theta)^3 \cdot r_{i,\text{unpois}} \quad (6)$$

$$r_{p,\text{pois}} = (1-\theta_{av})^\alpha \cdot r_{p,\text{unpois}} \quad (7)$$

Other Poisons. Alkali metals and silica are sometimes present in the feed streams and both are poisons for the prereforming catalyst. Silica acts as a pore mouth poison by physically blocking the entrance to the pore system and restricting the access of gas to the pore system and the active catalyst surface. Thereby, the overall catalyst activity is decreased. Alkali metals reduce the turnover frequency and Rostrup-Nielsen (2) studied the influence of the contents of alkali metals on the intrinsic reaction rate. Potassium has a larger deactivating effect than sodium and the poisoning effect of alkali metals is stronger on less acidic supports. Addition of, e.g. 3000 ppm of potassium to a steam reforming catalyst can result in a decrease of the intrinsic activity by a factor 10 (2).

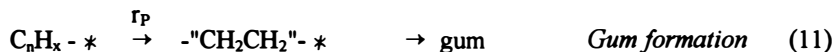
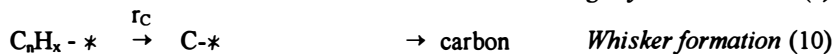
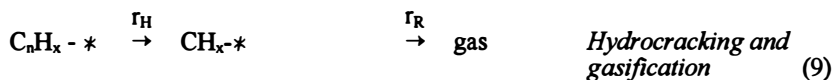
Carbon Formation. Carbon formation can take place by two major routes; whisker carbon and gum formation. *Whisker carbon* formation has been described by Rostrup-Nielsen (2) and is normally avoided by proper selection of catalyst type and of operating conditions (temperature and steam-to-carbon ratio). For given feedstock and process conditions, whisker carbon formation is formed above a certain temperature, $T > T_c$ (1,2).

Gum formation, which is a polymerization of hydrocarbons (especially aromatic compounds) on the catalyst surface, is a deactivation phenomenon that takes place at low temperature. Therefore, an investigation of the appearance of gum on steam reforming catalysts used at prereforming conditions is very relevant. Deactivation by gum formation can proceed several times faster than ordinary sulphur poisoning.

The gum phenomenon was studied in detail 10-25 years ago. The composition of "gum deposits" was studied by extracts of deactivated catalysts. Jackson *et al.* (10) found that the chemical structure of gum deposits on catalysts deactivated in laboratory tests was independent of the reacting hydrocarbons and consisted of $-\text{CH}_2-$ polymers, whereas Bhatta and Dixon (11) found aromatics in extracts from

industrially used catalysts. However, it is likely that the paraffinic structure observed by Jackson *et al.* (10) is slowly converted into an aromatic structure. This is in accordance with observations by Frennet and Lienard (12) that adsorbed hydrocarbons are gradually dehydrogenated into less reactive residues on the metal surface. Similar observations were made in methanation units for production of substitute natural gas (13). At certain conditions (high partial pressure of carbon monoxide and low temperature), the nickel catalyst was deactivated resulting in a displacement of the temperature profile. The activity could be almost restored (13) by treatment in hydrogen at elevated temperature (around 500°C) and the amount of carbon removed during the regeneration corresponded roughly to one monolayer of the total surface area or five monolayers on the nickel surface. The encapsulating carbon was related to the β -carbon identified by surface studies by McCarty and Wise (14).

A model for gum formation in steam reforming can be formulated from a simplified kinetic sequence (2,15):



Assuming that the process conditions have been selected to avoid whisker carbon formation ($r_C = 0$), the rate of gum formation can be expressed by equation 12:

$$r_P = r_A - r_H \quad (12)$$

The activation energy for adsorption of hydrocarbons on nickel is about 40 kJ/mole (16) and the activation energy for hydrocracking is in the range 160-200 kJ/mole (17). This means that below the temperature, T_P , at which $r_A > r_H$, i.e. $r_P > 0$, gum formation takes place. To ensure trouble free operation the prereformer must operate within the temperature window of $T_P < T < T_C$.

Models for Performance Prediction

Prediction of the deactivation rate can be made by empirical as well as by computational methods. The models can be used at two stages:

- In the *design phase*; for proper sizing of the reactors and for determination of the necessary catalyst volume for the required operating period.
- In the *plant operation*; for observation of the actual deactivation progress and determination of the optimal time for catalyst change out.

Empirical Methods. The *graphical deactivation plot* is a very useful empirical method for prediction of the catalyst performance and for estimation of catalyst lifetime (18,19). The deactivation plot shows the length of the reaction front as a function of time. This illustrates the movement of the temperature profile caused by the progressive deactivation of the catalyst. The method is illustrated in Figure 3. The temperature increase over the catalyst bed is calculated as $\Delta T = T_{\text{exit}} - T_{\text{inlet}}$ and a certain percentage hereof, e.g. 90% (ΔT_{90}) is calculated. The axial distance in the

catalyst bed corresponding to this temperature increase, usually called z_{90} , is then read from the temperature profile. The deactivation plot is made by depicting z_{90} as the length of the reaction front versus time-on-stream. The inverse slope of the deactivation plot is called the resistance number, R , defined as kg hydrocarbon feed required to deactivate one gram of catalyst. At slow deactivation a large resistance number is obtained and a small resistance number at fast deactivation.

The impact of the process parameters on the rate of gum formation has been reported by Moseley *et al.* (19) in terms of the resistance number R . A large resistance number was obtained with high steam-to-carbon feed ratio, high hydrogen partial pressure and with high H/C ratio of the hydrocarbon feed, whereas particularly low temperature caused a decrease in R . A high content of aromatic compounds was also found to decrease R and this can be explained by the aromatic hydrocarbons having high r_A and low r_H .

Computational Methods. *Mathematical models* describing the interaction between pore diffusion, poisoning and catalyst activity are essential for reactor design and for performance prediction. Mathematical models combining reaction kinetic and catalyst poisoning models have been developed and built into the computer programs, REFRAD and SPOIS (1,20). The models have proven useful in describing observed performance of adiabatic prereformers in bench-scale operation as well as in industrial operation (1,6).

Experimental Methods for Characterization of Catalyst Deactivation

Chemical Analyses. A spent and deactivated catalyst can be characterized by *chemical analysis* of carbon and poisons (S, Si, K, Na) deposited on the catalyst. The average sulphur coverage, θ_{av} , can be calculated when the total sulphur chemisorption capacity of the catalyst has been determined. The sulphur chemisorption capacity is proportional to the nickel surface area and methods for determining the sulphur capacity by chemisorption of H_2S have been developed by Rostrup-Nielsen (2). Due to the pore diffusion restriction of the reactions, the sulphur is chemisorbed in the outer shell of the catalyst pellet according to equation 5. The average sulphur coverage of the pellet, θ_{av} , is remarkably lower than the equilibrium coverage, θ , until the chemisorption front has moved to the centre of the pellet. The radial distribution of the sulphur and other poisons can be measured by a scanning electron microprobe. A radial profile of the sulphur coverage in a catalyst pellet taken from the top of a prereformer catalyst bed illustrating the shell poisoning nature is shown in Figure 4. For further characterization of the deactivation phenomena, advanced laboratory testing methods such as *TPR (Temperature Programmed Reaction)* and *intrinsic activity measurements* are used.

TPR (Temperature Programmed Reaction). Characterization of the carbon types formed on catalysts during operation can be made by use of TPR. Tests are performed by heating the reactor linearly from ambient to $1000^\circ C$ while flowing pure hydrogen through the catalyst bed (21). The carbon is reacting with the hydrogen and methane is formed as the most predominant compound and is detected as a function of temperature.

Carbon morphologies found on prereforming catalysts have been investigated in TPR studies (22). Prereforming catalysts, Ni supported by MgO , that have exhibited various deactivation phenomena during operation in industrial and laboratory adiabatic reactors, have been selected for the investigation. The catalysts had been in operation with feed mixtures of naphtha, steam and hydrogen with a steam-to-carbon ratio in the range 1.5-3.0 and in a temperature range of $400-530^\circ C$. The peaks observed on the TPR curves for the prereforming catalysts are characterized by their

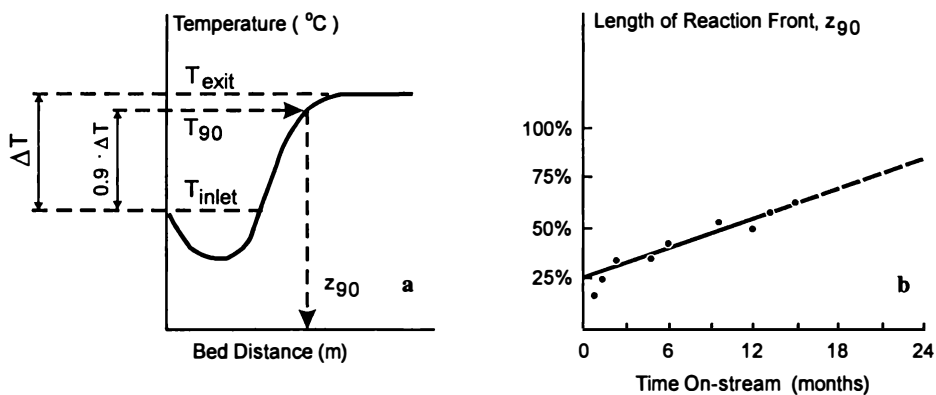


Figure 3. Graphical deactivation plot for performance prediction.

- Estimation of length of reaction front, z_{90} from temperature profile
- Deactivation plot

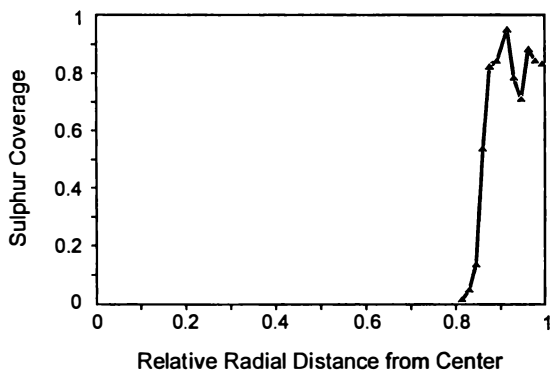


Figure 4. Measured radial sulphur distribution in a prereforming catalyst pellet from top of a bed after 1130 hours of operation with naphtha feed at $H_2O/C = 1.5$ and inlet temperature = $450^\circ C$.

peak temperature; Table II. McCarty *et al.* (21) have by model studies characterized the different carbon morphologies found after exposure of nickel catalysts to carbon monoxide and to ethylene. The peaks listed in Table II have been assigned a carbon morphology according to the nomenclature used by McCarty *et al.* (21). The carbon morphology found reacting at high temperature, 630-720°C, has been assumed related to the platelet/pyrolytic ϵ -carbon described by McCarty *et al.* (21). In total six different classes of carbon morphologies have been observed for the prereforming catalysts exposed to various feeds and operating conditions (22).

Table II Carbon Morphologies on Adiabatic Prereforming Catalysts found by H₂-TPR. Heating Rate = 6°C/min

Class	Peak Temperature (°C)	Type	Carbon Morphology Nomenclature according to McCarty <i>et al.</i> (21)
1	190-205	α'	Chemisorbed carbon
2	260-300	α	Chemisorbed carbon
3	420-530	β	Gum / β carbon film
4	570-600	δ	Filamentous carbon
5	630-720	ϵ	Platelet / Pyrolytic carbon
6	950-1000	G	Graphitized carbon

The individual catalyst sample typically shows the presence of 2-4 peaks and Figure 5 shows a TPR diagram for a catalyst that has been in operation for 6 months in an adiabatic prereformer with a naphtha feedstock at relative low temperature. Three peaks have been identified for this catalyst and they are ascribed to chemisorbed carbon (α -type) at 300°C, gum (β -type) at 480°C and the platelet/pyrolytic carbon (ϵ -type) at 650°C. In addition some graphitized carbon is also observed as a weak peak at high temperature around 950°C.

The normal unpoisoned prereforming catalyst contains only α -type and ϵ -type. For prereformer operation it is of special interest to study whether carbon is formed as gum (β -carbon) or as whiskers (δ -carbon) dependent on the feedstock, operating conditions and catalyst. Filamentous whisker carbon has only been seen by electron microscopy examinations (TEM) on catalysts with δ -type carbon. Catalysts, that judged on activity measurements are deactivated by gum formation, all have a TPR peak in the range of the β -carbon. The gum peak is often a very broad peak. The broad nature of the gum peak could be caused by variations in the hydrogen content of the polymerization deposits and some transformation with time could also change the peak temperature. McCarty *et al.* (21) found that the peak temperature of the β -carbon increased with increasing coverage.

The temperature intervals for the TPR peaks of the prereforming catalysts are for most of the types the same as found in the studies by McCarty *et al.* (21) when differences in the TPR heating rate are considered. The variations seen can most likely be explained by the differences in hydrocarbon feed and exposure conditions. Catalyst support can also effect the peak temperature, especially for the adsorbed surface carbon types (α - and β -carbon). McCarty *et al.* (21) reported large peaks of Ni-carbide (Ni₃C, γ -carbon) when the catalyst was exposed to ethylene at the very low temperature of 300°C. This type of carbon is not expected to be present at the prereforming conditions as it is not stable at temperatures above 330°C, due to decomposition (21), nor has it been identified by X-ray diffraction examinations of prereforming catalysts.

Intrinsic Activity Measurements. Measurement of the intrinsic reaction rate is a standard test to characterize prereforming catalysts. The catalyst is exposed to steam

reforming of ethane at isothermal conditions in a gradient-less plug flow micro-reactor (20). The activity measurements can be used for screening tests in development of new catalysts and for measurement of the degree of deactivation. In the catalyst bed of the adiabatic prereformer, the steam reforming reactions are controlled by pore diffusion, so application of intrinsic activity measurements must be done with great caution. The effectiveness factor for reforming of higher hydrocarbons is below 10-15% in most parts of the prereformer.

Catalyst samples exposed to prereforming conditions in bench-scale tests have been investigated for their catalyst activity. The samples have been collected from various positions in the catalyst beds and after various operating periods ranging from 50 to 1200 hours. Catalysts with a broad range of sulphur coverages have in this way been obtained. The standard test involves measurement of the intrinsic reaction rate for ethane steam reforming at 500°C and a feed ratio of $H_2O/C = 4.0$ applying crushed down catalyst of 0.3-0.5 mm sieve fraction. In Figure 6 the reaction rate is plotted versus $(1-\theta_{sv})$. Activities have been normalized with the activity of unpoisoned catalysts.

Sulphur poisoning of a steam reforming catalyst takes place as a shell poisoning and the sulphur coverage in the shell is typically 80-90% at prereforming conditions, as Figure 4 illustrates. The intrinsic activity throughout the pellet is given by equation 6 and the activity in the sulphur poisoned shell is therefore very low. When the activity of such a prereforming catalyst is measured on crushed-down catalysts, it can be shown that the measured intrinsic activity ideally is a straight line versus $(1-\theta_{sv})$, as shown on Figure 6. The catalysts are divided into two groups by this activity test method; normal sulphur poisoned catalysts and catalysts deactivated by gum in combination with sulphur poisoning. Some of the catalysts had been exposed to gum formation due to special operating conditions and feedstocks. For these catalysts a larger decrease in the catalyst activity is observed than can be ascribed to sulphur poisoning alone. The reaction rate is still proportional to the sulphur poisoning, but equation 6 is no longer valid. Figure 6 shows that the additional gum deactivation factor on the intrinsic reaction rate is in the range 2-5.

The TPR examinations of prereforming catalysts showed that the gum deposits (β -carbon) are relatively reactive. New methods have been developed combining a standard activity measurement with temperature programmed treatment of the catalyst in hydrogen or a hydrogen-containing gas. These regeneration tests can be used for verification of deactivation type; sulphur or gum. Sulphur is very slowly regenerable in H_2 , whereas gum can be gasified at moderate temperatures.

In Figure 7 the regenerative effect of the treatment with pure hydrogen is shown dependent on the regeneration temperature ranging from 450 to 650°C. All activity measurements were made for steam reforming of methane at 500°C after 3 hours of treatment at the regeneration temperature. It is seen that a sulphur poisoned catalyst is not regenerable. According to equation 4 sulphur poisoning is reversible, but in practise it is a very slow process at low temperature. Both examples of gum formation shown in Figure 7 are regenerable but it takes a longer time to restore the catalyst activity for a gum poisoned catalyst that has been exposed to long-term operation. It is most likely that the nature of the gum changes with time as the TPR analyses showed that the amount of β -carbon on the 100-hour old gum poisoned catalyst was 50-60% of the amount found on the 6-month old catalyst.

Bench-scale Testing as a Method for Investigation of Catalyst Deactivation

Testing in bench-scale equipment is a valuable experimental method for investigation of the impact of deactivation on the catalyst performance when full-size catalyst pellets, industrial mass velocity and pressure are used. Bench-scale testing is often

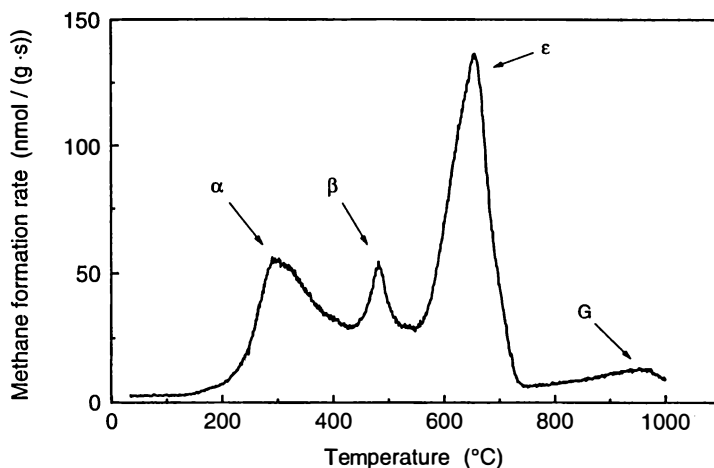


Figure 5. TPR (Temperature Programmed Reaction) of an adiabatic pre-reforming catalyst after 6 months of operation with naphtha feedstock. Heating rate: 6°C per min.

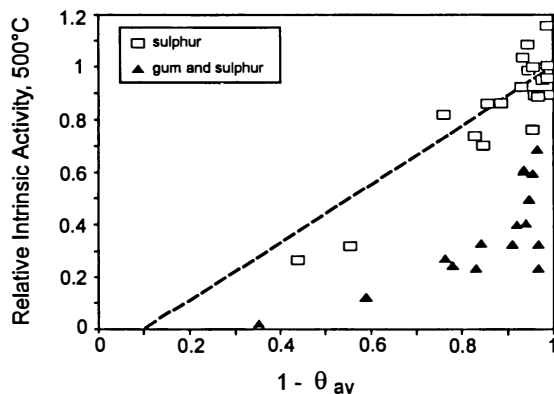


Figure 6. Intrinsic reaction rate in dependence of sulphur poisoning for a) normal catalysts (\square), b) gum deactivated catalysts (\blacktriangle). The dotted line represents the ideal relation for the average intrinsic activity of a normal shell poisoned catalyst, $\theta = 0.9$. Steam reforming of ethane, $\text{H}_2\text{O}/\text{C} = 4.0$, $P = 1$ bar. Activities normalized with activity of unpoisoned catalyst.

used to test new process concepts, new catalysts as well as for catalyst performance on special feedstocks (20).

Testing of adiabatic processes with large temperature gradients over the catalyst bed in bench-scale units is often misleading due to the heat loss, however, application of pseudo-adiabatic reactors with controlled heat loss compensation ensures reliable adiabatic testing (18). The compensation heat is controlled so the temperature drop over the insulation layer between the reactor and the heater elements is zero, as illustrated in Figure 8 for one heater zone. During catalyst deactivation the reactor wall temperature and the heater temperature will adjust to the level of the catalyst. In this way, the heat-input balances the heat loss. The reactor is equipped with a number of separate heater zones along the catalyst bed to minimize deviations from adiabatic operation (18).

Investigation of deactivation by gum formation and estimation of resistance numbers as a function of operating conditions and feedstock type are examples of bench-scale tests in which an insufficient heat loss compensation may spoil the results.

The prereformer performance for a given, heavy naphtha feed (IBP/FBP = 80/205°C) was investigated in a bench-scale pseudo-adiabatic prereformer at a low inlet temperature of 400°C and at a H₂O/C-ratio of 2.0. The test showed an extreme case of deactivation by gum formation illustrating what happens when $T < T_p$. The temperature profiles are shown in Figure 9. A satisfactory conversion was observed just after start-up; the exit gas contained no higher hydrocarbons and the temperature profile corresponded to the expected conversion of the higher hydrocarbons. Nevertheless, already within the first 24 hours of operation a fast deactivation took place so the temperature profile had moved far down in the catalyst bed and after only 72 run hours a breakthrough of higher hydrocarbons was observed. The resistance number was only a few per cent of the resistance numbers obtained at higher temperatures for the same feedstock. The test showed that for this given naphtha feedstock the low inlet temperature of 400°C was outside the allowed window of operation. It also shows the importance of having detailed knowledge of the feedstock properties.

When gum formation proceeds, the minimum temperature in the catalyst bed decreases with time. This could be explained by a shift in the reaction mechanism so more endothermic reaction steps are prevailing. The decrease in the bed temperature speeds up the deactivation by gum formation. This aspect of gum formation is also seen on the temperature profiles in Figure 9. Calculations with a heterogenous reactor model have shown that the decreasing minimum catalyst bed temperature could also be explained by a change of the effectiveness factors for the reactions. The radial poisoning profiles in the catalyst pellets influence the complex interaction between pore diffusion and reaction rates and this results in a shift in the overall balance between endothermic and exothermic reactions.

Another example of the capability of bench-scale testing is a performance test converting a heavy, straight-run naphtha (IBP/FBP = 90/185°C) with 18 wt% aromatic compounds at a very low H₂O/C-ratio of 1.5 in an adiabatic prereformer for production of a CO-rich gas (6). The test was carried out in a pseudo-adiabatic reactor and lasted 1130 hours (1½ months). The test was carried out at higher space velocity compared with industrial reactors and thus it simulates the upper part of the prereformer. The displacement of the temperature profile is seen in Figure 10 and it shows that a satisfactory conversion of the hydrocarbons was obtained throughout the test. The graphical deactivation plot has been used for evaluation of the performance, as illustrated in Figure 11. The deactivation is fastest during the first approx. 200 hours whereupon it stabilizes at a lower level. This behaviour is explained by the initial sulphur poisoning of the outer surface of the catalyst pellets having the highest impact on the activity. The overall resistance number has been

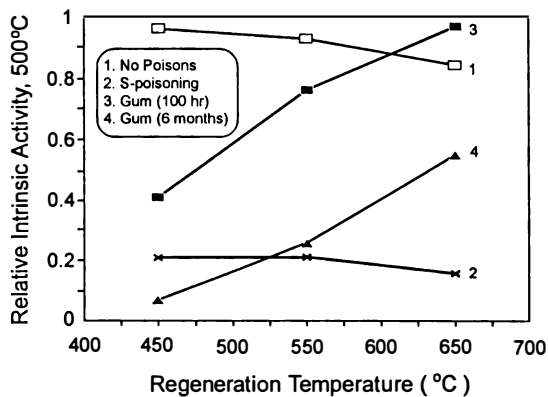


Figure 7. Regenerative effect of H₂ treatment. Method combining activity measurements for steam reforming of methane (H₂O/C = 4.0, P = 1 bar, 500°C) with temperature programmed treatment in H₂. Activities normalized with activity of unpoisoned catalyst.

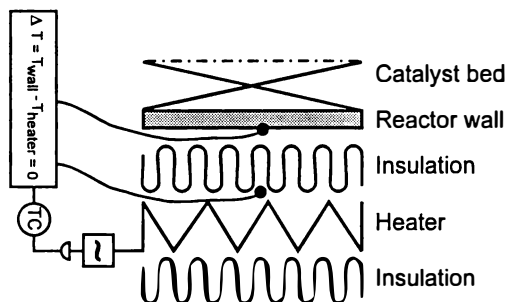


Figure 8. Principle lay-out of the pseudo-adiabatic reactor (one heater zone)

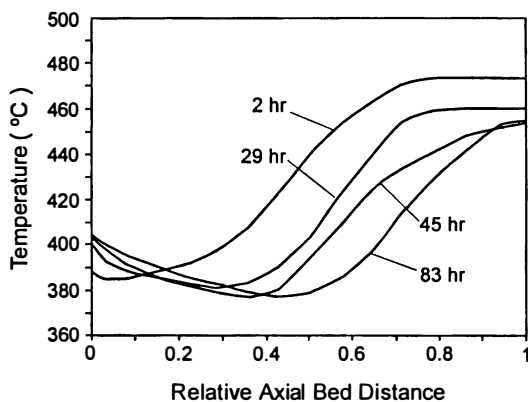


Figure 9. Temperature profile for an extreme case of gum poisoning with a heavy naphtha feed. $H_2O/C = 2.0$; $P = 18$ bar.

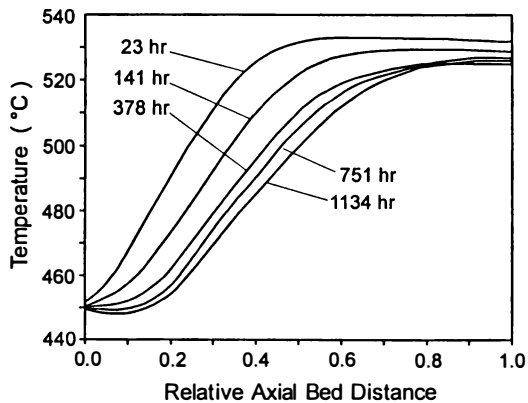


Figure 10. Performance test of adiabatic prereforming on naphtha feed. Temperature profiles from an pseudo-adiabatic prereformer. $H_2O/C = 1.5$; $P = 25$ bar; Topsøe RKNGR Catalyst.

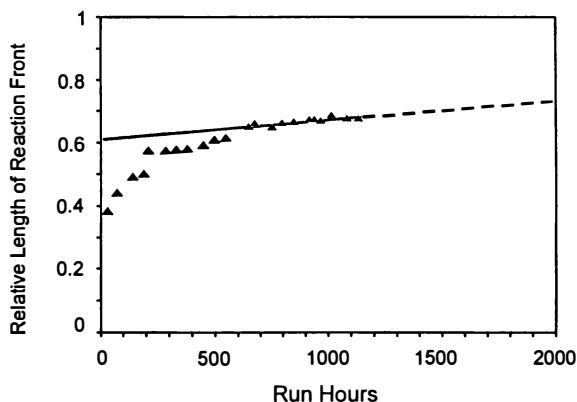


Figure 11. Performance test of adiabatic prereforming on naphtha feed. Graphical deactivation plot for the performance test of Figure 10.

estimated to 40 (kg hydrocarbon feed per g catalyst deactivated) and this is in the normal range. A more detailed look at the temperature profiles shows indication of gum formation. This is seen as the appearance of an endothermic dip on the temperature profile and as the decrease of this minimum bed temperature. Thus, some gum formation is taking place at a low rate, but in spite of this a satisfactory resistance number was obtained. Analyses of the spent catalyst revealed that the deactivation was caused by sulphur poisoning in combination with gum formation. The sulphur distribution in a catalyst pellet is shown in Figure 4. The effect of gum formation has been estimated by intrinsic activity measurement showing a gum deactivation factor of 1.3-1.9 for the upper approx. 15% of the bed. A slight increase in the inlet temperature could in this example further diminish the effect of gum formation and reduce the deactivation rate.

These examples show the importance of performing bench-scale tests as part of the process and catalyst development, but it also illustrates the importance of applying the pseudo-adiabatic reactor principle to observe the deactivation phenomena and to ensure reliable, adiabatic bench-scale tests when providing data for industrial design.

Conclusion

Deactivation plays an important role in the adiabatic prereforming process and fundamental knowledge is necessary for making a safe design of the process unit. The effect of deactivation can be diminished by proper selection of the operating conditions and catalyst. To ensure trouble free operation, the prereformer must be fed with a purified feed and operated within the temperature window; $T_p < T < T_c$. This window mainly depends on the feed properties, H_2O/C -ratio and H_2 -recycle. Experimental methods, such as bench-scale tests, activity measurements and Temperature Programmed Reaction as well as mathematical models for performance predictions are all valuable tools in defining the design limits. In the operation of adiabatic prereformers the graphical deactivation plot provides a simple method easy to use for the prediction of the deactivation rate and of the residual lifetime of the catalyst.

Literature Cited

1. Christensen, T.S.; Bak Hansen, J.-H., Proc. 2nd Nordic Symposium on Catalysis, Lyngby, Denmark, November 1989.
2. Rostrup-Nielsen, J.R., In: "Catalysis, Science and Technology", Anderson J.R., Boudart, M., Eds.; Springer, Berlin, 1984, Vol. 5, p.1.
3. Vannby, R.; Winter Madsen, S.E.L., Ammonia Plant Safety, **1992**, *32*, 122.
4. Davies, H.S.; Humphries, K.J.; Hebden, D.; Percy, D.A., Inst.Gas Eng. J., **1967**, *7*, 708.
5. Rostrup-Nielsen, J.R.; Christensen, T.S.; Bak Hansen, J.-H., In: Proc. Eurogas 94, Holmen, A.; Magnussen, B.F., Eds., Trondheim, March 1994, p. 1.
6. Christensen, T.S., Appl.Catal.A, in press.
7. Rostrup-Nielsen, J.R., Stud.Surf.Sci.Catal. **1988**, *36*, 73.
8. Rostrup-Nielsen, J.R.; Højlund Nielsen, P.E.; Kegel Sørensen, N.; Carstensen, J.H., Ammonia Plant Safety **1993**, *33*, 184.
9. Alstrup, I.; Rostrup-Nielsen, J.R.; Røen, S., Appl. Catal. **1981**, *1*, 303.
10. Jackson, S.D.; Thomson, S.J.; Webb, G., J.Catal. **1981**, *70*, 249.
11. Bhatta, K.S.M.; Dixon, G.M., Trans. Faraday Soc. **1967**, *63*, 2217.
12. Frennet, A.; Lienard, G.; Surface Sci. **1969**, *18*, 80.
13. Gierlich, H.H.; Fremery, M.; Skov, A.; Rostrup-Nielsen, J.R., Stud.Surf.Sci.Catal. **1980**, *6*, 459.
14. McCarty, J.G.; Wise, H., J.Catal. **1979**, *57*, 406.
15. Rostrup-Nielsen, J.R.; Tøttrup, P.B., Proc. Symposium on Science of Catalysis and its Application in Industry, FPDIL, Sindri, India, 1979, p.379.
16. Hayward, D.O.; Trappnell, B.M.W., Chemisorption, Butterworths, London, 1964.
17. Freel, J.; Galwey, A.K., J.Catal., **1968**, *10*, 277.
18. Rostrup-Nielsen, J.R.; Skov, A.; Christiansen, L.J., Appl. Catal., **1986**, *22*, 71.
19. Moseley, F.; Stephens, R.W.; Stewart, K.D.; Wood, J., J.Catal., **1972**, *24*, 18.
20. Rostrup-Nielsen, J.R.; Christiansen, L.J.; Bak Hansen, J.-H., Appl. Catal., **1988**, *43*, 287.
21. McCarty, J.G.; Hou, P.Y.; Sheridan, D.; Wise H., In: "Coke Formation on Metal Surfaces"; Albright L.F.; Baker, R.T.K., Eds., ACS Symposium Series **1982**, *202*, 253.
22. Christensen, T.S.; Törnqvist, E.O., unpublished results.

Mechanism of Deactivation in Reforming Catalysts at Start of Run

Yaofang Liu, Guoqing Pan, and Jiujin Yang

Department of Chemical Engineering, University of Petroleum,
Changping, Beijing 102200, China

The deactivating factors and their mechanisms for PtRe/Al₂O₃ catalysts at start-of-run of a reforming unit were investigated. It was found that among the many factors, hydrocarbons and oxygen contained in the nitrogen during the dehydration step were of most importance for the practical activities of the catalysts for the reforming reactions.

It is well known that the real activity of a reforming catalyst depends not only on its manufacture but also on the operating conditions during start-of-run. In general, the affecting parameters include temperature, water concentration, treating time, hydrogen purity etc., however less work has been reported on the influence of oxygen and individual hydrocarbons on the catalyst performance.

The catalytic functions of the platinum is the most important one for reforming reactions because it can not be restored after start-of-run damage unless the run is stopped and the catalyst is regenerated. Therefore this work stressed the effect of the gas composition during the dehydration and the reduction of catalysts on the catalytic functions of the platinum.

Experimental Part

Catalysts. Some commercial PtRe catalysts listed in Table I were used in this study as well as some PtSn catalysts on which were reported elsewhere (1). The fresh catalysts B-6, B-7 and B-8 made in China are white because they are unreduced. Catalyst 803 made by Engelhard Corp. was grey because it had been reduced by the manufacturer.

Characterization of the Platinum Functions. It was reported that the hydrogen adsorption represented as H/Pt measured by H₂-O₂ titration at 90°C was proportional to the dehydrogenation activity of a catalyst (1), even when the chlorine content varied greatly. Therefore the catalytic platinum functions was characterized by this

titration method. The relative dispersion "Rel.D.", i.e., the relative platinum function is the ratio of the hydrogen adsorption of a treated catalyst to that of its fresh catalyst. For a check, some of the catalysts were evaluated by the dehydrogenation reaction of methyl-cyclohexane in a microreactor-GC system at 471°C under 1.0MPa, 5.7 mol ratio of hydrogen to hydrocarbon and a WHSV of 15.4h⁻¹. The relative activity is expressed as the conversion of the treated catalyst divided by that of the fresh catalyst.

Table I. Fresh Catalysts

Catalyst	B-6	B-7	B-8	803
Pt , m%	0.30	0.21	0.15	0.22
Re , m%	0.27	0.44	0.30	0.44
color	white	white	white	grey
Reduction	no	no	no	yes
H ₂ adsorbed at 90°C, H/Pt	1.08	1.33	1.16	1.00

Results

Effect of Temperature on the Platinum Functions. The catalysts of Table I were treated at the traditional temperatures in dehydration and reduction stages, 482°C and 494°C, in N₂ of 3600 h⁻¹ with a water concentration of 18000 ppm for 4 hrs. The results are listed in Table II.

Table II. Effect of Temperature at N₂ Purging on the Platinum Functions*

Catalyst	Temperature , °C	Color	Rel. D.
B-6	482	grey	1.05
	494	black	0.30
B-7	482	white	1.36
	494	black	0.51
B-8	482	black	0.34
	462	black	0.45
803	482	grey	1.03
	494	black	0.18

* Treated in N₂ with water of 18000 ppm for 4hr by space velocity of 3600h⁻¹.

It can be seen that treated at 482°C, all catalysts except B-8 did not have a visible change in the relative dispersion although the catalyst B-6 and 803 became

grey. When treated at 494°C, all catalysts suffered a decrease in the relative dispersion and became black. This indicates that most of PtRe-catalysts would start sintering at around 480°C in N₂ and sinter severely at higher temperature. In order to get good activity, this catalyst temperature should be lower than 480°C in N₂. For some special catalyst, such as B-8, the temperature should be even lower.

Effect of Oxygen on the Platinum Functions. On the basis of the mechanism of sintering in a non-hydrogen atmosphere (2) and in order to protect the platinum functions of the catalysts, we treated them at 482 ~ 494°C with different oxygen concentration from 0 to 21% in N₂ for 4 ~ 8 hrs. The results are shown in Table III.

Table III. Effect of Oxygen on the Platinum Functions

Catalyst	Treating Conditions				Rel. D.	Color
	O ₂ , %	H ₂ O, ppm	T, °C	Time, hr		
B-6	0.00	18000	494	4	0.30	black
	3.15	18000	494	4	0.88	grey
	3.15	18000	494	8	0.79	grey
	21.0	18000	494	4	1.05	white
B-7	0.00	18000	494	4	0.51	black
	3.15	18000	494	4	1.28	white
B-8	0.00	18000	482	4	0.34	black
	1.85	18000	482	4	1.30	white
	3.15	36000	482	4	1.06	white
	4.20	18000	482	4	1.21	white
	4.20	18000	482	8	1.28	white
	21.0	18000	482	8	1.30	white

It can be seen that the treated catalysts were white and had higher relative platinum dispersion than 1.0 if the oxygen concentrations in the used medium were higher than the stoichiometric, for example, 21%O₂ for B-6 and 3.15%O₂ for B-7 at 494°C, 1.85%O₂ for B-8 at 482°C. It indicates that different catalysts have different stabilities and a high oxygen concentration may protect the metallic functions of the reforming catalysts. It is believed that using a high oxygen-containing gas as the medium during dehydration in start-of-run will keep the catalyst in a high activity condition.

Effect of Hydrocarbons in N₂ on the Platinum Functions. In a commercial reforming unit some hydrocarbons are always present in the system. In order to examine their effects, the individual hydrocarbons, --- CH₄, C₂H₆, and n-C₆H₁₄---in N₂ were used to treat catalysts under simulating conditions of dehydration which was 482°C in N₂ or air, 3600 h⁻¹ for 4 hrs. The results are listed in Table IV.

Table IV. Effect of Hydrocarbons in Nitrogen on the Platinum Functions of Catalysts B-7 and B-8

No.	Medium	Color	Rel. D.	Rel. Activity	Coke %
1	No treatment	white	1.00	1.00	—
2	N ₂ , 41850ppm H ₂ O	white	0.96	1.01	—
3	16.6v% CH ₄ in N ₂	brown	—	0.95	—
4	7.2v% C ₂ H ₆ in N ₂	black	0.11	0.12	0.08
5	7.2v% C ₂ H ₆ in air	brown	0.29	0.33	0.05
6*	8.78v% n-C ₆ H ₁₄ in N ₂	bright-black	< 0.10	—	9.04
7*	8.78v% n-C ₆ H ₁₄ in air	bright-black	< 0.10	—	18.11
8*	1.32v% n-C ₆ H ₁₄ in air	grey	0.79	—	0.02

* Catalyst B-8.

The fresh catalysts B-7 and B-8 without treatment are white and we define their relative dispersions and relative activities as 1.0. When treated with 16.6v% CH₄ , B-7 was only little changed in its activity. But 7.2v% C₂H₆ decreased B-7 catalyst both in the relative dispersion and in the relative activity in N₂ as well as in air, forming 0.05~0.08% coke on the catalyst. Catalyst B-8 treated with 8.78% of n-C₆H₁₄ lost almost all capacity for adsorbing hydrogen. The n-C₆H₁₄ formed 9.04% coke in N₂ and 18.0% coke in air on the catalyst. It is clear that in a N₂ atmosphere, methane has a lower effect on the platinum, ethane affects it more and n-hexane has a severe effect on the platinum and the activities. Their deactivating mechanisms should be the formation of coke on the catalysts. Even a little of coke formed in N₂ , such as 0.05% and 0.08%, gives a high deactivation. Air may decrease the effect of hydrocarbons because it would oxidize them into CO₂ and H₂O. But it is strange that 8.78%n-C₆H₁₄ in air formed 18.11% coke (No.7) but formed 9.04% coke in N₂ (No.6). It is probably due to a selective oxidative dehydrogenation reaction going on on the catalyst when there was an excess of hydrocarbons in the system.

Effect of the Hydrogen Purity on the Catalysts . It is well known that the purity of the hydrogen in the reduction step affects the catalytic activities. In order to get some details about that, we reduced the catalysts at 482°C for 4hrs with hydrogen of various purities, containing N₂ , O₂ and/or hydrocarbons. Table V shows the results obtained in a reduction with N₂ in H₂ . With the concentration of N₂ in H₂ even up to 40% , the relative dispersion of the catalyst is still on a high level, more than 1.0. For checking the real dehydrogenation activity, the catalyst B-7 was reduced with 30% N₂ in H₂ , followed by dehydrogenation of methyl-cyclohexane. The relative activity obtained was 1.02. This shows that the high relative dispersion truly represents a high metallic catalytic activity.

Table V. Effect of N₂ in H₂ on the Platinum Functions during Reduction*

No.	N ₂ in H ₂ , v%	Color	Rel. D.	Rel. Activity
9	10	light grey	1.36	—
10	20	light brown	1.16	—
11	30	light brown	1.20	1.02
12	40	brown	1.11	—

* Reduction condition : 482°C, 1atm, 4hrs.

Usually, the colour of a well-reduced catalyst is a dark gray or black . In Table V, only the catalyst(No.9) reduced with 10% N₂ in H₂ is gray and all others are brown. It implies that these catalysts are not completely reduced. The high dispersion and high dehydrogenation activity might result from the further reduction with pure hydrogen during H₂-O₂ titration and dehydrogenation reaction . But anyway, it indicates that the nitrogen contained in hydrogen does not damage the activity of the reforming catalyst during its reduction but affects its extent of reduction . It was proved by other experiments that the catalyst could be well reduced with higher hydrogen partial pressures than 0.2 MPa even if the concentration of N₂ in H₂ was up to 30% .

Table VI shows the effects of oxygen and hydrocarbons in H₂ on the platinum functions of the catalyst B-7 after reduction at 482°C. The oxygen concentration up to 10% in H₂ keeps the catalyst still in good dispersion and high activity. It was proved by another experiment that all oxygen completely formed water, when a mixture of 10%O₂ and 90% H₂ was passed through the catalyst at 482°C. It indicates that some oxygen contained in hydrogen dose not give visible effect on the platinum dispersion and its catalytic functions during the reduction stage.

Table VI. Effect of Oxygen and Hydrocarbons on the Platinum Functions during Reduction of B-7*

No.	Gas in H ₂	Rel. D.	Rel. Activity
13	5.0 v% O ₂ + 41860ppm H ₂ O	1.04	1.05
14	10.0 v% O ₂	1.06	1.05
15	3.0 v% C ₂ H ₆	0.93	0.96
16	5.0 v% O ₂ + 5.0 v% C ₂ H ₆	—	1.04
17	1.53 v% n-C ₆ H ₁₄	0.67	0.02 % coke

* Reduction conditions : 482°C, 1atm, 4hrs.

Among the hydrocarbons in H₂ ethane gave a small effect on the catalyst with 0.96 relative activity but n-C₆H₁₄ gave more effects, decreasing the relative dispersion to 0.67 because of 0.02m% coke formed on the catalyst. This suggests that the more carbon atoms the hydrocarbon has, the greater the effect is.

Conclusion

1. The composition of the gas during dehydration and reduction at start-of-run affects the practical activities of reforming catalysts.
2. Most reforming catalysts would start platinum sintering at around 480°C in N₂, but any oxygen present may protect the catalysts from sintering during the dehydration step.
3. A small amount of ethane and the higher hydrocarbons in N₂ affect severely the metallic catalytic functions, and the larger the hydrocarbon molecule is, the more severe the effect is because of coke formation on the catalyst. High concentration of oxygen in N₂ may decrease the effect of hydrocarbons on the metallic function.
4. Nitrogen and oxygen in the presence in H₂ do not give considerable effect on the metallic function during catalyst reduction .
5. Hydrocarbons higher than ethane in H₂ will decrease the activity because of coke formation on the catalyst. But the effect of hydrocarbons in H₂ is less than that in N₂.

Literature Cited

- (1) Liu, Y. F.; Pan, G. Q., et.al., *Petroleum Processing*, 1990, 21, No.8, pp.37-42
- (2) Liu, Y.F.; Pan, G. Q.; Yang, J. J., *Petroleum Processing*, 1992, 23, No.9, pp.1-5

DEACTIVATION
OF HYDROPROCESSING CATALYSTS

Catalyst Deactivation in Commercial Residue Hydrodesulfurization

Hiroki Koyama¹, Eiichi Nagai, and Hideaki Kumagai¹

Mizushima Oil Refinery, Japan Energy Corporation, 2-1 Ushio-dori,
Kurashiki-shi, Okayama 712, Japan

It has been proposed that, as an increase in the conversion of vacuum residue in the commercial fixed-bed reactors, a coke-controlled catalyst deactivation regime appears in the last bed, where coke blocks the active sites as well as decreases the diffusivity. The activity and diffusivity tests were conducted for aged and regenerated catalysts, which were used in the commercial reactors, to investigate mechanisms of the deactivation by coke and metal deposition. The effects of residue conversion, reactor position, and time on-stream on the deactivation were investigated, comparing the catalysts aged at different conditions.

The Mizushima Oil Refinery of Japan Energy Corporation first implemented a high conversion operation of vacuum residue, versus a constant desulfurization operation, in the commercial residue hydrodesulfurization unit equipped with fixed-bed reactors, to produce more middle distillates as well as fuel oil with lower viscosity. The catalysts will be replaced when the sulfur content in the product oil reaches the allowable limit. Since we have believed that an increase in the residue conversion decreases the catalyst activity by coke deposition, we have been interested in controlling the coke deactivation to maximize the residue conversion during a scheduled operating period.

Though a number of researchers have proposed deactivation mechanisms and models of the residue hydrodesulfurization catalysts, most of them are correlated with the amount and distribution of Ni and V deposited on the catalyst surface (1, 2, 3, 4). Newson has proposed a semi-quantitative deactivation model accounting for pore plugging by both coke and metal sulfides (5). Bartholdy and Cooper studied the catalyst deactivation at a constant desulfurization operation and a high temperature operation (6). They suggest that a high temperature operation causes an initial larger activity loss due to coke deposition. Meyers et al. examined the effects of coke and metal sulfides on residue catalyst deactivation in three-stage expanded-bed reactors with a high residue conversion operation, and observed the largest deactivation in the

¹Current address: Petroleum Refining Research and Technology Center, Japan Energy Corporation, 3-17-35 Niizo-Minami, Toda-shi, Saitama 335, Japan

third bed due to coke deposition (7). They have proposed a simple deactivation model, in which the activity loss is proportional to the amount of coke and metal sulfides.

Those deactivation models accounting for both coke and metal sulfides are rather simple. Coke and metals foul residue hydrodesulfurization catalysts simultaneously via different processes, and decrease both intrinsic reaction rate and effective diffusivity. They never uniformly distribute in the commercial reactors. We have examined the activity and diffusivity of the aged and regenerated catalysts which were used at the different conditions as well as during the different periods. This paper describes the effects of vacuum residue conversion, reactor position, and time on-stream on the catalyst deactivation. Two mechanisms of the catalyst deactivation, depending on residue conversion level and reactor position, are also proposed.

Commercial Residue Hydrodesulfurization Unit.

Reactors and Catalysts. The reactor configuration consists of two reactor trains of two reactors in series each with two beds (8). Since the reactors are adiabatic, each bed temperature, except the first bed, is controlled by recycle hydrogen gas. However, as shown in Figure 1, the bed temperatures increase with reactor depth. A maximum reactor inlet temperature is set to avoid coking in the furnace coil and the first bed. A maximum reactor outlet temperature is limited by reactor shell metallurgy. The hydrodesulfurization catalyst, which occupies about 70% of a total catalyst volume, is packed in a lower half of the second bed and the whole third and fourth beds. The rest is the hydrodemetallation catalyst. We have used Orient Catalyst HOP-802 as the hydrodesulfurization catalyst, which contains about 2% Ni and 8% Mo on an alumina support.

Operations. Table I shows average properties of the feedstock, which is mostly the vacuum residue from a mixture of the Middle East crude oil. Figure 2 shows changes in the weight average bed temperature. The temperature is increased in a few weeks high enough to convert vacuum residue into low viscosity fuel oil. We normally start with atmospheric residue, and replace it with vacuum residue gradually while the temperature is increased. After that, the temperature is increased to compensate for the gradual decrease in catalytic residue conversion activity. Since the desulfurization activity decreases faster than the conversion activity, the product sulfur level increases with time. The operation conditions are carefully scheduled and controlled so that the product sulfur content does not exceed the specification by the end of a run. Though we normally conduct a high residue conversion operation shown in Figure 2, we once experienced a medium residue conversion operation, lowering the reactor temperature to cope with a temporary hydrogen shortage. We studied an effect of the residue conversion on the catalyst deactivation, comparing the catalyst used in both operations.

Table I. Feedstock of the Residue HDS Unit

Average Feedstock Properties		
Specific Gravity	15/4°C	1.04
Sulfur	wt%	4.9
Conradson Carbon	wt%	21
Nickel	wt ppm	40
Vanadium	wt ppm	125

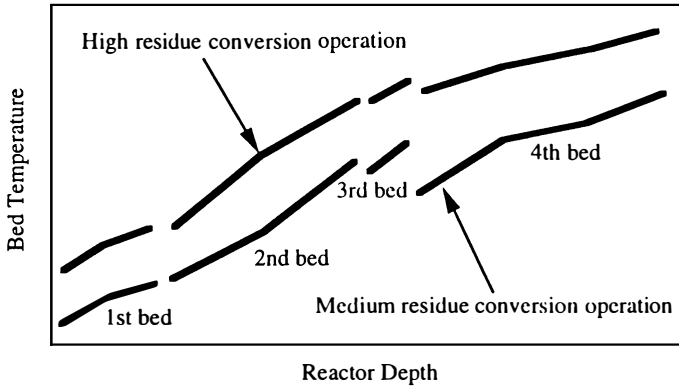


Figure 1. Reactor temperature profiles at the end of the runs.

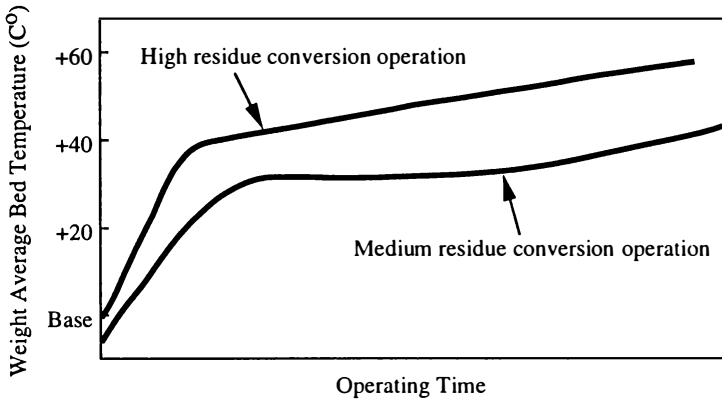


Figure 2. Changes in the reactor temperature with time.

Experimental

Catalyst Sampling and Preparation. The hydrodesulfurization catalysts used in the commercial reactors were sampled from different reactor positions after five-month operation, except one which was taken from the third bed two weeks after the start of the operation. During this short period, we did not charge vacuum residue at all. The used catalysts were Soxhlet-extracted with toluene followed by drying at 80 °C in vacuum. After the chemical analysis of those catalysts, the catalysts representing each bed were selected for the following activity and diffusivity tests. For the medium conversion operation, only the catalyst in the fourth bed was tested. The selected used catalysts were regenerated with 5 vol% oxygen in nitrogen, while a temperature is increased to 450 °C. Then, after holding the temperature for two hours, an oxygen content was increased to 21 vol% in four hours for complete coke removal.

Chemical and Physical Analysis. Carbon on the aged catalysts was determined by combustion, and metals were determined by wet chemical analysis and atomic absorption. Surface areas and pore volumes were measured by the standard BET method using nitrogen and the mercury porosimetry, respectively. All analyses were given on a fresh catalyst basis.

Activity Tests with Atmospheric Residue. Activity tests with Arabian Heavy atmospheric residue were conducted for the fresh and aged catalysts in a fixed-bed reactor with 100 cm³ catalyst bed at a temperature of 360 °C, pressure of 12 MPa, and a LHSV of 1.0 Hr⁻¹. Such a mild reaction condition was chosen to keep from further coke build-up during the test runs. The catalysts were presulfided with carbon disulfide in light gas oil up to 300 °C. A product sample was taken 18 hours after an operation condition was settled.

Activity Tests with Model Compounds. Activity tests with model compounds were also carried out for the fresh, regenerated, and aged catalysts in a fixed bed reactor under a vapor phase condition at 5.0 MPa. 3 cm³ of crushed catalyst (0.35 - 0.5mm) was diluted with 9 cm³ of inactive alumina particles. Catalyst activities, such as hydrodesulfurization (HDS), hydrodenitrogenation (HDN), and hydrogenation (HG), were measured, feeding a mixture of 1 wt% carbon dioxide, 1wt% dibenzothiophene, 1 wt% indole, and 1 wt% naphthalene in n-heptane. The catalysts were presulfided with a 5% H₂S/H₂ mixture at 400 °C for two hours and aged with a liquid feed at a reaction condition for 24 hours. Tests for HDS and HDN reactions were conducted at 275 °C, while those for a HG reaction were done at 325 °C. Condensed liquid products were analyzed with gas chromatography. Since all the reactions took place with the crashed catalysts in the vapor phase, we assumed that effectiveness factors were unity (9).

Diffusivity Tests. Diffusivity tests were conducted for crushed catalysts (0.18 - 0.26 mm) using the technique demonstrated by the previous workers (9). Changes in coronene concentration from 30 mg/cm³ in cyclohexane with time were measured in a tank stirred at 600 r.p.m. at an ambient temperature and pressure. Cyclohexane was dried with molecular sieve before use. The catalyst of about 200 to 300 mg, which was dried at 200 °C for three hours, was contained in the basket attached on the stirring shaft, and was soaked with 400 cm³ of the coronene solution in the tank. 2 cm³ of the solution was taken several times at a certain interval in five hours, and changes in the coronene concentration were measured with a UV spectroscopy. Coronene uptake was calculated from a change in its concentration in the tank.

Equilibrium uptake was measured in the separate tests, where the catalysts were soaked with the coronene solution in small bottles for eight days.

Results

Catalyst Inspections. Chemical analysis and physical properties of the used catalysts are shown in Table II, comparing the fresh catalyst. Maximum average bed temperatures where the catalysts were exposed are also shown relative to that of the third bed catalyst aged only for two weeks. Coke on the catalyst after the complete operation increased from the second bed to the fourth bed, while metals on the catalysts decreased conversely. A decrease in the surface area and pore volume with reactor depth implies a larger effect of coke deposition. Coke deposited more on the fourth bed catalyst used at the high residue conversion operation (catalysts F and G) than that used at the medium residue conversion operation (catalyst H), while similar amounts of metals accumulated on both catalysts. However, no large difference in amounts of coke and metals on the second and third bed catalysts was observed between those two operations. Comparing an amount of coke on the catalyst B with the catalyst D or E, in the third bed, coke did not increase after two weeks, but it seems to have slightly decreased as metal accumulated.

Table II. Chemical and Physical Analyses of Catalyst Samples

Age	Catalyst Samples						
	Fresh	2 weeks	21 weeks		22 weeks		
Ave. 1100°F Conversion			46% (High)		38% (Medium)		
Catalyst Bed		3rd	2nd	3rd	4th	4th	
Catalyst No.	A	B	C	D/E	F/G	H	
Deposits							
C	g/100g cat.	-	16.8	12.1	15.7/13.0	25.1/22.2	17.3
Ni+V	g/100g cat.	-	0.5	21.2	15.2/14.8	6.5/ 6.8	7.8
C/H	mol/mol	-	0.62	0.61	- /0.82	1.18/1.08	0.87
Physical Properties							
Surface Area	m ² /g	205	187	187	169/169	147/160	-
Pore Volume	cm ³ /g	0.57	0.40	0.38	0.35/0.35	0.32/0.34	-
Max. Bed Temp.	C°	-	Base	+25	+35	+35	+25

Catalyst Activities. Figure 3 shows the residue hydrodesulfurization activities of the aged catalysts relative to the fresh catalyst. Though no large change in the amount of coke on the aged catalyst was observed after the tests, 11 wt% coke built on the fresh catalyst during the test. Therefore, the activity of the fresh catalyst was close to that of the third bed catalyst used for two weeks (catalyst B). The activities of all the catalysts, except the fourth bed catalysts used at the high residue conversion operation (catalyst F and G), lay on the same asymptotically declining curve, versus amounts of metals. The large activity drops of the catalyst F and G from the curve imply a large effect of coke deposition.

Figure 4 shows the dibenzothiophen conversion activities of the aged and regenerated catalysts relative to the fresh catalyst, versus amounts of metals. The activities are considered to be proportional to the remained active sites on the catalyst surface because effectiveness factors are assumed to be unity in this test. An activity loss of the regenerated catalysts is considered to be caused by metal poisoning,

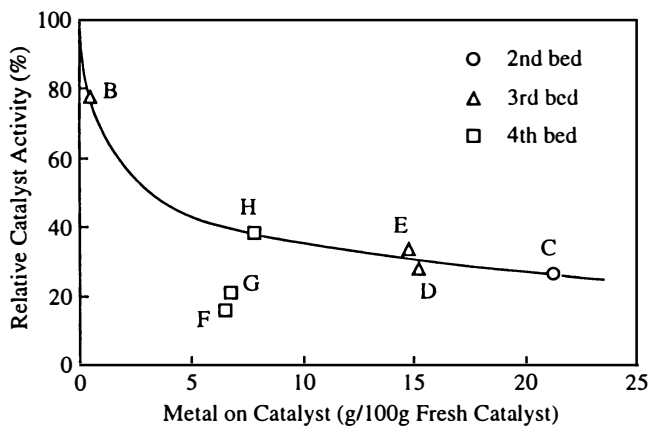


Figure 3. Residue hydrodesulfurization activities.

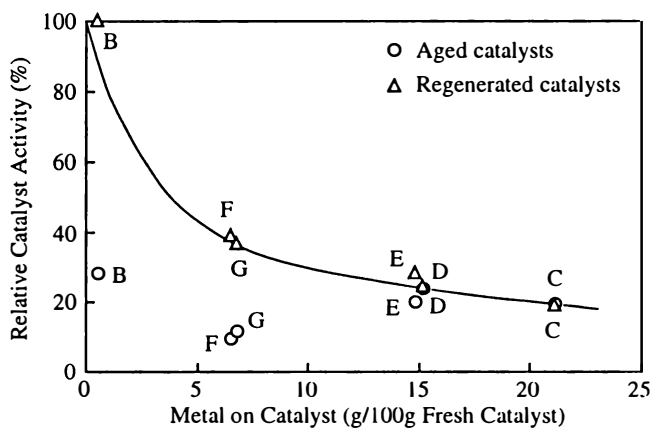


Figure 4. Dibenzothiophene conversion activities.

assuming neither agglomeration of the active sites nor activity of the metal sulfides. The third bed catalyst (catalyst B) lost 70% of the active sites by coke deposition within two weeks. After the run, it lost 80% of the active sites, which were mostly poisoned by metal sulfides instead of coke (catalyst D and E). Only 10% of the active sites were remained in the fourth bed catalysts (catalyst F and G) after a high residue conversion operation. 60% of the active sites were poisoned by metal sulfides, while 30% was fouled by coke. Figure 5 shows the activity loss for hydrodesulfurization, hydrodenitrogenation, and hydrogenation by coke and metal sulfides for the catalyst C, E, and F. A HDN means a conversion of a C-N bond from Indoline (10). A HDN activity was most sensitive to coke fouling, while a HG activity was least. On the contrary, a HG activity was most sensitive to metal poisoning, while a HDN activity was least. These results imply that HDS, HDN, and HG reactions may need different active sites.

Catalyst Diffusivity. Figure 6 shows changes in the fractional uptake of coronene with time for the fresh, aged, and regenerated catalysts. A decrease in the diffusivity decreases a rate of the coronene uptake, or increases a time to reach an equilibrium, where the fractional uptake is unity. Since the catalysts were crushed, it may make an influence of pore mouth plugging by metal sulfides smaller. However, since we did not observe any sharp decrease in the activity during the end of the runs, we do not believe that pore mouth plugging occurred. Therefore, an increase of the diffusivity after the regeneration fairly shows an effect of coke deposition.

The diffusivity of the second bed catalyst (catalyst C) was increased by the regeneration, but it was still lower than that of the fresh catalyst (catalyst A). This indicates that both coke and metal sulfides have a responsibility for a decrease of the diffusivity. Comparing the diffusivity between the catalyst B, on which only coke deposited, and the regenerated catalyst C, the initial coke deposit lowers the diffusivity more than the ultimate metal deposit. The fourth bed catalyst (catalyst F) showed the least diffusivity due to a large amount of coke deposit.

Discussion.

Catalyst Deactivation at a High Residue Conversion Operation. The chemical analysis (Table II) and the residue activity test (Figure 3), clearly show that, during a high conversion operation of vacuum residue, the hydrodesulfurization catalyst in the fourth bed is most deactivated due to a large amount of coke deposit. The model compound activity test (Figure 4) and the diffusivity test (Figure 6) also demonstrate that coke decreases both active sites and diffusivity, respectively. Comparing the operations of two different conversions, it is suggested that an increase in a conversion of vacuum residue increases an amount of coke deposit on the catalyst in the fourth bed, causing a decrease of the activity (Table II and Figure 3). As shown in Figure 3, the catalyst activity in the fourth bed used at the medium residue conversion operation (catalyst H) seems to lie on the curve tied with those in the second and third beds. This implies that there may exist a regime of coke-controlled deactivation in the fourth bed at a high conversion of vacuum residue, a boarder of which may be between 40 and 45%.

Generally, an amount of coke on the catalyst increases from the entrance to the exit of the fixed bed reactors in residue hydroprocessing (1, 6, 7). Tamm et al. showed the highest remained catalyst activity at the outlet of the bench-scale fixed-bed reactor after a constant desulfurization operation (1), while Myers et al. found the highest catalyst deactivation rate in the last stage of three-stage pilot-scale expanded-bed reactors after a 60 - 70% vacuum residue conversion operation (7). These results from two typical reactor operations support that the catalyst deactivation in a lower

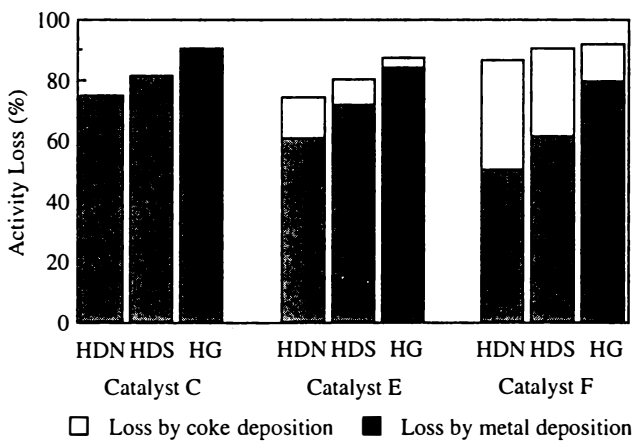


Figure 5. Activity losses of HDS, HDN, and HG reactions by coke and metal sulfides deposition.

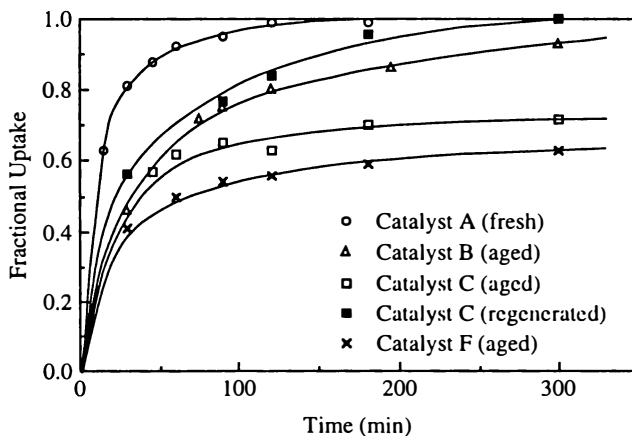


Figure 6. Fractional uptake of coronene versus time.

bed of the reactor is controlled by coke deposition at a high residue conversion region.

Roles of Coke and Metals on Catalyst Deactivation. The model compound activity test (Figure 4) and the diffusivity test (Figure 6) clearly show that both coke and metal sulfides have a responsibility for decreasing intrinsic reaction rate and effective diffusivity. However, the former test suggests that coke and metal sulfides do not independently affect the active sites. As shown in Figure 4, in the third bed, coke rapidly covered more than 70% of the original active sites at the start of the run. However, after the run, the ratio of the coke-covered active sites to the original ones dropped drastically to less than 10%, while that of the metal-poisoned active sites became around 70%. This indicates that the metal sulfides deposit on part of the active sites which coke initially covers and permanently poison them.

Coke preferentially deposits on the alumina support, growing in thickness, and blocks the active sites (11). As shown in Table II, a slight decrease in the amount of coke on the catalyst in the third bed with time implies that metal sulfides may reveal the coke which blocks the active sites when they deposit on the catalyst surface. The electron microprobe analysis also showed a decrease in coke with metal deposition (1). Therefore, we assume that part of the coke which blocks the active sites may be hydrogenated by metal sulfides and taken off.

Figure 5 shows that coke deactivates a HDN activity more than a HG activity. If acidic sites favor hydrogenolysis of a C-N bond like a hydrocracking reaction, loss of the acidic sites of an alumina support by coke deposition will decrease the HDN activity. Therefore, this result may support preferential deposition of coke on an alumina support.

Deactivation Process. There exists three stages of catalyst deactivation in residue hydrodesulfurization, such as an initial rapid deactivation stage, an intermediate slow deactivation stage, and an ultimate fast deactivation stage. Usually the last stage is attributed to pore plugging with metal sulfides (1, 2, 4). However, we have not observed this stage in the commercial operations. This may be because coke fouling determines the catalyst life rather than pore mouth blockage by metal sulfides at a high residue conversion operation. Therefore, we discuss the initial and intermediate deactivation stages in the commercial operation.

Initial Catalyst Deactivation. The horizontal axis in Figure 4 is not a cumulative amount of metal sulfides on the same catalyst but their ultimate amount on the different used catalysts. However, if we can assume that the catalyst activity loss is simply a function of an amount of metal sulfides on the catalyst surface, Figure 4 will show a change in a relative activity with metal accumulation. This graph shows that the activities of the regenerated catalysts lie on the single curve decreasing asymptotically with metal accumulation. This nonlinear correlation implies that not all the metal sulfides which deposit on the catalyst surface poison the active sites. We propose two stages of metal deactivation. During the first stage, metal sulfides preferentially deposit on the active sites and poison them. Since the diffusion of organic metal compounds in the catalyst pore is slow, the poisoning progress from the pore mouth toward the center. During the second stage, metal sulfides build up with a multilayer near the pore mouth and restrict the diffusion of reactants. However, since this further restricts the diffusion of the organic metal compounds to the center, a progress of the poisoning becomes slower. This is consistent with the models proposed previously (1, 2, 3, 4)

As shown in Figure 4, in the third bed, after coke covers 70% of the active sites during the initial short period, 10% of the active sites were further lost by the end. Since no more coke built on the third bed catalyst after the initial deposition, we

assume that metal poisoning causes this further loss of the active sites during the first stage of the metal deactivation. According to the residue activity test (Figure 3), after the rapid coke deactivation, the activity of the third bed catalyst dropped to a half by the end. This magnitude of the activity loss is larger than that of the active-site loss. This suggests that a decrease of the diffusivity due to metal deposition also decreases the activity of residue desulfurization.

We roughly estimated a change in the desulfurization activity of each bed with metal accumulation, assuming a correlation between hydrodesulfurization and a bed temperature rise and a simple increase in metals on the catalyst with time. As shown in Figure 7, the catalyst activity curves in the second and third beds consist of the initial fast deactivation period and the following slow deactivation period, while that in the fourth bed shows much faster deactivation after the initial period.

Since initial coke deposition is so rapid, we propose that metal poisoning has a major responsibility for this initial fast deactivation period. This is consistent with the deactivation mechanism proposed by Tamm et al. (1).

Intermediate Catalyst Deactivation. Except the coke-controlled regime, an increase in the metal layer thickness in the pore mouth may be a major cause of the slow deactivation following the initial fast deactivation period as pointed out, though Figure 4 shows a slight decrease in the active sites due to metal poisoning during this period.

Figure 7 shows that the catalyst activity of the fourth bed at a high residue conversion continuously decreased throughout the run. Therefore, in the coke-controlled regime, we believe that coke steadily increases throughout the run. Bartholdy and Cooper suggest that coke becomes more graphitic with time and may cover more active sites even if an amount of coke does not increase after the initial deposition (6). Table II shows that the highest aromaticity of coke on the fourth bed catalyst after the high residue conversion operation. However, Meyers et al shows that coke steadily increased in the third reactor while it reached equilibrium soon in the first reactors during a 30-day high residue conversion operation. This result is very similar to our observation in the commercial reactors. We also observed a steady increase in coke after the initial deposition at the exit of the bench-scale fixed-bed reactor with a high temperature operation (12).

It has been believed that coke is produced by the precipitation of large molecular hydrocarbons such as asphaltenes when their solubility in oil is lowered (13, 14). An increase in the conversion of vacuum residue increases the aromaticity of the asphaltenes and decreases the aromaticity of the maltenes (15). Consequently, the solubility of the asphaltenes in the maltenes decreases. Absi-Halabi et al. propose that absorption of asphaltenes on the acidic sites of an alumina support is a major cause of the initial rapid coke deactivation, while a decrease in asphaltene solubility causes the following steady coke build-up (14). This explains that an amount of coke increases from the entrance to the exit of the reactors as asphaltene solubility decreases and that an increase in the residue conversion increases an amount of coke in the reactor exit.

Conclusions

A study on the residue hydrodesulfurization catalysts used in the commercial reactors has suggested that there exists two deactivation mechanisms such as metal-controlled deactivation and coke-controlled deactivation, depending on a residue conversion level. In the second and third bed, the deactivation is controlled by metal deposition. However, in the fourth bed, a coke-controlled deactivation appears at a high residue conversion. We also have proposed that there exist two stages in the metal-controlled deactivation. During the first stage, metal sulfides partially poison the active sites and

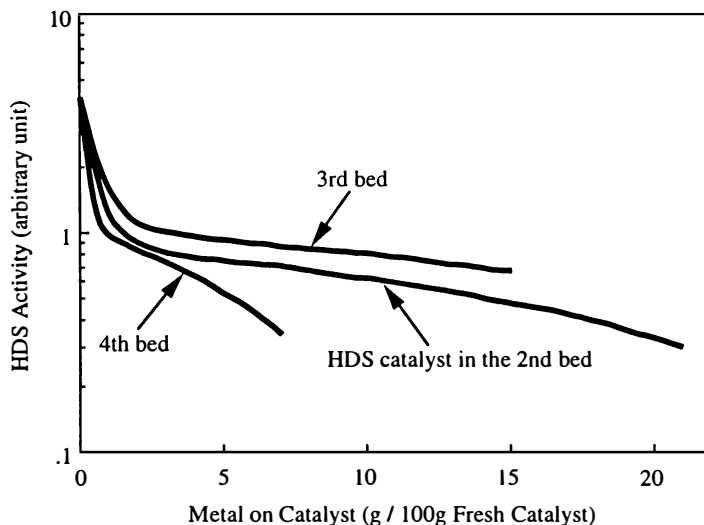


Figure 7. Deactivation curve of HDS catalyst in each bed.

causes fast deactivation. The metal sulfides deposit not only on the fresh active sites but also on the active sites which coke initially covers. During the following stage, metal sulfides build up with a multilayer near the pore mouth and restrict the diffusion of reactants, causing slow deactivation.

References

1. Tamm, P. W.; Harnsberger, H. F.; Bridge, A. G. *Ind. Eng. Chem. Proc. Des. Dev.* **1981**, *20*, 262.
2. Dautzenberg, F. M.; Van Klinken, J.; Pronk, K. M.; Sie, S.T.; Wijffles, J. B. *Chem. React. Eng. Cong.* **1981**, *21*, 254.
3. Hannerup, P. N.; Jacobsen, A. C. *ACS Prepr. Div. Petrol. Chem.* **1983**, *28*, 576
4. Ahn, B-J; Smith J. M. *AIChE J.* **1984**, *30*, 739.
5. Newson, E. *Ind. Eng. Chem. Proc. Des. Dev.* **1975**, *14*, 27.
6. Bartholdy, J.; Cooper, B. H. *ACS Prepr. Div. Petrol. Chem.* **1993**, *38*, 386
7. Myers, T. E.; Lee, F. S. Myers, B. L.; Fleisch, T. H.; Zajac, G. W. *AIChE Symp. Series* **1989**, *85*, 21.
8. Koyama, H.; Nagai, E., Torii, H.; Kumagai, H. *NPRA Annual Meeting* **1995**, AM-95-43
9. Johnson, B. G.; Massoth, F. E.; Bartholdy, J. *AIChE J.* **1986**, *32*, 1980.
10. Muegge, B. D.; Massoth, F. E. *Fuel Processing Technology*; Elsevier Science: Amsterdam, 1991, Vol. 29.; pp 19-30.
11. Deiz, F.; Gates, B. C. Miller, J. T.; Sajkowski, D. J.; Kukes, S. G. *Ind. Eng. Chem. Res.* **1990**, *29*, 1999.
12. Unpublished
13. Wiehe, I. A. *Ind. Eng. Chem. Res.* **1993**, *32*, 2447
14. Absi-Halabi, M.; Stanislaus, A.; Trimm, D. L. *Applied Catalysis*; Elsevier Science: Amsterdam, 1991, Vol. 72.; pp 193-215.
15. Takatsuka, T.; Wada, Y.; Hirohama, S.; Fukui, Y. *J. Chem. Eng. Japan*, **1986**, *22*, 298

Deactivation of Light Naphtha Aromatization Catalyst

S. Fukase¹, N. Igarashi¹, K. Aimoto¹, and K. Kato²

¹Petroleum Refining Research and Technology Center, Japan Energy Corporation, 3-17-35 Niizo-Minami, Toda-shi, Saitama 335, Japan

²Petroleum Refining Department, Japan Energy Corporation, Toranomon, Minato-ku, Tokyo 105, Japan

Deactivation of light naphtha aromatization catalyst based on zeolite was studied, by kinetic analysis, micropore volume analysis and model reactions. Coke accumulates at the entrance of zeolite channel, blocks it and hinders reactant molecule to access active sites in zeolite channel. Our own stabilization technique passivates coke-forming sites at the external surface of the zeolite. This minimizes the coke formation at the entrance of zeolite channel and increases on-stream stability. The stabilized catalyst enabled us to develop a new light naphtha aromatization process using an idle heavy naphtha reformer that is replaced by CCR process.

Aromatics are produced mainly by the catalytic reforming of heavy naphtha in the petroleum refining industry. In recent years, light hydrocarbons have become an alternative source of aromatics. Several processes have been developed for this reaction : Cyclar (1), Z-former (2) and Aroformer (3). Zeolitic catalysts with MFI structure are generally chosen for this reaction, because of their lower coking tendency. However the operating conditions required for the process results in a catalyst carbon lay-down rate which is unsuitable for a conventional fixed bed catalytic operation. Thus development of those processes was directed towards continuous or swing-type regeneration because of rapid decline of catalyst activity.

The economics of light hydrocarbon aromatization processes do depend on the initial investment cost, mainly construction cost, and the price difference between the feedstock and aromatics. Due to the massive construction cost and no expected widening in the feedstock/BTX price difference, the payout years of a construction cost would be lengthy.

One solution of this problem is to develop a new aromatization process using a conventional fixed bed, thus avoiding the need to construct CCR type or swing type reactor unit. Currently in many refineries, conventional "semi-regenerated type" heavy naphtha reformers have been replaced by CCR reformers. A number of these units are currently unused and available for another use of light naphtha aromatization. Modernization of these units to aromatize light naphtha may prove economically justifiable. The objective of the development of "LNA" process, thus, is to develop a new catalyst having extended stability which enables us to use conventional fixed bed reactors, minimizing initial construction cost.

The deactivation of acid zeolite catalysts is mainly due to the coke deposit within

the pores or on the external surface of the crystallites. The prevention of coke deposit is the key to success for the development of LNA process.

Under these circumstances, Japan Energy Corporation has conducted extensive research on the development of a new aromatization catalyst that exhibits high activity and excellent inhibition of coke formation (4, 5). On the basis of this fundamental research, we have operated the LNA demonstration plant. The present work describes the phenomena responsible for the deactivation of LNA catalyst.

Experimental.

Catalyst. Zinco-aluminosilicates (Si/Al = 30) were prepared by the method described elsewhere (6). Subsequently, the zeolites were stabilized by our proprietary technique of steaming. HZSM-5 having Si/Al ratio of 40 obtained from PQ Zeolite (CBV 8020) was also used to study the effect of steaming on deactivation.

Catalytic Activity Measurement. The reaction was carried out in a stainless steel microflow reactor. In each run, 2 g catalyst was placed in the reactor and heated to 520 °C under a nitrogen stream. The nitrogen stream was replaced by a light naphtha vapor fed by a micro plunger pump. The reaction was carried out at 520 °C, under various pressures and WHSVs without any hydrogen addition. The products were analyzed periodically by gas chromatography. The properties of the light naphtha are shown in Table I.

Table I Properties and components of the Feedstock

Density	(g/cm ³)	0.6591
Sulfur	(ppm)	<0.1
Nitrogen	(ppm)	<0.3
H ₂ O	(ppm)	13
<hr/>		
Components	(wt%)	
n-C5		32.3
i-C5 + C5 naphthene		17.8
n-C6		15.1
i-C6 + C6 naphthene		24.9
n-C7		2.1
i-C7 + C7 naphthene		5.4
n-C8		0
i-C8		0.1
Benzene + Toluene		2.3

Reproduced with permission from ref. 7. Copyright 1995

Micropore Size Distribution Analysis. Low pressure nitrogen adsorption and desorption of fresh and coked catalysts were carried out using an Omicron Technology Omnisorp 100CX. The data for the adsorption isotherms were collected at very low partial pressures of nitrogen ($P/P_0 < 10^{-1}$) to determine the BET surface area and the micropore volume. The micropore volume was estimated from the t-plots. The desorption isotherm was obtained to measure meso and macro pore volume which correspond to the pore volume larger than pore radius of 1nm.

Probe Molecule Reaction. Two probe molecules, cumene and 1, 3, 5-triisopropylbenzene were chosen to study the active sites on the zeolite. Triisopropylbenzene molecule is too bulky to penetrate into intracrystalline micro pore of MFI type zeolite, thus the cracking reaction takes place only on the external surface of the

zeolite. On the other hand, the intracrystalline pore of MFI zeolite is large enough to accommodate cumene molecule. Accordingly, the reaction of cumene cracking can be used to study the active site of both in the intracrystalline pore and on the external surface of the zeolite, while triisopropyl-benzene can be a probe molecule to detect active sites on the outer surface of the zeolite.

The reactions were carried out in a microflow reactor at 270 °C, under the partial pressure of the reactant of 0.1 kg/cm²G (nitrogen balance).

Results and discussion.

Stability of Various Catalysts. Experiments were conducted to investigate deactivation of the various catalysts. The conversion of light naphtha is defined here by the following equation:

$$\text{Conversion} = (\text{Products} - \text{AR}_0) / (1 - \text{AR}_0) \quad (1)$$

where,

AR₀ = fraction of aromatics in the feed naphtha
 Products = (H₂ + (C₁ to C₄) + (C₅₌ + C₆₌) + aromatics) in product

We examined the activity of various catalysts without any stabilization under weight hourly space velocity of 0.7 hr⁻¹ at 3 kg/cm²G. Hydrothermally synthesized zinco-aluminosilicate showed the best stability among those as was reported elsewhere (7). Even if zinco-aluminosilicate demonstrated fairly good stability, it deactivated after 150 hrs. This is not long enough to be used in a conventional fixed bed unit. Therefore we carried out further study to enhance the stability of the zinco-aluminosilicate catalyst.

Deactivation of the Catalyst after Stabilization Treatment. We studied the effect of stabilization treatment on the deactivation of zinco-aluminosilicate. Figure 1 shows variation of light naphtha conversion with time on stream under weight hourly space velocity of 5 hr⁻¹ at 3 kg/cm²G of total pressure over two catalysts, stabilized and unstabilized zinco-aluminosilicates, respectively. Higher space velocity was employed here to accelerate catalyst deactivation. The catalyst without stabilization showed rapid decline of activity compared with stabilized one. The analysis of coke deposit on the unstabilized catalyst suggested coke yield of 0.066 wt% on feed, which was about 6 times higher than that of the stabilized catalyst. Stabilization was found to be very effective in minimizing coke formation.

Acid Strength Distribution After Stabilization Treatment. The acid strength distributions of the zeolites were determined by temperature-programmed desorption of ammonia equipped with a thermal conductivity detector. The detailed procedure has been given in the early paper (6).

A comparison of the TPD spectra shown in Figure 2 indicates a large reduction in both the weak and strong acid sites of the zinco-aluminosilicate after the stabilization treatment. The decrease in the total number of acid sites is expected to be the result of the removal of aluminum from the zeolite matrix.

Kinetics of Catalyst Deactivation. In order to study the kinetics of the deactivation of stabilized catalyst, we carried out several sets of experiment varying pressure, with constant space velocity and with constant contact time, respectively. We assumed that reaction rate of light naphtha conversion conforms to first-order kinetics with respect to light naphtha concentration and that the decreasing rate of active site, which is caused by coke deposition, is expressed by first order. Then catalyst activity is described as exponential deactivation (8).

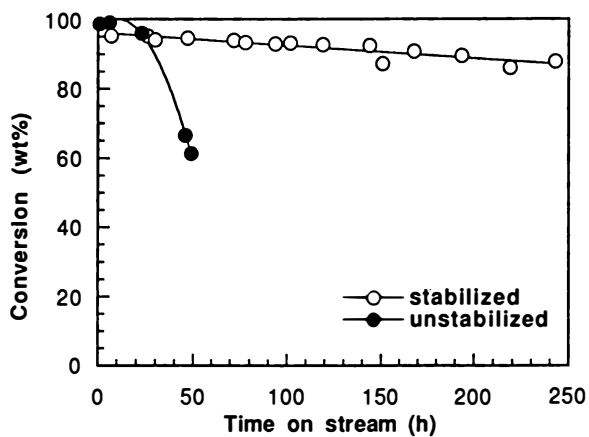


Figure 1. Deactivation of the catalyst with stabilization treatment.

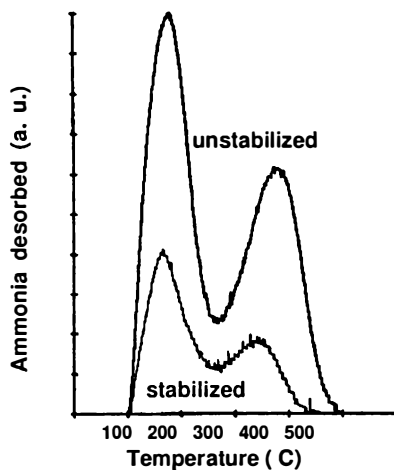


Figure 2. Ammonia TPD spectra of the stabilized and unstabilized catalysts. (Reproduced with permission from reference 7. Copyright 1995 Elsevier.)

$$k = k_0 \exp(-\alpha t) \quad (2)$$

where k = rate constant of light naphtha conversion
 α = aging rate constant
 t = time-on-stream

Figures 3 and 4 show catalyst deactivation under various pressures, with constant space velocity and with constant contact time, respectively. The linear relationships between kinetic constant and time-on-stream in both figures indicate that decreasing rate of active site on the stabilized catalyst is expressed as first-order kinetics with respect to concentration of active site.

Figure 3 shows variation of rate constant with time-on-stream at WHSV of 2.0 hr⁻¹. The figure suggests that aging rate constant does not depend on reaction pressure within the range of 3 - 8 kg/cm²G. Higher reaction pressure decreased initial rate constant of light naphtha conversion.

Figure 4 shows the result at the constant contact time of 17.5 second. In this experiment the space velocity was adjusted to have the same contact time with increasing pressure. The figure indicates that aging rate becomes greater with increasing pressure. This is considered to be due to the increased space velocity. However, the initial rate constants for three experiments are nearly equal.

The fact that deactivation of the stabilized catalyst is expressed as first-order kinetics with respect of concentration indicates that site coverage is responsible for the deactivation of the stabilized catalyst.

Rate constants of the unstabilized and stabilized catalyst shown in Figure 1 were calculated. The result indicated that the unstabilized catalyst deactivated faster than expected from exponential deactivation. This suggests that the deactivation mechanism of the unstabilized catalyst is different from simple site coverage.

Micropore Analysis by Nitrogen Adsorption. Low pressure nitrogen adsorption of stabilized and unstabilized catalyst was carried out to analyze micropore volume. Coked catalysts discharged from the experiment shown in Figure 1 were examined. The analysis suggests 16% of coke on catalyst for both samples. The nitrogen adsorption isotherms in the low pressure range up to p/p_0 of 0.01 are presented in Figure 5. The physical properties of those catalysts are shown in Table II.

Table II Properties of Coked Catalysts

	unstabilized		stabilized	
	fresh	coked	fresh	coked
Coke (wt%)	-	16.6	-	16.1
BET surface area (m ² /g)	387	74	355	285
Micropore volume (ml/g)	0.083	0.014	0.099	0.070
Meso & macro PV (ml/g)	0.27	0.15	0.24	0.17

Low pressure nitrogen adsorption isotherms of coked catalysts, in Figure 5 showed smaller amount of volume adsorbed in the coked unstabilized catalyst than stabilized catalyst samples. This is due to a large difference in micropore volume, shown in Table II.

A comparison of the micropore volume of the coked catalyst samples, shown in Table II, clearly illustrates that the coked-stabilized catalyst sample possesses 70% of internal pore volume, which is almost free of coke and is accessible to nitrogen. On the other hand, the coked-unstabilized catalyst sample showed large reduction of micropore. This indicates a virtual blocking of the internal pores in the coked sample

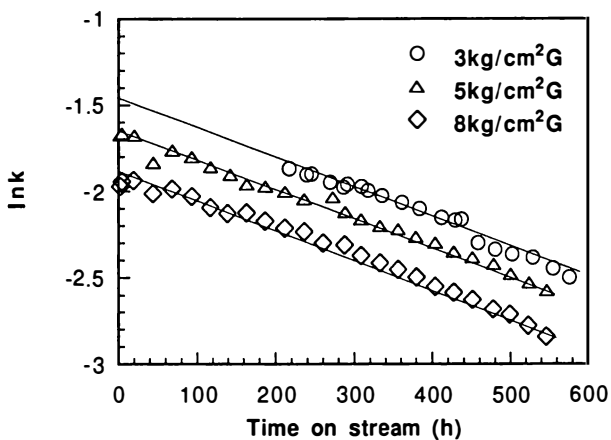


Figure 3. Variation of rate constant of light naphtha conversion with increasing pressure under constant space velocity over the stabilized catalyst.

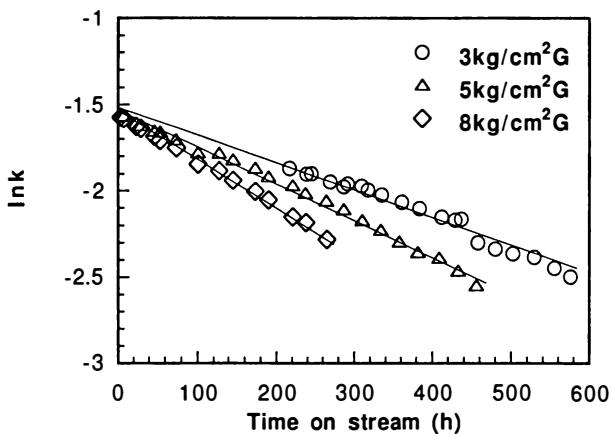


Figure 4. Variation of rate constant of light naphtha conversion with increasing pressure under constant contact time over the stabilized catalyst.

of unstabilized catalyst. Hence, the coke is considered to block the channel entrance of the unstabilized catalyst. This hinders free access of nitrogen to internal pore. Therefore, we believe that the stabilization treatment suppresses the coke formation at the zeolite channel entrance.

Larger amount of reduction in meso and macro pore volume was observed with the unstabilized catalyst than the stabilized catalyst after coking. The volume occupied by coke in the meso and macro pore region decreased by the stabilization treatment.

Surface Characterization of the Stabilized Catalyst by Probe Molecule Reaction. HZSM-5 obtained from PQ Zeolite was chosen to study the mechanism of stabilization in light naphtha aromatization. The reactions of both molecules were carried out over stabilized and unstabilized HZSM-5. We assumed first order kinetics with respect to each reactant concentration and first order decay of each reaction, and calculated initial rate constants. Figure 6 shows the initial rate constants of cumene cracking and triisopropyl-benzene cracking over the stabilized and the unstabilized catalysts.

The figure shows the large reduction in the rate constants of triisopropyl-benzene cracking. This suggests that large number of the acid sites on the external surface of the zeolite was removed by the stabilization, while the majority of the acid sites in the intracrystalline micro pore remained.

Modification of Acidity by Stabilization Treatment. Steaming of zinc-aluminosilicate can modify its acidity and enhances its stability as was shown above. However, steaming can also change the location and the activity of zinc species, and might lead to the better stability of the catalyst. It is known that migration and redispersion of metal species provide good on-stream stability of the aromatization catalyst (9). In order to clarify this by separating acid function from metal function, reaction of n-pentane was carried out over stabilized and unstabilized HZSM-5. The enhancement of catalyst stability because of acid modification can be clearly illustrated by using HZSM-5. The same stabilization treatment was performed to HZSM-5 and similar reduction in the total number of acid sites was observed. We performed several sets of experiments, varying time on stream at 520 °C, under various 3kg/cm²G and WHSV of 2 hr⁻¹ without any hydrogen addition. The catalyst was discharged after each experiment and coke content was analyzed.

Figure 7 shows an improvement of catalyst stability after the stabilization treatment. This clearly indicates that modification of acidity by steaming can enhance the stability of HZSM-5. The coke deposited on the catalysts were analyzed and divided by the total number of acid sites determined by ammonia TPD. It was expressed as the amount of coke per number of acid site and the result is shown in Figure 8. The figure demonstrates that there is no change in the amount of coke produced by the acid site after the stabilization treatment. This may suggest the nature of coke-forming sites for both stabilized and unstabilized catalysts are identical. Therefore we do not expect predominant passivation of some of the acid sites with certain strength and nature.

We have not determined the change in the location of zinc and its nature. Accordingly, our results do not contravene the contribution of zinc modification. However, we believe that modification of acid property plays an important role in increasing the catalyst stability.

Above studies suggest following thing. Large decline of coke-forming rate by the stabilization is considered to be due to the reduction of acid site density on the external surface. And the chance of pore mouth blocking is remarkably reduced by this external passivation. It is known that at high temperature coke molecules trapped in HZSM-5 channels overflow onto the external surface (10). The overflowed coke

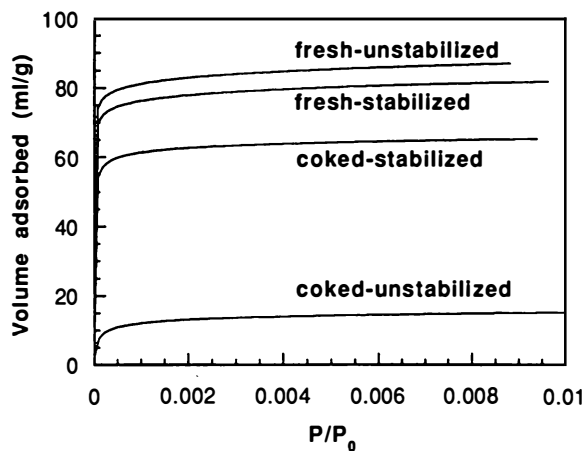


Figure 5. Low pressure nitrogen adsorption isotherms of catalysts.

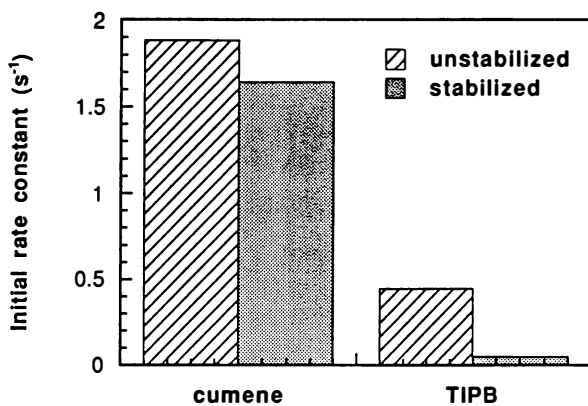


Figure 6 Effect of the stabilization on probe molecule reaction.

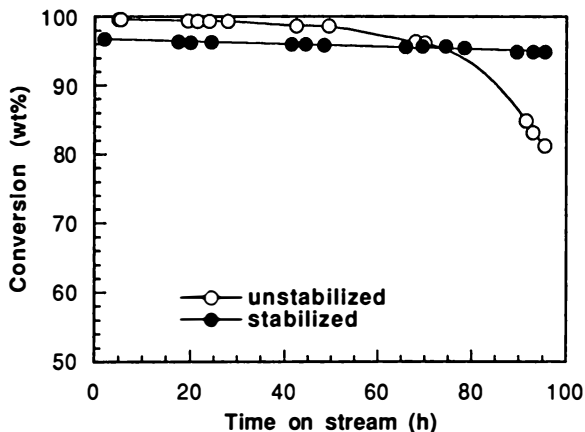


Figure 7. Improvement of stability after the stabilization treatment of HZSM-5.

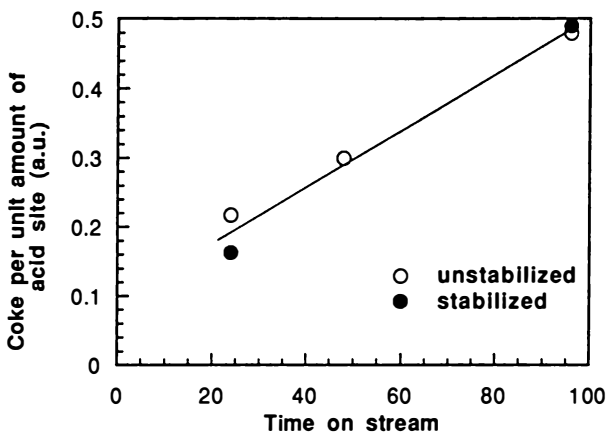


Figure 8. The amount of coke per number of acid site.

molecules will not further polymerize because acid site density of the external surface is greatly reduced by the stabilization treatment hence bimolecular reactions which growth coke molecules are restricted. The deactivation of stabilized catalyst proceeds gradually due to the site coverage inside the channel while most of the coke molecules overflow onto external surface and may grow in a manner which block the access only to a part of the volume.

On the other hand, pore blockage has much more pronounced deactivating effect with the unstabilized catalyst due to higher acid site density on the external surface. The coke molecules can easily grow into polyaromatics due to higher acid site density of external surface and block the access of all internal pores.

Development of a catalyst with long-term stability for LNA process. The above results indicate that it is necessary to dealuminate extra surface of the zeolite to obtain a catalyst having long-term stability. Extensive effort to improve catalyst stability resulted in a very stable catalyst compared to those employed in other processes. More than 90 % conversion was obtained for 2000 hrs at 520 °C under WHSV of 0.7 h⁻¹ with this catalyst, and more than 50 wt% aromatics was observed for that period.

Design of a Demonstration Plant and its Operation.

On the basis of the results of the fundamental and scale-up studies, a 2,250 BSD demonstration plant was designed and was operated at Japan Energy's Mizushima Oil Refinery in Japan to aromatize light naphtha. The plant achieved long-term operation without any trouble. We confirmed the good stability of the catalyst (7).

Conclusion.

A new catalyst with long-term stability was developed for the aromatization of light naphtha. Our proprietary technique of steaming reduced acid site density of the external surface of the catalyst and minimized coke formation. The new catalyst enabled us to develop a new light naphtha aromatization (LNA) process using a conventional fixed bed unit. Idle heavy naphtha reformer can be converted to this process without large modification.

Acknowledgments. The authors thank Mr.Minatoya and Mr.Yamashita for assistance in performing this work. The authors wish to thank Professor T. Inui of Kyoto University for his valuable suggestions. The demonstration plant work was sponsored by Petroleum Energy Center in Japan, which is supported by Japanese Ministry of International Trade and Industry.

Literature Cited

1. Gosling, C. D., Wilcher, F. P., Sullivan L., Mountford, R. A. *Hydrocarbon Processing*; **1991** Vol.70, pp 69-72.
2. Saito,S., Hirabayashi, K., Shibata,S., Kondo,T., Adachi, k. , Inoue,S., *Paper presented at 1992 NPRA annual meeting*, New Orleans, March 22-24, **1992**, AM- 92-38
3. Barbier, J. C., Minkkinen, A. *Paper presented at 1990 JPI Petroleum Refining Conference*, Tokyo, October, **1990**.
4. Kato, K. and Fukase,S., *J. Japan Petrol. Inst.* **1994**, vol.37 pp77-83 .
5. Kato, K., Fukase, S., Nomura, T. and Ishibashi,Y., *Paper presented at 1994 AIChE Annual Meeting*, San Francisco, November, **1994**.
6. Fukase, S., Kumagai H., Suzuka,T. *Appl. Catal. A: General*,**1992** vol.93 pp35-45.
7. Fukase, S., N. Igarashi, Kato, K., Nomura, T. and Ishibashi, Y., *Proceedings of the 2nd International Conference on Catalysts in Petroleum and Petrochemical Industries, Kuwait, 22-26, April 1995*, Studies in Surface Science and Catalysis, (in press).
8. Levenspiel, O., *Chemical Reaction Engineering*, John Wiley & Sons, New York **1972** pp 544
9. Le Van Mao, R., Yao, J., *Appl. Catal. A: General*, **1992** vol.86 pp127-138.
10. Guisnet, M., Magnoux, P., *Catalyst Deactivation*, Delmon, B., Froment, G. F., Studies in Surface Science and Catalysis, Elsevier Science, Amsterdam, **1994**, vol.88, pp53-68.

Effect of Process Conditions and Catalyst Properties on Catalyst Deactivation in Residue Hydroprocessing

M. Absi-Halabi and A. Stanislaus

Petroleum Technology Department, Petroleum, Petrochemicals, and Materials Division, Kuwait Institute for Scientific Research, P.O. Box 24885, Safat 13109, Kuwait

A comprehensive study of catalyst deactivation during hydroprocessing of Kuwait vacuum residue in trickle-bed reactors was carried out. The influence of selected process and catalyst parameters including temperature, hydrogen pressure, liquid hourly space velocity, presulfiding and catalyst pore size on coke and metals deposition was investigated. Increasing reactor temperature increased both coke and metal deposition on the catalyst, while increasing pressure decreased coke deposition. Vanadium deposition on the other hand increased with increasing pressure. Increasing feed flow rates increased the rate of deactivation by metals, but decreased coke deposition. Catalyst pore size distribution had a significant effect on catalyst deactivation. The rate of deactivation by both coke and metals deposition was found to be higher for catalysts having predominantly narrow pores. Presulfiding of the catalyst reduced coking and led to better distribution of foulant metals within the catalyst pellet. The effect of the studied parameters on surface area and pore volume of the catalyst was determined. Mechanistic arguments are presented to explain the results.

Rapid catalyst deactivation is a serious problem in heavy oil upgrading by hydroprocessing. It is generally accepted that the deactivation is caused by the accumulation of carbonaceous residues and metal (V, Ni and Fe) deposits (1,2). Coke is believed to be primarily responsible for the rapid decline in catalyst activity during the early period of the run (3-6). After this initial period, coking slows down while metals gradually build up on the catalyst throughout the run. Both coke and metals deposition contribute to diffusional resistance to the reacting molecules in the heavy oils by constricting the catalyst pore diameter and thereby reducing effective catalyst life (1,4,7).

Since rapid catalyst deactivation is undesirable to refiners from an economic point of view, intensive efforts have been directed towards controlling and minimizing the deactivation problem. Studies have shown that the mechanism of catalyst deactivation is very complex, particularly, in residual oil processing where both coke and metals deposition contribute to deactivation (1,2,8). The key to controlling catalyst activity decline is to understand the factors that influence the deposition of coke and metal foulants. A recent review on the subject indicates that studies related to the factors influencing catalyst deactivation in residual oil hydroprocessing are very limited, and the available information is often incomplete or conflicting (8). In the present study, attention was focused on determining the extent of catalyst fouling by coke and metal deposition under varying operating conditions during hydroprocessing of Kuwait vacuum residue. The influence of catalyst pore size on the deposition of the foulant materials was also investigated. In addition, the effect of presulfiding of the catalyst in suppressing catalyst deactivation was examined as part of the study.

Experimental

The experiments were conducted in a fixed bed reactor using Kuwait vacuum residue as feedstock (API gravity = 6.8; S = 5.2 Wt.%; N = 0.44 Wt.%; V = 94 ppm; Ni = 26 ppm; asphaltenes = 9.2 Wt.%; CCR = 19.2 Wt.%). A 50 ml sample of the catalyst, diluted with an equal amount of carborundum, was charged into a tubular reactor. Thermocouples inserted into a thermowell at the center of the catalyst bed were used to monitor the reactor temperature at various points. After loading the catalyst, the system was purged with nitrogen, and the temperature was increased to 150 °C gradually. Then the system was purged with hydrogen and pressurized to 120 bar. Under these conditions the presulfiding feed (recycle gas oil) was fed and presulfiding was carried out using standard procedures (9).

When presulfiding was completed, the feed (Kuwait vacuum residue) was injected and the conditions were adjusted to desired operating temperature, pressure, hydrogen flow and LHSV. Run duration was 240 hours. In a few selected experiments the feed was introduced without formal catalyst presulfiding. At the end of each run, the aged catalyst was removed, Soxhlet extracted with toluene, then dried. The washed and dried spent catalyst samples were analyzed for carbon and vanadium. The BET surface areas of different catalyst samples were measured with a Quantasorb Adsorption unit. A mercury porosimeter (Quantachrome Model-Autoscan 60) was used to determine pore volume and pore size distribution. In selected samples, the distribution of the major metal foulant (i. e. vanadium) within the pellet was determined using a scanning electron X-ray microprobe analyzer (Camebax). The properties of the used catalysts reported in the results and discussion section are averaged values of composite samples representative of the total bed.

Results And Discussion

Temperature Effect. The data presented in Figure 1 show that the amount of both carbon and vanadium deposited on the catalyst increases steadily with increasing operating temperature in the range 380- 450 °C. Coke deposition on the catalyst is particularly high at temperatures above 410 °C. Reactor temperature is known to enhance the rates of various hydrotreating reactions (10). In fixed bed industrial hydrotreating the reactor temperature is normally increased with the time on stream to compensate for the loss of catalyst activity. Bartholdy and Cooper (11) observed that more coke builds up and deactivation by coke occurs each time the operating temperature is increased to compensate for the loss of activity during the process. Our results indicate that in addition to coking, metal deposition is also severe at higher temperatures. Electron microprobe analysis of the distribution of the deposited vanadium within the catalyst pellets showed a relatively high concentration of vanadium near the outer surface of the pellet for the high temperature (>430 °C) runs. Such dense accumulation of vanadium deposits near the external surface of the catalyst is detrimental to the catalyst life as it can cause pore mouth plugging (4,6,12). A remarkably large loss in the catalyst's surface area (Figure 1) and pore volume is consistent with this.

Pressure Effect. The operating pressure was varied between 70 bar and 135 bar to study its influence on both carbon and metals deposition on the catalyst. The results presented in Figure 2 indicate that increasing pressure has a favorable effect in suppressing coke formation. It is interesting to note that the pressure effect in reducing coke deposition is more pronounced up to 100 bar above which the effect is negligible. In contrast the amount of vanadium deposited on the catalyst continues to increase with increasing pressure. These results are in accordance with the enhancing effect of pressure on the hydrogenation and HDM reactions (7,10). The surface area is found to improve with increasing operating pressure, despite the increase in vanadium deposition at higher pressures, indicating that the surface area loss of the catalyst is more influenced by coke than by the vanadium deposits (Figure 2b).

Coke on the catalyst is, thus, largely responsible for catalyst deactivation by loss of surface area, and this could be minimized by increasing the hydrogen pressure. However, increasing pressure has been reported to increase vanadium deposition more near the exterior surface of the catalyst pellet (13,14). In essence, an increase in the hydrogen pressure has a beneficial effect in suppressing coke formation, but can lead to shorter catalyst life due to rapid accumulation of vanadium at pore mouths.

LHSV Effect. Figure 3 illustrates the influence of feed space velocity on the deposition of carbon and vanadium on the catalyst during hydroprocessing of Kuwait vacuum residue. It is seen that the vanadium on the catalyst increases while the amount of carbon decreases with increasing feed space velocity. The loss in catalyst surface area is substantially high at low feed flow rates (Figure 3b), presumably due to increased carbon deposition. Considering these results, it is reasonable to conclude

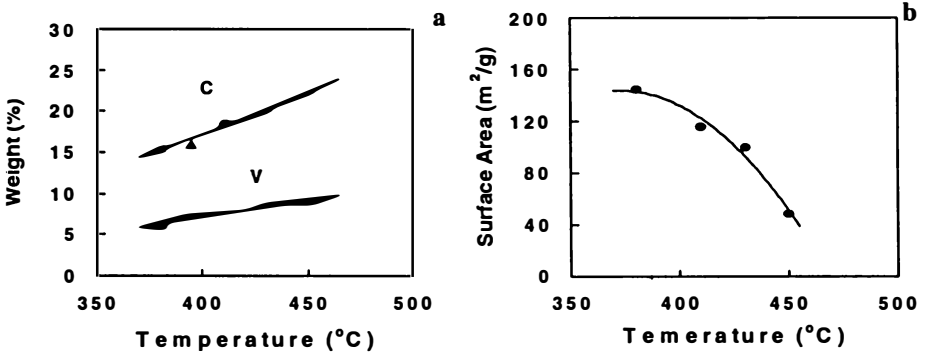


Figure 1. Effect of operating temperature on (a) coke and metal deposition, and (b) catalyst surface area (Run duration = 240 h).

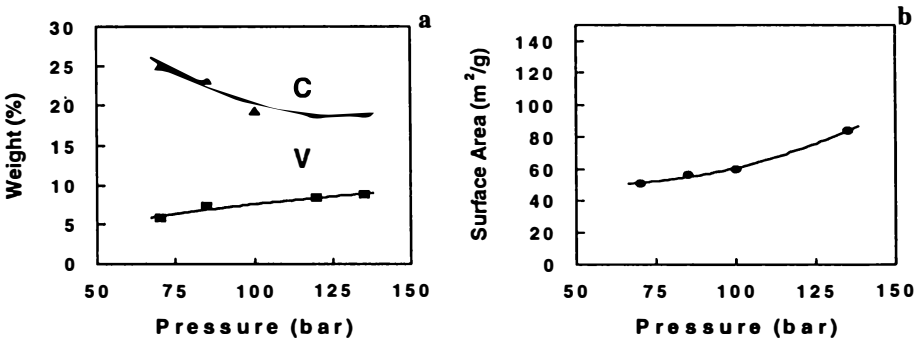


Figure 2. Effect of hydrogen pressure on (a) coke and metal deposition, and (b) catalyst surface area (Run duration = 240 h).

that increasing feed space velocity in residue hydroprocessing operations increases the rate of catalyst deactivation by metals, but has an opposite effect on the deactivation by coke. The linear relationship observed between feed space velocity and the catalyst's vanadium content (Figure 3a) could possibly be used for predicting catalyst life based on short duration runs. It is possible to calculate the amount of feed that could be processed over a given catalyst from the amount of vanadium accumulated during the short duration test, provided the catalyst maximum tolerable capacity for metals is known.

Influence of Catalyst Presulfiding. Presulfiding of hydrotreating catalysts has been widely practiced by refiners in distillate hydrotreating operations. It is generally believed that presulfiding of hydrotreating catalysts plays an important role in creating the essential surface requirements for optimum activity. In residue hydroprocessing, studies on the influence of presulfiding on catalyst performance are relatively scarce, despite the industrial importance of the process. In the present work, a detailed investigation of the effect of presulfiding on catalyst deactivation during hydroprocessing of Kuwait vacuum residue was undertaken. Catalysts with and without formal presulfiding were used to examine the effect of sulfidation on coke and metals deposition. The results revealed that presulfiding reduces the extent of early deactivation of the catalyst by coke deposition (15). Furthermore, the presulfided catalysts showed improved distribution of the major metal foulant vanadium within the pellet (15).

The exact reasons for this improvement are not clear. It is likely that passivation of the highly active acidic sites by presulfiding reduces the coke forming tendency. In addition, the small amount of coke deposited on the catalyst during the sulfidation process may also have a passivating effect on the highly active hydrogenation and hydrogenolysis sites allowing deeper diffusion of the metal-bearing molecules in the feedstock into the pellet.

Table I. Meso- and Macro-Pore Distributions in Various Catalysts

Catalyst	Pore Volume (ml/g)	Meso-Pore Distribution(%)			Macro-Pore Distribution(%)		
		30-100Å	100-250 Å	250 -500 Å	500 - 1000 Å	1000 - 3000 Å	>3000Å
P	0.53	38	60.5	1.5	0	0	0
Q	0.60	4	11	27	15	43	0
R	0.73	7	34	19	6	16	18
S	0.75	55	8	8	6	21	2

Influence of Catalyst Pore Size. In the present work, four Ni-Mo/Al₂O₃ catalysts with different pore size distributions were used to assess the effect of catalyst pore size on deactivation by coke and metals deposition. Table I summarizes the pore size distribution of the four catalysts used in the present work. The amount of carbon and

vanadium deposits formed on various catalysts together with the surface area and pore volume losses are included in Table II. The highest amount of carbon deposition is found for the bimodal pore Catalyst (S) that has a large percentage (55%) of very narrow pores ($<100\text{\AA}$). It is likely that the large molecular species in the feed, that have a high coke forming tendency, spend a longer time within the narrow pores of the catalyst. This is probably due to slow diffusion resulting in further cracking and coking. The lowest amount of carbon deposits found on Catalyst (Q) that contains predominantly macro-pores is in line with this argument. It is interesting to note that Catalyst (P), that has a monomodal pore size distribution with pore maximum in medium meso-pore range (100- 200 \AA), exhibits a low coke forming tendency similar to the large pore Catalyst (Q).

Table II. Concentration of Carbon and Vanadium Deposited on Different Catalysts

Catalyst	Carbon (wt %)	Vanadium (wt %)	Loss of Surface Area (%)	Loss of Pore Volume (%)
P	15.8	6.8	39.7	55.0
Q	15.5	11.0	20.5	36.5
R	19.7	9.6	44.5	67
S	21.2	8.7	50.0	80.0

In the catalytic processing of residual oil, the ability of the feedstock molecules to diffuse through the catalyst particles to the active sites inside the pores is a key factor in determining the effectiveness of the catalyst (12,16). The diffusivity is predominantly determined by the pore size of the catalyst. Increasing the pore size of the catalyst, which is normally accompanied by a decrease in surface area, improves diffusion. For maximum activity, it is desirable to have a maximum possible surface area compatible with the absence of diffusional limitations. Catalyst pore size can also have a significant effect on the rate of deactivation. Molecular size distribution of the macromolecular species (e.g. asphaltenes) present in the residual oils indicates that this range of pore size is large enough for unrestricted diffusion of such species. Molecular sizes ranging from 26-150 \AA have been reported for asphaltenes in Kuwait residual oil (17,18). In addition, Catalyst (P) was found to have high hydrogenation activity (19), which may also be partly responsible for the reduced coking tendency of this catalyst.

Vanadium concentrations on the spent catalysts, presented in Table II, show that the large unimodal pore Catalyst (Q) has accumulated more vanadium than the others. This is consistent with the highest HDM activity of this catalyst (19). Furthermore, the vanadium distribution within the pellet is more uniform for this catalyst than the others (Figure 4). For the narrow pore unimodal Catalyst (P), the vanadium concentration near the outer edge of the pellet is substantially higher than that near the center. Similarly among the bimodal pore catalysts, a more uniform distribution of the

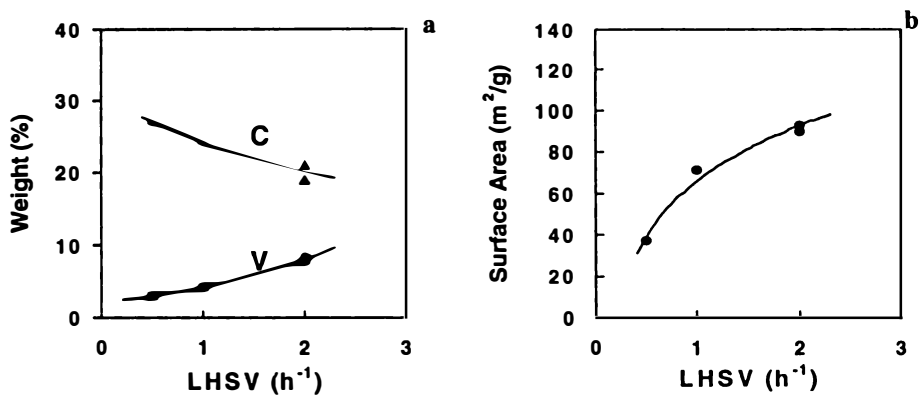


Figure 3. Effect of LHSV on (a) coke and metal deposition, and (b) catalyst surface area (Run duration = 240 h).

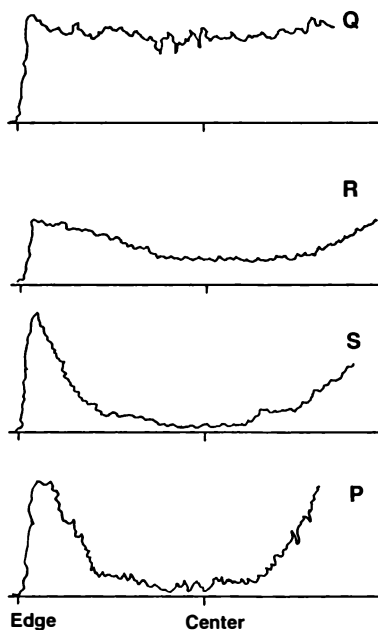


Figure 4. Distribution profile of vanadium within the catalyst pellets for catalysts with different pore size distributions

deposited vanadium is noticed for the large pore Catalyst (R) compared with the narrow pore Catalyst (S).

The percentage reduction in pore volume and surface area for the four used catalysts are in the order: $S > R > P > Q$. The pore volume loss is generally caused by the deposition of coke and metals in the pore. In catalysts with a large amount of small pores the deposited metals can cause pore mouth plugging leading to a large loss in pore volume and surface area.

The highest loss of pore volume and surface area observed for the predominantly small pore Catalyst S is therefore not surprising. Similarly, in catalysts with macropores, the metals penetration into the catalyst pellet is high and they are deposited evenly on the pore surface throughout the catalyst pellet without causing pore blockage. The lowest loss of pore volume and surface area noticed for the large pore Catalyst Q is in agreement with this.

Summary and Conclusions

The influence of some important process parameters, such as operating temperature, hydrogen pressure, liquid hourly space velocity, and selected catalyst parameters, such as catalyst pore size distribution and presulfiding, on catalyst fouling by coke and metals deposition was investigated during hydroprocessing of Kuwait vacuum residue. Increasing reactor temperature increased both coke and metals deposition, while increasing hydrogen pressure decreased coke deposition. Vanadium deposition on the other hand increased with increasing pressure. Coke deposition contributed more to the surface area loss than the metals deposition. Increasing feed flow rates enhanced the rate of deactivation by metals, but decreased coke deposition. Catalyst pore size distribution had a significant effect on catalyst deactivation. The deposition of both coke and metals was found to be higher for catalysts having predominantly narrow pores. Presulfiding of the catalyst reduced coking and led to better distribution of foulant metals within the catalyst pellet.

References

1. Absi-Halabi, M., Stanislaus, A., and Trimm, D. L., *Appl. Catal.*, 72, 193(1991)
2. Thakur, D. S., and Thomas, M. G., *Appl. Catal.*, 45, 197(1985)
3. Ternan, M., and Kriz, F., *Stud. Surf. Sci. Catal.*, 6, 283(1980)
4. Sie, S. T., *Stud. Surf. Sci. Catal.*, 6, 545(1980)
5. Gaulda, G. and Kasztelan, S., *Stud. Surf. Sci. Catal.*, 88, 145(1994)
6. Bridge, A. G., *Stud. Surf. Sci. Catal.* 53, 363(1990)
7. Hannerup, P., and Jacobson, A. C., *Preprints, Div. of Petrol. Chem., ACS*, 28(3), 576 (1988)
8. Bartholomew, C. H., In "Catalytic Hydroprocessing of Petroleum and Distillates" (Edited by M. C. Obella and S. S. Shih), Marcel Dekker, New York, (1994), pp 1-32.

9. Absi-Halabi, M., Stanislaus, A., Owaysi, F., and Khan, Z., *Stud. Surf. Sci. Catal.* 53, 201(1990)
10. Stanislaus, A., Absi-Halabi, M., Owaysi, F., and Khan, Z., "Effect of Temperature and Pressure on Hydroprocessing of Kuwait vacuum Residues". KISR Publication No. 2754 (1988)
11. Bartholdy, J., and Cooper, B. H., Preprints, Div. of Petroleum Chemistry, 205th National ACS Meeting, (1993) 386-390.
12. Quan, R. J., Ware, R. A., Hung, C. W., and Wei, J., *Advances in Chem. Eng.* 14, 95(1988)
13. Pazos, J. M., Vonzalex, J. C., and Salazar, A. J. *Ind. Eng. Chem. Process Des. Dev.* 22, 653 (1983).
14. Tamm, P. W., Harnsberger, H. F., and Bridge, A. G., *Ind. Eng. Chem. Process Des. Dev.* 20, 262 (1981).
15. Absi-Halabi, M., Stanislaus, A., Qamra, A., and Chopra, S. Paper Presented at the 2nd International Conference on Catalysts in Petroleum and Petrochemical Industries, April 22-26, 1995, Kuwait.
16. Ternan, M., *Can. J. Chem. Eng.*, 61,689(1983)
17. Baltus, E W., and Anderson, J. L., *Chem. Eng. Sci.*, 38,1959(1988)
18. Speight, J. G., *Stud. Surf. Sci. Catal.*, 19, 551(1984)
19. Stanislaus, A., Absi-Halabi, M., Mughni, T., Khan, S., and Qamra, A., Proceedings of Joint Kuwaiti-Japanese Symposium on Catalytic Processes for the Petroleum Refining and Petrochemicals Industries (J. Bishara, H. Qabazard, and M. Absi-Halabi, Editors), Kuwait Institute for Scientific Research, Kuwait, (1993), pp. 13-25.

Catalyst Deactivation in Hydrodemetallization

J. P. Janssens, A. D. van Langeveld, S. T. Sie, and J. A. Moulijn

Industrial Catalysis Section, Faculty of Chemical Technology and
Materials Science, Delft University of Technology, Julianalaan 136,
2628 BL Delft, Netherlands

Metal deposition in hydrotreating of heavy oils is one of the most important phenomenon causing catalyst deactivation. Present work focuses on the modeling of hydrodemetallisation catalyst deactivation by model compound vanadyl-tetraphenylporphyrin. Intrinsic reaction kinetics, restrictive diffusion and the changing catalyst porous texture are the relevant phenomena to describe this deactivation process. The changing catalyst porous texture during metal deposition can be described successfully by percolation concepts. Comparison of simulated and experimental metal deposition profiles in catalyst pellets show qualitative agreement.

In the hydrotreating processing of heavy oils heteroatoms, such as sulphur, nitrogen, oxygen and metals, are catalytically removed. These metals, mainly vanadium and nickel, remain in the reactor as solid deposits accumulating on the catalyst surface after decomposition of the organo-metallic compounds. The loss of catalyst activity through metal deposition can be attributed to the interaction of the deposited metals with the active sites of the catalyst (*'active site poisoning'*) and the loss of pore volume due to the obstruction of catalyst pores (*'pore plugging'*) as depicted in Figure 1.

Key-issue in hydrodemetallisation (HDM) process design and operation is the development of catalyst deactivation models which give reliable predictions of catalyst life-time and activity, thus providing a tool for designing optimized catalysts.

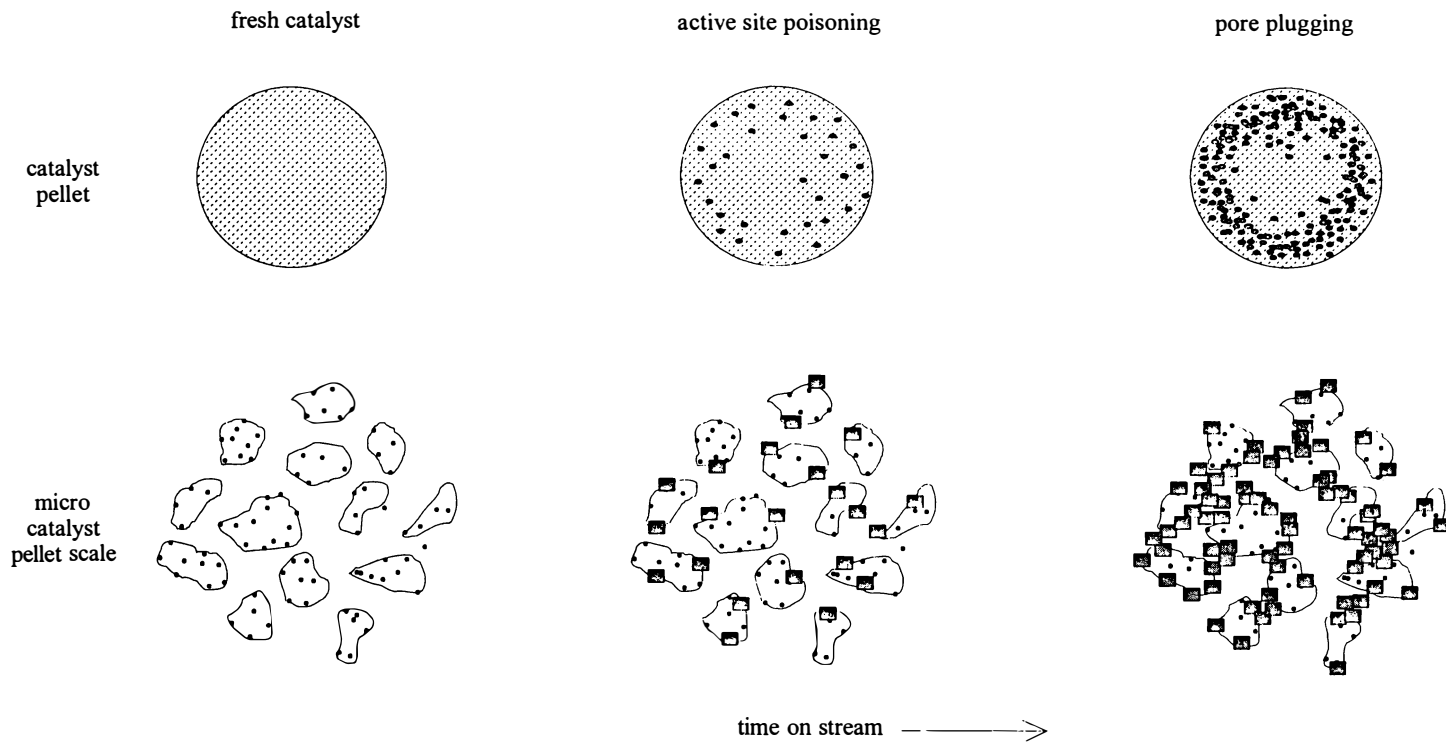


Figure 1. A schematic representation of catalyst deactivation phenomena.

Approach for Modelling HDM Catalyst Deactivation

The general approach for modelling catalyst deactivation is schematically organised in Figure 2. The central part are the mass balances of reactants, intermediates, and metal deposits. In these mass balances, coefficients are present to describe reaction kinetics (reaction rate constant), mass transfer (diffusion coefficient), and catalyst porous texture (accessible porosity and effective transport properties). The mass balances together with the initial and boundary conditions define the catalyst deactivation model. The boundary conditions are determined by the axial position in the reactor. Simulations result in metal deposition profiles in catalyst pellets and catalyst life-time predictions.

HDM Reaction Kinetics and Diffusion.

A significant proportion of the metal compounds in heavy oil residua is complexed in porphyrins. The use of porphyrinic model compounds in reaction kinetics research eliminates many of the complicated and competing reactions encountered with heavy oil residua, thus enabling a clearer picture of the reactions to be ascertained. The hydrodemetallisation of porphyrinic model compounds involves a sequence of hydrogenations and hydrogenolysis steps. Figure 3 depicts the HDM reaction mechanism for vanadyl-tetraphenylporphyrin (VO-TPP) (1).

Bonné et al. (1) studied reaction kinetics of tetraphenylporphyrin model compounds over several catalysts and concluded that hydrogenation and hydrogenolysis occur on two different sites. Therefore, the reaction mechanism of VO-TPP hydrodemetallisation is described by a two-site model. It was also found that a Langmuir-Hinshelwood type of kinetics applies with small inhibition by hydrogen.

The HDM reaction mechanism of model compounds is found to be unique to the type of porphyrin and independent of the type of catalyst employed (1). This makes HDM of VO-TPP useful for screening and testing of different catalyst systems.

Prerequisite for hydrodemetallisation is the diffusion of these large porphyrins into the catalyst porous texture. Diffusion of these molecules can be limited by geometric exclusion and hydrodynamic drag. When the solute molecular size is significant as compared to the pore size, a restrictive factor should be introduced to account for the reduction in diffusivity. As a consequence, clarification of detailed HDM reaction kinetics may be obscured by diffusion limitations.

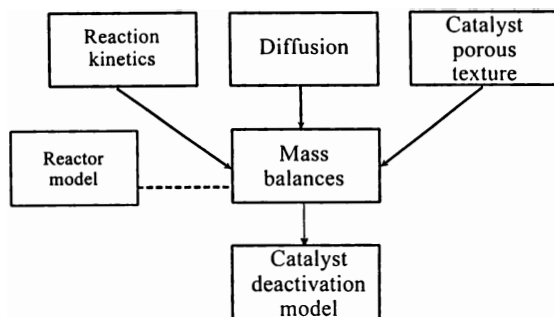


Figure 2. General approach for modelling HDM catalyst deactivation.

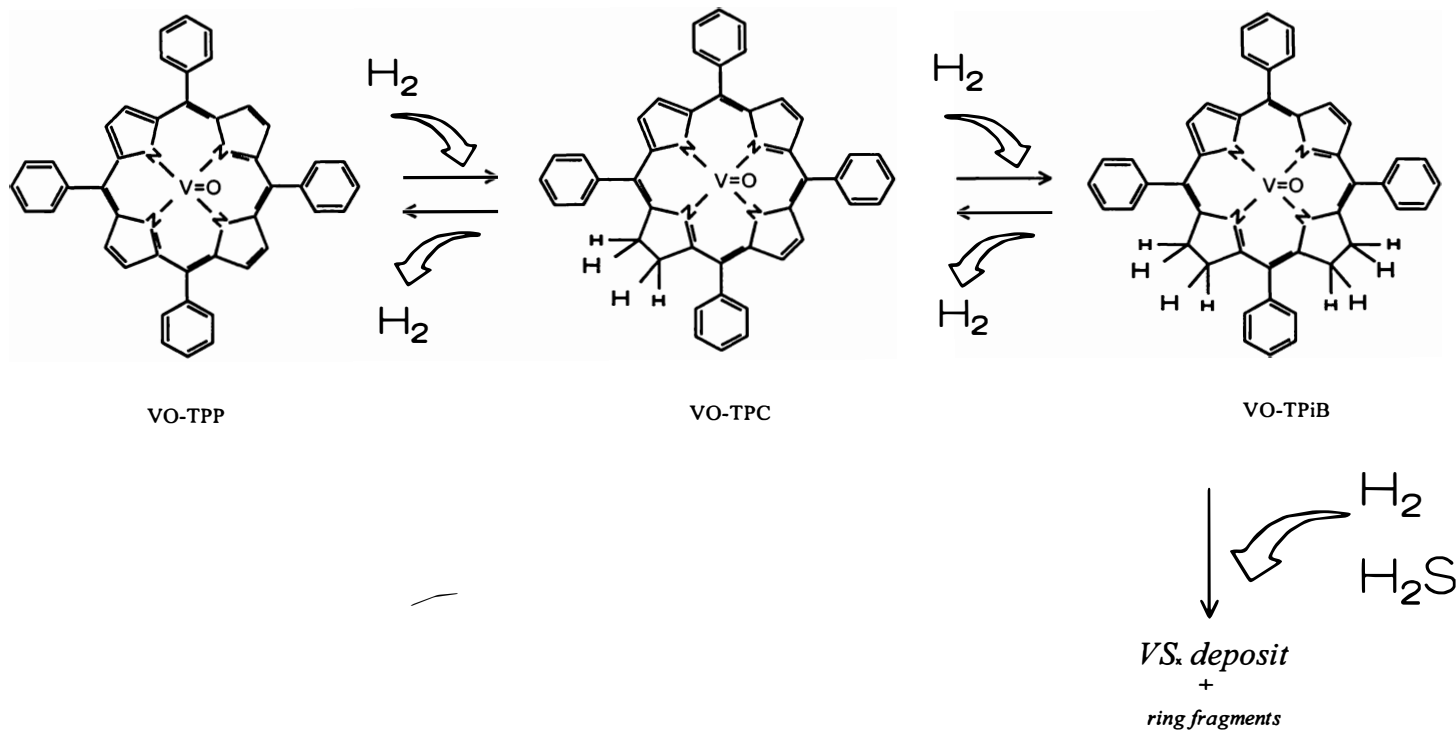


Figure 3. HDM reaction mechanism of model compound vanadyl-tetraphenylporphyrin. (TPP: tetraphenylporphyrin, TPC: tetraphenylchlorin, TPiB: tetraphenylisobacteriochlorin)

Catalyst Porous Texture.

The initial porous texture of a catalyst pellet and the change in texture caused by metal deposition can be described using the percolation theory. In the percolation approach the pellet is constructed as a binary interdispersion of void space and (deposited) solid material. In this binary interdispersion, the void space can exist as (a) isolated clusters surrounded by solid material or (b) sample overspanning void space that allows mass transport from one side to the other. The total void space ϵ can be split into the sum of the volume fraction of isolated clusters ϵ^I and the volume fraction of accessible void space ϵ^A . If ϵ is below a critical value, the so-called percolation threshold ϵ_c , all the void space consists of isolated clusters and transport through the pellet is impossible.

A quantity relevant to (diffusional) transport is the effective transport voidage ϵ^E . If the accessible void space would be arranged in parallel layers, then ϵ^E equals ϵ^A . However, in disordered interdispersions the accessible void space for transport may be tortuous and have inactive dead-ends, so that in general $\epsilon^E \leq \epsilon^A$.

Two types of percolation models are mentioned in literature to describe the local porosity in catalyst pellets, (a) topologically-disordered networks in a continuous system (tessellation models) and (b) regular discrete networks (Bethe networks) (2). In tessellation models, the interdispersion represents void and solids distributed as for example cubes. The composite shown in Figure 4a is a random tessellated space with identical cubes. The metal deposition process can be envisaged as an increase in the number of random tessellated cubes.

A Bethe network is a branching structure defined by nodes and bonds, as shown in Figure 4b. The metal deposition process can be envisaged as a uniform deposition of metals in the pores of the network. The dependence of ϵ^I , ϵ^A , and ϵ^E on the total void space ϵ during the metal deposition process can be determined by analytical relations (3).

A disadvantage of the Bethe network is that it lacks physical reality, e.g. the presence of closed loops, whereas closed loops are present in the tessellation models. The presence of closed loops is considered to be an important aspect in describing the metal deposition process in catalyst pellets. Therefore, the tessellation approach is favoured over the Bethe network.

Mass Balances and Model Equations.

The mass balances for the reactants, intermediates, and metal deposits are given for a spherical catalyst particle. By defining Fick's law, the generalized mass balance results in

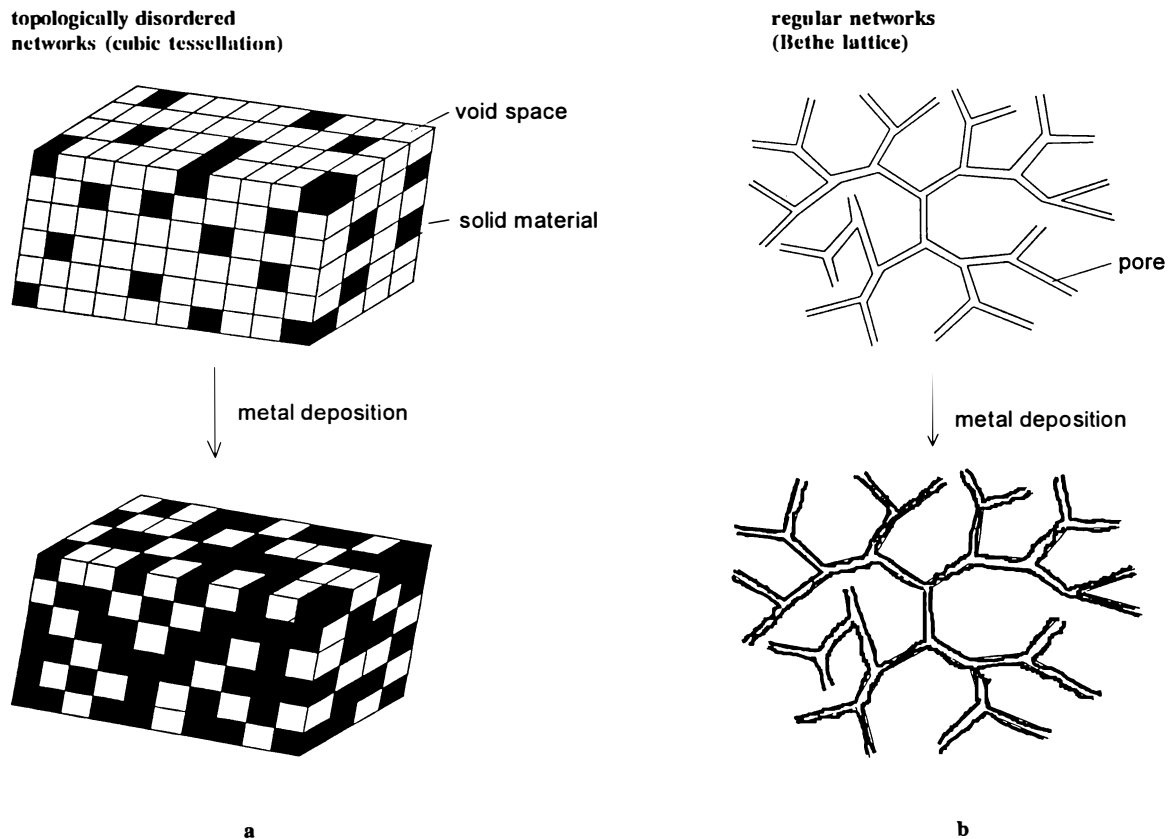


Figure 4. Catalyst porous texture as described by the cubic tessellation model and the Bethe network: a- by cubic tessellation model, b- Bethe network.

$$C \frac{\partial \epsilon^A}{\partial t} + \epsilon^A \frac{\partial C}{\partial t} = \frac{1}{r^2} \frac{\partial}{\partial r} \left[r^2 \epsilon^E D_{\text{eff}} \frac{\partial C}{\partial r} \right] - S_v R \quad (1)$$

The mass balance for the metal deposits results in

$$\frac{\partial W_M}{\partial t} = \alpha M_M S_v R \quad (2)$$

The initial and boundary conditions are:

$$t = 0, 0 \leq r \leq R_c: \quad t > 0, r = R_c: C = C_{\text{bulk}}$$

$$C = 0 \text{ and } W_M = 0 \quad r = 0: \frac{\partial C}{\partial r} = 0$$

In the mass balances, the variables S_v , ϵ^A , and ϵ^E occur. These are the variables characterizing the porous texture of the catalyst pellet during metal deposition and can be described using the percolation approach.

EXPERIMENTAL

HDM Reaction Kinetics.

Intrinsic reaction kinetic parameters for the hydrodemetallisation of model compound VO-TPP on a sulfided vanadium on silica catalyst are determined. The experiments are carried out with *o*-xylene as solvent in a 250 ml batch autoclave. The HDM reaction is carried out at industrial conditions, ~ 578 K and 10 MPa H₂ pressure. Kinetic parameters and activation energies are given elsewhere (4).

Catalyst Deactivation.

Catalyst deactivation experiments are carried out in a micro-flow reactor using a wide- and a narrow-pore silica with a pellet diameter of 1.7 mm. An industrial feedstock containing 61 ppm V is continuously fed to the reactor at 15 MPa H₂ pressure and 673 K. After the run a catalyst pellet is collected from the catalyst bed and the average vanadium deposition profiles determined with EPMA (Electron Probe Micro Analysis).

RESULTS AND DISCUSSION

Catalyst Deactivation: Experimental and Modelling.

Figure 5 shows the influence of the bulk diffusion coefficient, D_b , on the vanadium deposition profiles using the reaction kinetics of VO-TPP and a wide pore silica catalyst. The simulations are performed at reactor inlet conditions, which implies that the concentration of intermediates is equal to zero outside the catalyst pellet. Obviously, by decreasing the diffusivity the metal deposition process becomes more diffusion rate-limited. With a decreasing diffusion coefficient the transport of reactant and intermediates is more limited resulting in a less deep penetration into the catalyst pellet. Therefore, the vanadium deposition maximum is shifted further to the exterior of the pellet. According to literature (5), a bulk diffusion coefficient of 10^{-8} m^2/s is an accurate value for the diffusion of porphyrins.

Figure 6 shows the influence of the axial position of the catalyst pellet in the reactor. As can be observed, the vanadium deposition profiles shift from a M-shaped profiles to a more U-shaped profile. This is due to the increasing presence of intermediates outside the catalyst pellet when going further downstream in the reactor. Experimental work by Ware & Wei (6) showed a similar shift in the shape of the metal deposition profile.

Figure 7 shows the influence of the initial pore radius, in the case of a wide- and narrow-pore silica catalyst, on the vanadium deposition profiles at an average axial position in the reactor. Both cases show the presence of deposition maxima, indicating that the deposition process is diffusion rate-limited. In the case of the narrow-pore silica the core volume of the pellet potentially available for vanadium deposition cannot be reached by reactant and intermediates and is lost for vanadium deposition.

If we compare the simulations from Figure 7 to experimental vanadium deposition profiles, depicted in Figure 8, it's clear that there is qualitative agreement. Apparently, model simulations using reaction kinetics of model compound VO-TPP give identically shaped vanadium deposition profiles. The Thiele modulus, which determines the shape of the deposition profiles, is apparently for both cases (the model compound and the industrial feedstock) identical. Since the bulk diffusion coefficient of an industrial feedstock is about two orders of magnitude lower than for a model compound (7), the reaction rate of a model compound should be two orders of magnitude higher than for an industrial feedstock. Therefore, one should bear in mind that the metal deposition rate using a model compound is much higher than with an industrial feedstock, which implies that catalyst life-times using model compounds will be much shorter.

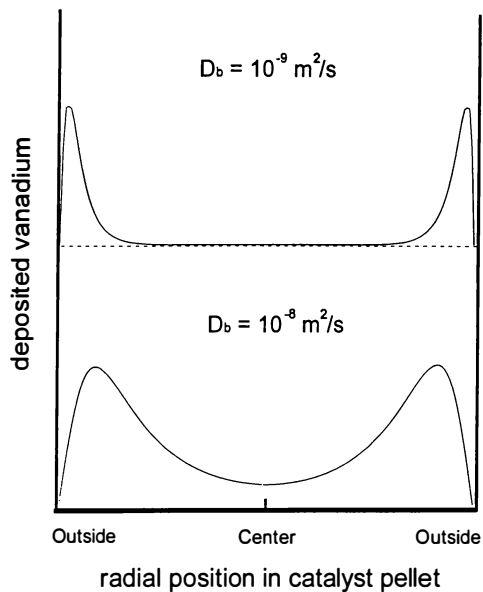


Figure 5. Influence of the bulk diffusion coefficient, D_b , on the vanadium deposition profile in a wide pore silica catalyst pellet at reactor inlet conditions. (Model compound VO-TPP, 673 K, 10 MPa H_2 , initial pore radius: 30 nm, catalyst pellet radius: 0.85 mm)

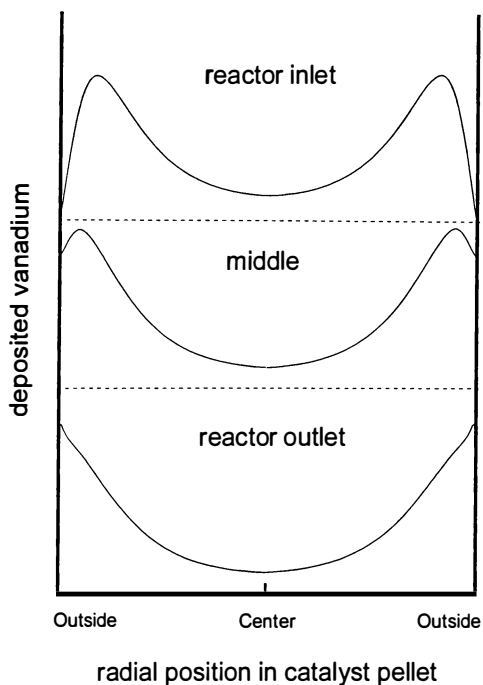


Figure 6. Influence of axial position in the reactor on the vanadium deposition profile in a wide pore silica catalyst pellet.

(Model compound VO-TPP, 673 K, 10 MPa H_2 , $D_b=10^{-8}$ m²/s, initial pore radius: 30 nm, catalyst pellet radius: 0.85 mm)

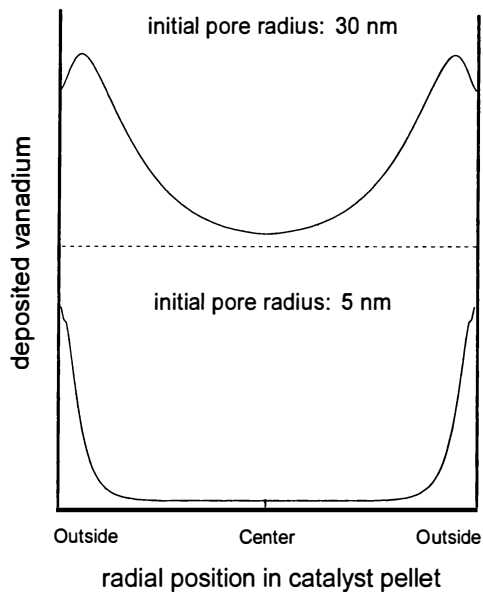


Figure 7. Influence of the initial pore radius on the vanadium deposition profile (wide- and narrow pore silica catalyst pellet) at an average axial position in the reactor.

(Model compound VO-TPP, 673 K, 10 MPa H_2 , $D_0=10^{-8}$ m²/s catalyst pellet radius: 0.85 mm)

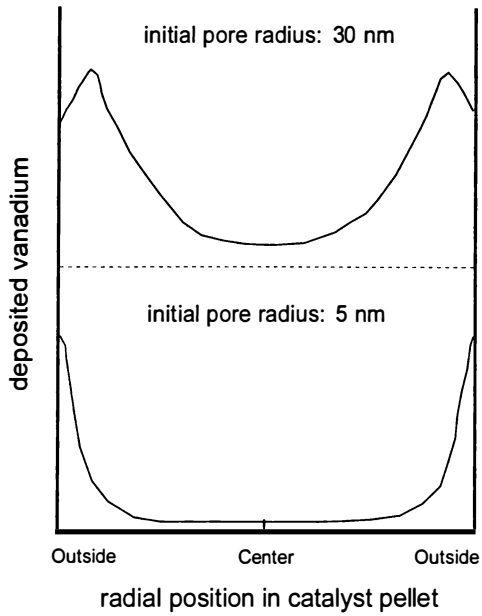


Figure 8. Experimental vanadium deposition profiles for wide- and narrow pore silica catalyst. (Industrial feedstock containing 61 ppm V, 673 K, 15 MPa H_2 , catalyst pellet radius: 0.85 mm)

CONCLUSIONS

Intrinsic reaction kinetics, restrictive intraparticle diffusion and the (changing) catalyst porous texture are the relevant phenomena to describe HDM catalyst deactivation .

The use of porphyrinic model compounds in reaction kinetics research is a convenient tool in screening and testing of different catalyst systems.

Percolation concepts can be successfully applied to describe the changing catalyst porous texture during HDM.

Comparison of HDM catalyst deactivation simulations and experimental deposition profiles in catalyst pellets shows that the metal deposition process can be reproduced.

Acknowledgments

The authors gratefully acknowledge the Koninklijke/Shell Laboratory, Amsterdam (KSLA) for their financial support and Dr. B. Scheffer (KSLA) for stimulating discussions.

Notation

α	: ratio of number of metal atoms in deposit to number of metal atoms in porphyrin precursor	-
C	: concentration	mol/m ³
D_b	: bulk diffusion coefficient in liquid phase	m ² /s
D_{eff}	: effective or restrictive diffusion coefficient	m ² /s
ϵ	: total void space or total porosity	-
ϵ^A	: fraction of accessible void space or accessible porosity	-
ϵ_c	: percolation threshold	-
ϵ^E	: effective transport voidage	-
ϵ^I	: fraction of isolated void space or isolated porosity	-
M_M	: molecular weight of metal deposit	kg/mol
r	: radial length coordinate from centre of catalyst pellet	m
R	: reaction rate	mol/m ² ·s
R_c	: radius of catalyst pellet	m
ρ_M	: density of metal deposit	kg/m ³
S_v	: surface area per unit volume of catalyst pellet	m ² /m ³
σ	: dimensionless deposited vanadium, $W_M / \rho_M \epsilon^A$	-
t	: time	s
W_M	: mass concentration of metal deposit	kg/m ³

Literature Cited

1. Bonné, R.L.C.; Steenderen, P. van; Moulijn, J.A. *Bull. Soc. Chim. Belg.*, **1992**, 100 (11-12), pp. 877.
2. Sahimi, M.; Gavels, G.R.; Tsotsis, T.T. *Chem. Eng. Sci.*, **1990**, 45, pp. 1443.
3. Mohanty, K.K.; Ottino, J.M.; Davis, H.T. *Chem. Eng. Sci.*, **1982**, 37, pp. 905.
4. Janssens, J.P.; Bezemer, B.J.; Langeveld, A.D. van; Sie, S.T.; Moulijn, J.A., in *Studies in Surface Science and Catalysis* (B. Delmon and G.F. Froment, Eds.), Elsevier Science B.V., 1994, Vol. 88, pp. 335.
5. Chung, H. Tsai; Massoth, F.E.; Lee, S.Y.; Seader, J.D. *Ind. Eng. Chem. Res.*, **1991**, 30, pp.22.
6. Ware, R.A.; Wei, J. *J. Catal.*, **1985**, 93, pp. 100.
7. Chantong, A; Massoth, F.E. *AIChE J*, **1983**, 29, pp. 725.

TESTING OF CATALYST PERFORMANCE

Activity and Coking Rate of Catalysts Deactivated by Fast-Coking Species Added to the Feed

Dady B. Dadyburjor, Zhenyu Liu, Shigeki Matoba, Shinichi Osanai, and Tetsuya Shirooka

Department of Chemical Engineering, West Virginia University,
P.O. Box 6102, Morgantown, WV 26506-6102

The time required to test a catalyst for stability towards coke can be decreased by adding to the feed a component known to form copious amounts of coke. The effect of adding two such additives, decane and naphthalene, separately and in various amounts, to a cumene feed is investigated here over a zeolite catalyst. Coke levels and the rate of coke formation in general increase with the amount of naphthalene added, and decrease with the amount of decane added. The parameters of the coking kinetics are correlated with the amount of the two additives, using the aromatic ring percent as the independent variable. The changes in the initial activity of the catalyst and its sensitivity to coke depend upon the type of additive used. If (as is usual) the species added is more-rapidly coking, then the activity parameters are independent of the additive concentration.

The laboratory and the pilot plant are often constrained in the amount of time available to study the effect of deactivation of a catalyst. Consequently, deactivation by coking is frequently studied by adding "coke generators" to the feed. These components, generally multi-ring compounds, deposit coke at a much faster rate than do the regular components of the feed. Hence, the effect of coke level on the catalyst performance can supposedly be obtained in shorter clock times during this accelerated coking than would be possible if only the regular components of the feed were used.

However, the information obtained from such experiments has, at least, the potential to be misleading. Can the kinetics of coke deposition from the actual feed be estimated from a knowledge of the coke deposition rate during this accelerated coking process? How is the rate of reaction of the actual feed (as a function of coke level) changed by the presence of coke from the fast-coking species? Does one need to account for the reaction(s) of the fast-coking additive? We have started to answer these and other questions in our laboratory, using relatively simple reactions and simple fast-coking additives. Preliminary information has been presented earlier (1,2).

TABLE I. Properties of Rare-Earth Exchanged HY Zeolite Catalyst

Residual Na ₂ O	0.88 wt%
Surface Area	780 m ² /g
Ammonia Chemisorbed	8.6 ml/g

Experimental

The reactor and some details of the experimental procedure have been described earlier (3). In brief, the reactor consists of a microbalance configured as a pulse-flow reactor. Approximately 5mg of the catalyst is placed in the sample pan and pretreated. Under reaction conditions (500°C), He carrier gas flows over the sample pan at around ambient pressure, and a 2- μ l pulse of the reactant(s) is introduced into the inlet. The exit stream flows to an integral sample collector in a liquid-nitrogen bath; (virtually) all of the reactants and products are condensed, and (virtually) only He flows out of the collector. After a given period of time, the incremental change in weight of the sample pan contents can be related to the coke deposited on the catalyst. At this point, the collector is isolated, the bath is removed and the collector is electrically heated. When the collector contents are in the vapor phase, a stream of high-pressure He forces them into the gas chromatograph. The process is then repeated with another pulse of reactant(s). The advantages of this approach are that the reaction is carried out at ambient pressure, while the product analysis is carried out at sufficiently high pressures to allow unambiguous determination of the species present. Further, the activity and selectivity of the catalyst can be determined at well-defined levels of coke.

In the present work, a rare-earth-exchanged HY zeolite was used as the catalyst. The catalyst was steamed. Other properties of the catalyst can be found in Table I. The cracking of cumene (to benzene and propylene) was used as the probe reaction; side reactions could be neglected under the conditions used. Naphthalene was the fast-coking species used; its condensed two-aromatic-ring structure is expected to generate coke in larger amounts than does cumene, which has only one aromatic ring. Another additive used was decane, which has the same number of carbon atoms as naphthalene, but has no ring structures.

The conversion of aromatics can be obtained by using the so-called benzene-ring balance, *i.e.*, by assuming that the aromatic ring does not crack. Details of this technique have been given in Ref. (1). The conversion of decane obviously cannot be obtained by this method, but can be obtained by comparing peak areas from the chromatograph with and without the catalyst. Values of the cumene conversion obtained from the benzene-ring balance and from the peak-areas technique are not identical, but show consistent trends; similarly values for naphthalene conversion are different by these two methods, but consistent. The latter method is more prone to error and scatter since it involves two separate runs, one with catalyst and the other without; nevertheless, it must be used for decane. Consequently, the benzene-ring balance was used to obtain the conversion for cumene cracking; while the peak-areas technique was used for both the additives, naphthalene and decane.

In order to quantify the results using cumene - naphthalene and cumene -

decane mixtures, a single term should be used to describe various compositions of both these reactant pairs. Accordingly, we defined the aromatic ring percent, \underline{A} , as:

$$\underline{A} = \underline{C} + 2 \underline{N} \quad (1)$$

where \underline{C} represents the percentage of cumene present in the reactant mixture and \underline{N} represents the percentage of naphthalene present. Then mixtures of cumene and decane will have values of \underline{A} no greater than 100, whereas naphthalene - cumene mixtures will have \underline{A} values greater than or equal to this number. The parameter \underline{A} can be taken to be an indicator of the number of rings per 100 moles of feed, regardless of whether the rings are on a one-ring compound or a two-ring compound (or a no-ring compound).

The limitations of this parameter should be noted. We do not necessarily expect that \underline{A} is a unique indicator. For example, feeds with $\underline{A} = 100$ could be obtained with pure cumene and also with a decane - naphthalene mixture. We do not claim that these two feeds would necessarily behave similarly. At this point, \underline{A} is simply a way to present our data for cumene - decane and cumene - naphthalene mixtures on the same plot.

Results and Discussion

Coking Kinetics. These results are described elsewhere (1) in more detail. Nevertheless, for the sake of completeness, a summary is provided here.

We continue to rely extensively on the two-step (initiation - propagation or autocatalytic) model (4) to evaluate data on coking rates. Two rate constants are involved: \underline{k}_1 for the deposition of coke on a "clean" surface, *i.e.*, with no coke around; and \underline{k}_2 when coke is deposited adjacent to another coke deposit. The former rate constant is for an initiation step (or "non-catalytic" coking), while the latter is for the propagation step (or coking catalyzed by the presence of the coke "product"); hence, typically, $\underline{k}_2 > \underline{k}_1$. A third parameter used in the model is \underline{M} , which represents the maximum amount of coke which can be deposited on the catalyst. In terms of these three parameters, the coke level \underline{c} expected in a pulse reactor after the passage of \underline{R} amount of reactant is given by:

$$\underline{c} = \frac{\underline{M}(1 - \exp[-\underline{k}_1\{1 + (\underline{k}_2/\underline{k}_1)\underline{M}\underline{R}\}])}{1 + (\underline{k}_2/\underline{k}_1)\underline{M} \exp[-\underline{k}_1\{1 + (\underline{k}_2/\underline{k}_1)\underline{M}\underline{R}\}]} \quad (2)$$

The values of the three parameters can be obtained by fitting the experimental data to Equation 2. The form of $\underline{c}(\underline{R})$ is S-shaped, and the location of the inflexion point (the maximum "rate" of coke deposition) plays an important role in the coke / activity / selectivity behavior of a catalyst in general (4). The coke level, \underline{c}_m , at the inflexion point of the curve can be obtained from the fitted values of the three parameters.

Curves of the experimental data on coke level as a function of the amount of reactant used, $\underline{c}(\underline{R})$, were obtained when the feeds were decane - cumene mixtures and cumene - naphthalene mixtures. Compositions ranged from 100% decane ($\underline{A} = 0$) through 100% cumene ($\underline{A} = 100$) upto 70%cumene - 30%naphthalene ($\underline{A} = 130$). (Larger fractions of naphthalene are not soluble in cumene.) The coking curves are

shown in Figures 1 and 2. As expected, the amount of coke deposited increases with the amount of naphthalene added to the cumene, and decreases with the amount of decane added to the cumene.

Values of k_1 , k_2 and M were obtained from fitting these curves to Equation 2. These values and the corresponding values of c_m are shown in Figures 3-6 as functions of changing feeds (changing values of A).

From Figures 3 and 4, it can be seen that the values of M and c_m are independent of A . The invariance of these two parameters with feed concentrations is as expected since these values, particularly M , are characteristics of the catalyst surface rather than the feed.

The values of the rate constants depend strongly on the feed compositions. From Figure 5, the value of k_1 increases slightly with A for decane - cumene mixtures, but then increases to a much greater extent with increasing A when cumene - naphthalene mixtures are used. In other words, the slope of the $k_1(A)$ curve increases sharply around $A = 100$. Hence the increase in k_1 with the aromatic ring percent, *i.e.*, on a per-ring basis, is greater for the addition of a two-ring compound than when a one-ring compound is added. On a mole-of-feed basis, the increase in k_1 when a two-ring additive is used would be more than twice that when a one-ring additive is used.

The value of k_2 , Figure 6, increases more-or-less linearly with A through the entire range. The slope of the $k_2(A)$ curve is intermediate between the two values for the $k_1(A)$ curve. Hence the increase in k_2 is the same on a per-ring basis whether one-ring additives or two-ring additives are used. On a mole-of-feed basis, the increase in k_2 when a two-ring additive is used would be twice that when a one-ring additive is used.

Under these conditions, the evaluation of k_1 , k_2 , and M from coking kinetics experiments in the presence of fast-coking species will allow the estimation of these parameters, *i.e.*, the determination of coking kinetics, for the actual feed alone.

Activity. We concentrate on the conversion of the "actual" feed reactant, cumene, as the measure of activity. We note how the conversion changes when different amounts of different coking additives (decane, naphthalene) are mixed with the feed, and pulsed over a catalyst of different coke levels. We also report data on the conversions of the additives decane or naphthalene under the same conditions. As mentioned earlier, cumene conversion is obtained by carrying out a benzene-ring balance on the contents of the sample collector after each pulse procedure, while conversions of naphthalene or decane are obtained by comparing peak areas with and without catalyst.

Our previous results with the pulse microreactor indicate that the conversion, X , decreases linearly with the coke level c , at least upto c_m . At larger values of the coke level, the conversion drops more rapidly, and tends towards zero around $c = M$. For the linear portion of the $X(c)$ curve, we can write:

$$X = a - b.c \quad (3)$$

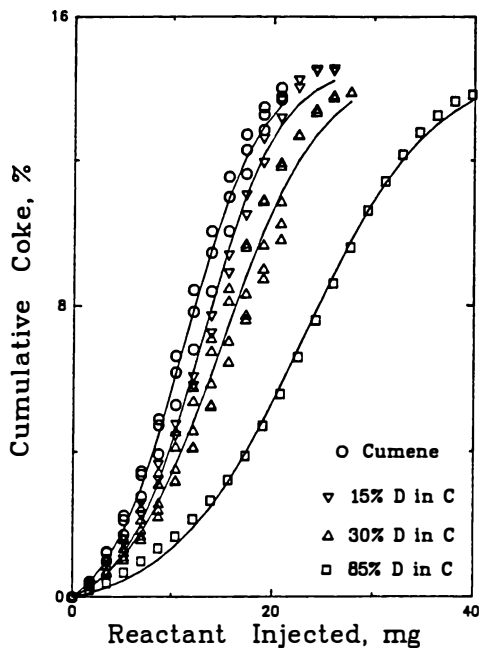


Figure 1. Coke deposited after pulses of cumene-decane mixtures. (Reproduced with permission from Ref. 1. Copyright 1994 Elsevier.)

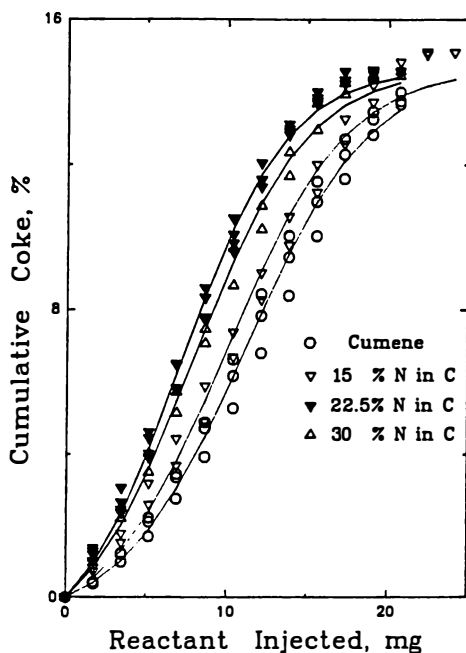


Figure 2. Coke deposited after pulses of cumene-naphthalene mixtures. (Reproduced with permission from Ref. 1. Copyright 1994 Elsevier.)

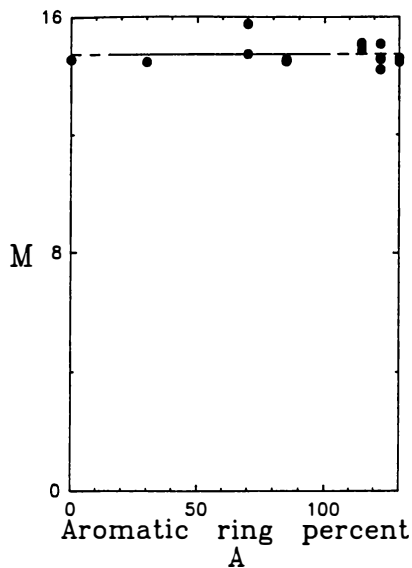


Figure 3. Effect of aromatic ring percent, Δ , on maximum coke deposited, M . (Reproduced with permission from Ref. 1. Copyright 1994 Elsevier.)

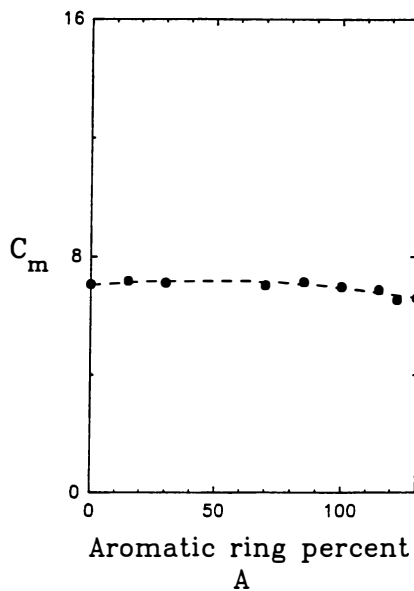


Figure 4. Effect of aromatic ring percent, Δ , on the coke level at the maximum deposition "rate", C_m . (Reproduced with permission from Ref. 1. Copyright 1994 Elsevier.)

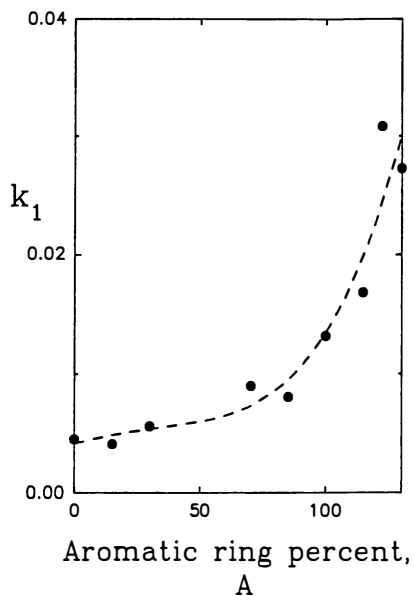


Figure 5. Effect of aromatic ring percent, A , on the initiation (non-catalytic) rate constant for coking, k_1 . (Reproduced with permission from Ref. 1. Copyright 1994 Elsevier.)

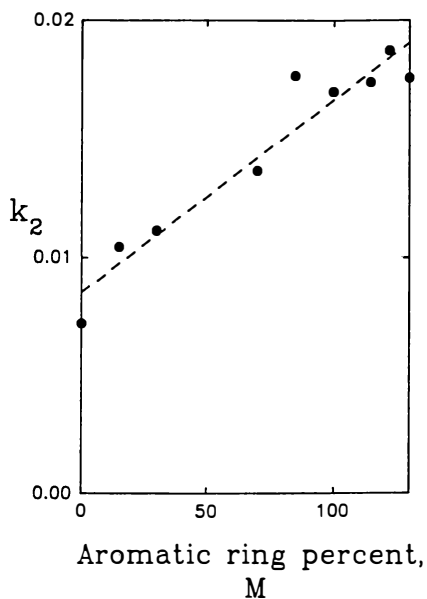


Figure 6. Effect of aromatic ring percent, A , on the propagation (autocatalytic) rate constant for coking, k_2 . (Reproduced with permission from Ref. 1. Copyright 1994 Elsevier.)

Here \mathbf{a} is the conversion corresponding to the fresh, uncoked, catalyst while \mathbf{b} denotes a measure of the sensitivity of the catalyst activity to coke level. We use the parameters \mathbf{a} and \mathbf{b} to quantify the role of the added species on the catalyst activity,

For each of the experimental runs used above, *i. e.*, for each value of \mathbf{A} above, the value of the conversion of cumene was obtained. For most of the runs, the conversions of the additive was also obtained. Values of \mathbf{a} and \mathbf{b} were obtained by fitting the experimental values of \mathbf{X} corresponding to coke levels \mathbf{c} less than or equal to \mathbf{c}_m ($\approx 7\text{wt}\%$).

For the cumene - naphthalene feeds, Figure 7, the $\mathbf{X}(\mathbf{c})$ lines all lie within a relatively tight band. The corresponding values of \mathbf{a} and \mathbf{b} are shown in Table II. As expected from Figure 7, the values of \mathbf{a} and \mathbf{b} are relatively constant with increasing \mathbf{A} . For the cumene - decane feeds, Figure 8, the $\mathbf{X}(\mathbf{c})$ lines are different. The corresponding values of \mathbf{a} and \mathbf{b} are shown in Table III. Both parameters increase with increasing values of \mathbf{A} .

Conversions of the decane component (in the decane - cumene mixture) and the naphthalene component (in the naphthalene - cumene mixture) have been analyzed similarly. Figure 9 represents the data for the conversion of decane in a mixture of 85% decane and 15% cumene. Also shown in the figure is the straight line obtained by fitting the data at coke levels of less than \mathbf{c}_m ($\approx 7\text{wt}\%$). The corresponding values of \mathbf{a} and \mathbf{b} are given in Table IV. Because of the greater scatter of the points, they are not shown for the rest of the cumene - decane mixtures. Instead, the corresponding straight lines are shown in Figure 10. The values of \mathbf{a} and \mathbf{b} are again given in Table IV. It can be seen that there is no consistent trend in the values of \mathbf{a} and \mathbf{b} as the value of \mathbf{A} increases. In all cases, however, the value of \mathbf{b} is remarkably small, indicating that the coke deposited (by cumene, predominantly) affects very little the activity of the catalyst for decane cracking.

Figure 11 similarly represents the data for naphthalene in naphthalene - cumene mixtures, with the corresponding values of \mathbf{a} and \mathbf{b} given in Table V. In this case, as the value of \mathbf{A} increases, the value of \mathbf{a} decreases monotonically.

From Tables III and V, it would appear that, for the component of the feed which is more-rapidly coking, the activity and the coke resistance of the catalyst change with the amount of that component in the feed. From Tables II and IV, conversely, for the component of the feed which is less-rapidly coking, the behavior of the catalyst is apparently unchanged.

If these observations are generally true, a strong case can be made for the usefulness of the accelerated-coking technique. Since one would add a species which is more-rapidly coking than the feed, the activity and the coke resistance of the catalyst for the (less-rapidly coking) actual feed would have (close to) the same value as if no fast-coking species had been added. While the catalyst performance for the fast-coking species may well be different when it is added to the feed than when it is present by itself, this is of relatively little consequence, at least as long as the actual products from the actual feed and the additive can be separated in some manner.

Summary and Conclusions

We report the effect on the kinetics of coking and on the activity of the deactivated catalyst when a species with a different propensity to coke formation is added to the feed. Steamed REHY zeolite was used as the catalyst, and feeds containing various

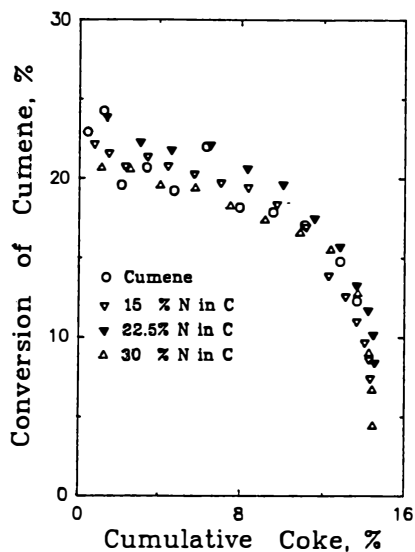


Figure 7. Activity of catalyst for cumene conversion (by benzene-ring balance) in cumene - naphthalene mixtures as a function of coke on the catalyst.

TABLE II. Performance of Catalyst for Cumene Cracking Using Cumene - Naphthalene Feeds

A, aromatic ring percent of feed; a, initial conversion; b, sensitivity to coke

<u>A</u> , %	<u>a</u> , %	<u>b</u> , %/wt%
100	21.7	0.570
115	21.4	0.481
122.5	21.3	0.413
130	21.6	0.488

TABLE III. Performance of Catalyst for Cumene Cracking
Using Cumene - Decane Feeds

A, aromatic ring percent of feed; a, initial conversion; b, sensitivity to coke

<u>A</u> , %	<u>a</u> , %	<u>b</u> , %/wt%
30	15.2	0.325
70	21.0	0.483
100	23.4	0.597

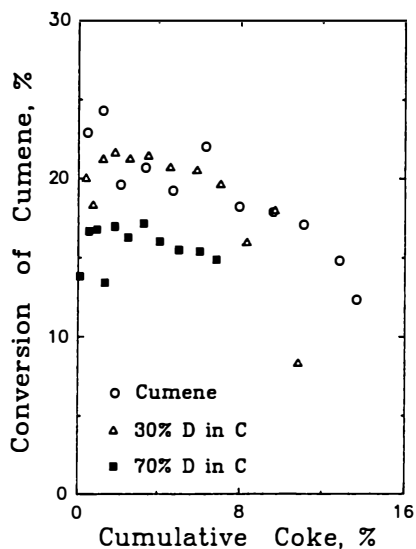


Figure 8. Activity of catalyst for cumene conversion (by benzene-ring balance) in cumene - decane mixtures as a function of coke on the catalyst.

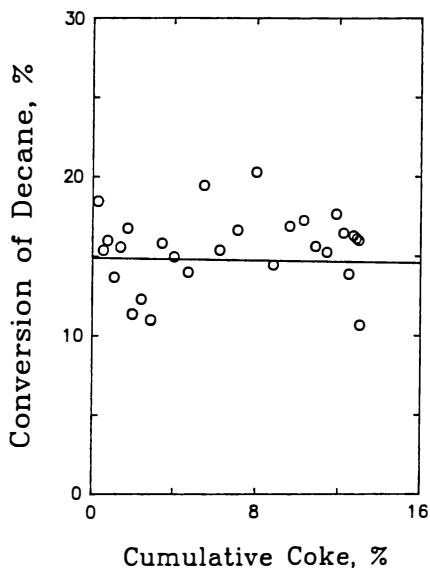


Figure 9. Activity of catalyst for decane conversion (by comparison with non-catalytic run) in 15%cumene - 85%decane mixture as a function of coke on the catalyst. The straight line indicates the best fit for coke levels less than 7%.

TABLE IV. Performance of Catalyst for Decane Cracking
Using Cumene - Decane Feeds

A, aromatic ring percent of feed; a, initial conversion; b, sensitivity to coke

<u>A</u> , %	<u>a</u> , %	<u>b</u> , %/wt%
15	14.9	0.020
70	12.0	0.428
85	13.1	0.066

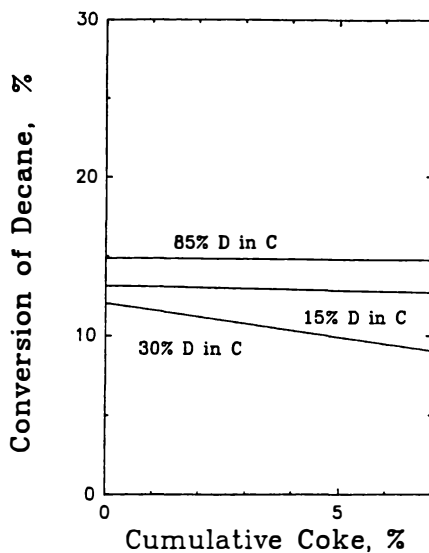


Figure 10. Activity of catalyst for decane conversion (by comparison with non-catalytic run) in cumene - decane mixtures as a function of coke on the catalyst. The straight lines indicate the best fit for coke levels less than 7%.

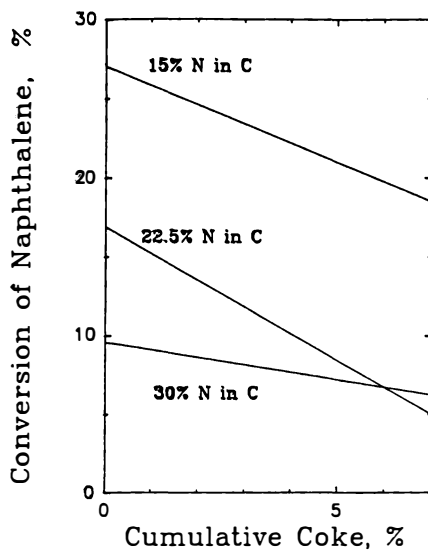


Figure 11. Activity of catalyst for naphthalene conversion (by comparison with non-catalytic run) in cumene - naphthalene mixtures as a function of coke on the catalyst. The straight lines indicate the best fit for coke levels less than 7%.

**TABLE V. Performance of Catalyst for Naphthalene Cracking
Using Cumene - Naphthalene Feeds**
A, aromatic ring percent of feed; **a**, initial conversion; **b**, sensitivity to coke

<u>A</u> , %	<u>a</u> , %	<u>b</u> , %/wt%
115	27.0	1.22
122.5	16.9	1.70
130	9.56	0.480

amounts of decane in cumene and feeds containing various amounts of naphthalene in cumene were used.

Coke levels and the rate of coke formation on the catalyst increase with the amount of naphthalene added, and decrease with the amount of decane added. In the two-step (initiation/propagation or autocatalytic) model of coke formation, the maximum coke level of the catalyst, M , and the coke level at the maximum deposition "rate", c_m , are independent of the feed used. However, the two rate constants depend strongly on the feed composition, as quantified by the aromatic ring percent, A . Both rate constants increase with increasing A . However, the initiation rate constant, k_1 , has a greater increase, per ring, for a two-ring additive than for a one-ring additive; while the increase per ring for the propagation rate constant, k_2 , is approximately the same for both types of additives. With this behavior in mind, and knowing the values of the parameters k_1 , k_2 and M (and c_m) for the feed containing the fast-coking species, one can obtain the coking parameters for the actual feed.

The performance of the coked catalyst is quantified by the initial conversion, a , and the sensitivity to coke, b , viz., the intercept and slope of the conversion - coke relationship, at least for coke levels less than c_m . The effect of reaction mixtures on a and b depends upon the nature of the feed and the species added. When the additive is less-rapidly coking, then values of a and b for the feed itself change with additive concentration. When the species added is more-rapidly coking, then a and b for the feed itself are independent of the additive concentration, i.e. independent of A . But since only a more-rapidly coking species would be an additive for a typical accelerated-coking test, it can be concluded that the presence of the added species does not influence the activity, at least upto coke levels equal to c_m .

Acknowledgments

We thank Professor M. Kobayashi, Kitami Institute of Technology, Kitami, Japan, for his support and encouragement of this research. The REHY catalyst and its characterization were supplied by W.R. Grace and Co., Inc.

Literature Cited

1. Dadyburjor, D.B., Liu, Z., Matoba, S., Osanai, S. and Shiro-oka, T. In *Catalyst Deactivation 1994*; Delmon, B. and Froment, G.F., Eds.; Stud. Surf. Sci. Catal.; Elsevier: Amsterdam, 1994, Vol. 88; pp 273-280.
2. Dadyburjor, D.B., Liu, Z., Matoba, S., Osanai, S. and Shiro-oka, T., *Prepr. - Amer. Chem. Soc. Div. Petr. Chem. 1995*, vol, pp.
3. Dadyburjor, D.B. and Liu, Z., *J. Catal.* **1993**, *141*, 148.
4. Dadyburjor, D.B. and Liu, Z., *Chem. Eng. Sci.* **1992**, *47*, 645.

Pilot Reactor Testing of the Effect of Naphtha Boiling Point in Catalytic Reforming

K. Moljord¹, K. Grande², I. Tanem¹, and A. Holmen³

¹SINTEF Applied Chemistry, N-7034 Trondheim, Norway

²STATOIL Research Centre, N-7004 Trondheim, Norway

³Department of Industrial Chemistry, Norwegian Institute of Technology, N-7034 Trondheim, Norway

Naphthas with different initial and final boiling points were compared by pilot reactor testing. The pilot reactor unit consisted of isothermal, once-through reactors with on-line GCs for full product analysis and octane number determination. Octane numbers, reformat yields and composition as well as gas yields were measured as a function of reaction temperature at 16 bar reaction pressure and a molar H₂/HC ratio of 4.3. Catalyst deactivation was studied over two weeks periods at high severity conditions, i.e. 102.4 RON and a H₂/HC ratio of 2.2. Test results, with emphasis on the yields of benzene and other aromatics, reformat and hydrogen yields as well as catalyst deactivation, are presented.

Catalytic reforming is an important process for conversion of low-octane naphthas into high-octane gasoline. Catalytic reforming is also an important source of hydrogen for a number of refinery processes. Legislation is limiting the amount of benzene and other aromatics allowed in gasoline. At the same time the demand for hydrogen in the refineries increases as a result of increased hydrotreating in order to meet lower fuel sulfur specifications. Reformer units might be run at lower severity to produce less aromatics, but lower octane numbers and hydrogen production will result. Refiners will then have to examine carefully the alternatives within the refinery to meet the new demands for cleaner fuels. For the reformer, optimized hydrogen production may be the best solution. The reformer operating conditions as well as feedstock are worth considering.

In this paper we report the results of a pilot reactor testing of naphthas with different initial as well as different final boiling points. Increasing the initial boiling point (IBP) is one way of reducing benzene formation by removing benzene precursors from the naphtha. It is, however, of interest to know exactly how efficient this strategy is, and to specify the effect on reformat and hydrogen yields as well as on the cycle length. Decreasing the final boiling point (FBP) of the naphtha is a way of reducing the ASTM 90% distillation (T90) of the gasoline. Again a firm

relation between naphtha FBP and heavy ends of reformat should be established, and the effect on yields and cycle length specified.

The study was carried out in relatively small isothermal reactors without recycle, constructed for testing and comparison of different catalysts and feedstocks. Detailed information about catalyst performance under different conditions can be efficiently obtained under very controlled conditions in such equipment (1). However, exact predictions of the performance of a commercial reformer unit consisting of 3-4 adiabatic reactors will need detailed kinetic and reactor modeling, which is not included in this paper.

Experimental

Reactor Unit. The pilot reactor unit consists of three once-through isothermal reactors in parallel, designed for simultaneous testing of three different catalysts (or feedstocks). The reactors are heated in three separate baths of circulating molten salt (an eutectic mixture of KNO_3 , NaNO_3 and NaNO_2), assuring very high rates of heat transfer and good temperature control, as reported by Van Trimpont et al. (2) and Lox et al. (3). Each reactor tube has an internal diameter of 19 mm and a length of 750 mm, and is equipped with a 6.4 mm diameter axial thermowell, leaving ca. 190 cm^3 of reactor volume. Further details on the pilot reactor unit is given elsewhere (4).

In order to minimize the temperature drop at the reactor inlet caused by the rapid, endothermic naphthene dehydrogenation, the catalyst bed was diluted by a low-surface, chloride-free alumina. The degree of dilution was varied in three different zones of the reactor, with the highest dilution at the reactor inlet. The first zone, comprising 33% of the reactor volume, contained only 6% of the total amount of catalyst. The temperature drop at the reactor inlet, measured with the axial thermocouple, did not exceed 5°C.

The reactor effluent was analyzed by on-line GC-analysis prior to condensation. Each reactor line was equipped with a HP 5890 GC with flame ionization detector (FID), interfaced with a PC for data handling and storage. The method of analysis, based on HP's PONA analysis, included all important hydrocarbons up to C_{11} . Heavier components than this were only present in trace amounts, and were not analyzed. Research octane numbers (RON) were calculated from GC-analysis based on an adapted version of the method presented by Anderson et al. (5). The hydrogen yield was calculated from GC-analysis as the hydrogen balance over the reactor.

The critical operating variables (temperatures and pressures) were monitored continuously by an in-house programmed PC. The unit would be shut down automatically by the computer if certain limits were exceeded. Hence unmanned operation of the unit was possible.

Test Procedures. The tests were performed with 35 g of catalyst in the reactor, and the catalyst was oxychlorinated, reduced and sulfided in the reactor prior to testing. Oxychlorination was carried out in order to ensure uniform chloride content as well as a highly dispersed metal function on the catalyst. Oxychlorination was carried out at 500°C in an air stream containing H_2O and HCl at a given ratio, before "rejuvenation" of the metal function in dry air. The catalyst was then reduced in H_2

at 10 bar, with a temperature ramping of +20°C/h from 400 to 480°C, which was kept for 2h. Finally the catalyst was presulfided with H₂S in H₂ at 425°C until breakthrough of H₂S. After flushing with pure H₂, naphtha was introduced at 400°C, and the reactor temperature was slowly raised to 480°C.

The tests were carried out at WHSV=2.03, a molar ratio H₂/hydrocarbon of 4.34 and a reactor pressure of 16 bar. After "lining out" the fresh catalyst at 480°C for minimum 50 h, octane numbers and yields were examined as a function of reaction temperature at 480, 495 and 510 °C. Subsequently, catalyst deactivation was studied at high severity in order to obtain sufficient catalyst deactivation during 14 days of operation. This was achieved by lowering the H₂/HC ratio to 2.17 at a severity of 102.4 RON, which was maintained by continuously increasing the reactor temperature.

Calculated RON values corresponded to engine values of debutanized reformate samples (25 samples) with a standard deviation of 0.55 RON units, which is close to the accuracy of engine measurements. By carrying out a number of repeated test runs, the reproducibility taken as the standard deviation for the measured reformate and hydrogen yields were determined as 0.25 and 0.02 wt%, respectively, and 0.25 units for RON. In order to achieve this a detailed calibration of the GC system was carried out, and the reactor thermocouples, the hydrogen mass flow controllers and naphtha feed pumps were thoroughly calibrated between each test run.

The tests were carried out with a commercial, balanced Pt-Re (0.3 wt% Pt and 0.3 wt% Re) reforming catalyst, supplied and used in the form of 1/16" extrudates. After each test the catalyst was analyzed for chloride content at four different points through the reactor to ensure that overchloriding or chloride loss did not occur. Each sample differed by less than 0.15 wt% and the mass averaged value for each reactor by less than 0.05 wt% from the original 1.00 wt% Cl on the fresh catalyst. This proves good chloride control during testing.

Feedstock. A hydrotreated, straight-run naphtha from a North Sea crude was used as a base feedstock in the test program. By distillation (according to ASTM D-2892, with 15 theoretical plates and a reflux ratio of 5:1) three naphthas with different initial boiling points (IBP) and three naphthas with different final boiling points were produced. The boiling point properties of the base and the derived naphthas are given in Table I. The composition of the different naphthas was determined by GC analysis.

The hydrotreated base naphtha contained less than 0.5 ppm sulfur. The naphthas were dried over molecular sieve and stored under an inert gas (Ar) prior to use in the pilot unit. Using Karl-Fischer analysis the water content of the dried naphthas was measured to be 5-8 wt ppm. In order to compensate for the effect of the remaining water on the chloride content of the catalyst, 0.8 wt ppm chloride as 1,1,2-trichloroethane was added to the naphthas. H₂ (99.995%, Norsk Hydro), supplied from gas cylinders, was passed over a deoxo catalyst (BASF R3-11) at 70°C and a 4A molecular sieve to remove traces of oxygen and water, respectively. The deoxo catalyst as well as the molecular sieve were regenerated between each test run.

Table I: The boiling point properties of the base naphtha and the naphthas derived from this by distillation (ASTM D-2892)

	Naphtha						
	Base	IBP 97	IBP103	IBP114	FBP149	FBP132	FBP116
IBP	76 °C	97°C	103°C	114°C	77°C	72°C	68°C
5%	96°C	107°C	112°C	121°C	93°C	88°C	82°C
10%	100°C	110°C	114°C	123°C	97°C	92°C	84°C
50%	122°C	125°C	128°C	134°C	114°C	105°C	94°C
90%	155°C	155°C	158°C	160°C	137°C	123°C	106°C
95%	164°C	163°C	166°C	167°C	143°C	127°C	109°C
FBP	177°C	172°C	177°C	178°C	149°C	132°C	116°C

Naphtha Analysis

Effect of IBP. The removal of the C₅, C₆ and C₇ components with increasing IBP in the boiling range of 76 to 114 °C is shown in Figure 1. The C₈ components were not removed in this interval. While all the C₅ components were totally removed at IBP 97°C, the C₇ components were removed only above this temperature. Of the C₇ components, toluene was the last to be removed, due to the highest boiling point. The toluene concentration was reduced only at an IBP above 105 °C.

Effect of FBP. By decreasing the FBP, the naphtha concentration of n-paraffins and naphthenes increased as a result of the removal of the aromatics-rich heavy end of the base naphtha. Above FBP 149 °C, only C₉₊ components were removed. Below this temperature the C₈ aromatics were affected, and first of all the xylenes (Figure 2). Because of a higher boiling point, o-xylene is the first C₈ aromatic component to be removed from the naphtha when the FBP is lowered. Ethylbenzene is the last C₈ aromatic component to be removed due to a lower boiling point (136.2 °C, compared with 138-144 °C for the xylenes).

Test Results.

Aromatics. RON is strongly dependent on the concentration of aromatics in the reformat. A linear correlation has been reported for a given feedstock with changing operating variables such as reaction temperature and pressure (6). The results given in Figure 3 demonstrate that a single linear correlation holds also for feedstocks with different boiling point properties. However, the amount of each aromatic component varies with the boiling point properties, Figure 4.

The general trend, not surprisingly, is that the heavier (C₈ and C₉₊) aromatics become more important the higher the initial boiling point of the naphtha. The yield

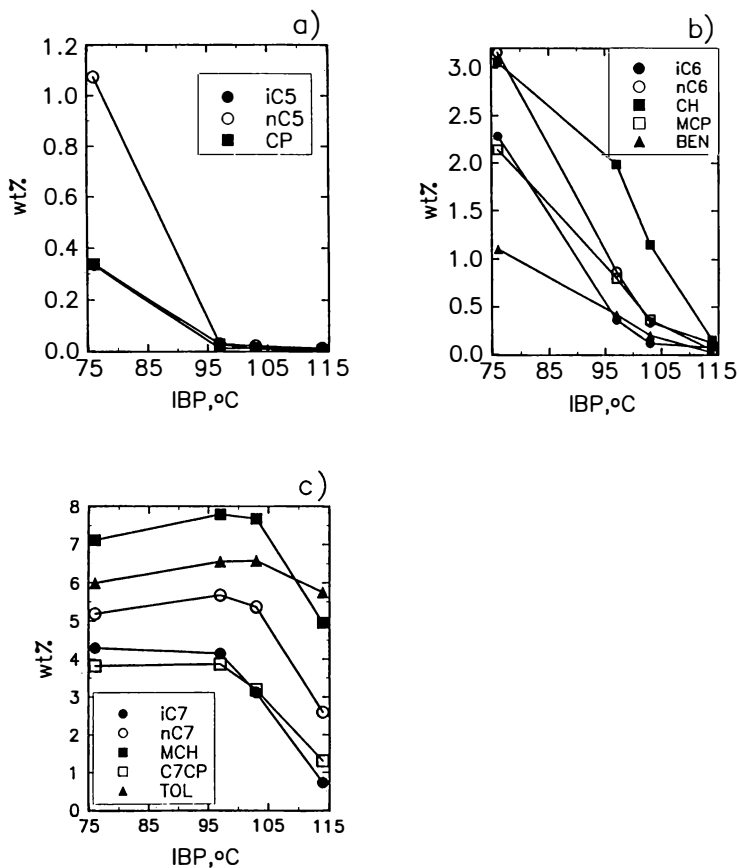


Figure 1. The content of a) C₅; b) C₆ and c) C₇ components in the naphthas as a function of the initial boiling point (IBP). CP=cyclopentane; MCP=methylcyclopentane; C7CP=dimethyl- and ethyl -cyclopentane; CH=cyclohexane; MCH=methylcyclohexane; BEN=benzene; TOL=toluene.

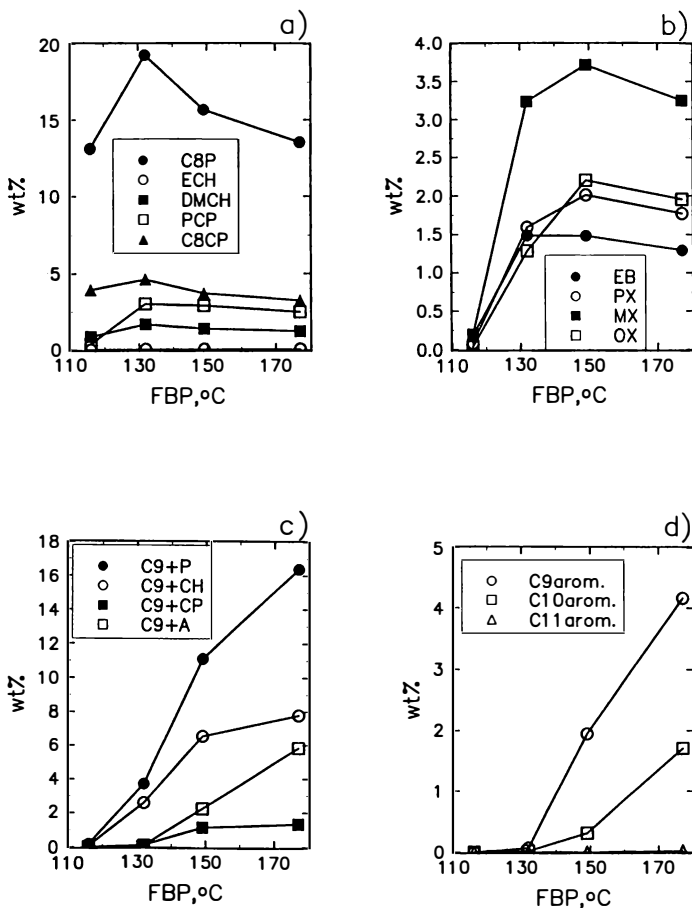


Figure 2. The content of a) C₈ paraffins and naphthenes; b) C₈ aromatics; c) C₉₊ components and d) C₉₊ aromatics in the naphthas as a function of the final boiling point (FBP). C8P=C₈ paraffins; PCP=propylcyclopentane; C8CP=ethylmethyl- and trimethyl-cyclopentanes; ECH=ethylcyclohexane; DMC=dimethylcyclohexane; EB=ethylbenzene; PX,MX,OX=xylenes.

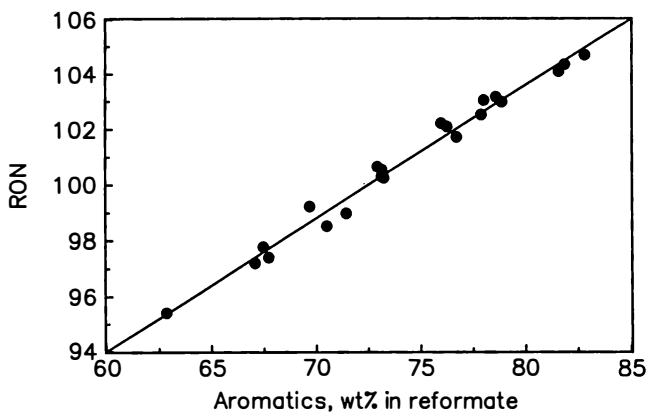


Figure 3. RON as a function of the concentration of aromatics in the reformat for the different naphthas.

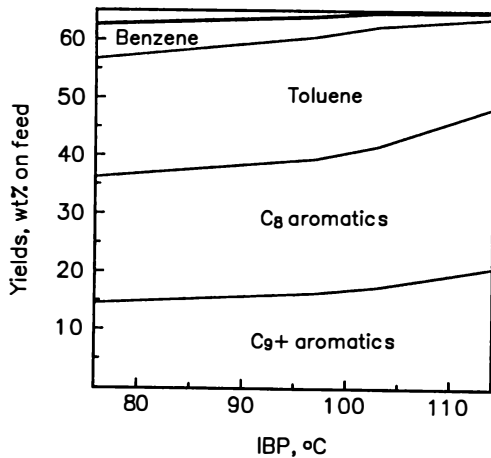


Figure 4. The distribution of aromatics as a function of naphtha IBP at 100 RON.

of benzene diminish with increasing IBP, while the yield of toluene is constant for an IBP up to 103 °C. In order to obtain a given RON a certain total yield of aromatics is necessary, but by changing the naphtha IBP the type of aromatics will change. The yield of benzene can be significantly reduced, but the benzene reduction is accompanied by a corresponding increase in the yield of heavier aromatics if RON is to be maintained.

Toluene is the most important single aromatic component independent of severity. Benzene, toluene and C₈ aromatics are favoured at high severity, compared to the C₉₊ aromatics, as a result of more hydrodealkylation. As expected, this effect is more pronounced at higher reaction pressures (7). In particular, a significant amount of benzene is produced from heavier aromatics at high severity. As shown in Figure 5, between 1.0 and 1.5 weight% benzene was produced, depending on the severity, even when all the C₆ cyclics were removed from the naphtha. At a given severity, the benzene yield increases linearly with the C₆ cyclics content of the naphtha. The selectivity towards benzene of the C₆ cyclics, i.e. cyclohexane, methylcyclopentane and benzene, can therefore be defined as the slope of those straight lines. For severities between 99 and 102 RON this benzene selectivity varied between 75 and 79 %.

Reformate yield. Reformer feedstock is often characterized by its (N+A) or (N+2A), where N signifies naphthenes and A aromatics, in liquid vol% (8). Feedstocks with high content of naphthenes are easy to reform due to the high naphthene selectivity to aromatics. As RON is nearly proportional to the concentration of aromatics in the reformate, naphthenic naphthas produce high octane numbers with good reformate yields. Aromatics pass virtually unconverted through the reactor, except from some hydrodealkylation of side chains at high severities.

In Figure 6 the reformate yield (wt% on feed) is given as a function of the (N+2A) wt% determined by GC analysis for the different naphthas. Obviously the weight% reformate yield is linearly dependent of the weight% (N+2A) for the heavier naphthas, i.e. the naphthas with different IBP. A linear correlation between reformate yield and (N+2A) for naphthas with different boiling points signifies that differences in aromatics selectivity for paraffins, naphthenes and aromatics are accounted for, and that differences in selectivity for components with different carbon number do not affect reformate yield. When removing the heavy end of the base naphtha (i.e. for the case of the naphtha with FBP 149°C), the reformate yield was lower than expected, possibly because of the particularly high aromatic and low naphthenic content of this C₉₊ fraction (Figure 2). The fraction between 132 and 149 °C was rich in naphthenes (Figure 2), and the reformate yield of the naphtha with FBP 132°C corresponded to the value obtained by extrapolating the line obtained for the heavier naphthas.

The very light naphtha (FBP 116°C) consisting of 4 wt% C₅, 24 wt% C₆, 54 wt% C₇ and the rest C₈ components (no C₈ aromatics), produced lower reformate yields than expected just from the extrapolated (N+2A) parameter. This can be explained considering the lower aromatization selectivity of C₆ and C₇ than of C₈ paraffins and cyclopentanes (9). However, within certain limits, the parameter (N+2A) describes the changes in feedstock "richness" with changing boiling points well. As the selectivity to aromatics is much lower for paraffins than for cyclopentanes and in particular cyclohexanes and aromatics, also dependent on carbon

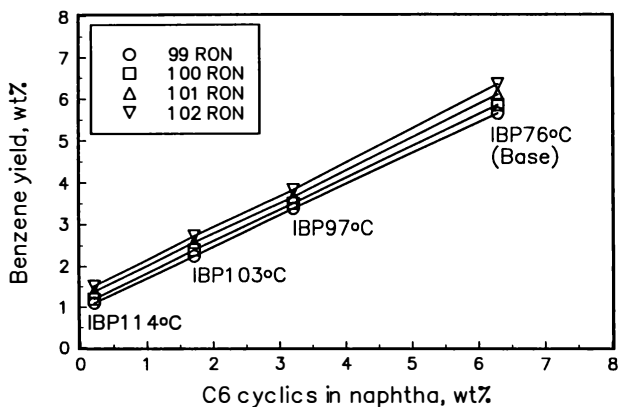


Figure 5. The yield of benzene (wt% on feed basis) as a function of the sum of the benzene, cyclohexane and methylcyclopentane in naphtha.

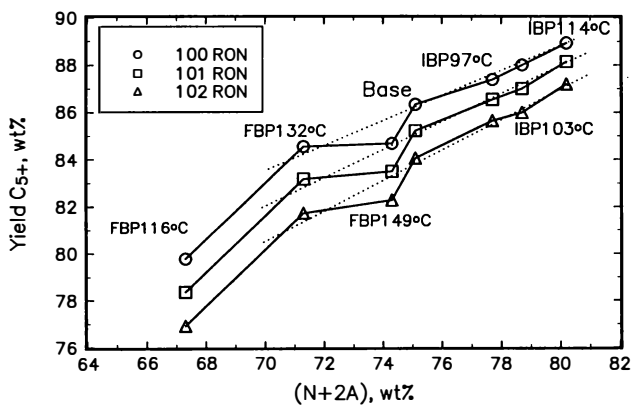


Figure 6. The reformate yield (wt% on feed) as function of (N+2A) wt% in the naphtha. (N=total naphthenes, A=aromatics).

number (9), it is clear that such a correlation is not suited for extrapolation beyond those limits. As can be seen from Figure 6, the slope of wt% reformat yield vs. wt% (N+2A) also depends on the severity, increasing from 0.53 at 100 RON to 0.65 at 102 RON.

Hydrogen. For a given feedstock the yield of hydrogen depends on the balance between the hydrogen producing and the hydrogen consuming reactions. Dehydrogenation and dehydrocyclization are the most important hydrogen producing reactions, while hydrocracking and hydrogenolysis, both undesired reactions which lower the reformat yield, are hydrogen consuming. However, the content of hydrogen in the feedstock is important for the H₂ yield in the reforming process. The hydrogen content of naphtha is determined mainly by the relative amount of aromatics, naphthenes and paraffins, as an unsaturated -CH- contains 7.7 wt% hydrogen while a saturated -CH₂- contains 14.3 wt% hydrogen. The chain length is of minor importance, as for example a C₆ paraffin contains 16.3 wt% and a C₁₀ paraffin 15.5 wt% hydrogen.

The hydrogen content of the different naphthas, calculated from GC analysis, is shown in Figure 7. There is a nearly linear negative correlation between hydrogen content and the concentration of aromatics. Therefore the naphtha hydrogen content diminishes with increasing IBP but increases with lower FBP.

The hydrogen yields are shown as a function of RON for the different naphthas in Figure 8. Hydrogen yields between 1.8 and 2.2 wt% were found, depending both on the feedstock and on the severity. By increasing the severity the hydrogen yield increases, but much less for the lighter naphthas than for the heavier ones. This can be explained by higher cracking selectivities and therefore hydrogen consumption with increasing temperature for the C₆ and C₇ -rich light naphthas. The heaviest naphtha (IBP 114°C) has the lowest hydrogen content (Figure 7) and gives the lowest hydrogen yield. The lightest naphthas (FBP 116 and 132°C) have the highest hydrogen contents and produce the highest hydrogen yields at normal severities. However, due to a weaker temperature response the difference in hydrogen yield diminish with increasing severity.

Catalyst deactivation. Catalyst deactivation due to coke formation is strongly dependent on the operating conditions as well as on the nature of the feedstock. Coke formation is favoured by low hydrogen partial pressures (low H₂ to hydrocarbon ratios) (10) and by high reaction temperatures (11). Certain components in naphtha are considered as important coke precursors. Cyclopentanes are known coke precursors in the initial boiling range of naphtha, while alkylbenzenes and bicyclic aromatics are the most important coke precursors in the heavy end (11).

Catalyst deactivation was studied at high severity (102.4 RON) and low partial pressure of hydrogen in order to obtain reasonable deactivation over periods of two weeks. In Figure 9 the necessary temperature rise to maintain a constant RON as the catalyst loses activity is presented. The base naphtha gave the highest catalyst deactivation. By increasing IBP from 76 to 97 °C a significant reduction in catalyst deactivation was obtained, while a further increase in IBP above 97 °C gave only marginal additional improvements in catalyst stability. By lowering the FBP from

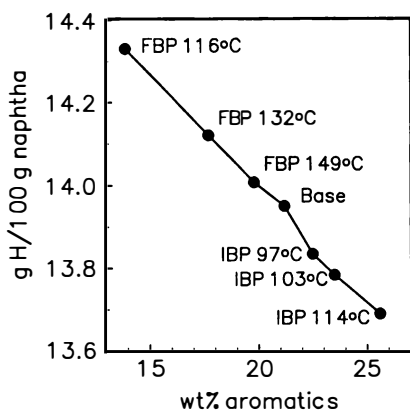


Figure 7. The hydrogen content as a function of the content of aromatics in the naphtha.

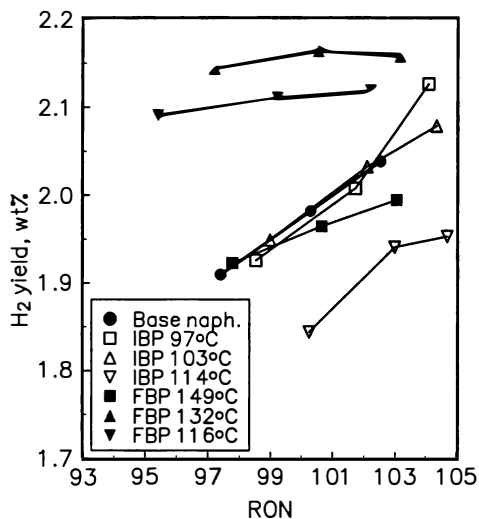


Figure 8. Hydrogen yields (wt% on feed basis) as a function of RON.

177 to 149 °C an even greater improvement was observed in catalyst stability measured as the necessary temperature increase. Again a further reduction of FBP had only a minor effect on catalyst deactivation.

The heavier naphthas (IBP 97, 103 and 114 °C) with high N+2A produced the desired RON at lower temperatures than the base naphtha: The extrapolated starting temperatures are 6, 9 and 12 °C lower, respectively (Figure 9). The amount of cyclopentanes in the naphthas was reduced from 13.4 to 11.1 wt% when the IBP was increased from 76 to 114 °C. This is probably too limited to account for the observed reduction in catalyst deactivation when the IBP was increased. This is supported by the observation of only slightly higher coke contents for the naphthas with higher cyclopentanes content, limited also to a very narrow zone at the reactor inlet. Except for the inlet there were no axial coke profiles through the reactors after testing. The lower catalyst deactivation with increasing IBP is therefore probably related to lower reaction temperatures, an effect of a "richer" feedstock as the N+2A increases.

The effect of reduced FBP on catalyst deactivation is not related to the reaction temperature as this was similar for the naphthas with different FBP (Figure 9). Therefore the amount of coke precursors in the heavy end is the important factor. Table II presents the identified C₁₀ aromatics (the heaviest components present in more than just trace concentrations) in the reformat at 102.4 RON. There is a distinct difference between the base naphtha and the FBP 149 °C naphtha with respect to feedstock as well as reformat content of propyl-toluenes and n-butylbenzene, which both can form bicyclic aromatics through direct side-chain cyclization.

The effect of naphtha FBP on catalyst deactivation is further illustrated in Figure 10, where relative rates of deactivation, expressed as the rate of temperature

Table II: Identified C₁₀ aromatics in the reformat at 102.4 RON (16 bar; H₂/HC=2.2; WHSV=2.0)

	Naphtha			
	FBP 177	FBP 149	FBP 132	FBP 116
n-butylbenzene	0.26 wt%	0.05 wt%	0.01 wt%	0.01 wt%
sec-butylbenzene	0.05 wt%	0.00 wt%	0.00 wt%	0.00 wt%
t-butylbenzene	0.00 wt%	0.00 wt%	0.00 wt%	0.00 wt%
propyl-toluenes (5 isomers)	0.79 wt%	0.20 wt%	0.03 wt%	0.01 wt%
diethylbenzenes (2 isomers)	0.19 wt%	0.05 wt%	0.01 wt%	0.01 wt%
ethyl- dimethylbenzenes (1 isomer)	0.18 wt%	0.06 wt%	0.01 wt%	0.01 wt%
tetramethylbenzenes (1 isomer)	0.24 wt%	0.09 wt%	0.01 wt%	0.00 wt%
Total	1.71 wt%	0.45 wt%	0.07 wt%	0.04 wt%

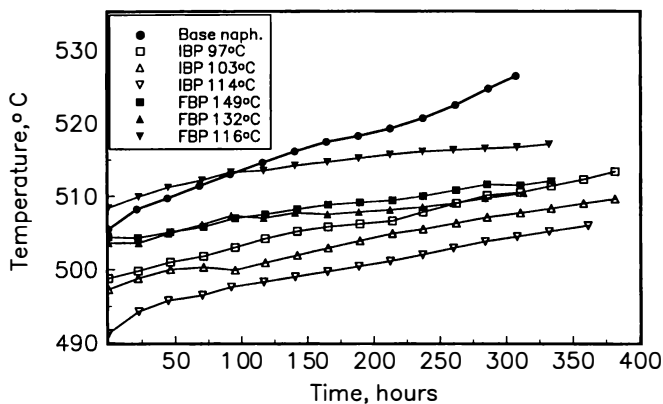


Figure 9. The temperature rise needed to maintain 102.4 RON during the periode of accelerated deactivation: 16 bar pressure and $H_2/HC=2.2$.

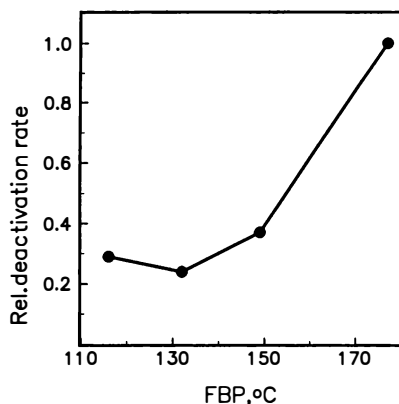


Figure 10. The deactivation rate relative to the one for the base naphtha, as a function of naphtha FBP. The deactivation rate was measured as the temperature rise needed to maintain 102.4 RON.

rise to maintain RON, is given as a function of FBP. The catalyst deactivation is most influenced by naphtha FBP around 177 °C, i.e. in the boiling range where the most notorious coke precursors are located. In this region an approximate deactivation rate reduction of 2% (compared to the base naphtha with FBP 177°C) for each °C of naphtha FBP reduction was observed. At FBPs below 149 °C obviously the most important coke precursors are removed and deactivation depends less on naphtha FBP.

Conclusion

By varying both initial and final boiling points of the feedstock, octane numbers, reformat yields and composition as well as gas yields were measured in a once-through, isothermal pilot reactor. The effect of the feedstock boiling point properties on catalyst deactivation was also studied.

As RON depends on the total concentration of aromatics in the reformat, the benzene yield (and concentration in the reformat) can be reduced significantly by increasing the naphtha initial boiling point, but a corresponding amount of heavier aromatics is needed to maintain RON. However, even when all the C₆ cyclics were removed from the naphtha, between 1.0 and 1.5 wt% (on feed) benzene, depending on severity, was produced by dealkylation of heavier aromatics.

The reformat yields of the different naphthas depended primarily on their content of naphthenes and aromatics, and could within certain limits be expressed by the (N+2A) wt%, determined by GC analysis. The hydrogen yields depended strongly on the hydrogen content of the naphtha, which increased as the naphtha became lighter and more paraffinic with decreasing FBP. The heaviest naphtha (IBP 114 °C) had the lowest hydrogen content and gave the poorest hydrogen yield.

The base naphtha (IBP 76 °C - FBP 177 °C) gave the highest catalyst deactivation. When IBP was increased the naphthas became "richer" and the same octane number could be achieved at lower reaction temperatures and therefore with less catalyst deactivation. When FBP was decreased less deactivation resulted from the removal of notorious coke precursors in the heavy end of the base naphtha.

Acknowledgement

The authors are grateful to Statoil for supporting this work and for the permission to publish the results.

Literature cited

- (1) Sie, S.T.; Blauwhoff, P.M.M. *Catalysis Today* **1991**, *11*, 103.
- (2) Van Trimpont, P.A.; Marin, G.B; Froment, G.F. *Ind.Eng.Chem.Res.* **1988**, *27*, 51.
- (3) Lox, E.; Coenen, F.; Vermeulen, R.; Froment, G.F. *Ind.Eng.Chem.Res.* **1988**, *27*, 576.
- (4) Moljord, K.; Hellenes, H.G.; Hoff, A.; Tanem, I.; Grande, K.; Holmen, A. Submitted for publication in *Ind.Eng.Chem.Res.*

- (5) Anderson, P.C.; Sharkey, J.M.; Walsh, R.P. *J.Inst.Petrol.* **1972**, *58*, 83.
- (6) McCoy, R.D. *Catalytic Reformer Product Octane Measurement via Total Aromatics*, ISA Transactions, 1973, p.187.
- (7) de Bruin, P.J. and van Broekhoven, E.H.; *Fuel Reformulation* 1993, *3*, 42.
- (8) Little, D.M. *Catalytic Reforming*, PennWell Publishing Company, Tulsa, 1985, p.24.
- (9) Tamm, P.W.; Mohr, D.H.; Wilson, C.R. In *Catalysis 1987*, Ward, J.W., Ed.; Elsevier Science Publ., Amsterdam, 1988, p.335.
- (10) Bournonville, J.P.; Franck, J.P. In *Hydrogen Effects in Catalysis*, Paál, Z.; Menon, P.G., Eds., Chem.Ind.; vol.31, Marcel Dekker, New York, 1988, p.653.
- (11) Parera, J.M.; Figoli, N.S. In *Catalysis Volume 9*, Spivey, J.J., Ed.; The Royal Society of Chemistry, Cambridge, 1992, p.65.

Vanadium Mobility in Fluid Catalytic Cracking

Richard F. Wormsbecher¹, Wu-Cheng Cheng¹, Gwan Kim¹, and Robert H. Harding²

¹Grace Davison and ²Research Division, W. R. Grace and Company—Conn., 7500 Grace Drive, Columbia, MD 21044

Previous work has shown that the poison precursor for vanadium poisoning of fluid cracking catalysts is a volatile species, vanadic acid, H_3VO_4 , formed in the regenerator from the interaction of H_2O vapor and oxides of vanadium in the V^{+5} oxidation state. The vapor pressure of the vanadic acid is very low, and may not be high enough to explain the *mobility* of vanadium in the regenerator. Some authors have suggested that the vanadium is transferred throughout the catalyst inventory by inter-particle transfer, through an unspecified collision mechanism. In this work, the mobility of vanadium is studied by measuring the rate of vanadium transfer to a vanadium trap. By varying the particle size distribution, and consequently the number density of particles, the collision frequency can be changed. In these experiments, the rate of vanadium transfer was shown to be independent of collision frequency. Mass transfer calculations for a volatile species in a fluid bed show that even very low vapor pressures are sufficient to support mass transfer in the bed. The experimental data are best fit by the model that a vanadium species undergoes volatile transfer, where the vapor pressure fits a second order Freundlich isotherm. Because the catalyst surface is inhomogeneous, these results suggest that the vapor pressure of the vanadic acid is governed by a coverage dependent heat of adsorption.

The poisoning of fluid cracking catalysts (FCC) by vanadium is well known (1, 2). In general, vanadium is deposited on the cracking catalyst as coke by vanadyl porphyrins in the feed. During regeneration, the coke is burned off, and vanadium can be oxidized to the V^{+5} oxidation state. Woolery et al. (3) have shown that the oxidation state of the vanadium can alternate between +4 to +5 in

the cracking regeneration cycle, but that the predominant state is +5 in the FCC regenerator. These oxides of vanadium then react with the H_2O vapor in the regenerator to form vanadic acid, H_3VO_4 , which is volatile (4). Zeolites are known to be sensitive to acid-catalyzed hydrolysis, which destroys the zeolite framework. The vanadic acid apparently catalyzes this reaction in the presence of steam in the regenerator (4). Pine (5) has shown that this reaction is a solid state transformation that is catalyzed by a vapor phase species. Vanadium is also known to be very mobile throughout the catalyst inventory (1). Other work (4) has shown that steam is necessary for intra-particle transfer, and for the poisoning of the cracking activity by vanadic acid.

Although the poison precursor of vanadium poisoning was shown to be volatile vanadic acid, because of its very low vapor pressure, it may not explain the observed inter-particle mobility of vanadium. Kugler and Leta (6) have shown that the distribution of vanadium in equilibrium catalysts is consistent with either a volatile or inter-particle transfer mechanism. von Ballmoos et al. (7) have suggested that the mobility of vanadium is due to particle-to-particle collisions. What is currently known about the mobility of vanadium is that it is dependent on the vanadium being in the V^{+5} oxidation state, and that water vapor is present at the conditions of regeneration. Also, V_2O_5 melts at 943 K, which is below the operating temperature of most regenerators, 970 - 1020 K. Presumably, if particle-to-particle collisions are responsible for the transport, then the water vapor must lower the surface tension of the liquid species sufficiently to facilitate the transport.

It is the purpose of this paper to study which mechanism, particle-to-particle or vapor phase transport, is responsible for the mobility of vanadium in the FCC unit. The approach used in this work is to measure the rate of vanadium transport to a basic oxide "vanadium trap" in fluid bed experiments. By varying the particle size distribution, the collision frequency can be changed and the rate of transport determined. Also, calculations of the mass transfer of a vapor species in a fluid are performed.

Experimental

The catalyst chosen for this study is a 40 wt% USY catalyst bound in an alumina sol/kaolin matrix, similar to GRACE Davison's DA catalyst family. It contains no rare earth, and is therefore considered to be an octane catalyst. The trap used in this experiment is a 40 wt% MgO based trap bound in a $\text{La}_2\text{O}_3/\text{Al}_2\text{O}_3$ matrix (8). The trap has been shown to have a high affinity for vanadic acid. Fluid bed steaming experiments were performed in temperature controlled sand bath reactors using the conditions given in Table I. Staged bed steaming experiments were performed in a fixed bed reactor, using the conditions given in Table I. Density separations of catalyst from trap in the fluid bed experiments were performed by a procedure similar to that in earlier work (9, 10). Particle size measurements were performed using a light scattering technique from a Malvern 3600E particle size analyzer. Chemical analysis was performed by ion coupled plasma analysis, standardized to NIST standards.

Table I. Fluid and Staged Bed Experiments

Conditions	45 gr. catalyst/.5 gr. trap 5 hr. @ 1088 K 95% Steam 8.5 cc/min N ₂ 7.5 cc/hr. liquid H ₂ O	
	Catalyst	Trap
Before Steam		
wt% V	0.5	0
After Steam	Float (Catalyst)	Sink (Trap)
wt% V	0.186	2.58
% V transferred	64	
<u>Staged Bed Experiment</u>		
Conditions	9 cc/hr. liquid H ₂ O 10 cc/min N ₂ 5 hrs. @ 1088 K	
	Catalyst	Trap
Before Steam		
wt% V	0.509	0.02
After Steam		
wt% V	0.511	0.02

Results and Discussion

The mobility of vanadium in a fluidized bed is illustrated by a fluid bed steaming experiment using a "vanadium trap" which will react with the mobilized vanadium and render it immobile (4). Traps which are effective for reacting with vanadic acid are basic oxides, such as MgO and is very effective for reacting with vanadic acid. In this experiment, 90 wt% catalyst/ 10 wt% trap blend is steamed for 4 hours at 1088 K, 95% vol. H₂O vapor, in a fluid bed. Only the catalyst is impregnated to 0.5 wt% V prior to blending and steaming. After steaming, the catalyst and trap fractions, which have different densities, are separated by the sink/float technique, and analyzed for vanadium. The results (Table I) show that the catalyst retained 0.186 wt% V, while the trap gained 2.58 wt% V. Essentially 64% of the vanadium was transferred from the catalyst to the trap.

A staged bed transpiration experiment was also performed. In this case, the catalyst was again impregnated with 0.5 wt% V and loaded into a fixed bed reactor. A layer of glass wool was placed over the catalyst, and the trap was layered on top of the glass wool. In this way, there was no contact between the beds. Steam vapor was flowed through the catalyst bed then up to the trap bed at 9 cm³/h liquid, 10 cm³/min. N₂. Results (Table I) show that the catalyst did not lose vanadium, nor did the trap gain vanadium so that there was no

transpiration of vanadium between the beds. The equilibrium vapor pressure of H_3VO_4 over pure V_2O_5 at 1088 K and 1 atm water vapor pressure is 2.9×10^{-5} atm (11). Assuming the gas phase is saturated with H_3VO_4 vapor, in the staged bed experiment, the vanadium on the catalyst should have decreased from 5000 ppm to 4750 ppm, a change which is well within the detection limit of analysis.

There is an apparent paradox from these experiments: vanadium moves readily from catalyst to trap in a fluid bed, yet vanadium transpiration is negligible under the same conditions. This result would suggest that the mechanism of transport is by particle-to-particle collisions in the bed. Still, an alternate question arises, what are the requirements for mass transfer of vapor phase vanadium in a fluid bed? Following the correlation of Richardson and Szekely (12), the mass transfer coefficient, k_m , in a fluid bed can be calculated from the Sherwood number, Sh , and a knowledge of the particle Reynolds number, Re , in the bed by,

$$Sh = k_m d_p / D = \begin{matrix} 0.374 Re^{1.18} & Re < 15 \\ 2.01 Re^{0.5} & 15 < Re, \end{matrix} \quad (1a)$$

$$(1b)$$

where d_p is the particle diameter and, D is the vapor phase diffusivity of the transporting species (13). The particle Reynolds number is

$$Re = d_p v \rho / \mu, \quad (2)$$

where v is the superficial fluidizing vapor velocity, ρ is the fluidizing vapor density, and μ is the fluidizing vapor viscosity. Using values appropriate for the conditions for the fluid bed experiment given in Table I,

$$v = 2.24 \text{ cm s}^{-1}, \quad (3a)$$

$$d_p = 7 \times 10^{-3} \text{ cm}, \quad (3b)$$

$$\rho = 2.2 \times 10^{-4} \text{ g cm}^{-3}, \quad (3c)$$

$$\mu = 2 \times 10^{-4} \text{ g cm}^{-1} \text{ s}^{-1}, \text{ (estimated from (14))} \quad (3d)$$

$$D = 10 \text{ cm}^2 \text{ s}^{-1}, \text{ (estimated from (15))} \quad (3e)$$

the Reynolds number is, $Re = 0.014$. From (Equation 1a) this translates to Sherwood number, $Sh = 0.0024$, and a mass transfer coefficient, $k_m = 3.5 \text{ cm s}^{-1}$.

The mass transfer rate is given by,

$$\text{mass transfer rate} = k_m A_{trap} (C_{H_3VO_4, gas} - C_{H_3VO_4, trap}), \quad (4)$$

where A_{trap} is the external area of the trap, $C_{H_3VO_4, gas}$ is the concentration of vanadium vapor in the gas phase, and $C_{H_3VO_4, trap}$ is concentration of vanadium vapor over the trap. If it is assumed that $C_{H_3VO_4, trap} \ll C_{H_3VO_4, gas}$, namely that the vapor pressure of vanadic acid is very low at the surface of the trap due to the chemistry of the interaction, then $C_{H_3VO_4, gas}$ can be calculated from the experimental data given in Table I,

$$C_{H_3VO_4, gas} = 1.05 \times 10^{-11} \text{ mol cm}^{-3}, \quad (5)$$

$$P_{H_3VO_4, gas} = 9.4 \times 10^{-7} \text{ atm}. \quad (5a)$$

The calculated vapor pressure of vanadic acid is a factor of 30 lower than the equilibrium vapor pressure of vanadic acid over pure V_2O_5 . At this vapor pressure of vanadic acid, the transfer of V to trap is rapid while the removal of V by transpiration is negligible. Approximately 64% would be transferred from catalyst to trap, and about 0.05% removed by transpiration. This is rationalized by noting that the velocity of the vanadic acid vapor (calculated from the kinetic theory of gases), $4.4 \times 10^4 \text{ cm s}^{-1}$, is four orders of magnitude higher than the superficial velocity of the fluidizing gas, Equation 3a. From these calculations it is clear that mass transfer of vapor phase vanadic acid in a fluid bed is sufficient to account for the transport of vanadium from catalyst to trap.

Although vapor phase mass transfer of vanadium is consistent with all our data, further experiments were performed to test the particle-to-particle mechanism. In this case, the rate of vanadium transfer is expected to be proportional to the collision frequency in the bed,

$$V \text{ transfer rate} = k_{\text{collision}} N_{\text{catalyst}} N_{\text{trap}} \gamma \quad (6)$$

where N_{catalyst} and N_{trap} are the number densities of the catalyst and trap particles, respectively and γ is the amount of vanadium transferred per collision, which is a function of the concentration of the vanadium on the catalyst. The number densities can be varied by varying the particle size distribution. In these experiments, the catalyst was split into two fractions by screen classification. Table II gives the particle size distributions for both the coarse and fine catalyst, as well as the trap distribution. By assuming spherical particles of uniform particle density, the number density can be determined, and is shown in Table II. The ratio of the particle densities for the fine and coarse fractions is

$$N_{\text{fine}} / N_{\text{coarse}} = 6.5. \quad (7)$$

Catalyst and trap blends were steamed in a fluid bed using the same conditions as in Table I. Weight blend ratios with 95/5, 90/10, 85/15 of catalyst trap for both the fine and the coarse fractions were steamed, and the sink/float technique was again used to measure the rate of vanadium transfer. The results (Table III) show that there is not a strong dependence of the vanadium transfer rate on particle size. The rate enhancement, which is the rate of the fine catalyst / rate of the coarse catalyst, only varies by 10%, whereas the number density varied by a factor of 6.5. This experiment shows that the rate of vanadium transfer from catalyst to trap is only weakly dependent on the particle density, and it implies that particle-to-particle collisions are not the dominant mode of vanadium transfer.

Table II. Particle Size Distributions of Fine and Coarse Fraction of Catalyst

	Catalyst Coarse	Catalyst Fine	Trap
Volume % in			
0-20 microns	0	0.3	1.8
0-40	0.7	10.8	14.9
0-60	1.8	57.2	29.6
0-80	15.5	87.4	56.9
0-105	41.6	96.6	80.6
0-125	59.6	98.5	89.6
0-150	75.6	99.5	94.9
0-200	93.7	99.8	99
0-320	99.5	100	100
APS/microns	113	57	75
# Particles/cm ³	1.70E+06	1.05E+07	2.30E+07

Table III. Coarse and Fine Catalyst/Trap Blends
5000 PPM V on Catalyst/5 hrs. @ 815 °C/95% Steam/Fluid Bed

Nominal wt. catalyst/wt. trap blend	95/5 Blend		90/10 Blend		85/15 Blend	
	float (cat.)	sink (trap)	float (cat.)	sink (trap)	float (cat.)	sink (trap)
Separated Fraction						
Coarse Catalyst/Trap Blend						
wt. fraction	0.94	0.06	0.90	0.10	0.83	0.17
wt%V normalized	0.29	3.83	0.21	2.75	0.14	1.80
V transfer rate (g V h ⁻¹ g cat ⁻¹) X 10 ⁻⁴	4.5		6.1		7.2	
Fine Catalyst/Trap Blend						
wt. fraction	0.94	0.06	0.90	0.10	0.84	0.16
wt%V normalized	0.25	4.13	0.17	2.90	0.14	1.98
V transfer rate (g V h ⁻¹ g cat ⁻¹) X 10 ⁻⁴	5.1		6.7		7.3	
Rate Enhancement: rate fine/rate coarse	1.1		1.1		1.0	

On the contrary these results support the interpretation that gas phase vanadic acid is in pseudo-equilibrium with vanadium on the FCC catalyst, and the rate limiting step in vanadium transfer is the adsorption of vanadic acid vapor onto the trap. Since the rate of vanadium transfer is independent of catalyst particle size, intraparticle vanadium transfer must be very fast compared with interparticle vanadium transfer. The vanadium transfer experiments can provide information on the vapor pressure of vanadic acid, using the same techniques as outlined above. Equation 4 can be rewritten as,

$$V \text{ transfer rate} = k' P_{H_3VO_4} C_{trap} \quad (8)$$

where C_{trap} is the concentration of the trap in the blend. If one assumes that the equilibrium between H_3VO_4 vapor and surface vanadium follows the Langmuir isotherm, then at low vanadium levels, the vapor pressure of vanadium is approximately linearly dependent on the vanadium concentration, then,

$$P_{H_3VO_4} = K V_{catalyst} \quad (9)$$

where $V_{catalyst}$ is the concentration of V on the catalyst and K is the equilibrium constant for adsorption. By substituting Equation 9 into Equation 8 and integrating over time gives the concentration dependence of vanadium on the catalyst as a function of the ratio of trap concentration to the catalyst concentration in the blend,

$$V_{catalyst} = V_{catalyst}^o \exp\left(-k_1 \frac{C_{trap}}{C_{catalyst}}\right), \quad (10)$$

where rate constant k' , the adsorption constant K and time, which are constant for all the experiments, have been lumped into the new constant k_1 .

It is also possible that, because the surface of the catalyst is inhomogeneous, the equilibrium between H_3VO_4 vapor and surface vanadium may not follow the Langmuir isotherm. In this case, the vapor pressure can be modeled by a Freundlich isotherm,

$$P_{H_3VO_4} = \alpha V_{catalyst}^n \quad (11)$$

Substituting Equation 11 into Equation 8 and integrating over time gives,

$$\left(\frac{1}{-n+1}\right) \left[(V_{catalyst}^o)^{-n+1} - (V_{catalyst})^{-n+1} \right] = k_2 \frac{C_{trap}}{C_{catalyst}}, \quad (12)$$

where time has again been lumped into the constant k_2 .

The best fit curves of both models to the vapor pressure data extracted from the coarse blends (Table III) are shown in Figure 1. In the case of the Freundlich isotherm, an exponent value of 2 gave the best fit. As can be seen, the second order Freundlich isotherm is a closer fit to the observed data than the linear model. Similar plots are obtained for the fine catalyst experiments. This fact indicates that the heat of adsorption of vanadium in the V^{+5} oxidation state is coverage dependent. This result is more clearly seen by the plot of "vanadium pick-up factor", $V_{\text{trap}}/V_{\text{catalyst}}$, versus trap/catalyst concentration (Figure 2). This plot shows the strong dependence on the second order model, again verifying the inhomogeneous nature of the catalyst surface for vanadium.

A second set of experiments was performed to determine the rate of transfer as a function of vanadium loading. In these experiments the entire blend, with 10% trap, was impregnated at different vanadium levels. The blend was then fluid steamed using a cyclic procedure, which switches between oxidizing and reducing conditions using propylene, in much the same spirit as occurs in normal FCCU operation. The steaming procedure is described in detail in (15). The data are shown in Table IV. Because of pore volume differences between the catalyst and trap, the initial % V on the catalyst is corrected. Figure 3 shows the vanadium concentration on the catalyst after steaming versus the initial % V on catalyst before steaming. As before, the data were fitted to the two models and again the second order Freundlich isotherm best fits the data. Figure 4 shows the vanadium pickup factor, which as before show a strong dependence for the second order model.

The rate of vanadium mobility in FCCU's is dependent on many operating factors. These might be whether the unit is operated in full or partial combustion, which will effect the average oxidation state of the vanadium. Other factors will be "freshness" of the vanadium, presumably older vanadium has had more of an opportunity to react with the catalyst matrix and become immobile. Steam concentration in the regenerator, catalyst make-up rate, temperature, and two-stage regeneration will all effect the mobility of vanadium.

Conclusion

The results of this work show that even though the vapor pressure of vanadium is low, the transfer velocity of vanadium vapor is high and the rate of mass transfer in a fluidized bed is high. A high rate of vanadium transport to traps and a low rate of vanadium transport by transpiration are consistent with the vapor phase transport model. The vapor pressure of the vanadic acid follows a second order Freundlich isotherm, which reflects a coverage dependent heat of adsorption. The rate of vanadium transfer from catalyst to trap is only weakly dependent on the number density of the catalyst or trap particles. This lack of dependence suggests that inter-particle collisions are not the dominant mechanism for vanadium transfer. Vanadium mobility in FCCU's is a complex issue dependent on many operating variables.

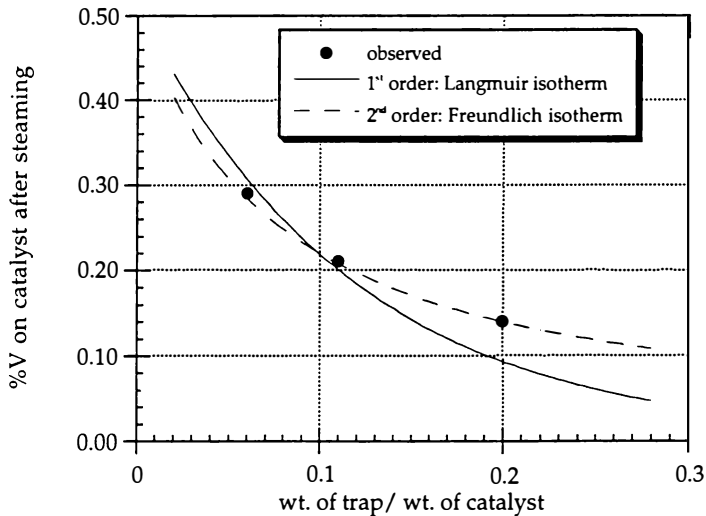


Figure 1. Vanadium Concentration on the Catalyst as a Function of Trap Content. Blends of Coarse Catalyst with Trap.

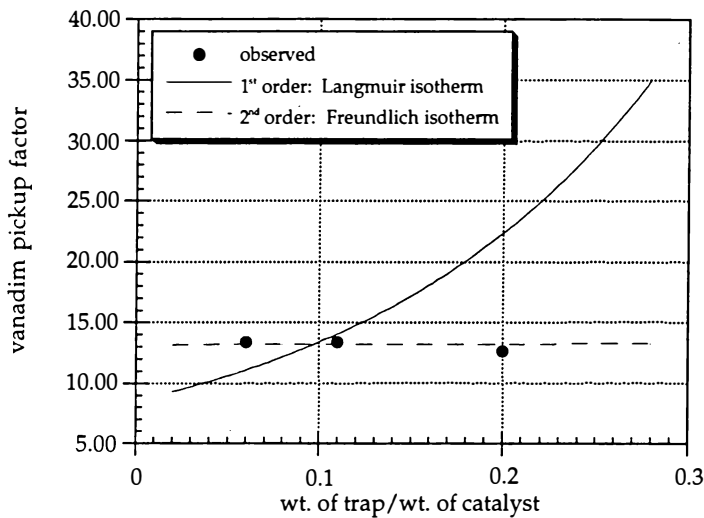


Figure 2. Vanadium Pickup Factor as a Function of Trap Content. Blends of Coarse Catalyst with Trap

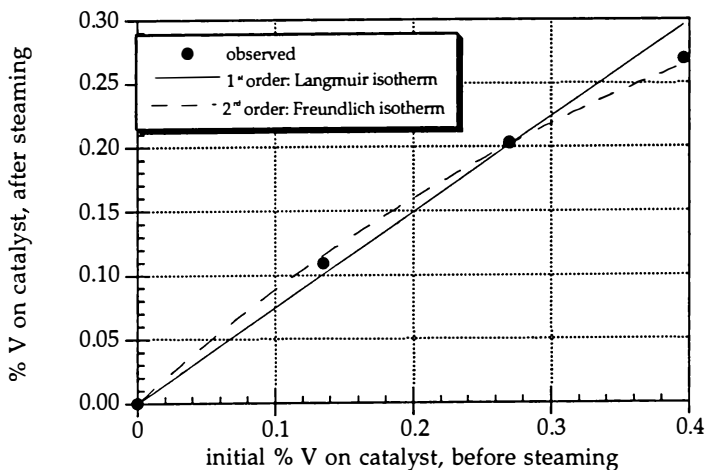


Figure 3. Vanadium Concentration on the Catalyst as a Function of Vanadium Loading.

Table IV. 90% Catalyst/10% Trap Blends for Co-Impregnated Samples At Different Vanadium Loadings

Initial Blend wt% V	Initial wt. % V corrected on catalyst	Float (cat.) wt% V	Sink (trap) wt% V	Pickup Factor % V Trap/% V Cat.
.172	.135	.109	.715	6.6
.343	.270	.203	1.47	7.2
.503	.396	.269	2.59	9.6

After cyclic propylene steam: 30 cycles with 60% volume H₂O cycled between balance gas of 5% wt. C₃H₆ in N₂, and air with 4000 ppm SO₂, total time 20 hrs., T = 771°C, Fluid Bed

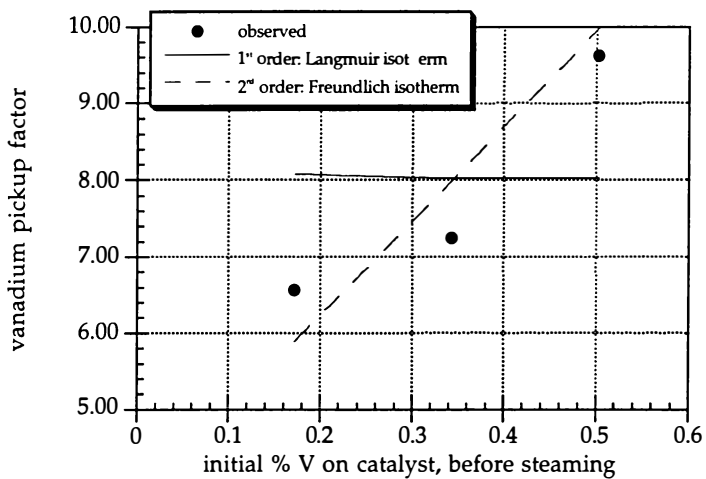


Figure 4. Vanadium Pickup Factor as a Function of Vanadium Loading.

Literature Cited

1. Nielsen, R. H; Doolin, P. K. in *Fluid Catalytic Cracking: Science and Tech.*, Magee, J. S. and Mitchell, M. M., Ed.; Elsevier Science Publishers B.V.: New York, 1993, pp 339-384.
2. Ritter, R. E.; Rheume, L.; Welsh, W. A. and Magee, J. S., *Oil & Gas J.*, 1981, July 6, pp. 103-110.
3. Woolery, G. L.; Chin, A. A.; Kirker, G. W. and Huss, A. in *Fluid Catalytic Cracking - Role in Modern Refining*; Occelli, M. L., Ed.; ACS Symposium Series 375; American Chemical Society: Washington, DC, 1988, pp. 215-228.
4. Wormsbecher, R. F., Peters, A. W. and Maselli, J. M., *J. Catal.*, 1986, Vol. 100, pp. 130-137.
5. Pine, L. A., *J Catal.*, 1990, Vol. 125, pp. 514-524.
6. Kugler, E. L. and Leta, D. P. *J. Catal.*, 1988, Vol. 109, pp. 387-395.
7. von Ballmoos, R.; Deeba, M.; Macaoay, J. M. and Murphy, M. A., *Annual NPRA Mtg.*, San Antonio, TX, 1993, Vol. AM-93-30.
8. Kim, G. U.S. Patent 5,407,878 (1995).
9. Palmer, J. L. and Cornelius, E. B., *Appl. Catalysis*, 1987, Vol. 35, pp. 217-235.
10. Beyerlein, R. A.; Tamborski, G. A.; Marshall, C. A.; Meyers, B. L.; Hall, J. B. and Huggins, B. J. in *Fluid Catalytic Cracking II - Concepts in Catalyst Design*; Occelli, M. L., Ed.; ACS Symposium Series 452; American Chemical Society: Washington, DC, 1991, pp. 109-143.
11. Yannopoulos, L.N., *J. Phys. Chem.*, 1968, Vol. 72 (9), pp. 3293-3296.
12. *Fluidization Engineering*; Kunii, D. and Levenspiel, O., Ed.; Robert E. Krieger Publishing Company: Huntington, New York, 1977, Vol. 534.
13. Richardson, J. F. and Szekely, J., *Trans. Inst. Chem. Engrs.*, 1961, Vol. 39, pp. 212.
14. *Perry's Chemical Engineers' Handbook*; Perry, R. H. and Green, D. W., Ed., 6th Ed., McGraw-Hill, Inc., 1984.
15. Fuller, E. N.; Schettler, P. D. and Giddings, J. C., *Ind. Eng. Chem*, 1966, Vol. 58 (5), pp. 18.
16. (Boock, L. T., Petti, T. F., and Rudesill, J. A., *International Symposium on Deactivation and Testing of Hydrocarbon Conversion Catalysts*, ACS Annual Meeting, Chicago, IL, August 1995)

Improved Methods for Testing and Assessing Deactivation from Vanadium Interaction with Fluid Catalytic Cracking Catalyst

Bruce Lerner and Michel Deeba

Engelhard Corporation, 101 Wood Avenue, Iselin, NJ 08830-0770

Test methods for studying the effect of vanadium on FCC catalyst have been developed. Vanadium tolerance is important as it relates to catalyst deactivation. A simple, effective, and inexpensive test has been developed which takes the best features from other test methodologies and combines them; the test is termed the Engelhard Transfer Method (ETM). Results from the test have provided data which may be used to infer the mechanism of vanadium transport in these systems. It appears that vanadium moves via a solid state interparticle transfer and not by liquid or gas phase movement. The test design also allows for the incorporation of other feed contaminants such as sulfur or nitrogen oxide gases. The importance of including sulfur in vanadium trap evaluation is shown by demonstrating its effect on trap materials.

In recent years the refining industry has addressed the importance of upgrading the "bottom of each barrel" to optimize refinery economics based on the changing product slate and price structure of crude. An increased number of oil refineries are now processing at least a portion of resid or heavy crude as a feed stock (1). Processing resid can negatively affect yields of valuable products relative to a light feed. To counter this, catalyst design must address the following aspects: upgrading bottoms, minimize coke and gas formation, maximize catalyst stability, and minimize deleterious selectivity due to contaminant metals such as nickel and vanadium. Particular attention must be paid to the mediation of contaminant metals.

Nickel and vanadium are contained within the crude oil as their respective porphyrins and naphthenates (2). As these large molecules are cracked, the metals are deposited on the catalyst. Nickel which possesses a high intrinsic dehydrogenation and hydrogenolysis activity drastically increases the production of coke and dry gas (particularly H_2) at the expense of gasoline. Vanadium on the other hand interacts with the zeolitic component of a cracking catalyst and leads to destruction of its crystallinity. This results in reduced activity as well as an increase in non-selective amorphous silica-alumina type cracking. Supported vanadium also has an intrinsic

dehydrogenation activity which increases hydrogen and coke make, albeit it is significantly less than the contribution due to nickel.

A long compilation of open and patent literature attests to the effort and quantity of research which has been directed towards resolving metals tolerance. Advances in this area have been nicely reviewed by several authors (3,4,5).

So far nickel has been most successfully controlled by addition of an antimony additive in a process developed by Phillips Petroleum in the late 1970's (6). This technology remains a practiced method for nickel control particularly in low to moderate levels, however in recent years the concern over the toxicity of antimony to the environment has reemphasised the need for effective yet benign nickel passivators.

Vanadium passivation has been a more difficult challenge to overcome. In reviewing the literature it is quickly realized that a host of materials have been studied for vanadium passivation and some have been commercialized. However, not all materials perform equally. In fact, actual unit performance may vary significantly from that predicted by testing methods commonly used in many laboratories.

The ultimate performance of an FCC catalyst in the presence of vanadium is related to the chemistry and thermodynamics of the catalysts' trapping system and the affinity for vanadium over competitive species. The testing of candidate materials is important in order to judge their relative performance. Different test methods approach the reality of actual unit conditions to varying degrees. The desire to mimic the actual unit is often offset by considerations of complexity, time, and cost. One aspect of the present paper will be to discuss a simplified, yet elegant test procedure called the Engelhard Transfer Method (ETM) (7) which can easily and realistically assess the interaction of vanadium with FCC catalyst. The test is a rapid, efficient, and cost-effective way of testing for vanadium tolerance.

In designing a working catalyst or catalyst component a fundamental understanding of the chemistry or mechanism at hand is extremely useful. It has become accepted that aluminum, alkali, or rare earth vanadate formation is the end result of vanadium-zeolite interaction. Whether this is due to eliminating charge neutrality of the sieve resulting in structural collapse or creation of a low melting eutectic composition (8) is still a matter of opinion although probably neither is exclusive. The means by which vanadium makes its way to a site of potential interaction is also debated. In general two camps exist: one which contends vanadium pentoxide is formed and is transported as a liquid, upon melting, through the catalyst (9); the other proposes that vanadic acid is formed which is volatile and travels via gas phase transport (10). Data presented herein from the development of ETM suggest a third mechanism which may offer a more accurate model of vanadium migration.

Many of the materials used to trap vanadium by chemical reaction also share a similar chemistry with the oxides of sulfur a prevalent contaminant in FCC feed stocks. Sites which trap vanadium are thereby competed for by sulfur species. Results obtained by incorporating a feed contaminant, such as sulfur, in a competition with vanadium demonstrate the importance of including sulfur in vanadium tolerance testing and will be discussed. The ETM test offers the ability to study what happens under just such a competition.

Experimental. Two catalysts were used in this study. The first is a standard Engelhard commercial fluid cracking catalyst whose typical properties are given in Table 1. In vanadium trapping studies this catalyst was combined with a commercial Engelhard vanadium trap based on MgO in a 70:30 ratio cat:trap. Others catalyst samples are laboratory prototypes for this study, and were prepared by combining 25% USY in a SiO₂-Al₂O₃-Kaolin matrix. 5 wt% of Barium or Strontium Titanate, vanadium passivators, were included in two samples. A control sample which has 75% of its composition as the matrix formulation and no trap component was also prepared. Properties of the control and the titanate containing catalysts were essentially identical and are also given in Table 1.

Table 1.
Physical and Chemical Properties of Catalysts

Property	Commercial Catalyst	Lab Catalyst
SiO ₂ (wt%)	65.6	64.7
Al ₂ O ₃ (wt%)	29.6	26.5
Na ₂ O (wt%)	0.28	0.16
ReO (wt%)	1.02	1.18
Total Surface Area ¹ (m ² /g)	224	170
Zeolite Surface Area ¹ (m ² /g)	154	118
Pore Volume (cc/g)	0.274	0.145

1 - Steamed 1500F/4h/100% stm

Metals impregnation was done according to the Mitchell Method (11). In this method the catalyst sample is impregnated with vanadium naphenate (ALFA) diluted with cyclohexane. After air drying for several hours the sample is calcined at 600 F for 1 hour and then at 1100 F for 1 hour. The samples are subsequently steamed for 4 hours at 1450 F in an atmosphere of 90% steam and 10% air.

The Engelhard Transfer Method makes use of the same steaming apparatus as is conventionally used to steam deactivate FCC catalyst. Simply, a bed of material is supported on a frit in a quartz tube and the tube placed vertically inside a three zone tube furnace. Steam, air, and nitrogen (if desired) flow upwards through the bed and fluidize it. In the method inert particles of calcined clay are impregnated with 10,000 - 15,000 ppm V by the Mitchell method and are abbreviated as V/in. These particles are highly calcined kaolin clay microspheres with a very low surface area (<5 m²/g) and are catalytically inert. The V/in material is physically mixed with the catalyst and placed into the steamer. The amount of V/in material used is usually constant at a 70:30 ratio of catalyst :V/in and the amount of V on the inert is varied as necessary to provide a proper level of V for a given target metals level. In the case of vanadium trapping experiments where a separate particle vanadium trap is used, the ratio of V/in:Trap:Cat was 30:20:50.

Fixed Fluid Bed Cyclic Metallation was conducted by spiking a gas oil with vanadium naphenate so as to provide enough vanadium to reach a target level of V in 20 cycles of oil contact followed by oxidative regeneration after each cycle. In some cases during the regeneration step SO_x gas was admitted under dry conditions so as not to form sulfuric acid and unduly deactivate the sample. Each time after

regeneration at a temperature of 1350 F the catalyst was again contacted with oil at a temperature of 1150 F.

X-ray Photoelectron Spectroscopy (XPS) data were collected on samples which were pressed into pellets and mounted with double sided tape on a nickel charge dispersion screen. The spectrometer used was a Fisons/SSX 206 ESCA system. This instrument uses a monochromatized Al Ka (1486.6eV) excitation, a spot size of 600 microns, and a pass energy of 100V. The pressure in the analysis chamber was maintained at 2×10^{-7} Pa or less during data collection. The XPS has attached to it a sample preparation chamber constructed of Hastelloy and which may be heated. Samples in the chamber may be exposed to various gas atmospheres and after exposure the preparation cell is evacuated to UHV conditions and the pellet transferred to the analysis chamber through an interlock. A spectrum was recorded for the "as is" pellet and then the samples were heated in a variety of atmospheres and their spectra recorded. The chosen atmospheres were either nitrogen, 10% oxygen in He, 10% CO in He, 10% CO₂ in He, 20% CO/10% CO₂ bal He, or 2% O₂/7.5% CO balance He and the temperature was ramped to 800 C. Binding energy shifts of 0.2 eV are considered to be significant based on analysis of standards. Calibration data for peak position of vanadium +5 from purchased high purity vanadium were in agreement with those published in The Handbook of X-Ray Photoelectron Spectroscopy, Wagner *et al.* Eds., Perkin-Elmer Corporation, 1979.

Analytical methods including surface area and vanadium levels were also performed. Nitrogen BET surface areas were evaluated with an Autosorb-6 by the multi point BET method and the matrix contribution determined. An ARL 3410 ICP was used to determine vanadium, sodium, and rare earth content after decomposing the sample in HF.

Results and Discussion

Test Methods. Since its inception, the Mitchell Method (MM) or slight variations (often referred to as the Modified Mitchell Method) have been employed by researchers evaluating FCC catalyst as a simple, inexpensive, and fast procedure by which to simulate the effect of contaminant metals on catalyst performance. As a fallout of more sophisticated catalytic testing in fixed fluid bed reactors, the method of cyclic metals deposition (CMD) has also emerged as a useful method for introducing metal contaminants.

Each of these two methods has advantages and disadvantages associated with them. Since the Mitchell method involves a passive liquid impregnation of the metal solution at room temperature, various artifacts arise which may not be present in true unit operation. The liquid material is absorbed throughout the catalyst making the metal very well dispersed and accessible to all components of the catalyst. Differences in catalyst porosity effect the absorption of the liquid and the subsequent dispersion of the metals. In actual unit operation the metals are deposited on or close to the exterior of the catalyst surface where the large molecules containing the metals are initially cracked at elevated temperature. SIMS imaging of equilibrium catalyst displays this deposition phenomena (12). Nickel contaminants are essentially immobilized on the catalyst surface while vanadium species tend to migrate from the surface into the particle structure (13). This mobility is however not instantaneous and is governed by

a rate which depends on unit conditions. The CMD method tries to mimic this deposition by running multiple cracking cycles with a metal (V and/or Ni) contaminated oil. The metals are deposited via the cracking reaction. Furthermore since only a portion of the total metals are deposited with each cycle, the metals are "aged" with each increasing cycle simulating the gradual increase in metals concentration on the catalyst found in commercial operation. The "older" metals are less active due to induced sintering and oxide formation and the last metals which impinge on the sample are the "newest and freshest", being the most well dispersed and active. In the Mitchell Method all the metals are the same age; fresh and highly active. While the CMD technique appears more technically appealing, the great disadvantage is the rather large cost associated with the equipment and the time required to run each sample. A typical 20 cycle deposition may take up to a day per sample making it a cumbersome, inefficient screening tool.

It would be desirable to have available a simpler testing tool which could imitate many of the aspects of the cyclic deposition particularly the impingement of the metals on the catalyst surface with the simplicity, efficiency, and cost of the Mitchell Method. One such test, at least so far developed for vanadium interaction, is what we termed above as the Engelhard Transfer Method (ETM) (7).

Transfer Method. The efficiency of the transfer was tested by physically blending a clean FCC catalyst with vanadium impregnated inert (V/in) particles and steaming the two materials together. Before steaming the vanadium and rare earth content of the blend was assessed. Furthermore the catalyst was prescreened so that the blend contained catalyst particles which were 200-325 mesh in size and V/in particles which were 100 - 170 mesh. After steaming the material was collected and both the blend and each component were analyzed for vanadium and rare earth. The results are given in Table 2 and show

Table 2.

Blend and Component Characteristics of Sample Experiencing V Transfer

	Before Steaming		After Steaming	
	<u>Blend</u>	<u>Cat</u>	<u>Blend</u>	<u>Cat</u>
REO (wt%)	0.7	1.02	0.7	1.01
V (ppm)	5600	200	5575	5085

clearly that selective loss of mixed components does not occur. The catalyst fraction retains all of the rare earth illustrating no migration of this species. However, the vanadium level of the catalyst is significant after steaming, demonstrating that vanadium was transferred from the inert particles to the catalyst. Figure 1 displays that for a target quantity of 5000 ppm vanadium the transfer is rapid but not instantaneous; this allows for a small range of age distribution of the vanadium to occur. The sample depicted was blended with V/in containing 16,572 ppm V in a 70:30 ratio (cat:V/in) to achieve 5000 ppm V on catalyst. After one hour the transfer is 86% complete and after 3 hours is quantitative. MAT evaluation of the sample and physical characteristics of the catalyst subjected to transfer more closely resemble those of the cyclic deactivated sample than the MM. These data appear in Table 3 and support the conclusion that the MM is more severe on the catalyst sample, a result also observed in the direct comparison of cyclic and MM deactivation relative to commercial e-cat (14).

Table 3.
**Comparison of Properties of the Same Catalyst¹ Metallated by MM, Cyclic
 Deposition and ETM**

	MM	ETM	Cyclic
V level (ppm)	4550	5085	4655
MAT conv. ² (%)	64	72	69.5
Coke/Act	2.86	2.51	2.30

1-Commercial Catalyst, 2- cat:oil = 5, 910F, WHSV=15, cat wt.=6.0g, contact time=48s, oil wt. 1.2g

General Requirements for Vanadium Transfer. Several interesting observations were made from ETM which have implications for the mechanism of vanadium interaction with FCC catalyst. It appears that both oxygen and steam are necessary to induce vanadium migration. Figure 2 displays the results of steaming a mixture of catalyst and V/in with pure nitrogen or pure oxygen. Catalyst deactivation is not nearly so severe when the sample is steamed in pure nitrogen. This implies that steam alone is not sufficient to facilitate vanadium destruction. Hettinger et al. (15) obtained a similar result for catalyst which was impregnated with vanadium and steamed independently in nitrogen and oxygen. The decline in zeolite surface area for the nitrogen steaming was only marginally greater than that due to steam alone without the presence of any vanadium contaminant. When a sample containing vanadium was steamed with oxygen the destruction was significantly more severe. By monitoring the amount of vanadium transferred by the ETM as a function of time on stream in the steamer, it can be shown that N₂ does not necessarily inhibit vanadium transfer and induced zeolite destruction, but rather that oxygen seems to promote a more effective transfer of vanadium (Figure 3). Steam may facilitate the catalyst deactivation via vanadium induced zeolite destruction by acting as a catalyst itself as was suggested by Pine (16). One may speculate that as steam causes zeolite dealumination, additional alumina sites are created which can react to form eutectic vanadates which then melt at low temperatures. This scenario is speculative and we have no proof for its existence, only the observation and conclusion that both steam and oxygen are necessary elements in the interparticle transfer of vanadium, and vanadium induced loss of zeolite.

Surface Enrichment of Vanadium. In an attempt to understand the role of oxygen in promoting this interparticle transfer an XPS study was done on a mixture of catalyst and V/in. The sample was pressed into pellets and observed both initially and after exposure to different atmospheres (described above) at elevated temperature. While no steam may be admitted to the XPS reaction chamber for practical operating considerations, the results under dry conditions were rather remarkable. Table 4 gives binding energy and surface concentration data for the samples after exposure to the various atmospheres. The "as is" sample at room temperature has a vanadium binding energy characteristic of V⁺⁵. After exposure to nitrogen this BE is slightly shifted towards that of a partially reduced V, but not completely to the position at which V⁺⁴ would come. The distribution of vanadium on the particles is the same as that for the initial state. When the sample is heated in oxygen the BE remains constant for V⁺⁵ but

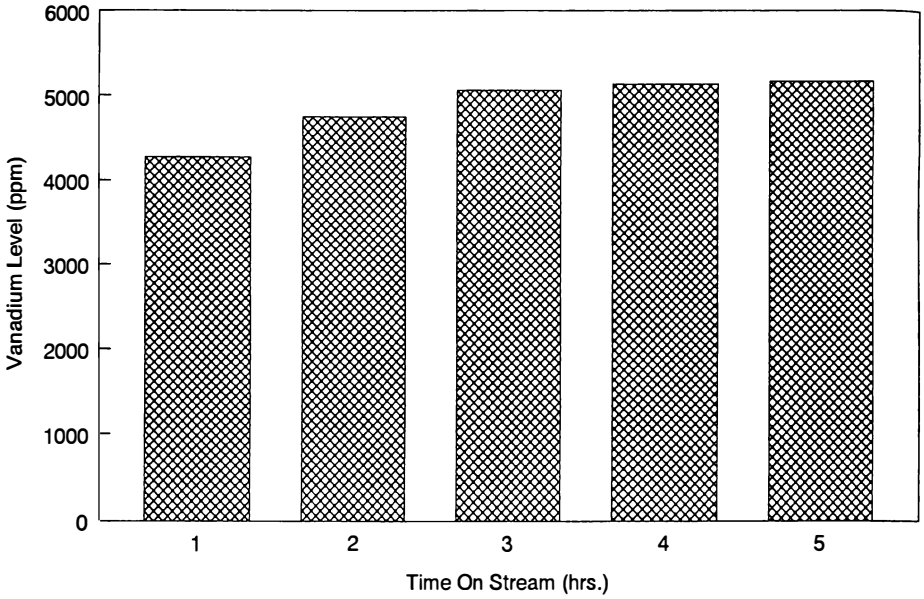


Figure 1. Vanadium accumulation during ETM as a function of time on stream. Target 5000 ppm on catalyst

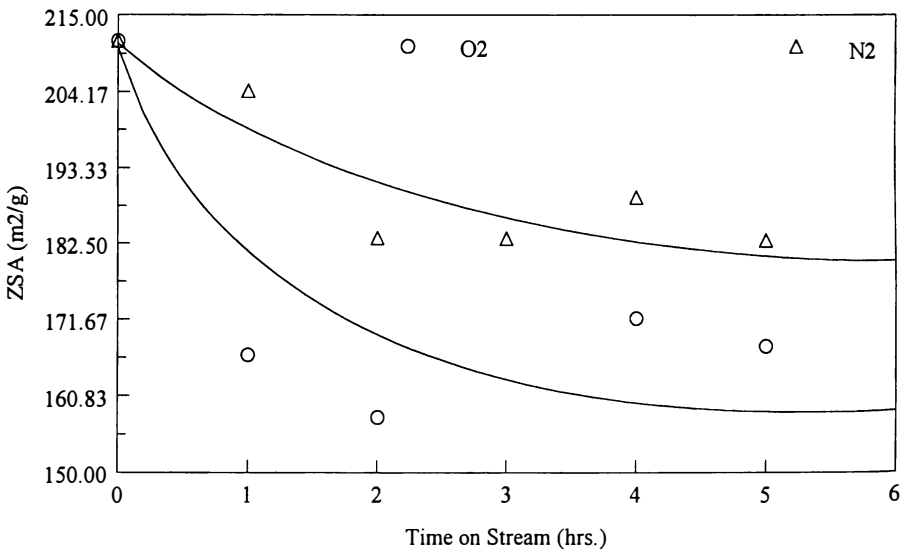


Figure 2. Effect of oxidative vs. inert atmosphere on vanadium induced loss of zeolite surface area (ZSA).

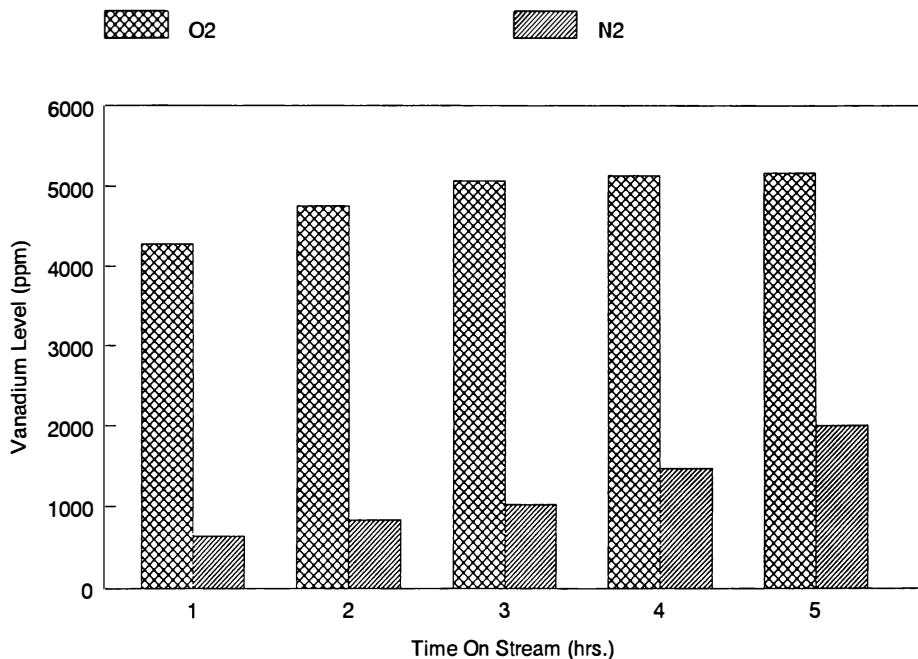


Figure 3. Effect of oxidative vs. inert atmosphere on vanadium transfer.

Table 4.

Binding Energies and Surface V Concentrations Under Various Atmospheres at 850 C

Conditions	Binding Energy ¹ (eV)	Al/M ²	Si/M	V/M
As is ³	517	0.37	0.62	0.01
N ₂	516.4	0.40	0.59	0.01
O ₂	517.7	0.31	0.61	0.08
CO	515.7	0.36	0.63	0.01
CO ₂	517.0	0.34	0.66	0.02
CO/CO ₂	516.2	0.35	0.65	0.01
CO/O ₂	517.9	0.32	0.68	0.07

1-referenced to Al2p = 74.3eV, 2-M = matrix = summation of Al2p + Si2p + V2p_{3/2}
atom percents, 3-Room Temp collection, no heating

now an enormous surface enrichment of vanadium is observed. Simply having an oxidizing atmosphere is not sufficient to induce this migration because CO_2 does not produce the same effect. When the sample is heated in CO a reduction of vanadium to V^{+4} is observed but no migration. V^{+4} has been inferred to not destructively interact with zeolite or FCC catalyst (15). It may be proposed that when V is reduced to lower oxidation states that migration is inhibited as well.

It now seems clear that after vanadium is deposited onto the catalyst it may be mobile in an atmosphere of steam and oxygen (from air). Mobile vanadia species migrate into the particles but may be enriched at the surface segment of low surface area particles such as our inert clay microspheres or old sintered equilibrium catalyst. Surface vanadyl groups are transferred to other FCC particles and migrate through them as well. Migration ceases when a reaction occurs with catalyst moieties, such as Al or rare earth, to form stable vanadates (17).

Mechanism of Vanadium Transfer. In previous literature two mechanisms of vanadium migration were postulated: liquid or gas phase vanadium transport. The results in this study lead us to propose a third alternative mechanism. It appears from our data that a more appropriate mechanism involves interparticle vanadium transport which occurs as a result of a solid state interaction between vanadium containing particles.

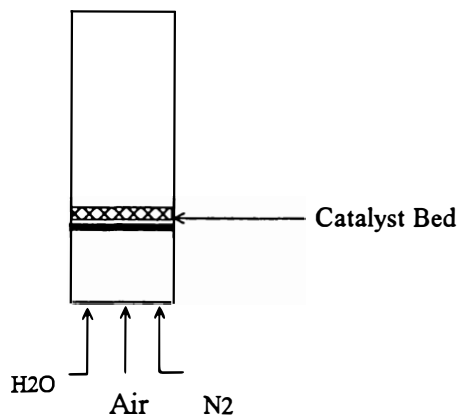
A conformation of this mechanism was sought by performing separated bed experiments as are schematically shown in Figure 4 and comparing these to a control where a sample was steamed without any vanadium present. The surface area and vanadium content of the catalyst was measured both before and after steaming. Different size sieve fractions of catalyst and V/in were used so that after steaming the catalyst could be separated from the V/in and analyzed. After steaming the mixed bed, vanadium had quantitatively deposited on the catalyst which resulted in a substantial loss of surface area. This could be compared to a catalyst sample which was steamed without any V/in as a control. In the separated bed experiment the V/in and the catalyst can not come in physical contact with each other during the steaming due to the presence of the quartz wool plug. After steaming the measured catalyst surface area and vanadium content were in perfect agreement with that of the control sample (Table 5) indicating no destructive contribution of vanadium. A trivial amount of vanadium was detected in the catalyst fraction and can be easily attributed to some V/in fines which were not sieved out of the cut. As a final check the quartz wool was also analyzed for vanadium to determine if any gas phase vanadium species had plated out on that material. A representative sample from the plug was analyzed, no vanadium was detected.

Table 5.

Properties of Catalysts from Separated and Unseparated Beds

	V_i (ppm)	V_f (ppm)	ZSA_i (m^2/g)	ZSA_f (m^2/g)
Control	200	200	298	202
Separated Bed	200	900	298	197
Mixed Bed	200	8131	298	103

Standard Exp.: Cat Bed = cat + VT + V/in



Modified Exp.: Cat Bed = cat + VT

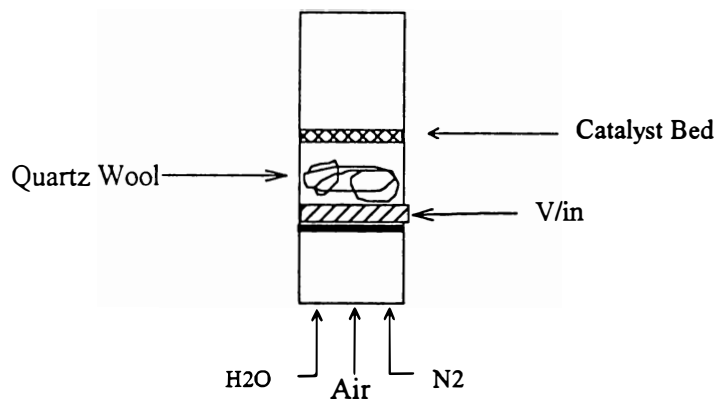


Figure 4. Separated Bed Experiments for V Migration Study

In early work (8,9) it was assumed that V_2O_5 readily formed from deposited vanadium under the oxidizing conditions of a FCCU regenerator and that this species was the culprit of vanadium induced zeolite destruction. The fact that V_2O_5 has a melting point considerably below that of typical regenerator operating conditions helped support the notion that V_2O_5 could melt and migrate via liquid diffusion throughout a particle. Work by Wormsbecher (10) which was supported by Elvin (18) demonstrated that V_2O_5 alone could not be the operating species since simple thermal treatment did not result in the observed destruction. Wormsbecher concluded that steam was a vital part to the mechanism and proposed that volatile vanadic acid was formed from the interaction of steam with V_2O_5 on the catalyst. This vanadic acid could then migrate throughout particles via gas phase transport.

Multiple papers in the open literature have presented work on the interaction of vanadium with model components which may be present in an FCC catalyst. These model systems mainly consisted of aluminas or silica aluminas which were doped with vanadium and studied by a host of analytical techniques. Ocelli and Stencel (19) physically combined alumina particles with a commercial cracking catalyst and introduced vanadium at different levels via impregnation. The levels of vanadium ranged from 0.5 wt% to 5 wt% and the samples were studied with Raman Spectroscopy, XRD, and XPS. The conclusion was drawn that only at the highest level of V was V_2O_5 formation detected. At lower levels *viz* 0.5 -1.5%, only discrete vanadyl units or surface coordinated divanadates were present. Steaming can condense some well dispersed discrete vanadia species into divanadates as the surface area of the support is sintered, placing species in closer proximity. In fact these monomeric and dimeric surface coordinated vanadium species have also been observed for other supports such as titania, other aluminas, and silica over a similar range of V loadings. The poly vanadate species and crystalline V_2O_5 were however not observed on silica (20,21), and V_2O_5 was absent until higher vanadium loadings (4-5%) for the other supports. In light of this descriptive work it is highly unlikely that any crystalline V_2O_5 is actually present on typical cracking catalysts. Furthermore the levels at which V is found on equilibrium catalyst rarely even come close to approaching the levels at which model systems are studied for favorable analytical reasons. It is common to find that 5000 ppm V (0.5 wt%) is a rather high level and quantities higher than this are the exception not the rule. While it is plausible that V_2O_5 phases may form in localized regions, for instance after reacting with zeolite to form destroyed zeolitic/vanadia phases, these would correspond to a reaction product and not the intruding vanadium precursor. In fact we have not been able to find any crystalline V_2O_5 present on a catalyst which has been impregnated to 5000 ppm V by either Laser Raman Spectroscopy, XRD, TPR, or ^{51}V NMR (Lerner, B.A.; Woltermann, G.M. To be published).

If V_2O_5 is not present on the catalyst how can it further react with steam to form the vanadic acidic entity? We do not contest that finely divided bulk V_2O_5 may be hydrolyzed in the presence of steam to form this volatile acid as in the case of the key experiment of Wormsbecher. Rather we simply assert that formation of vanadic acid from vanadia species on a cracking catalyst does not occur at all. Instead it is

evident from our data that vanadia species are transferred by a solid state mechanism due to particle-particle contact. If a volatile vanadic acid were present, the simple gas permeable separation of the mixture would not prevent the vanadium from contacting the catalyst material.

Competitive Adsorption and Vanadium Trapping. It is always a goal of both the catalyst manufacturer and the refinery to apply tests to catalysts which will most accurately rank performance in commercial units. Any measures which can be added to screening tests which will avoid disappointing results at late stage testing such as pilot unit evaluation is a large added benefit. The inclusion of feed contaminant sulfur on vanadium trapping studies is an important variable.

It has been found that compounds of the alkaline earth metals as well as rare earths are suitable for vanadium trapping. Patents relating to the use of titanates of calcium (22), barium (23), and strontium (24) have been issued. Equivalent stannates of calcium and strontium have also been recommended (24,25). Rare earths as separate particles (26) and in the same catalyst particle (27) have been proposed. Naturally occurring minerals such as Sepiolite and Dolomite which are rich in magnesium oxide and calcium oxide have been suggested (28).

Magnesium Oxide Based Trap Technology. The MgO based Engelhard vanadium trap picks up sulfur with a first order dependence as a function of temperature. When a catalyst/trap sample was exposed to 1% SO₂(g), 3% O₂(g), 10% steam, and the balance N₂, sulfur accrues on the trap. This quantity increases with both time on stream and increasing temperature. However, the same relative percent of sulfur is lost during reductive elimination in a MAT at 910 F (Table 6). At temperatures similar to the mix zone of the riser where hot catalyst just exits the regenerator and contacts fresh feed oil (ca. 1150F) the elimination is much greater, nearly quantitative. This reductive elimination of sulfur regenerates MgO sites and facilitates further vanadium trapping.

Table 6.
Sulfur Loss from Catalyst Under Pseudo Riser Conditions

Sulfation Temp F	Initial S (mmol/g)	Final S (mmol/g)	% Released
1250	9.16	3.38	63
1450	16.88	6.22	63

Irreversible poisoning occurring with more basic alkaline earths' such as Sr can be shown to have a different effect. Figure 5 shows the effect of sulfur on the SrTiO₃ containing lab prototype. A comparison is made after exposing the sample with and without SrTiO₃ to 5000 ppm vanadium via a 20 cycle cyclic. The third sample is the same SrTiO₃ material except sulfur has been spiked into the feed as thiophene to yield 1 wt% sulfur on catalyst after the 20 cycle cyclic metallation. Relative to the control SrTiO₃ clearly mitigates effects of V in the absence of sulfur. However, inclusion of sulfur completely removes its trapping ability and renders the material equivalent to the control with no trap at all.

Figure 6 demonstrates the same point by comparing the MgO based trap to the Barium Titanate lab prototype. Again loss of performance in the presence of sulfur is observed. For these experiments SO₂ gas was used to effect the sulfation during the regeneration mode of cyclic deactivation. SO₂ gas may also be bled into the system during the Transfer Method experiment allowing sulfur to directly compete with trap sites as in the above two studies.

Thermodynamics. In addition to the kinetic data given above, an evaluation of the thermodynamics of sulfur adsorption quickly shows the rather facile formation of very stable sulfates at regenerator conditions of all the alkaline and rare earths'. This problem is compounded by the fact that the reductive elimination of sulfur under typical riser temperatures is highly unfavorable. The only exception to this is for the case of magnesium and RE. In the case of Mg while the free energy of formation for magnesium sulfate is favored in the regenerator, at temperatures usually seen in the riser mix zone the reductive elimination of sulfur to regenerate MgO and form H₂S is also favored. The free energy data for the formation of sulfates and their subsequent reduction are given for a variety of compounds in Table 7. Alkaline earth sulfate formation has a free energy which becomes more favorable as the temperature increases and even at 1300 F is already quite substantial for the heavier members of the series. For the reverse reduction only magnesium has a negative free energy at 620 C, a typical mix zone temperature. The rare earths' will also reductively eliminate sulfur at these temperatures. The main disadvantage of rare earth traps is the cost of the material relative to compounds such as MgO, a poorer affinity for vanadium, the amount of moles of active material per weight is much lower, and unfavorable selectivity due to increased hydrogen transfer chemistry may be realized. The alkaline earths' are not without faults of their own. Incorporating the material into a catalyst offers serious manufacturing difficulties due to incompatibility with other materials in the formulation and because it may undergo unfavorable reactions itself during catalyst preparation.

Table 7.

Free Energy Values for Sulfate Formation and Reduction of Parent Oxides

MO	DG _(rxn) (KJ/mole)	
	Oxidative SO ₄ form ¹ .	Reductive H ₂ S elim. ²
Mg	-92	-193
Ca	-208	-77
Ba	-317	+33
Nd	-317 ³	-593

1- 780 C, MO + SO₃ = MSO₄

2- 500 C, MSO₄ + 8H₂=MO + H₂S + 3 H₂O

3- value @ 650 C

Conclusions. It is necessary to test a catalyst's stability and performance under high vanadium conditions for materials which will be processing metals laden feedstocks. The Engelhard Transfer Method offers the benefits of both the Mitchell Method and

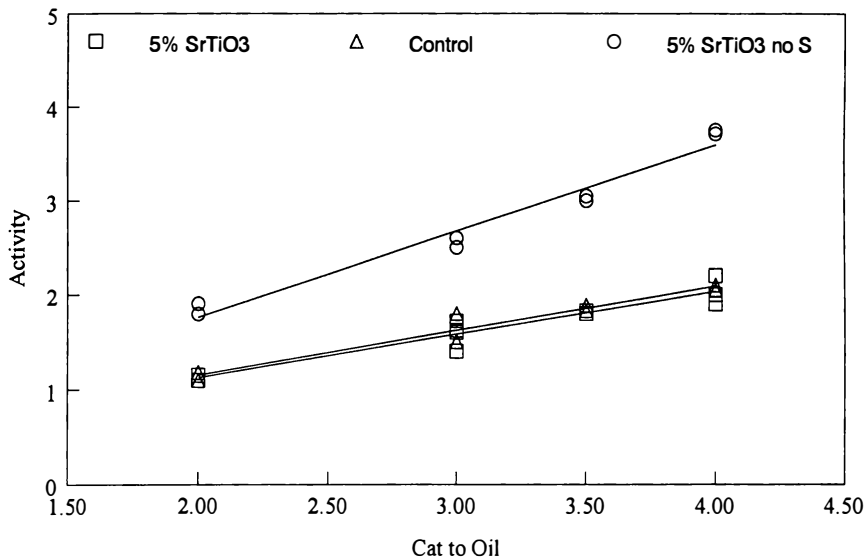


Figure 5. Effect of sulfur on the trapping ability of SrTiO₃ vanadium trap.

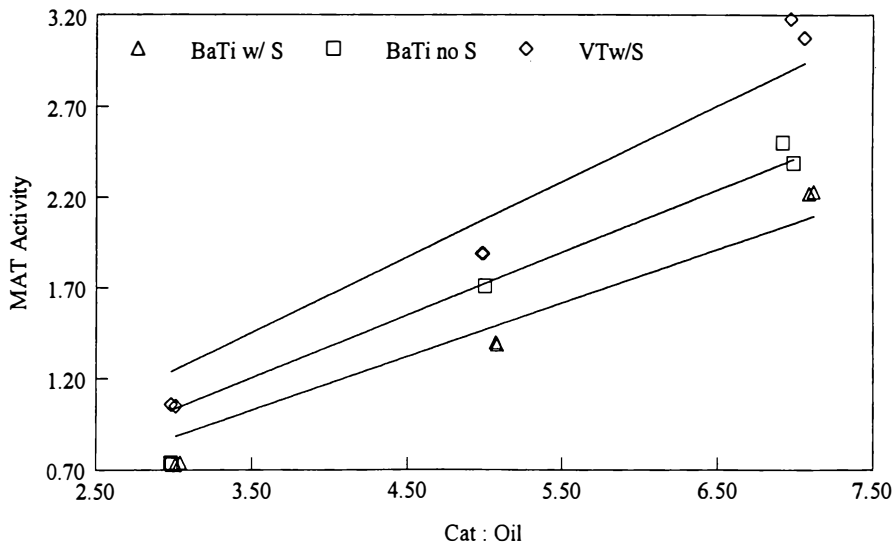


Figure 6. Comparison of MgO based trap to BaTiO₃ trap with and without sulfur.

the Cyclic Deactivation Method. Variations of the experiment allow for integrating other species such as sulfur or nitrogen oxides. Sulfur can be an extremely dangerous poison for many vanadium trap materials rendering them inactive despite their outstanding performance in the absence of sulfur.

Vanadium is transferred by interparticle solid state transport. The combination of oxygen or air plus steam promotes surface migration and enrichment of vanadia species which are not crystalline V_2O_5 . Interparticle contact is a requirement for vanadium transfer from particle to particle. Evidence for a volatile vanadic acid species could not be found.

Acknowledgments. We gratefully acknowledge the assistance of Dr. Nancy Brungard with XPS work and Ms. Stephanie Shedrick and Mr. Gary Smith for work with cyclic metallation studies. Also we acknowledge the detailed work of Mr. Glenn Zullo with ETM and steaming studies.

Literature Cited

1. Rush, J.B. NPRA paper AM-81-43. NPRA Meeting, San Antonio, TX; March 1981.
2. Argawal, B.B. and Gulati, F.B. *Pet. Hydrocarbons*. 1972, 6, 193.
3. Occelli, M.L. In *Fluid Catalytic Cracking II*. Occelli, M.L. Ed.; ACS Symp. Ser. American Chemical Society: Washington, D.C., 1991, vol 452.
4. Nielsen, R.H. and Doolin, P.K. In *Fluid Catalytic Cracking: Science and Technology*; Magee, J.S. and Mitchell, M.M. Eds.; Stud. Surf. Sci. Catal. Elsevier: Amsterdam, 1993, vol 76.
5. Bohmer, R.W.; McKay, D.L.; and Knopp, K.G. In *Fluid Catalytic Cracking II* Occelli, M.L. Ed.; ACS Symp. Ser. American Chemical Society: Washington, D.C., 1991, vol 452.
6. Dale, G.H. and McKay, D.L., *Hydrocarbon Proc.* 1977, 56, 97.
7. Deeba, M. *et al.* U.S. Patent 5,300,469; April 5, 1994.
8. Pompe, R.; Jaras, S.; Vannerberg, N.G. *Appl Catal.* 1984, 13, 171.
9. Rawlence, D.J.; Gosling, K.; Staal, L.H.; Chapple, A.P. In *Preparation of Catalysts V.*, Poncelet, G.; Jacobs, P.A.; Grange, P.; Delmon, B. Eds., Elsevier: Amsterdam, 1991.
10. Wormsbecher, R.; Peters, A.W.; Maselli, J.M. *J. Catal.* 1986, 100, 30
11. Mitchell, B.R. *Ind Eng Chem Prod. Res. Dev.* 1980, 19, 209.
12. Andersson, S.L.T.; Landin, S.T.; Jaras, S.; Otterstedt, J.E. *Appl. Catal.* 1984, 9, 317.
13. Leta, D.P. and Kugler, E.L., *Preprints ACS Div. Petr. Chem.* 1988, 33, 637.
14. Gerritsen, L.A.; Wijngaards, H.N.J.; Verwoert, J.; O'Connor, P. *Catal. Today.* 1991, 11, 61.
15. Hettinger, W.P.Jr.; Beck, H.W.; Cornelius, E.B.; Doolin, P.K.; Kmecak, R.A.; Kovach, S.M. *Preprints Div. Petr. Chem.* 1983, 28, 920.
16. Pine, L.A. *J. Catal.* 1990, 125, 514.
17. Anderson, M.W.; Occelli, M.L.; and Suib, S.L. *J. Catal.* 1990, 122, 374.
18. Elvin, F.J., *Oil and Gas J.*, Mar. 2, 1987, p. 42.

19. Occelli, M.L.; Stencel, J.M. In *Zeolites: Facts, Figures, Future*. Jacobs, P.A.; van Santen, R.A. Eds.; Elsevier: Amsterdam, 1989.
20. Went, G.T.; Oyama S.T.; Bell, A.T. *J. Phys. Chem.* 1990, 94, 4240.
21. Owens, L.; Kung, H.H. *J. Catal.* 1993, 144, 202.
22. Mitchell, B.R.; Vogel, R.F. US Patent 4,451,355 (1984).
23. Groenenboom, C.J. US Patent 4,791,085 (1988).
24. Chapple, A.P. US Patent 4,948,769, (1990).
25. Bartek, R.; Woltermann, G.M. US Patent 4,770,765 (1988).
26. Chin, A.A.; Sarli, M.S. US Patent 4,921,824 (1990).
27. Chu, P.; Huss, A. Jr.; Kirker, G.W. US Patent 5,001,096 (1991).
28. Kenedy, J.V.; Jossens, L.W. US Patent 5,002,653 (1991).

Riser Simulator: Testing of Adsorption Effects

Jacek Pruski¹, Ahmet Pekediz², and Hugo de Lasa

Faculty of Engineering Science, Chemical Reactor Engineering Center,
University of Western Ontario, London, Ontario N6A 5B9, Canada

Investigation of the adsorption phenomena present during fluidized catalytic cracking of hydrocarbons was conducted utilizing the Riser Simulator, a novel unit developed at CREC-UWO. A series of cracking experiments were carried out using commercial gas oils and cracking catalysts which resembled the ones used in industrial FCC units. Determination of the adsorption coefficients of the various hydrocarbon lumps was possible based on mass balance considerations. Based on the experimental results and subsequent analysis, the adsorption coefficients were related mainly to molecular weight and reaction temperature with other factors, such as catalyst/oil being of less importance.

Modelling catalytic cracking of hydrocarbons in industrial FCC units requires a thorough understanding of combined kinetic and adsorption phenomena. Cracking reactions considered in the technical literature are interpreted in terms of kinetic modelling as a pseudo-homogeneous reaction process. Two recent contributions emphasize the importance of this approach in a pulse microreactor (2) and in a continuous riser unit (3). These studies also highlight the critical interest of adsorption coefficients for adequate simulation of cracking reactions.

To this end, the Riser Simulator, a novel unit developed at CREC-UWO (1) was adapted and employed in the joint determination of these parameters. The use of accurate pressure monitoring devices allowed for good mass balances closures which in turn were crucial to the reliable determination of the other experimental parameters.

¹Current address: SACDA, Inc., 343 Dundas Street, Ontario N6B 1V5, Canada

²Permanent address: Chemical Engineering Department, Gazi University, Ankara, Turkey

Experimental Set-up

Experimental runs were performed in a 45mL Riser Simulator reactor in operation at CREC-UWO (Figure 1a). The reactor was connected to a 455mL vacuum system by means of a four-port valve whereby the cracked products were removed from the Riser Simulator at the end of the reaction period (Figure 1b). A four-port valve was controlled by a timer/actuator assembly linked to the gas oil injection system. The vacuum system was also connected to a manually operated six-port sampling valve which allowed for sample injections into the gas chromatograph. Both the reactor and the vacuum system were equipped with two pressure transducers which permitted for continuous pressure monitoring during the reaction and post-reaction evacuation periods. The Riser Simulator, the vacuum system as well as the connecting lines and valves were well insulated.

The gas oil injector system included a 1000 μ L glass syringe connected to the injection needle and to a m gas oil reservoir by means of a two-way valve (sample/inject). It was also equipped with electrically actuated switches which controlled the timer/actuator assembly on the four-port valve as well as the data acquisition system. The data acquisition system allowed for collecting the pressure profiles in the reactor and vacuum system as a function of time during the reaction and post-reaction evacuation periods.

A typical pressure profile obtained from the two transducers is presented in the Figure 2. Curve I along with points A, B and C illustrates the characteristic pressure profile observed during the operation of the reactor. Meanwhile, curve II depicts the pressure profile inside the vacuum chamber. Point A of curve I indicates the pressure condition inside the Riser Simulator just prior to the hydrocarbon injection. Point B gives the Riser Simulator pressure at the end of the reaction period (just before evacuation commences) and Point C represents the equilibrium pressure once the pressures between the vacuum chamber and the Riser Simulator have stabilized.

Experimental Procedure. FCC catalysts employing the submicron zeolite structure were used in this study. These catalysts were synthesized, spray-dried into 60 μ m pellets and impregnated with the metals by the incipient wetness technique at CREC-UWO.

The operating reaction conditions employed during this study closely resembled those present in commercial FCC installations. Several runs at various residence times (5-10s), reaction temperatures (500-550°C) and catalyst-to-oil ratios of 4 and 6 were performed. Each run involved loading the catalyst basket located inside the Riser Simulator with a pre-determined amount of catalyst, sealing the system and heating the reactor to the desired temperature. The vacuum system along with all its associated valves and lines were also heated to 250-350°C in order to prevent hydrocarbon condensation. The heating process was carried out under continuous flow of argon.

When equilibrium was attained, the flow of argon was cut off and the reactor at 15 psia was sealed off from the vacuum system. The pressure inside the vacuum system was subsequently reduced to 2 psia. The reaction was initiated by

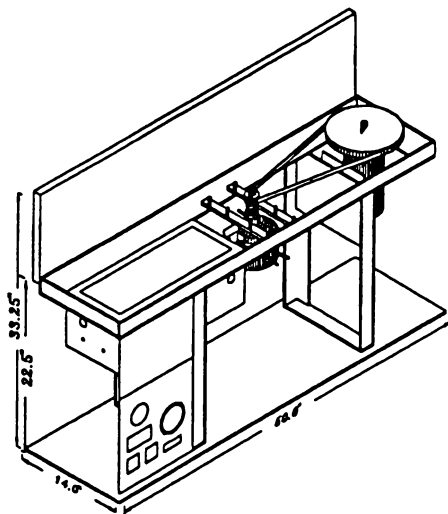


Figure 1a. Schematic of the Riser Simulator with a general view of the unit

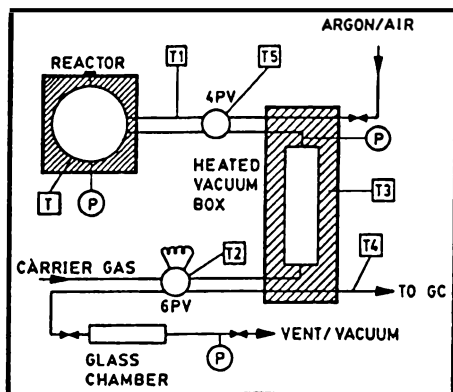


Figure 1b. Riser Simulator Components: reactor, vacuum box, glass chamber

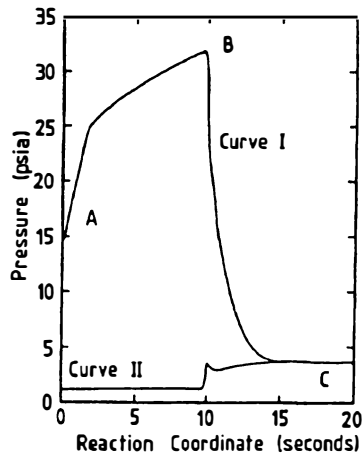


Figure 2. Curve I: Riser Simulator Pressure. (A) Prior to Injection, (B) Before Evacuation, (C) Equilibrium Pressure. Curve II: Vacuum Chamber Pressure.

the injection of a pre-determined amount of gas oil into the reactor. After the selected residence time, the reactor and the vacuum system were again connected. Because of the large pressure and volume difference between the two systems, all the contents of the reactor were effectively moved from the reactor into the vacuum system, thus terminating the reaction and preventing the possibility of overcracking. After achieving pressure equilibrium between the two systems, the reactor was again sealed off and a sample of the gaseous products held within the vacuum system was sent to the gas chromatograph for analysis.

The gas oil used was a typical hydrotreated fraction with a high content of aromatics. The detailed properties of the feedstock can be examined in Table I (5). Gas oil condensation in the sampling lines was found negligible from experimental observation. In addition, dew point calculations at temperatures and pressures prevalent, after sample evacuation, in the vacuum box confirmed the negligible condensation of hydrocarbons in the sampling system.

Modelling, Results and Discussion

Modelling catalytic cracking reactions involves a thorough understanding of kinetics and adsorption phenomena taking place simultaneously on catalyst surface while catalytic cracking reactions are progressing. Catalytic cracking reactions are heterogenous processes with significant adsorption of both reactants and products taking place on catalyst surface. This phenomenon has significant repercussions not only on the kinetic parameters but also on the modelling of continuous riser units. As a result of this adsorption phenomenon, riser volumetric flows and consequently, fluid dynamics can be severely affected. Therefore, if these facts are not properly taken into account, significant miscalculations in the fluid dynamics may occur.

In this study, we adopted a model with one balanced algebraic equation which incorporated various lumps (gas oil, cycle oil, gasoline, light gases) in both gas and solid phase. Hydrocarbons lumps are distributed and coexist between the two phases at all times during the reaction period (before product evacuation):

$$M_{hc,inj} = M_{hc,gas} + M_{hc,cat} + M_{coke} \quad (1)$$

At the same time, the total pressure in the vacuum chamber during pressure equalization as well as in the Riser Simulator during reaction is the sum of the partial pressure contributions of the various lumps:

$$\Delta P_{total} = p_{go} + p_{cy} + p_{ga} + p_{lg} \quad (2)$$

Furthermore, for each of the hydrocarbons lumps, given the relatively low pressures employed, the ideal gas law gives:

Table I. Feedstock properties

Metals in oil	V < 0.3 ppm
	Ni < 0.3 ppm
	Fe < 4.0 ppm
	Na < 0.5 ppm
	Cu < 0.1 ppm
Anilin Point	63.10 °C
Bromine Number	< 5.0
Conradson Carbon Residue	0.10 wt%
Density @15°C, densitometer	929.20 kg/m ³
Nitrogen, chemiluminescence	0.12 wt%
Sulphur, Leco SC32	0.76 wt%
NMR Aromaticity	25.00 %
C	87 wt%
H	11.7 wt%
Viscosity @40°C	29.27 CST
Low resolution mass spectrometry	%
Paraffins	10.62
Cycloparaffins	39.76
Monoaromatics	20.82
Diaromatics	15.32
Triaromatics	5.55
Tetraaromatics	2.16
Pentaaromatics	0.28
Aromatic sulphur	2.68
Polar compounds	2.80
Simulated distillation	°C
IBP	259
5 wt%	300
10 wt%	314
30 wt%	348
50 wt%	377
70 wt%	410
90 wt%	457
95 wt%	479
FBP	527

$$P_i = \frac{M_{i,\text{gas}} R T}{MW_i V_R} \quad (3)$$

Finally, hydrocarbons are distributed between the gas and the catalyst phases. Thus, for any given lump the following relation applies:

$$M_{i,\text{cat}} = \frac{K_i M_{i,\text{gas}} m_c}{V_R} \quad (4)$$

Thus, by combining Equations (1-4) the total pressure rise inside the Riser Simulator can be represented by the following equation:

$$\Delta P = \sum \frac{w_i M_{\text{hc},\text{inj}} RT}{[V_R + m_c K_i] MW_i} \quad (5)$$

It has to be stressed that this equation only contains partition coefficients (equilibrium constants), no kinetic parameters are required and can, thus, be solved independently of the particular kinetic model considered for modelling the cracking reaction.

Finally, introducing a proportionality factor K_o and the associated reference molecular weight $MW_o = 1$, as well as the following relationship between the coefficients and lump molecular weight,

$$K_i = K_o P \left[\frac{MW_i}{MW_o} \right]^\beta \quad (6)$$

the following relation is obtained for ΔP as a function of K_o and β :

$$\Delta P = \sum \frac{w_i M_{\text{hc},\text{inj}} RT}{[V_R + m_c K_o P (MW_i/MW_o)^\beta] MW_i} \quad (7)$$

In order to check various model assumptions a first step in the analysis requires to perform mass balance calculations involving the amount of gas oil injected and the amount of hydrocarbons obtained by pressure difference under vacuum conditions, with the key hypothesis that no hydrocarbons remain on catalyst surface at 2 psia. Given mass balance closure was within typically 5 - 7% error for all experiments conducted, the following was validated:

- a) the total mass of hydrocarbons including various lumps during the reaction period was very close to the amount injected, and therefore was considered equal for further analysis,
- b) the overall mass balance under vacuum conditions could be done with various partition coefficients (equilibrium constants) set to zero or no hydrocarbons remaining on catalyst surface.

Once these facts were established, the second phase of the analysis involved the use of Equation (7) with $\beta=0.5$, just before product evacuation. In these equations the contribution of various lumps in both gas and solid phases were accounted for simultaneously.

Using the above mentioned methodology lump fractions (gas oil, cycle oil, gasoline and light gases) obtained at three reaction times 5, 7.5 and 10 seconds, three reaction temperatures and two C/O, lump fractions, as reported by Pruski (4), were analyzed. Adsorption constants for the light gases, gasoline, cycle oil and gas oil lumps were determined and correlated with the total pressure, temperature and hydrocarbon molecular weight. Table II and Table III summarize results for two selected catalyst-to-oil (C/O) ratio, 4 and 6, and three temperature levels. Adsorption constants reported have a confidence span of $\pm 10\%$.

Comparing the results obtained in Table II and in Table III, it can be observed that the adsorption coefficients for cracking catalyst decrease moderately with temperature, are significantly affected by the specific lump considered ($K_{i,g}$ is about three times smaller than $K_{g,o}$) and are relatively insensitive to the C/O ratio.

Conclusions

- 1- Catalytic cracking reactions involve the combined effects of reaction and adsorption phenomena. Thus, adequate kinetic modelling should consider heterogeneous representations distinguishing between the chemical species, reactants and products, distributed between gas/solid phases.
- 2- The novel Riser Simulator is a suitable experimental tool for assessing adsorption parameters of various hydrocarbon lumps involved in the catalytic cracking process.
- 3- Given the magnitude of the adsorption constants and the adsorption parameters, as reported in this study, it can be advanced, as demonstrated by Martignoni and de Lasa (3), the significant influence of adsorption on large scale riser unit modelling and the importance of so-called "heterogeneous models" for FCC riser unit simulation.

Notation

K_i	adsorption constant for the lump i ($\text{cm}^3 \text{g}^{-1}$)
K_o	adsorption constant defined at the reference molecular weight $MW_o=1$ ($\text{cm}^3 \text{g}^{-1}$)
m_c	mass of catalyst (g)
M_{coke}	mass of coke (g)
$M_{\text{hc,inj}}$	total mass of hydrocarbons injected (g)
$M_{\text{hc,gas}}$	mass of hydrocarbons in the gas phase (g)
$M_{\text{hc,cat}}$	mass of hydrocarbons in the catalyst (g)
$M_{i,\text{cat}}$	mass of the lump i adsorbed in the catalyst phase (g)
$M_{i,\text{gas}}$	mass of lump i in the gas phase (g)
MW_i	molecular weight of the i lump (g mol^{-1})

Table II. Adsorption Coefficients in cm^3/g for $\text{C}/\text{O} = 4$ with $\beta = 0.5$

	K_{go}	K_{cy}	K_{ga}	K_{lg}
500°C	140	110	81	52
525°C	102	80	59	37
550°C	76	60	44	28

Table III. Adsorption Coefficients in cm^3/g for $\text{C}/\text{O} = 6$ with $\beta = 0.5$

	K_{go}	K_{cy}	K_{ga}	K_{lg}
500°C	119	94	68	44
525°C	89	70	52	33
550°C	75	59	43	27

MW _o	molecular weight of the reference component of molecular weight 1 (g mol ⁻¹)
p _i	partial pressure contribution if the lump i (kPa)
P	total pressure in the reactor (kPa)
R	universal gas constant (kPa cm ³ mol ⁻¹ K ⁻¹)
T	temperature (K)
V _R	reactor volume (cm ³)
w _i	weight fraction of a given lump
β	parameter involved in eq (6)
ΔP	total pressure rise in the Riser Simulator (kPa)

Subscripts

lg	light gases
cy	cycle oil
ga	gasoline
go	gas oil

References

- (1) de Lasa, H., *US Patent 5,102,628, 1992.*
- (2) Farag, H.; Blasetti A.; Ng, S.; de Lasa, H., *Ind. Eng. Chem. Res.*, **1995**, *33*, 3131.
- (3) Martignoni, W.; de Lasa, H., *Proc. Fluidization*, Tours, France, May 1995.
- (4) Pruski, J., *MESc Thesis*, Univ. Western Ontario, London, Ontario, Canada, 1995.
- (5) Blasetti, A., *PhD Thesis*, Univ. Western Ontario, London, Ontario, Canada, 1994.

Development of a Bench-Scale Fluid Catalytic Cracking Microriser

M. P. Helmsing, M. Makkee, and J. A. Moulijn

Faculty of Chemical Technology and Materials Science, Delft University of Technology, Julianalaan 136, 2628 BL Delft, Netherlands

Catalyst performance testing procedures for fluid cracking catalysts have been evaluated. A benchscale microriser is described and results are compared with those of a so-called microsimulation test. The two tests result in significant differences in light cycle oil, gasoline and LPG yield. The microriser experiments yielded a higher LPG olefinicity. This is explained by the dilution of the feed with the nitrogen carrier gas, which decreases the amount of bi-molecular hydrogen transfer reactions. Experiments at a very short contact time of 0.7 seconds were carried out. It is striking that the coke yield does not differ significantly from that in experiments performed at a much greater contact time of 5 seconds. This indicates that the majority all the coke formed during reaction is already deposited in the first few tenths of a second.

Catalyst performance testing for fluidised catalytic cracking (FCC) is of major importance for the profitability of a refinery, and it is not suprising that it draws a lot of attention (1,2). New and existing fields of interest for catalyst testing are catalyst development and performance, resid processing, metal (Ni and V) contaminations, and FCC environmental issues (e.g. sulfur transfer agents) (3-6). Due to the small margins and large throughput in an industrial FCC unit, a realistic assessment of test data is an absolute requirement. Adequate downscaling of the characteristics of the process is essential.

Several types of FCC testing equipment are described in literature, varying from the more traditional standardized micro activity test (MAT) and fluidised bed reactors to complete riser-regenerator combinations. Also other designs such as a pulse reactor, or a very short contact time reactor have been reported in literature (7-9).

A newly developed concept in this field is the microriser reactor developed at the Delft University of Technology. This riser reactor is a 'once through' reactor with variable length and well defined conditions matching industrial practice.

The quality of the experimental data is not only determined by the choice of reactor, but also by the catalyst pretreatment. A change in either one can lead to a different ranking of catalysts (10). On the other hand, several practical and economical constraints exist, such as the available amount of catalyst (*i.e.* in catalyst development), manpower needed to operate the testing rig (in the case of a large pilot plant) or experimental time needed for one run. This dilemma between quality demands and practical constraints can be a matter of reactor selection.

Aims of this chapter are to discuss (i) reactor selection, and (ii) the essentials for FCC catalyst testing. A case study will be presented concerning these subjects. In this case study, the microriser (MR) is compared with the so-called microsimulation test (MST) developed by Akzo Nobel (11). The discussions will be illustrated with experimental data obtained from the microriser and the microsimulation testing equipment.

FCC Catalyst Performance Testing

The success of FCC catalyst performance testing is determined by a combination of catalyst pre-treatment, choice of testing reactor, and interpretation of the experimental data collected. The evaluation of the experimental data has to be based on adequate modelling. Depending on the testing objectives different strategies can be chosen. Process optimisation puts different constraints and priorities on the testing equipment than catalyst development. With these backgrounds in mind a discussion will be given concerning reactor selection for FCC catalyst performance testing.

Reactor Selection. In the industrial fluidised catalytic cracking process, one aims at maximum gasoline yield, which is achieved by ideal contact of the catalyst with completely vaporised feed, in an adiabatic plug flow riser reactor, under optimal and well defined process conditions. In practice, this idealised goal is only approached. Reasons for this are that imperfections are present in the feed injection, a large residence time distribution of the catalyst exists due to annular core flow, a slip velocity between catalyst and feed is present. Furthermore, every individual industrial FCC riser reactor is different in design and process conditions, resulting in different hydrodynamics of feed and catalyst in the reactor, catalyst age distribution, possible composition of the injected feed, *etc.* In selecting the reactor and test conditions for catalyst testing, the aim is not to simulate the exact conditions in an actual FCC unit, because these conditions are clearly variable and not well defined. Likewise, a maximum production of gasoline is not required. Instead, the main idea is to scale down properly *viz.* to subject the catalyst to the right local chemical environment and to obtain intrinsic experimental data in a relevant kinetic regime, *i.e.* data essentially independent of the reactor used. Prediction of product yields is only possible with test reactors capable of yielding intrinsic kinetic data. Application of a reactor model for the industrial unit then translates the experimental data to an estimated product distribution. A test reactor capable of

producing intrinsic kinetic data is defined by several conditions. The experimental conditions should be well defined on both reactor and catalyst level. The desired mode of operation for solid and vapour phase in the reactor can be batch or continuous. The hydrodynamics determine the catalyst-feed contacting efficiency and the residence time distribution. As is generally the case, mass- and energy transport limitations should be minimal. The contacting efficiency has to be optimal and the contact time well defined. This sets constraints for the design and dimensions of the equipment. In general, the larger the equipment, the less control there is over the experimental conditions, and imperfections in hydrodynamics and contact efficiency are unavoidable.

The residence time distribution of the feed (and catalyst) should unambiguously correspond with a physically correct model, so that true kinetic parameters are determined by the catalyst. In practice, this means that each of the two phases should be represented by either a plug flow or ideally mixed flow model. Reactors behaving according to complex models are not advisable. Even a reactor behaving as a combination of a continuous stirred tank reactor (CSTR) and a plug flow reactor (PFR) can lead to erroneous results. This is illustrated by the classical example of a hypothetical first order series reaction network (see Figures 1a to 1f). The $E(t)$ versus t curves in Figures 1a and 1b are the residence time distributions derived for both combinations of reactors. Evidently, they are the same, but the conversion profile of A (Figs. 1c and 1d), and the selectivity profile of component B (Figs. 1e and 1f) are dependent on the reactor sequence. Although both combinations yield the same final conversion, the final selectivity towards B is different. Obviously, the residence time distribution is not sufficient to characterize the reactor even for these simple combination of linear rate equations.

Transient behaviour as occurs in a MAT unit should be avoided. The constantly changing conditions and catalyst properties throughout the reactor during the experiment, result in a badly defined experiment. Of course the MAT unit is popular for a good reason: it is very convenient experimentally.

The second level involves the heat fluxes. In order to assure well defined conditions isothermal operation is preferred. Also kinetic studies should be performed with isothermal conditions (1). Because in an industrial unit the hot catalyst is coming from the regenerator, preheating of the catalyst can be a necessity to mimic a correct temperature time history. Along these lines a benchscale reactor for FCC catalyst testing, called the Microriser, has been designed and developed.

Experimental

Design of the Microriser. The design of the microriser is based on an earlier design by Crosfield Chemicals Ltd (12). Figure 2 shows an outline of the unit. It consists of five sections: a catalyst feeder, a feed supply, a reactor, a separation of catalyst and products, and a condensing section. The catalyst is fed with a sophisticated metering device. The design of the feeder is similar to the design of Horsely *et al.* (13). It

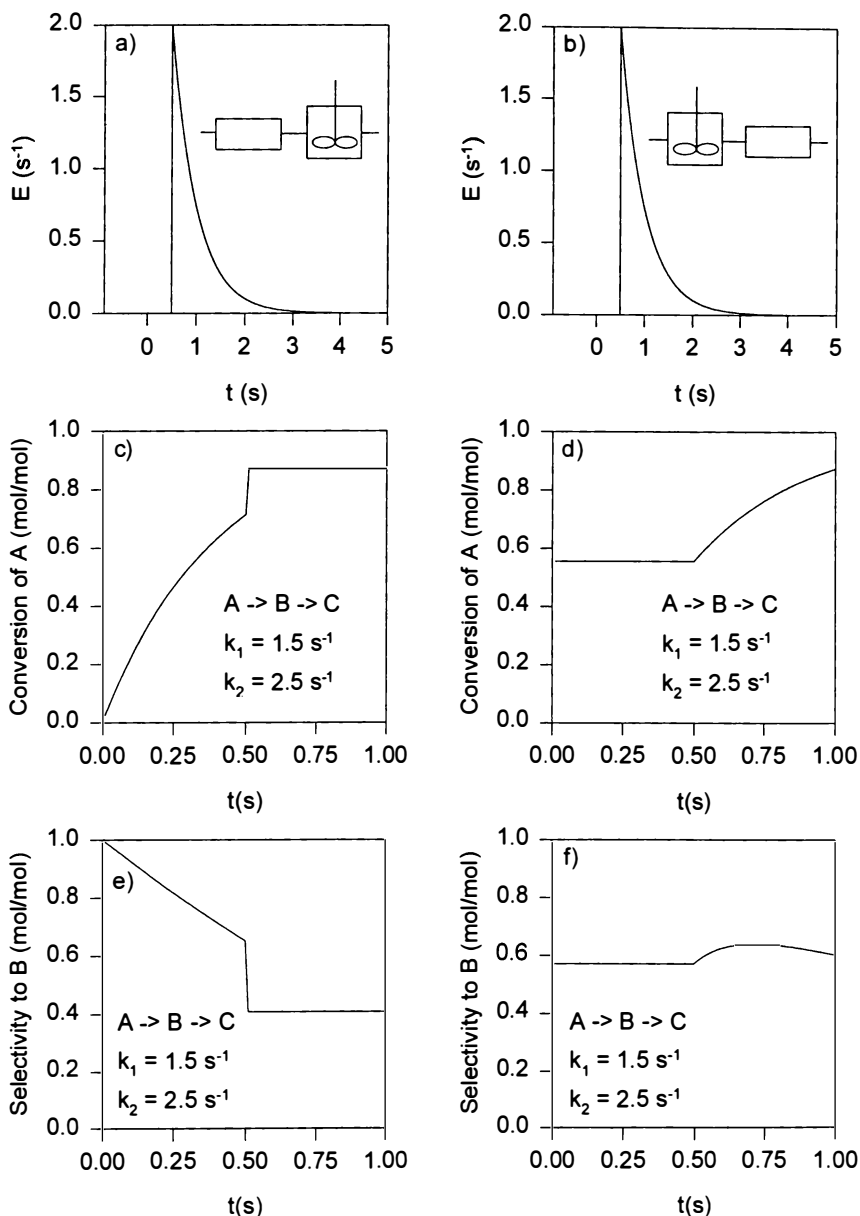


Figure 1. Reactor behaviour of two different combinations of a plug flow reactor (PFR) and a continuous stirred tank reactor (CSTR). The combinations are denoted in the figure. Fig. 1a and b are the corresponding $E(t)$ -curves, Fig. 1c and d are the conversion profiles, Fig. 1e and f are the selectivity profiles along the combination of reactors.

basically consists of a hopper filled with catalyst and a dosing wheel to control the flow rate. The catalyst flow can be varied from 2 to 20 g/min. Nitrogen acts as a carrier gas and transports the catalyst particles through the preheater to the reactor. The temperature in the preheater ranges from 873 to 1023 K. A pulse-free, accurate syringe pump (ISCO 500D) supplies the feed at constant flow, typically between 2 and 5 g/min, to the feed preheater. The temperature of the preheater is dependent on the type of feed, but a typical value would be 573 K. A 1/16" tube is used to inject the feed as a spray perpendicular to the catalyst flow in the reactor. The entrained flow reactor is built in an oven with internal forced convection and a maximum temperature of 833 K. The reactor is a folded tube made of inconel with bends of 180° (bend radius 0.09 m, ID 4 mm) and an adjustable length in steps of 2 meter up to a maximum of 20.6 meters. In FCC catalyst testing a folded tube reactor has been described before (14). Residence times from 0.1 to 5 seconds can be easily realized by varying the tube length and the carrier gas flow. The product mixture and catalyst are separated in a cyclone at typically 773 K. The catalyst is collected in a fluidised bed for post-run stripping with a nitrogen flow varying from 300-600 ml/min. Because of practical reasons the stripping of the hydrocarbons is batchwise, but in the near future the microriser will be modified for continuous stripping. The hydrocarbon vapours coming from the cyclone during the cracking and stripping period are condensed using a stage wise cooling system, consisting of an air cooler, a Liebig cooler and a two stage condenser immersed in a mixture of propanol and dry ice. The non-condensable vapours are collected in a tedlar gas bag with a capacity of 43 l.

Operation. The reactor of the microriser (MR) is folded for practical reasons. A cold flow model of the reactor was used to study the flow behaviour of the catalyst in the tubes and especially in the bends. Based on measured residence time distributions and modelling, it can be concluded that the reactor approaches plug flow very well (15). Another feature of the micro riser is its isothermal operation, although catalytic cracking is an endothermic process which would cause a temperature gradient along the reactor. Based on general design rules, there is no limitation of heat transfer to the reaction occurring within the reactor during the cracking operation. This results in a constant reaction temperature, as the catalyst and the oil contact, defined by the oven temperature. During experiments, a steady state can be obtained before the collection of the hydrocarbons has started. In this way, the effects of a start-up and close-down of an experiment are avoided. A process computer controls the necessary actions during an experiment and insures a well defined pre-specified runtime.

The Microsimulation test (MST). Modification of the operating procedure and experimental conditions of a convectional micro activity test (MAT) has led to the so-called microsimulation test (MST, see Figure 3). Basically, the reactor is a fixed bed with transient operation during the catalyst contact time. A complete description of the operation and design of the MST reactor is given by O'Connor in (11). Table I gives an overview of the main differences between the MR and the MST.

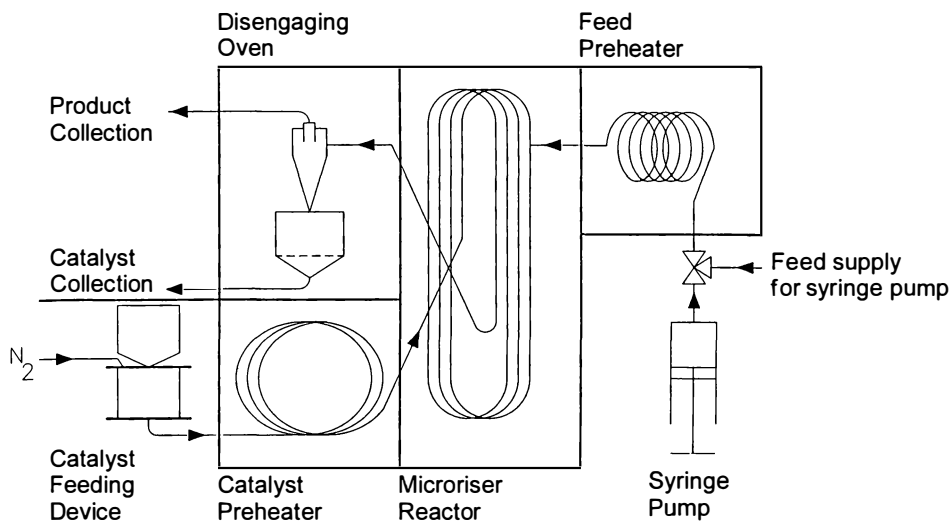


Figure 2. An outline of the microriser setup.

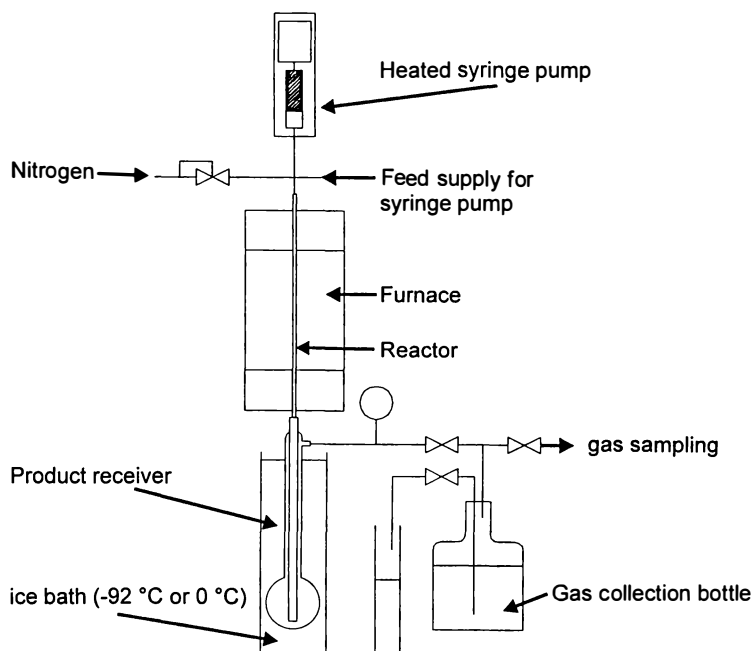


Figure 3. An outline of the microsimulation test equipment (Adapted from ref. 11.)

Table I : Differences between the MR and MST reactor

	<i>Microriser reactor (MR)</i>	<i>Microsimulation test (MST)</i>
Type of reactor	riser reactor	fixed bed reactor
Operation	steady state	transient
Catalyst fraction (vol%)	2 - 5	40 - 50
Dilution ratio (vol N ₂ /vol feed)	5	0
Ratio of Catalyst to oil contact time (s/s)	1	50-60

Feed and catalysts. A regular Kuwait vacuum gasoil was used as a feed. Its characteristics can be found in Table II. Three commercial cracking catalysts with an increasing rare earth and alumina content, *viz.* **A**, **B**, and **C**, were tested. All catalyst were presteamed and deactivated to an equilibrium level by its supplier. Larger catalyst particles were removed with a 150 μm sieve. This step is followed by either a calcination or regeneration. Fresh, but pre-steamed catalyst was calcined at 773 K for 1 h, while coked catalyst was regenerated at 873 K for 2 h.

Table II : Characteristics of the Kuwait Vacuum gasoil

<i>Feedstock characteristics</i>	
Conradson carbon content	0.48 wt%
Boiling range	643 - 835 K
Contaminations :	
Sulfur	2.93 wt%
Nitrogen (basic)	275 ppm
Nickel	1.0 ppm
Vanadium	1.0 ppm

Conditions. The catalyst and oil were preheated to 973 K and 673 K, respectively. The microriser reactor was operated at 833 K. The catalyst and the gaseous products were separated at 773 K. Mass balances were typically within a range from 92 to 96 wt%. The difference in mass balance found are mainly attributed to liquid product left behind in the glassware. The same feed and catalysts were also tested in the MST reactor at 833 K by Akzo Nobel. The analysis of the liquid products was done using a simulated distillation method. Cutpoints for the HCO, LCO and gasoline fraction are 616 K, 489 K, and 309 K respectively. The components of the gaseous products upto C₅ were analyzed using a GC method. The amount of coke was calculated using the analysis of the gases produced during a burn-off. In FCC, the conversion is usually defined as the yield in gasoline, LPG and fuelgas, but in this study, the conversion of an experiment is defined as the amount of heavy cycle oil (HCO) converted. This was done because the feed consists only of HCO and thus LCO would be a product. The conclusions drawn in this paper are not affected by this definition of conversion.

Different contact times. Three contact times were used in this research, viz. 0.7, 4.1 and 5.0 seconds based on the inlet conditions of the reactor. The residence time at the outlet of the reactor will slightly differ from the calculated residence time due to the expansion of the hydrocarbon fraction. The experimental settings used are tabulated in Table III.

Table III : Experimental settings for different contact times in the MR

	<i>Length of reactor (m)</i>	<i>Nitrogen flow (ml/min)</i>	<i>Oil flow (g/min)</i>	<i>Calculated residence time (s)</i>
Set 1	20.6	993	4.0	5.0
Set 2	14.6	850	4.0	4.1
Set 3	20.6	1338	4.0	4.1
Set 4	2.6	993	4.0	0.67

Results

Experiments with the same conditions were carried out in both the microriser (MR) and the microsimulation test (MST). The experimental results are tabulated in Table IV. The results for catalyst **B** are displayed in Figure 4a to 4f. The same trends, displayed in Figure 4, were also found for catalyst A and C.

Table IV : Experimental results at a conversion of 82.5 wt%

	Catalyst A		Catalyst B		Catalyst C	
	MR	MST	MR	MST	MR	MST
Conversion ^a	82.5	82.5	82.5	82.5	82.5	82.5
CTO ^b	4.2	3.5	3.6	2.1	3.1	2.6
Fuel gas	2.7	2.3	2.5	1.7	2.5	2.0
LPG	13.0	16.7	10.6	14.7	11.9	15.1
Gasoline	49.5	45.1	50.3	45.6	49.3	44.5
LCO	14.8	17.0	16.9	19.5	16.5	18.7
HCO	17.5	17.5	17.5	17.5	17.5	17.5
Coke	2.6	1.6	2.3	1.1	2.5	2.2

^a Conversion and all product fractions are given in wt% of the feed.

^b Catalyst-to-oil ratio (CTO) needed for a 82.5 wt% conversion in g catalyst/ g feed.

In Figure 4.a the activity data are plotted. In both the MR and the MST the conversion increases with a higher cat-to-oil ratio (CTO). A higher activity was found in the case of the MST.

The product yields are shown in figure 4b to 4f. The coke, LCO, gasoline, and LPG plots measured by the MR have the same curvature as the MST data, but there are significant differences, up to 5 wt% in the gasoline yield plot (see Figure 4d). The curves shown in graphs 4c to 4e reveal significantly less secondary cracking in the case of the MR : a combination of a higher gasoline and lower LPG yield was found in comparison

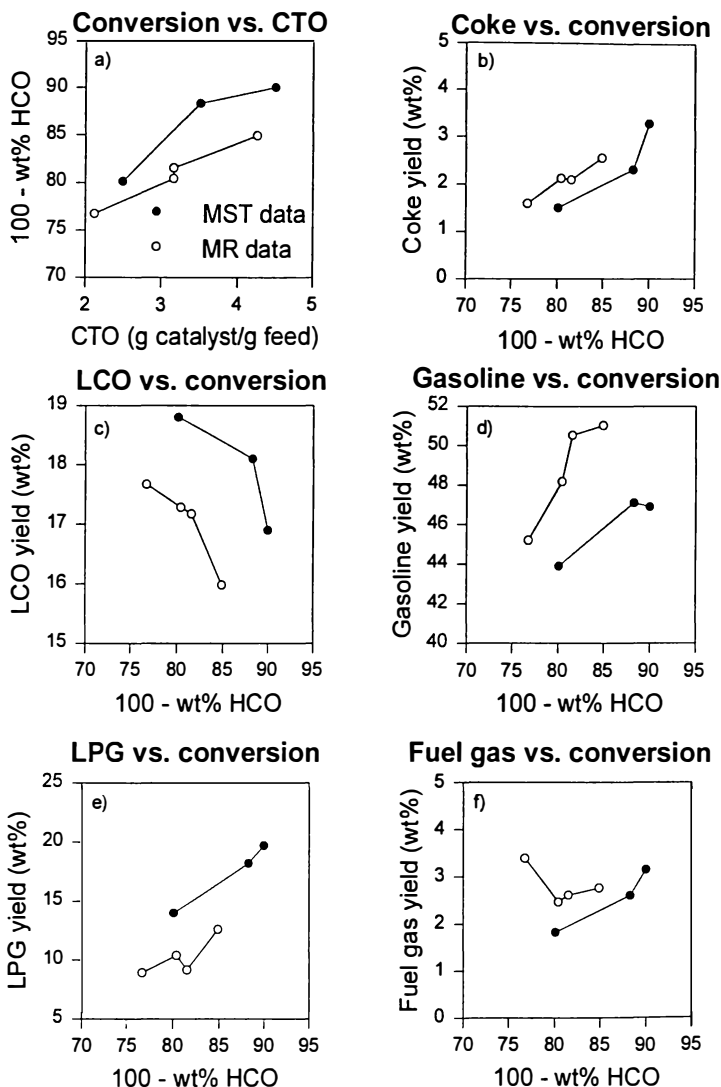


Figure 4. Activity and yield plots for catalyst **B** based on data from the Microriser (MR) and Microsimulation test (MST). The activity plot is shown in Figure 4a. The yield plots for coke, LCO, gasoline, LPG, and fuel gas are given in Figure 4b to 4f, respectively.

with the MST data. The LCO yield is somewhat lower for the MR than the MST. The gasoline formed via the LCO fraction is better retained in the MR.

The occurrence of fewer secondary cracking reactions in the MR is confirmed by the significant deviations in the LPG olefinicity. This is the ratio of unsaturated to saturated components in the LPG fraction and is a typical indicator for secondary hydrogen-transfer reactions. The definition of this ratio is given in equation 1. Figure 5 shows this

$$\text{LPG olefinicity} = \frac{\text{wt\% } C_3^= + \text{wt\% } C_4^=}{\text{wt\% LPG}} \quad (1)$$

ratio for the experimental values of both the MR and the MST. It is clear that a significantly higher ratio is found for the data determined with the microriser.

The trend found in the fuel gas yield plot originating from the MR experiments is independent of the conversion. The MST data show a correlation between conversion and fuel gas yield. Fuel gas consists of hydrogen, methane, ethane and ethene. These are all typical products resulting from thermal cracking reaction. The fuel gas yields are in the same order of magnitude for both reactors, indicating that the absolute amount of thermal cracking is about the same. Isobutane is a branched paraffin and a typical catalytic cracking product. The ratio of fuel gas to iso-butane can be used as an indicator for the ratio of thermal versus catalytic cracking (see Figure 6). It is clear that the ratio is larger for the microriser. Relatively less catalytic cracking occurs in relation to the amount of thermal cracking.

Discussion

The experimental data for catalyst A, B, and C all reveal systematic differences between the MR and the MST. As a consequence, the differences found are caused by the different reactor configurations and are far from negligible especially in view of the actual throughput in a FCC unit.

Activity. The differences found in activity of the catalyst are caused by two effects: the definition of the catalyst-to-oil (CTO) ratio and the feed partial pressure in both reactors. The CTO is time averaged over the reaction time and is not clearly defined in the MST. The contact between the catalyst and oil is not constant throughout the experiment. At the beginning of the MST experiment fresh feed encounters fresh catalyst. However, after some time fresh feed meets a partially deactivated catalyst with coke already deposited on it. At the end of the experiment the situation is the opposite of the contact between catalyst and oil in an industrial unit. This makes the definition of the CTO not unambiguous in the case of the MST and can lead to over- or underestimation of the CTO. However, the most important effect is the difference in partial pressure of the feed in both sets of equipment : the nitrogen carrier gas lowers the partial pressure in the MR. A lower partial pressure results in a lower conversion. With these two effects a higher activity for the MST can be expected.

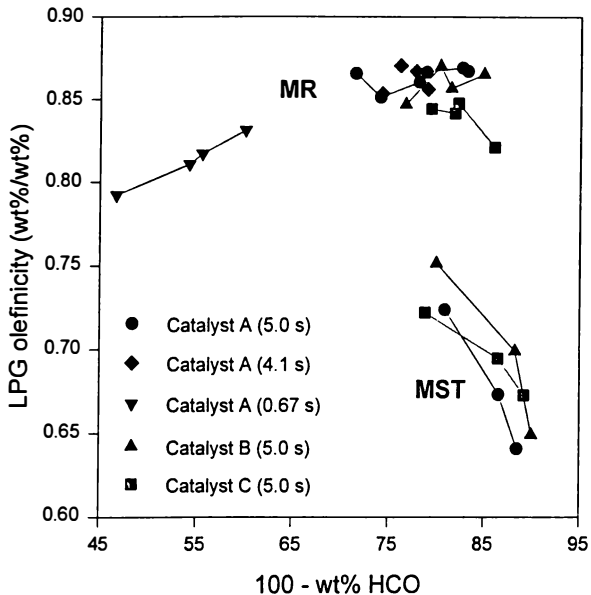


Figure 5. The LPG olefinicity versus conversion for all data sets in the Microriser (MR) and Microsimulation test (MST).

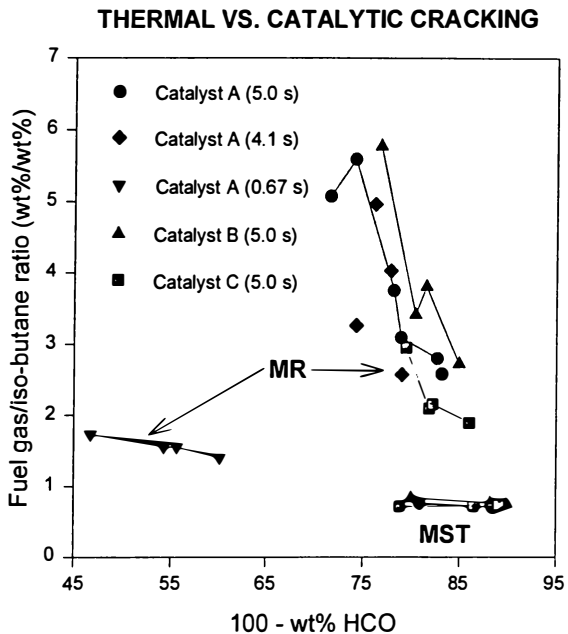


Figure 6. Ratios of fuel gas/isobutane for all experimental data obtained in the Microriser (MR) and the Microsimulation test (MST)

Coke yield. The coke yield plot in Figure 4b shows little difference between the MR and the MST data. Nevertheless, it will be shown that, in fact, the behaviour is physically quite different. When the relative amount of coke is plotted, *i.e.* the amount of coke per gram of catalyst, the difference becomes clear. Figures 7a and 7b show these data plotted against the catalyst-to-oil ratio. The MST data shows an increasing relative amount for all catalysts. This is not expected. It means that increasing the amount of catalyst at a constant amount of feed would lead to a higher coke yield per gram of extra added amount of catalyst. The MR data shows a constant or decreasing trend for all data. This is in agreement with expectations and the real life situation of an industrial cracker: additional active catalytic sites result in an equal or lesser amount of coke per weight of catalyst. Based on these observations, it is concluded that different coke build up mechanisms take place in the MR and the MST.

LCO, Gasoline and LPG yield : Secondary Cracking. Less secondary cracking and a higher LPG olefinicity was found in the case of the MR. A higher gasoline, and lower LCO and LPG yield was found for the MR indicating less secondary cracking. More saturated products signify more hydrogen transfer reactions and thus a lower LPG olefinicity. Evidently less secondary bi-molecular reactions are taking place in the MR. This is explained by the fact that the nitrogen transport gas used in the microriser suppresses the secondary bi-molecular cracking reactions. A fivefold dilution is the result of the use of the carrier gas (see Table I). Bi-molecular reactions are less likely to occur in a diluted reaction mixture.

Fuel Gas yield : Thermal vs. Catalytic Cracking. A higher ratio of fuel gas/iso-butane was found in the case of the MR, which is to be expected with a relatively low catalyst volume fraction and longer residence time of the hydrocarbons in the reactor (see Table I). With increasing catalyst fraction (or conversion) the ratio decreases due to the formation of more iso-butane. A reduction in contact time will also result in a lower ratio, because fewer thermal cracking reactions will take place.

Catalyst ranking. The MR and MST were directly compared in a catalyst ranking study. Only results for the gasoline, coke, and total gas selectivity are shown in Figure 8. Despite the scattering in the microriser data, a ranking is still possible. The MR shows catalyst **B** to have the highest selectivity for gasoline at high conversions. Based on the MST data catalyst **C** is the best. Although at first sight the differences may not seem to be large, in practice they correspond to a substantial economic margin. The same order in catalysts is found for the total gas selectivity. Catalyst **A** produces most gases in both cases. This can be a decisive factor in catalyst selection, because of the capacity limits of the gas compressor downstream an actual unit. Another crucial factor is the coke selectivity. In some cases, the regenerator temperature is limiting for the throughput of the FCC unit. Unfortunately, no clear answer can be given on the ranking with respect to coke selectivity due to a minimal overlap of data obtained at the same conversion.

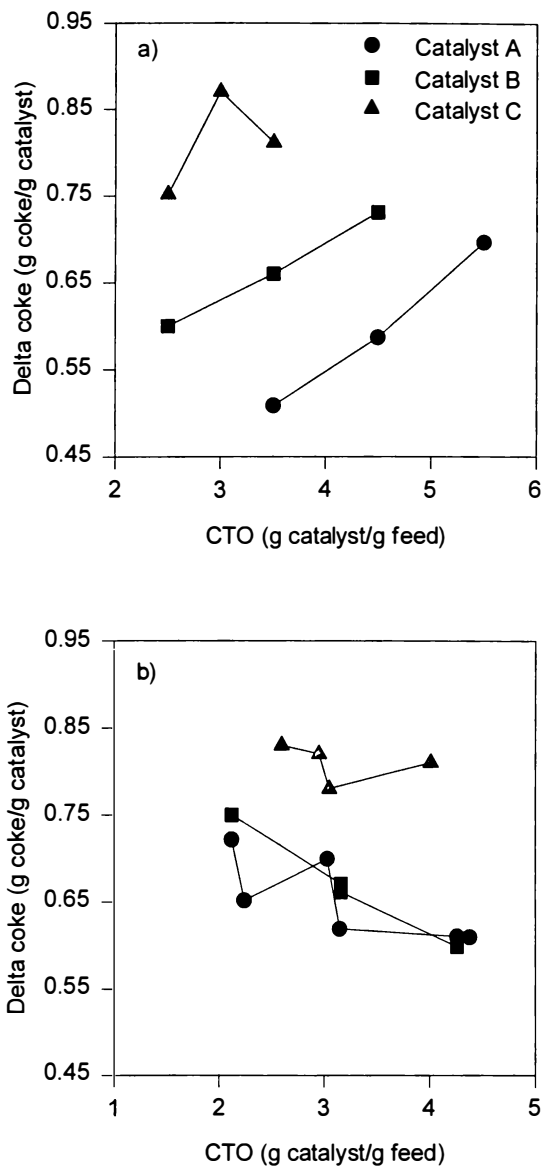


Figure 7. Coke yield as a function of catalyst-to-oil ratio for the Microsimulation test (MST, Figure 7a) and the Microriser (MR, Figure 7b)

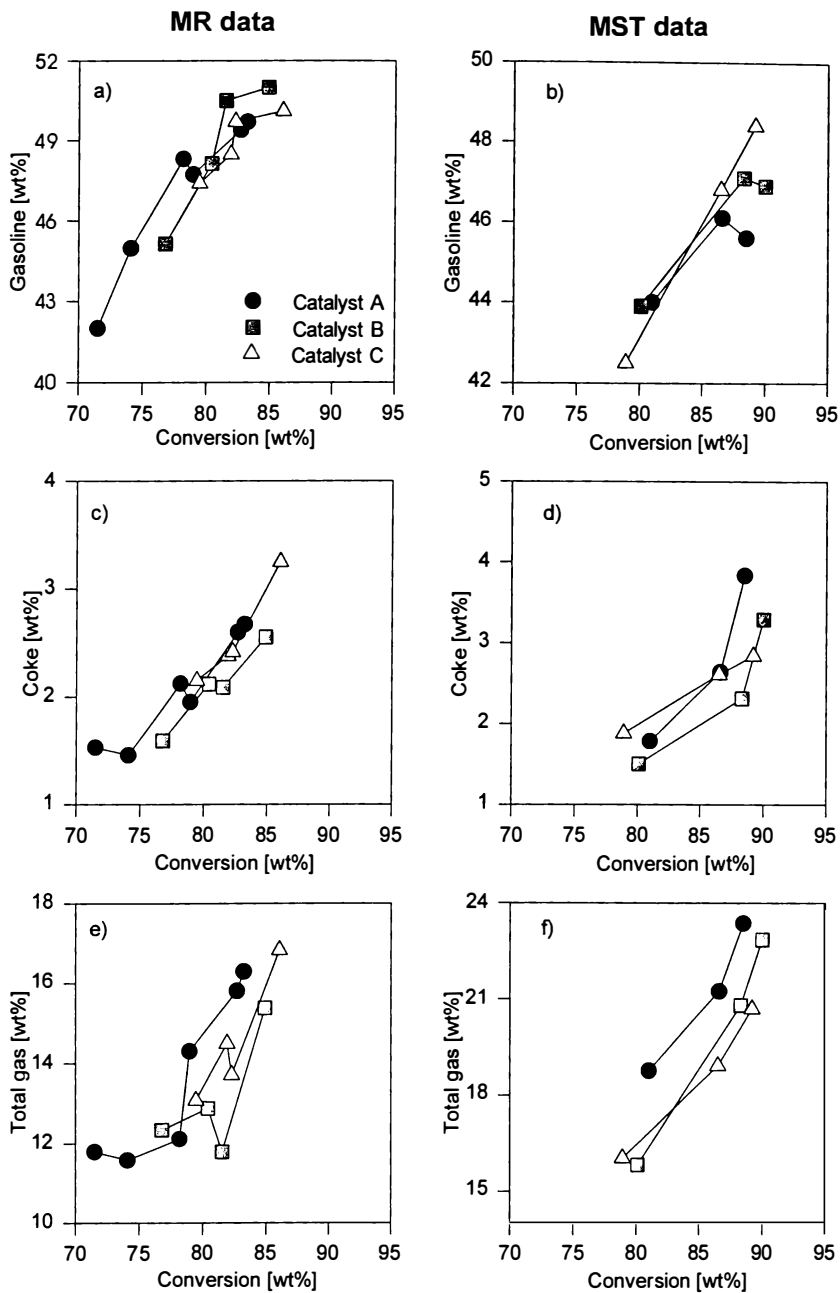


Figure 8. Gasoline (a and b), coke (c and d) and total gas ranking (e and f) for catalyst A, B, and C in both reactors.

Short contact times. A study was carried out to investigate the influence of the nitrogen carrier gas in the microriser experiments and to explore the most optimal kinetic regimes in FCC catalyst testing with the microriser. Only catalyst A was used in experiments with different contact times. Four experimental settings were used resulting in contact times of 0.67, 4.1 and 5.0 seconds (see Table III). The results of the MST experiments and the four MR data sets are shown in Figure 9. The activity plot (Figure 9a) displays the conversion behaviour of catalyst A at different contact times. The conversion found for the data obtained at 0.7 seconds contact time is much lower. The other data are in the same order of magnitude. The yield plots (Figures 9b to 9f) show the coke, LCO, gasoline, LPG, and fuel gas yield as function of the conversion. In all plots there is no significant difference between data obtained at 4.1 and 5.0 seconds. The coke yield plot shows a remarkable result. No significant difference in the coke yield is found for data at 0.7 seconds or higher. Only the MST data shows a higher coke production at higher conversions. The LCO yield at 0.7 s. differs considerably from that at higher contact times. Also the direction of the trend is changed. At higher conversions the trends are descending, while at low conversion the opposite is true. The gasoline and LPG yield plots reveal that the data at low contact time are in direct line with data at higher conversions. This indicates the validity of the data at low contact times. The fuel gas yield plot shows a much lower fuel gas production at lower contact times.

Influence of Nitrogen carrier gas. Two sets of experimental conditions were used to create a contact time of 4.1 seconds (see Table III). A striking result is that no significant difference was found with data obtained at 5.0 seconds. This implies that the catalyst is completely deactivated and no reactions take place after 4.1 seconds. The nitrogen flow does not influence the LPG olefinicity in comparison with previously described experiments (see Figure 6). As a consequence, these conditions are not the most optimal kinetic regime to carry out catalyst testing. Nothing happens anymore. The results of the experiments carried out at 0.7 seconds are also presented in Figure 9. A lower conversion of the catalyst was found indicating that not all reactions had gone to completion. The gasoline and LPG yield are on the same line as the experiments done at higher contact times. This in contrast with the other yields. The LCO yield shows an increasing trend at low conversions, but a decreasing trend at higher conversions. This is in agreement with a maximum in the LCO yield plot because of the series reaction kinetics. At first LCO is produced from HCO, but at higher contact times the cracking reactions lead to the consumption of LCO to form gasoline. The coke yield plot displays an interesting result. After 0.67 seconds there is no significant change in the formation of coke. This can be explained by a combination of three explanations. First, essentially all coke precursors in the feed have disappeared after 0.67 seconds, and therefore no more coke will be formed. A second explanation is based on the existence of multiple sites on the catalyst. If the most active sites will be deactivated by coke deposition, the remaining sites, where hardly coke deposition occurs, account for the activity left over to carry out the rest of the cracking reactions. A third cause of this phenomenon could be the initial contact of the injected feed with the fresh, hot catalyst. A local high concentration of

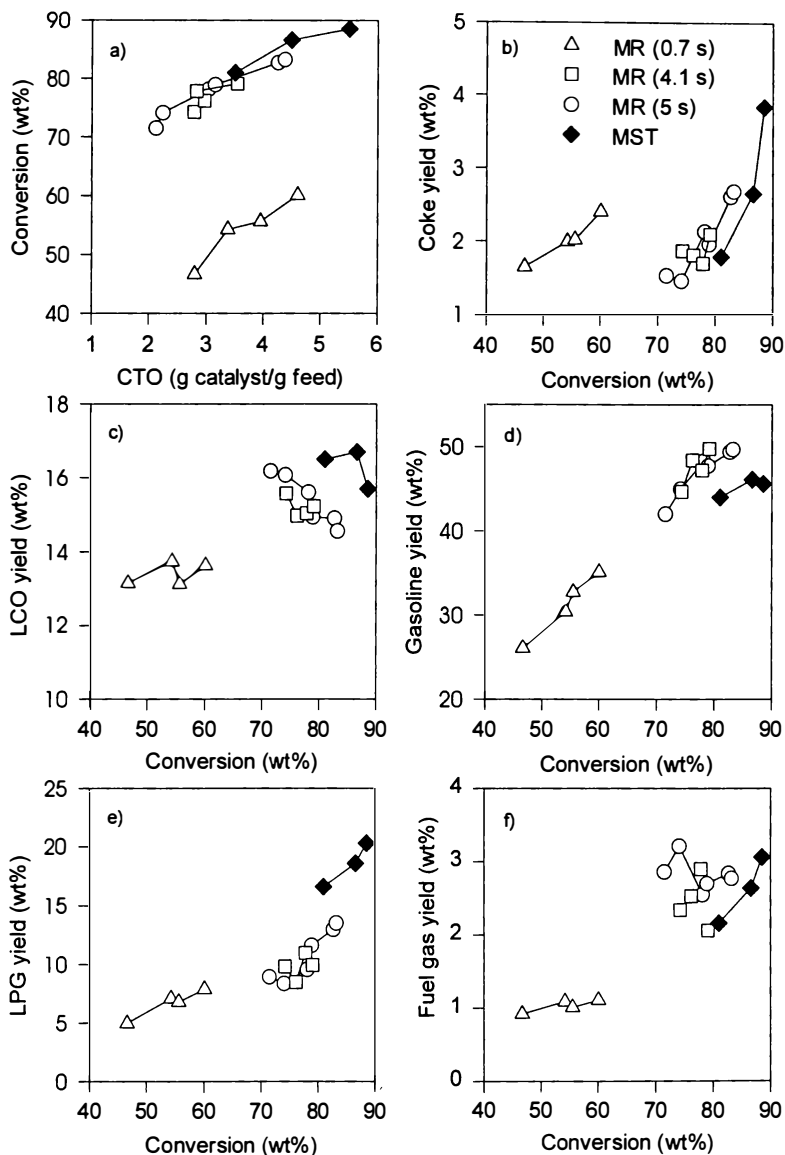


Figure 9. Experimental activity and yield plots for catalyst Δ determined with different contact times, viz. 0.7, 4.1 and 5.0 seconds, respectively.

very active catalyst and a not properly introduced feed could give the majority of the coke, while only small amounts of coke are formed during the cracking reactions.

The fuel gas yield is considerably lower because of the shorter contact time. This is also expressed in a much lower fuel gas/isobutane ratio (see Figure 6). The LPG olefinicity is in the same order of magnitude as other experiments (see Figure 5).

Conclusions

The microriser performs well and is as a riser pilot plant for FCC catalyst testing a very useful tool which provides intrinsic kinetic data. The microriser was compared with the microsimulation test with three catalysts. Significant differences in product distributions were found in the two tests. A higher LPG olefinicity and a larger contribution of thermal cracking were observed in the microriser. The catalyst carrier gas nitrogen is thought to be the main cause for less hydrogen transfer. The ranking of catalysts based on gasoline selectivity was changed with respect to the conclusions obtained from MST data. Short contact time experiments revealed deeper insight in the cracking phenomena and a kinetically more relevant time frame was explored. It is striking that coke yields at a low contact time (0.7 s) were not significantly different from those at higher contact time experiments (4 and 5 s). In fact, after about four seconds no further catalysed reaction takes place. The fuel gas yield was considerably lower. Other product yields corresponded well with trends observed at higher contact times.

Acknowledgments

The authors would like to thank Akzo Nobel Amsterdam for the feed, catalysts and analyses. In particular, the microsimulation test data are greatly appreciated and F.Olthof, E.Brevoord and P.O'Connor are thanked for the stimulating discussions. The Netherlands Technology Foundation (STW) is acknowledged for their financial support (project ACH99.1894).

Literature cited

- 1 Young, G. In *Fluid Catalytic Cracking: Science and Technology*; Magee, J.S.; Mitchell, M.M., Eds.; *Studies in Surface Science and Catalysis*, Elsevier, Amsterdam, **1993**, Vol. 76, pp. 257
- 2 Sapre, A.V.; Leib, T.M.; In *Fluid Catalytic Cracking II: concepts in Catalyst design*; Occelli, M.L., Ed.; ACS symposium series **1991**, Vol. 452, pp. 144
- 3 Occelli, M., In *Fluid Catalytic Cracking II: concepts in Catalyst design*; Occelli, M.L., Ed.; ACS symposium series **1991**, Vol. 452, pp. 343
- 4 Corma, A.; Palomares, A.E.; Rey, F., *Appl. Catal.* **1994**, B **4**, pp. 29
- 5 Elia, M.F.; Iglesias, E.; Martinez, A.; Perez Pascual, M.A., *Appl. Catal.* **1991**, **73**, pp. 195

- 6 Mitchell, M.M.; Hoffman, J.F.; Moore, H.F., *In Fluid Catalytic Cracking: Science and Technology*; Magee, J.S.; Mitchell, M.M., Eds.; *Studies in Surface Science and Catalysis, Elsevier, Amsterdam, 1993, Vol. 76*, 293
- 7 Wagner, M.C., Humes W.H., Magnabosco L.M., *Plant/Operations Prog.* **1984**, 3(4), 222
- 8 Kraemer, D.W.; deLasa, H.I.; *Ind.Eng.Chem.Res.* **1988**, 27, pp. 2002
- 9 Chen, N.Y.; Lucki, S.J.; *Ind.Eng.Chem.Process.Des.Dev.* **1986**, 25, pp. 814
- 10 Moorehead, E.L.; Margolis, M.J.; Mclean, J.B., *ACS symposium series 411 (1989)*, pp. 120
- 11 O'Connor, P.; Hartkamp, M.B., *ACS symposium series 411 (1989)*, pp. 135
- 12 Rawlence, D.J.; Gosling, K., *Appl. Catal.* **1988**, 43, pp. 213
- 13 Horsley, D.M.C.; Rothwell, E., *Powder Tech.* **1972**, 6, pp. 117
- 14 Humes, W.H., *Chem.Eng.Progr.* **1983**, 2, pp. 51
- 15 Helmsing, M.P.; Cybulski, A.; Makkee, M.; Moulijn, J.A., AICHe National Spring meeting, Alanta, 17-21 April **1994**, pp. 51d

Evaluation of Coke Selectivity of Fluid Catalytic Cracking Catalysts

E. Brevoord, A. C. Pouwels, F. P. P. Olthof, H. N. J. Wijngaards, and Paul O'Connor

Akzo Nobel Catalysts, Nieuwendammerkade 1–3, P.O. Box 37650, 1030 BE Amsterdam, Netherlands

In resid cracking the high feed metals and Conradson Carbon Residue (CCR) require careful consideration when assessing both catalyst design and performance evaluation. This paper addresses the issues of the latter with respect to coke, delta coke and catalyst deactivation.

Overall, evaluation of catalysts on resid feedstocks requires sophisticated and well integrated catalyst deactivation, catalyst stripping and cracking systems. It is important to determine not only the coke yield, but each of its components (Catalytic coke, contaminant coke, CCR coke and stripper (soft) coke). This paper provides details on how each of the components of the coke yield may be experimentally determined using catalyst metallation by cyclic deactivation, catalyst strippability measurements and modified catalytic cracking techniques.

In fixed-bed catalytic cracking tests the proper decreasing delta coke response as catalyst-to-oil is increased is possible if a constant catalyst load and a constant feed injection rate are maintained. As CCR increases above 4 wt%, however, fixed-bed cracking methods are suspect because the mass balance drops significantly and the cracking performance can be measured better using other techniques (e.g.s., circulating pilot plants or fluidized-bed reactors).

Introduction: Resid cracking and delta coke.

Since the early 80's the number of FCCU's processing resids has increased dramatically. New units are being built, designed for processing 100% atmospheric resid with a conradson carbon residue content up to 10%. Many units

are revamped to allow processing heavy feed. One of the major modifications is the implementation of a catalyst cooler, allowing a higher coke yield.

When processing resid, coke formation is often a major limit (1). Problems associated with processing heavy resid feeds are (1,2):

1. Poor atomization and vaporization of high boiling components.
2. More irreversible deactivation (hydrothermal, metals), if the feed is not hydrotreated.
3. A quick reversible deactivation in the riser through the adsorption and deposition of polars and coke, which are burnt off in the regenerator.

The types of coke formed in Resid FCC can be classified based on the length of time needed for their formation. Conradson carbon residue (CCR) coke will form nearly instantly at the inlet of the reactor and is therefore also called "entrance coke". The second type of coke is formed by the adsorption of highly aromatic and basic materials on even weakly acidic surfaces; this process also occurs rapidly. A part of the adsorbed polars can be stripped off, but still causes reversible deactivation. Finally, reaction or catalytic and dehydrogenation coke will form which are the slowest coke forming processes. Consequently, the relative importance of non reaction coke will increase in resid operations with a short contact time riser. In order to correctly evaluate the coke selectivity of a catalyst, it is necessary to distinguish between the types of coke made. In what follows we will also distinguish between hard and soft coke, whereby the hard coke is the coke after a long period of ideal stripping and the soft coke the difference between total and hard coke.

In summary, coke consists of several components (3):

1. Feed conradson carbon residue (CCR) coke.
2. Non strippable additive coke, being adsorbed aromatics and polars (AC).
3. Reaction or catalytic coke (RC).
4. Dehydrogenation or contaminant coke, caused by metals (DHC).
5. Soft coke (SC), being:
 - adsorbed hydrocarbons
 - trapped hydrocarbons caused by pore mouth blocking
 - hydrocarbons entrained in interstitial spaces

In this paper we tackle the issue on how to test and evaluate resid catalysts in respect to their coke make, consisting of:

$$\text{Coke} = \text{CCR} + \text{AC} + \text{RC} + \text{DHC} + \text{SC}$$

How to determine reaction or catalytic coke.

For light feedstocks and low metals operations, determining the coke selectivity by making use of yields from a Micro Activity Test (MAT) is generally the preferred route. Several modifications of the test and test procedures, for

instance the Micro Simulation Test (MST), have been proposed for improved relevancy of the test results (4, 5, 6).

In MAT/MST the conversion is usually varied by changing the cat/oil ratio, which is realized by varying either:

1. The amount of catalyst in the reactor and injecting a constant amount of feed
- or:
2. The amount of feed, increasing the feed flow at a constant feed injection time and catalyst content

Contrary to commercial performance, this results in an increase in delta coke versus cat/oil ratio. Catalytic coke yield (% on feed) is expected to be proportional with cat/oil ratio. Consequently that delta coke should remain constant or drop:

$$\begin{aligned} \text{Delta coke} &= \text{coke yield} / \text{cat/oil ratio} = (\text{CCR coke} + \text{catalytic coke}) / \text{cat/oil ratio} \\ &= (a + b * \text{cat/oil ratio}) / \text{cat/oil ratio} = a / \text{cat/oil ratio} + b \\ &\quad (a, b \text{ are constants}) \end{aligned}$$

Moreover, often catalyst ranking reverses with changing cat/oil ratio, especially if yields are evaluated at constant coke yield. This phenomena can be explained with the increasing pressure in the MST reactor, when the catalyst bed height is increased, as illustrated in figure 1. Pressure affects bimolecular reaction rates and consequently higher reactor pressures result in more hydrogen transfer and coke formation. Figure 2 shows that a good correlation exists between coke make and hydrogen transfer, a high LPG olefinicity being a sign of low hydrogen transfer.

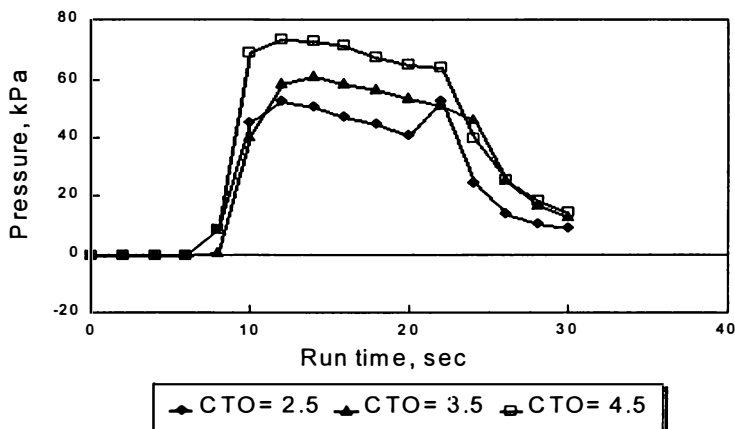


Figure 1. Impact cat. bed height on pressure in MST

To simulate a commercial unit, it would be better to have the same pressure profile for different cat/oil ratios. In table 1 and figure 3 is shown that delta coke drops slightly with increasing cat/oil ratio, if variable feed injection is applied, keeping the catalyst bed height and feed flow rate constant. To change cat/oil the amount of feed and feed injection time is varied.

The consequence of variable feed injection is that the liquid contact time varies with cat/oil ratio. This can be circumvented by injecting a fixed amount of feed in fixed time, and varying the amount of catalyst as is done traditionally, and keeping the catalyst bed height constant by adding inerts. This is a good method to obtain a constant pressure, but is a rather laborious testing method as quantities of catalyst and inerts must be weighted in accurately.

Table 1. MST results using different methods to increase cat/oil ratio

<i>Case</i>	<i>Lower bed height</i>	<i>Base</i>	<i>Const. bed height</i>
Cat/oil (t/t)	3.5 ---->	4.5	<---- 3.5
Cat. bed (gram)	3.5	4.5	4.5
Feed pumping time (sec)	15	15	19
Conversion (wt%)	69.6	74.0	72.3
Coke yield (wt%)	3.39	4.85	3.82
Delta coke (wt%)	0.97 --->	1.08	<--- 1.09

How to determine dehydrogenation or contaminant coke

The performance of a commercial FCCU is affected by the equilibrium catalyst quality, which is a mixture of particles with a wide age distribution. The average catalyst residence time in the FCCU measures up to several months, during which time the particles undergo thousands of regeneration cycles. Traditionally this was simulated in the laboratory by a simple steaming of fresh catalyst at elevated temperatures to accelerate the hydrothermal aging which occurs in a commercial operation. A wide range of steaming conditions are applied worldwide, all attempting to match some major catalyst properties like MAT activity, unit cell size and/or surface area. In addition, the metal resistance of cracking catalysts is often studied by metal impregnation, followed by calcination and steaming. The result is a homogeneous metals distribution throughout the catalyst particle. The metals in a FCC unit mainly deposit on the

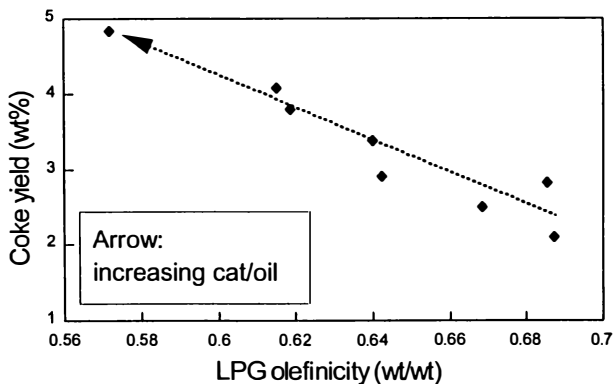


Figure 2. Impact of hydrogen transfer on coke make yields at various cat/oil ratio's

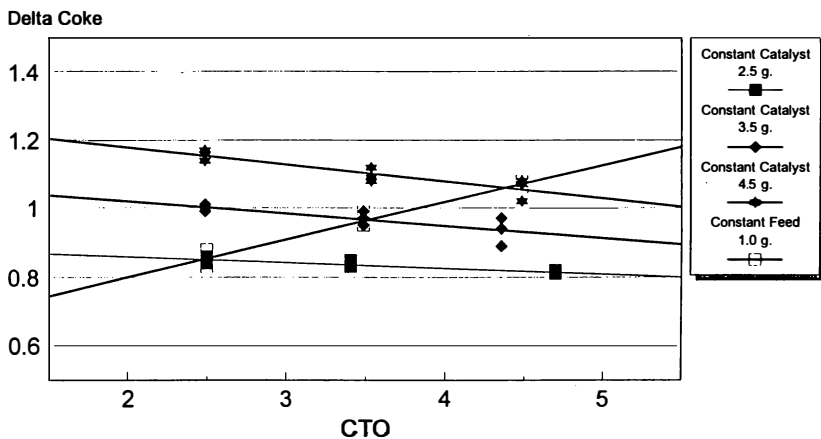


Figure 3. Constant feed versus constant catalyst

external catalyst surface. Through migration, vanadium distributes itself gradually over the catalyst, but nickel remains predominantly on the outer surface. The catalyst to metal interaction obtained will be completely different for the two deactivation conditions. Pore plugging by metals will only be observed for the heterogeneous distributed metal. Also, in the regenerator the oxidized form of vanadium (V₂O₅) is mobile in the presence of steam, while in the reactor vanadium is reduced and much less destructive.

The MAT and MST can be effectively utilized to study the effect of metals deactivation and deactivation conditions on delta coke. We can demonstrate for instance, that nickel has a considerable dehydrogenation activity and that fresh, homogeneously distributed nickel is much more active than nickel, deposited on the external surface of the catalyst particle. Therefore the hydrogen and coke yield are much higher for a deactivated catalyst after a pore volume impregnation method than for cyclic deactivation (see table 2). The cyclic deactivation (CD) unit consists of a fixed fluidized bed reactor, in which the catalyst is deactivated during repeated cycles of cracking, stripping and regeneration (for test procedures, see ref.7). As a result the catalyst is aged during a number of alternating cycles of reduction and oxidation (Redox cycles).

Table 2. MST performance of Ni-deactivated catalysts

<i>Deactivation</i>	<i>Comm.</i>	<i>Cyclic Deact.</i>	<i>Pore</i>
Nickel, ppm	4634	4907	5164
Vanadium, ppm	223	1111	1037
<u>Yields at conv = 68%</u>			
H ₂ /C ₁ , vol/vol	3.1	2.8	5.6
Coke, wt%	2.7	3.1	4.4

The possibility to evaluate the coke selectivity of metal resistant catalyst has been essential for the development of resid catalyst. In table 3 the coke yields are given for two catalysts after different deactivation conditions. The equilibrium catalyst originates from an unit switching from the base catalyst to the improved version. A considerable improvement in coke selectivity was observed, reducing the regenerator temperature 10°C at 40% change out of the catalyst inventory.

Table 3. MST results:Coke yield at 68% conversion after several deactivations

<i>Catalyst</i>	<i>Base</i>	<i>Improved</i>
E-cat (3000/5800 ppm Ni/V)	3.5	3.2 (at 40% change out)
Steam Deactivation (5 hrs, 788°C, no metals)	2.1	2.0
Mitchell method (1500 ppm Ni)	2.3	2.1
Cyclic Deactivated (5000/1000 ppm Ni/V)	2.8	2.2

The MST is a very suitable test to measure the nickel and vanadium tolerance of properly deactivated resid catalysts (8). Clear differences in hydrogen and coke make, as well as activity maintenance are observed. That test conditions play an important role, is shown in figure 4, being the result of testwork on a great variety of resid catalysts, being suitable for high bottoms conversion. All grades have a high matrix activity and have been cyclic deactivated to 6000 ppm Ni+V, creating a high dehydrogenation activity. For this test program, the high dehydrogenation activity resulted in a high H₂ make, increasing the volume of wet gas with approximately 50%, compared with a standard, no metal tests. This results in a considerable increase in back pressure. Consequently the coke make at constant conversion strongly depends on the activity of the catalyst, or, the cat/oil ratio at which a certain conversion is obtained. Moreover, at low cat/oil ratio's the MST reactor contains less catalyst, and consequently less active metal (Ni+V) sites are available, affecting dehydrogenation activity. In the pilot riser this trend in coke selectivity is not observed. In the pilot riser a constant pressure can be maintained for all catalysts and operating conditions. Consequently we recommend to test catalysts having a high metals content at a constant pressure. This can be achieved through variable feed injection in MST, or by using a reactor with a fluidized bed.

How to determine Conradson carbon coke

Conradson carbon coke deposits shortly after feed introduction. If high conradson carbon feed is processed in a MST unit, coke will deposit shortly after feed introduction. As the MST reactor consists of a fixed bed reactor, the feed will still meet clean catalyst after passing the first zone, where CCR coke deposits. Consequently the mechanism is different compared to commercial units. It can also be shown that material boiling above the MST reactor temperature does not leave the reactor, resulting in a low mass balance (9, 10). Therefore it is recommended to test high CCR feeds ($CCR > 4-5\%$) in a fluidized bed system or in a riser unit.

One of our pilot riser units (PRU) is a modified Arco FCC design. When processing resid feedstocks, problems were encountered with coke formation in the reactor riser. Consequently the feed injection system was modified, allowing feed CCRs of 10% or more. To get a better insight of what is happening in the bottom of the riser, the vaporization time was calculated in a similar way as described by Buchanan (11). We conclude that the time to vaporize the feed depends mainly on the oil droplet size after atomization. For a droplet size of 100 micrometers, less than 10 milliseconds is required to vaporize 75% of the feed, being sufficient for our purposes. Though the catalyst return temperature does not seem of great importance for the vaporization time, it does of course affect the percentage of feed which is vaporized and thus the percentage of liquid cracking that is taking place.

Test results have shown so far that coke make is very sensitive to dehydrogenation activity, when processing high CCR feed, using catalysts with high nickel and vanadium. In figure 5 is shown how the coke make relates to dehydrogenation activity.

As CCR coke deposits immediately after feed introduction and no catalytic cracking is required for CCR coke deposition, we can distinguish between CCR coke and other types of coke by extrapolating the coke yield to $cat/oil\ ratio = 0$ (12) (figure 6). As expected the CCR coke mostly depends on the feed CCR. From figure 7 it can be calculated that more than 100% of feed CCR is converted to coke. This was caused by too much backmixing and too low temperature of the catalyst/feed mixing zone. By improving the design of the feed inlet, the percentage of CCR converted to coke dropped to 80-85%, being much closer to commercial practice.

How to determine soft delta coke

The hydrocarbons which are entrained or adsorbed by the catalyst and are not stripped off before the catalyst enters the regenerator, will clearly contribute to the total delta coke. Fast and effective stripping will therefore be essential in

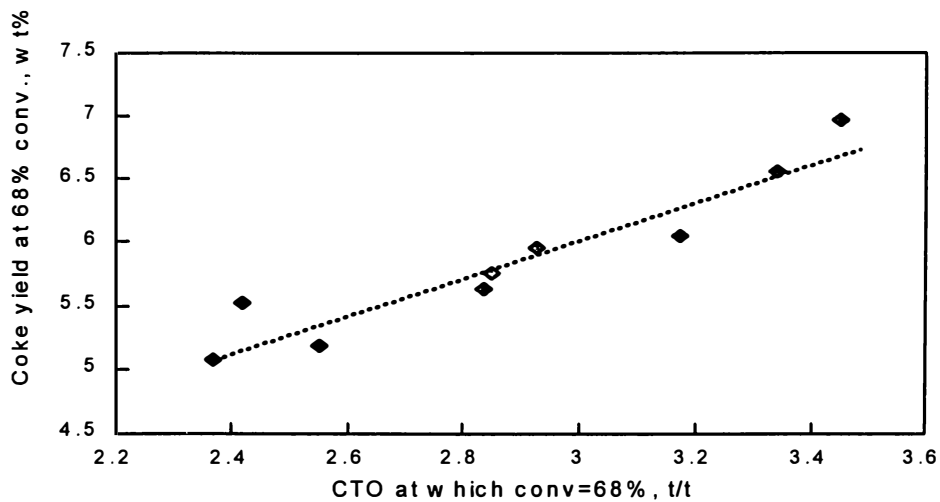


Figure 4. Dehydrogenation coke

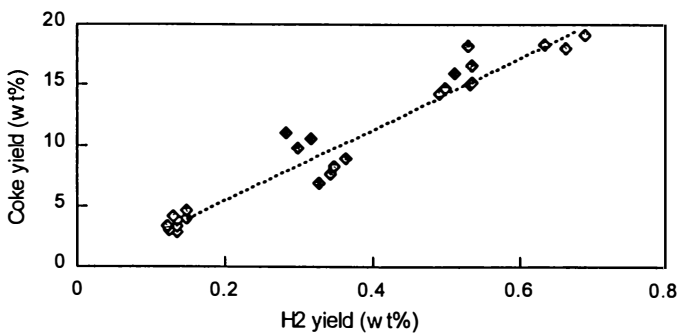


Figure 5. Dehydrogenation activity in PRU

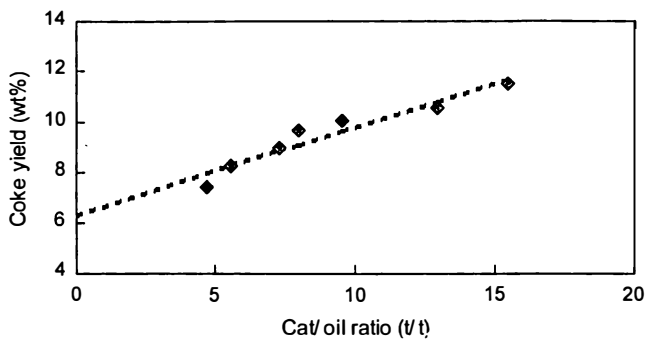


Figure 6. Determination of CCR coke

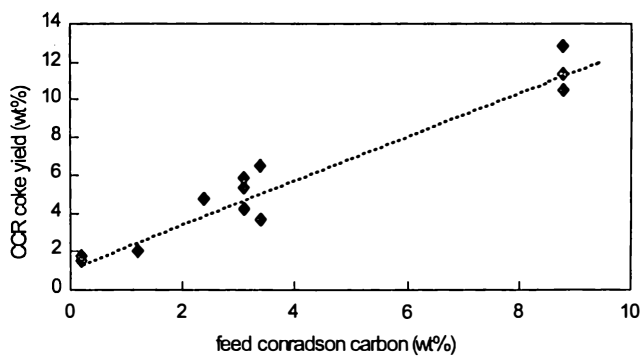


Figure 7. CCR coke (Pilot riser results)

order to minimize the soft delta coke. Akzo Nobel has developed a strippability test which can be performed during the stripping stage in a cyclic deactivation unit (3,7). The cyclic deactivation unit consists of a fixed fluidized bed. After feed introduction and coke deposition, the catalyst is stripped with nitrogen at reactor temperature and the catalyst coke content is monitored with time (figure 8). The coke removed during stripping is considered to be soft coke, the remaining coke is hard coke. The rate with which the coke content drops is a measure for the catalyst strippability. The curves obtained can be described well by first order kinetics:

$$\text{Coke}(t) = C_{\text{hard}} + C_{\text{soft}} \times \exp(-K_s \times t), \text{ or:}$$

$$d\text{Coke}(t)/dt = -K_s \times (\text{Coke}(t) - C_{\text{hard}})$$

$\text{Coke}(t), \text{ wt\%} =$ function for coke content vs time

$K_s, \text{ sec}^{-1} =$ stripping rate

The $K_{s,50}$ shown in the tables is calculated with the formula:

$$K_{s,50} = (\text{Coke}(50) - \text{Coke}(100)) / (\text{Coke}(100) - C_{\text{hard}}) / 50$$

$\text{Coke}(50), \text{ wt\%} =$ coke yield after 50 sec stripping

$K_{s,50}, \text{ sec}^{-1} =$ stripping rate

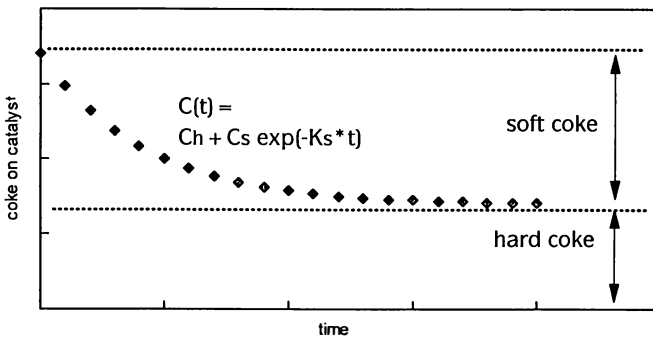


Figure 8. Soft coke

Table 4. Impact of accessibility on strippability

<i>Catalyst</i>	<i>A</i>	<i>B</i>	<i>C</i>
Accessibility	high	high	low
Y content	low	high	highest
MST activity (wt%)	70	68	69
C hard (wt%)	0.76	0.67	0.69
C soft (wt%)	0.49	0.71	0.69
$K_{s,50} * 1000$ (sec ⁻¹)	9.4	12.0	9.0

Our investigations show that catalyst composition and architecture can have a significant effect on the initial quantity of adsorbed hydrocarbons, i.e. soft delta coke, as well as on stripping rate (table 4). A high zeolite content usually results in a high soft coke make, but not necessarily in a low stripping rate (cat. A vs B). At a constant activity, hard and soft coke make, the stripping rate increases with accessibility (cat. B vs C).

In some cases it was hard to find a good explanation for the stripping behavior, based on the physical properties of the catalyst. We presumed that this was caused by catalytic properties, as soft coke may be converted to hard coke during the cracking and stripping stage. Therefore the same catalyst was tested after various steaming severities. As steaming also has an impact on physical properties, the activity of the catalyst was also reduced by depositing some hard coke on the catalyst prior to the test (=precoke). The results in tables 5&6 show that active catalyst indeed converts soft coke to hard coke. At low conversion levels, more heavy molecules are available, and thus the soft coke content is higher.

Table 5. Impact of steaming severity on strippability

<i>Steaming time (hrs)</i>	<i>C hard+soft (wt%)</i>	<i>C-hard (wt%)</i>	<i>C-soft (wt%)</i>	$K_{s,50} * 1000$ (sec ⁻¹)	<i>MST act. (wt%)</i>
2	1.73	1.04	0.69	9.3	73.9
5	1.72	0.85	0.87	14.4	72.0
17	1.68	0.51	1.17	15.8	66.3

Table 6. Impact of pre-coke on strippability

<i>Pre-coke (wt%)</i>	<i>Hard Coke deposited (wt%)(*)</i>	<i>C-hard (wt%)</i>	<i>C-soft (wt%)</i>	<i>K_{s,50} *1000 (sec⁻¹)</i>	<i>MST activity (wt%)</i>
0	0.85	0.85	0.87	14.4	72.0
0.32	0.72	1.04	1.20	14.9	71.8
0.54	0.61	1.15	1.40	12.8	70.8
0.87	0.49	1.36	1.75	12.5	66.6

(*): Hard Coke deposited = C_{hard}- pre coke

The stripping rate shows an optimum versus the pre-coke content (table 6). Pre-coke reduces activity, increasing stripping rates similar to the trends shown in table 6. An explanation for the lower stripping steam rates at high pre-coke levels might be that pore mouth blocking reduces stripping rates.

Conclusions and recommendations

For obtaining a good impression of the coke selectivity of resid catalysts, all contributions to the total coke make must be determined properly:

Reaction or catalytic coke: Can be measured properly in MST if a constant pressure profile is maintained. This can be achieved by using a constant catalyst bed height and constant feed injection flow rate.

Dehydrogenation coke: Representative deactivation of fresh catalyst to obtain the equilibrium catalyst properties is required. The cyclic deactivation unit allows deposition of metals on the outer surface. Aging of the metals and catalyst takes place via many alternating reduction / oxidation cycles, resulting in a much better simulation of the deactivation in a commercial unit and a more realistic interaction between metals and catalyst. Also for determining the dehydrogenation coke in MST, a constant pressure profile is essential.

Conradson carbon coke: Catalyst testing with very high CCR feedstocks can be done successfully in a fluidized bed system, if the feed is introduced properly. MST can be used for feedstocks with a CCR up to 4-5%. The contribution of CCR coke can be calculated by extrapolation to cat/oil ratio=0.

Soft coke: The contribution of soft coke can be determined in the cyclic deactivation unit. The soft coke make depends both on physical and chemical properties, such as activity and catalyst accessibility. The initial soft coke is expected to increase with the zeolite content, stripping rates are higher for the very accessible catalysts.

References

1. Mauleon, J.L., Sigaud, J.B.,
"Characterization and selection of heavy feeds for upgrading through FCC", 12th World Petroleum Congress, Houston 1987, John Wiley & Sons Ltd.
2. O'Connor, P., Gevers, A.W., Humphries, A.P., Gerritsen, L.A., Desai, P.H.,
"Concepts for Future Residuum Catalyst Development, ACS Symposium Series 452, Washington 1990.
3. O'Connor, P., Yanik, S.,
"Resid FCC operating regimes and catalyst selection", Akzo Catalyst Symposium 1994
4. Mauleon, J.L., Courcelle, J.L., *Oil&Gas J.*, Oct.21 1985, p. 64
5. O'Connor, P., Hartkamp, M.B.
"A Microscale Simulation Test for FCC", ACS Symposium Series 411, Washington 1988.
6. Moorehead, E.L., Margolis, M.J., McLean, J.B.,
"Evaluation of FCC Catalysts", ACS Symposium Series 411, Washington 1988.
7. Gerritsen, L.A., Wijngaards, H.N.J., Verwoert, J., O'Connor, P.,
Catalysis Today, 11, 1991.
8. O'Connor, P., Pouwels, A.C., Wilcox, J.R.,
"Evaluation of Resid FCC catalysts", paper 242E, Nov.1992, AIChE Annual meeting.
9. Pouwels, A.C., Olthof, F.P.P., Wijngaards, H.N.J.,
"A Review of FCC Catalyst Testing", Akzo Nobel Catalysts Symposium 1994, p. 25.
10. Ho, T.C.,
"Study of coke formation in resid catalytic cracking", *Ind.Eng.Chem.Res.* 1992, vol. 31, no. 10.
11. Buchanan, J.S.,
"Analysis of heating and vaporization of feed droplets in FCC Risers", *Ind.Eng.Chem.Res.*, 33, 1994, 3104.
12. Fisher, I.P.,
"Residuum catalytic cracking: influence of diluents on the yield of coke", *Fuel* April 1986, vol. 65.

Correlation of Catalyst Performance Between Laboratory Tests and Commercial Units for Hydrotreating Residual Oil

Yoshimitsu Miyauchi¹, Takeshi Hashiguchi^{1,3}, Naoto Kimbara², and
Katsuhisa Fujita²

¹Nippon Ketjen Company Ltd., Sumitomo Fudosan Shiba, Number 2
Building, 5-9 1-chome, Shiba, Minato-ku 105, Japan

²Research and Development Center, Niihama Division, Nippon Ketjen
Company Ltd., 17-4 Isoura-cho, Niihama-shi, Ehime 792, Japan

70 lbs/ft²·hr (0.10 kg/m²·s) in minimum as liquid mass velocity utilized in a pilot plant test and a correction method involving mainly effects of feedstock properties on desulfurization activity are proposed to get better agreement in evaluating aging performance and cycle length of a catalyst system with multiple catalysts between pilot and commercial units.

Catalyst lives were compared with reactor metal distribution, obtained from micro, pilot and commercial units. It was found that a micro reactor with low liquid mass velocity caused metal pass-through to down stream catalysts, resulting in a shorter life of catalyst system than that in the commercial operation. Therefore in this paper, effects of liquid mass velocity and feedstock properties on catalyst aging performance of the catalyst system are discussed.

The role of resid desulfurization units introduced into Japan in the latter half of the 1960s has changed to the feed pretreatment for resid fluid catalytic cracking (RFCC) and the mild resid hydroconversion as well as the desulfurization of heavy oil since the oil crises.

Resid hydrotreating catalysts, developed in 1987 have been used together with a scale-and iron-removing catalyst for (1) the cracking and desulfurization of atmospheric residue, (2) the pretreatment of RFCC and (3) the cracking of vacuum residue. Approximately 7000 tons of industrial catalysts have been used in commercial units so far.

A qualitative criterion for simulation of an industrial reactor on laboratory

³Current address: Akzo Nobel Chemicals Pte. Ltd., 510 Thomson Road, Number 15-01/02
SLF Building, Singapore 1129

scale has been discussed by Mears(1), Gierman(2) and Sie(3) etc. It is reported to be a satisfactory agreement between activities found in laboratory test and in commercial operation. However, these activity data for the comparison were generally obtained from an initial period of catalyst cycle length. This paper discusses the correlation of catalyst aging performance and cycle length as a function of on-stream time (or metal deposition on catalysts) between laboratory tests and commercial operations for resid hydrotreating with fixed catalyst beds and with multiple catalyst grades.

Correlation in Catalyst Life between Laboratory and Commercial Units

Catalyst Testing Units. The catalyst aging performance and cycle length by a laboratory-test unit does not always agree with that by a commercial unit with fixed catalyst beds. The comparison of various factors between the tests and commercial units is shown in Table I. Both units are mainly different from each other in the following points:

- a) Differences inherent in the laboratory-test units and the commercial units including liquid mass velocity, the performance of oil distributor and the temperature distribution in the reactor.
- b) Difference in the properties of feedstock caused by changing the feed origin and mixing ratios of the various resid in the commercial unit from in the test units.

Particularly in the test units, the resistance of liquid film is high and the oil diffusion rate into the catalyst pore is low due to the velocity approximately 1/100 to 1/10 as low as that in the commercial unit, thereby decreasing the reaction efficiency. Satterfield(4) reported that the reaction efficiency was increased by increasing the liquid mass velocity, reaching the desirable mass velocity of 2000 lbs/ft² hr (2.7 kg/m²s).

For correcting the shortcoming of the low liquid mass velocity in the test units, an oil upflow method and a dilution method of catalyst beds for substantially increasing the flow rate of feed oil on the surface of catalyst particles by filling the void in the catalyst beds with inert particles were proposed(5)(6). The contacting efficiency of feed and catalyst particles can be improved by the upflow method of the feed. Although the dilution method is useful for the test of the fraction lighter than the vacuum gas oils, it has shortcomings that metals contained in the feedstock are deposited on the surface of inert particles, so the demetallization activity cannot be sometimes exactly determined, and that the long-term life test of a catalyst system has to be frequently discontinued due to pressure drop built up in the reactor. The aging performance test has, therefore, to be made by the downflow method of feedstock without diluting the catalyst beds.

Relationship between Liquid Mass Velocity and Catalyst Life. The laboratory test units were operated with a catalyst system composed of demetallization and

desulfurization catalysts, to hydrocrack Iranian Heavy (IH) and Arabian Heavy (AH) atmospheric residue at high temperature. Almost the same catalyst system was used in a commercial unit. The distributions of vanadium and nickel deposited on the spent catalysts in the laboratory and the commercial reactors are illustrated in Figure 1. The axis of ordinate is graduated in a relative value calculated by dividing metal content deposited on the catalyst at a specified position by the average metals on the whole spent catalysts. The properties of feedstock and the operating conditions are shown in Table II and III, respectively.

Figure 1 reveals that the metals are removed by the upstream catalyst in the commercial reactor, while it is removed by the downstream catalyst as well as by the upstream catalyst in the micro-reactor because of low liquid mass velocity.

Figure 2 illustrates the relationship in the micro-, pilot- and commercial reactors between the desulfurization activities and metal on catalysts (MOC). In the micro-reactor, the metal which cannot be sufficiently removed by the upstream catalyst due to low liquid mass velocity deactivated the downstream desulfurization catalyst, thereby shortening the life of the catalyst system.

It is, therefore, required to hydrotreat the feedstock at a liquid mass velocity above a certain level to evaluate the life of the catalyst system in the resid hydrotreating. This level is proposed to be more than 70 lbs/ft²hr (0.10 kg/m²s) at which the pilot test was done.

Correlation of Catalyst Performance between Pilot and Commercial Operations

Since different origins of resid feedstock are hydrotreated in the commercial fixed bed unit, an issue how to correct the commercial result is raised to compare them with pilot test results. The difference in the liquid mass velocity and the oil distributor efficiency between the pilot and commercial units is another important issue for determining the correlation between both units. The performance of catalyst was, therefore, evaluated under the normalized conditions applicable to the results of both units.

Assuming that the correction with the feedstock properties includes all the differences between the pilot and commercial unit, and that each commercial unit has the optimum correction equations with the feedstock properties, pilot test results obtained at a liquid mass velocity of above 70 lbs/ft²hr and commercial results were corrected with the feedstock properties to get the optimum correlation between two.

Properties of Feedstock and Desulfurization Reactivity. Various feedstocks were hydrotreated through the pilot reactor under the constant desulfurization conditions to determine the reaction temperature required for 0.27 wt% sulfur product. The relationship between the contents of various impurities in the feedstock and the relative reaction temperature are illustrated in Figure 3 to 6. The feedstocks to be tested are atmospheric residue (AR) of AM, AH, Upper

Table I. Comparison of Laboratory and Commercial Units

	Laboratory unit	Commercial unit
• Scale factors		
Catalyst volume	5 ~ 1,000cc	100 ~ 1,600 m ³
Reactor diameter	10 ~ 30 mm	3 ~ 4 m
Catalyst bed length, m	0.1 ~ 4	10 ~ 130
Linear velocity, m/hr	0.1 ~ 0.6	5 ~ 13
Superficial liquid mass velocity, lbs/ft ² hr	30 ~ 300	1,200 ~ 2,300
kg/m ² ·S	0.04 ~ 0.40	1.6 ~ 3.1
• Quench	No	Yes
• H ₂ supply	Once through	Recycle
• Reactor temperature	Isothermal	Non isothermal
• Oil distributor	Distributed by inert balls	Yes
• Feed origin	Constant	Variety
• Type of oil flow	Down or up	Down

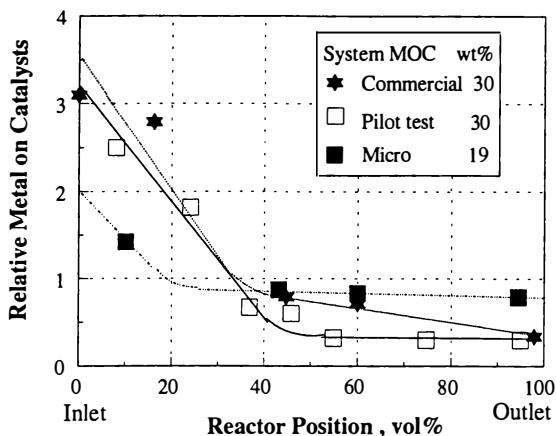


Figure 1. Reactor Metal Distribution of Spent Catalysts

Table II. Properties of Feedstocks

Feedstock	Mainly Iranian Heavy Atmospheric Residue	Mainly Arabian Heavy Atmospheric residue
Density , g/cc@15° C	1.00	1.01
Viscosity , cst@50° C	12,600	26,700
Sulfur , wt%	3.5	4.6
Vanadium , ppm	202	116
Nickel , ppm	62	41
Con. carbon residue, wt%	16	18

Table III. Process Conditions for Catalyst Performance Evaluation

Unit type	Micro reactor	Pilot reactor	Commercial reactor
Catalyst volume, cc	100	500	200 x 10 ⁶
Catalyst combination A/B/C *1), vol%	33/17/50	33/17/50	40/20/40
Type of oil flow	Down	Down	Down
Catalyst bed	Non dilution	Non dilution	Non dilution
Feedstock	IH,AH-AR	IH, AH-AR	IH, AH-AR
Operating conditions			
WAT, °C	408	410	405 - 415
LHSV, 1/hr	0.35	0.32	0.32 - 0.38
H ₂ /Oil, nl/l	900	900	900 - 1000
Superficial liquid mass velocity,lbs/ft ² ·hr	30	70	1600
	kg/m ² ·S	0.10	2.2

*1) A, B and C are industrial catalysts and demetallization, demetallization/desulfurization and desulfurization catalyst, respectively.

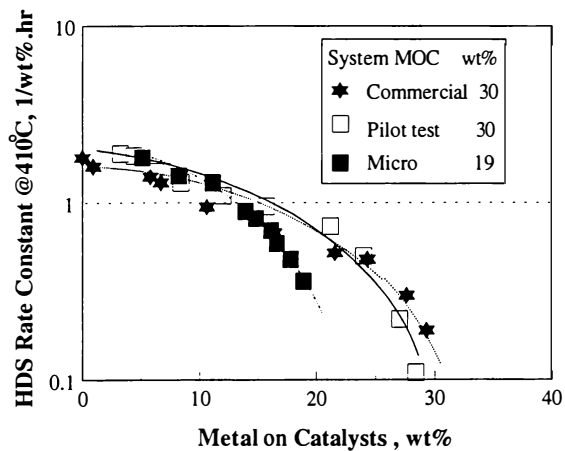


Figure 2. Hydrodesulfurization Stability

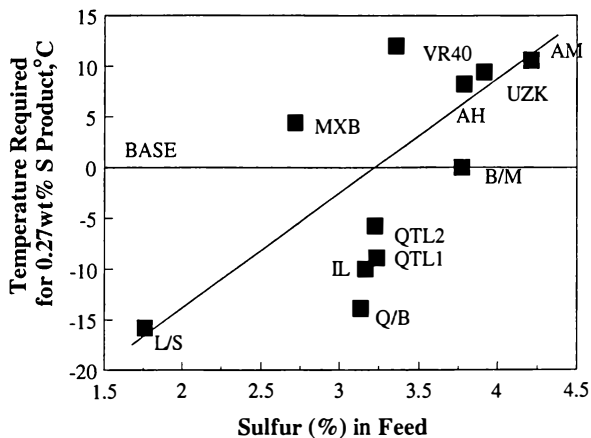


Figure 3. Effect of Feed Sulfur on HDS Reactivity

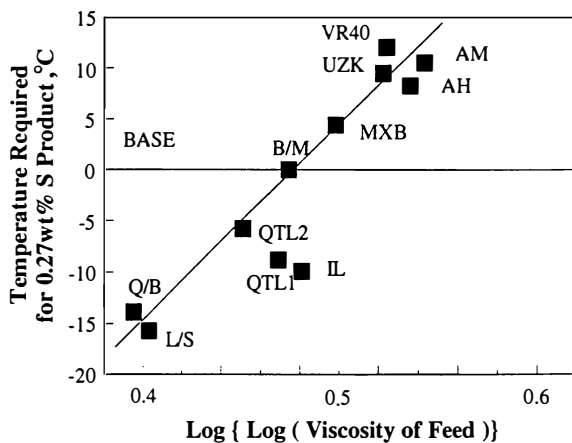


Figure 4. Effect of Feed Viscosity on HDS Reactivity

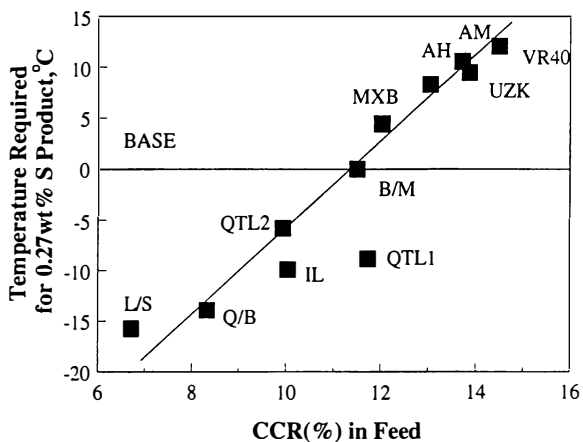


Figure 5. Effect of Feed CCR on HDS Reactivity

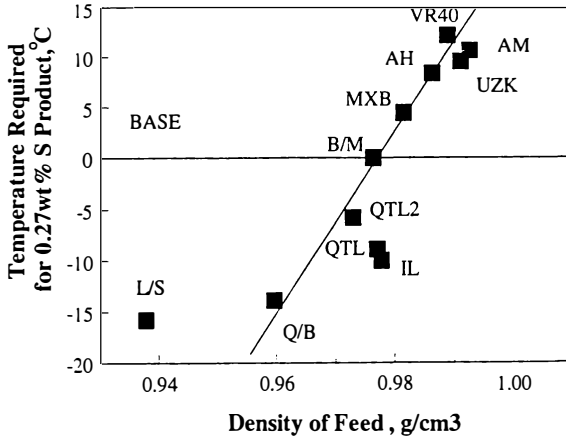


Figure 6. Effect of Feed Density on HDS Reactivity

Zakum (UZK), Mexican blends(MXB), Iranian Light (IL), mixture of Light and Mexican blends (B/M) and, blends of Qatar and Basla Light (Q/B), low sulfur crude AR (L/S) and 40% blended vacuum residue (VR40).

Figure 3 reveals that the desulfurization reactivity is deteriorated with the increase of sulfur content in the feedstock as generally known. The viscosity, the Conradson carbon residue (CCR) content and the density of the feedstock are relatively closely correlated with the desulfurization reactivity as illustrated in Figure 4 to 6, respectively. It is necessary to raise the reaction temperature by approximately 4°C with increasing of the carbon residue content by 1%, and by approximately 8°C with increasing of the density by 0.01 g/cm³. Although those relationship between the properties of feedstock and the desulfurization reactivity are mentioned above, they vary also according to the origin of feed oil, the desulfurization conditions and the sulfur content in the product.

Reaction Rate Equation and Correction with Feedstock Properties. The correlation of the pilot test data with the commercial data is generally made comparing the desulfurization reaction temperature in both operations under the normalized conditions. The reaction temperature under the normalized conditions can be calculated from the following reaction rate equation:

$$\frac{1}{n-1} \left(\frac{1}{S_{p0}^{n-1}} - \frac{1}{S_0^{n-1}} \right) \times \text{LHSV}_0 = k_0 \quad \text{----- (1)}$$

The reaction rate constant, k_0 , is corrected by introducing the correction terms of feedstock for Arrhenius equation, then

$$k_0 = A(S_0)^a(D_0)^b(\log\log\text{VIS}_0)^c e^{-E/RT_0} \quad \text{---- (2)}$$

The reaction rate equations under the operating conditions are expressed by the same equations as Eqs.(1) and (2) by replacing the suffix of zero by unit. The normalized temperature, T_0 , is expressed as follows:

$$T_0 = \frac{1}{1/T_1 - R/E \text{Ln}k'_0/k'_1} \quad \text{---- (3)}$$

Then,

$$\frac{k'_0}{k'_1} = \frac{k_0}{k_1} \times \left(\frac{S_1}{S_0}\right)^a \left(\frac{D_1}{D_0}\right)^b \left(\frac{\log\log\text{VIS}_1}{\log\log\text{VIS}_0}\right)^c \quad \text{---- (4)}$$

where

S_p	= Product sulfur,	wt%
S	= Feedstock sulfur,	wt%
n	= Reaction order	
E	= Activation energy,	cal/mol
R	= Gas constant,	1.897 cal/molK
T	= Absolute temperature,	K
VIS	= Viscosity,	cst
D	= Density,	g/cm ³

It is not so easy to determine the parameters including n , E , a , b , and c in Eqs.(1)(2)(3) and (4) by the trial and error method. Accordingly, those parameters were determined in such a way that moving average in the vicinity of a specified normalized temperature was determined and the difference between the moving average and the corresponding normalized temperature was squared to obtain the square of deviation. Applying the procedure to all the points, the sum of squares deviation was calculated and it was collectively minimized by variously changing the value of each parameter with care taken not to largely deviate the moving average of the normalized temperature from the graph.

Case Studies. The weighted average reaction temperature (WAT) required for 1.0 wt% sulfur bottom product under the normalized conditions without correcting with the feedstock are plotted in Figure 7. AH atmospheric residue with the most run average properties of a commercial operation was hydrotreated in the

middle of the commercial run. The reaction temperature of AH atmospheric residue is almost the same as that in the pilot unit. However, at the start of the pilot run, the reaction temperatures of IH atmospheric residue are approximately 13°C different from that of AH atmospheric residue. A continuous deactivation curve of the catalyst system is, therefore, unable to be drawn for the pilot run.

Normalized WAT of the commercial operation were corrected with the properties including sulfur content, density and viscosity of the feedstock by the above mentioned procedure. Normalized WAT of the pilot test operations were also corrected in the same manner as above. The parameters were determined so as to minimize the sum of squares deviation of the desulfurization reaction temperatures under the normalized conditions in the pilot and commercial units as shown in Table IV. The result is illustrated in Figure 8.

None of the curves drawn in Figure 8 have a discontinuous point. The figure reveals that the correlation in the results from the start to the end of the runs between the pilot and commercial units is considerably improved from that in Figure 7. The figure can be used for predicting the remaining life of the catalyst system, because the deactivation of the catalyst system at the end of the commercial run can be estimated.

The deactivation curve of the catalyst system in the cracking and the deep desulfurization of atmospheric residue are illustrated in Figure 9 and 10, respectively. The curves for the pilot and commercial units in both cases almost fall on each other. Those figures reveal, therefore, that the pilot test results correlate with the commercial operation results. The information concerning the

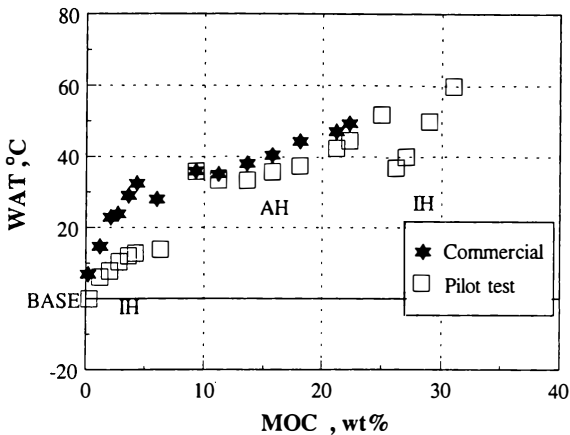


Figure 7. Normalized WAT (Conventional) in Case-1

Table IV. Normalized Conditions

Case No.	1	2	3
Feedstock	AH-AR	AM-AR	AM-AR
Mode of operation	Constant HDS ^{*1)}	MHC ^{*2)}	Constant HDS
Figure No.	8	9	10
Process Conditions			
LHSV, l/hr	0.41	0.42	0.20
H ₂ /Oil, nl/l	1100	845	1100
Feedstock properties			
Density, g/cm ³ @15° C	1.000	0.975	0.983
Viscosity, cst@50° C	11,600	800	2,300
Sulfur, wt%	4.7	3.8	4.1
Bottom sulfur for normalization, wt%	1.0	0.80	0.27

*1)HDS: Hydrodesulfurization

*2)MHC: Mild hydroconversion

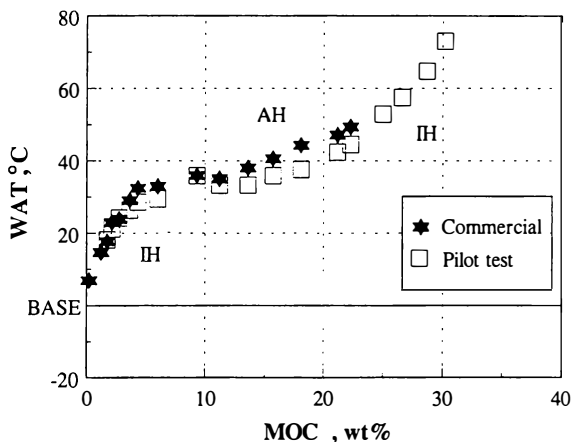


Figure 8. Normalized WAT in Case-1

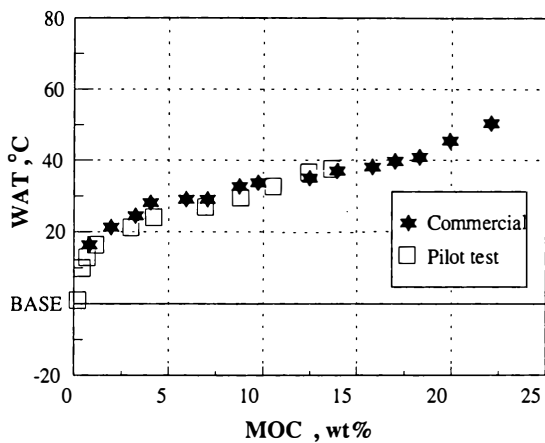


Figure 9. Normalized WAT in Case-2

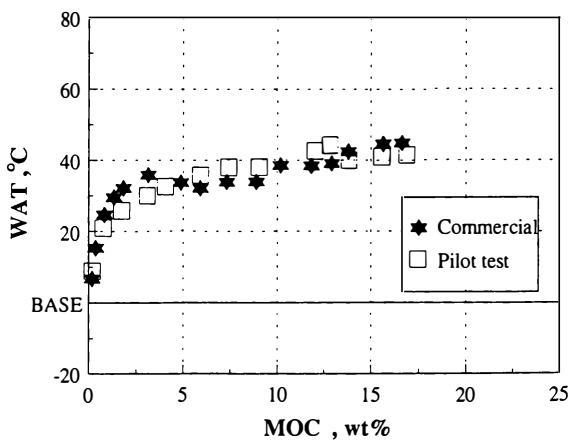


Figure 10. Normalized WAT in Case-3

remaining catalyst activity inferred from the long run pilot test data based on the correlation is now available.

The results of the pilot and commercial units do not completely agree with each other even by the correction mentioned above. Probably this is because the correction equation by the feedstock does not take the carbon residue content largely affecting the desulfurization reactivity into consideration. Although the carbon residue content is not routinely analyzed in the commercial operations, improved correction equations will be derived by incorporating the correction of the carbon residue content.

The procedure is applicable to the desulfurization of vacuum gas oils and gas oils as an effective tool for analyzing the operating data.

Conclusions

Discrepancies in catalyst aging performance between laboratory tests and commercial units are often observed. Different liquid mass velocity and/or type of feedstock can be reasons for the discrepancies.

(1) Catalyst lives were compared with reactor metal distribution, obtained from micro, pilot and commercial units. It was found that the micro reactor with low liquid mass velocity caused metal pass-through to the down stream catalysts. As a result, a life of catalyst system was shorter than that of the commercial operation because of metal deactivation of the down stream catalysts. Liquid mass velocity above a certain level is required for the catalyst life evaluation to avoid aforementioned discrepancy. This level is proposed to be 70 lbs/ft²hr (0.10 kg/m²s) in minimum.

(2) Proposal was made on a correction method which involves mainly the effects of feedstock properties on desulfurization activity. It shows much better agreement in catalyst aging performance between the pilot and commercial operations.

Literature Cited

- (1) Mears, D., Chem. Eng. Sci., 26, 1361 (1971)
- (2) Gierman, H., Appl. Catal., 43, 277 (1988)
- (3) Sie, S., Preprints Symposia, Am. Chem. Soc., 40, 463 (1995)
- (4) Satterfield, C. N., A. I. Ch. E. J., 21, 209 (1975)
- (5) de Bruijn, A. Petrotec (JPI), 2, 65 (1979)
- (6) de Bruijn, A. Proc. 6th Int. Cong. Cot., London, 352 (1976)

Life Testing of Light Hydrocarbon Aromatization Catalysts

K. Hirabayashi¹, F. Igarashi¹, and T. Kondou²

¹Petroleum Research Laboratory, Mitsubishi Oil Company Ltd.,
4-1 Ohgimachi, Kawasaki-ku, Kawasaki 210, Japan

²Research and Development Center, Chiyoda Corporation,
3-13 Moriyacho, Kanagawa-ku, Yokohama 221, Japan

In aromatization processes of light hydrocarbons, the deposition of coke on the catalyst proceeds faster than in other processes such as naphtha reforming. The catalyst must thus be regenerated by burning the coke from the catalyst enabling it to be reused. Catalyst activity gradually decreases, however, due to repeating reaction and regeneration in multiple cycles. The authors have made an automated experimental apparatus that is able to evaluate the life of aromatization catalysts in a relatively short time. The lives of several types of representative catalysts were tested using this apparatus by selecting accelerated coking and regeneration conditions. This paper will describe the selection of these accelerated coking and regeneration conditions, discuss comparisons of the decreases in catalyst activity between accelerated deterioration experiments and compare them to a demonstration test using a pilot plant (200BPD). Finally we have tried to elucidate the causes of the decrease of catalyst activity resulting from a thorough characterization of the spent catalysts.

Light hydrocarbon aromatization is a process whereby light hydrocarbons e.g. propane and butane, the main components of LPG, and light naphtha, consisting mainly of paraffins having 5 to 7 carbon atoms, are converted into aromatics consisting mainly of benzene, toluene and xylene, with hydrogen produced as a by-product. This process is able to convert light hydrocarbons into BTX; conventional catalytic reformers can only convert C6 & C7 paraffins. Thus, it gives diversification to the BTX sources and so increases the added value of LPG and light naphtha.

In the aromatization process of light hydrocarbons, the deposition of coke on the catalyst proceeds rapidly in comparison with other processes such as naphtha

reforming. Consequently, the catalyst is regenerated more often by burning and removal of the coke deposited on its surface, and restoration of the activity for re-use.

This catalyst regeneration operation is performed using published processes, examples of which include the use of a fixed bed switching reactor system in the case of the Z-Forming process(1), and the use of a continuous catalyst regeneration system in the case of the Cyclar process(2). However, catalyst activity gradually decreases due to the repeated reaction and regeneration. Catalyst life, therefore, is considered terminated at the point where its activity falls below the point at which it is able to maintain a pre-set aromatic yield.

The authors fabricated a computer-controlled experimental system that is able to predict the life of an aromatization catalyst in a relatively short span of time. Using this system, the catalyst life of several types of representative aromatization catalysts was evaluated by selecting accelerated coking and accelerated regeneration conditions. This paper reports on the selection of those accelerated coking and regeneration conditions, the results of a comparison of catalyst activity in this test, and on a demonstration test using a large pilot plant (200 BPD); further more on the causes of the decreased catalyst activity based on characterizations of spent catalysts.

Experimental

Catalyst. H-ZSM-5 was synthesized according to the well-known Arganer & Landolf Mobil patent(3). Metal-loaded H-ZSM-5 was prepared by refluxing NH_4^+ -ZSM-5 powder in an aqueous solution of $\text{Ga}(\text{NO}_3)_3$ or $\text{Zn}(\text{NO}_3)_2$ for 24 hours followed by drying. H-Ga-Silicate was synthesized in the same manner as H-ZSM-5 with the exception of using gallium nitrate for the gallium source. Alumina powder was then added to the zeolite or metallosilicate prepared in the above manner to obtain substances having a final alumina content of 27 wt%. After kneading and extrusion molding, the substances were calcined for 3 hours at 550°C in the presence of air to obtain the catalysts. The properties of the catalysts obtained in this manner are shown in Table I.

Catalyst Activity Test. Catalyst activity tests were conducted using a fixed bed flow-type microreactor, shown in Fig. 1. 7 ml of catalyst (16-28 mesh) were filled into a stainless steel reactor (i.d. 10.2 mm) and treated for 1 hour at 538°C with argon gas passed through air. n-Hexane was fed under conditions of a mean catalyst layer temperature of 538°C, atmospheric pressure and LHSV of 2h^{-1} . The entire effluent from the reactor was analyzed with an on-line FID-type gaschromatograph equipped with a capillary column and a TCD-type gaschromatograph equipped with a packed column, connected to the reactor by means of sampling valves. Product components were grouped using a data processor based on the resulting chromatographs followed by calculation of the conversion and the product yields. In this system, the products can also be separated and analyzed off-line followed by determination of the conversion and the product yields. A material balance of 97% by weight or better is obtained in this case.

Table I. Characteristics of the Zeolite Catalyst Samples

Catalyst	Zeolite		Metal Loaded (wt% on catalyst)	
	SiO ₂ /Al ₂ O ₃	SiO ₂ /Ga ₂ O ₃	Zn	Ga
H-ZSM-5	63	—	—	—
Zn/H-ZSM-5	63	—	0.35	—
Ga/H-ZSM-5	63	—	—	0.25
H-Ga-Silicate	—	68	—	—

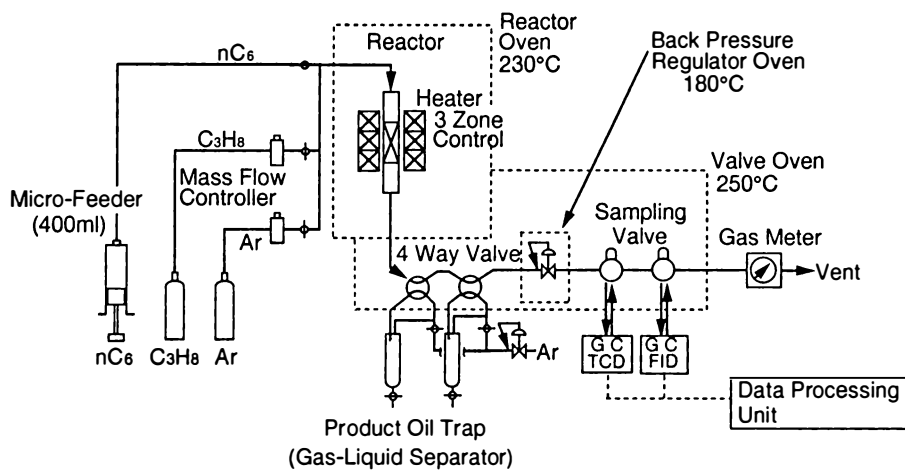


Figure 1. Schematic drawing of catalyst activity test unit.

Accelerated Catalyst Aging Test. The accelerated catalyst deterioration testing system based on cycling of reaction and regeneration under accelerated conditions is shown in Fig. 2. This system is composed of a reaction feed supply unit, a regeneration gas supply unit, a reaction (regeneration) unit and a control unit. The reactor uses the same type of microreactor used for evaluation of the catalyst activity as described above. The reaction/regeneration cycle consists of four steps, namely reaction, purging, regeneration and another purge; these operations are automatically controlled by the computer.

Two modes of displays are used for computer input and output. One mode displays a time sequence table while the other provides a display of the operating status. Sequence conditions can be altered and the operating status at that time can be determined by switching between these two mode displays. Switching between reaction and regeneration lines for each step as well as setting of conditions for temperature, flow rate and so forth are performed by key entry on the time sequence table. Reaction and regeneration cycles proceed automatically in accordance with the sequence conditions that have been set. The required number of cycles of reaction and regeneration are entered in advance on the operating status display. During operation, the number of cycles that have elapsed until that time along with the feed supply rate in the reaction step are displayed on the monitor. Changes in catalyst activity as the reaction and regeneration cycles is progressing are determined by stopping the system for every fixed number of cycles, removing the reactor after sealing with argon gas, transferring the reactor to a microreactor for evaluation of catalyst activity, and assaying catalyst activity according to the catalyst activity test. This system consists of three reaction (regeneration) series (the first series is shown in Fig. 2), enabling us catalyst life prediction testing simultaneously on three types of catalysts.

Coking and Decoking Experiments. Coking and decoking experiments were performed using either the microreactor used for catalyst activity evaluation or the catalyst accelerated deterioration testing system for various types of feeds or under various regeneration conditions.

Catalyst Characterization. Analysis of the constituent elementary composition of the catalysts was carried out by first dissolving the sample in hydrofluoric acid and diluting, followed by atomic absorption analysis for Al, Zn, and Ga or the absorptiometric method for Si. Catalyst X-ray diffraction patterns were analyzed using the Rigaku Gigerflex RAD-1A. Analysis of coke deposited on the catalyst was measured for C and H using the Perkin-Elmer 240B. Catalyst surface area was measured according to the BET method using the Shimadzu ASAP 2000. For measurement of ^{29}Si -MAS-NMR we use the JEOL JMS-DX300.

Results and Discussion

Catalyst Activity. Fig. 3 shows the results of the catalyst activity test. The reaction was carried out at standard conditions consisting of a mean catalyst bed temperature of 538°C , atmospheric pressure and LHSV of 2h^{-1} . The left graph indicates the results for conversion, total aromatics and BTX yields versus time on

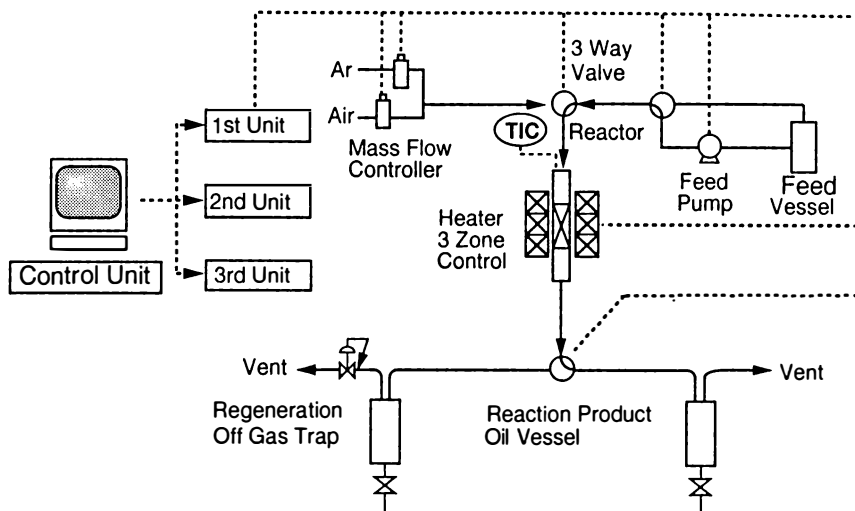


Figure 2. Schematic drawing of catalyst aging test unit.

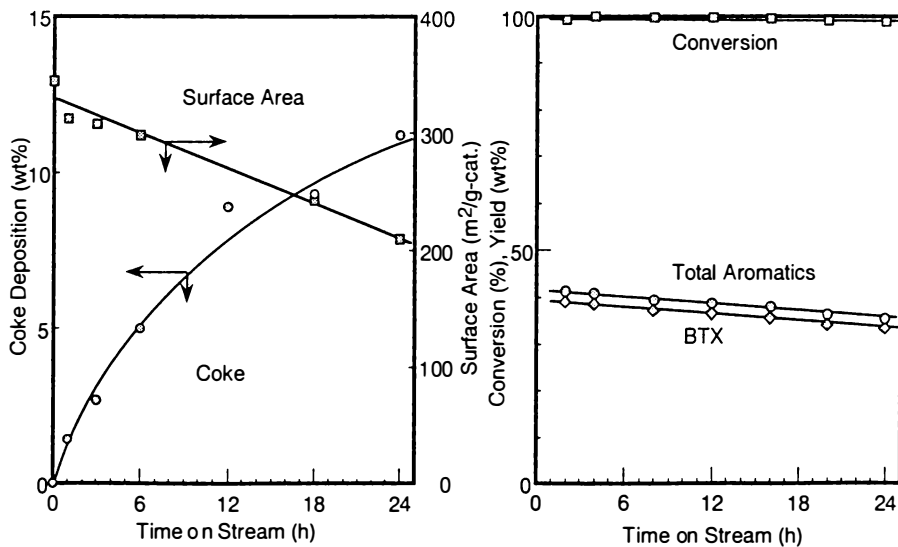


Figure 3. Change of catalyst activity with time on stream.

stream. The right graph shows the changes in coke deposition on the catalyst and in the specific surface area of the catalyst also versus time on stream. Coke deposition on the catalyst increases with time on stream. This is accompanied by a decrease in specific surface area.

Although slight, total aromatics and BTX yields decrease steadily. In catalyst evaluation testing, therefore, it was decided to determine the 24-hour mean values for total aromatics as a catalyst activity.

Coke Formation. An example of the change in the amount of coke formed with respect to time on stream under the aromatization reaction conditions of several types of hydrocarbons on the H-Ga-silicate prototype catalyst is shown in Fig. 4. In this figure, feed rate was set to be uniform at an LHSV of 2h^{-1} in terms of the n-hexane equivalent to compare the amount of coke formed. The major components of light paraffin consist of n-butane and n-hexane, while ethylene, cyclohexane and toluene are compounds that contribute largely to the amount of coke formed.

In the case of pure toluene, since there is little gas produced and the deposition of coke on the catalyst is not uniform, it was supplied after dilution with n-heptane. As the mole ratio of toluene to n-heptane increased from 40/60 to 50/50 to 90/10, the amount of coke formed increased in 20-30% increments. The data for a mole ratio of 90/10 is shown in Fig. 4.

According to this graph, when the feed that contributes to coke formation is used, it is possible to promote a coking rate that is 2-4 times greater than in the case of n-butane or n-hexane. The H/C atomic ratio of the formed coke changes depending on the amount of coke deposited. The H/C atomic ratio is known to be large at low coke levels(4). According to the results of coking experiments conducted using various types of feed at coke levels of 5-15 wt%, the H/C atomic ratio is within a range of 0.4-0.7, as seen in Table II. These results were essentially identical to those for coke deposited on catalysts in a bench-scale plant experiment (0.1 BPD) as well as in a demonstration plant experiment (200BPD) for aromatization of light hydrocarbons. The relationship between the amount of coke deposition on catalysts and their BET specific surface area is shown in Fig. 5. This relationship apparently holds irrespective of the type of feed used. This finding indicates that there are no large differences in the mode of coke formation between the feed which contributes to a large amount of coke formed, and the usual light hydrocarbon of the aromatization process.

Coke Removal. Regeneration of aromatization catalyst was performed using a supply gas having a low oxygen concentration while pressurizing under mild conditions in which the concentration of formed moisture was minimized to prevent its detrimental effects on the zeolites. In this method, the majority of the coke was first removed slowly by burning at a relatively low temperature. Next, the temperature was raised and the remaining coke was removed by burning in a relatively short period of time. In the bench-scale plant and demonstration plant experiments, the coke level on the catalyst was 10-15 wt% when switching between reactors every several days of operation. Thus, the coke level at which it is possible to maintain a prescribed aromatic yield is considered to be within this range.

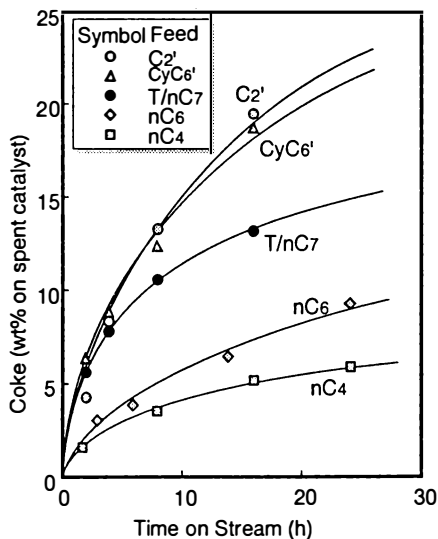


Figure 4. Coking rate for various feeds. Catalyst: H-Ga-Silicate.

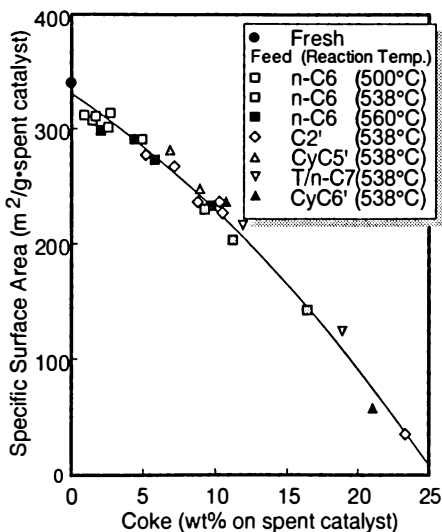


Figure 5. Relationship between amount of coke deposition and specific surface area of coke deposited catalyst. Catalyst: H-Ga-Silicate.

Table II. The Atomic H/C Ratio of Coke

Reactor	Bench Scale Plant ¹			Microreactor ²		
	Feed	C3	C4	L't Naphtha	n-C6	T/n-C7
Temp.(°C)		538	520	520	538	538
Press.(Kg/cm ² G)		3	3	3	0	0
LHSV(h ⁻¹)		1.5	1.5	1.5	2	1.44
Time on stream(h)		48	48	96	24	16
H/C		0.50	0.45	0.35	0.50	0.40

Catalyst : H-Ga-Silicate

¹Catalyst volume ; 250 ml

²Catalyst volume ; 7 ml

In order to select accelerated decoking conditions, feed in the form of T/n-C7 (90/10, mole/mole) was allowed to flow through H-Ga-Silicate catalyst for 13.5 hours at an LHSV n-hexane equivalent of 2h^{-1} and reaction temperature of 538°C to obtain a catalyst with a coke level of 12.5 wt% on catalyst. Decoking experiments were then performed under various conditions using this coke deposited catalyst. As one example of a catalyst regeneration, an experiment under conditions of low oxygen concentration and high GHSV is shown in Fig. 6. This graph shows the changes over time in the composition of the off gas of decoking during catalyst regeneration. Although the majority of the coke is removed in 10 hours at a set reactor temperature of 450°C , a small amount of coke still remains at this level of heating. The coke is then completely removed by baking at the second level of 550°C . Another example of catalyst regeneration, Fig. 7 shows the data for catalyst regeneration under the relatively severe conditions of a high oxygen concentration at normal pressure. The majority of the coke is removed in roughly 4 hours, and the remaining coke is completely removed by a second round of heating at 570°C . The complete absence of coke was confirmed by removing the catalyst from the reactor following completion of the experiment.

The results of catalyst regeneration experiments under various conditions are summarized in Table III. The activity of catalysts regenerated by coke burning can be seen to have recovered to nearly the level of fresh catalyst.

Accelerated Catalyst Aging Test. Based on the study results of coking and decoking conditions described above, a sequence of steps was designed allotting 24 hours per cycle using toluene/n-C7 (90/10 mole/mole) for the feed. Each complete cycle consisted of a reaction step under conditions of LHSV of 2h^{-1} in terms of the n-hexane equivalent, reaction temperature of 538°C and atmospheric pressure, a first purge step using argon gas, a two-stage regeneration step at 500°C and 570°C at an oxygen concentration of 8 vol%, and a second purge step also using argon gas. The catalyst used in the demonstration operation was then submitted to an accelerated deterioration experiment using the system shown in Fig. 2. Comparison of the results of the accelerated catalyst aging test with the catalysts used in the Z-Former demonstration test, and the activity of the catalysts sampled from the reactor of the demonstration test is shown in Fig. 8. In the case of the demonstration test, catalysts were sampled after 24 cycles of reaction and regeneration, and then compared by plotting the mean catalyst activity on the same graph. As seen in this graph, the logarithm of catalyst activity and the number of reaction/regeneration cycles exhibits a good linear relationship. Although reaction/regeneration conditions were not all the same in the demonstration test, the coke level was within a range of 10-15% by weight. In the accelerated catalyst aging test, testing was carried out by matching the coke level to that mean value. As seen from the graph, despite there being only one point, the plot of the demonstration test can be seen to closely agree with the results of the accelerated catalyst aging test.

Thus, the accelerated catalyst aging test can be considered to accurately reproduce the tendency of catalyst deterioration in the Z-Former demonstration test. In the case of a sequence consisting of 24 hours per cycle, it is possible to predict catalyst life in 1/4 to 1/8 the time required by the demonstration test assuming reaction/regeneration in

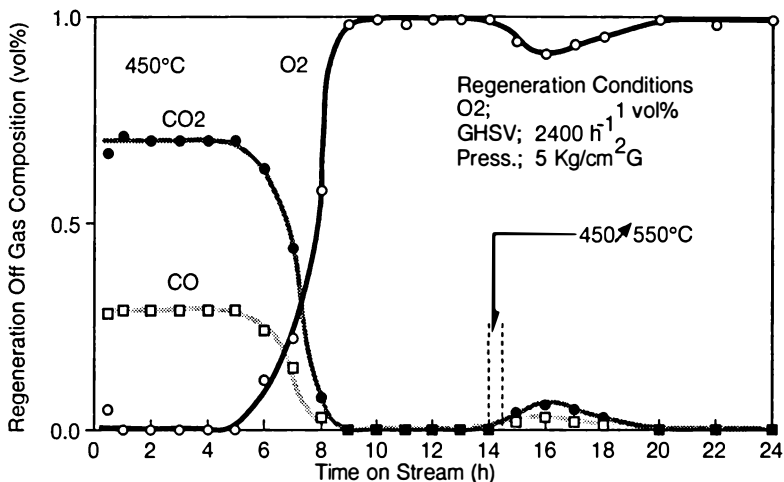


Figure 6. Regeneration of spent catalyst under mild conditions.
Coked catalyst: H-Ga-Silicate.
Coke level; 12.5 wt%.

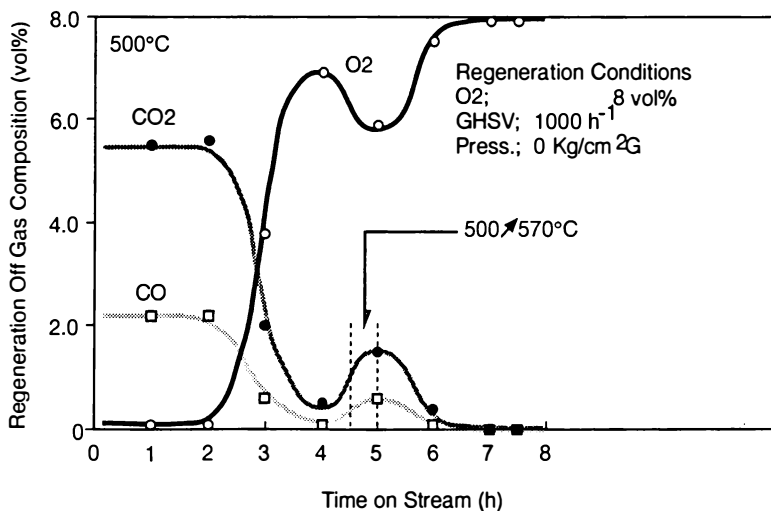


Figure 7. Regeneration of spent catalyst under severe conditions.
Coked catalyst: H-Ga-Silicate.
Coke level; 12.5 wt%.

the demonstration test is carried out for 2 to 4 days. Accelerated catalyst aging tests were carried out on the four types of catalysts for aromatization of light paraffins that we prepared. Based on the results of the catalyst activity test and accelerated coking test, there are no large differences in the amount of coke deposition between these catalysts used in the demonstration test. Consequently, the aging test was carried out for 24 hours per cycle with results as shown in Fig. 9. Also for these catalysts, the logarithm of catalyst activity and the number of reaction/regeneration cycles demonstrates a good linear relationship. The change in catalyst activity accompanying reaction and regeneration in the accelerated deterioration experiment can be expressed with the simple equation $A=A_0 \cdot X^n$, where A, A_0 , X and n respectively represent catalyst activity, activity of the fresh catalyst, the deterioration coefficient and the catalyst deterioration cycles.

Although the relative catalyst lives of these four catalysts can be easily predicted from the slopes of the lines, an estimation of the actual catalyst life is not considered to be that easy. As one means of attempting this, the estimation of catalyst life is attempted on the bases of a relatively rough hypothesis. It is assumed we compensate for a decrease in activity of roughly 10%, as evaluated with the catalyst activity test in this reaction, by raising the reactor temperature as is done in the demonstration test. The number of cycles of reaction and regeneration equivalent to fresh catalyst activity of 90% was determined from these lines. The lives indicated in this graph were then estimated from the ratio with roughly 55 cycles of reaction and regeneration for 1 year of operation of 3 days stream on average. The life of the low activity, proton type ZSM-5 catalyst was estimated at roughly 1 year, while that of the relatively highly active, proton type gallo-silicate catalyst was roughly 0.2 years.

In order to investigate the causes of changes in catalyst activity accompanying cycles of reaction and regeneration, the spent catalysts used in the accelerated deterioration experiment were analyzed. Some of those representative results are shown in Table IV. There are hardly any differences in the X-ray diffraction pattern of the spent catalysts with that of the fresh catalysts, thus indicating that the zeolite structure is maintained. Although specific surface area is slightly smaller in the spent catalysts in all cases, the differences are not large. Although these catalysts contain 27% alumina as binder, based on the results of their chemical analysis, there are no remarkable changes in the Si, Al and Ga contents. In addition, in the case of the Zn/H-ZSM-5 and Ga/H-ZSM-5 catalysts, although the levels of Zn or Ga, respectively, decrease slightly as a result of the repeated reaction and regeneration cycles, there are no large changes observed as in example (5) of elution of Zn or Ga resulting from long-term treatment in a hydrogen atmosphere at high temperatures (1100 °F).

On the other hand, information about the framework of zeolite can be obtained from the ^{29}Si -MAS-NMR spectrum. In the case of the high silica-type zeolite used here, the Si/metal ratio in the zeolite framework is determined from the relative values of Si(0M) and Si(1M). As is seen in Table IV, this ratio becomes larger in comparison with that of the fresh catalyst for all spent catalysts, thus indicating that some active components in the form of Al or Ga are being eliminated from the framework by the reaction and regeneration cycles. Based on this finding, the major

Table III. Catalyst Regeneration Conditions and Activity of Regenerated Catalysts

O ₂ Concentration (vol%)	Regeneration Conditions				Coke Remaining (wt% on catalyst)	Relative Activity of Regenerated Catalyst*
	GHSV (h ⁻¹)	Press. (Kg/cm ² G)	Temp. (°C)	Time (h)		
1	2400	5	500	24	0.3	0.98
1	2400	5	450	14	0.0	0.99
			550	0.5		
			550	9.5		
1	2400	5	500	14	0.0	0.99
			550	0.5		
			550	9.5		
6	400	0	450	16	0.0	0.99
			570	0.5		
			570	7.5		
8	1000	0	500	7.75	0.4	0.98
8	1000	0	500	4.5	0.0	0.99
			570	0.5		
			570	2.75		

Catalyst sample: coked H-Ga-Silicate (coke: 12.5wt% on catalyst)

* Activity of the regenerated catalyst / Activity of the fresh catalyst

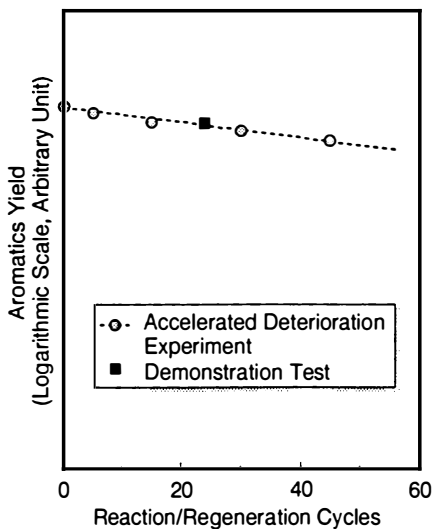


Figure 8. Change in catalyst activity with reaction/regeneration cycles.

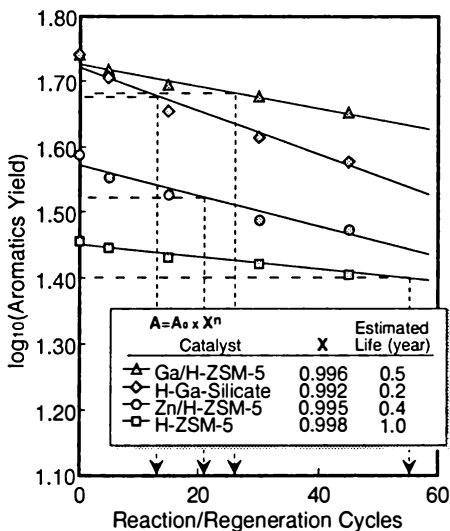


Figure 9. Change in catalyst activity with accelerated reaction/regeneration cycles for various catalysts.

Table IV. Characterization of Zeolite Catalysts

<i>Catalyst</i>	<i>Chemical Analysis</i>				<i>MAS NMR</i>		<i>Surface Area</i> (m ² /g cat.)
	<i>Si</i>	<i>Al</i>	<i>Zn</i>	<i>Ga</i>	<i>Si/Metal</i> (atom/atom)	<i>Si/Metal</i> (atom/atom)	
H-ZSM-5 Fresh	31.9	14.5	—	—	—	35	344
H-ZSM-5 Spent	32.0	14.4	—	—	—	40	329
Zn/H-ZSM-5 Fresh	31.8	15.1	0.36	—	—	35	359
Zn/H-ZSM-5 Spent	31.8	14.7	0.34	—	—	40	329
Ga/H-ZSM-5 Fresh	31.1	13.0	—	0.25	—	40	341
Ga/H-ZSM-5 Spent	31.0	12.7	—	0.24	—	50	335
Ga-Silicate Fresh	30.9	14.0	—	2.21	35	35	326
Ga-Silicate Spent	30.7	13.9	—	2.22	34	40	321

factor behind catalyst deterioration is surmised to be the elimination of active metal from the zeolite framework by the mentioned cycling.

Conclusion

In order to estimate the life of aromatization catalysts of light hydrocarbons, an accelerated catalyst deterioration testing system was fabricated in which reaction and regeneration are repeated continuously under computer control. Using this system, catalyst life estimation tests were conducted by selecting the conditions for reaction (accelerated coking) and regeneration (accelerated decoking). In these tests, results were obtained that matched the level of catalyst activity in a large demonstration pilot plant.

With this method, we can estimate the catalyst life in roughly 1/4 to 1/8 the time of operating the actual plant that we expect to be used.

Catalyst life estimation tests were also conducted on four different catalysts used for aromatization of light hydrocarbons in this system, namely H-ZSM-5, Zn/H-ZSM-5, Ga/H-ZSM-5 and H-Ga-silicate. Based on the results of characterization of the spent catalysts, the primary cause of deterioration of catalyst activity is the elimination of active metal from the zeolite framework.

Literature Cited

- (1) Saito, S., Hirabayashi, K., Shibata, S., Kondoh, T., Adachi, K. and Inoue, S., "Z-Forming Process: Conversion of LPG and Light Naphtha to Aromatics" 1992 NPRA Annual Meeting, New Orleans, LA, March 22-24, 1992.
- (2) Mowly, J. R., Anderson, R. F. and Johnson, J. A., *Oil and Gas J.*, 83(48), 128(1985), Scruton, M., *Petroleum Review*, 45(533), 270(1991).
- (3) US Patent 3, 702, 886 and 3, 756, 942.
- (4) Gnep, N.S., Roger, P., Magnoux, P. and Guisnet, M. PREPRINT Div. of Petrol Chem., ACS, 38(1), 87(1993).
- (5) US Patent 4, 392, 989.

Performance Testing of Hydroconversion Catalysts

W. H. J. Stork

Shell Research and Technology Centre, Amsterdam, Shell International Chemicals B. V., P.O. Box 38000, 1030 BN Amsterdam, Netherlands

Performance testing of hydroconversion catalysts is reviewed, with the emphasis on the use in catalyst development. This necessitates application of procedures to accelerate reaching a steady state performance, and also to determine long term deactivation. Catalyst deactivation phenomena in hydroconversion, especially in distillate desulfurization, hydrogenation, distillate hydrocracking and residue hydroconversion are discussed in detail. It is argued that at the present state-of-the-art performance testing in small scale equipment under realistic conditions, supported by process modelling, is the most effective approach. Examples are given, and areas for further study identified.

1. Introduction

Catalyst deactivation has been extensively studied, and excellently reviewed in many places, for example by Butt and Petersen (1). Much attention has been given to the area of hydroconversion (particularly residue hydroprocessing) (2). In general, however, these reviews have focussed on the description and understanding of deactivation, with little consideration to the point of view of the process or catalyst developer. In this review the deactivation phenomena in the various areas of hydroconversion and their modelling will be considered. Options for performance testing of catalysts that are meaningful without being excessively lengthy will be derived.

Catalyst performance is determined by activity, selectivity and stability. Whereas activity is indispensable, selectivity is often of prime importance (e.g. lube base oil yield in catalytic dewaxing), particularly if an improved selectivity can break a bottleneck in a unit (e.g. by lower gas makes which break up the gas train bottleneck in a hydrocracking unit). Catalyst life is determined both by the start of run activity and deactivation rate. With high activity catalysts in low severity duty (e.g. naphtha hydrotreating), catalyst life can be very long (e.g. 5–10 years), and in some cases the

total cycle length is determined by a fouling of a top layer of the catalyst rather than by deactivation. (This fouling can be counteracted by applying dedicated top-bed materials with higher tolerance of foulants, particulates, scale, etc. (3)). Such long catalyst lifecycles may seem desirable, but an earlier catalyst replacement, e.g. in case of deteriorating selectivities, may be attractive. Also, a more severe operation of the catalyst, e.g. by increasing feedstock heaviness (such as can be envisaged in hydrocracking or residue conversion) or by increasing severity/operating temperature (such as by going from VGO HDS to MHC (4)), thereby decreasing feedstock costs or increasing product value, may be economically much more attractive than a longer catalyst life. This is obvious when one considers that most catalysts are regenerable and the availability of presulfurized catalysts and off-site regeneration often allow shorter downtimes of the processing units.

2. Catalyst Poisoning and Catalyst Deactivation

In the following, catalyst poisoning and deactivation through coking and metals deposition will be considered, but not fouling by salt deposition, etc.

a. Reversible Poisoning. In hydroprocessing oil fractions, the feedstocks and products are complex mixtures of hydrocarbon molecules of different molecular weight, shape, aromaticity, and heteroatom (S, N, O, Ni, V, etc.) content. As a result of this vast range of molecular species, a reaction such as hydrodesulfurization is in fact the overall sum of the desulfurization reactions of the different individual sulfur species. Some of these (or other) species will also act as a catalyst poison for the reaction of e.g. lower molecular weight species. Such poisoning effects can be expressed for the example of desulfurization over one type of active site, and neglecting pore diffusion effects, by Equations 1 and 2,

$$r_{\text{HDS}} = -\frac{d[\text{S}]}{dt} = k_{\text{emp}} S_f^n \quad (1)$$

$$r_{\text{HDS}} = \frac{\sum_i k_i(T) K_i(T) S_i(\xi) p_{\text{H}_2}(\xi)}{1 + \sum_j K_j(T) S_j(\xi) + \sum_k K_k(T) A_k(\xi)} \quad (2)$$

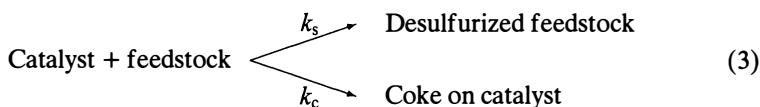
where Equation 1 simply defines the empirical overall rate constant according to a power law with reaction order n . In practice n often equals 2, with the individual components having an order of 1 (as in Equation 2), which is a consequence of multicomponent kinetics (5). Equation 2 expresses in detail that (i) HDS is the sum of many individual reactions (each taken first order in hydrogen partial pressure), which (ii) are poisoned by absorption of S molecules j and other molecules k on the active site, to a degree (iii) that depends on conversion (ξ , location in the reactor) and temperature T , in case of non-isothermal reactors again dependent on ξ .

The importance of such poisoning can be illustrated by, for example, the poisoning of gasoil HDS by addition of N compounds (6), or the reduction in activity for gasoil/thiophene HDS of a catalyst after a short period of processing residual feedstocks (7). As stated earlier by Somorjai (8), catalysis is the science of dirty surfaces.

Poisoning as defined by Equation 2 is due to an equilibrium adsorption to active sites, and is in principle completely reversible, as has been shown for instance for nitrogen compounds in gasoil HDS (6). (This is also the basis for the common practice of blocking-in feedstocks/conditions in pilot plant testing). Nevertheless, it may take a long time to achieve total equilibrium adsorption over the entire catalyst bed, because, e.g., the concentration of the poisons in the feedstock is low or the adsorption/desorption processes are slow, especially at low temperatures. An example is the second, cracking stage of hydrocracking unit running under low ammonia/low organic nitrogen levels in the feed (“two stage”), where it may take some 2000 h to reach a stationary state (Figure 1) (9). Slow desorption of adsorbed species is also the basis for the common practice of processing lighter feedstocks before heavier ones in blocked-in pilot plant experiments. In the coke deactivation both catalyst poisoning through adsorption of polyaromatics (“RCT”) in the feed and deactivation through condensation reactions can play a role.

Kinetic effects of a different nature occur if the strong catalyst poisons diffuse so slowly that at first only the outer parts of the catalyst particles are poisoned (shrinking-core model, as discussed for dewaxing (10)) or that these poisons are converted in the outer layers of the catalyst, leaving a clean active core (11).

b. Irreversible Deactivation. If the species such as deposited metals, silicon and coke that poison the active sites do not desorb, a different situation exists, and a progressive, irreversible deactivation, as expressed by Equations 3 to 5, will often occur.



$$r_{\text{HDS}} = -\frac{d[\text{S}]}{dt} = k_s(t, \xi)S^n \quad (4)$$

$$k_s(t, \xi) = k_{s,0} \cdot X(t, \xi) \quad (5)$$

Here the rate constant for HDS becomes time dependent, the degree of deactivation $X(t, \xi)$ also being dependent on the location in the reactor/conversion. X can sometimes be directly correlated to the amount of metals or coke deposited on the catalyst; in other cases a definition has to be based on the total “history” of the catalyst (according to Equations 6 and 7), instead of simply its state.

$$X(t, \xi) = 1 - \int_0^t k_{\text{coking}}(\xi)X(t, \xi) dt \quad (6)$$

$$\frac{dk_s}{dt} = -k_{\text{coking}}(\xi)k_s \quad (7)$$

Again, the degree of deactivation can be expected to depend on the temperature and conversion level, as expressed by Equations 4 and 5. Indeed, coke profiles over isothermal laboratory reactors (12) show such differences, primarily due to a reduction in hydrogen partial pressure. Metals deposition over residue catalysts beds show a decrease with conversion simply because of depletion of the reactant (2,13,14).

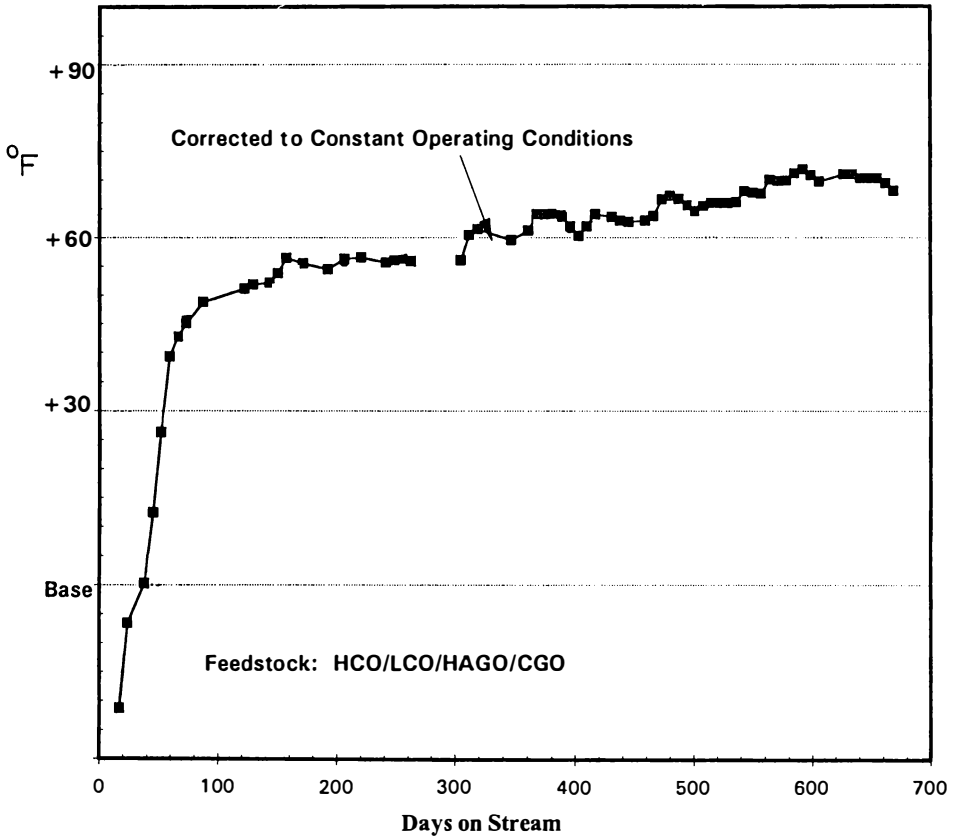


Figure 1. Activity ($^{\circ}\text{F}$) versus catalyst age for Z 753 in a commercial hydrocracker. (Reproduced with permission from reference 9. Copyright 1994 Safa George.)

Similar to the situation with poisoning, the permanent deactivation may be non-uniform over the catalyst particle, which can sometimes be used to advantage, as for instance in residue HDS catalysts where the metals are deposited at the periphery of the particles and the core remains “clean” and active for HDS (15–17).

Permanent catalyst deactivation effectively leads to a reduction in the number of active sites available for reaction (and poisoning). In commercial practice, catalyst deactivation is generally coped with by increasing the reaction temperature, expressed as degrees Celsius (Fahrenheit) per 1000 run-hours. This experimental measure is related to the fundamental deactivation parameters discussed above through the apparent activation energy. A high activation energy results in a lower temperature increase requirement for a given fractional deactivation X . The strongly poisoned systems often have high apparent activation energies, as follows from Equation 2, since the degree of poisoning decreases with increasing temperature. Thus in a practical application a strongly poisoned system can have excellent long-term stability (although not always good short-term reactor temperature stability).

c. Separation of Reversible and Irreversible Deactivation. Taking together the adjustment of the catalyst to the feedstock, and the irreversible deactivation generally gives a plot as shown in Figure 1 for catalyst activity (expressed as temperature required for a desired conversion) versus runtime. From Figure 1 it can be seen that at times shorter than about 100 days the catalyst is still reaching stationary state. Obviously this separation of these two stages may not always be easy or complete. A catalyst that has not yet been poisoned to its stationary state may, however, be very active for coking, etc. If a catalyst is quickly brought to its stationary operating temperature, it may suffer a higher deactivation than with a more careful start-up. This is possibly the basis for procedures such as “soft start-up” in first-stage hydrocracking (18).

The challenge now is to arrive at such an understanding of the processes and the poisoning and deactivation phenomena that the catalyst performance during its entire life, often with a variety of feedstocks and conditions, can be reliably predicted on the basis of short performance tests. Because of the complexities noted above, modelling, as an expression of an understanding of the process, will have to play a major role here. Before discussing the desired rapid performance tests, we will therefore look at the individual process areas separately, and then briefly review modelling.

3. Hydroprocessing

a. Distillate Desulfurization. In HDS of distillates such as naphtha, gasoil, etc., the traditional CoMo on alumina catalysts are used because of their high stability. Alternative catalyst formulations, such as CoMo supported on mixed oxides containing titania, have been studied (19), but so far their high initial activity was accompanied by a high deactivation rate. Hence the main emphasis in catalyst development has been a further optimization of the traditional CoMo alumina systems in terms of start-of-run activity. With the tightening sulfur specifications

for gasoline and distillates, deep desulfurization for which alternative catalysts might be developed is now being studied (20).

The current HDS catalysts clearly operate in a state of partial poisoning by reactants, nitrogen compounds, H_2S , etc. These phenomena have been extensively studied (21,22). Fortunately, the steady state is generally reached quickly (see Figure 2), and often reversibly. A deactivated catalyst can have a change in selectivity with respect to one that is fresh: a NiMo alumina catalyst poisoned by nitrogen compounds had increased selectivity to HDS relative to hydrogenation (23), and recently Texaco claimed the use of partially deactivated catalysts for selective processing of naphtha (24). This suggests that at least two types of active sites are present (cf. Section 2), a feature most recently discussed by van Veen et al. (25).

The structure and activity of coked catalysts exposed for a short time to aromatic feedstocks has been studied (26). It was concluded that coke is primarily located on the bare alumina support, and that the Ni(Co)Mo sulfides have a "self-cleaning" capability; with increasing coke content, coke gradually approaches the (active) edges of the NiMoS function. At a coke level of 10%, catalyst activity decreased by some 75%. It has been shown (27) that the nature of the coke not only depends on conditions but also on the type of catalyst.

b. Sulfur-Tolerant Hydrogenation. The hydrogenation of aromatics in middle distillates is done to comply with regulatory specifications on middle distillates as are now established in places such as Sweden and California (28). The mixed sulfides, because of their low activity, can only operate at high temperature, and for thermodynamic reasons require a high hydrogen pressure. The much more active noble metal catalysts that have been equipped with an enhanced resistance to sulfur poisoning are therefore preferred. These catalysts operate in a regime where the large majority of the metal sites are poisoned by S, even when sulfur tolerance has been improved by choosing modern metals and support functions (29). Thus these catalysts are currently used only in situations of relatively low sulfur contents, such as the Shell Middle Distillate Hydrogenation Process (30,31) and the SYNSAT process (32); in both cases the majority of the sulfur compounds have been eliminated by processing over a NiMo catalyst, and the noble metal catalyst operates in a low S/H_2S environment. Noble metal catalysts that can operate in a stacked-bed operation with a NiMo catalyst without intermediate H_2S removal have not yet been reported.

Laboratory tests (Figure 3) (28) and commercial experience (30,31) show that the catalysts need considerable time to reach the stationary state, after which further deactivation is very slow. This is related to the high sensitivity of the catalyst to poisons, and their necessarily low concentration.

c. Hydrocracking. The area of hydrocracking is particularly complex, because it involves both denitrogenation and cracking, because multiple catalyst systems are generally used, because hydrocracking itself is based on bifunctional catalysis, and because product recycle is often applied.

Generally the feedstock is first denitrogenated over NiMo alumina catalysts to reduce the poisoning of the cracking catalyst (33). This step is very similar

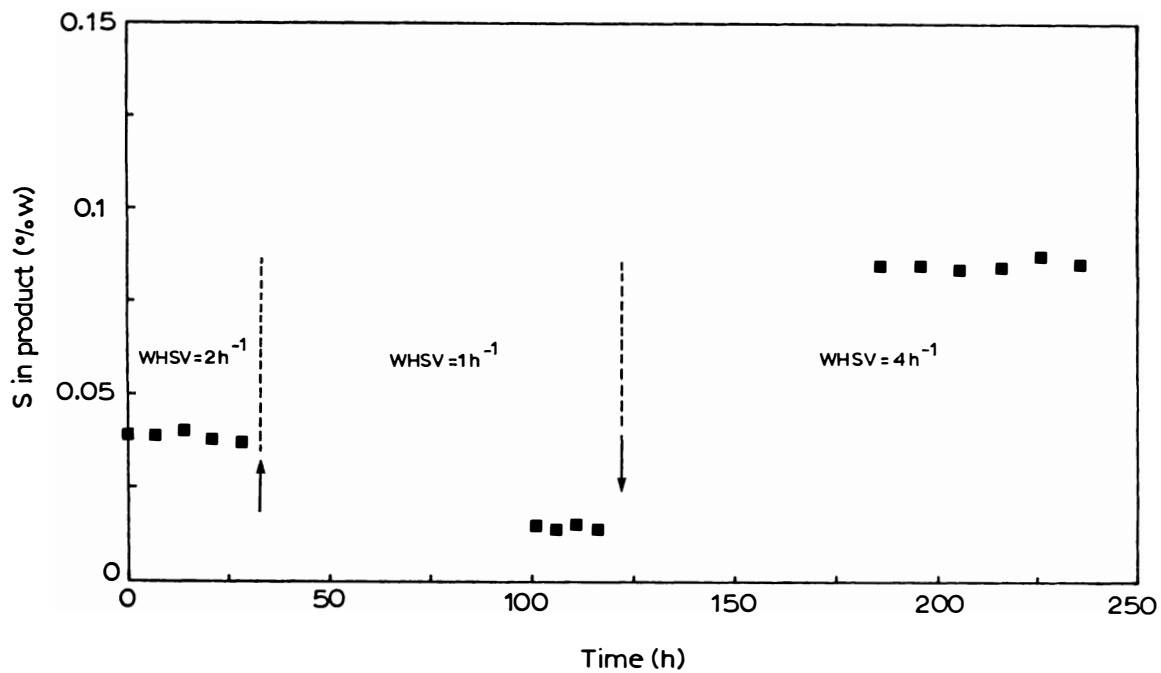


Figure 2. Stabilization of a high activity HDS catalyst, DC 130, in HDS of gasoil at 3 space velocities.

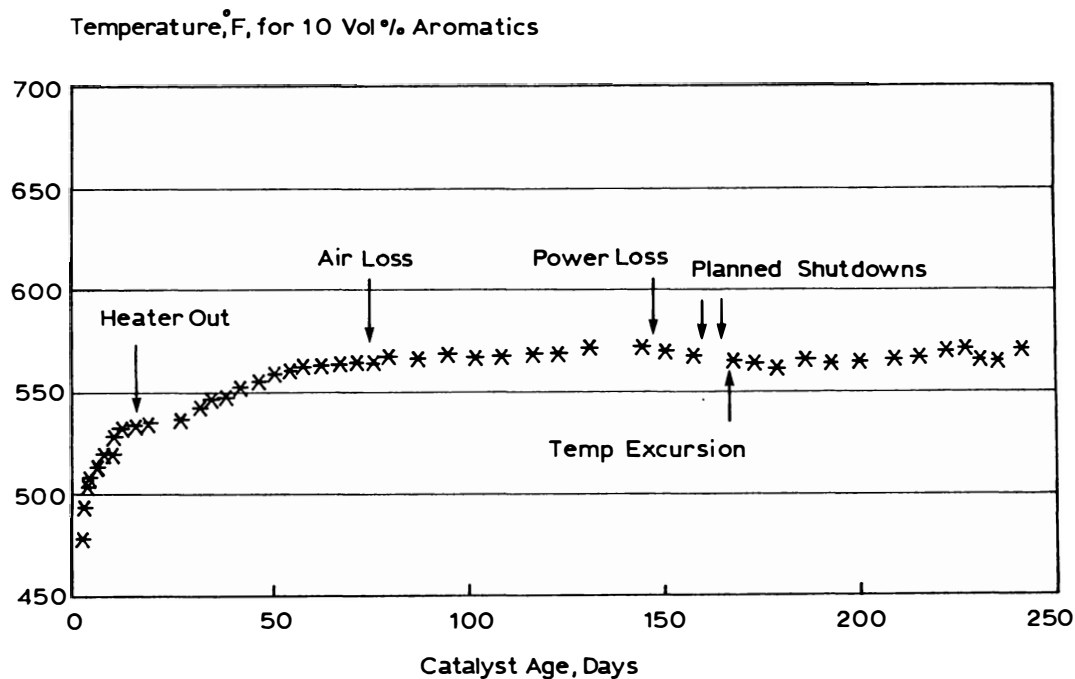


Figure 3. 242 Day stability test with hydrotreated West Coast diesel (35.1 vol.% aromatics; 19 ppm N; 156 ppm S; 700 psig; 2.0 LHSV). (Reproduced with permission from reference 28. Copyright 1994 B. D. Murray.)

to distillate HDS, although attaining the stationary state may sometimes take as long as 1000 h depending on feedstock and conditions. Similar to the situation in hydrogenation, equilibrium effects may occur in HDN, with the consequence that increasing temperature above a given value will not be effective in increasing the reaction rate (34). Clearly one must not confuse this inherently lower response to temperature increase with a supposedly high rate of deactivation. At least part of the denitrogenation is often also carried out over NiMo(W) catalysts with an acidic support such as amorphous silica alumina (ASA) or a zeolite (34,35); these catalysts often have a higher activation energy (33,34) that favours stability (see Section 2), as well as a higher cracking activity.

Hydrocracking itself is based on bifunctional catalysis, with a (de)hydrogenation function (mixed sulfides or noble metals) and a cracking function (zeolite, ASA) combined in one catalyst. In the fresh catalyst these have been well balanced for the given duty, as has been described by Ward (36,37). A change in stabilization of zeolite Y can markedly affect both selectivity and stability of a hydrocracking catalyst (38). Deactivation of the catalyst can affect each function differently, and result in a change in selectivity. Butt and coworkers (39) have studied in detail a series of commercially deactivated catalysts consisting of CoMo/ASA/Ultra Stable Y sieve supplied by Amoco. The activities of both functions were studied separately using several methods, and it was established that both deactivated during commercial operation, with the acidic function more affected. A catalyst cannot be expected to operate constantly in terms of product yields and properties during its lifetime, which is in agreement with observations (40) (see however Refs. (9,35) where selectivity is very constant).

In two-stage operation, where in the second (hydrocracking) stage the denitrogenated feed (from the first stage) is cracked at low ammonia partial pressure and at low temperature, it takes a very long time to reach the stationary state, as is illustrated in Figure 1 (9). In series-flow operation, where the first-stage effluent is cracked at high ammonia partial pressures and high temperatures, steady state is reached much faster. Obviously the poisoning by ammonia has major consequences (41): higher temperature requirements and different selectivities such as a higher middle distillate selectivity. These effects are related to a changed ratio in hydrogenation over cracking activity, and to an enhanced evaporation of cracked products at higher temperatures (42).

Hydrocracking is special in that often a recycle of unconverted feedstock is applied. Since hydrocracking catalysts generally do not convert all compounds with the same activity, e.g. due to the size exclusion effects occurring with zeolites such recycles can easily lead to the build-up of "inert" species, the nature of which depends on the catalyst used (Figure 4) (43). Sometimes such species can even be further generated (44). These recycle effects were studied in detail by Yan (45–47) who concluded that addition of a NiWASA catalyst, either separately in the recycle stream or in a ASA/zeolite composite catalyst (35), could reduce or eliminate the recycle effects which otherwise occur when processing cycle oils (end point 450°C; see Figure 5). It is interesting to note that a later publication reports that a (noble) metal REX catalyst instead of its Ni/W analogue does not lead to build-up effects, which is attributed to the much smaller volume taken up by the noble metals than the mixed sulfide, thus resulting in higher diffusion coefficients. Whether such

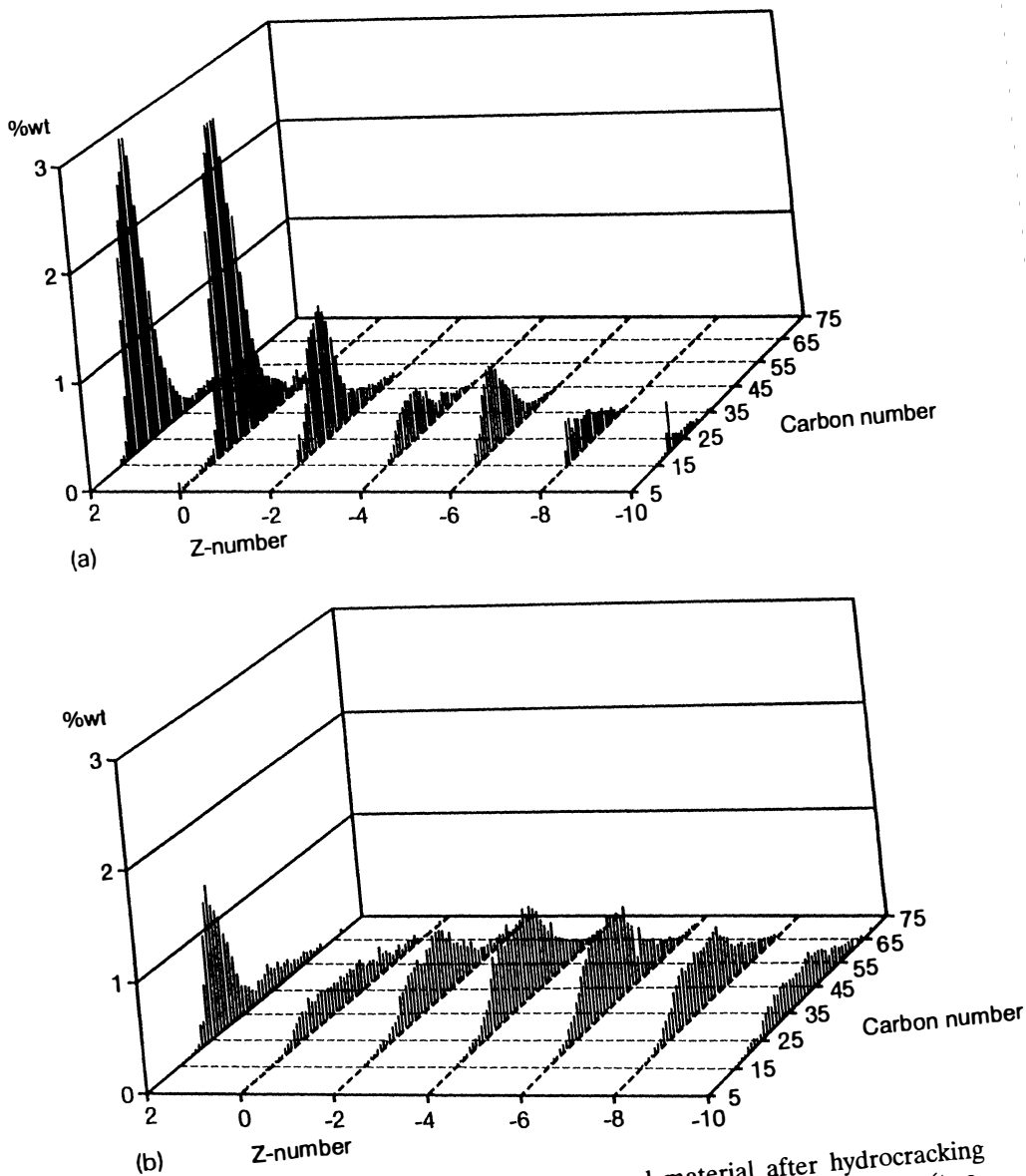


Figure 4. FIMS spectra of the unconverted material after hydrocracking treated VGO over (a) all-amorphous, and (b) all-zeolitic catalysts (two-stage operation), Z indicates the hydrocarbon stoichiometry, C_nH_{2n+Z} , i.e. (poly)naphthenes occur for $Z \leq -4$, and aromatics are possible at $Z \leq -4$. (Reproduced with permission from reference 35. Copyright 1994 T. Huizinga.)

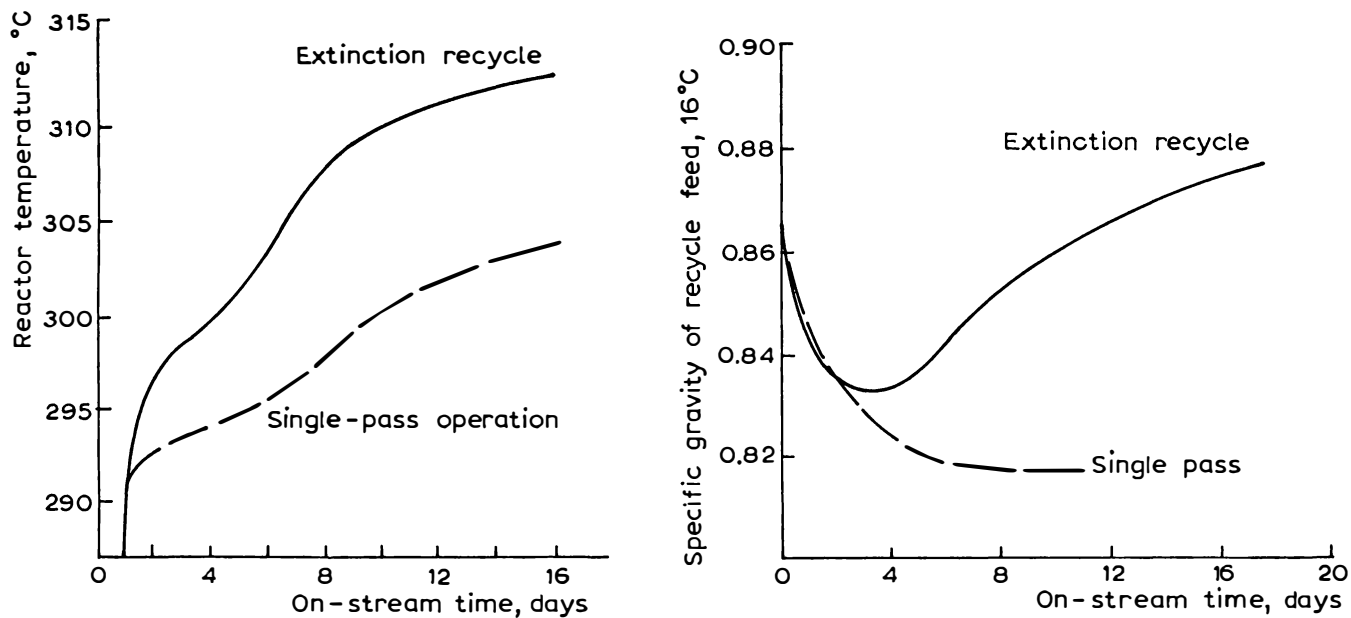
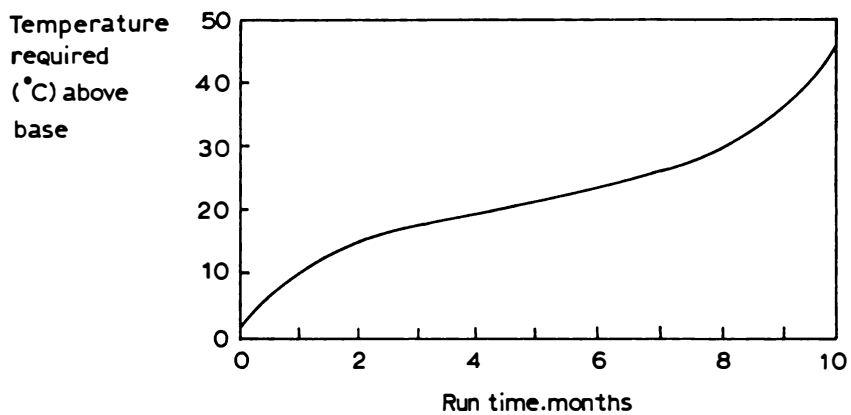


Figure 5. Reactor temperature and specific gravity of the recycle feed as a function of time-on-stream for recycle-to-extinction and single-pass modes of hydrocracking using NiW/RE-X catalyst. (Reproduced from reference 45. Copyright 1983 American Chemical Society.)

catalysts would also be adequate to avoid recycle effects with heavier feedstocks is not known. Abdul Latif (48) approached the recycle problem from the point of view of the refiner, showing that in recycle operation the polynuclear aromatics build-up causes catalyst deactivation and heat exchanger fouling (“red death”). PNA removal from the recycle stream leads to a clear increase in catalyst lifetime. Options include a bleed stream, a recycle of unconverted product to the vacuum column, or adsorption to a dedicated guard bed. These findings illustrate the importance of avoiding unrealistically large bleeds (e.g. due to sampling) in small-scale laboratory testing.

d. Fixed-Bed Residue Hydroprocessing. Process-wise fixed-bed residue hydroprocessing is relatively simple compared to hydrocracking: it is a once-through operation using a number of multi-bed reactors; in some cases the catalyst can be continuously replaced on-line (49,50). Catalyst deactivation is much more pronounced than in the process-wise similar distillate hydrotreating (Figure 6). Fouling by salt, scale, etc., is more pronounced but generally coped with by using (double) desalting (51) and special guard beds with high-porosity material (3), or by using on-stream catalyst replacement (49,50). The presence of asphaltenes and metals (especially Ni and V) in residue leads to severe progressive deactivation, which has been extensively studied primarily by Chevron (Gulf) and Shell, and often reviewed (2,13,50): generally coke deactivation rapidly reaches a stationary state (51,52), the deactivation becoming more severe with conversion and increasing temperature, while metals deactivation is progressive, through a combination of poisoning of sites active for HDS, and closure of the pore mouth (1,2,14,50,52). This pore-mouth plugging model (14) was later extended to active site poisoning (14), and has been extended by several other groups (53–55), which also considered metals poisoning more explicitly (56), pore size distribution effects (57), bimodal catalysts (58), interstitial deposition (59), and combined coke and metals deactivation (60). The interference between coke deactivation and metals deposition has been noted but is difficult to describe quantitatively.

In general an attempt is made to first remove the larger part of the metals using catalysts with a high metals uptake capacity but low HDS activity — generally wide-pore or bimodal catalysts with a rather low intrinsic activity. After this the demetallized feedstock is processed over dedicated HDS catalysts with smaller pores/higher surface area, where the core is not poisoned by metals (and less by coke), which also have a higher intrinsic activity. If desired this approach can be extended to more than two catalysts. In all cases pore diffusion plays a major role (it has been shown that diffusion coefficients of molecules such as coronene are reduced by a factor of about 500 — depending on pore diameter — in spent residue catalysts, relative to fresh ones (61)), and the pore texture is one of the prime characteristics in developing optimized catalysts (62). Product properties such as asphaltenes solubility may indirectly be correlated with catalyst stability. Upon residue hydroconversion the solvency of the maltenes for asphaltenes generally decreases, and at a given stage asphaltenes precipitate. This can result in bed plugging, interstitial growth, products with insolubles, indirect deactivation of the catalyst bed, and in general limits attainable conversion both in fixed- and in ebullating-bed operation. Catalysts that allow a higher conversion before



Case: 90% HDM:A/B/C catalyst system

Figure 6. Residue test. (Reproduced with permission from reference 50. Copyright 1989 Elsevier.)

asphaltenes precipitation sets in are therefore more stable at the higher conversion level and extremely valuable, as reported in Ref. (63) for ebullating-bed operation.

A more recent development in fixed bed residue processing is the use of zeolitic cracking catalysts. These have been developed primarily in Japan, and are quite stable according to the literature (64).

4. Modelling

In a (rapid) catalyst screening test, conditions will in general be different from those in actual operation, and experience and understanding of the particular process is essential for defining a test that is relevant, and for the translation of its results to the actual operation. The total process "know how" that has been obtained can be captured in an accessible form in a process model. One should not necessarily expect this model to be perfect, however, and extrapolations to conditions, feedstocks and catalysts that are outside the experimental base from which the model was constructed should be made with caution. This does not detract from the fact that, given the proper expertise, process models are extremely useful. In principle, two types of process models can be distinguished. In correlative models the effect of certain process (or catalyst) variables has been incorporated in mathematical formulae, which in themselves may be without physical meaning. They are an abbreviated form of the experimental database, relatively easy to set up, convenient to use, but sometimes difficult to expand. More ambitious, and generally more time-consuming to set up, are the kinetic models, in which the feedstock is split into certain (groups of) components, which then react according to a kinetic scheme for which parameters have been fitted. An example of such an approach for gasoil HDS has been reported (65), where the oil is split into 26 components, which are followed in the reactor, which has been split into 10 segments, on the basis of a detailed analysis. Between all these segments heat effects, evaporation, etc., can be taken into account. A similar approach of segmenting the reactor was described by De Jong et al. (66). This molecular approach can be extended and ultimately used to evaluate entire refining schemes (67).

In general such models focus on the description of the stationary state, predicting reaction rates, product yields, product quality, etc. as a function of feedstock and conditions. Catalyst deactivation usually does not have a prominent place in these models, and is based on a simple description, again because the available database is limited. In the example quoted above (65), however, a dedicated series of experiments on catalyst aging at different conditions was carried out to model the catalyst deactivation.

Ideally one would therefore choose a model, similar to that of described in Ref. (65), in which the reactor is split into a number of sectors, and in which for each the activity of the catalyst is calculated as a function of time. This is essentially what the RESIDS model (14,50) does for residue hydroprocessing: it correlates local catalyst activity/deactivation with local reaction rates for HDM, HDS, etc. Thus, at any time and location in the reactor, the actual state and activity of the catalyst are defined, allowing predictions of complex multi-catalyst/multi-bed systems over a range of feedstocks and conditions. For this the catalyst activity and

deactivation parameters have to be determined in dedicated experiments — see Section 5 — a complex task generally only undertaken by major oil companies. However, once these performance parameters can be correlated with the physical and chemical properties of the catalysts in their fresh (or stationary) state, the way will be open to “catalyst design”.

5. Catalyst Performance Testing

An unequivocal determination of catalyst activity and stability is of crucial importance in the design of a new processing unit or sometimes even when introducing a new catalyst package in an existing unit, and to this end often lengthy, dedicated pilot plant tests are carried out before a design is finalized. For catalyst development this is not realistic, and shorter tests, which are still relevant, must be used. Ideally activity and deactivation of catalyst particles should be measured in one well defined, uniform environment. This can be achieved by using a differential reactor (possibly with external recycle), as was done in Shell’s work on residue catalyst deactivation by metals (15). Even in this extensive study, however, metals deposition on the catalyst was accelerated by using high metals feedstocks at high spatial velocity and temperature, and still necessitated translation to the real conditions (15,50).

Often such an extensive effort cannot be justified, and one has to be satisfied with deactivation experiments that measure the average over a catalyst bed where a considerable conversion is achieved, hence where the catalyst is definitely not operating in a uniform environment. Examples are the variations in metals in or over the catalyst bed in residue hydroprocessing, and in organic nitrogen in hydrocracking; for both cases dedicated top-bed catalysts which are more stable under high concentrations of metals (HDM catalysts, ABC concept (15,50)) or nitrogen (Z 763 specifically developed from Z 753 for improved nitrogen tolerance in top-bed duty (68)) are used commercially. [In principle the variation in deactivation in the axial direction might be derived from the temperature (heat generation) profiles over the catalyst bed, but this is easier for adiabatic industrial reactors than for the isothermal laboratory scale ones.] The translation to situations with different conversions, etc., will remain difficult, however. Indeed, the definition of a relevant rapid screening test is generally a major task, and many tests in the end give results that are not relevant. When determining catalyst activity and stability, one will want to accelerate both the approach to the stationary state and the (subsequent) long-term deactivation; also it will remain crucial to have a good separation of the two, otherwise too high apparent deactivation rates are reported (see Section 2 and Figure 3).

Thus, when the considerations of the earlier sections are taken into account, the following points can be made on setting up a screening test:

a. Feedstock. Clearly, performance testing should be done using feedstocks that closely resemble the intended one. Use of feedstocks with a different boiling point will influence catalyst activity differences as well as catalyst stability; in addition, cracked feedstocks generally lead to faster catalyst deactivation because of the high aromatics content. In practice, therefore, one generally uses one screening

feedstock for catalyst development, and then assesses the performance of the promising candidates with a range of other feedstocks.

Performance testing in trickle-flow operation invariably takes longer than in gas-phase tests with model compounds. Testing with model compounds such as thiophene can be an effective contribution to fast screening, e.g. for the effectiveness of catalyst functions in a defined context, but should not be taken beyond that.

b. Accelerating the Reaching of the Stationary State. As was discussed in Section 2, the stationary state is reached reasonably quickly in situations where the feedstock contains a high concentration of catalyst poisons, such as in gasoil HDS, first-stage hydrocracking and in residue hydroprocessing. In sulfur-tolerant hydrogenation experiments and in second-stage hydrocracking at low ammonia levels, however, this takes much longer. The poisons in the feed are strongly absorbed at the catalyst, and at the same time converted over it. The “equilibration time” can be shortened by several means, such as blocked-in periods with high feed rates, or with higher contaminant levels, or even a total screening with a feedstock with a higher concentration of poison. These procedures can give a useful ranking test, but the translation to the envisaged application must be confirmed. Too often such a test develops into something which ultimately is merely a complicated titration rather than a determination of catalytic activity.

c. Long-Term Catalyst Deactivation. Obviously here also accelerated tests to measure deactivation by coke and by metals are required in a catalyst screening stage. The accelerated coking is achieved by operation at lower hydrogen partial pressures and/or higher temperatures, as described in Ref. (65).

Accelerated deactivation tests in hydrocracking have been reported (38), where a constant conversion mode was run at much higher space velocity (and hence temperature) than under actual operation conditions. Differences in deactivation were measured that were later substantiated in commercial operation (38). Although all these approaches aim at accelerating the catalyst deactivation reaction in Equation 7, such tests should obviously not be applied to catalyst systems that — at the high space velocity — operate at such high temperatures that very high polyaromatics concentrations prevail.

In residue hydroprocessing, however, coke is often set at a quasi-stationary level dictated by factors such as temperature, so here this approach must be followed with care (51–53,69). Metals deactivation can be accelerated by using a high metals feedstock, higher space velocity (to get a higher overall loading) and higher temperature. This was studied for instance by Altag (69): in a “normal” test, at normal temperature, blocked-in conditions were used with high space velocity, high temperature and high metals feedstock (Hondo, Maya), such that although most of the time the test is run under normal feed/conditions, most of the metals are deposited in the blocked-in periods. The amount of deposition is a good measure of activity/deactivation for HDM, although possible feedstock effects need to be taken into account, Maya AR giving larger than expected deactivation in the quoted reference (attributed to stronger coke make and hence larger diffusion hemming). For HDS the result was different, and the blocked-in experiments always gave lower HDS activity, including the check-back periods. A

fair representation of the deactivation by metals for HDS was obtained by simply impregnating Ni and V onto the catalyst.

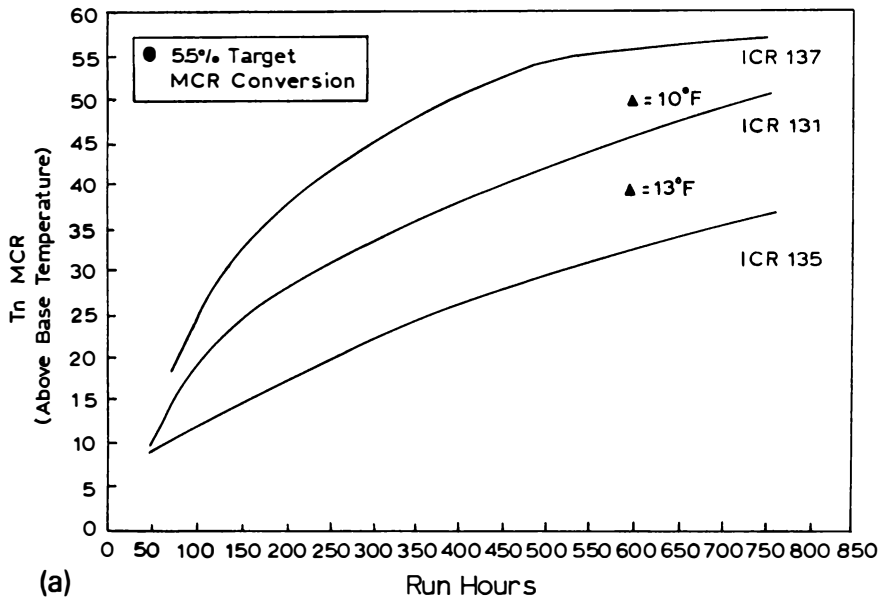
d. Modelling. In Section 4 the importance of modelling was stressed. In practical terms the following examples can be quoted: in Ref. (49) test results with improved catalysts are given, the new catalyst apparently having a lower start-of-run temperature and stability for HDS. It is only by considering the total dual catalyst system that the advantage of the improved HDM catalyst, emerges (Figure 7); obviously models predict these phenomena far more effectively than experiments. Also, Shell has reported on a dedicated test for residue catalyst screening, where a series of temperatures was applied that is closely linked to their RESIDS model (14,50) (Figure 8), also using correlations between metals deactivation and metals penetration into the catalyst particles. An occasional confirmatory experiment then suffices to validate the results and complete the catalyst development.

e. Recycle Operation. The recycle in hydrocracking poses special problems because it has a clear effect on catalyst performance, dependent on the formulation of the catalyst. The preferred option to cope with this is to carry out recycle tests using small-scale equipment with realistic feeds and conditions (43). The deactivation can be accelerated by the usual means, lower gas rates and pressures, higher space velocities and temperatures, and heavier feedstocks. In our experience this is an excellent procedure for catalyst development (43). An alternative is to carry out once-through experiments with feedstocks that contain recycle material, obtained either directly from a commercial hydrocracker or by separate blending of first stage effluent and a recycle stream. Obviously this set-up is experimentally easier; at the same time it is less rigorous in that build-up effects with the catalyst under study are not really monitored.

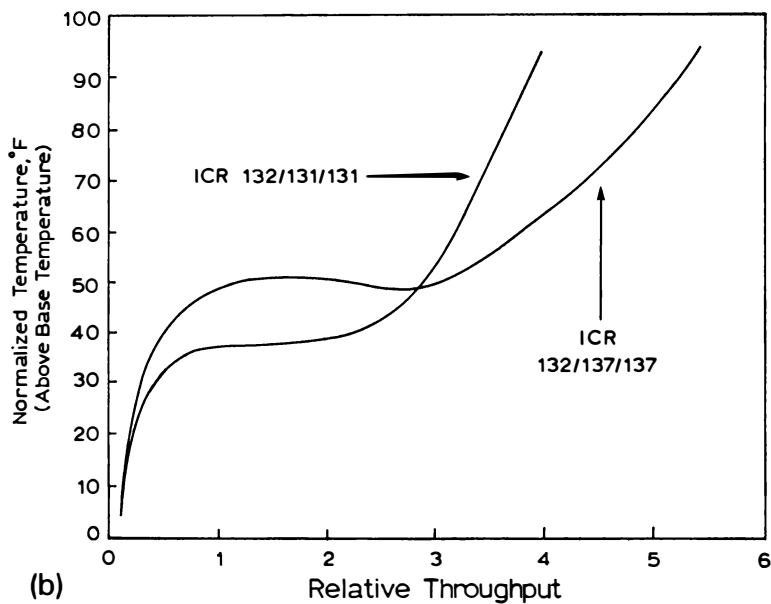
f. Further Development. Clearly the design of accelerated tests hinges on a good understanding of the process. Nevertheless, the slow approach to stationary state in some of the above-mentioned applications would in particular lend itself to modelling. This would lead to generic procedures to shorten such periods that are nevertheless more specific than those quoted earlier. For the acceleration of coking and metals deposition the approach and dangers are clear, and here less basic work is necessary. Modelling will become increasingly more important, but we are still a long way from the stage where deactivation can be predicted theoretically with a reasonable precision. Hence it is necessary to continue to develop and implement cost-effective small-scale equipment to measure catalyst performance, in conjunction with process models for interpretation of the data. A review of reliable small-scale testing methods is presented by S.T. Sie in this symposium (70).

6. Conclusions

Performance testing is essential in the development and application of catalysts, and the preferred approach will depend on the target to be reached. Thus for a final process evaluation long and detailed pilot plant tests will be carried out whereas for catalyst development this is not realistic. In the latter process simple



(a)



(b)

Figure 7. a. MCR Conversion activity for ICR catalysts (Arabian Heavy AR). b. Normalized temperature for MCR removal (55% conversion target in whole liquid product). (Reproduced with permission from reference 49. Copyright 1993 Elsevier.)

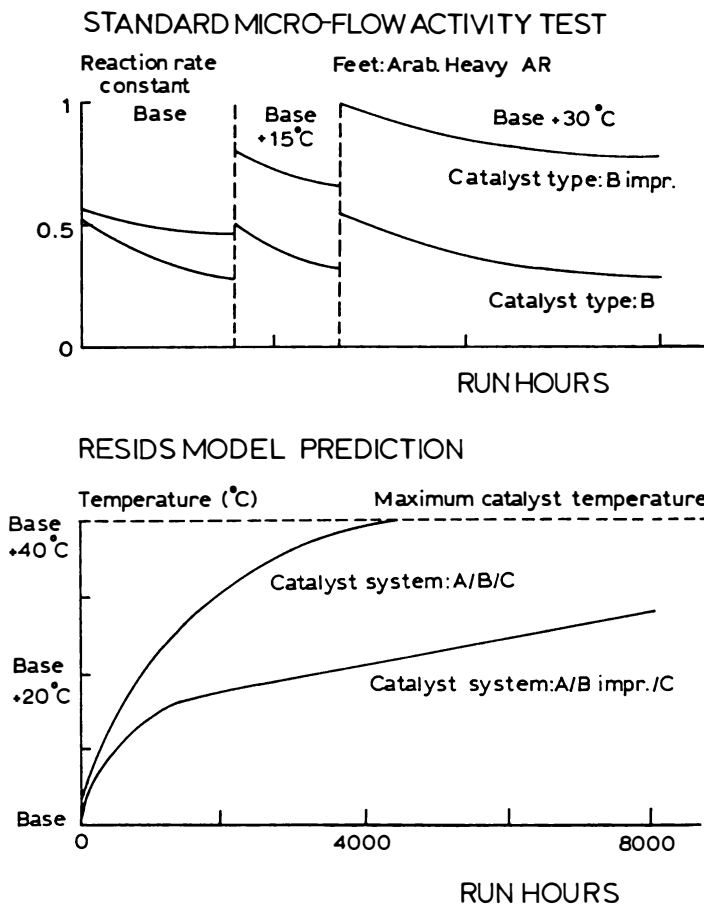


Figure 8. Testing and prediction of catalyst performance. (Reproduced with permission from reference 50. Copyright 1989 Elsevier.)

screening tests, both for initial performance and for stability, will have to be selected carefully on the basis of an adequate process knowledge, and preferably supported by process models. In this situation the use of small-scale equipment that is nevertheless able to reliably mimic the essential features of the process, including product recycles, is of great value.

Acknowledgments

The author is indebted to his colleagues at KSLA (in particular Dr. J.W. Gosselink) and WTC for many stimulating and critical discussions on the subject of this paper.

Literature Cited

1. Butt, J.B.; Petersen, E.E. *Activation, Deactivation and Poisoning of Catalysts*; Academic Press: New York, 1988.
2. Bartholomew, C.H. In *Catalytic Hydroprocessing of Petroleum and Distillates*; Oballa, M.C. and Shih, S.S., Eds.; Marcel Dekker: New York, 1994.
3. Fujita, K.; Torihara, N.; Miyauchi, Y.; Inoue, Y. *Catalytic Science Technology*; Kodansha: Tokyo, 1991; Vol. 1, p. 347.
4. Gosselink, J.W.; Stork, W.H.J.; de Vries, A.F.; Smit, C.H. In *Catalyst Deactivation 1987*; Delmont, B.; Froment, G.F., Eds.; Elsevier: Amsterdam, 1987; p. 279.
5. Gosselink, J.W.; Stork, W.H.J. *Chem. Eng. Process.* **1987**, *22*, 157; and references therein.
6. Kaernbach, W.; Kisielow, W.; Warzecha, L.; Miga, K.; Klecan, R. *Fuel* **1990**, *69*, 221.
7. Richardson, R.L.; Riddick, F.C.; Ichikawa, M. *Oil Gas J.* **1977**, *May 28*, 80.
8. Somorjai, G.A. *Chemistry in Two Dimensions*; Cornell University Press: Ithaca, 1981.
9. George, S.E.; Boardman, S.R.; Foley, R.M.; Sanborn, L.J.; Johnson, P.S.; Webb, A.; Gallagher, A.; Gualtieri, P.K.; Mok W.S.; Nash, D. *Paper AM 94-19*, NPRA Meeting, March 20–22, 1994, San Antonio
10. Kennedy, C.R.; LaPierre, R.B.; Pereira, C.J.; Mikovsky, R.J. *Ind. Eng. Chem. Res.* **1991**, *30*, 12.
11. Sie, S.T. In *Advanced Zeolite Science and Applications*; Jansen, J.C.; Stoecker, M.; Karge H.G.; Weitkamp, J., Eds.; Elsevier: Amsterdam, 1994.
12. Maxwell, I.E.; Stork, W.H.J.; Schaper, B.; Lundquist, L.E.O.; Yoguchi, M. *Petrotech (Tokyo)* **1982**, *5(9)*, 816.
13. Tamm, P.W.; Harnsberger, H.F.; Bridge, A.G. *Ind. Eng. Chem. Process. Des. Dev.* **1981**, *20*, 262.
14. Adams, C.T.; del Paggio, A.A.; Schaper, H.; Stork, W.H.J.; Shiflett, W.K. *Hydrocarbon Process.* **1989**, *Sept.*, 57.
15. Sie, S.T. In *Catalyst Deactivation*; Delmon, B.; Froment, G.F., Eds.; Elsevier: Amsterdam, 1980.
16. v. Zijll Langhout, W.C.; Ouwkerk, C.; Pronk, K.M.A. *Paper at AiChE Meeting*, June 1980, *Oil Gas J.* **1980**, *Dec.*, 1.

17. Dautzenberg, F.M.; van Klinken, J.; Pronk, K.M.A.; Sie, S.T.; Wijffels; J.-B. *Chem. Eng. Sci.* 1978, 254.
18. Smegal, J.; et al. *US Patent 5006224*; April 9, 1991.
19. Daly, F.P.J. *Catal.* **1989**, 116, 600; and references therein.
20. European Patent Application 0573973A1; 1992
21. Satterfield, C.N. *Heterogeneous Catalysis in Industrial Practice*; McGraw Hill: New York, 1991.
22. van Gestel, J.; Leglise J.; Duchet, J.-C. In *Catalytic Hydroprocessing of Petroleum and Distillates*; Oballa, M.C.; Shih, S.S., Eds.; Marcel Dekker: New York, 1994; p. 357.
23. Nagai, M. *Ind. Eng. Chem. Prod. Res. Dev.* **1985**, 24, 489.
24. US Patent 5286373; 1992.
25. van Veen, J.A.R.; Colijn, H.A.; Hendriks P.A.J.M.; van Welsenens, A.J. *Fuels Process. Technol.* **1993**, 35, 137.
26. Diez, F.; Gates, B.C.; Miller, J.T.; Sajkowski, D.J.; Kukes, S.G. *Ind. Eng. Chem. Res.* **1990**, 29, 1999.
27. de Jong, K.P.; Kuipers, H.P.C.E.; van Veen, J.A.R. In *Catalyst Deactivation 1991*; Bartholomew, C.H.; Butt, J.B., Eds.; Elsevier: Amsterdam, 1991; p. 289.
28. Murray, B.D.; Winqvist, B.H.C.; Sanborn, L.J.; Milan, S.N.; Foley, R.M.; Johns, W.F.; Schofield, D.P. *Paper 243d*, AIChE Meeting, November 1994.
29. Naber J.E.; Stork, W.H.J. Paper, JECAT 1991, Tokyo.
30. van den Berg, J.P.; Lucien, J.P.; Germaine, G.; Thielemans, G.L.B. *Fuels Process. Technol.* **1993**, 35, 119.
31. van den Berg, J.P.; Germaine, G.; Verloop, J.; Elfring, M. *Presentation at Summer Conference Royal Dutch Chemical Society*, Delft, September 1–2, 1994.
32. Suchanek A.J.; Granniss, E.L. *Paper AM 95-40*, NPRA Meeting, San Francisco, March 19–21, 1995.
33. Gosselink, J.W., van der Paverd, A.; Stork, W.H.J. In *Catalysts in Petroleum Refining*; Trimm, D.L.; Akashah, S.; Absi-Halabi, M.; Bishara, A., Eds.; Elsevier: Amsterdam, 1990; p. 385.
34. Minderhoud, J.K.; van Veen, J.A.R. *Fuels Process. Technol.* **1993**, 35, 87.
35. Huizinga, T.; Teunissen, J.M.H.; Minderhoud, J.K.; van Veen, J.A.R.; Springett, H.J. *Paper at AIChE Meeting*, San Francisco, November 15, 1994.
36. Ward, J.W. In *Design and Preparation of Catalysts*; Elsevier: Amsterdam, 1983; p. 587.
37. Ward, J.W. *Fuels Process. Technol.* **1993**, 35, 55.
38. Hoek, A.; Huizinga, T.; Esener, A.A.; Maxwell, I.E.; Stork, W.H.J.; van den Meerakker, F.J.; Sy, O. *Oil Gas J.* **1991**, 89(16), 77.
39. Hadjiloizou, G.C.; Butt, J.B.; Dranoff, J.S.; *J. Catal.* **1992**, 135, 481; and references therein
40. Reno, M.E.; Schaefer, B.L.; Penning, R.T.; Wood, B.M. *NPRA Paper AM 87-60*.
41. Dufresne, P.; Quesada A.; Mignard, S. In *Catalysts in Petroleum Refining*; Trimm, D.L.; Akashah, S.; Absi-Halabi M.; Bishara, A., Eds.; Elsevier: Amsterdam, 1990; p. 301.

42. Sie, S.T.; Eilers, J.; Minderhoud, J.K. In *Proceedings 9th Congress on Catalysis*; Vol. 2, Calgary 1988; Phillips, M.J.; Ternan, M., Eds.; Chem. Institute Canada: Ottawa, 1988; p. 743.
43. van Dijk, A.; de Vries, A.F.; van Veen, J.A.R.; Stork W.H.J.; Blauwhoff, P.M.M. *Catal. Today* **1991**, *11*, 129.
44. Sullivan, R.F.; Boduszynski, M.M.; Fetzer, J.C. *Energy and Fuels* **1989**, *3*, 603.
45. Yan, T.S. *Ind. Eng. Chem. Process. Des. Dev.* **1983**, *22*, 154.
46. Yan, T.S. *Ind. Eng. Chem. Res.* **1989**, *28*, 1463.
47. Yan, T.S. *Ind. Eng. Chem. Res.* **1990**, *29*, 1995.
48. Abdul Latif, N.M. In *Catalysts in Petroleum Refining*; Trimm, D.L.; Akashah, S.; Absi-Halabi, M.; Bishara, A., Eds.; Elsevier: Amsterdam, 1990, p. 349.
49. Scheuerman, G.L.; Johnson, D.R.; Reynolds, B.E.; Bachtel, R.W.; Threikel, R.S. *Fuels Process. Technol.* **1993**, *35*, 39.
50. Oelderik, J.M.; Sie, S.T.; Bode, D. *Applied Catal.* **1989**, *47*, 1.
51. Hohnholt, J.F.; Fausto, C.Y. *Oil Gas J.* **1986**, *Jan. 6*, 63.
52. Myers, T.E.; Lee, F.S.; Myers, B.L.; Fleisch, T.H.; Zajac, G.W. *AIChE Symposium Series 273*, Vol. 85; 1989, p. 21.
53. Ammus, J.M.; Androutsopoulos, G.P.; Tsetsekou, A.H. *Ind. Eng. Chem. Res.* **1987**, *26*, 1312.
54. Ahn, B.-J.; Smith, J.M. *AIChE J.* **1984**, *30*, 739.
55. Khang S.-J.; Mosby, J.F. *Ind. Eng. Chem. Process. Des. Dev.* **1986**, *25*, 437.
56. Rautiainen, E.P.H.; Wei, J. *Chem. Eng. Comm.* **1990**, *98*, 113.
57. Tsakalis, K.S.; Tsotsis, T.T.; Stiegel, G.J. *J. Catal.* **1984**, *88*, 188.
58. Pereira, C.J.; Beeckman, J.W. *Ind. Eng. Chem. Res.* **1989**, *28*, 422.
59. Kissinger, S.L.; Khang, S.-J. *Chem. Eng. Sci.* **1989**, *44*, 417.
60. Chao, Y.-C.; Liaw, H.-J.; Huang, H.-P. *Chem. Eng. Comm.* **1991**, *104*, 267.
61. Johnson, B.G.J.; Massoth, F.E.; Bartholdy, J. *AIChE J.* **1986**, *32*, 1980.
62. Beuther, H.; Larson, O.A.; Perrotta, A.J. In *Catalyst Deactivation*; Delmon, B.; Froment, G., Eds.; Elsevier: Amsterdam, 1980; p. 271.
63. Nongbri, G.; Clausen, G.A.; Huang, J.R.; Self, D.E.; Paul, C.A.; Rodarte, A.I. In *Catalytic Hydroprocessing of Petroleum and Distillates*; Oballa M.C.; Shih, S.S., Eds.; Marcel Dekker: New York, 1994; p. 55.
64. Nakamura, I.; Iwamoto, R.; Iino, A. In *New Aspects of Spillover Effects in Catalysis*; Inui, T.; et al., Eds.; Elsevier: Amsterdam, 1993, p. 77.
65. US Patent 5 341 313; 1994.
66. de Jong, K.P.; Reinalda, D.; Emeis, C.A. In *Catalyst Deactivation 1994*; Delmon, B.; Froment, F.G., Eds.; Elsevier: Amsterdam, 1994; p. 155.
67. van der Eijk, H.; Vink, K.J. *Paper presented at the 8th Int. Symposium on Large Chemical Plants*, Antwerp, Belgium, 1992.
68. George, S.E.; Foley, R.M. *Paper AM 91-13*, NPRI Meeting, March 17-19, 1991, San Antonio.
69. Altag, A.W. *AIChE Symposium Series 273*; Vol. 85; 1989, p. 32.
70. Sie, S.T. *Paper T1*, Int. Symp. on the Deactivation and Testing of Hydrocarbon Conversion Catalysts, August 20-25, 1995, Chicago.

Development of a Test Procedure To Evaluate Fluid Catalytic Cracking Catalyst Regenerability

V. L. N. Murthy, S. Debnath, M. Rama Rao, S. K. Ray, A. K. Das, and
S. Ghosh

Research and Development Centre, Indian Oil Corporation Ltd.,
Sector 13, Faridabad 121007, India

Regeneration of spent catalyst is an important step in FCC. The regenerability or intrinsic coke burning rate of the catalyst is affected by its physico-chemical properties and the presence of different constituents which influence the accessibility of oxygen to the coked site. Knowledge of regenerability helps in catalyst selection, simulation and trouble shooting. A novel Batch Fluidized bed Regenerator (BFR) has been developed for studying catalyst regenerability, in which coking, stripping and regeneration of catalyst can be carried out in situ. The test conditions were optimized to minimize axial gradients and the effect of catalyst sampling.

The present study reveals that the regenerability is strongly dependent on the ratio of micro to macro pore surface area. A critical coke concentration (C_{cr}) is also identified, below which the regeneration behavior differs significantly from the initial first order kinetics. Studies on this unit also explain the impact of catalyst changes on coke on regenerated catalyst (CRC), in a commercial plant. The present test effectively distinguishes catalysts with varying regenerabilities.

Fluid Catalytic Cracking (FCC) is a major secondary conversion process in the petroleum refinery. In this process, heavy petroleum fractions (vacuum gas oils) are catalytically cracked into a host of valuable products from LPG to diesel. The feed vapors are brought into contact with fluidized catalyst in the riser-reactor, resulting in catalytic cracking. The catalyst is stripped of interstitial hydrocarbon vapors in the stripper, before it enters the regenerator. The coke deposited on the catalyst is burnt off, in presence of air, in the regenerator. The catalyst is circulated through these vessels resulting in a complex interaction among different process variables.

Regeneration of coked catalyst is an important step in FCC operation as the effective activity of the catalyst entering the riser is determined by the coke on regenerated catalyst

(CRC). Thus the CRC should be maintained at an optimum level to fully exploit the selectivity and activity functions of the catalyst. Moreover, as FCC unit is guided by a delicate heat balance, regenerator operation has significant impact on the overall operation of the unit. In fact, the capacity and performance of a particular FCC unit is often governed by the efficiency of regeneration.

The coke burning rate in a commercial regenerator is strongly influenced by the regenerability of the catalyst, the hydrodynamics (gas-solid mixing) and operating conditions. The unit hardware largely determines the extent of non-idealities in the distribution of gas and solid phases. Thus for a given hardware with constant operating limits like air blower capacity etc., the catalyst regenerability becomes a crucial parameter in determining the unit coke burning capacity. The impact of regenerability is more pronounced in partial combustion mode regenerators where a significant amount of CO will be present in flue gas. Any deterioration in regenerability of the catalyst results in the burning of CO in the dilute region, leading to severe after-burning.

Fig. 1 shows the effect of catalyst regenerability on CRC and after-burning. This study has been conducted using an in-house simulation package the details of which could be found elsewhere (1). The regenerator model can predict CRC and gas concentration profiles in the dense and dilute regions. It can be clearly seen from Fig. 1 that an increase in intrinsic coke burning rate constant results in reduced CRC and after-burning and vice versa. It is worth while to mention here that the model assumes ideal contacting patterns, both in the dense and dilute regions. It is needless to say that the oxygen break through due to improper catalyst and gas mixing would further aggravate the problem of increased CRC and after-burning.

In India all the FCC units operate under low severity in order to maximize the yield of middle distillates. The regenerators operate in partial combustion mode, frequently facing the problems as discussed earlier. In the context of Indian FCC operations, identification and use of catalysts with better regenerability is of paramount importance for enhancing operational efficiency. A priori knowledge of the regenerability of a catalyst helps in modeling and analysis of regeneration operation. In addition, it plays a significant role in choosing a catalyst for FCC unit.

A considerable amount of work had been done to understand the effects of the physico-chemical properties of the catalyst on its activity and selectivity. However, there is a paucity of information on the coke burning behavior of different FCC catalysts and its effect on catalyst properties. This gap is further widened by the advent of a variety of zeolite based catalysts, with widely different physico-chemical and morphological properties.

Weisz (2) carried experiments on silica- alumina beads (many times the size of an average FCC particle). He observed that the intrinsic coke burning rate was independent of the coke composition and the catalyst characteristics but dependent on initial coke level and the diffusivity. Weisz (3) in another study, found that the CO_2/CO ratio during intrinsic coke burning is only a function of temperature. He also observed that this ratio is affected by the presence of trace metals like iron and nickel etc. Even though this study was elaborate, it was limited to only silica-alumina catalysts in the form of beads.

Wang (4) et al studied regeneration kinetics on a zeolite catalyst using pulse and continuous flow techniques. They proposed a parallel -consecutive reaction mechanism

for coke burning. This study was limited to a single zeolite catalyst with an objective to identify a rate expression. Hano (5) et al studied the kinetics over a zeolite based catalyst and estimated the kinetic parameters.

It can be generally concluded that the works of many authors were confined to amorphous or a single zeolite based FCC catalyst. The effect of catalyst properties on regenerability has not received the due importance in the above studies.

The work of Magnoux (6) was to some extent oriented in this direction. He studied the coke burning behavior over HZSM-5, HY and H-mordenite. The burning rates observed with mordenite was much higher because of free movement of oxygen in the supercages, where coke is located. In HZSM-5, the burning rate is severely diffusion-limited. The observations were largely qualitative and no attempt was made to correlate the effect of catalyst properties on regenerability.

With this background, the present work is initiated at the Indian Oil Corporation R&D Centre. The broad objectives of this work are as given below.

- to study the dependence of the regeneration behavior of different zeolite based FCC catalysts in respect of various physico-chemical properties.
- to develop a simple procedure for testing FCC catalysts (both equilibrium and steamed) for regenerability

A Batch Fluidized bed Regenerator (BFR) with the facility for in-situ coking of catalysts has been designed and fabricated in house. Different FCC catalysts have been coked and regenerated in this unit. The results of the studies clearly distinguish catalysts with different regenerabilities. A few simple studies in this unit could clearly explain the changes in CRC level of catalyst in a commercial FCC unit with catalyst changes.

Experimental Section

Setup. The sketch of the experimental setup used in the present study is shown in the Fig.2. The regenerator (R) consists of a one inch stainless steel column with a wire mesh distributor (D) at the bottom. Measured quantities of air and nitrogen pass through the preheater zone (H1) before entering the regenerator bottom. The flow of N_2 or air through the system is achieved by changing the position of the three way valve (V1). The regenerator vessel is heated with a heating tape. Thermocouples (TC1-TC5) are fitted to monitor the temperature at different axial positions. For in-situ coking of catalysts, a feed injection system (F1) is provided which has the facility for different injection rate and injection time settings. The feed is preheated (H3) before it enters the regenerator and reacts on the catalyst. The feed line is constantly purged with N_2 to avoid plugging. All heaters are controlled by PID controllers.

Experimental Conditions. As the aim of the present study is to understand the intrinsic coke-burning behavior of FCC catalysts, extreme care has been taken in selecting experimental conditions so that no transport resistances influence the results. Minimizing the oxygen axial concentration gradient and obtaining sufficient kinetic data are the two

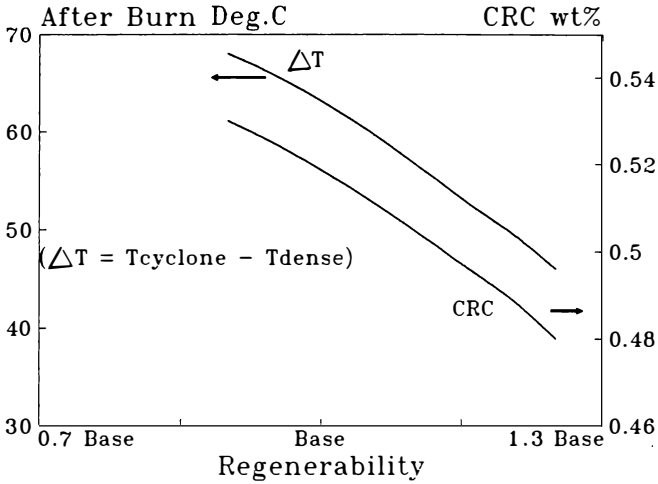


Fig.1. Effect of Catalyst Regenerability On CRC and After-burning

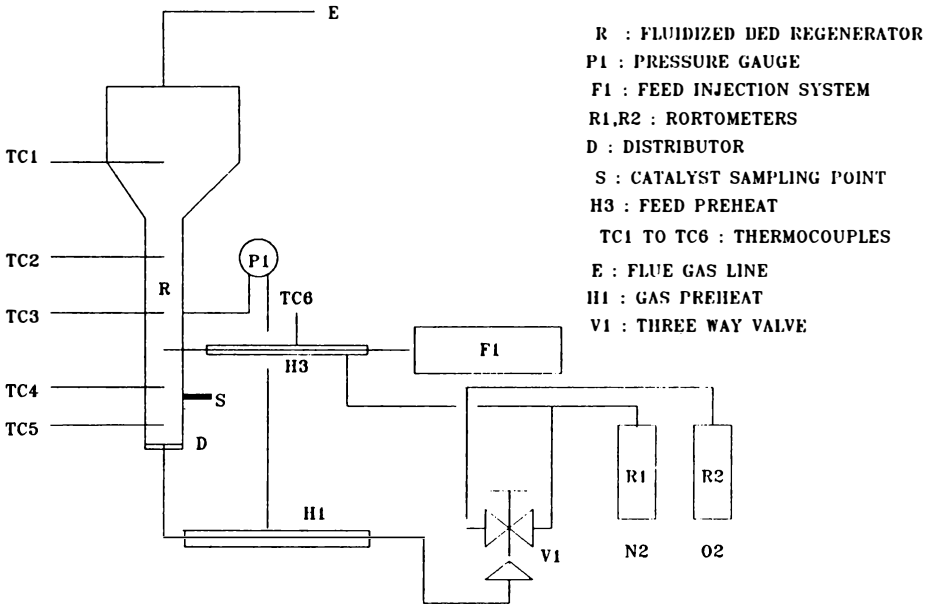


Fig.2. Schematic of Fluidized bed Regenerator

important concerns in the design of the test methodology. It is worth while to note that the minimum O_2 concentration gradient ensures homogeneity of the CRC at any bed position during regeneration. Experimental conditions follow.

Coking

Catalyst Inventory (W_c) : 50 gms
 Temperature of coking : 495 deg.c
 Feed (VGO) injection time : 120 s
 Total feed quantity injected : 5.7-5.8 gms

Stripping

Strip time : 15 min. using nitrogen as stripping medium

Regeneration

Regeneration Temperature : 585 deg.C
 Catalyst Sampling interval : 1 min.
 Regeneration medium: Air/Nitrogen

Experimental Methodology. The experimentation broadly involves three steps, coking, stripping and regeneration, each of which is described in detail below.

Coking. 50 gms of FCC catalyst (steamed or coke free equilibrium) is loaded in the regenerator. Continuous flow of nitrogen is maintained to keep the catalyst in a good fluidized condition. The regenerator is heated up to 495 deg.C and allowed for 20 min. to attain the steady state. The feed injection system is activated at this point and the desired quantity of feed is injected in 120 s.

Stripping. The nitrogen flow is continued for another 15 min. to strip off any volatile hydrocarbons left on the catalyst or regenerator walls. The temperature of the regenerator is brought down to about 400 deg.C and the coked catalyst is drained off the regenerator. The vessel temperature is raised to 620 deg.C, simultaneously switching on air flow in order to burn off any coke deposited inside the regenerator.

Regeneration. The valve V1 is turned for N_2 flow to flush out any traces of oxygen left in the regenerator and the temperature is set to 585 deg.C. Then the desired quantity of coked catalyst is loaded into the regenerator. Once the steady temperature is attained, the first coke sample is collected. Air flow is switched on and catalyst sampling is done every minute up to the first five minutes. Subsequently, the interval is increased to 2 min. The samples are analyzed in a Carbon Analyzer which measures the coke concentration (wt of coke/wt of catalyst). The same methodology is followed for any catalyst studied in the setup.

Data Analysis It has been established by many authors(4,5) that the rate of coke burning is first order with respect to coke on catalyst (C_c) and oxygen partial pressure (P_{O_2}), is given below.

$$r_c = K^* C_c P_{O_2} \quad (1)$$

Here K_c^* is the intrinsic coke burning rate constant.

Under the present experimental conditions P_{O_2} remains almost constant throughout the bed. (The change in O_2 partial pressure is very small i.e 21% at the inlet and 20% at the exit of the regenerator). This reduces the rate equation further to

$$-dC_c/dt = r_c = K_c C_c \quad (2)$$

which is a first order rate expression.

Upon integration,

$$-\ln(1-X) = K_c t \quad (3)$$

where,

$$K_c = K_c^* P_{O_2}$$

$$X = 1 - (C_c/C_{c_0})$$

t = reaction time

& C_{c_0} = the initial concentration of coke.

In the present study K_c is used as a characteristic of intrinsic kinetics (Regenerability) for comparison of different catalysts.

Results & Discussions

Table-I gives the properties of different steamed catalysts used in the present study. Catalyst AM is the amorphous catalyst while all others (Z1-Z4) are zeolite based catalysts. All the steamed catalysts have been analyzed (in ASAP-2000 of Micromeritics) for the surface area of micro and macro pores. In the present study, all the pores below 30 Å are considered as micro pores while those above this are lumped into macro pores. The ratio of surface areas of micro to macro pores (S_z / S_m) is used in the data analysis.

Table I. Properties of Different Catalysts

Catalyst	AM	Z1	Z2	Z3	Z4
BET Surface Area, m ² /g	159.0	128	88	123.72	57.08
BJH Surface Area, m ² /g	167.0	12.24	17.38	29.35	8.1941
Micro Pore Area, m ² /g	12.5	118	72.09	97.44	41.391
BJH Comp Pore Vol, cc/g	0.632	0.089	0.111	0.119	0.139
Micro Pore Vol, cc/g	0.0060	0.0537	0.0369	0.0492	0.020
S_z / S_m	0.0853	11.8	4.531	3.708	2.638

Table-II shows the experimental data for the steamed catalysts. A third order polynomial is used for fitting and smoothing of the data. This fit is used whenever interpolation of data is required. For calculating the kinetic constants data of first 5 (five) minutes of the reaction is used.

Table II. Kinetic Data of FCC Catalysts (Steamed)

Rxn.Time (Min)	AM	Z1	Z2	Z3	Z4
	<-----CRC----->				
0	0.801	0.728	0.757	0.757	0.648
1	0.571	0.571	0.574	0.562	0.456
2	0.378	0.446	0.430	0.411	0.387
3	0.249	0.348	0.320	0.299	0.282
4	0.179	0.275	0.240	0.221	0.145
5	0.131	0.222	0.185	0.170	0.106
6	0.103	0.186	0.150	0.140	0.089
7	0.082	0.163	0.130	0.127	0.088
8	0.079	0.150	0.121	0.125	0.096
9	0.063	0.142	0.118	0.128	0.107
10	0.057	0.137	0.117	0.129	0.114
11	0.051	0.130	0.111	0.125	0.111
12	0.046	0.117	0.097	0.109	0.091
13	0.044	0.096	0.070	0.075	0.048

Figs.3&4 are the plots of kinetic data of for steamed and equilibrium catalysts respectively. It is very clear from the Figs.3&4 that all the catalysts exhibit 1st order behavior with respect to the concentration of coke up to about 5 minutes of reaction time. The deviation from the 1st order behavior becomes significant after about 6 minutes of reaction time. The concentration of coke at which the deviation from the 1st order behavior takes place is termed as critical coke concentration (C_{cr}).

At this juncture, it is presumed that the regeneration order and kinetic constant or in general, the regeneration behavior changes due to significant transport resistance or oxygen accessibility limitation.

Effect of Catalyst Properties on Regenerability Fig.5 shows the effect of micro to macro poresurface area S_z/S_m on regenerability. It can be seen that there exists a strong relationship between the regenerability and S_z/S_m . It can be concluded that the increase in zeolite content (in terms of micro surface area & micro pore volume) has a tendency to reduce the regeneration kinetic constant.

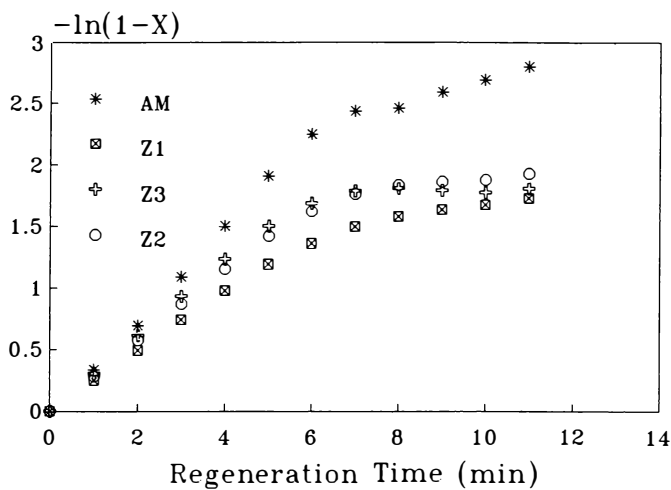


Fig.3. Kinetic Data of Steamed Catalysts
[Regeneration Time vs $-\ln(1-X)$]

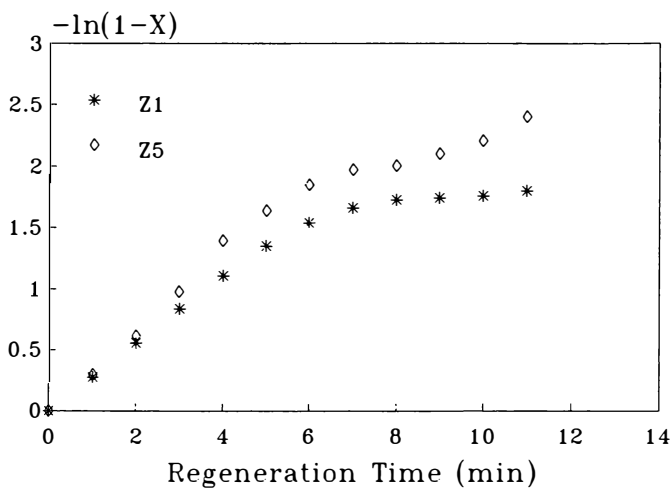


Fig.4. Kinetic Data of Equilibrium Catalysts
[Regeneration Time vs $-\ln(1-X)$]

Effect of Catalyst Properties on Critical Coke. Fig.6 shows the effect of Sz/Sm on the critical coke level. Increase in Sz/Sm ratio increases C_{cr} . This may be attributed to the increased oxygen diffusional/accessibility limitations to the coked sites.

Effect of Catalyst Equilibration. Fig.7 shows the kinetic data of a steamed catalyst and of the equilibrated sample of the same catalyst, from the refinery FCCU. The equilibrium catalyst exhibits a significantly higher regenerability when compared with the steamed. The destruction of zeolite, consequently lower Sz/Sm, may be considered as the main cause for this behavior.

Effect of Regenerability in Commercial FCC Regenerator Operation. Fig.8 shows the plant data for three different catalysts. This data spans over a period of 5 years covering the two catalyst switching from AM to Z1 & from Z1 to Z2. It has been observed that CRC has increased considerably due to these catalyst switch-overs, which in fact resulted in operational problems. Earlier, it was not possible to explain this phenomena. Laboratory studies on these catalysts clearly revealed the lower regenerabilities $Z2 < Z1 < AM$. This explains the increase in CRC and extent of after-burning in the commercial unit. Prior testing of these catalysts for regenerability would have averted these problems.

Role of Regenerability in Catalyst Screening. IOCR&D has incorporated Regenerability studies as a part of its routine catalyst screening and selection methodology. Steamed catalyst samples are tested for their regenerability, in addition to the routine MAT selectivity. The proprietary in-house FCC simulation package suitably scales up the regenerability to take care of higher regenerator temperature and predicts the performance of the catalyst from simulated MAT data. Table-III shows the performance of three catalysts (A1, A2, and A3) in one of our commercial plant. While the switch-over

Table III. Effect of Regenerability on Overall Performance of FCC Unit

<i>Catalyst</i>	<i>A1</i>	<i>A2</i>	<i>A3</i>
Regenerability	Base	1.3 x Base	1.5 x Base
CRC wt%	0.62	0.45	0.30
Regenerator Dense Temp.°C	662	651	657
MAT Activity	67	64	61
ΔT^* Deg.C	35	27	15
Bottom Yield wt%	15.0	12.0	8.0

* ΔT is the difference in Dense and Cyclone bed temperatures

from A1 to A2 had taken place some time back, the other, namely from A2 to A3 has been the most recent. The regenerability of these catalysts are in the increasing order. While the operation with A1 is most inefficient with high after-burning (35 Dec. C) the performance of A3 is much better. The CRC with these catalysts has also reduced significantly from

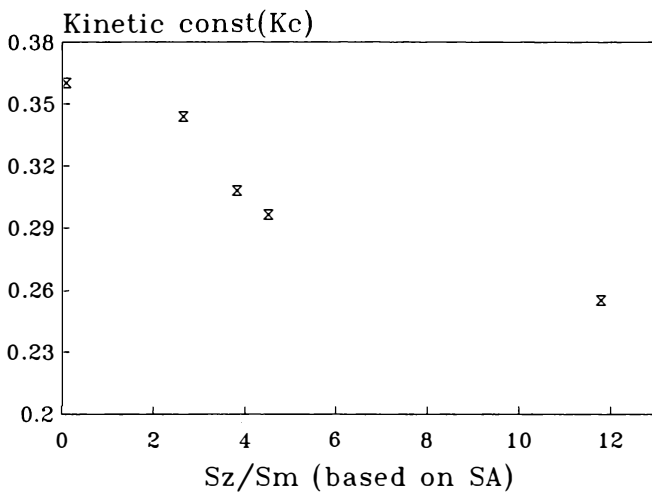


Fig.5. Effect of Sz/Sm on Regenerability

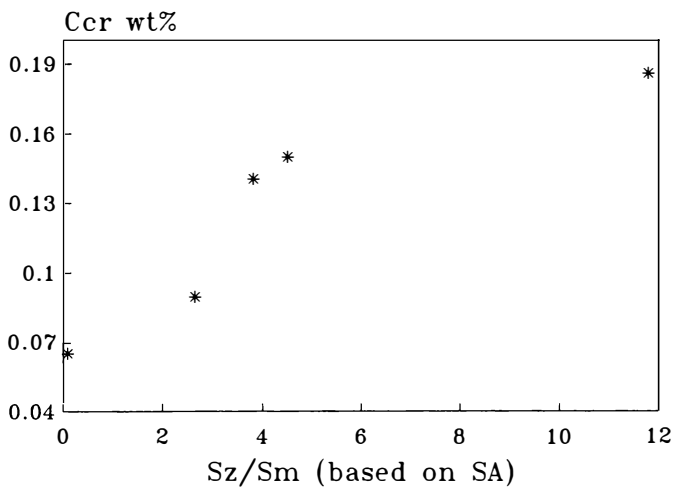


Fig.6. Effect of Sz/Sm on Critical Coke on Catalyst (Ccr)

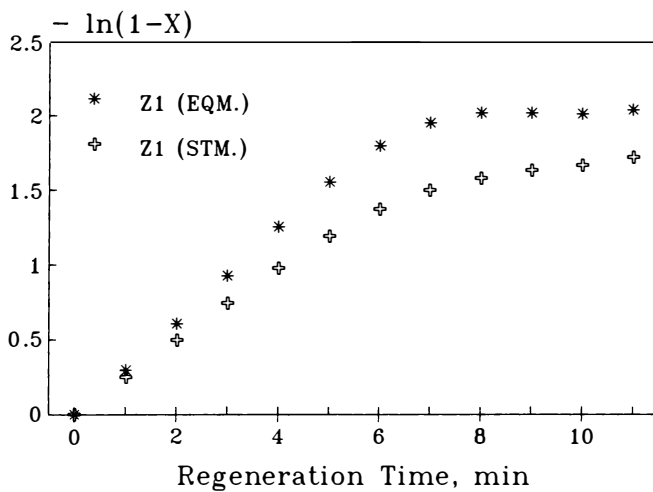


Fig.7. Comparison of Kinetic Data of Equilibrium and Steamed Catalysts

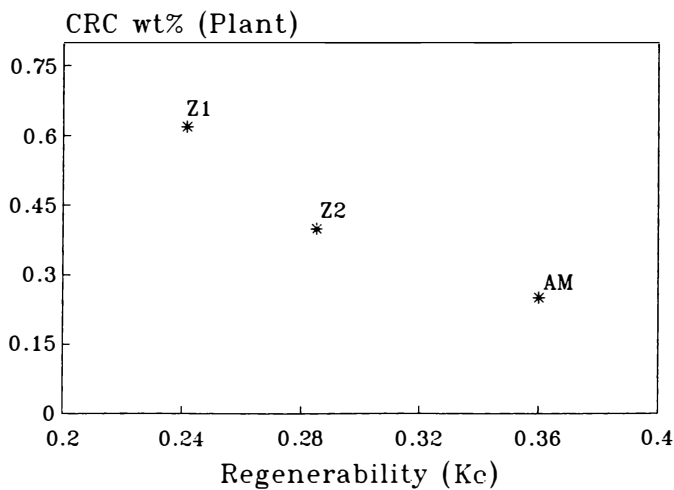


Fig.8. Effect of Catalyst Regenrability on the Performance of a Commercial Unit

0.62 to 0.30 due to improved regenerabilities. The better bottom selectivity coupled with lower CRC due to better regenerability has a synergistic effect in reducing bottom yield of A3 catalyst.

Conclusions

Understanding the regeneration behavior of FCC catalysts is of great significance in simulation, modeling, analysis of FCC process and also for proper evaluation and selection of FCC catalysts. The physico-chemical properties of different FCC catalysts influence their regenerabilities and in turn affect the coke on regenerated catalyst and the level of after-burning.

In the present study a fluidized bed regenerator is designed and fabricated for testing the regenerabilities of different catalysts. The operating conditions are selected to minimize axial gradients and the effect of sampling. The analysis of data shows that catalyst properties such as micro pore surface area and micro pore volume have significant influence on regenerability. Studies conducted with different catalysts amply reflect the efficacy of the present test setup and methodology. Studies in this unit could also explain certain impacts of catalyst switch-overs in the commercial unit, which hitherto were not explainable.

IOC R&D has incorporated the above methodology in its catalyst evaluation program for selecting a catalyst with optimal cracking and regeneration functions. This has greatly improved process of catalyst evaluation, especially for low severity FCC operation, prevalent in India.

Acknowledgments

The authors wish to express their deep sense of gratitude to the management of Indian Oil Corporation Limited for allowing the publication of this work.

Literature Cited

1. Murthy, V.L.N; Singh, S.; Das, A.K.; Ghosh, S. Presented in *Chemical Engineering Congress, 1992*, Manipal, India.
2. Weisz, P.B; and Goodwin, R.D. *J. Catal.*, **1963**, 2, 397.
3. Weisz, P.B; and Goodwin, R.D. *J. Catal.* **1966**, 6, 425.
4. Guang- Xun Wang; Shi-Xlong Lin; Wel-Tian Mo; Chun-Lan Peng; Guang-Hua Yang. *Ind. Eng. Chem. Des. Dev.* **1988**, 25, 3, 626.
5. Hano, T; Nakashio, F; Kusunoki, K. *J. Chem. Eng. Japan*, **1975**, 8, 127.
6. Magnoux; Guisnet, M. *Appl. catal.* **1988**, 38, 341-352.

MODELING OF CATALYST PERFORMANCE

A Catalyst Deactivation Model for Residual Oil Hydrodesulfurization and Application to Deep Hydrodesulfurization of Diesel Fuel

Toru Takatsuka, Yukitaka Wada, and Shin-ichi Inoue

Chiyoda Corporation, 3-13 Moriya-cho, Kanagawa-ku,
Yokohama 221, Japan

Hydrodesulfurization processes play a dominant role in the modern refineries to upgrade residual oils either by removing the heterogeneous atoms or by hydrocracking the bottoms to distillate products. A practical model is proposed to predict the catalyst life, which is of great interest to these processes. The catalyst is deactivated in the early stages of the operation by coke deposition on the catalyst's active sites. The ultimate catalyst life is determined by pore mouth plugging depending on its metal capacity. The phenomena are mathematically described by losses of catalyst surface area and of effective diffusivity of the feedstock molecules in the catalyst pores. The model parameters were collected through pilot plant tests with various types of catalysts and feedstocks.

The concept of this model for catalyst deactivation is also applicable to hydrotreating of other petroleum fractions. An example of such applications for the case of deep hydrodesulfurization of diesel fuel is also presented.

The Simulation Model

Kinetics. When the diffusion rate of reactants in a catalyst pore affects the reaction rate, the rate equations can be represented for desulfurization r_s and vanadium removal r_v , respectively by:

$$r = \rho_{\text{cat}} A E_f k C_{\text{h}_2}^n \quad (1)$$

, where E_f is the effectiveness factor and k is the intrinsic rate constant.

The model for coke deposition on the catalyst is expressed by Eq. (2) with the assumption that deposited coke can also be decreased by hydrogenation:

$$r_c = \rho_{\text{cat}} A k_{c1} - \rho_{\text{cat}} A_c k_{c2} C_{\text{h}_2} \quad (2)$$

, where A_c is the coked surface area of the catalyst. Eq. (2) indicates that a reduction of an active surface area A gives a negative value to r_c ; thus, causing a decrease in the coke content on the catalyst.

The hydrogen concentration in the residue is affected by both reaction pressure and temperature, and the solubility of hydrogen employed in the model is :

$$C_{h_2} = 8.91 \times 10^{-6} P + 4.16 \times 10^{-6} (T-273) - 1.40 \times 10^{-3} \quad (3)$$

$$\text{for } 50 \text{ kg/cm}^2 < P < 180 \text{ kg/cm}^2, 573 \text{ K} < T < 733 \text{ K}$$

The Effectiveness Factor. The effectiveness factor used in Eq. (1) depends on the reactant concentration in the catalyst pores as defined by Eq. (4), which is affected by diffusion in a porous medium.

$$E_f = \frac{A \int 4\pi R^2 C^n dR}{\frac{4}{3} \pi R_0 A C_0^n} \quad (4)$$

The mass balances of reactants in the catalyst pores are calculated as follows in the case of a spherical catalyst:

$$\frac{1}{R^2} \frac{d}{dR} \left(R^2 D \frac{d\rho_{oil} C}{dR} \right) = \rho_{oil} A k C_{h_2} C^n \quad (5)$$

The hydrogen concentration is postulated to be the same in and out of the catalyst pores. Eq. (5) is converted to a non dimensional differential equation as follows:

$$\frac{d^2 \phi}{d\eta^2} + \frac{2}{\eta} \frac{d\phi}{d\eta} = h^2 \phi^n \quad (6)$$

, where ϕ is the dimensionless concentration ($\phi = C/C_0$), and η is the dimensionless distance ($\eta = R/R_0$) from the pellet center.

The Thiele-modulus h is defined by Eq. (7).

$$h = R_0 \sqrt{\frac{\rho_{cat} A k C_{h_2} C_0^{n-1}}{\rho_{oil} D}} \quad (7)$$

The boundary conditions are:

$$\begin{aligned} \frac{d\phi}{d\eta} &= 0 & \text{at} & \eta = 0 \\ \phi &= 0 & \text{at} & \eta = 1 \end{aligned} \quad (8)$$

If the reaction is first order, the following solution is obtained:

$$E_f = \frac{3}{h^2} \{h \coth(h) - 1\} \quad (9)$$

The dimensionless differential equation Eq. (6) for other orders than first order

reaction is solved by use of the Thomas method¹⁾, and the distribution of concentration along the pellet radius is obtained to give E_f with Eq. (10).

$$E_f = 3 \int \eta^2 \phi^n d\eta \quad (10)$$

Consequently, the relation between the effectiveness factor and the Thiele-modulus is obtained as shown in Figure 1. The figure indicates that an approximate value of the effectiveness factor is obtained by Eq. (9) even for reactions of other orders than first order and that the sensitivity of the effectiveness factor towards a change of the Thiele-modulus is almost the same for any order of reaction.

Catalyst Deactivation. In the model, the catalyst deactivation is postulated to be caused by the deposition of metals and coke. For convenience the demetallization is represented by vanadium removal and the effect of nickel on deactivation is included in the parameters. The quantities of vanadium Q_v and coke Q_c accumulated are given with Eqs. (1) and (2):

$$Q = \int r d\theta / \rho_{cat} \quad (11)$$

This is rearranged to dimensionless forms to obtain Ψ_v and Ψ_c for vanadium- and coke deposition as follows:

$$\Psi_v = Q_v / (P_v \rho_v) \quad (12)$$

$$\Psi_c = Q_c / (P_v \rho_c) \quad (13)$$

, where P_v is the catalyst pore volume, and ρ_v , ρ_c are the densities of vanadium and coke, respectively. Ψ_v and Ψ_c are the volumes of contaminants per unit pore volume.

If the active surface area is considered to be proportional to the catalyst surface area, the reduced active surface area for reactions can conveniently be expressed by the following equations:

$$A = A_0 (1 - \alpha_v \Psi_v - \alpha_c \Psi_c) \quad (14)$$

, where α_v , α_c are the parameters defined for each reaction; they include the effect of nickel deposition and so on.

Coked surface area defined for Eq. (2) is similarly calculated.

$$A_c = A_0 \beta_c \Psi_c \quad (15)$$

Another deactivation factor is the deposited substances that hinder intraparticle diffusion of reactants. The vanadium deposition is supposed to have a significant effect on the effective diffusivity in the catalyst pores. The decline of the effective diffusivity is expressed by the following equations for sulfur D_s and vanadium D_v , respectively:

$$D = D_0 (1 - \delta_{v1} \Psi_v - \delta_{v2} \Psi_v) \quad (16)$$

, where δ_{v1} and δ_{v2} are parameters which represent the effect of a distribution of vanadium deposition in the catalyst pore on the diffusivity of sulfur or vanadium compounds. Since larger amounts of vanadium deposit in the outer parts of a pellet than in the central part, the effective diffusivity is not constant throughout the pellet.

The Reactor Model. The material balances of sulfur C_s and vanadium C_v in a plug-flow reactor are derived as follows:

$$U_1 \frac{dC}{dz} + \varepsilon r = 0 \quad (17)$$

The solution is obtained by a numerical integration of Eq. (17) by taking into account the distribution of catalyst deactivation along the direction of catalyst bed from the inlet to outlet.

Discussion

Catalyst deactivation with diffusion-controlled reactions. The studies were carried out with the model to find the effect of metal- and carbon depositions on the catalyst deactivation, when the reaction is controlled by the diffusivity of the reactants.

When metal is accumulated on the catalyst, the effective diffusion coefficients are affected. If the catalyst fouling caused by a loss of active surface area is not accounted for, the apparent catalyst activity changes as shown in Figure 2. It shows that catalyst activity changes significantly from SOR (start of run) to EOR (end of run) due to a decrease of the effective diffusivity at low effectiveness factors. On the contrary a high degree of deactivation is not predicted for the catalyst with a high effectiveness factor, but rapid deactivation is predicted at EOR.

Figure 3 shows calculated catalyst deactivation results caused by a loss of active surface area without a change in the effective diffusion coefficient. Catalyst fouling is proportional to a loss of active surface area if diffusion does not control the reaction rate, so with a high effectiveness factor. On the other hand, a loss of active surface area is compensated to a certain extent in the apparent reaction rate when the effectiveness factor is small, because the effectiveness factor increases with the loss of surface activity.

Figure 4 shows the typical trends of catalyst fouling with metal- and coke deposition on the catalyst. Both cause a change in the effective diffusivity and a loss of surface activity. It indicates that the initial fouling brought about by coke laydown on the catalyst is accompanied by a loss of surface activity. The ultimate catalyst life is determined by metal deposition which decreases the effective diffusivity of reactants into catalyst pores.

Experimental results and discussion. The HDS tests were carried out for five catalysts with typical physical properties as shown in Table 1. The catalysts were prepared in the laboratory. The properties of the feedstocks are tabulated in Table 2. All the HDS tests were made under isothermal conditions. The feed was brought together with hydrogen gas in an upflow reactor. Hydrogen gas was passed once through. A reactor of the following dimensions was used: reactor inner diameter 25.4 mm; thermowell diameter in the center of the reactor 6.35 mm; catalyst bed volume 400 cm³. Figure 5 shows that the experimental results for Catalyst "A", "B" and "C" are well simulated by the catalyst deactivation model and the catalyst life depended greatly upon the catalyst properties.

Catalyst "A" with a small pore size rapidly lost its activity due to plugging of the catalyst pores from SOR to EOR. This type of catalyst is not strongly deactivated by coke deposition, because asphaltenic compounds, which easily make coke on the catalyst surface, are not allowed to diffuse into the catalyst pores. However, this catalyst is easily deactivated through pore plugging by metal deposition.

Catalyst "C" with the largest ave. pore diameter was deactivated mostly by coke laydown on its active surface sites, but did not show signs of pore plugging. The catalyst with too big pore diameters is susceptible to coking and loses its activity before its pores are plugged.

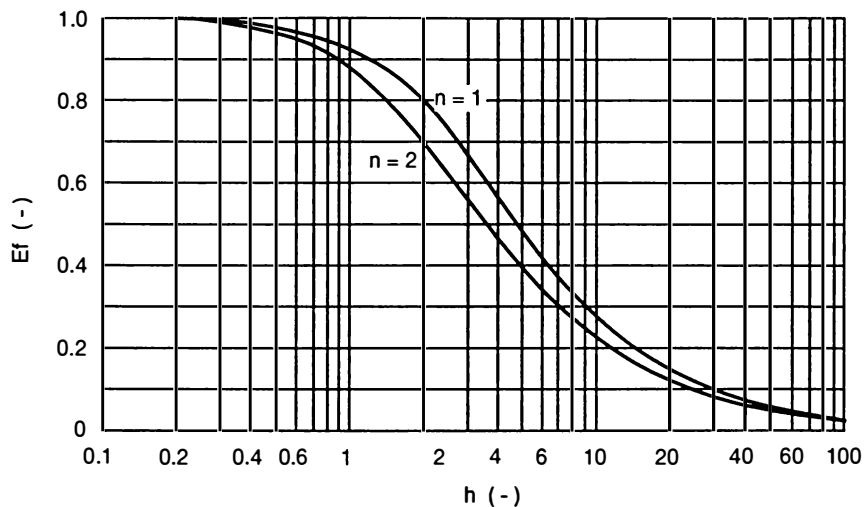


Figure 1 Thiele Modulus and Effectiveness Factor

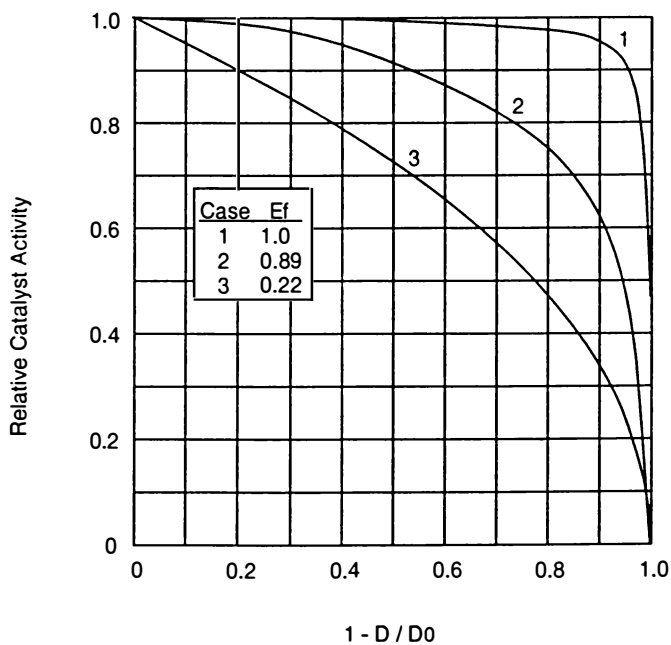


Figure 2 Catalyst Deactivation due to Pore Plugging

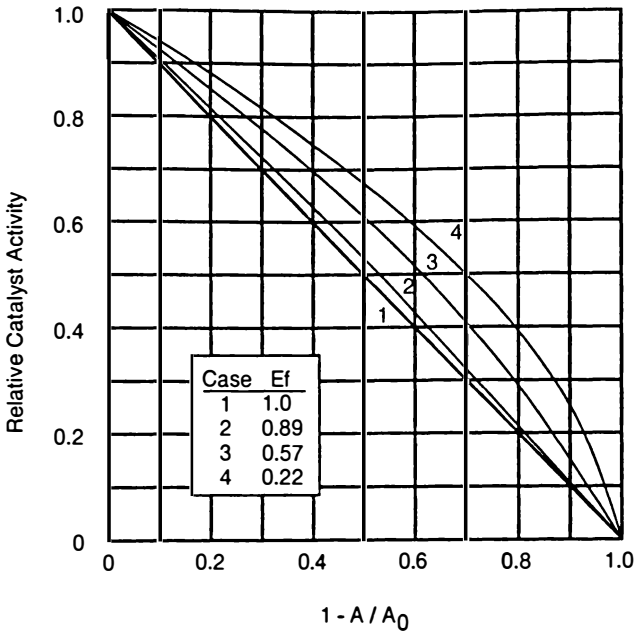


Figure 3 Catalyst Deactivation due to a Loss of Surface Area

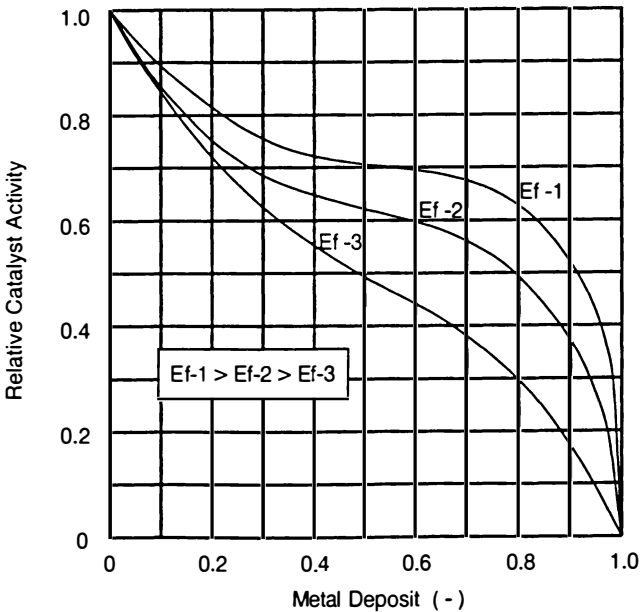


Figure 4 Typical Trends of Catalyst Fouling

Table 1 Physical Properties of HDS Catalysts

Catalyst	Type	Pore Volume (cm ³ /g)	Surface Area (m ² /g)	Equivalent Diameter (mm)
A	Ni-Co-Mo	0.440	280	1.16
B	Co-Mo	0.601	155	1.34
C	Co-Mo	0.786	341	1.59
D	Ni-Co-Mo	0.500	180	1.41
E	Ni-Co-Mo	0.558	161	1.22

Table 2 Properties of Feedstock

		Iranian Heavy V.R.
Specific Gravity (15/4°C)		1.0379
Viscosity at 100°C	cSt	2,890
Carbon Residue	wt%	21.6
Asphaltene Content	wt%	8.2
Sulfur Content	wt%	3.67
Nitrogen Content	wt%	0.76
Metals		
Vanadium	ppm	270
Nickel	ppm	92
Sodium	ppm	4
Iron	ppm	13

Catalyst "B" with a medium pore diameter was deactivated by coke deposition at SOR, but showed a stable performance in MOR (middle of run); it began to lose its activity due to pore plugging towards the EOR. It is regarded to have well balanced properties against catalyst deactivation by either coke or metal accumulation in the catalyst pores. The parameters obtained in the data fitting were also found to be significantly dependent on the properties of the catalyst. Figure 6 with including parameters other than for Catalyst "A", "B", "C" indicates that the apparent catalyst activity for vanadium removal depends on the catalyst properties which affect the effective diffusivity, but not the rate constant.

Application of the Model to Deep Desulfurization of Diesel Fuel

This model for catalyst deactivation is widely applicable in hydrotreating of other petroleum fractions. The model is inevitably complicated in the case of bottom upgrading, because there exists a distribution of catalyst activity in the reactor and even in the catalyst pores due to metal contaminants.

In the case of distillate hydrotreating the simulation models are simply described even for the complicated reaction scheme employed in the reaction model as discussed in the later section, because the catalyst deactivation is not necessarily predicted for local sites in the system. And the assumption confirmed in the previous discussion that the relationship between the Thiele-modulus and effectiveness factor is approximately represented by that of a first order reaction for any reaction order makes the simulation model simpler and easier to develop.

Catalyst Deactivation by Coke Deposition. The catalyst employed in deep desulfurization of diesel fuel is deactivated by coke deposition onto the catalyst. Coke deposition affects not only the surface activity but also the diffusivity of the reactants, because the pore diameter is relatively small in this case. The catalyst deactivation data suggest that the effectiveness factor is smaller than 1.0.

The reaction order n defined in Eq. (1) is 1.7. For simplicity, Eq. (9) is employed to calculate the effectiveness factor E_f , instead of predicting the exact value of E_f by numerical integration of Eq. (6) and (10).

Eqs. (18) and (19) are used instead of Eqs. (14) and (16) in the model for diesel hydrodesulfurization.

$$A = A_o (1 - \alpha_c \Psi_c) \quad (18)$$

$$D = D_o (1 - \delta_c \Psi_c') \quad (19)$$

It seems that there are two types of coke on the catalyst, "soft" or "hard" coke. The coke deposition Ψ_c defined as soft coke in Eq. (18) has equivalent characteristics to that defined in Eq. (14). The rate of coke deposition is simulated by Eq. (2) where coke is defined as "hydrogenable". This coke is speculated to be adsorbed polyaromatics rather than coke. Hard coke Ψ_c' defined in Eq. (19), on the contrary, is steadily produced with a deposition rate of Eq. (2); this affects the diffusivity of reactant.

The example of data fitting results are shown in Figure 7. It shows that predicted results represent experimental data well throughout the operation though operating conditions are frequently changed.

Color Degradation of Diesel Fuel in Deep Desulfurization. The color of diesel fuel is degraded in the higher reactor temperature range of deep desulfurization.²⁾ The color bodies (fluorescence compounds) are thought to be polyaromatics which are

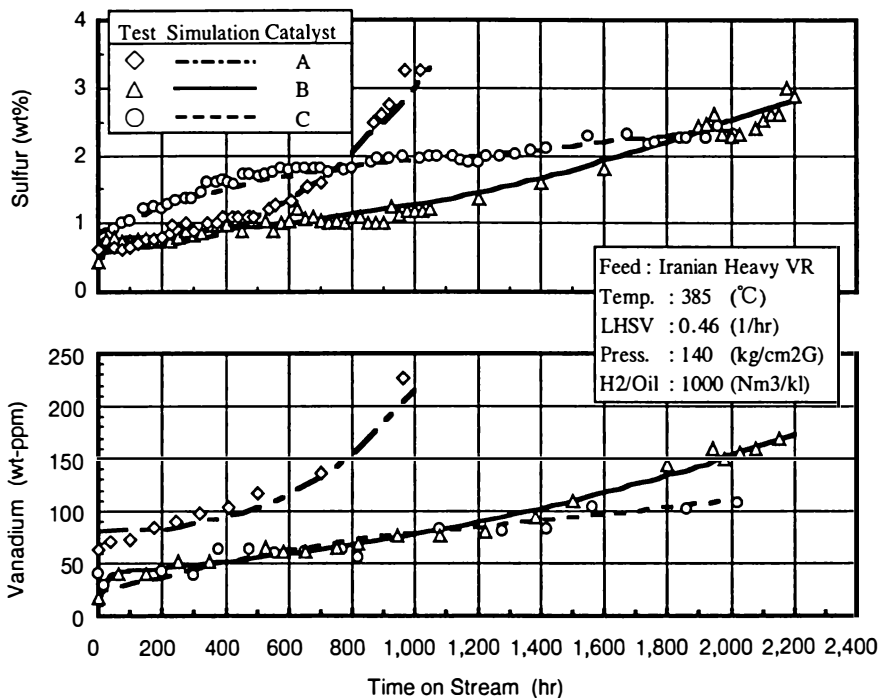


Figure 5 Simulation for Catalyst Aging Tests

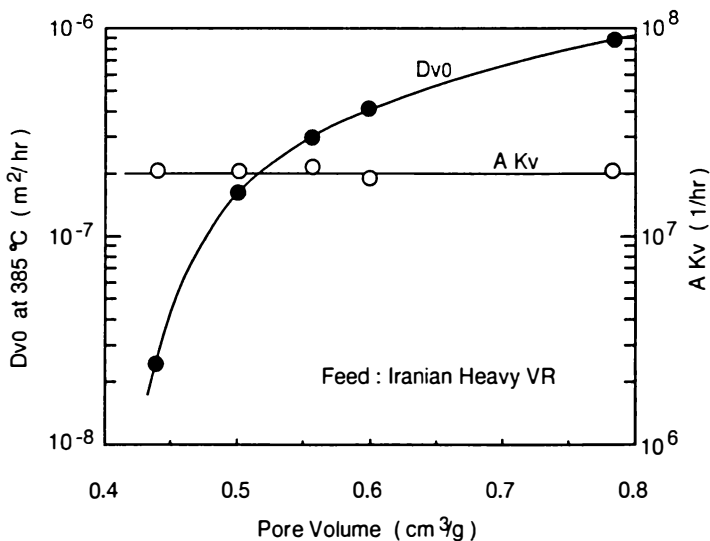


Figure 6 Relation between Catalyst Pore Volume and Parameters

produced as a by-product from desulfurization of dibenzothiophenes and heavier sulfur compounds as shown in the reaction model of Figure 8. These color bodies are hydrotreated to extinction in the further stages of hydrotreating. The proposed color degradation scheme represents the complex phenomena very well as shown in Figure 9. The rate of color body production also decreases along with a deactivation of catalyst but with a different aging rate from hydrodesulfurization. The reaction model of the color degradation is not simple as shown in Figure 8. However, the catalyst deactivation is simply incorporated for the reaction rate of k_3 in the model. The assumptions that the reaction is represented by the first order reaction and that the degree of catalyst deactivation is the same for the whole reactor make the simulation model easier to develop. The structure of the catalyst deactivation model is the same as discussed in previous section for the desulfurization.

Figure 10 shows the nice fit of these catalyst deactivation results. It indicates that the reaction of color degradation decreases rapidly in the early stages of the operation. And the parameters obtained in the data fitting demonstrate that catalyst deactivation for color degradation is caused by a rapid decrease of the diffusion coefficients.

Figure 11, the effect of temperature on color degradation, also reveals that the color degradation is strongly controlled by the diffusivity of the reactants. The apparent activation energy of used catalyst was 3/4 of that of fresh catalyst.

Conclusions

A practical model is proposed to predict the catalyst life in hydrodesulfurization processes which are of great interest to the refinery operations.

The phenomena are mathematically described by losses of catalyst surface area and a decline in the effective diffusivity of feedstock molecules in the catalyst pores.

The model was basically developed for hydrodesulfurization of residual oil with a high level of catalyst contaminants causing pore mouth plugging of catalyst.

This model for catalyst deactivation, with certain simplifications, is more widely applicable to hydrotreating of also other petroleum fractions.

The relationship between the Thiele-modulus and effectiveness factor represented here for a first order reaction can also be applied to other reaction orders for approximations in practical use. This makes the model simpler and easier to use and develop quantitatively.

Nomenclature

A	surface area of catalyst	m^2/kg
C	concentration	$\text{kg} /$
D	effective diffusivity of sulfur	m^2/hr
E_f	effectiveness factor	-
h	Thiele-modulus	-
k	intrinsic rate constant	$\text{kg}/\text{m}^2.\text{hr}$
P	pressure	kg/cm^2
P_v	pore volume of fresh catalyst	m^3/kg
Q	quantity of contaminant on catalyst	kg/kg
R	distance from pellet center	m
R_o	equivalent radius of catalyst pellet	m
r	reaction rate	$\text{kg}/\text{m}^3.\text{hr}$

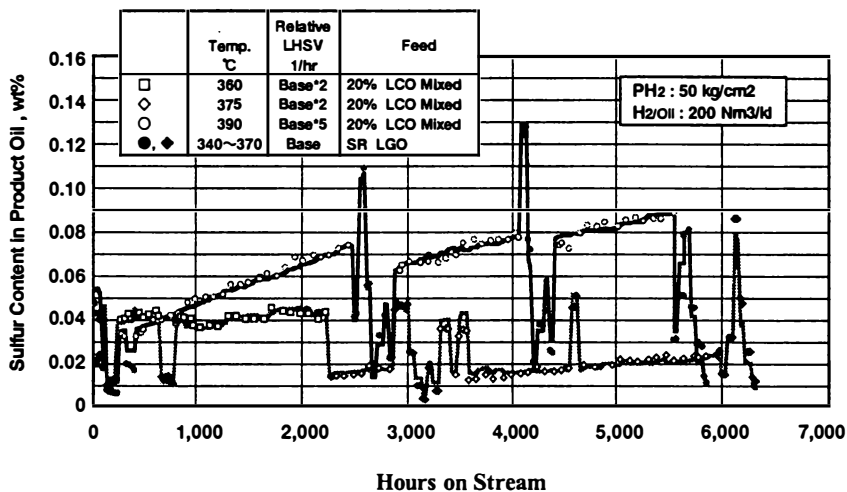


Figure. 7 Pilot Plant Tests of Deep HDS of Diesel Fuel

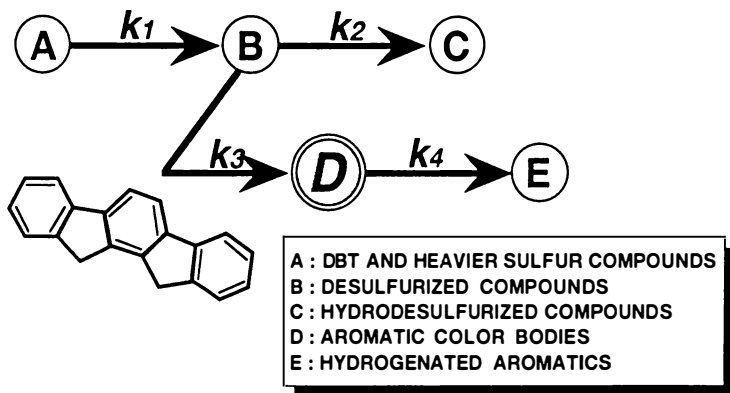


Figure 8 Proposed Reaction Model Color Degradation of Diesel Fuel in Deep HDS

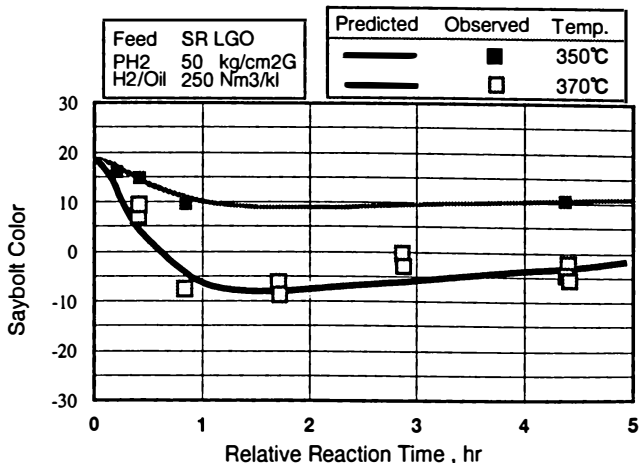


Figure 9 Prediction of Color Degradation of Diesel Fuel by Proposed Model

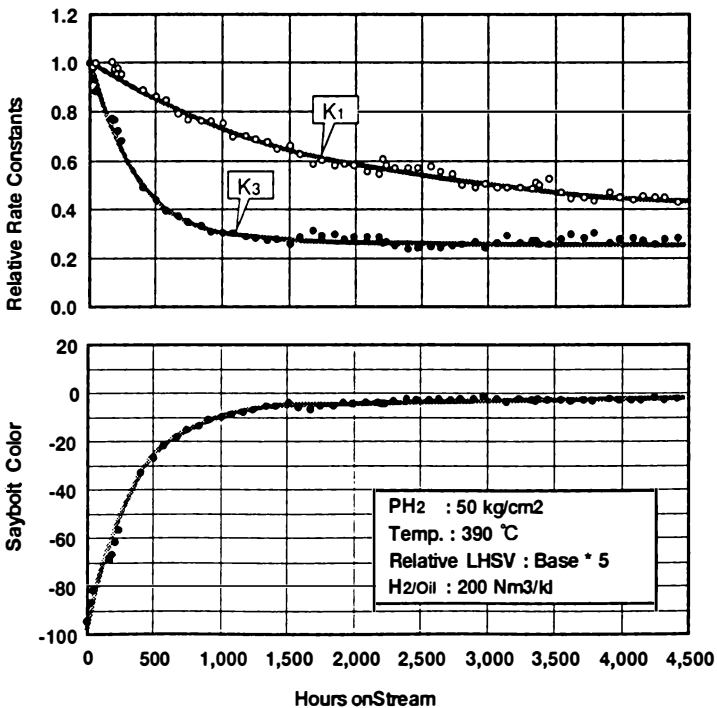


Figure 10 Catalyst Deactivation in Color Degradation Model for Deep HDS of Diesel Fuel

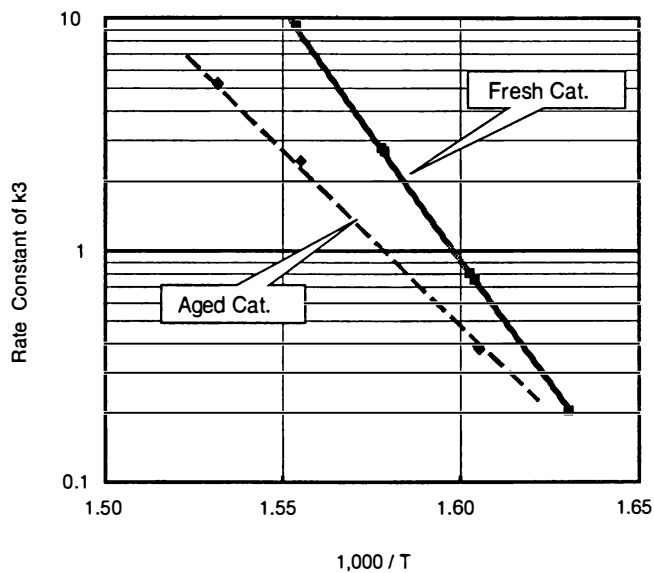


Figure 11 Effect of Catalyst Aging on Apparent Activation Energy of K_3 in Color Degradation Model

T	temperature	K
U	flow rate	kg/m ² .hr
Z	distance from reactor inlet	m

Greek Letters

α	parameter expressed in Eq. (14), (18)	
β	parameter expressed in Eq. (15)	
δ	parameter expressed in Eq. (16), (18)	
ϵ	catalyst charge volume	m ³ /m ³
η	dimensionless distance from pellet center	
θ	process time	hr
ρ	density	kg/m ³
ϕ	dimensionless concentration	
ψ	dimensionless quantity of contaminant on catalyst	

Subscripts

c	coke,coked
c ₁	coke formation
c ₂	coke hydrogenation
cat	catalyst
h ₂	hydrogen
l	liquid phase
s	sulfur
oil	oil phase
v	vanadium
o	fresh catalyst,feed,inlet

Reference

- 1) Lapidus,L., "Digital Computation for Chemical Engineers", (1962) , McGraw-Hill.
- 2) Takatsuka,T. et al., J.Jpn.Pet.Inst.,35,179,1992.

Modeling Catalytic Deactivation of Benzene Hydrogenation

Paul F. Meier and Marvin M. Johnson

Phillips Research Center, Phillips Petroleum Company,
Bartlesville, OK 74004

Theoretical equations, which predict the loss of catalyst activity due to sulfur poisoning in hydrogenation reactions, are presented in this paper. The integration of the partial differential equations resulting from a consideration of sulfur poisoning, hydrogenation, and a catalyst active site balance leads to an analytical solution. When these equations were applied to deactivation data obtained for commercial benzene hydrogenation catalysts, conversions measured experimentally as a function of time were fit quite well by these equations.

Benzene hydrogenation to cyclohexane is an important industrial reaction which has received extensive attention in the literature. Much of the reported work was done at low pressures and conversion, but industrial reactors operate at high pressures (20-30 atm) and conversions near 100%. Some examples of high pressure, high conversion studies are the work of Aben et al. (1), Prasad et al. (2), and Marangozis et al. (3). Many discussions have been presented on the hydrogenation mechanism, leading to rate equations of various orders for benzene and hydrogen. Some of these are discussed later in the Derivation of Rate Equations section.

A progressive loss in catalytic activity occurs in the plant reactor from small amounts of thiophene present in the feed. The sulfur acts as an irreversible poison of the metallic catalyst. It has been suggested that hydrogen sulfide is the sulfiding agent, and mechanistically this occurs from desulfurization of thiophene to hydrogen sulfide on the catalyst (4).

Theoretical equations developed in this paper are intended to model benzene hydrogenation in an industrial reactor and account for the loss of catalyst activity due to sulfur poisoning. The approach used to develop the equations results in an analytical solution for the partial differential equations describing hydrogenation, sulfur poisoning, and a catalyst active site balance. The solution, which accounts for thiophene

consumption in the gas phase and accumulation on the catalyst, is identical in form to that obtained by Johnson et al. (5) for oxygen consumption and carbon content during catalyst regeneration and also to that obtained by Bohart and Adams (6) for chlorine consumption and absorbance capacity of charcoal.

Derivation of Rate Equations

The development begins with the following six postulates:

1. The reaction is zero-order in benzene and first-order in both hydrogen and unpoisoned sites.
2. Deactivation is first-order in thiophene concentration and unpoisoned sites. The catalyst surface behaves ideally, meaning that poisoning of the surface does not affect unpoisoned sites with respect to the main reaction.
3. Deactivation is slow, and a steady-state assumption is made to solve the mass balance equations.
4. Mass transfer is neglected, and the system is treated as homogeneous.
5. Axial dispersion is neglected since the reaction order for benzene is assumed to be zero.
6. Experiments were conducted (see Experimental Section) in a fixed-bed reactor at isothermal conditions with reactants in the gas phase.

The first two postulates deserve some discussion. Many mechanisms are proposed in the literature for benzene hydrogenation with widely different assumptions and conclusions. Coenen et al. (7) reported reaction orders from 0.5 to 0.8 for hydrogen, indicative of a Langmuir-type of behavior. However, the reaction was found to be zero-order for benzene. Dissociative adsorption of hydrogen was assumed, and the addition of the second hydrogen, through a six-step addition, was found to be the rate determining step. Mass transfer was not important. In a later paper, van Meerten and Coenen (8) examined three possible mechanisms involving various types of hydrogen addition, and found that they were essentially indistinguishable based on the statistical fit of experimental data. Reaction orders as high as three were reported for hydrogen in this paper. Marangozis et al. (3) examined a power law rate equation and a Langmuir-type model. For the power law equation, fractional values were obtained for both hydrogen and benzene; the value for hydrogen increases while that for benzene decreases with temperature. The Langmuir-type model postulated a reaction between hydrogen gas and adsorbed benzene, leading to a zero-order reaction with respect to benzene at high pressure. Prasad et al. (2) indicate that at high pressure, a Rideal-type mechanism occurs with reaction of six adsorbed hydrogen atoms simultaneously. Many other papers can be cited in the literature with varying opinions about the mechanism of hydrogen addition and whether it occurs as an adsorbed species or from the gas phase. However, at high pressure the kinetics seems to be well described by a reaction which is approximately first-order in hydrogen and zero-order in benzene.

An interesting discussion of catalyst deactivation through thiophene is given by Aguinaga et al. (4) which supports our second postulate. In this study, they suggest that hydrogen sulfide is the actual deactivation agent and that thiophene is first hydrogenolyzed to hydrogen sulfide. A linear relationship was observed between activity

and the fraction of catalyst surface remaining unsulfided. This supports the concept of an ideal catalyst surface where chemisorption and reaction of both the reactant and poison molecules are not affected by poisoning of the rest of the surface.

The one-dimensional, homogeneous material balances for thiophene and benzene may be written as follows:

$$\frac{\varepsilon \rho_g}{M_g} \left(\frac{\partial y_s}{\partial t} \right) + \frac{F}{A} \left(\frac{\partial y_s}{\partial z} \right) = -r_p \rho_B \quad (1)$$

$$\frac{\varepsilon \rho_g}{M_g} \left(\frac{\partial y_B}{\partial t} \right) + \frac{F}{A} \left(\frac{\partial y_B}{\partial z} \right) = -r_p \rho_B \quad (2)$$

As stated in the postulates, the deactivation reaction is assumed to be first-order in both thiophene and unpoisoned sites. Also, since the loss of active sites is slow with respect to reaction, the deactivation will be treated as a pseudo steady-state.

$$\frac{F}{A} \left(\frac{\partial y_s}{\partial z} \right) = -\rho_B k_s \Pi y_s (C^\circ - C) \quad (3)$$

In terms of catalyst mass, equation 3 may be rewritten.

$$F \left(\frac{\partial y_s}{\partial m} \right) = -k_s \Pi y_s (C^\circ - C) \quad (4)$$

To make the equation dimensionless, let $V = \left(\frac{(C^\circ - C)}{C^\circ} \right)$ and

$m' = \frac{k_s \Pi C^\circ m}{F}$. Then, in dimensionless form equation 4 may be written as

$$\left(\frac{\partial \left(\frac{y_s / y_s^\circ}{\partial m'} \right)} \right) = -V \left(\frac{y_s / y_s^\circ}{\partial m'} \right) \quad (5)$$

The rate of increase for poisoned sites may also be written as first-order in thiophene and unpoisoned sites.

$$\left(\frac{\partial C}{\partial t} \right) = k_s \Pi y_s (C^\circ - C) \quad (6)$$

To write in dimensionless form, let $T = k_s \Pi y_s^\circ t$. With this substitution, equation 6 becomes

$$\left(\frac{\partial V}{\partial T}\right) = -V \left(\frac{y_s / y_s^\circ}{y_s^\circ}\right) \quad (7)$$

For equations 5 and 7, $(y_s / y_s^\circ) = 1$ at $m' = 0$ for all T and $V = 1$ at $T = 0$ for all m' . Equations 5 and 7 may be combined to give

$$\frac{\partial (y_s / y_s^\circ)}{\partial m'} = \frac{\partial V}{\partial T} \quad (8)$$

Integration gives the following solutions.

$$\left(\frac{y_s}{y_s^\circ}\right) = \frac{1}{1 + e^{-T}(e^{m'} - 1)} \quad (9)$$

$$V = \frac{1}{1 + e^{-m'}(e^T - 1)} \quad (10)$$

In terms of catalyst mass and conversion, equation 2, the mass balance equation for benzene, may be rewritten. As in the case of thiophene, a pseudo steady-state is assumed. Also, since hydrogen is in an excess and the change in hydrogen through reaction is small, constant pressure is assumed.

$$y_B^\circ F \left(\frac{dx}{dm}\right) = k_B \Pi (C^\circ - C) \quad (11)$$

Substituting the solution for V from equation 10 and rearranging gives equation 12.

$$dx = \frac{C^\circ k_B \Pi}{F y_B^\circ} \left[\frac{1}{1 + e^{-m'}(e^T - 1)} \right] dm \quad (12)$$

Since $m' = \frac{k_s \Pi C^\circ m}{F}$, equation 12 may be rewritten as

$$dx = \frac{k_B}{k_s y_B^\circ} \left[\frac{1}{1 + e^{-m'}(e^T - 1)} \right] dm' = \frac{k_B}{k_s y_B^\circ} \left[1 + \frac{1}{1 + e^{-m'}(e^T - 1)} - 1 \right] dm'$$

$$= \frac{k_B}{k_s y_B^o} \left[1 - \frac{e^{-m'} (e^T - 1)}{1 + e^{-m'} (e^T - 1)} \right] dm' \quad (13)$$

At the entrance to the catalyst bed (where $m' = 0$), the conversion is also zero. Integration yields

$$\begin{aligned} x &= \frac{k_B}{k_s y_B^o} m' - \frac{k_B}{k_s y_B^o} \int_0^{m'} \frac{e^{-m'} (e^T - 1)}{1 + e^{-m'} (e^T - 1)} dm' \\ &= \frac{k_B}{k_s y_B^o} m' + \frac{k_B}{k_s y_B^o} \ln \left[\frac{1 + e^{-m'} (e^T - 1)}{e^T} \right] \end{aligned} \quad (14)$$

Substituting back m for m' and setting $\alpha = \frac{k_B}{k_s y_B^o}$ yields the final form of the previous equation.

$$x = \frac{k_B C^o \Pi m}{F y_B^o} - \alpha T + \alpha \ln[1 + e^{-m'} (e^T - 1)] \quad (15)$$

Values for m , y_B^o , y_s^o , and F are determined from experimental conditions. The product $k_B C^o$ can be determined at $t = 0$. For short deactivation times when $(e^T - 1) \approx 0$, the initial slope gives a method for calculating k_B^o . Values of k_s were determined to give the best statistical fit to the experimental data. A discussion of the experiments is given next.

Experimental Section

The conversion of benzene to cyclohexane as a function of time was determined in an accelerated sulfur poisoning test using thiophene. A fixed-bed reactor, 2 ft long and constructed with 3/4" OD stainless steel tubing and containing a 1/8" thermowell, was used. Experiments were conducted in a three-zone furnace. The catalyst weight in the reactor was 2.4g, ± 0.1 g and the particle sizes used were 20-40 mesh (425-850 μ m). The small particle sizes should minimize any Thiele modulus effects. A liquid feed rate of 19.8 cc/hr (6.6 WHSV) was used with a composition of 25% benzene and 75% cyclohexane. Thiophene present in the feed was 95 ppm, approximately 150 times that in commercial reactors. The hydrogen feed rate was 518 cc/min or about 1.39 moles/hr. All experiments were conducted at 14.6 atm and normally at a temperature of 250°C; however, for active catalysts, the reaction temperature was dropped to 200°C. Catalyst pretreatment was a hydrogen reduction at atmospheric pressure for 9 to 16 hours at 400°C and a flow rate of 200 cc/min. Benzene conversion was determined using thermal conductivity gc at approximately two-hour intervals.

The metal surface area for one of the catalysts, catalyst A, was determined by hydrogen chemisorption. Prior to the adsorption experiment, the sample was reduced in hydrogen at 370°C for 16 hours and then evacuated for one and a half hours. The adsorption experiment was conducted at room temperature using one gram of catalyst.

Results and Discussion

Deactivation data for three different catalysts were used to test the applicability of the rate equations derived previously. Calculated rate constants for hydrogenation, sulfur poisoning, and the catalyst active site concentration are shown in Table I along with some catalyst properties. The product $k_B C^\circ$ was determined at $t = 0$ while k_B° was calculated from the slope from 0 to 2 hours when long-term deactivation, reflected through the term $(e^T - 1)$, is essentially zero. Values of k_s were determined to give the best fit to the experimental data. Figure 1 compares deactivation curves determined from the model equations with the experimental data for all three catalysts. The good fit of the model with the experimental data indicates that the model properly accounts for the effect on activity from sulfur retained on the catalyst. It also supports the assumption of a zero-order rate with respect to benzene.

Table I. Catalyst rate constants and properties

Calsicat Catalyst	Catalyst A	Catalyst B	Catalyst C
k_B°	7.29	8.26	5.35
C°	1.78×10^{-4}	1.74×10^{-4}	2.52×10^{-4}
Metal Surface Area, moles of sites/g	5×10^{-4}		
k_s	545	350	110
Reaction Temperature, °C	250	250	200
wt % Sulfur (a)	0.57	0.56	0.82
ρ_B	0.86	1.04	0.88
Ni, wt %	43	56	41
Surface Area, m ² /g	155	160	250

a. Sulfur content at complete deactivation based on C° .

As shown in Table I, complete deactivation for these three catalysts occurs around 0.6 to 0.8 wt% sulfur, based on the active site content. These values are typical for complete deactivation in a commercial reactor. The metal surface area measured by hydrogen chemisorption is almost three times the active site concentration determined from the fit of the model to the accelerated aging data. Some of this difference may be due to a poor separation of the product $k_B C^\circ$ into the individual constants. How-

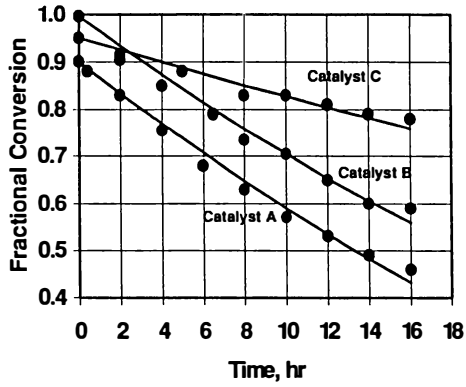


Figure 1 - Fractional Conversion versus Time

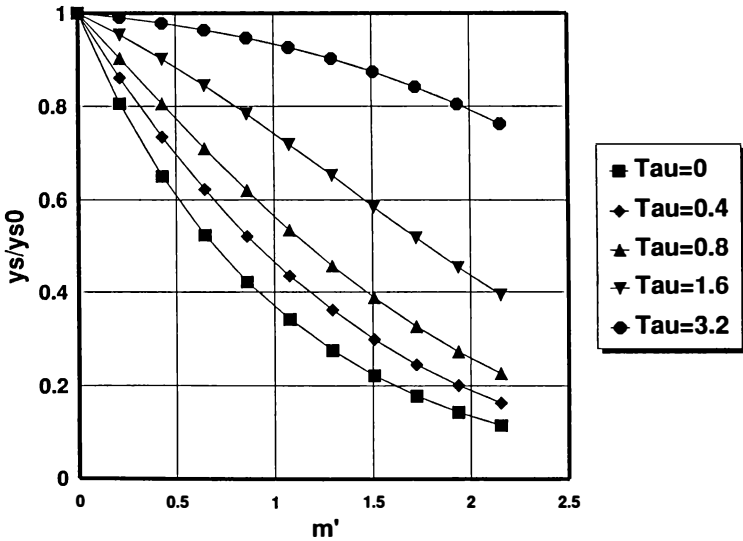


Figure 2 - y_s / y_s^0 versus m' for Catalyst A at Different τ 's

ever, it is also possible that the number of active sites determined by hydrogen chemisorption will be greater than that measured for benzene adsorption, if a larger metal crystallite size is necessary for the adsorption of benzene.

An examination of the rate constants extracted from the experimental data explains differences between the three catalysts. For example, catalyst C, tested at a 50°C lower temperature, is less active initially than catalyst B, because of the lower activity for hydrogenation. However, because of the greater active site concentration and greater resistance to poisoning, long-term activity is better. Catalyst A and B have comparable active site concentrations and deactivation behavior. However, the higher hydrogenation constant for catalyst B accounts for the higher overall activity.

Equations 9 and 10 show how the thiophene mole fraction in the gas and the concentration of unpoisoned sites varies with time (T) and position (m') in the reactor and both of these equations can be graphed using the calculated values for the rate of thiophene poisoning and active site concentration as well as the experimental conditions. Figures 2 and 3 show the ratio of the instantaneous to initial thiophene mole fraction and active site balance, respectively, as a function of reduced length down the bed at several different reduced times for Catalyst "A". Figures 4 and 5 show the same ratios for Catalyst "C".

Thiophene conversion is known to be less than 100% since the amount of thiophene fed to the reactor over these 16 hour experiments exceeds the amount of sulfur needed to cover all active sites by a factor of five to seven. For Catalyst "A", the thiophene conversion is initially projected to be about 90% at $T=0$ but it drops to around 60% at $T=1.6$ (about 18 hours). After long exposure to thiophene, the front part of the reactor is essentially inactive. Above a value of $T=1.6$, the rate of thiophene disappearance increases as the thiophene goes through the catalyst bed, resulting in a change for the shape of the curve.

The value of k_s for Catalyst "C" indicates that thiophene conversion will be much less than for Catalyst "A", and Figure 4 shows that the conversion of thiophene is only about 50% on the fresh catalyst. In fact, the disappearance of thiophene and the active site concentration as a function of axial bed position for Catalyst "C" is nearly linear. Indeed, Figure 5 suggests a fairly uniform profile for active sites as a function of axial position.

A comparison of Figures 1 and 2 shows that at 16 hours ($T=1.44$), the benzene conversion for Catalyst "A" is around 45% but greater than 60% for thiophene. Similarly, a comparison of Figures 1 and 4 shows that at 16 hours ($T=0.29$) for Catalyst "C", benzene conversion is still about 78% but the conversion of thiophene is around 40%. These results suggest that Catalyst "C" is less susceptible to thiophene poisoning which results in better benzene conversion over the life of the catalyst. This makes Catalyst "C" a good choice for benzene hydrogenation unless the amount of residual sulfur in the product exceeds specifications.

Conclusions

The catalyst deactivation model developed in this paper accounts for the nonsteady-state activity of commercial catalysts measured using accelerated sulfur aging experi-

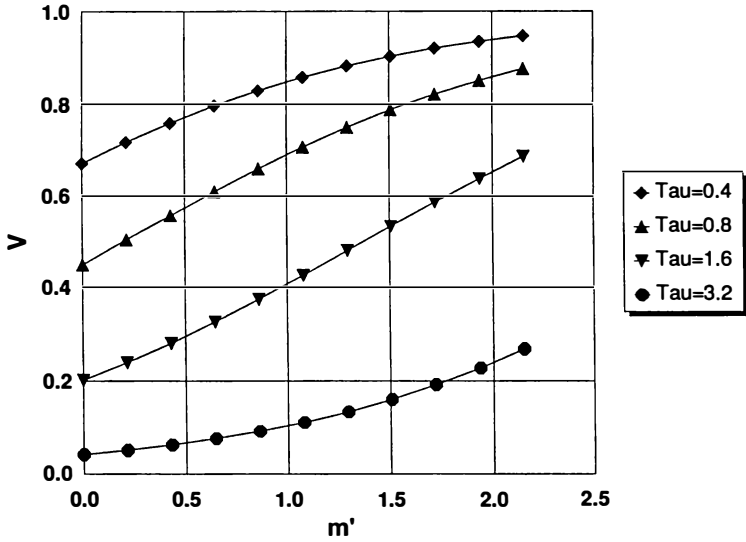


Figure 3 - V versus m' for Catalyst A at Different Tau's

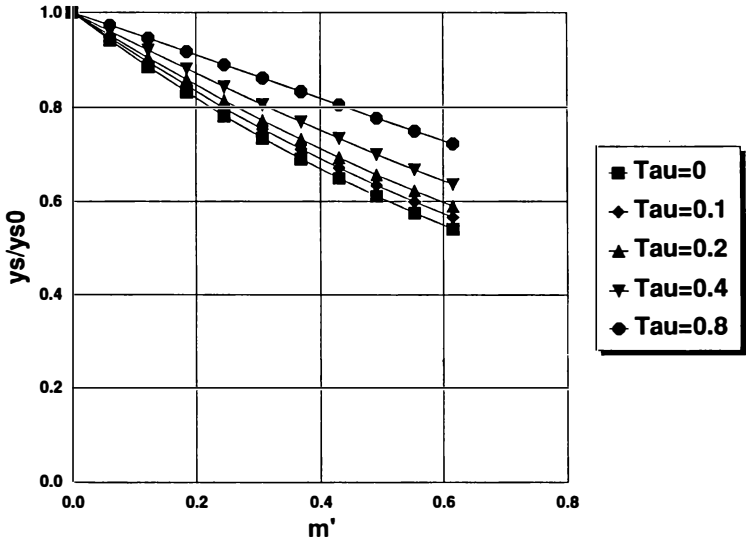


Figure 4 - y_s / y_s^0 versus m' for Catalyst C at Different Tau's

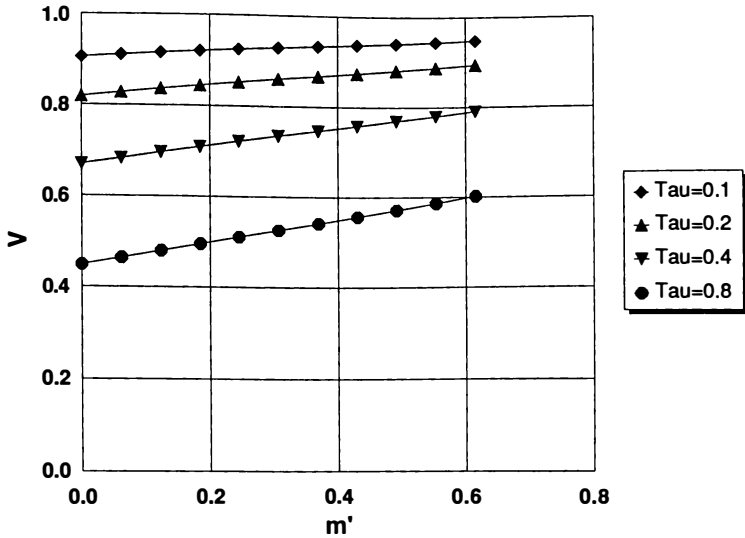


Figure 5 - V versus m' for Catalyst C at Different Tau's

ments. The model solution, an analytical one, provides an easy method to calculate benzene hydrogenation activity, active site concentration, and the rate of poisoning.

This type of solution method is possible for reactions where deactivation is slow, and a pseudo steady-state assumption can be made when solving the mass balance equations. Thus, these equations are applicable to reactions where the activity loss is first-order in both the poison and the active sites, and where deactivation is slow compared to the main reaction. A similar type of approach was taken by Johnson et al. (5), for oxygen consumption and carbon content during catalyst regeneration and by Bohart and Adams (6), for chlorine consumption and absorbance capacity of charcoal.

Symbols

A = cross sectional area, cm^2

C^o = initial concentration of active sites, moles of sites/g

C = poisoned active sites, moles of sites/g

F = molar flow rate, moles/hr

k_B = rate constant for hydrogenation, moles/(hr-atm-moles of sites)

k_s = rate constant for deactivation, moles/(hr-atm-moles of sites)

m = mass of catalyst, g

M_g = molecular weight of gas, g/mole

r_p = global rate, moles/(mass-hr)

t = time, hr

- x = fractional molar conversion of benzene
 y_B = mole fraction of benzene
 y_B^o = initial mole fraction of benzene in feed
 y_s = mole fraction of thiophene
 y_s^o = initial mole fraction of thiophene in feed
 z = axial distance, cm

Greek Symbols

- ε = void fraction
 ρ_B = bulk density of catalyst, g/cm³
 ρ_g = gas density, g/cm³
 Π = total pressure, atm

Acknowledgments

The authors wish to thank the Calscat Division of Mallinckrodt, Inc. for allowing us to use their benzene hydrogenation test data in this paper. The authors also wish to thank Joe Smith of the University of California, Davis, and Fil Pennella of Phillips Petroleum Company for many useful discussions.

Literature Cited

1. Aben, P.C., Platteeuw, J.C., and Stouthamer, B., *Reci. Trav. Chim. Pays-Bas*, **1970**, *89*, 449.
2. Prasad, K.H.V., Prasad, K.B.S., Mallikarjunan, M.M., and Vaidyeswaran, R., *J. Catal.*, **1983**, *84*, 65.
3. Marangozis, J.K., Mantzouranis, B.G., and Sophos, A.N., *Ind. Eng. Chem. Prod. Res. Dev.*, **1979**, *18(1)*, 61.
4. Aguinaga, A., Montes, M., de la Cal, J.C., and Asua, J.M., *Ind. Eng. Chem. Res.*, **1992**, *31(1)*, 155.
5. Johnson, B.M., Froment, G.F., and Watson, C.C., *Chem. Eng. Sci.*, **1962**, *17*, 835.
6. Bohart, G.S. and Adams, E.Q., *J. Am. Chem. Soc.*, **1920**, *42*, 523.
7. Coenen, J.W.E., van Meerten, R.Z.C., and Rijnten, H.Th., **1972**, *5th Int. Congr. on Catal., Miami Beach, FL*, 1, 671.
8. van Meerten, R.Z.C. and Coenen, J.W.E., *J. Catal.*, **1977**, 46, 13.

Author Index

- Absi-Halabi, M., 229
Aimoto, K., 219
Al-Lamy, A., 42
Andresen, J. M., 117
Barrage, M. C., 99
Bonardet, J. L., 99
Boock, Lori T., 171
Brevoord, E., 147,340
Cheng, Wu-Cheng, 159,283
Christensen, Thomas S., 186
Dadyburjor, Dady B., 254
Das, A. K., 401
de Lasa, Hugo, 312
Debnath, S., 401
Deeba, Michel, 296
Fraissard, J., 99
Fujita, Katsuhisa, 354
Fukase, S., 219
Ghosh, S., 401
Grande, K., 268
Guisnet, M., 77
Harding, Robert H., 283
Hashiguchi, Takeshi, 354
Hashimoto, K., 62
Helmsing, M. P., 322
Hirabayashi, K., 367
Holmen, A., 268
Hughes, R., 117
Hutchings, G., 117
Igarashi, F., 367
Igarashi, N., 219
Inoue, Shin-ichi, 414
Janssens, J. P., 238
Johnson, Marvin M., 428
Kato, K., 219
Khalaf, K., 42
Kim, Gwan, 283
Kimbara, Naoto, 354
Kondou, T., 367
Koon, C. L., 117
Koyama, Hiroki, 208
Kumagai, Hideaki, 208
Lerner, Bruce, 296
Liu, Yaofang, 201
Liu, Zhenyu, 254
Magnoux, P., 77
Makkee, M., 322
Mann, R., 42
Masuda, T., 62
Matheson, M., 91
Matoba, Shigeki, 254
McGhee, B. J., 117
Meier, Paul F., 428
Miyachi, Yoshimitsu, 354
Moljord, K., 77,268
Moulijn, J. A., 238,322
Murthy, V. L. N., 401
Nagai, Eiichi, 208
O'Connor, Paul, 2,147,340
Olthof, F. P. P., 340
Osanai, Shinichi, 254
Pan, Guoqing, 201
Pekediz, Ahmet, 312
Petti, Thomas F., 171
Pouwels, A. C., 147,340
Pruski, Jacek, 312
Rao, M. Rama, 401
Ray, S. K., 401
Rice, N. M., 134
Rostrup-Nielsen, Jens, 186
Rudesill, John A., 171
Sermon, P. A., 91
Shirooka, Tetsuya, 254
Sie, S. T., 6,238
Snape, C. E., 117
Stanislaus, A., 229
Stork, W. H. J., 379
Takatsuka, Toru, 2,414
Tanem, I., 268
van Langeveld, A. D., 238
Vong, M. S. W., 91
Wada, Yukitaka, 414

Wijngaards, H. N. J., 147,340
 Wojciechowski, B. W., 134
 Woolery, Geoffrey L., 2

Wormsbecher, Richard F., 283
 Yang, JiuJin, 201
 Zhao, Xinjin, 159

Affiliation Index

Akzo Nobel Catalysts, 2,147,340
 Brunel University, 91
 Chiyoda Corporation, 2,367,414
 Delft University of Technology, 6,238,322
 Engelhard Corporation, 296
 Haldor Topsøe A/S, 186
 Indian Oil Corporation Ltd., 401
 Japan Energy Corporation, 208,219
 Kuwait Institute for Scientific
 Research, 229
 Kyoto University, 62
 Liverpool University, 117
 Mitsubishi Oil Company Ltd., 367
 Mobil Technology Company, 2
 Nippon Ketjen Company Ltd., 354
 Norwegian Institute of Technology, 268

Phillips Petroleum Company, 428
 Queen's University, 134
 SINTEF Applied Chemistry, 77,268
 STATOIL Research Centre, 268
 Shell International Chemicals B. V., 379
 Université de Poitiers, 77
 Université Pierre et Marie Curie, 99
 University of Manchester Institute
 of Science and Technology, 42
 University of Petroleum, 201
 University of Salford, 117
 University of Strathclyde, 117
 University of Western Ontario, 312
 W. R. Grace and Company—Conn.,
 159,171,283
 West Virginia University, 254

Subject Index

A

Accuracy, small-scale testing of catalysts
 for fixed-bed processes, 31,33–38
 Acid catalytic sites for hydrocarbon
 reactions, deactivation by coking, 91–97
 Acid sites, coke deposition effect, 72,75f
 Acid zeolite catalysts
 coke composition determination methods,
 78–79
 coke formation modes, during *n*-heptane
 cracking on protonic zeolites, 79–84
 deactivation modes
 coke content effect, 84f,85
 pore blockage, 85–87,88f,89
 site coverage, 84f,87,88f,89
 types, 83,85
 zeolite effect, 84f,85
 Activation, catalyst coking, 91–97

Activity

catalyst deactivation by fast-coking
 species added to feed, 254–267
 role in catalyst performance, 379–380
 Adiabatic prereforming
 advantages, 187
 applications, 186
 bench-scale testing of catalyst
 deactivation, 194,196–199
 deactivation of prereforming catalyst,
 187–190
 experimental methods for
 characterization of catalyst
 deactivation, 191–195,197
 installation of prereformer units,
 187,188f
 models for performance prediction,
 190–191,192f
 temperature profiles, 186,188f

- Adsorption effect, testing using Riser simulator, 312–320
- Advantages, small-scale testing of catalysts for fixed-bed processes, 6–41
- Aging of catalyst, *See* Catalyst aging
- Aging tests for catalysts, simulation, 417,421,422*f*
- ²⁷Al-NMR studies, coking of zeolite catalysts, 105
- Alkali metal poisoning, catalyst deactivation in adiabatic prereforming, 189
- Applications, small-scale testing of catalysts for fixed-bed processes, 6–41
- Aromatic compounds, production in petroleum refining industry, 219
- Aromatic concentration, role in pilot reactor testing of naphtha boiling point effect in catalytic reforming, 271,274–275,276*f*
- Aromatic ring percent, 255–256
- Aromatization catalyst, light hydrocarbon, life testing, 367–378
- Aromatization catalyst deactivation, light naphtha, *See* Light naphtha aromatization catalyst deactivation
- Aromatization process of light hydrocarbon, catalyst regeneration, 367–368
- Available time, 16
- Axial convective diffusion, role in small-scale testing of catalysts, 11,14,15*f*
- Axial diffusivity, 16
- Axial molecular diffusion, role in small-scale testing of catalysts, 11,12*f*,13*t,f*
- Axial position of catalyst pellet, role in catalyst deactivation in hydrodemetallization, 246,248*f*
- B**
- Bench-scale fluid catalytic cracking microriser, 322–338
- Bench-scale testing, characterization of catalyst deactivation in adiabatic prereforming, 194,196–199
- Benzene hydrogenation, catalytic deactivation modeling, 428–437
- Bulk diffusion coefficient, role in catalyst deactivation in hydrodemetallization, 246,247*f*
- Burning rate of coke, influencing factors, 402
- C**
- ¹³C NMR
- characterization of fluid catalytic cracking catalyst coke, 117–131
- studies of coking of zeolite catalysts, 99–105
- Carbon formation, catalyst deactivation in adiabatic prereforming, 189–190
- Carbonaceous deposits
- Pt/alumina, 91–92,93*f*,97
- Pt/silica, 92,94*f*,97
- silica–alumina, 92,95–97
- Catalyst(s)
- hydrocarbon, *See* Hydrocarbon catalysts
- hydrocarbon conversion, *See* Hydrocarbon conversion catalysts
- metal deactivation and metal dehydrogenation effects during cyclic propylene steaming, 177–183
- small-scale testing for fixed-bed processes, 6–41
- testing conditions, 6–7
- Catalyst aging, role in catalyst activity and selectivity, 147,150*t*
- Catalyst coking
- activation, 91–97
- deactivation, 91–97
- Catalyst contacting, small-scale testing of catalysts for fixed-bed processes, 19,22,23*f*
- Catalyst cracking, catalyst decay as side reaction of chain processes, 134–145
- Catalyst deactivation
- by coke, 62–131
- by fast-coking species added to feed activity, 257,261–267
- catalyst properties, 255

Catalyst deactivation—*Continued*

by fast-coking species added to feed—

Continued

coking kinetics

decane effect, 256–257,258f

feed concentration effect, 257,259–260f

naphthalene effect, 256–257,258f

experimental procedure, 255

cyclic propylene steaming, 177–183

in adiabatic prereforming

alkali metal poisoning, 186

bench-scale testing, 194,196–199

carbon formation, 189–190

experimental methods for

characterization

chemical analyses, 191,192f

intrinsic activity measurements,

193–194,195f,197f

temperature-programmed reaction,

191,193,195f

models for performance prediction

computational methods, 191

empirical methods, 190–191,192f

use at stages, 190

silica poisoning, 189

sintering, 187

sources, 187

sulfur poisoning, 189

in commercial residue hydrodesulfurization

at high residue conversion operation,

214,216

catalyst activities, 212–214

catalyst diffusivity, 214,215f

catalyst inspections, 212

coke effect, 216

experimental description, 209,211–212

hydrodesulfurization unit

catalysts, 209,210f

operations, 209,210f

reactors, 209,210f

metal effect, 216

process

initial catalyst deactivation,

216–217,218f

intermediate catalyst deactivation,

217,218f

reason for interest, 208

Catalyst deactivation—*Continued*

in fluid catalytic cracking

deactivation by poisons and deposits,
148–149,150t

evaluation

catalyst deactivation by coke, 154–155

high poisoning power of nitrogen, 154

hydrothermal deactivation, 147–148

mechanism, 147,150t

simulation

catalyst poisoned by metals, 151–153

low metals catalyst deactivation,

149,151

in hydrodemetallization

axial position of catalyst pellet effect,
246,248f

bulk diffusion coefficient effect, 246,247f

catalyst porous texture, 243,244f

experimental vs. modeling, 246,250f

experimental procedure, 245

initial pore radius effect, 246,249f

mass balances, 243,245

model equations, 245

modeling approach

diffusion, 240

reaction kinetics, 240

reaction mechanism, 240,242f

schematic representation, 240,241f

in residual oil hydrodesulfurization

application to deep hydrodesulfurization

of diesel fuel

catalyst deactivation by coke

deposition, 421,424f

color degradation, 421,423,424–426f

catalyst deactivation with diffusion-

controlled reactions

catalyst fouling trends, 417,419f

pore clogging, 417,418f

surface area, 417,419f

catalyst pore volume vs. parameters,

421,422f

catalyst properties, 417,420t

feedstock properties, 417,420t

simulation for catalyst aging tests,

417,421,422f

simulation model

catalyst deactivation, 416

- Catalyst deactivation—*Continued*
in residual oil hydrodesulfurization—
Continued
simulation model—*Continued*
effectiveness factor, 415–416, 418f
kinetics, 414–415
reactor model, 417
in residue hydroprocessing
catalyst pore size effect, 233–236
catalyst presulfiding effect, 233
experimental description, 230
feed space velocity effect,
231, 233, 235f
pressure effect, 231, 232f
temperature effect, 231, 232f
pilot reactor testing of naphtha boiling
point effect in catalytic reforming,
277, 279–281
role of nickel and vanadium, 296–297
- Catalyst decay
as side reaction of chain processes of
catalytic cracking
coke formation mechanism,
136–138, 139f
experimental description, 134
kinetics
assumptions, 138, 140
first-order decay, 140–141
mixed-order decay, 145
second-order decay, 142–145
minor product formation mechanism,
136–138, 139f
kinetics and mechanism, 135
processes leading to loss of activity,
135–136
- Catalyst equilibration, role in fluid
catalytic cracking catalyst
regenerability, 409, 411f
- Catalyst fouling, role in catalyst
activity and selectivity, 147, 150f
- Catalyst life
liquid mass velocity effect, 355–359
termination, 368
- Catalyst performance
influencing factors, 379–380
modeling, 414–437
- Catalyst performance correlation between
laboratory tests and commercial units
for resid hydrotreating
applications, 366
catalyst life
liquid mass velocity vs. catalyst
life, 355–359
testing units, 355, 357f
- Catalyst performance
case studies, 362–366
feedstock properties vs. desulfurization
reactivity, 356, 359–361, 363
reaction rate equation, 361–362
experimental description, 355
- Catalyst performance testing
acceleration of reaching stationary
state, 394
data generation in laboratory, 3–4
evolution in hydrocarbon conversion
processes processes, 4–5
feedstock, 393–394
long-term catalyst deactivation,
394–395
miniaturization trend, 4
modeling, 395, 396–397f
philosophical issues, 2–3
recycle operation, 395
- Catalyst poisoning and deactivation
irreversible deactivation, 381, 383
reversible poisoning, 380–381, 382f
role in catalyst activity and
selectivity, 147, 150f
separation of reversible and
irreversible deactivation, 383
- Catalyst pore size, role in catalyst
deactivation in residue
hydroprocessing, 233–236
- Catalyst porous texture, role in catalyst
deactivation in hydrodemetallization,
243, 244f
- Catalyst presulfiding, role in
catalyst deactivation in residue
hydroprocessing, 233
- Catalyst properties, role in fluid
catalytic cracking catalyst
regenerability, 406–407, 409, 410f

- Catalyst ranking, role in fluid catalytic cracking performance testing, 333,335f
- Catalyst regenerability, role of coke on regenerated catalyst and after-burning, 402,404f
- Catalyst regeneration, aromatization process of light hydrocarbons, 367–368
- Catalyst screening, role of regenerability, 409,412
- Catalyst-to-oil ratio, 331
- Catalytic coke
determination, 341–344,352
formation, 341
- Catalytic cracking of hydrocarbons in industrial fluid catalytic cracking units, modeling requirements, 312
- Catalytic cracking reaction, modeling using Riser simulator, 312–320
- Catalytic deactivation modeling of benzene hydrogenation
active site balance vs. reduced length down the bed, 435,436–437f
applications, 437
catalyst properties, 433
experimental description, 428–429,432–433
fractional conversion vs. time, 433,434f
rate constants, 433
rate equation derivation, 429–432
sulfur amount for complete deactivation, 433,435
thiophene mole fraction vs. reduced length down the bed, 434f,435
- Catalytic disproportionation of two normal adjacent carbenium ions, cause of decay in cracking catalysts, 134
- Catalytic function, importance of pore sizes, 42–43
- Catalytic reforming
applications, 268
pilot reactor testing of naphtha boiling point effect, 268–281
- Chain mechanism of cracking, 135
- Chain processes of catalytic cracking, catalyst decay as side reaction, 134–145
- Chemical analyses, characterization of catalyst deactivation in adiabatic prereforming, 191,192f
- CH_n coke, *n* value vs. coke loading, 63,66f
- Coke
catalyst deactivation, 62–131
components, 341
definition, 78
evaluation of catalyst deactivation, 154–155
from *n*-hexadecane feeds
¹³C-NMR analysis, 130–131
MS analysis, 126,128–129f
from refinery feeds
¹³C-NMR analysis, 120–126
MS analysis, 126,127f
role
catalyst deactivation in commercial residue hydro-desulfurization, 216
rapid catalyst deactivation, 229
zeolite deactivation, 77
zeolite catalyst deactivation, 62–75
- Coke burning rate, influencing factors, 402
- Coke content, role in coke deactivation, 84f,85
- Coke deactivation modes
coke content effect, 84f,85
pore blockage, 85–87,88f,89
site coverage, 84f,87,88f,89
types, 83,85
zeolite effect, 84f,85
- Coke deposition
catalytic property effect, 65–75
process, 63,64f
relative activity effect, 63,64f
- Coke formation
during *n*-heptane cracking on protonic zeolite, 79–84
mechanism, 136–138,139f
requirements, 79
- Coke selectivity of fluid catalytic cracking catalysts
catalytic coke determination, 341–344,352
Conradson carbon coke determination, 347,348–349f,352
contaminant coke determination, 344–346,348f,352

- Coke selectivity of fluid catalytic cracking catalysts—*Continued*
soft delta coke determination, 347,350–352
- Coke yield, role in fluid catalytic cracking performance testing, 333,334*f*
- Coked zeolite, diffusivity effect, 67,69–75
- Coking
acid zeolite catalysts, 77–89
deactivation of metallic and acid catalytic sites for hydrocarbon reactions, 91–97
definition, 79
zeolite catalysts, NMR techniques for studying, 99–115
- Coking rate, catalyst deactivation by fast-coking species added to feed, 254–267
- Commercial residue hydrodesulfurization, catalyst deactivation, 208–218
- Commercial units, correlation of catalyst performance with laboratory tests for resid hydrotreating, 354–366
- Computational models for performance prediction, catalyst deactivation in adiabatic prereforming, 190–191,192*f*
- Computer images of sectioned three-dimensional stochastic network, evaluation of pore structure and morphology of hydrocarbon conversion catalysts, 52,54–60
- Conradson carbon coke, determination, 347,348–349*f*,352
- Conradson carbon residue coke, formation, 341
- Contact times, role in fluid catalytic cracking catalyst performance testing, 336,337*f*
- Contaminant coke
determination, 344–346,348*f*,352
formation, 341
- Contaminant metal deactivation, cyclic propylene steaming of fluid catalytic cracking catalysts, 177–183
- Cracking catalysts, causes of decay, 134
- Cyclic metal decomposition method, 299–300
- Cyclic metal impregnation, 172
- Cyclic propylene steaming
advantages, 172
disadvantages, 172
fluid catalytic cracking catalysts
advantages, 183
deactivation
comparison to equilibrium catalyst, 173,174*f*,175*f*,*t*
procedure, 173
factors affecting metal tolerance catalysts, 173,176,177*f*
low oxygen cyclic propylene steaming deactivation, 178,180,181*f*
metal oxidation state, 176,178,179*f*
final metal oxidation state effect on deactivation, 180,181*f*
V oxidation state effect on deactivation, 180,182–183
- D
- Data, generation in laboratory, 3–4
- Data collection, catalyst performance testing, 3
- Deactivation
acid zeolite catalysts, 77–89
catalyst coking, 91–97
catalyst in hydrodemetallization, 238–250
fluid catalytic cracking catalyst, 134–183
fluid catalytic cracking catalyst during oil transformation, 99
forms, 147,150*t*
hydroprocessing catalysts, 208–250
light naphtha aromatization catalyst, 219–228
reforming catalysts, 186–205
role of fast-coking species added to feed, 254–267
See also Catalyst deactivation
- Deactivation assessment, vanadium interaction with fluid catalytic cracking catalyst, 296–309
- Deactivation mechanism in reforming catalysts at start of run
experimental description, 201–202

- Deactivation mechanism in reforming catalysts at start of run—*Continued*
 hydrocarbons in N₂ effect on platinum functions, 203–204
 hydrogen purity effect on platinum functions, 204–205
 oxygen effect on platinum functions, 203
 temperature effect on platinum functions, 202–203
- Deactivation modes, coke, *See* Coke deactivation modes
- Decane, role in catalyst deactivation, 254–267
- Decay in catalytic cracking, influencing factors, 135
- Dehydrogenation, metal, cyclic propylene steaming of fluid catalytic cracking catalysts, 177–183
- Dehydrogenation coke, determination, 344–346,348f,352
- Desulfurization reactivity, role of feedstock properties, 356,359–363
- Diesel fuel, catalyst deactivation model, 421,423,424–426f
- Diffusion, catalyst deactivation in hydrodemetallization, 240
- Distillate desulfurization, 383–384,385f
- E
- Effectiveness factor, role in residual oil hydrosulfurization, 415–416,418f
- Empirical methods for performance prediction, catalyst deactivation in adiabatic prereforming, 190–191,192f
- Engehard transfer method
 advantages, 297
 competitive adsorption and vanadium trapping, 307
 experimental procedure, 298–299
 function, 296
 magnesium oxide based trap technology kinetics, 307–308,309f
 thermodynamics, 308
 process, 300–301,302f
 surface enrichment of vanadium, 301,303–304
- Engehard transfer method—*Continued*
 vanadium transfer mechanism, 304–307
 vanadium transfer requirements, 301,302–303f
- F
- Fast-coking species added to feed, role in catalyst deactivation, 254–267
- Feed, catalyst deactivation by added fast-coking species, 254–267
- Feed partial pressure, 331
- Feed space velocity, role in catalyst deactivation in residue hydroprocessing, 231,233,235f
- Feedstock, role in pilot reactor testing of naphtha boiling point effect in catalytic reforming, 270–271
- Feedstock properties, role in desulfurization activity, 356,359–361,363
- Fine inert particles, catalyst bed dilution, 22,24,25f,t
- First-order decay, catalyst decay as side reaction of chain processes of catalytic cracking, 140–141
- Fixed-bed processes, small-scale testing of catalysts, 6–41
- Fixed-bed reactors, usage, 6
- Fixed-bed residue hydroprocessing, 390–392
- Fluid catalytic cracking
 catalyst deactivation, 147–155
 description, 401
 importance
 petroleum refining, 117
 regeneration of coked catalyst, 401–402
 mechanisms of coke formation, 117
 vanadium mobility, 284–294
- Fluid catalytic cracking catalyst(s)
 coke selectivity, 340–352
 contaminant metal deactivation and metal dehydrogenation effects during cyclic propylene steaming, 177–183
 deactivation, 134–183
 description, 160
 poisoning by vanadium, 283–284
 sodium deactivation, 159–170

- Fluid catalytic cracking catalyst coke
 characterization by ^{13}C NMR
 and MS
 ^{13}C -NMR analysis of cokes
n-hexadecane feed, 130–131
 refinery feeds
 aliphatic structure, 125–126
 aromatic structure, 120, 125
 quantitative aspects, 120–125
 ^{13}C -NMR measurement procedure,
 119, 125*t*
 experimental description, 118–119
 MS
 cokes
 from *n*-hexadecane microactivity
 test runs, 126, 128–129*f*
 from refinery feeds, 126, 127*f*
 measurement procedure, 119
- Fluid catalytic cracking catalyst
 deactivation, *See also* Catalyst
 deactivation in fluid catalytic cracking
- Fluid catalytic cracking catalyst particle,
 scanning electron microscopic image,
 42, 44*f*
- Fluid catalytic cracking catalyst
 performance testing
 applications, 322
 catalyst ranking, 333, 335*f*
 coke yield, 333, 334*f*
 contact times and experimental
 settings, 329
 design of microriser, 324, 346, 327*f*
 experimental conditions, 328
 factors affecting activity, 331
 feed and catalysts, 328
 LPG olefinicity, 331, 332*f*
 microriser results, 329–331
 microsimulation test
 procedure, 326, 327–328
 results, 329–331
 nitrogen carrier gas effect, 336, 338
 operation, 326
 reactor selection, 323–324, 325*f*
 secondary cracking, 333
 short contact times, 336, 337*f*
 thermal vs. catalytic cracking,
 331, 332*f*, 333
- Fluid catalytic cracking catalyst
 regenerability evaluation, test
 procedure, 401–412
- Fluid catalytic cracking units
 modeling requirements, 312
 operating conditions in India, 402
- Fluid catalytic cracking unit's processing
 resid
 coke formation limitation, 341
 types of cokes formed, 341
- Formation of coke, *See* Coke formation
- Fouling of catalyst, *See* Catalyst fouling
- Fresh zeolite, coke deposition effect on
 diffusivity, 65, 67, 68*f*
- G
- Ga/H-ZSM-5 zeolite, life testing, 367–368
- Gas adsorption, porosity measurement of
 particle, 42
- Graphical deactivation, graphical
 deactivation in adiabatic prereforming,
 190–191, 192*f*
- Gum formation in steam reforming,
 model, 190
- H
- H-Ga-silicate, life testing, 367–368
- H-mordenite, ^{13}C -NMR studies, 99–105
- ^1H -NMR studies, coking of zeolite
 catalysts, 106–110
- H-ZSM-5 zeolite, life testing, 367–368
- Heavy crude, processing problems, 296
- n*-Heptane cracking, protonic zeolites,
 79–84
- HY zeolites
 ^{27}Al -NMR studies, 105
 ^{13}C -NMR studies, 99–105
 ^1H -NMR studies, 106
 ^{29}Si -NMR studies, 105
 ^{129}Xe -NMR studies, 111–114
- Hydrocarbon aromatization catalysts,
 light, life testing, 367–378
- Hydrocarbon catalysts, performance
 testing, 379–397

- Hydrocarbon conversion, deactivation by coking, 91–97
- Hydrocarbon conversion catalysts, pore structure and morphology, 42–60
- Hydrocarbon conversion processes, evolution, 4–5
- Hydrocarbons in N₂, role in platinum functions, 203–204
- Hydrocracking, 384,387–390
- Hydrodemetallization, catalyst deactivation, 238–250
- Hydrodesulfurization, catalyst deactivation, 208–218,414–426
- Hydrogen content, role in pilot reactor testing of naphtha boiling point effect in catalytic reforming, 277,278f
- Hydrogen purity, role in platinum functions, 204–205
- Hydrogenation of benzene, catalytic deactivation modeling, 428–437
- Hydrometallization process design and operation, development of catalyst deactivation models, 238
- Hydroprocessing
distillate desulfurization, 383–384,385f
fixed-bed residue hydroprocessing, 390–392
hydrocracking, 384,387–390
sulfur-tolerant hydrogenation, 384,386f
- Hydroprocessing catalysts, deactivation, 208–250
- Hydrothermal deactivation, catalysts in fluid catalytic cracking, 147–148
- Hydrotreating, resid, catalyst performance correlation between laboratory tests and commercial units, 354–366
- Hydrotreating processing of heavy oils, heteroatom removal, 238
- Hypothesis, catalyst performance testing, 3
- HZSM-5 zeolites
¹H-NMR studies, 106
²⁷Al-NMR studies, 105
¹³C-NMR studies, 99–105
²⁹Si-NMR studies, 105
- Impregnation, low melting point alloy, *See* Low melting point alloy impregnation
- Initial catalyst deactivation, process, 216–217,218f
- Initial pore radius, role in catalyst deactivation in hydrodemetallization, 246,249f
- Intermediate catalyst deactivation, process, 217,218f
- Intrinsic activity measurements, characterization of catalyst deactivation in adiabatic prereforming, 193–194,195f,197f
- Irregular cubic three-dimensional pore network, pictorial representation, 47,48f
- K
- Kinetics of catalyst deactivation hydrodemetallization, 240
residual oil hydrodesulfurization, 414–415
- L
- Laboratory deactivated catalysts, simulation problems, 172
- Laboratory tests, correlation of catalyst performance with commercial units for resid hydrotreating, 354–366
- Life testing of light hydrocarbon aromatization catalysts
accelerated catalyst aging test, 374,376–378
catalyst activity, 370–372
catalyst activity test procedure, 368–369
catalyst properties, 368,369t
coke formation, 372,373f,t
coke removal, 372,374,375f,377t
experimental description, 368,370
- Light hydrocarbon aromatization, description, 367
- Light hydrocarbon aromatization catalysts, life testing, 367–378

Light naphtha aromatization catalyst deactivation
acidity modification by stabilization treatment, 225,227
conversion of light naphtha, 221
design of demonstration plant and operation, 228
development, 219–220,228
economics, 219
experimental procedure, 220–221
micropore analysis of nitrogen adsorption, 223,225,226f
stability of catalysts
acid strength distribution after stabilization treatment, 221,222f
catalyst deactivation after stabilization treatment, 221,222f
kinetics of catalyst deactivation, 221,223,224f
surface characterization of stabilized catalyst by probe molecule reaction, 225,226f
Limitations, small-scale testing of catalysts for fixed-bed processes, 6–41
Liquid mass velocity, role in catalyst life, 355–356,357f,358t,359f
Low melting point alloy impregnation, 47,49–51
Low metals, catalyst deactivation, 149,151
LPG olefinicity, 331,332f

M

Magnesium oxide based trap technology
kinetics, 307–308,309f
thermodynamics, 308
Mass balances, catalyst deactivation in hydrodemetallization, 243,245
Mathematical models for performance prediction, catalyst deactivation in adiabatic prereforming, 191
Mercury porosimetry
evaluation of pore structure and morphology of hydrocarbon conversion catalysts, 43–46,48
porosity measurement of particle, 42

Metal(s)
catalyst deactivation, 151–153
loss of catalyst activity through deposition, 238,239f
role in catalyst deactivation in commercial residue hydrodesulfurization, 216
Metal contaminants, 171–172
Metal deactivation, cyclic propylene steaming of fluid catalytic cracking catalysts, 177–183
Metal dehydrogenation, cyclic propylene steaming of fluid catalytic cracking catalysts, 177–183
Metal-loaded H-ZSM-5 zeolite, life testing, 367–368
Metal oxidation state, role in cyclic propylene steaming of fluid catalytic cracking catalysts, 177–183
Metallic catalytic sites for hydrocarbon reactions, deactivation by coking, 91–97
Micropore analysis of nitrogen adsorption, light naphtha aromatization catalyst deactivation, 223,225,226f
Microriser, development, 322–338
Microsimulation test, comparison to bench-scale microriser for fluid catalytic cracking catalyst performance testing, 322–338
Miniaturization trend, catalyst performance testing, 4
Mitchell method, 299–300
Mitchell method steam deactivation procedure, 172
Mixed-order decay, catalyst decay as side reaction of chain processes of catalytic cracking, 145
Mobility of vanadium in fluid catalytic cracking, *See* Vanadium mobility in fluid catalytic cracking
Modeling
catalyst deactivation
benzene hydrogenation, 428–437
hydrodemetallization, 240–242
catalyst performance, 414–437
catalytic cracking reaction, use of Riser simulator, 312–320

- Modeling—*Continued*
 performance testing of hydroconversion catalysts, 392–393
- Morphology of pores of hydrocarbon conversion catalysts, *See* Pore structure and morphology of hydrocarbon conversion catalysts
- MS, characterization of fluid catalytic cracking catalyst coke, 117–131
- N
- Naphtha aromatization catalyst deactivation, light, *See* Light naphtha aromatization catalyst deactivation
- Naphtha boiling point effect in catalytic reforming, pilot reactor testing, 268–281
- Naphthalene, role in catalyst deactivation, 254–267
- Nickel
 laboratory catalyst deactivation by cyclic propylene steaming, 177–183
 role in catalyst deactivation, 296–297
- Nitrogen, evaluation of high poisoning power, 154
- Nitrogen carrier gas, role in fluid catalytic cracking catalyst performance testing, 336–338
- NMR
 deactivation studies, 117–118
 study of coking of zeolite catalysts
²⁷Al NMR, 105
¹³C NMR, 99–105
¹H NMR, 106–110
²⁹Si NMR, 105
¹²⁹Xe NMR, 110–115
- Nucleation growth process, coking of zeolites, 79–84
- O
- Oxygen, role in platinum functions, 203
- P
- Parallel bundles of pores, 46
- Particle size, limiting factor for applicability of small laboratory reactors for representative catalyst testing, 22
- Performance testing of hydroconversion catalysts
 catalyst performance testing
 acceleration of reaching stationary state, 394
 feedstock, 393–394
 long-term catalyst deactivation, 394–395
 modeling, 395,396–397f
 recycle operation, 395
- catalyst poisoning and deactivation
 irreversible deactivation, 381,383
 reversible poisoning, 380–381,382f
 separation of reversible and irreversible deactivation, 383
- Physicochemical properties of catalyst, role on activity and selectivity, 402–403
- Pilot reactor testing of naphtha boiling point effect in catalytic reforming
 aromatic concentration effect, 271,274–275,276f
 catalyst deactivation, 277,279–281
 experimental description, 268–269
 feedstock, 270–271
 hydrogen content effect, 277,278f
 naphtha analysis, boiling point effect, 271–273f
 reactor unit, 269
 reformat yield effect, 275–277
 test procedures, 269–270
- Poison(s), catalysts deactivation, 148–149,150r
- Poisoning of catalyst, *See* Catalyst poisoning
- Pore blockage, role in coke deactivation, 85–87,88f,89
- Pore size
 importance for catalytic function, 42–43
 role in catalyst deactivation in residue hydroprocessing, 233–236
- Pore size distribution, three-dimensional stochastic network, 52,53f

- Pore structure and morphology of hydrocarbon conversion catalysts
computer images of sectioned three-dimensional stochastic network, 52,54–60
development, 43
low melting point alloy impregnation, 47,49–52
mercury porosimetry, 43–46,48
pore size distribution for three-dimensional stochastic network, 52,53f
stochastic pore network application, 46–47,48–49f
- Pore volume of catalysts, role in residual oil hydrodesulfurization, 421,422f
- Porous texture of catalyst, role in catalyst deactivation in hydrodemetallization, 243,244f
- Pressure, role in catalyst deactivation in residue hydroprocessing, 231,232f
- Presulfiding of catalyst, role in catalyst deactivation in residue hydroprocessing, 233
- Process conditions, role in catalyst deactivation in residue hydroprocessing, 229–236
- Processes with reactants in gas phase, accuracy, 31,33–34t
- Properties of catalyst, role in catalyst deactivation in residue hydroprocessing, 229–236
- Propylene steaming of fluid catalytic cracking catalysts, cyclic. *See* Cyclic propylene steaming of fluid catalytic cracking catalysts
- Protocol, catalyst performance testing, 3
- Protonic zeolites, coke formation during *n*-heptane cracking, 79–84
- Pt/alumina, development and properties of carbonaceous deposits, 91–92,93f,97
- Pt/silica, development and properties of carbonaceous deposits, 92,94f,97
- PtRe/Al₂O₃ catalysts, deactivation mechanism at start of run, 201–205
- Pyrolytic elimination of hydrogen, cause of decay in cracking catalysts, 134
- R
- Rapid catalyst deactivation, 229–230
- Rate equation, catalytic deactivation modeling of benzene hydrogenation, 429–432
- Rate of coking, catalyst deactivation by fast-coking species added to feed, 254–267
- Reaction coke, determination, 341–344,352
- Reformate yield, role in pilot reactor testing of naphtha boiling point effect in catalytic reforming, 275–277
- Reforming catalysts
deactivation, 186–205
factors affecting activity, 201
pilot reactor testing of naphtha boiling point effect, 268–281
- Regenerability, role in catalyst screening, 409,412
- Regeneration
catalysts
aromatization process of light hydrocarbons, 367–368
partial and total oxidation of coke, ¹²⁹Xe-NMR studies, 114–115
coked catalyst, 401–402
- Regular cubic three-dimensional pore network, pictorial representation, 47,48f
- Research octane numbers, pilot reactor testing of naphtha boiling point effect in catalytic reforming, 268–281
- Resid, processing problems, 296
- Resid desulfurization units, 354
- Resid hydrotreating, catalyst performance correlation between laboratory tests and commercial units, 354–366
- Resid hydrotreating catalysts, applications, 354
- Residence time distribution, small-scale testing of catalysts for fixed-bed processes, 11–21
- Residual oil hydrodesulfurization, catalyst deactivation model, 414–426
- Residue hydrodesulfurization, catalyst deactivation, 208–218

- Residue hydroprocessing, role of process conditions and catalyst properties on catalyst deactivation, 229–236
- Riser simulator
 experimental procedure, 313,314*f*,316
 feedstock properties, 316,317*t*
 function, 312
 modeling of catalytic cracking reactions
 analysis, 318–319,320*t*
 theory, 316,318
 pressure profile, 313,315*f*
- S**
- Screening of catalysts, role of regenerability, 409,412
- Second-order decay, catalyst decay as side reaction of chain processes of catalytic cracking, 142–145
- Secondary cracking, role in fluid catalytic cracking performance testing, 333
- Selectivity, role in catalyst performance, 379–380
- ²⁹Si NMR, studies of coking of zeolite catalysts, 105
- Silica–alumina, development and properties of carbonaceous deposits, 92,95–97
- Silica poisoning, catalyst deactivation in adiabatic prereforming, 189
- Simulation of metals deactivation,
 Mitchell method steam deactivation procedure, 172
- Sintering, catalyst deactivation in adiabatic prereforming, 187
- Site coverage, role in coke deactivation, 84*f*,87,88*f*,89
- Small-scale testing of catalysts for fixed-bed processes
 accuracy
 processes with reactants in gas phase, 31,33–34*t*
 temperature definition
 adiabatically operated reactors, 28,30–31,32*f*
 isothermally operated reactors, 26–28,29*f*
 types, 24,26
 trickle-flow processes, 31,34–38
- Small-scale testing of catalysts for fixed-bed processes—*Continued*
 advantages, 38
 allowable spread in residence time, 10,12*f*
 applications, 41
 catalyst bed dilution with fine inert particles, 22,24,25*f*,*t*
 catalyst contacting, 19,22,23*f*
 categories of laboratory reactors, 7,8*t*
 feed requirements vs. reactor class, 7,8*t*
 incentives, 7–8
 limitations, 38
 microflow reactor examples, 38–40
 residence time distribution
 axial convective diffusion effect, 11,14,15*f*
 axial molecular diffusion effect, 11,12*f*,13*t*,*f*
 erasure of transbed velocity profile by molecular diffusion, 16,18–19,20–21*f*
 transverse macroscopic velocity effect, 14,16,17*f*
 simulation of industrial reactor on laboratory scale, 9–10
- Sodium, interparticle and intraparticle mobility, 166,167*t*,*f*
- Sodium deactivation of fluid cracking catalyst
 experimental procedure, 160–161
 feedstock properties, 161,162*t*
 influencing factors, 159–160
 interparticle and intraparticle mobility of sodium, 166,167*t*,*f*
 matrix and zeolite deactivation for laboratory deactivated catalysts, 163,165*f*
 mechanisms, 159
 sodium effect on fresh and steam-deactivated catalysts, 166,168–169
 sodium effect on matrix and zeolite surface areas, 161–163,164–165*f*
 source of sodium, 159
- Soft delta coke, determination, 347,350–352
- Soluble coke, components, 80
- Stability
 light naphtha catalysts, 221–224
 role in catalyst performance, 379–380

- Steam-deactivated catalysts, sodium effect, 166,168–169
- Stochastic pore networks, 46–47,48–49*f*
- Stripper coke
determination, 347,350–352
formation, 341
- Structure of pores of hydrocarbon conversion catalysts, *See* Pore structure and morphology of hydrocarbon conversion catalysts
- Sulfur poisoning, catalyst deactivation in adiabatic prereforming, 189
- Sulfur role
in catalytic activity, 428–437
in vanadium interaction with fluid catalytic cracking catalyst, 296–309
- Sulfur-tolerant hydrogenation, 384,386*f*
- T
- 10×10×10 network, pictorial representation, 47,48*f*
- Taylor diffusivity, 16
- Temperature definition, accuracy, 24,26–28,29*f*
- Temperature-programmed reaction, characterization of catalyst deactivation in adiabatic prereforming, 191,193,195*f*
- Temperature role
in catalyst deactivation in residue hydroprocessing, 231,232*f*
in platinum functions, 202–203
- Test procedure for fluid catalytic cracking catalyst regenerability evaluation
catalyst equilibration effect, 409,411*f*
catalyst properties
vs. critical coke, 409,410*f*
vs. regenerability, 407,410*f*
data analytical procedure, 405–406
experimental description, 403–405
kinetics, 407,408*f*
regenerability effect in commercial operation, 409,411*f*
role of regenerability in catalyst screening, 409,412
- Testing
catalyst(s) for fixed-bed processes, small scale, *See* Small-scale testing of catalysts for fixed-bed processes
catalyst performance, 254–412
philosophical overview, 2–5
vanadium interaction with fluid catalytic cracking catalyst, 296–309
See also Catalyst performance testing
- Thiele modulus, relationship to effectiveness factor, 415–416,418*f*
- Thiophene, loss in catalytic activity, 428–437
- Three-dimensional stochastic network
computer images, 52,54–60
pore size distribution, 52,53*f*
- Transbed velocity profile, erasure, 16,18–19,20–21*f*
- Transverse macroscopic velocity, role in small-scale testing of catalysts, 14,16,17*f*
- Trickle-flow processes, accuracy, 31,34–38
- V
- Vanadic acid, formation in fluid catalytic cracking catalyst regenerator, 283–284
- Vanadium
laboratory catalyst deactivation by cyclic propylene steaming, 177–183
poisoning of fluid catalytic cracking catalysts, 283–284
role in catalyst deactivation, 296–297
- Vanadium interaction with fluid catalytic cracking catalyst
development of test methods, 296–207
experimental procedure, 298–299
test methods
cyclic metals decomposition method, 299–300
Engelhard transfer method, 300–309
Mitchell method, 299–300
- Vanadium mobility in fluid catalytic cracking
catalyst concentration effect, 291,292*f*
experimental procedure, 284–285

- Vanadium mobility in fluid catalytic cracking—*Continued*
- mass transfer requirements of vapor-phase vanadium fluid bed, 286–287
- operating condition effect, 291
- particle-to-particle transfer of vanadium, 287–289
- staged bed transportation experiment, 285–286
- trap experiment, 285
- vanadium loading effect, 291,293*f,t*,294*f*
- vanadium vapor adsorption onto trap as rate-limiting step in vanadium transfer, 290–291
- vapor pressure of vanadic acid, 291
- Vanadium transfer
- mechanism, 304–307
- requirements, 301,302–303*f*
- W
- Wall effect, 14,16,17*f*
- Washburn equation, 43,46
- X
- ¹²⁹Xe-NMR studies, coking of zeolite catalysts, 110–115
- Y
- Y zeolites, ¹³C-NMR studies, 99–105
- Z
- Zeolite(s)
- applications, 77
- coke effect on function, 62
- pore structures, 62–63
- role in coke deactivation, 84*f*,85
- sodium deactivation, 159–170
- Zeolite catalysts, NMR techniques for studying coking, 99–115
- Zeolite catalyst deactivation by coke
- amount of coke deposition vs. relative activity, 63,64*f*
- coke deposition process, 63,64*f*
- diffusivity effect on coke deposition
- coked zeolite, 67,69–75
- fresh zeolite, 65,67,68*f*
- shape selectivity, 65,66*f*
- mechanism, 72
- n* value of CH_{*n*} coke vs. coke loading, 63,66*f*
- pore structures of zeolites, 62–63
- Zn/H-ZSM-5 zeolite, life testing, 367–368
- ZSM-5 zeolites, ¹³C-NMR studies, 99–105